

APR 29 1989

NAS 1.55:3031/pt.2

mf - 2830 - H-10)

330

NASA Conference Publication 3031
Part 2

4

Recent Advances in Multidisciplinary Analysis and Optimization

*Proceedings of a symposium held in
Hampton, Virginia
September 28-30, 1988*

6

NASA

5

VL

NASA Conference Publication 3031
Part 2

Recent Advances in Multidisciplinary Analysis and Optimization

Jean-Francois M. Barthelemy, Editor
NASA Langley Research Center
Hampton, Virginia

Proceedings of a symposium cosponsored by
NASA Langley Research Center, NASA Lewis
Research Center, and the Wright Research
Development Center, and held in
Hampton, Virginia
September 28-30, 1988



National Aeronautics and
Space Administration
Office of Management
Scientific and Technical
Information Division

1989

I

BLANK PAGE

H

PREFACE

This publication contains papers presented at the Second NASA/Air Force Symposium on Recent Advances in Multidisciplinary Analysis and Optimization held September 28-30, 1988 in Hampton, Virginia. The symposium was cosponsored by NASA Langley, NASA Lewis, and the Wright Research Development Center. The meeting was attended by 195 participants, with 41% from industry, 35% from academia, and 24% from government organizations.

The aim of the symposium was to provide a forum for researchers, software developers, and practitioners of multidisciplinary analysis and optimization to learn of the latest developments and to exchange experiences in this burgeoning field of engineering.

Ninety-two papers were presented (83 of which are published here). Of the papers originally presented, 58% discussed method development, 30% applications, and 12% software development or implementation. Most (72%) of the contributions to the symposium were strictly multidisciplinary. There were 15 papers dealing with the combination of structures and control systems, 10 with aeroelastic problems, and 5 with aeroservoelastic problems. Eight papers dealt with generic developments in multidisciplinary design. The keynote address was a review of the role of knowledge-based systems in analysis and optimization.

The papers are grouped by sessions and are identified in the Contents. Papers were edited to conform to the technical standards set by NASA for conference publications. A list of addresses of all registered participants is included.

Jean-François M. Barthelemy
Technical Program Chairman

BLANK PAGE

CONTENTS

PREFACE	iii
ATTENDEES	xiii

Part 1*

Session 1: Plenary **Chairman: Owen P. Hughes**

APPLICATIONS OF INTEGRATED DESIGN/ANALYSIS SYSTEMS IN AEROSPACE	
STRUCTURAL DESIGN	3
Philip Mason, Edwin Lerner, and Lawrence Sobel	
INTEGRATED DESIGN OPTIMIZATION RESEARCH AND DEVELOPMENT IN AN INDUSTRIAL ENVIRONMENT	39
V. Kumar, M. D. German, and S.-J. Lee	
OPTIMIZATION BY DECOMPOSITION: A STEP FROM HIERARCHIC TO NON-HIERARCHIC SYSTEMS	51
Jaroslav Sobieszczanski-Sobieski	
OVERVIEW OF DYNAMICS INTEGRATION RESEARCH (DIR) PROGRAM AT LANGLEY RESEARCH CENTER: Goals and Progress	79
Steven M. Sliwa and Irving Abel	

SESSION 2: HELICOPTERS **Chairmen: D. Anderson and R. G. Kvaternik**

AN INITIATIVE IN MULTIDISCIPLINARY OPTIMIZATION OF ROTORCRAFT	109
Howard M. Adelman and Wayne R. Mantay	
STRUCTURAL OPTIMIZATION OF ROTOR BLADES WITH STRAIGHT AND SWEPT TIPS SUBJECT TO AEROELASTIC CONSTRAINTS	145
Peretz P. Friedmann and Roberto Celi	
OPTIMIZATION OF ROTOR BLADES FOR COMBINED STRUCTURAL, PERFORMANCE, AND AEROELASTIC CHARACTERISTICS	163
David A. Peters and Y. P. Cheng	
TRANSONIC AIRFOIL DESIGN FOR HELICOPTER ROTOR APPLICATIONS	181
Ahmed A. Hassan and B. Jackson	
EFFICIENT SENSITIVITY ANALYSIS AND OPTIMIZATION OF A HELICOPTER ROTOR	195
J. W. Lim and I. Chopra	
STRUCTURAL OPTIMIZATION OF ROTOR BLADES WITH INTEGRATED DYNAMICS AND AERODYNAMICS	205
Aditi Chattopadhyay and Joanne L. Walsh	

*Presented under separate cover.

MULTI-OBJECTIVE/LOADING OPTIMIZATION FOR ROTATING COMPOSITE FLEXBEAMS	235
Brian K. Hamilton and James R. Peters	

SESSION 3: ARTIFICIAL INTELLIGENCE
Chairmen: K. H. Abbott and P. Hajela

NEW DIRECTIONS FOR ARTIFICIAL INTELLIGENCE (AI) METHODS IN OPTIMUM DESIGN	259
Prabhat Hajela	
DEVELOPMENT OF A MICRO-COMPUTER BASED INTEGRATED DESIGN SYSTEM FOR HIGH ALTITUDE LONG ENDURANCE AIRCRAFT	275
David W. Hall and J. Edward Rogan	
DEMONSTRATION OF DECOMPOSITION AND OPTIMIZATION IN THE DESIGN OF EXPERIMENTAL SPACE SYSTEMS	297
Sharon L. Padula, Chris A. Sandridge, Raphael T. Haftka, and Joanne L. Walsh	
STRUTEX - A PROTOTYPE KNOWLEDGE-BASED SYSTEM FOR INITIALLY CONFIGURING A STRUCTURE TO SUPPORT POINT LOADS IN TWO DIMENSIONS	317
James L. Rogers and Jaroslaw Sobieszczanski-Sobieski	
TRUSS: AN INTELLIGENT DESIGN SYSTEM FOR AIRCRAFT WINGS	333
Preston R. Bates and Daniel P. Schrage	
REAL-TIME APPLICATION OF KNOWLEDGE-BASED SYSTEMS	357
Randal W. Brumbaugh and Eugene L. Duke	
THE DESIGNER OF THE 90'S: A LIVE DEMONSTRATION	373
Tommy L. Green, Basil M. Jordan, Jr., and Timothy L. Oglesby	

SESSION 4: AEROELASTIC TAILORING
Chairmen: B. A. Rommel and T. A. Weisshar

STRUCTURAL TAILORING OF COUNTER ROTATION PROPPANS	389
K. W. Brown and D. A. Hopkins	
COMPOSITE SIZING AND PLY ORIENTATION FOR STIFFNESS REQUIREMENTS USING A LARGE FINITE ELEMENT STRUCTURAL MODEL	403
N. A. Radovcich and D. P. Gentile	
AEROELASTIC TAILORING AND INTEGRATED WING DESIGN	431
Mike Love and Jon Bohlmann	
INTEGRATED AERODYNAMIC-STRUCTURAL DESIGN OF A FORWARD-SWEPT TRANSPORT WING	445
R. T. Haftka, B. Grossman, P. J. Kao, D. M. Polen, and J. Sobieszczanski-Sobieski	
STATIC AEROELASTIC ANALYSIS AND TAILORING OF MISSILE CONTROL FINS	465
S. C. McIntosh, Jr., and M. F. E. Dillenius	

EFFECTS OF NONLINEAR AERODYNAMICS AND STATIC AEROELASTICITY ON MISSION PERFORMANCE CALCULATIONS FOR A FIGHTER AIRCRAFT	477
Gary L. Giles, Kenneth E. Tatum, and William E. Foss, Jr.	
OPTIMUM STRUCTURAL DESIGN WITH STATIC AEROELASTIC CONSTRAINTS	497
K. B. Bowman, R. V. Grandhi, and F. E. Eastep	
OPTIMUM DESIGN OF SWEEP-FORWARD HIGH-ASPECT-RATIO GRAPHITE-EPOXY WINGS	509
M. J. Shuart, R. T. Haftka, and R. L. Campbell	

PART 2

SESSION 5: SOFTWARE I

Chairmen: G. W. Vanderplaats and R. E. Pulton

ASTROS - A MULTIDISCIPLINARY AUTOMATED STRUCTURAL DESIGN TOOL	529
D. J. Neill	
A GENERALIZED SOFTWARE EXECUTIVE FOR MULTIDISCIPLINARY COMPUTATIONAL STRUCTURAL DYNAMICS	545
Alex Berman	
RESEARCH ON OPTIMIZATION-BASED DESIGN AT THE ENGINEERING DESIGN METHODS LAB, BRIGHAM YOUNG UNIVERSITY	565
R. J. Balling, A. R. Parkinson, and J. C. Free	
RECENT EXPERIENCES USING FINITE-ELEMENT-BASED STRUCTURAL OPTIMIZATION	58
B. K. Paul, J. C. McConnell, and M. H. Love	
THE SIZING AND OPTIMIZATION LANGUAGE (SOL) - A COMPUTER LANGUAGE TO IMPROVE THE USER/OPTIMIZER INTERFACE	601
S. H. Lucas and S. J. Scotti	
ROBUST COMPUTER-AIDED SYNTHESIS AND OPTIMIZATION OF LINEAR MULTIVARIABLE CONTROL SYSTEMS WITH VARYING PLANT DYNAMICS VIA AUTOCON	621
C. P. Lefkowitz, J. A. Tekawy, P. K. Pujara, and M. G. Safonov	
COMPUTERIZED DESIGN SYNTHESIS (CDS), A DATA BASE-DRIVEN MULTIDISCIPLINARY DESIGN TOOL	639
D. M. Anderson and A. O. Bolukbasi	

SESSION 6: SENSITIVITY ANALYSIS

Chairmen: R. T. Haftka and B. Prasad

ON EQUIVALENCE OF DISCRETE-DISCRETE AND CONTINUUM-DISCRETE DESIGN SENSITIVITY ANALYSIS	653
Kyung K. Choi and Sung-Ling Twu	
AN INVESTIGATION OF USING AN RQP BASED METHOD TO CALCULATE PARAMETER SENSITIVITY DERIVATIVES	673
Todd J. Beltracchi and Gary A. Gabriele	

GRID SENSITIVITY CAPABILITY FOR LARGE SCALE STRUCTURES	697
Gopal K. Nagendra and David V. Wallerstein	
ITERATIVE METHODS FOR DESIGN SENSITIVITY ANALYSIS	713
A. D. Belegundu and B. G. Yoon	
RESULTS OF AN INTEGRATED STRUCTURE/CONTROL LAW DESIGN SENSITIVITY ANALYSIS	727
Michael G. Gilbert	
ON THE CALCULATION OF DERIVATIVES OF EIGENVALUES AND EIGENVECTORS IN THE SIMULTANEOUS DESIGN AND CONTROL OF STRUCTURES	747
Luis Mesquita and Manohar P. Kamat	
TREATMENT OF BODY FORCES IN BOUNDARY ELEMENT DESIGN SENSITIVITY ANALYSIS	759
Sunil Saigal, R. Aithal, and Jizu Cheng	
DESIGN SENSITIVITY ANALYSIS OF BOUNDARY ELEMENT SUBSTRUCTURES	777
James H. Kane, Sunil Saigal, and Richard H. Gallagher	

SESSION 7: CONTROL OF AEROELASTIC STRUCTURES

Chairmen: I. Abel, and N. A. Radovcich

AEROSERVOELASTIC TAILORING FOR LATERAL CONTROL ENHANCEMENT	803
Terrence A. Weisshaar and Changho Nam	
RESULTS OF INCLUDING GEOMETRIC NONLINEARITIES IN AN AEROELASTIC MODEL OF AN F/A-18	815
Carey S. Buttrill	
FLUTTER SUPPRESSION USING EIGENSPACE FREEDOMS TO MEET REQUIREMENTS	837
William M. Adams, Jr., Robert E. Fennell, and David M. Christhilf	
AEROELASTIC MODELING FOR THE FIT TEAM F/A-18 SIMULATION	861
Thomas A. Zeiler and Carol D. Wieseman	
DIGITAL ROBUST CONTROL LAW SYNTHESIS USING CONSTRAINED OPTIMIZATION	879
Vivekananda Mukhopadhyay	
AN INTEGRATED APPROACH TO THE OPTIMUM DESIGN OF ACTIVELY CONTROLLED COMPOSITE WINGS	897
E. Livne	
CONTROL SURFACE SPANWISE PLACEMENT IN ACTIVE FLUTTER SUPPRESSION SYSTEMS	919
E. Nissim and J. J. Burken	

SESSION 8: STRUCTURES

Chairmen: R. Levy and P. Papalambros

AN APPROXIMATION FUNCTION FOR FREQUENCY CONSTRAINED STRUCTURAL OPTIMIZATION	937
R. A. Canfield	

STRUCTURAL OPTIMIZATION OF FRAMED STRUCTURES USING GENERALIZED OPTIMALITY CRITERIA	955
R. M. Kolonay, V. B. Venkayya, V. A. Tischler, and R. A. Canfield	
FINITE ELEMENT FLOW-THERMAL-STRUCTURAL ANALYSIS OF AERODYNAMICALLY HEATED LEADING EDGES	971
Pramote Dechaumphai, Allan R. Wieting, and Ajay K. Pandey	
INVOLUTE COMPOSITE DESIGN EVALUATION USING GLOBAL DESIGN SENSITIVITY DERIVATIVES	991
J. K. Hart and E. L. Stanton	
OPTIMIZING FOR MINIMUM WEIGHT WHEN TWO DIFFERENT FINITE ELEMENT MODELS AND ANALYSES ARE REQUIRED	1009
Jeffrey C. Hall	

PART 3*

SESSION 9: LARGE ENGINEERING SYSTEMS Chairman: G. L. Giles

ENGINEERING APPLICATIONS OF HEURISTIC MULTILEVEL OPTIMIZATION METHODS	1029
Jean-François M. Barthelemy	
RECENT DEVELOPMENTS IN MULTILEVEL OPTIMIZATION	1039
G. N. Vanderplaats and D-S Kim	
A DECOMPOSITION-BASED DESIGN OPTIMIZATION METHOD WITH APPLICATIONS	1055
S. Azarn, M. Pecht, W.-C. Li, and S. Praharaj	
MULTILEVEL DECOMPOSITION OF COMPLETE VEHICLE CONFIGURATION IN A PARALLEL COMPUTING ENVIRONMENT	1069
Vinay Bhatt and K. M. Ragsdell	

SESSION 10: SHAPE OPTIMIZATION Chairman: G. A. Gabriele

DESIGN OPTIMIZATION OF AXISYMMETRIC BODIES IN NONUNIFORM TRANSONIC FLOW	1085
C. Edward Lan	
PROCEDURES FOR SHAPE OPTIMIZATION OF GAS TURBINE DISKS	1097
Tsu-Chien Cheu	

SESSION 11: ENGINEERING SYSTEM DESIGN Chairmen: M. D. German and D. P. Schrage

A DECISION-BASED PERSPECTIVE FOR THE DESIGN OF METHODS FOR SYSTEMS DESIGN	1111
Farrokh Mistree, Douglas Muster, Jon A. Shupe, and Janet K. Allen	

*Presented under separate cover.

THE ART OF SPACECRAFT DESIGN: A MULTIDISCIPLINARY CHALLENGE	1137
P. Abdi, H. Ide, M. Levine, and L. Austel	
HYPersonic AIRBREATHING VEHICLE CONCEPTUAL DESIGN (FOCUS ON AERO-SPACE PLANE)	1157
James L. Hunt and John G. Martin	
OPTIMIZING CONCEPTUAL AIRCRAFT DESIGNS FOR MINIMUM LIFE CYCLE COST	1195
Vicki S. Johnson	
AIRCRAFT DESIGN OPTIMIZATION WITH MULTIDISCIPLINARY PERFORMANCE CRITERIA	1219
Stephen Morris and Ilan Kroo	

SESSION 12: METHODS

Chairmen: M. P. Kamat and J. E. Rogan

AN INTERPRETATION AND SOLUTION OF ILL-CONDITIONED LINEAR EQUATIONS	1239
I. U. Ojalvo and T. Ting	
GENERALIZED MATHEMATICAL MODELS IN DESIGN OPTIMIZATION	1253
Panos Y. Papalambros and J. R. Jagannatha Rao	
OPTIMUM DESIGN OF STRUCTURES SUBJECT TO GENERAL PERIODIC LOADS	1265
R. Reiss and B. Qian	
FUZZY SET APPLICATIONS IN ENGINEERING OPTIMIZATION	1279
Alejandro R. Diaz	
A PENALTY APPROACH FOR NONLINEAR OPTIMIZATION WITH DISCRETE DESIGN VARIABLES	1291
Dong K. Shin, Z. Gurdal, and O. H. Griffin, Jr.	
MULTIPLIER-CONTINUATION ALGORITHMS FOR CONSTRAINED OPTIMIZATION	1303
Bruce N. Lundberg, Aubrey B. Poore and Bing Yang	

SESSION 13: SOFTWARE II

Chairmen: R. A. Canfield and J. L. Rogers, Jr.

A LARGE SCALE SOFTWARE SYSTEM FOR SIMULATION AND DESIGN OPTIMIZATION OF MECHANICAL SYSTEMS	1319
Bernhard Dopker and Edward J. Haug	
THE ROLE OF OPTIMIZATION IN THE NEXT GENERATION OF COMPUTER-BASED DESIGN TOOLS	1335
J. E. Rogan	
AN OVERVIEW OF THE DOUGLAS AIRCRAFT COMPANY AEROELASTIC DESIGN OPTIMIZATION PROGRAM (ADOP)	1359
Alan J. Dodd	
MEETING THE CHALLENGES WITH THE DOUGLAS AIRCRAFT COMPANY AEROELASTIC DESIGN OPTIMIZATION PROGRAM (ADOP)	1369
Bruce A. Rommel	

SESSION 14: DYNAMICS AND CONTROL OF FLEXIBLE STRUCTURES

Chairmen: J.-N. Juang and E. Livne

OPTIMIZATION OF STRUCTURE AND CONTROL SYSTEM	1381
N. S. Khot and R. V. Grandhi	
STRUCTURAL OPTIMIZATION AND RECENT LARGE GROUND ANTENNA INSTALLATIONS	1393
Roy Levy	
A NOVEL IMPLEMENTATION OF METHOD OF OPTIMALITY CRITERION IN SYNTHESIZING SPACECRAFT STRUCTURES WITH NATURAL FREQUENCY CONSTRAINTS	1417
B. P. Wang and F. H. Chu	
COMPUTATIONAL EXPERIMENTS IN THE OPTIMAL SLEWING OF FLEXIBLE STRUCTURES	1427
T. E. Baker and E. Polak	
OPTIMAL PLACEMENT OF EXCITATIONS AND SENSORS BY SIMULATED ANNEALING	1441
M. Salama, R. Bruno, G-S. Chen, and J. Garba	
EXPERIENCES IN APPLYING OPTIMIZATION TECHNIQUES TO CONFIGURATIONS FOR THE CONTROL OF FLEXIBLE STRUCTURES (COPS) PROGRAM	1459
Joanne L. Walsh	
AN IMPROVED ALGORITHM FOR OPTIMUM STRUCTURAL DESIGN WITH MULTIPLE FREQUENCY CONSTRAINTS	1489
Oliver G. McGee and Khing P. Phan	

ADDITIONAL PAPERS

The following paper is being included in this publication although time restrictions did not permit its presentation at the September conference.

STRUCTURAL DAMAGE ASSESSMENT AS AN IDENTIFICATION PROBLEM	1507
P. Hajela and P. J. Soeiro	

The following paper arrived during the printing process and was originally included in Session I.

RECENT DEVELOPMENTS IN LARGE-SCALE STRUCTURAL OPTIMIZATION	1521
V. B. Venkayya	

BLANK PAGE

ATTENDEES

Mrs. Kathy H. Abbott
NASA/Langley Research Center
MS 156A
Hampton, VA 23665-5225

Mr. Irving Abel
NASA/Langley Research Center
MS 242
Hampton, VA 23665-5225

Mr. William M. Adams Jr.
NASA/Langley Research Center
MS 489
Hampton, VA 23665-5225

Dr. Howard K. Adelman
NASA/Langley Research Center
MS 246
Hampton, VA 23665-5225

Dr. Don Anderson
McDonnell Douglas Helicopter Co.
Bldg. 530/B327
5000 E. McDowell Rd.
Mesa, AZ 85205

Mr. Ernest S. Armstrong
NASA/Langley Research Center
MS 499
Hampton, VA 23665-5225

Prof. Shapour Azarm
The University of Maryland
Department of Mechanical
Engineering
College Park, MD 20742

Dr. Richard J. Balling
Brigham Young University
Engineering Design Methods
Laboratory
368R Clyde Building
Provo, UT 84602

Dr. Dey Banerjee
McDonnell Douglas Helicopter Co.
Bldg. 530, MS/B 346
5000 E. McDowell Rd.
Mesa, AZ 85205

Mr. Paul Barnhart
Sverdrup Technology, Inc.
P.O. Box 30650, Midpark Branch
Middleburg Heights, OH 44130

Dr. Bruno Barthelemy
Ford Research and Engineering
Center
Room E3184/SCI-LAB
P. O. Box 2053
Dearborn, MI 48121-2053

Dr. Jean-Francois M. Barthelemy
NASA/Langley Research Center
MS 246
Hampton, VA 23665-5225

Mr. Oscar Barton, Jr.
Howard University
Department of Mechanical
Engineering
2308 6th St. N.W.
Washington, DC 20059

Mr. P. R. Bates
Georgia Institute of Technology
School of Aerospace Engineering
P. O. Box 30302
Atlanta, GA 30332-0150

Prof. Asbok D. Belegundu
Penn State University
Mechanical Engineering
University Park, PA 16802

Mr. Todd J. Beltracchi
Rensselaer Polytechnic Institute
2418 Huntington Lane #3
Redondo Beach, CA 90278

Dr. Leslie Berke
NASA/Lewis Research Center
MS 4907
21000 Brookpark Road
Cleveland, OH 44135

Mr. Alex Berman
Kaman Aerospace Corp.
Old Windsor Road
P.O. Box 2
Bloomfield, CT 06002

Mr. Vinay Bhatt
University of Missouri-Columbia
Mechanical and Aerospace
Engineering
1080 Engineering UMC
Columbia, MO 65201

Mr. Robert Blackwell
Sikorsky Aircraft
No. Main Street
Stratford, CT 06401-1381

Mr. Chris Borland
Boeing Military Airplane Co.
P.O. Box 3707
Mail Code 33-04
Seattle, WA 98124

Mr. Keith Bowman
US Air Force
AFWAL/FIRCA
Wright AFB
Wright-Patterson AFB, OH 45433

Mrs. Lynn M. Bowman
Planning Research Corporation
303 Butler Farm Rd, Suite 100
Hampton, VA 23666

Mr. Kenneth W. Brown
Pratt & Whitney Aircraft
400 Main Street, M.S. 163-09
East Hartford, CT 06108

Mr. Randal W. Brumbaugh
Planning Research Corporation
PO Box 271
NASA Dryden Bldg. 4839
Edwards, CA 93323

Mr. Christopher W. Batten
Digital Equipment Corporation
4417 Corporation
Virginia Beach, VA 23462

Mr. Carey N. Buttrill
NASA/Langley Research Center
MS 494
Hampton, VA 23665-5225

Mr. Charles Canarda
NASA/Langley Research Center
MS 396
Hampton, VA 23665-5225

Mr. Frank Campisano
Northrop Corporation
One Northrop Ave
Hawthorne, CA 90250

Capt. Robert A. Canfield
AF Wright Aeronautical
Laboratories
AFWAL/FIRRA
Wright-Patterson AFB, OH
45433-6553

Mr. Richard G. Carter
ICASE
NASA/Langley Research Center
MS 132C
Hampton, VA 23665

Mr. Jeffrey A. Cerro
Planning Research Corporation
303 Butler Farm Rd, Suite 100
Suite 100
Hampton, VA 23666

Dr. Christos C. Chamis
NASA/Lewis Research Center
MS 49-8
21000 Brookpark Road
Cleveland, OH 44135

Prof. A. Chandra
University of Arizona
Aerospace and Mechanical
Engineering
Aero Bldg #16
Tucson, AZ 85721

Dr. Kwan J. Chang
Planning Research Corporation
303 Butler Farm Rd, Suite 100
Hampton, VA 23666

Dr. Mladen Chargin
NASA/Ames Research Center
MC 213-3
Moffett Field, CA 94035

Dr. Aditi Chattopadhyay
Analytical Services and
Materials Inc.
NASA/Langley Research Center
MS 246
Hampton, VA 23665-5225

Dr. Tsu-Chien Chou
Textron Lycoming, Dept. LSK-5
550 S. Main Street
Stratford, CT 06497

Prof. Kyung K. Choi
The University of Iowa
Dept. of Mechanical Engineering
2132 Engineering Bldg
Iowa City, IA 52242

Mr. Choon T. Chou
Ford Motor Company
S-1108, SRL
P.O. Box 2053
Dearborn, MI 48121

Prof. Inderjit Chopra
University of Maryland
Dept. of Aerospace Engineering
College Park, MD 20742

Mr. David M. Christhilf
Planning Research Corporation
NASA/Langley Research Center
MS/489
Hampton, VA 23665-5225

Mr. Ching-Hung Chuang
Old Dominion University
937 Rockbridge Ave. #244
Norfolk, VA 23508

Prof. Young W. Chun
Villanova University
Dept. of Mechanical Engineering
Villanova, PA 19085

Mr. Robert D. Consoli
General Dynamics
P. O. Box 748
Fort Worth, TX 76102

Mr. Mark W. Davis
United Technologies Research
Center
MS 19
Silver Lane
E. Hartford, CT 06108

Mr. Randall C. Davis
NASA/Langley Research Center
MS 396
Hampton, VA 23665-5225

Dr. Pramote Dechaumphai
NASA/Langley Research Center
MS 395
Hampton, VA 23665-5225

Prof. Alejandro Diaz
Michigan State University
Dept. of Mechanical Engineering
Room 200, Engineering Building
East Lansing, MI 48824-1226

Mr. Alan J. Dodd
Douglas Aircraft Company
C1-E84, Mail Code 212-10
3155 Lakewood Blvd.
Long Beach, CA 90815

Mr. Augustine R. Dovi
Planning Research Corporation
303 Butler Farm Rd, Suite 100
Hampton, VA 23666

Mr. Rodney Dreisbach
The Boeing Company
P. O. Box 707
Mail Stop 9W-22
Seattle, WA

Mr. Delmar W. Drier
NASA/Lewis Research Center
MS 86-12
21000 Brookpark Road
Cleveland, OH 44135

Dr. Ernest D. Eason
Modeling & Computing Services
1153 Bordeaux Drive
Suite 107
Sunnyvale, CA 94089

Dr. Peter A. Fenyas
General Motors Research
Laboratories
Engineering Mechanics Department
30500 Mound Rd Dept 15
Warren, MI 48090-9055

Mr. Brian Fite
NASA/Lewis Research Center
21000 Brookpark Road
MS 86-10
Cleveland, OH 44135

Dr. Donald Flaggs
Lockheed Palo Alto Research
Laboratory
Lockheed M&S 93-30/251
3251 Hanover ST.
Palo Alto, CA 94304

Prof. Claude Fleury
University of California
Dept. of Mech. Aero. & Nuclear
Engrg.
5732 Boelter Hall
Los Angeles, CA 90024

Mr. Williard E. Foss Jr.
NASA/Langley Research Center
MS 412
Hampton, VA 23665

Prof. Joseph Free
Brigham Young University
Department of Mechanical
Engineering
242 Clyde Building
Provo, UT 84602

Prof. Peretz P. Friedmann
University of California-Los
Angeles
5732H Boelter Hall
Los Angeles, CA 90024

Prof. Robert E. Fulton
Georgia Institute of Technology
Mechanical Engineering
Atlanta, GA 30332

Dr. Gary A. Gabriele
Rensselaer Polytechnic Institute
Dept. of Mechanical Engineering
Johnson Engineering Center,
Rm. 4026
Troy, NY 12180-3590

Mr. James E. Gardner
NASA/Langley Research Center
MS 246
Hampton, VA 23665

Mrs. Marjorie German
G. E. Research and Development
1 River Road, Bldg. K-1, Room
3A20
Schenectady, NY

Mr. D. Ghosh
Planning Research Corporation
303 Butler Farm Rd, Suite 100
Hampton, VA 23665

Mr. Daniel P. Giesy
Planning Research Corporation
303 Butler Farm Rd, Suite 100
Suite 100
Hampton, VA 23666

Mr. Michael G. Gilbert
NASA/Langley Research Center
MS 243
Hampton, VA 23665-5225

Dr. Gary L. Giles
NASA/Langley Research Center
MS 246
Hampton, VA 23665-5225

Mr. David E. Glass
Analytical Services & Materials
107 Research Drive
Hampton, Va 23666

Prof. Ramana Grandhi
Wright State University
Mechanical Systems and
Engineering
Dayton, OH 45435

Mr. Philip C. Graves
Vigyan Research Association
30 Research Drive
Hampton, Va 23666

Mr. Tommy L. Green
LTV Aerospace and Defense
Company
Aircraft Products Group
P.O. Box 655907, MS 194-24
Dallas, TX 75265-5907

Mr. William H. Greene
NASA/Langley Research Center
MS 190
Hampton, VA 23665-5225

Prof. Bernard Grossman
Aerospace and Ocean Engineering
VPI & SU
Blacksburg, VA 24061

Prof. Zafer Gurdal
VPI & SU
Engineering Science and
Mechanics Dept.
Norris Hall
Blacksburg, VA 24061

Prof. Raphael T. Haftka
VPI&SU
Dept. of Aerospace & Ocean
Engineering
Blacksburg, VA 24061

Prof. Prabhat Hajela
University of Florida
Dept. of Aero. Eng., Mech. and
Eng. Sci.
231 Aerospace, Aero
Gainesville, FL 32611

Mr. David W. Hall
David Hall Consulting
1158 South Mary Avenue
Sunnyvale, CA 94087-2103

Dr. Jeffrey C. Hall
General Dynamics Corp./Elec.
Boat Div.
Department 443
Eastern Point Road
Groton, CT 06340

Mr. Stephen A. Hambric
David Taylor Research Center
Code 1844
Bethesda, MD 20084

Dr. M. Nabil Hamouda
Planning Research Corporation
NASA/Langley Research Center
MS 340
Hampton, VA 23665-5225

Mr. Jonathan K. Hart
PDA Engineering, Inc.
2975 Redhill Avenue
Costa Mesa, CA 92626-5923

Mr. Ahmed A. Hassan
McDonnell Douglas Helicopter
Company
5000 E. McDowell
Bldg 530, MS B346
Mesa, AZ 85205-9797

Mr. T. K. Hasselman
Engineering Mechanics Assoc.,
Inc.
3820 Del Amo Boulevard, Suite
318
Torrance, CA 90503

Ms. Jennifer Heeg
Planning Research Corporation
303 Butler Farm Rd, Suite 100
Hampton, Va 23666

Mr. Charles Holland
AF Office of Scientific Research
Department of the Air Force
Bolling Air Force Base, DC
20332-6458

Prof. Jean Win Hou
Old Dominion University
Dept. Mech. Engineering and
Mechanics
Norfolk, VA 23462

Prof. Owen F. Hughes
VPI & SUN
1745 Jefferson Davis Highway
STE 300
Arlington, VA 22202

Mr. Amir Izadpanah
Vigyan Research Association
NASA/Langley Research Center
MS 340
Hampton, VA 23665

Mr. Burton H. Jackson
McDonnell Douglas Helicopter
5000 E. McDowell
Mesa, AZ

MS. Cheryl C. Jackson
Old Dominion University
Dept. of Mech. Eng. and Mech.
Norfolk, VA 23529-0247

Mr. Benjamin B. James III
Planning Research Corporation
303 Butler Farm Rd, Suite 100
Hampton, VA 23666

Ms. Vicki Johnson
NASA/Langley Research Center
MS 412
Hampton, VA 23665-5225

Mr. B. M. Jordan, Jr.
LTV Aerospace & Defense Company
P.O. Box 655907
MS 194-24
Dallas, Texas 75265-5907

Mr. Suresh M. Joshi
NASA/Langley Research Center
MS 161
Hampton, VA 23665-5225

Dr. Jer-Man Juang
NASA/Langley Research Center
MS 230
Hampton, VA 23665-5225

Prof. Manohar P. Kamat
Georgia Institute of Technology
School of Aerospace Engineering
Atlanta, GA 30332

Mr. James Kane
Clarkson University
Mech. and Ind. Engineering Dept.
Potomac, NY 13676

Mr. Pi-Jen Kao
VPI&SU
Dept. of Aerospace & Ocean
Engineering
Blacksburg, VA 24061

Mr. Mordechai Karpel
Technion -Israel Institute of
Technology
Dept. of Aero Engineering
Haifa 32000 Israel

Mr. Sean P. Kenny
Old Dominion University
Norfolk, VA 23508

Mr. Suresh Khandelwal
Sverdrup Technology
16530 Commerce Ct.
Middleburg Hts, OH 44130

Prof. Noboru Kikuchi
University of Michigan
Department of Mechanical
Engineering
Ann Arbor, MI 48109

Prof. Rex K. Kincaid
College of William and Mary
Dept. of Mathematics
Williamsburg, VA 23185

Dr. Norman F. Knight, Jr.
NASA/Langley Research Center
MS 244
Hampton, VA 23665-5225

Mr. Raymond M. Kolonay
AF Wright Aeronautical
Laboratories
AFWAL/FIBRA
Wright-Patterson AFB, OH 45433

Prof. Ilan Kroo
Stanford University
Dept. of Aero/Astro
Stanford, CA 94305

Dr. Raymond G. Kvaternik
NASA/Langley Research Center
MS 340
Hampton, VA 23665-5225

Prof. C. Edward Lan
The University of Kansas
Aerospace Engineering Dept.
Room 2004, Learned Hall
Lawrence, KS 66045

Mr. Jerry Lang
NASA/Lewis Research Center
21000 Brookpark Rd.
Cleveland, OH 44135

Mr. M. Levine
Rockwell International
P.O. Box 92098
Los Angeles, CA 90245

Dr. Roy Levy
Jet Propulsion Laboratory
MS 144-201
4800 Oak Grove Drive
Pasadena, CA 91109

Mr. Joon W. Lim
University of Maryland
College Park, MD

Mr. Kyong B. Lim
Planning Research Corporation
303 Butler Farm Rd
Suite 100
Hampton, VA 23666

Mr. Eli Livne
University of California Los
Angeles
4531 Boelter Hall, UCLA
Los Angeles, CA 90024

Mr. Andrew Logan
McDonnell Douglas Helicopter Co.
Bldg. 503, MSB 325
5000 E. McDowell Rd.
Mesa, AZ 85205

Mr. Michael G. Long
Cray Research, Inc.
1333 Northland Drive
Mendota Heights, MN 55120

Dr. Robert V. Lust
General Motors Research
Laboratories
Engineering Mechanics Department
30500 Mound Road, MS 256 Rm B
Warren, MI 48090-9057

Mr. Peiman G. Maghami
Old Dominion University
Norfolk, VA 23508 23508

Mr. Wayne R. Mantay
US Army Aerostructures
Directorate
NASA/Langley Research Center
MS 266
Hampton, VA 23665-5225

Mr. Carl J. Martin
Planning Research Corporation
303 Butler Farm Rd, Suite 100
Hampton, VA 23666

Mr. John G. Martin
Planning Research Corporation
303 Butler Farm Rd, Suite 100
Hampton, VA 23666

Mr. Zoran W. Martinovic
Analytical Mechanics
Associates, Inc.
17 Research Drive
Hampton, VA 23666

Mr. Philip Mason
Grumman Aerospace Corp.
B-35, Dept. 430
Stewart Ave.
Bethpage, NY 11714

Mr. Oliver G. McGee
Ohio State University
Department of Civil Engineering
417B Hitchcock Hall
Columbus OH 43210

Mr. Niki Mahta
Old Dominion University
Dept. of Mechanical Eng. and
Mechanical

College of Engineering and
Technology
Norfolk, VA 23529-0247

Prof. Luis Mesquita
University of Nebraska
Department of Engineering
Mechanics
217 Bancroft
Lincoln, NE 68588

Prof. Farrokh Mistree
University of Houston-Univ. Park
Dept. of Mechanical Engineering
4800 Calhoun Road
Houston, TX 77204-4792

Dr. Hiro Miura
NASA/Ames Research Center
Ames Research Center
Attn: 237-11
Moffett Field, CA 94035

Mrs. Arlene A. Moore
Planning Research Corporation
303 Butler Farm Rd, Suite 100
Hampton, VA 23666

Prof Subrata Mukherjee
Cornell University
Dept of T & AM
Kimball Hall
Ithaca, NY 14853

Dr. T. Sreekanta Murthy
Planning Research Corporation
MS 340
NASA/Langley Research Center
Hampton, VA 23665-5225

Mr. Evhen M. Mychalowycs
Boeing Vertol Company
MS F32-15
P. O. Box 16858
Philadelphia, PA 19142

Dr. Gopal K. Nagendra
MacNeal-Schwandler Corp.
815 Colorado Blvd.
Los Angeles, CA 90041-1777

Mr. Changho Nam
Purdue University
School of
Aeronautics/Astronautics
West Lafayette, IN 47907

Mr. D. J. Neill
Northrop Corporation, Aircraft
Division
Dynamics & Loads Research
3854/82
One Northrop Avenue
Hawthorne, CA 90250

Dr. Elli Nissim
NASA Dryden
CODE OFV
Edwards, CA 93523-5000

Mr. Kevin W. Noonan
NASA/Langley Research Center
MS 266
Hampton, VA 23665-5225

Dr. Ahmed K. Noor
The George Washington University
NASA/Langley Research Center
MS269
Hampton, VA 23665-5225

Mr. T. L. Oglesby
LTV Aerospace & Defense Company
P. O. Box 655907
MS 194-24
Dallas, TX 75265-5907

Prof. Irving U. Ojalvo
University of Bridgeport
Dept. of Mechanical Engineering
Bridgeport, CT 06601

Mrs. Sharon L. Padula
NASA/Langley Research Center
IRO Office
MS 246
Hampton, VA 23665

Mr. Ajay K. Pandey
Planning Research Corporation
303 Butler Farm Rd, Suite 100
Hampton, VA 23666

Prof. Alan Parkinson
Department of Mechanical
Engineering
Brigham Young University
242 CB
Provo, UT 84602

Mr. Bernhard Pepker
CCAD, EB
University of Iowa
Iowa City, IA 52242

Prof. David Peters
Georgia Institute of Technology
School of Aerospace Engineering
Atlanta, GA 30332

Mr. James Peters
McDonnell Douglas Helicopter Co.
Bldg. 530/B346
5000 E. McDowell Rd.
Mesa, AZ 85205-9797

Prof. Lucian Elijah Polak
University of California
Dept. of Electrical Engineering
565 Cory Hall
Berkeley, CA 94720

Mr. Dave Polen
VPI&SU
Dept. of Aerospace & Ocean
Engineering
400 H. Foxridge
Blacksburg, VA 24061

Prof. Aubrey Poore
Colorado State University
Dept. of Mathematics
Fort Collins, CO 80523

Dr. Biren Prasad
Electronic Data Systems
Corporation
5555 New King Street
Troy, MI 48007-7019

Dr. Thomas K. Pratt
Pratt & Whitney
Engineering Building, 161-16
400 Main Street
East Hartford, CT 06108

Dr. W. A. Radovcich
Lockheed Aeronautical Systems
Co.
D/76-12, Bldg 63-G, Plant A-1
P.O. Box 551
Burbank, CA 91520

Mr. Charles C. Rankin
Lockheed Missiles and Space
Palo Alto Research Lab.
0/93-30 B/251
Palo Alto, CA 94304-1191

Dr. S. M. Rankin
Mathematics Dept.
Worcester Poly. Tech.
Worcester, MA 01609

Mr. Jagannatha Rao
The University of Michigan
2212 G. G. Brown Lab.
Ann Arbor, MI 48109

Mr. John J. Rehder
NASA/Langley Research Center
MS 365
Hampton, VA 23665-5225

Prof. Robert Reiss
Howard University
Department of Mechanical
Engineering
2300 Sixth Street, N.W.
Washington, DC 20059

Mr. J. Edward Rogan
Georgia Institute of Technology
School of Aerospace Engineering
Atlanta, GA 30332-0150

Mr. James. L. Rogers
NASA/Langley Research Center
IRO Office
MS 246
Hampton, VA 23665

Mrs. V. Aileen Rogers
Planning Research Corporation
303 Butler Farm Rd, Suite 100
Hampton, VA 23666

Mr. Bruce A. Rommel
Douglas Aircraft Company
CI-284, Mail Code 212-10
3855 Lakewood Blvd.
Long Beach, CA 90846

Dr. Sunil Saigal
Worcester Polytechnic Institute
Mechanical Engineering
Department
Institute Road
Worcester, Mass 01069

Dr. Mektar Salama
Jet Propulsion Laboratory
Applied Mechanics Div. - MS
157-316
California Institute of
Technology
Pasadena, CA 91109

Mr. Chris A. Sandridge
VPI & SU
Aerospace & Ocean Engineering
Blacksburg, VA 24061

Prof. Lucien A. Schmit
University of California, Los
Angeles
4531K Boelter Hall
Los Angeles, CA 90024

Prof. Daniel P. Schrage
Georgia Institute of Technology
School of Aerospace Engineering
250 Drummen Ct
Atlanta, GA 30332-0150

Mr. Stephen J. Scotti
NASA/Langley Research Center
MS 396
Hampton, VA 23665-5225

Mr. Jeen S. Sheen
Old Dominion University
Dept. of Mechanical Eng. and
Mechanics
College of Engineering and
Technology
Norfolk, VA 23529-0247

Mr. Joram Shenhar
Planning Research Corporation
303 Butler Farm Rd, Suite 100
Hampton, VA 23665

Dr. Mark J. Shuart
NASA/Langley Research Center
MS 190
Hampton, VA 23665-5225

Mr. J. A. Shupe
B. F. Goodrich
9921 Brecksville Road
Brecksville, OH 44141

Mr. Walter A. Silva
Planning Research Corporation
303 Butler Farm Rd, Suite 100
Hampton, VA 23666

Mr. James A. Simak
General Dynamics
Data Systems Division
P.O. Box 748
Fort Worth, TX 76102

Dr. Jaroslaw Sobieski
NASA/Langley Research Center
MS 246
Hampton, VA 23665-5225

Mr. Andy N. Soediono
Georgia Institute of Technology
P. O. Box 34091
225 North Avenue
Atlanta, GA 30332

Dr. James H. Starnes, Jr.
NASA/Langley Research Center
MS 120
Hampton, VA 23665-5225

Mr. Frank J. Tarzanin
Boeing Vertol Company
MS P32-15
P. O. Box 16858
Philadelphia, PA 19142

Mr. Kenneth E. Tatum
Planning Research Corporation
SSD/ATD
303 Butler Farm Rd., Suite 100
Hampton, VA 23666

Mr. Rajiv Thareja
Planning Research Corporation
303 Butler Farm Rd, Suite 100
Hampton, VA 23666

Prof. Garret N. Vanderplaats
University of California, Santa
Barbara
Dept. of Mechanical &
Environmental Eng.
Santa Barbara, CA 93160

Dr. Vipperla B. Venkayya
AF Wright Aeronautical
Laboratories
AFWAL/FIBR
Wright-Patterson AFB, OH 45433

Dr. A. V. Viswanathan
Boeing Commercial Airplane Co.
P. O. Box 3707
Seattle, WA 98124

Mr. A. Von Flotow
MIT
37-335, MIT
Cambridge, MA 02139

Ms. Joanne L. Walsh
NASA/Langley Research Center
MS 246
Hampton, VA 23665-5225

Prof. Bo Ping Wang
The University of Texas
Dept. of Mechanical Engineering
P.O. Box 19023
Arlington, TX 76019

Mr. Bryan Watson
Spectragraphics Corporation
9125 Rehco Road
San Diego, CA 92121

Prof. Terrence A. Weisshaar
Purdue University
School of
Aeronautics/Astronautics
West Lafayette, IN 47907

Mr. W. H. Weller
United Technologies Research
Center
M. S. 19, Silver Lane
East Hartford, CT 06108

Ms Carol D. Wieseman
NASA/Langley Research Center
MS 243
Hampton, VA 23665-5225

Mr. James L. Williams
NASA/Langley Research Center
MS 499
Hampton, VA 23665-5225

Mrs. Jessica A. Woods
Planning Research Corporation
NASA Langley Research Center
Mail Stop 243
Hampton, VA 23665-5225

Mr. Gregory A. Wrenn
Planning Research Corporation
NASA/Langley Research Center
MS905
Hampton, VA 23665-5225

Mr. Ren-Jye Yang
Ford Motor Company
Scientific Research Labs
P. O. Box 2083, RM E-1134
Dearborn, MI 48212

Dr. E. Carson Yates
NASA/Langley Research Center
MS 246
Hampton, VA 23665-5225

Mr. Chao-Pin Yeh
Georgia Tech
Atlanta, Georgia 30332

Mr. John W. Young
NASA/Langley Research Center
MS 499
Hampton, VA 23665-5225

Mrs. Katherine C. Young
NASA/Langley Research Center
IRO Office
MS 246
Hampton, VA 23665

Mr. Rudy Turkovich
McDonnell Aircraft Co.
P.O. Box 516
St. Louis, MO 63166

Dr. Thomas A. Zeiler
Planning Research Corporation
NASA/Langley Research Center
MS 243
Hampton, VA 23665-5225

PART 2

SESSION 5: SOFTWARE I

Chairmen: G. N. Vanderplaats and R. E. Fulton

ASTROS - A MULTIDISCIPLINARY AUTOMATED STRUCTURAL DESIGN TOOL

D. J. Neill
Northrop Corporation, Aircraft Division
Hawthorne, California

INTRODUCTION

ASTROS (Automated STRuctural Optimization System) is a finite-element-based multidisciplinary structural optimization procedure developed under Air Force sponsorship to perform automated preliminary structural design. The design task is the determination of the structural sizes that provide an optimal structure while satisfying numerous constraints from many disciplines. In addition to its automated design features, ASTROS provides a general transient and frequency response capability, as well as a special feature to perform a transient analysis of a vehicle subjected to a nuclear blast.

The motivation for the development of a single multidisciplinary design tool (Figure 1) is that such a tool can provide improved structural designs in less time than is currently needed. The role of such a tool is even more apparent as modern materials come into widespread use. Balancing conflicting requirements for the structure's strength and stiffness while exploiting the benefits of material anisotropy is perhaps an impossible task without assistance from an automated design tool. Finally, the use of a single tool can bring the design task into better focus among design team members, thereby improving their insight into the overall task.

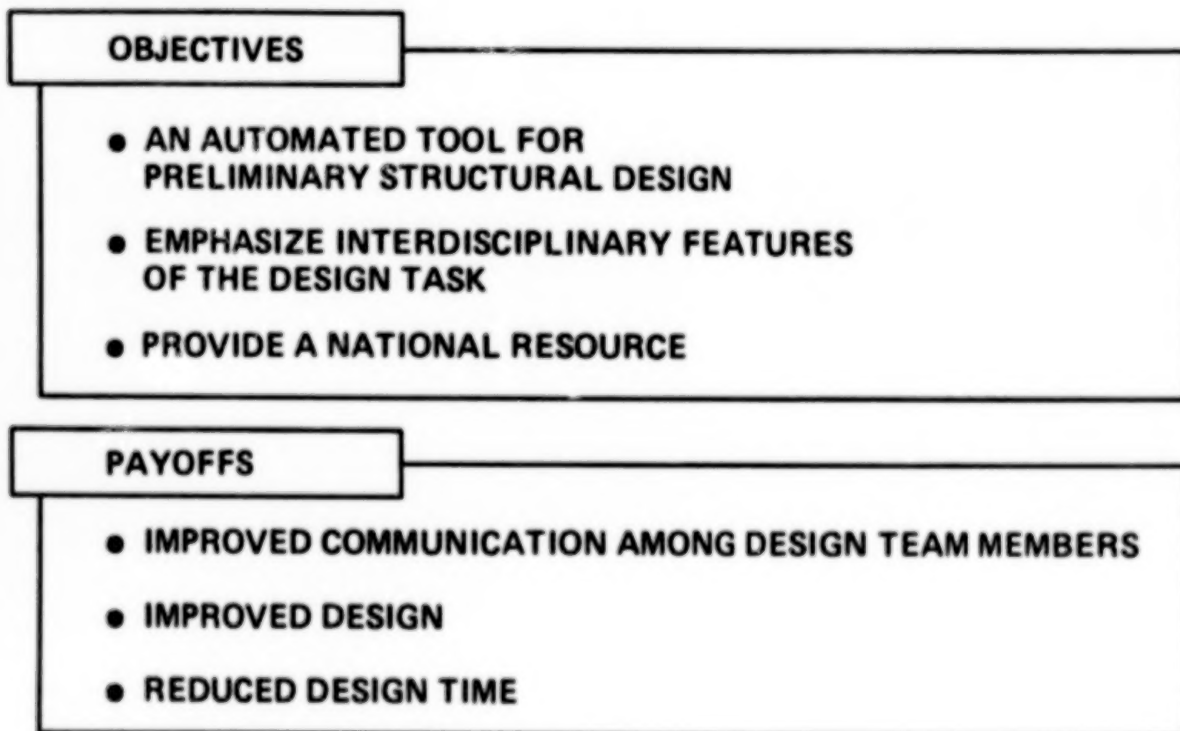


Figure 1

ENGINEERING DISCIPLINES

At the core of the ASTROS engineering disciplines (Figure 2) is finite-element structural analysis. This central analysis discipline is augmented by steady aerodynamic loads analysis, unsteady aerodynamics and aeroelastic stability analysis, as well as a limited control response capability. In addition, the automated design features of ASTROS include an analytical sensitivity analysis for the available design constraints and a battery of optimization methods.

The development of the ASTROS system has been predicated on the use of existing software resources whenever possible. The NASTRAN (Ref. 1) system has served as the most substantial resource for the ASTROS development although in many cases, it proved expedient to program the NASTRAN algorithm rather than modify the NASTRAN code and, in all cases, substantial modification of the NASTRAN software was required. USSAERO (Ref. 2) and MICRO-DOT (Ref. 3) played a similar role for the steady aerodynamic analysis and optimization methods, respectively, although fewer modifications were made to integrate them. In addition to these software resources, earlier automated design systems served to guide the design of the ASTROS system in the area of multidisciplinary optimization. Most notable among these are the TSO (Ref. 4) and FASTOP (Ref. 5) systems.

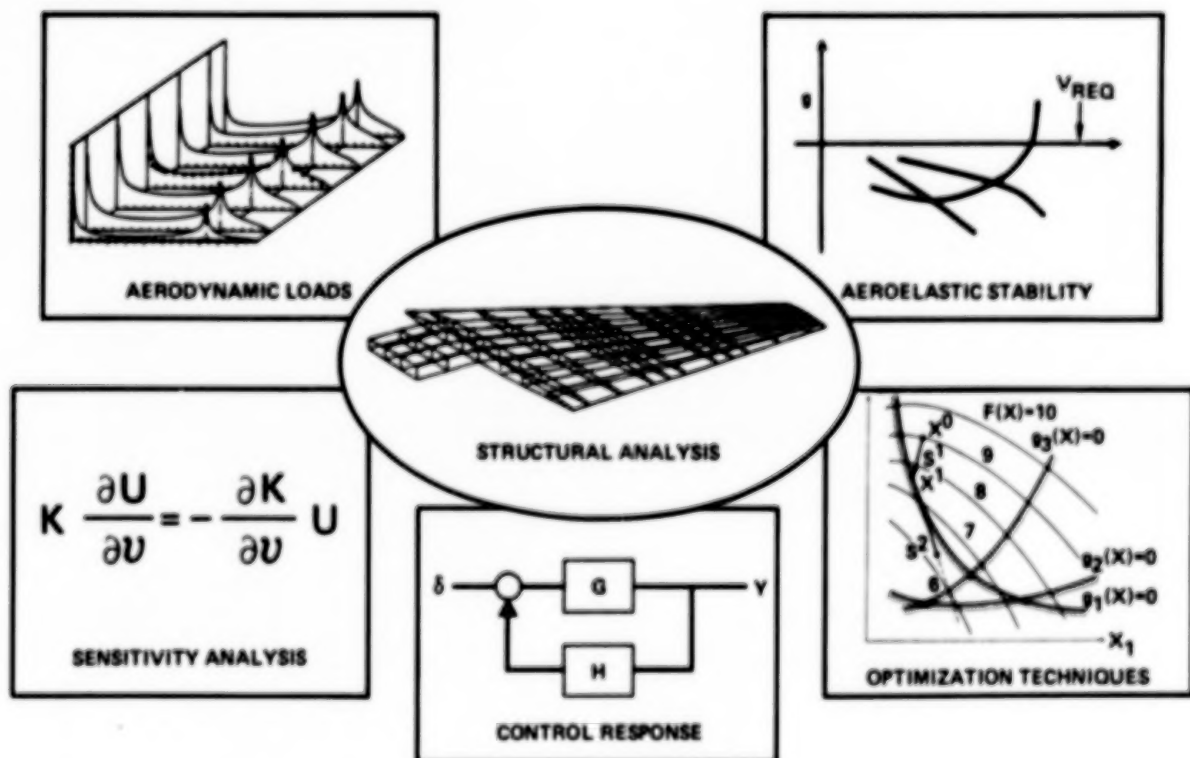


Figure 2

STRUCTURAL ANALYSES

The structural analyses in ASTROS (Figure 3) include statics, normal modes, transient response and frequency response using either modal or direct coordinates. The statically applied loads can be composed of any combination of mechanical (i.e., discrete forces, moments and pressures), gravitational or thermal loads.

In addition to the structural analyses, the steady aerodynamic loads capability in ASTROS is used to generate aerodynamic loads and aeroelastic corrections which are then used to perform symmetric or antisymmetric aeroelastic trim analyses. Finally, a pair of unsteady aerodynamics analyses is used to provide a p-k flutter analysis capability. The subsonic unsteady aerodynamics uses the Doublet Lattice Method (DLM) (Ref. 6) while the supersonic aerodynamics uses the Constant Pressure Method (CPM) (Ref. 7). The unsteady aerodynamics analyses are also used to provide harmonic gust loads for the frequency response and to provide frequency dependent aerodynamic forces for the nuclear blast analysis.

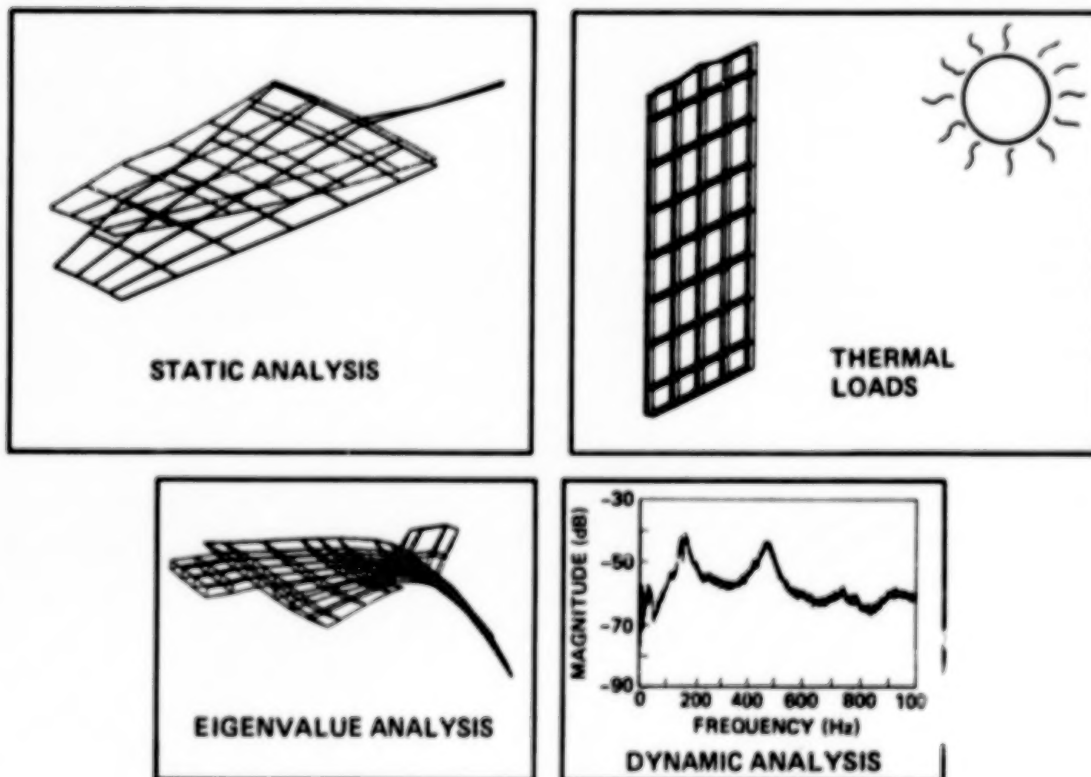


Figure 3

DESIGN PARAMETERS

The local or physical design variables in ASTROS (Figure 4) are such that the stiffnesses and masses are linear functions of the design variable. For the bar, this requires that the bar area and inertia be coupled by a user specified relationship and that the bending and extensional behavior be treated separately. ASTROS supports three methods of design variable linking, in which the physical variables are linked to global variables that are actually used in the redesign process. The linking schemes include unique linking and physical linking, in which the global variable controls one or more local variables, and shape function linking in which each local variable is a linear combination of several global variables. In the latter case, the global variables are weighting factors on a "shape" such as a linear taper or a uniform thickness distribution.

The design constraints in ASTROS are standard for an aerospace structural design task and include stress, strain and displacement constraints for statics and/or static aeroelastic disciplines, modal frequency constraints for a normal modes analysis, aeroelastic effectivenesses for the steady aeroelastic analysis discipline and flutter constraint for the aeroelastic stability analysis. Any or all of these constraints types and any number of each type may be combined in a single optimization run in order to achieve an optimal design satisfying all the required design constraints.

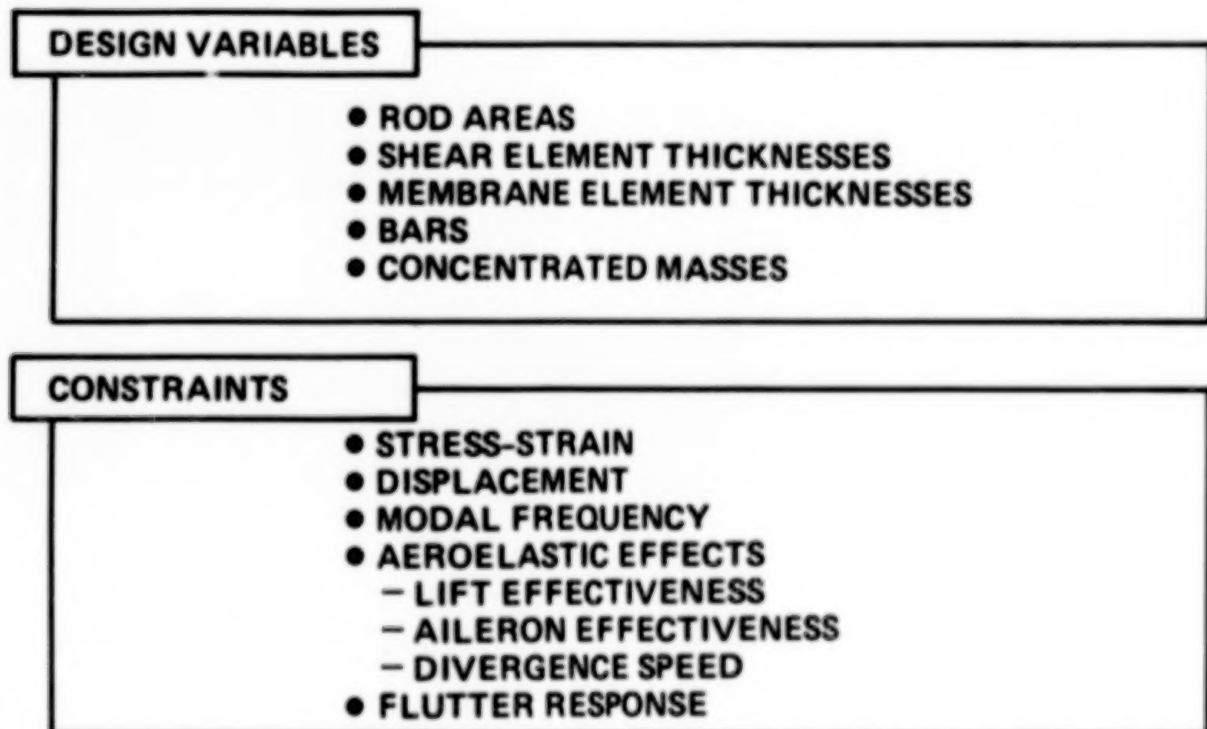


Figure 4

MULTIDISCIPLINARY OPTIMIZATION

The effective application of automated optimization methods to structural design requires the simultaneous consideration of all conditions that are critical in determining the final design. Figure 5 presents a schematic diagram of the ASTROS program flow for the automated design task. It indicates that there are three phases to the design task in ASTROS. In the first phase, the required engineering analyses are performed for the current design. Any number of boundary conditions may be applied and within each boundary condition any number of disciplines (i.e., statics, normal modes, etc.) may be analyzed. Further, any number of "subcases" (e.g., load conditions or flight conditions) may be analyzed in each discipline. As indicated in the figure, each of these analyses generate constraints that must be satisfied for the design to be considered acceptable.

In the second phase, those constraints that are most critical for the current redesign are chosen and their sensitivities computed. This constraint screening process is desirable in order that the optimization remain tractable while still capturing the critical design constraints. An important benefit of such a step is that entire boundary conditions or disciplines may be eliminated from the computationally intensive sensitivity evaluation. Finally, in the third phase, the information on the objective function (which is the weight in ASTROS) and the active constraints and their sensitivities are used to perform a redesign to satisfy the constraints while minimizing the objective function.

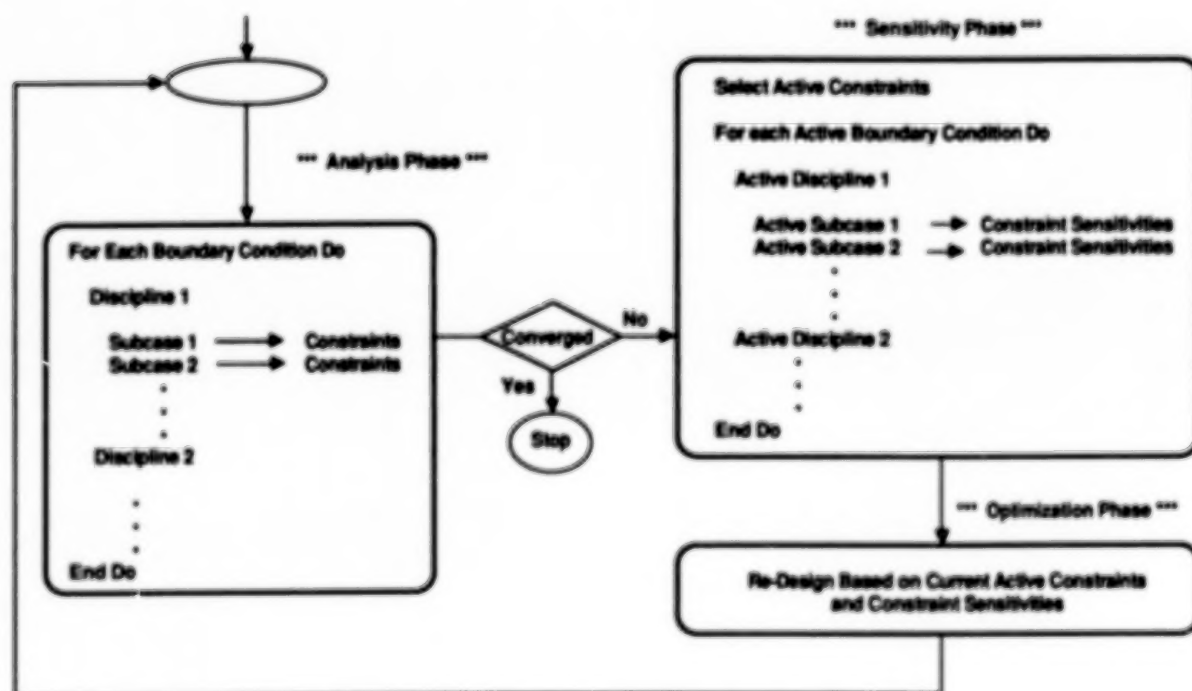


Figure 5

AN ARCHETYPICAL ASTROS APPLICATION

The ASTROS system has been delivered to the Air Force and is available for application to "real world" preliminary structural design problems. Figure 6 shows one such problem that may be considered archetypical of the problem for which the ASTROS procedure was developed. Given the structural configuration and materials represented by a finite-element model and a set of design requirements, the ASTROS procedure will determine the structural sizes of the designed elements to minimize the weight of the structure while satisfying the potentially numerous multidisciplinary constraints.

One should not limit ASTROS, however, by this single example. The true potential for an optimization system such as ASTROS lies in its ability to generate additional information that allows a rapid assessment of the quality of competing design concepts through the comparison of "optimal" solutions. In addition, ASTROS enables the designer to accommodate conflicting constraints at a much earlier stage in the design cycle, thereby avoiding potentially serious conflicts later. Finally, the use of formal optimization in the preliminary design enables the designer to develop nonintuitive solutions to the complex interdisciplinary design problems that can occur in modern aerospace structural design.

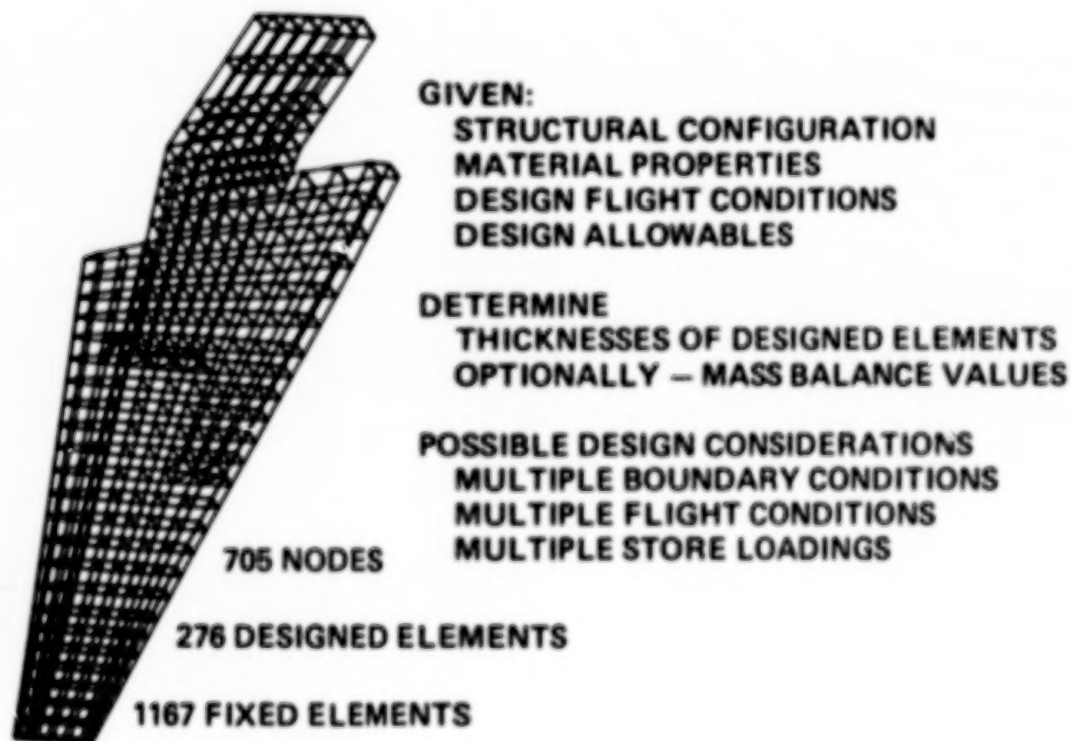


Figure 6

INTERMEDIATE COMPLEXITY WING EXAMPLE - GEOMETRY

As an example of the ASTROS system, the Intermediate Complexity Wing (ICW) problems that were developed to test the FASTOP system were duplicated in the ASTROS system. These tests both confirm the accuracy of the ASTROS system and serve to highlight the differences in the treatment of multidisciplinary constraints in these two systems.

The ICW structural model, shown in Figure 7, uses quadrilateral and triangular membrane elements to model the composite wing skins and shear panels to model the substructure. Rod elements are used as posts to complete the interconnection of the upper and lower surfaces. The model is cantilevered at the root and all rotational degrees of freedom are constrained at each node. The substructure material is modeled as aluminum, while the wing skins are made of a graphite/epoxy composite.

No. of Nodes	No. of Elements	No. of DOF's
88	39 Rods	294 Constrained
	55 Shear Panels	<u>234</u> Unconstrained
	62 Quadrilateral Membrane	528 Total
	<u>2</u> Triangular Membrane	
	158 Total	



Figure 7

DESIGN REQUIREMENTS FOR THE INTERMEDIATE COMPLEXITY WING (ICW)

The design problem (Figure 8) minimizes the weight of the structure subject to the material stress allowables and gauge constraints under two static loads representing a subsonic and a supersonic air load and subject to a minimum required flutter speed of 925 KEAS at Mach 0.80. To examine the behavior of different design variable linking options, two different design models were used in ASTROS. The first was developed to emulate the FASTOP results and links the upper and lower skin surfaces for each ply orientation (128 design variables), treats each spar element as a separate design variable (23 design variables) and links all the posts and rib shear panels together as two additional design variables for a total of 153 global design variables. In the second linking scheme, the ASTROS shape function design variable linking option was utilized. The shapes for each ply orientation for the wing skin elements were uniform, a linear spanwise taper, a quadratic spanwise taper and a linear chordwise taper with the upper and lower surfaces linked as before (16 design variables). A uniform and a linear spanwise taper were used for each of the three spars (6 design variables), and the posts and ribs are linked as before for a total of 22 shape function design variables and two physically linked design variables.

• FLUTTER CONSTRAINTS

$$\begin{aligned} V_f &\leq 925 \text{ knots} \\ \rho &= .0023769 \text{ slugs/ft}^3 \\ M &= 0.80 \end{aligned}$$

• ISOTROPIC MATERIAL IN SUBSTRUCTURE

$$\begin{aligned} E &= 10.5 \times 10^6 \text{ psi} & \rho &= 0.10 \text{ lb/in}^3 \\ \nu &= 0.30 & t_{\min} &= 0.02 \text{ in} \\ \sigma_T &\leq 67 \text{ ksi} \\ \sigma_C &\leq 57 \text{ ksi} \\ \tau_{xy} &\leq 39 \text{ ksi} \end{aligned}$$

• ORTHOTROPIC MATERIAL IN SKINS

$$\begin{aligned} E_1 &= 18.5 \times 10^6 \text{ psi} & \nu_{12} &= 0.25 & \rho &= 0.055 \text{ lb/in}^3 \\ E_2 &= 1.6 \times 10^6 \text{ psi} & G_{12} &= 0.65 \times 10^6 \text{ psi} & t_{\min} &= 0.00525 \text{ in} \\ X_T &= X_C = Y_T = Y_C & &= 1.15 \times 10^5 \text{ psi} \\ S &\leq 1.0 \times 10^{15} \end{aligned}$$

Figure 8

ICW STRENGTH DESIGN RESULTS

Figure 9 presents the ply counts for the final strength design obtained from FASTOP, ASTROS using "FASTOP" design variable linking (labeled "153" in the figure) and ASTROS with shape function linking (labeled "ELIST" in the figure). As expected, the final material distribution for ASTROS and FASTOP using identical design variable linking are very similar despite the use of mathematical programming methods in ASTROS and fully stressed design methods in FASTOP. The final objective function values do not compare as well but the ASTROS objective function represents a design with continuous design variables while FASTOP rounds up to the next whole ply prior to the objective function computation. In general, however, the agreement between ASTROS and FASTOP for this case gives confidence that the ASTROS system is functioning properly.

The shape function results are interesting in their own right even though it is not directly comparable to any external results. In this case, the limitations imposed by using shape functions results in the optimizer's selection of all zero degree fibers to satisfy the stress constraints with all other orientations going to minimum gauge. This result is illustrative of an "optimal" solution given external constraints like manufacturing limits or limits in the rates of ply drop-off. Further, compared to the FASTOP linked result, it clearly represents a radically different method of addressing the same set of physical constraints.

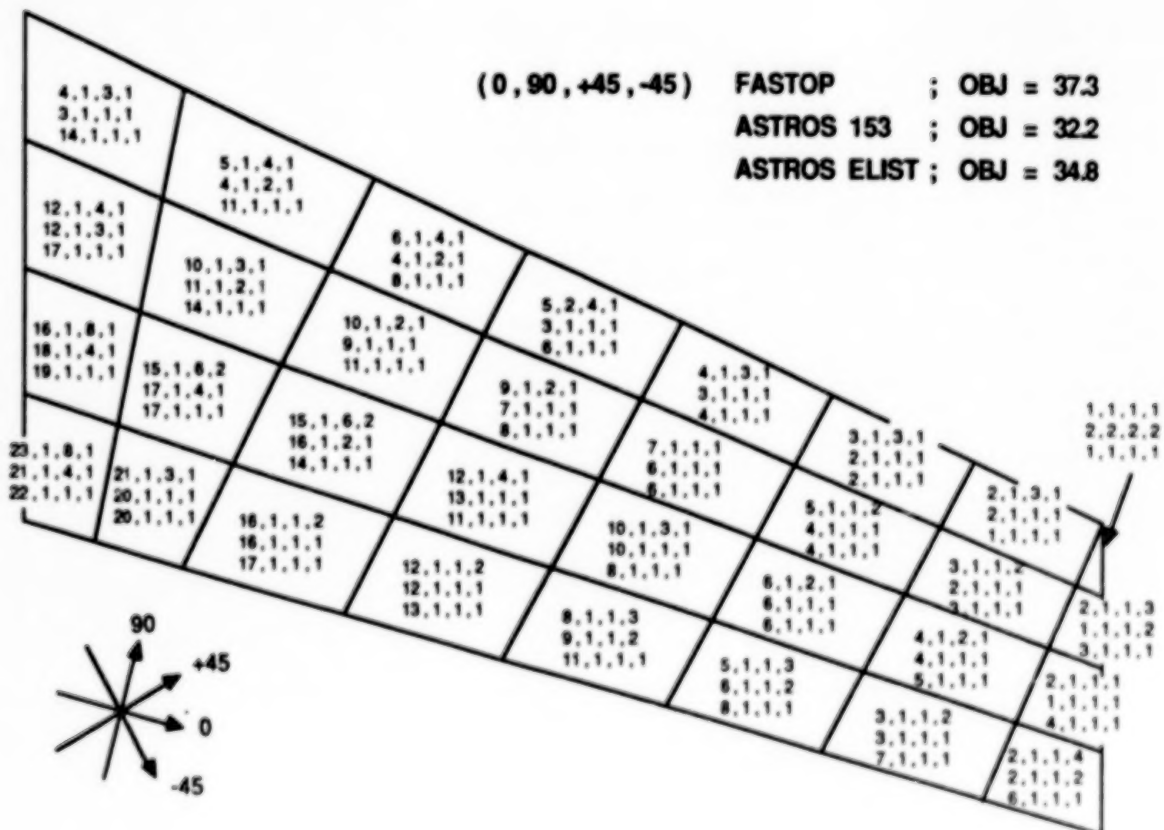


Figure 9

ICW STRENGTH/FLUTTER DESIGN RESULTS

Figure 10 presents the ply counts for the same three final designs obtained for the combined strength and flutter optimization. Unlike the case where the strength constraints were considered alone, there is little agreement between FASTOP and ASTROS in the resultant final design. The ASTROS result is significantly lighter even when the restrictive shape function variables are used. There are several possible explanations for the differences. First, and most important, is that ASTROS treats the strength and flutter constraints simultaneously at each iteration; whereas, the FASTOP algorithm treats each constraint type sequentially and applies ad hoc move limits on "flutter critical" and "strength critical" elements in between each cycle. It is known that such an algorithm does not necessarily lead to an optimal solution. A second important factor is that the two systems use different methods to couple the aerodynamic and structural deflections and may, therefore, produce different flutter results for the same model. A necessary check that has not been made is to analyze the ASTROS result in FASTOP to see if it meets the flutter requirement. Finally, the objective function computations are different due to the rounding to whole plies that takes place in FASTOP at each cycle of the optimization.

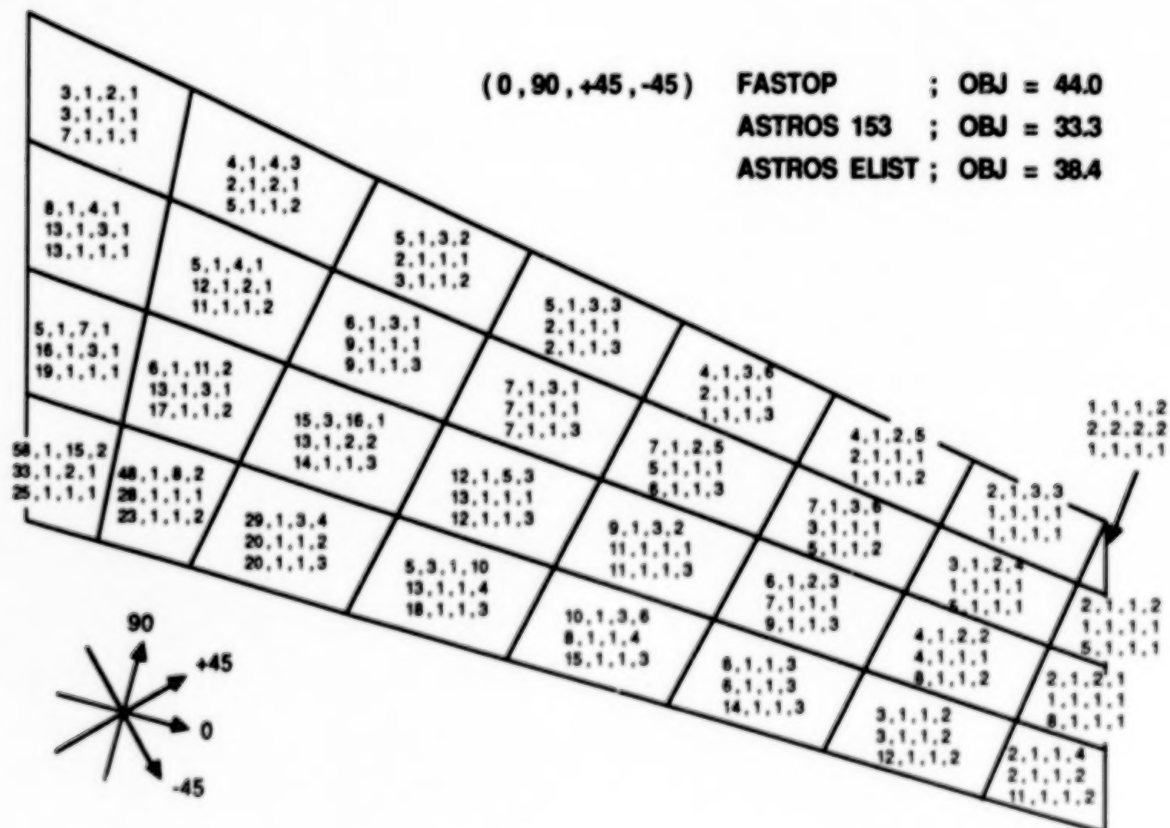


Figure 10

SOFTWARE CONTRIBUTIONS OF ASTROS

While the software development in ASTROS depended to a large degree on existing software systems, several noteworthy software contributions (Figure 11) were made in the course of the ASTROS development. Most importantly, an architecture was designed that is suited to multidisciplinary analysis and design. It includes a data base management system tailored to handle the engineering data common to matrix structural analysis methods, as well as to the design task. Another important contribution was the design of the ASTROS executive system and its control language, MAPOL (Matrix Abstraction Problem Oriented Language). Together, these provide nearly limitless flexibility in the application of the ASTROS system to tasks not explicitly designed into the procedure. Also important to the successful development of ASTROS was the exploitation of modern computer environments to integrate the software components developed by a dispersed development team and to manage the resultant system. The flexibility offered by the microcomputer to tailor the computer environment made the software management task tractable without a great deal of effort on the part of the developers.

- Framework For Multidisciplinary Analysis and Design
- Engineering Data Base
- High Level Executive System
- Obsolescence of Rigid Formats
- Unlimited Problem Size
- Exploitation of Microcomputers
- Built In Maintenance Features
- Improved Special Purpose Utilities
- Balanced Approach to Software Design
- Integration of Dispersed Development Team

Figure 11

ENGINEERING CONTRIBUTIONS OF ASTROS

In addition to its software contributions, ASTROS has made several key engineering contributions (Figure 12). The first and most important is the system's ability to perform multidisciplinary design. This means a simultaneous consideration of an unlimited number of constraints from a set of disparate engineering analyses to obtain an "optimal" design that meets very general design criteria. Included in this capability is an analytical sensitivity analysis for all the constraint forms, the incorporation of approximation concepts in a production optimization code and a number of design variable linking schemes. All these features result in the tractable optimization of large problems with many constraints from many disciplines.

Other engineering contributions include an innovative approach to the treatment of flutter constraints which does not require the expensive computation of the flutter speed and avoids the complex problems of tracking multiple flutter branches. ASTROS also includes a public domain quadrilateral bending plate element, incorporates improvements to dynamic reduction techniques and has integrated advanced aerodynamics for nuclear blast response analysis with finite-element structural analysis methods. Finally, ASTROS has adopted an improved supersonic unsteady aerodynamic analysis (CPM) and has included the computation of aerodynamic influence coefficients for the static aeroelastic analysis.

- Multidisciplinary Analysis and Design
- Analytical Sensitivity Analysis
- Approximation Concepts in a Production Code
- QUAD4 Element in the Public Domain
- Improved Supersonic Unsteady Aerodynamics
- Innovative Flutter Design Technique
- Nuclear Blast Analysis with Finite Elements and Advanced Aerodynamics
- Advanced Methods of Dynamic Reduction
- Design Variable Linking
- Aerodynamic Influence Coefficients For Static Aeroelasticity

Figure 12

CONCLUSIONS

The ASTROS system development is complete in the sense that the basic features desired in the system are in place and the code is available for application to real world problems. It provides a very general tool to perform automated preliminary structural design subject to multidisciplinary constraints. In addition to its design features, the code has been provided with a suite of dynamic analyses and special purpose analyses to improve its utility as a unified tool for structural design.

At this point, however, the ASTROS system is immature from a software standpoint and has known bugs with additional problems sure to show up with increased use. In anticipation of these problems, the Air Force has funded an enhancement effort that will address the quality assurance and software maintenance issues, as well as make several enhancements to the engineering aspects of the code. Among the enhancements are the inclusion of a triangular bending plate element, additional steady aerodynamic analysis features, improved aeroelastic analysis and enhanced treatment of the control system. Also included in this effort is the inclusion of general, multidisciplinary optimality criteria methods as an alternative to the current mathematical programming methods for the redesign task in ASTROS.

•

•

REFERENCES

1. MacNeal, R.H., The NASTRAN Theoretical Manual, NASA SP-221(01), April 1971.
2. Woodward, F., "USSAERO Computer Program Development, Versions B and C," NASA CR 3227, 1980.
3. Vanderplaats, G.N., "An Efficient Feasible Directions Algorithm for Design Synthesis," AIAA Journal, Volume 22, No. 11, November 1984, pp 1633-1640.
4. Lynch, R.W., Rogers, W.A., Braymen, G.W., and Hertz, T.J., "Aeroelastic Tailoring of Advanced Composite Structures for Military Aircraft, Volume III - Modifications and User's Guide for Procedure TSO," AFFDL-TR-76-100, Vol. III, February 1978.
5. Markowitz, J., and Isakson, G., "FASTOP-3: A Strength, Deflection and Flutter Optimization Program for Metallic and Composite Structures," AFFDL-TR-78-50, Vols. I and II, May 1978.
6. Giesing, J.P., Kalman, T.P., and Rodden, W.P., "Subsonic Unsteady Aerodynamics for General Configurations: Part II, Volume I - Application of the Doublet-Lattice Method and the Method of Images to Lifting-Surface/Body Interference," AFFDL-TR-71-5, Part II, Volume I, August 1971, Air Force Flight Dynamics Laboratory, Wright-Patterson Air Force Base, Ohio.
7. Appa, K., "Constant Pressure Panel Method for Supersonic Unsteady Airloads Analysis," Journal of Aircraft, Volume 24, October 1987, pp 696-702.

A GENERALIZED SOFTWARE EXECUTIVE FOR
MULTIDISCIPLINARY COMPUTATIONAL STRUCTURAL DYNAMICS

Alex Berman
Kaman Aerospace Corporation
Bloomfield, Connecticut

INTRODUCTION TO DYSCO

The objective of this presentation is to introduce the attendees to the DYSCO program. The emphasis will be on the features which make it "multidisciplinary."

DYSCO is a very general and versatile software program which couples and solves dynamic systems. It was initiated in the late '70s in response to a helicopter analysis requirement. The system development, however, resulted in an executive which was completely separated from any particular area of technology, except that of second order ODE. During the course of its development, it was funded by the Army Aviation Applied Technology Directorate, the Air Force Wright Aeronautical Laboratories, and by the Kaman Aerospace Corporation. It is completely written in FORTRAN and is operational on IBM and VAX computers. The size is indicated in figure 1.

- o DYNAMIC SYSTEM COUPLER (DYSCO)
- o INITIAL DEVELOPMENT - 1979
- o FUNDED BY ARMY, AIR FORCE, KAMAN
- o PRESENTLY OPERATIONAL ON IBM AND VAX
- o SIZE - 50000+ LINES OF CODE
350+ SUBROUTINES
4+ MEGABYTES OF STORAGE
- o INSTALLATIONS INCLUDE GOVERNMENT FACILITIES AND
UNIVERSITIES

Figure 1

DEFINITION OF DOMAIN OF DYSCO

The "domain" is the technical area in which the program is designed to operate. The domain of DYSCO is "coupled sets of second order ordinary differential equations." The Executive of DYSCO recognizes and manages: algorithms for computing equation coefficients; the necessary data; coupling constraints; coupling procedures; algorithms for solving the coupled equations; the resulting data.

Figure 2 illustrates the generic equation of a "component," the coupling constraints, the coupled equations of the system.

DYSCO COUPLES AND SOLVES SECOND ORDER ODE

$$0 \quad M_I \ddot{X}_I + C_I \dot{X}_I + K_I X_I = F_I \quad (\text{COMPONENT } I)$$

$$0 \quad X_I = T_I X_S$$

$$0 \quad M_S \ddot{X}_S + C_S \dot{X}_S + K_S X_S = F_S \quad (\text{SYSTEM})$$

Figure 2

DEFINITION OF COMPONENT

A component is anything represented by second order ODEs where the coefficients can be any computable function of present or past states of this and other components of the "model." The degrees of freedom (dependent variables) and the independent variable are completely arbitrary. (Figure 3.)

- o "COMPONENT" IS MORE GENERAL THAN "FINITE ELEMENT"
- o $M_I, C_I, K_I, F_I =$ ARBITRARY FUNCTIONS OF STATE
- o $X_I =$ ANY GENERALIZED DOF - PHYSICAL, MODAL, OTHER
- o COMPONENT MAY BE
 - FINITE ELEMENT
 - ASSEMBLY OF FINITE ELEMENTS (SUBSYSTEM, OUTPUT OF FE ANALYSIS)
 - SPECIAL SET OF EQUATIONS (E.G., HELICOPTER ROTOR, SPECIAL MECHANISM)
 - CONTROL ALGORITHM (MIMO, NON-SYMMETRICAL MATRICES, NONLINEAR)
 - FORCE ALGORITHM ($M, C, K =$ NULL, AERO, ELECTROMAGNETIC)
 - ETC., ETC.

Figure 3

DEFINITION OF MODEL

A "model" describes a system made up of coupled components. The description of each component includes the identification of the algorithm for computing the equation coefficients and the identification of the data to be used. In DYSCO the equations may be nonlinear but the coupling is limited to linear relationships between degrees of freedom. (Figure 4.)

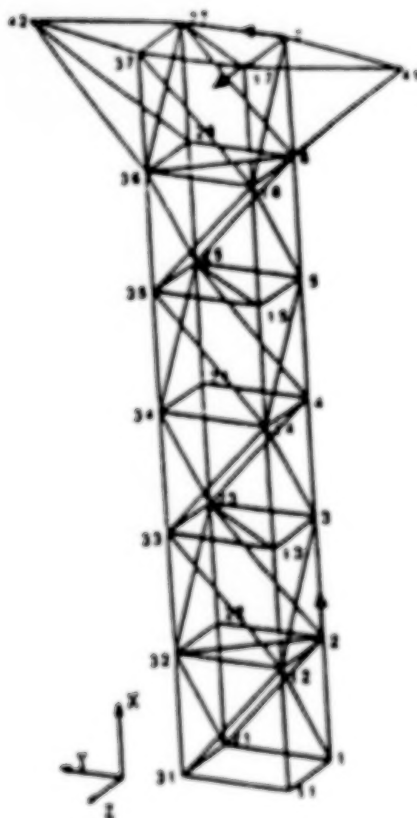
When the model is defined, the DYSCO command "RUN" assembles the equations and prepares for the execution of any user specified solution algorithm.

- o A MODEL IS A DESCRIPTION OF A COUPLED SET OF COMPONENT EQUATIONS
- o COMPONENT EQUATIONS ARE DEFINED BY
 - NAME OF THE ALGORITHM IN "TECHNOLOGY LIBRARY"
 - NAME OF DATA SET IN "MODELING DATABASE"
- o COMMAND "RUN" COUPLES EQUATIONS
- o NEXT STEP IS TO SPECIFY SOLUTION ALGORITHM

Figure 4

ILLUSTRATION OF A MODEL

In the illustration in figure 5, a truss structure is modeled with 10 "components." The component "CTR4" defines the equations for a truss bay consisting of 4 vertical members, 4 horizontal members and up to 8 diagonal members. The component number (NO.) represents a feature which automatically couples the components. Note that the odd numbered (as well as the even numbered) bays are identical and thus use the same "DATA SET." Component 9 represents a linear MIMO control algorithm and Component 10 applies single point constraints to ground the model at the base.



	<u>COMPONENT</u>	<u>NO.</u>	<u>DATA SET</u>
1	CTR4	1	ABCD1
2	CTR4	3	ABCD1
3	CTR4	5	ABCD1
4	CTR4	2	ABCD2
5	CTR4	4	ABCD2
6	CTR4	6	ABCD2
7	CSF1		TOPR
8	CSF1		TOPL
9	CSF1		CONTR
10	CLC1		GROUND

Figure 5

DYSCO SYSTEM OVERVIEW

On the next few figures, some of the features of the design of the system will be described. The Executive acts as an intelligent interface between the user, the "technology library," the data. The technology library contains all the algorithms for computing equation coefficients, forces, constraints, solution algorithms ("technology modules"). The database contains data to be used by the technology modules. It is identified by the name of the technology module which is to use it as well as a user supplied "data set" name. It also contains model descriptions and other pertinent types of data. The executive coordinates all the actions of the system: including input and editing of data, forming models, assembling models, solving models, retrieving local state vectors and all other necessary functions to make the system operable. (Figure 6.)

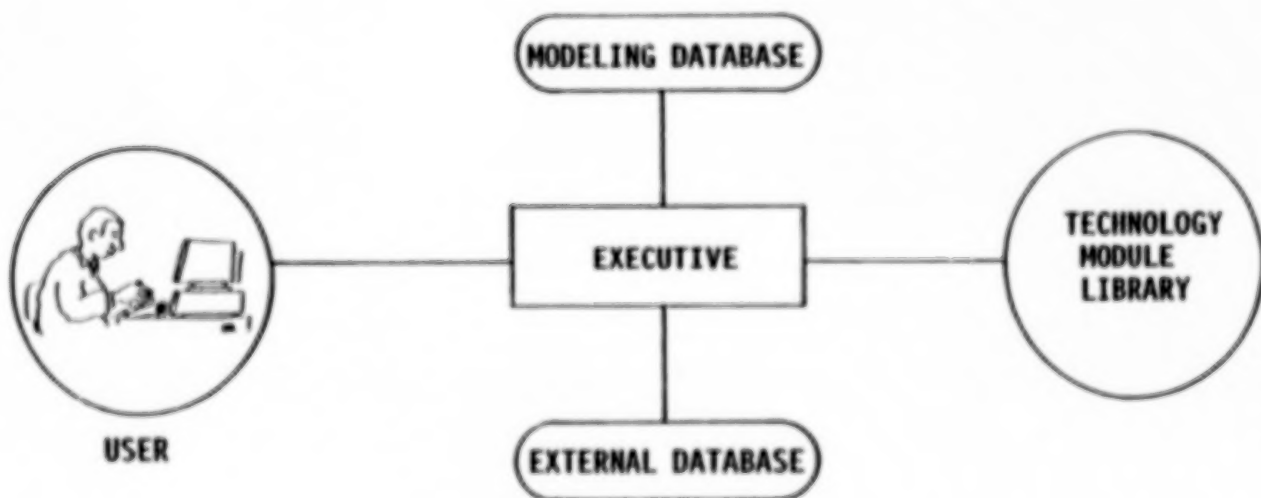


Figure 6

MODELING SCENARIO

Figure 7 is an illustration of the relationship between some of the modeling commands and the operation of the system. The NEW commands allow the user to input the data for a component, a force algorithm, or to define a model. The user specifies the name of the technology modules and is then guided through the input and/or edit process. This data is then stored on the modeling database. When defining a model, the user inputs information such as component algorithm and data set name. The executive validates the existence of this information before acceptance. The model is named and also stored on the database. When the RUN command is issued, the user supplies the model name and the executive then obtains the data, accesses the technology modules in the library, assembles the equations and carries out all preparations necessary to execute a solution module from the technology library, as specified by the user.

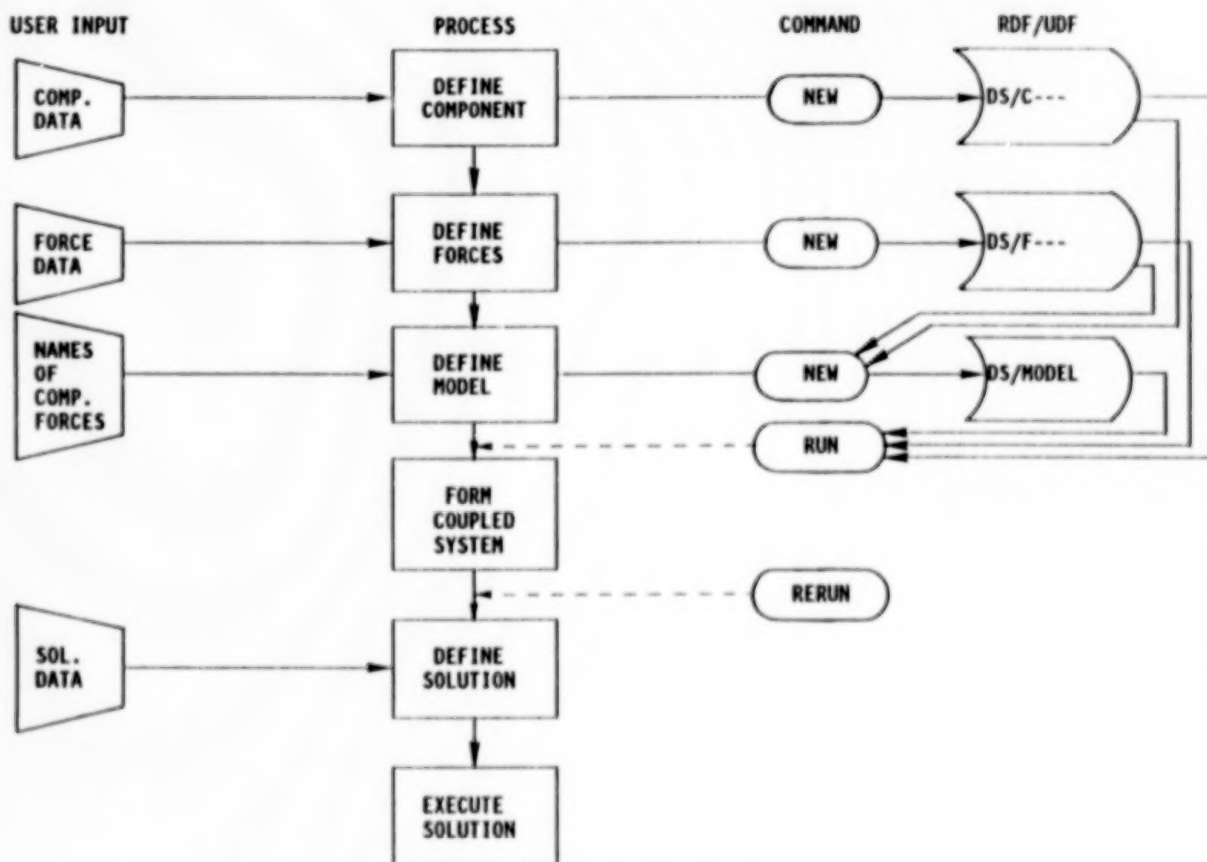


Figure 7

TECHNICAL MODULES

In order for the Executive to perform its functions and to simplify the installation of new components or solution, the technology modules are separated into functional modules as defined in figure 8. The relationships between the commands and the technical modules are shown on the following figure.

A technology module is given a 4 character name. The first character is C (for component), F (for force), S (for solution). The technical modules which comprise the technical modules use the same first 4 characters plus I, D, C, etc. as shown on figure 8. The specific functions of the individual modules are briefly categorized below.

---I	INPUT DEFINITION
---D	DEFINE DEGREES OF FREEDOM
---C	COMPUTE CONSTANT COEFFICIENTS IN EQUATIONS
---A	COMPUTE NON-CONSTANT COEFFICIENTS, FUNCTION OF TIME AND STATE
---O	OUTPUT
---L	INTERNAL LOADS, FUNCTION OF STATE

Figure 8

RELATIONSHIP BETWEEN MODELING SCENARIO AND TECHNICAL MODULES

Figure 9 illustrates how the Executive accesses the appropriate technical modules as necessary during various phases of the modeling and solution process.

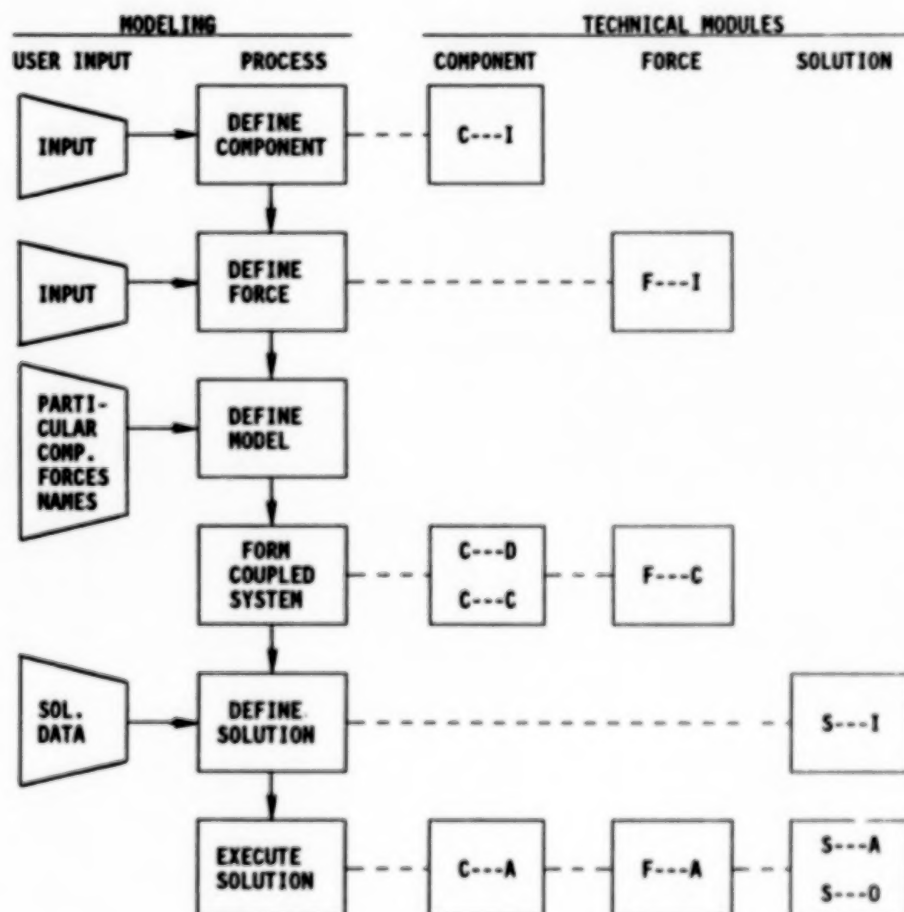


Figure 9

RUN COMMAND

Figure 10 illustrates the functions performed by the Executive after the command RUN. The only input required from the user is the command and the name of the model. All the operations are performed in a manner which is completely transparent to the user.

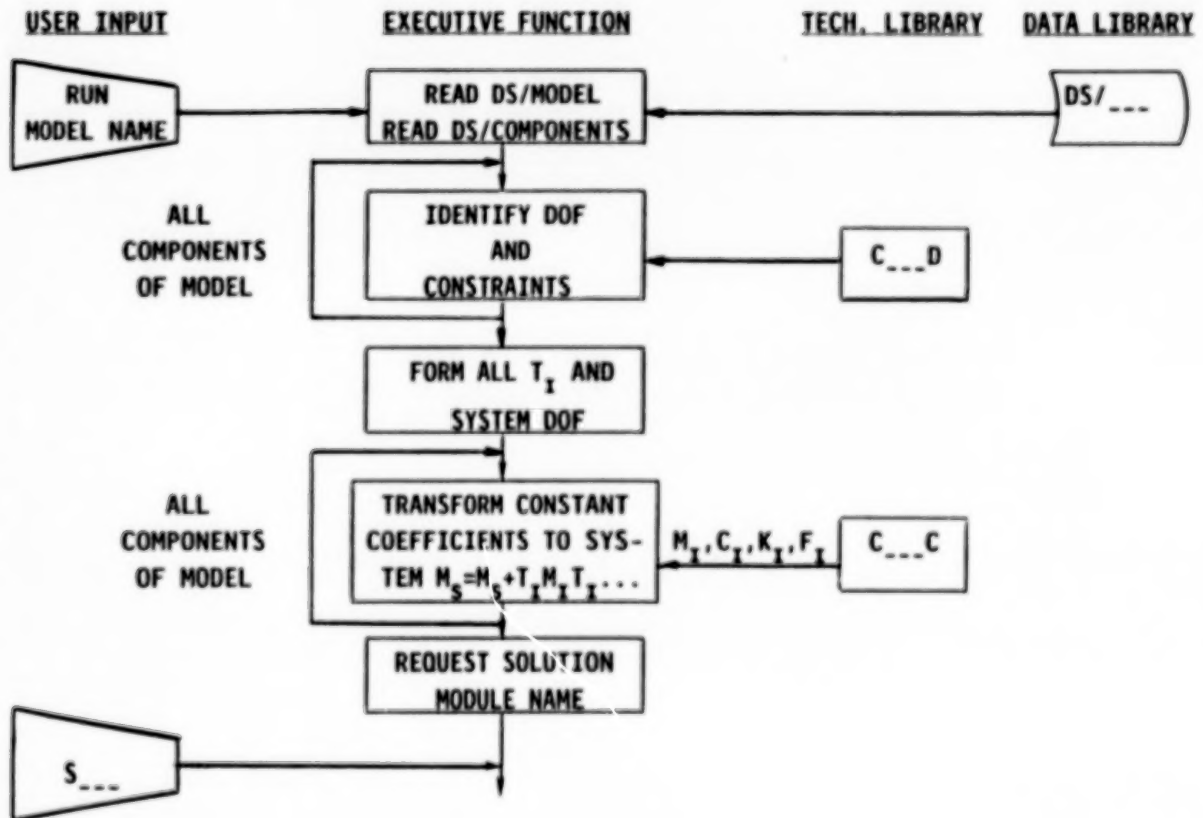


Figure 10

TIME HISTORY

Figure 11 is an illustration of a particular solution performed after execution of the RUN command. Functions such as retrieval of component state and the assembly of the varying matrix coefficients are performed as routine procedures in the Domain Executive.

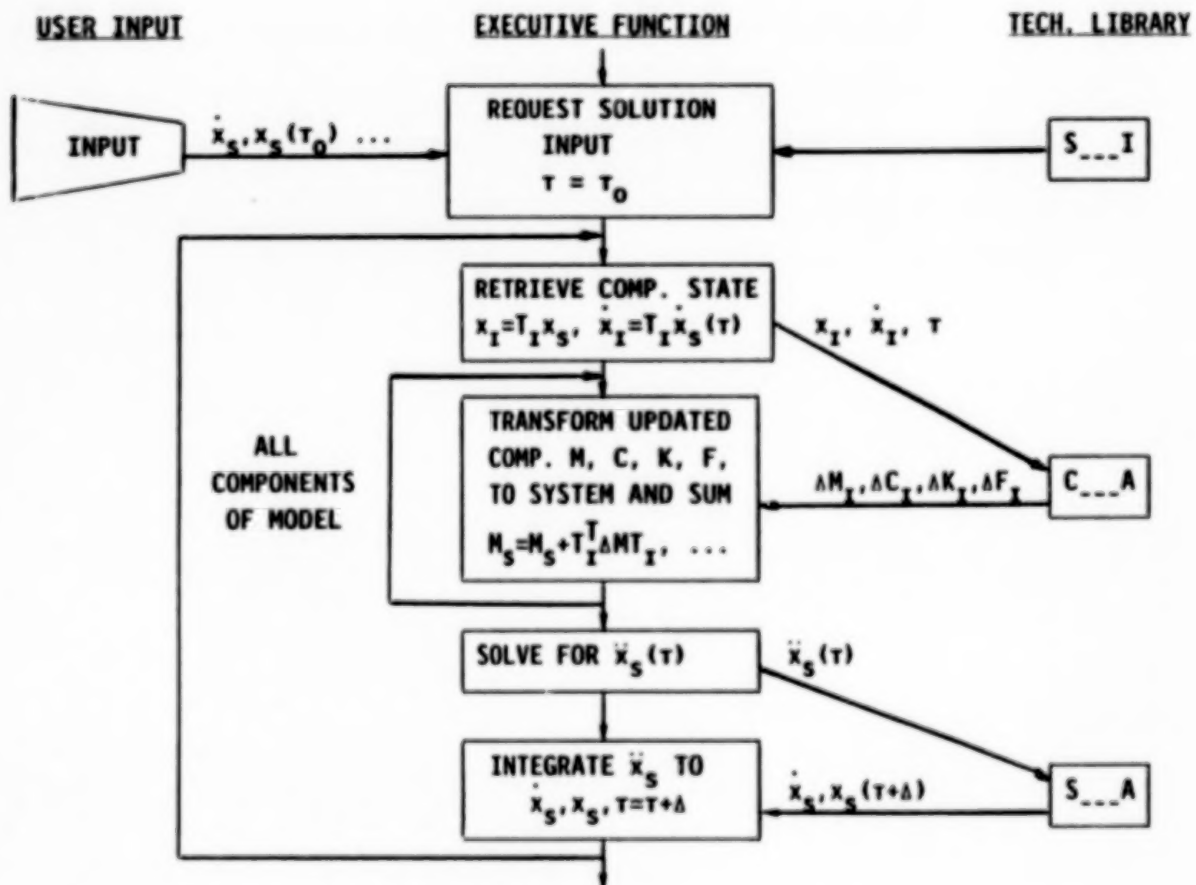


Figure 11

FEATURES OF THE EXECUTIVE

The principal executive characteristics are listed on figure 12. It performs all necessary operations without specific detailed instructions from the user. The Executive treats generic differential equations. None of its characteristics is related to any particular area of technology. This dependence is left to the specific modules in the Technology Library. Since the Technology Library may be readily expanded, any of a broad range of technologies may be treated alone or in conjunction with other technologies.

- o EXECUTIVE IS SPECIFICALLY BUILT TO MANAGE
STRUCTURAL DYNAMIC ANALYSIS**
- o IT UNDERSTANDS AND MANAGES**
 - INPUT: IDENTIFICATION, STORAGE, EDITING**
 - MODEL BUILDING: RETRIEVAL OF DATA, CALLS
TO TECHNOLOGY LIBRARY**
 - ASSEMBLY OF EQUATIONS: APPLIES MPC, SPC**
 - SOLUTION OF EQUATIONS: CALLS TO TECHNOLOGY
LIBRARY, RETRIEVAL OF LOCAL STATES,
INTERFACE LOADS**
- o EXECUTIVE INDEPENDENT OF ANY PARTICULAR AREA OF
TECHNOLOGY**
 - UNIFORM ABSTRACT INTERFACES TO TECHNOLOGY
LIBRARY**

Figure 12

FEATURES OF TECHNOLOGY LIBRARY

Figure 13 emphasizes many of the major features of the Technology Library. Because of the modularity and the uniform interfaces to the Executive, it is a simple procedure to add any capability (within the defined domain) to the program. This new capability then may be used in conjunction with all other capabilities which already exist in DYSCO.

- o NEW TECHNOLOGY EASILY ADDED
 - COMPONENT, FORCE, SOLUTION
 - UNIFORM INTERFACES TO EXECUTIVE
 - FORTRAN CODING

- o COMPONENTS ARE ANY SECOND ORDER ODE, SUCH AS,
 - SINGLE SPRING, DAMPER, OR MASS
 - ANY FINITE ELEMENT
 - COMPLETE NASTRAN MODEL
 - HELICOPTER ROTOR
 - MIMO CONTROL ALGORITHM

- o SOLUTIONS ACT ON MODEL EQUATIONS, E.G.
 - EIGENANALYSIS
 - FREQUENCY RESPONSE
 - TIME HISTORY
 - HELICOPTER TRIM (PERIODIC SHOOTING)
 - PERIODIC SYSTEM STABILITY
 - STATE FEEDBACK OPTIMIZATION

Figure 13

OTHER FEATURES

DYSCO contains a number of valuable features which are listed in figure 14. All of these make the program easy and safe to run. Safe means that data is all validated, in correct format, and that aborts or erroneous outputs due to inconsistent or missing data are not possible. The editing of both data and models allows easy modification or correction of data, configuration changes, damage analysis. The coupling procedures are also such that the user is relieved of much effort which is automatically performed by the Executive.

- o **VALIDATED INPUT AND EDITING**
 - **USES KNOWLEDGE TABLE: TYPE, CHARACTERISTICS, EXISTENCE, RANGE**
 - **PROMPTED INPUT**
 - **INSTANTANEOUS VALIDATION**
 - **ASSURED COMPLETE AND CONSISTENT DATA**
- o **SIMPLE EDITING OF MODEL**
 - **CONFIGURATION CHANGES**
 - **PARAMETER VARIATION**
 - **DAMAGE ANALYSIS**
- o **INTELLIGENT COUPLING PROCEDURES**
 - **RECOGNITION OF DOF NAMES**
 - **MPC OPTIONALLY AUTOMATICALLY FORMED**
 - **GENERAL MPC SOLVED FOR DOF EQUATIONS**

Figure 14

BASIC TECHNOLOGY MODULES - COMPONENTS

Figure 15 lists a number of general purpose components which are presently included in the Government version of DYSCO.

- o CSF1 - LINEAR FINITE ELEMENT
USER SUPPLIES: NAMES OF DOF
M, C, K, F
- o CFM3 - 3D MODAL STRUCTURE
RIGID BODY, ELASTIC MODES (ALL OPTIONAL)
DOF NAMES AUTOMATICALLY GENERATED
AUTOMATIC COUPLING AT SPECIFIED NODES
- o CSB2 - GENERAL BAR ELEMENT* (NOT AVAILABLE IN GOVT VERSION)
MAY BE USED AS A BEAM OR ROD ELEMENT
SHEAR FACTORS, CONSISTENT MASS, RAYLEIGH DAMPING
UP TO 12 DOF
- o CES1 - ELASTIC STOP
NONLINEAR SPRING, DAMPING, WITH GAP
- o CGF2 - GENERAL FORCE
 - POLYNOMIAL, FOURIER SERIES, OR TABULAR
 - PERIODIC
- o CLC0 - SINGLE POINT CONSTRAINTS
- o CLC1 - MULTIPOINT CONSTRAINTS
- o CLC2 - ADVANCED MULTIPOINT CONSTRAINT

32

Figure 15

BASIC TECHNOLOGY MODULES - SOLUTION

Figure 16 lists basic, general purpose solution routines which are also presently installed.

- o SEA4 - EIGENANALYSIS, REAL
- o SEA5 - COMPLEX EIGENANALYSIS
- o STH4 - TIME HISTORY
 - CONDITION CODES
- o SFD1 - FREQUENCY DOMAIN MOBILITY
 - RESPONSE PER UNIT FORCE
- o STC0 - OPTIMIZER FOR LINEAR STATE FEEDBACK* (NOT AVAILABLE IN GOVT VERSION)
 - SOLVES MATRIX RICCATI EQUATION
 - INTEGRATES SYSTEM STATE EQUATIONS
- o SII3 - INTERFACE AND INTERNAL LOADS
 - RESIDUAL FORCES AT INTERFACES
 - FORCES, STRAIN ENERGY, BENDING MOMENTS

Figure 16

SPECIALIZED TECHNOLOGY MODULES

On figure 17 is a listing of technology modules which were developed and installed to perform specialized representation and solutions.

- o CRR2, CRR3 - HELICOPTER ROTOR**
- o CCE0, CCE1 - ROTOR CONTROL SYSTEM**
- o CRD3 - ROTOR DAMAGE**
- o CFM2 - HELICOPTER FUSELAGE**
- o CLG2 - NONLINEAR LANDING GEAR**
- o CLS2 - LIFTING SURFACE**
- o FRA0, FRA2, FRA3 - ROTOR AERODYNAMICS**
- o FFA0, FFC2 - FUSELAGE AERODYNAMICS**
- o STH3 - TIME HISTORY, HELICOPTER CONTROLS**
- o STR3 - HELICOPTER TRIM**
- o SSF3 - FLOQUET STABILITY**

Figure 17

LIST OF ILLUSTRATIVE PROBLEMS

In conclusion, figure 18 is a list of actual diverse problems which have been modeled and solved using the DYSCO program.

- o PACOSS TOWER DYNAMIC ANALYSIS
- o TRUSS STRUCTURE WITH ACTIVE ELEMENTS - VIBRATION CONTROL
- o PIEZOELECTRIC SENSORS/ACTUATORS ON BEAM - VARY CONTROL LAWS, ADD ELASTIC STOP, STABILITY, TIME, FREQUENCY DOMAIN
- o POINTING-TRACKING SYSTEM - MOTOR DRIVEN MIRRORS - MOVING, ACCELERATING TARGET, VARY CONTROL GAINS
- o ROTORCRAFT TRIM - DAMAGED BLADE - INTERNAL LOADS
- o RAIL GUN PNEUMATIC ACCELERATOR - GAS PRESSURE - BOLT MOTION
- o ALGORITHM EVALUATION - REDUCED MODELS, SYSTEM IDENTIFICATION, SIMULATE EFFECTS OF MEASUREMENT ERRORS

Figure 18

RESEARCH ON OPTIMIZATION-BASED DESIGN
AT THE
ENGINEERING DESIGN METHODS LAB,
BRIGHAM YOUNG UNIVERSITY

R.J. BALLING
A.R. PARKINSON
J.C. FREE
BRIGHAM YOUNG UNIVERSITY
PROVO, UTAH

ENGINEERING DESIGN METHODS RESEARCH LAB

To develop engineering design methods which,

- 1) are domain-independent to a certain degree,
- 2) can be implemented on the computer.

THE OPTDES.BYU PACKAGE VERSION 4.0

A collection of general design methods that have been developed or collected by the Lab and implemented as software.

- 1) Use in the classroom -- about 80-100 students each year
- 2) Use in research -- about 12-15 graduate students each year
- 2) Use in industry -- about 90 company sites

* OPTDES.BYU / COMMERCIAL ANALYSIS PACKAGES

- 1) OPTDES/ACSL (MGA Associates, Concord, MA)
 - * simulation of dynamic systems
- 2) OPTDES/MECHANICAL ADVANTAGE (Cognition, Billerica, MA)
 - * mechanical design software
- 3) OPTDES/COSMOSM (SPAC, Santa Monica, CA)
 - * finite element analysis on microcomputers
- 4) OPTDES/CALIPER (Aptek, Colorado Springs, CO)
 - * interference calculation and packing of geometric shapes
- 5) OPTDES/CIVILPAK (BYU)
 - * design of land subdivisions, water distribution networks, steel frames, reinforced concrete systems
- 6) OPTDES/??? (Design Synthesis, Provo, UT)
 - * SBIR Phase I Award from Wright-Patterson AFB to develop an optimization, feature-based modeling system for the design of mechanical parts

STANDARD CAPABILITIES OF OPTDES.BYU

- 1) First-class optimization algorithms:
 - * Powell's Sequential Quadratic Programming Algorithm
 - * Our Own Hybrid SQP/GRG Algorithm — an SQP that stays feasible
 - uses the SQP search direction (updated hessian)
 - uses the GRG line search (hemstitching)
 - * SLP and Method of Centers
 - * Goldfarb/Idnani's Dual Algorithm for QP problems
 - * Revised Simplex Algorithm for LP problems
 - * BFGS Variable Metric Algorithm for unconstrained problems
- 2) Interactive Design Utilities
 - * Trial-And-Error Design (Set and Display)
 - * History Backtrack and History Plots
 - * 1D, 2D, and 3D Plots of Design Space or Subspace
- 3) Flexible Problem Setup
 - * Function Designation (as objectives or constraints)
 - * Many-to-One Variable and Function Mappings
 - * Bounds on Variables and Allowable Values on Constraints
 - * Log Variables and Functions
- 4) Interface with Analysis
 - * Conventional and Generalized Interfaces
 - * Programming-Free Interface

NEW AND DEVELOPING CAPABILITIES OF OPTDES.BYU

- 1) Manufacturing Considerations
 - * Optimization with variables that are available in discrete combinations
 - * Optimization in light of manufacturing tolerances on variables
- 2) Large-Scale Problems
 - * Approximations based on analyses according to statistical test plans
 - * Decomposition of optimization problems
- 3) Topological Optimization
 - * Use of AI heuristic search strategies
 - * Formal expert systems for generating topologies

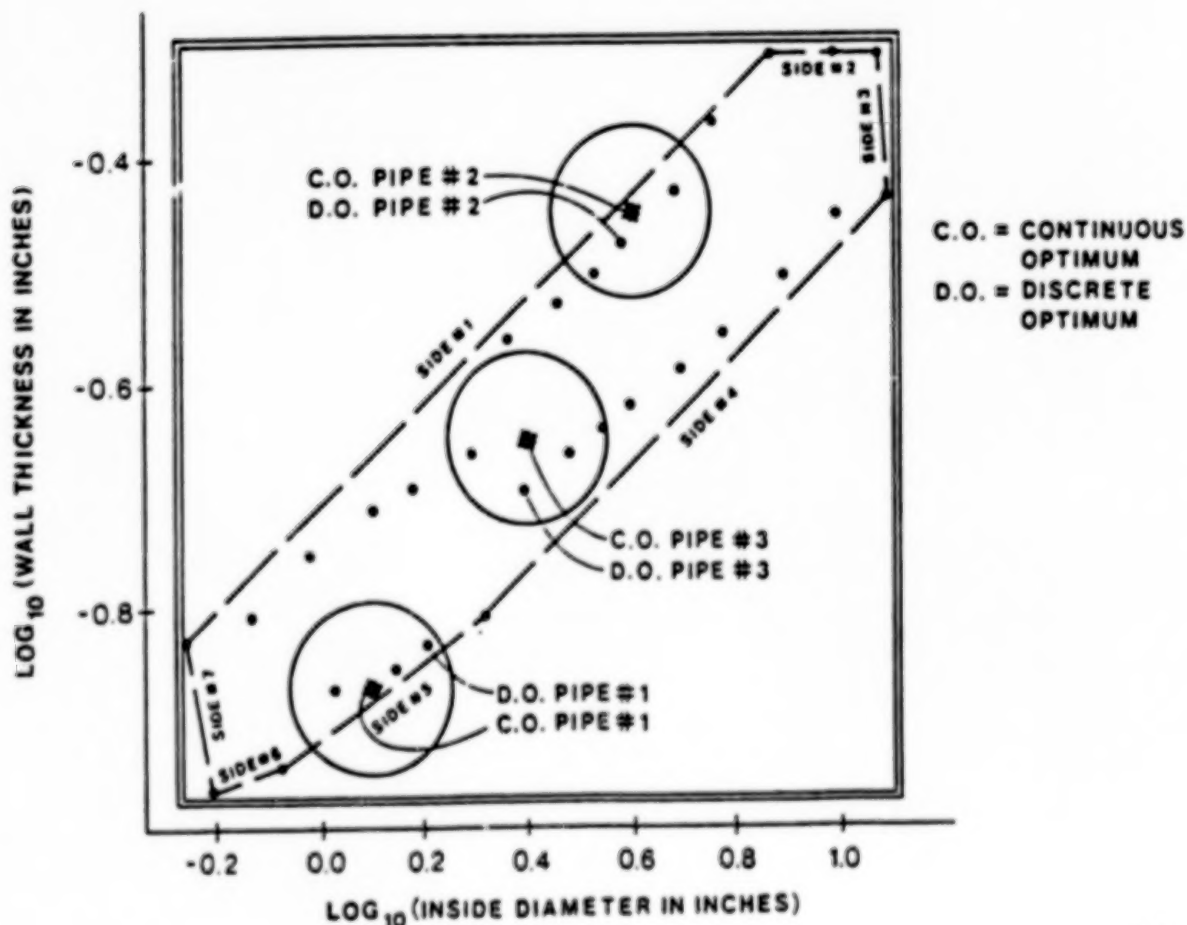
OPTIMIZATION WITH DISCRETE VARIABLES STEP 1: CONTINUOUS OPTIMIZATION WITH ENVELOPING CONSTRAINTS

In this illustrative example it is desired to find the optimum diameters and thicknesses for three pipes. Each dot represents an available pipe. Log values are used to make the spacing of the dots more uniform.

A convex set of linear constraints are collapsed around the available pipes. This means $7 \times 3 = 21$ constraints are added to the optimization problem. Constraints may be thrown out by the user in the order of smallest length (or area in 3D, or hyper-area in ND). In this problem side #6 would be the first to be thrown out, followed by side #2, then side #3, and so on.

The continuous optimization problem is solved, and continuous optimum values are indicated by asterisks.

Neighborhoods are constructed about continuous optimum values. The user selects the radii to be large enough to include a sufficient number of dots, but small enough to keep the computational search effort reasonable.



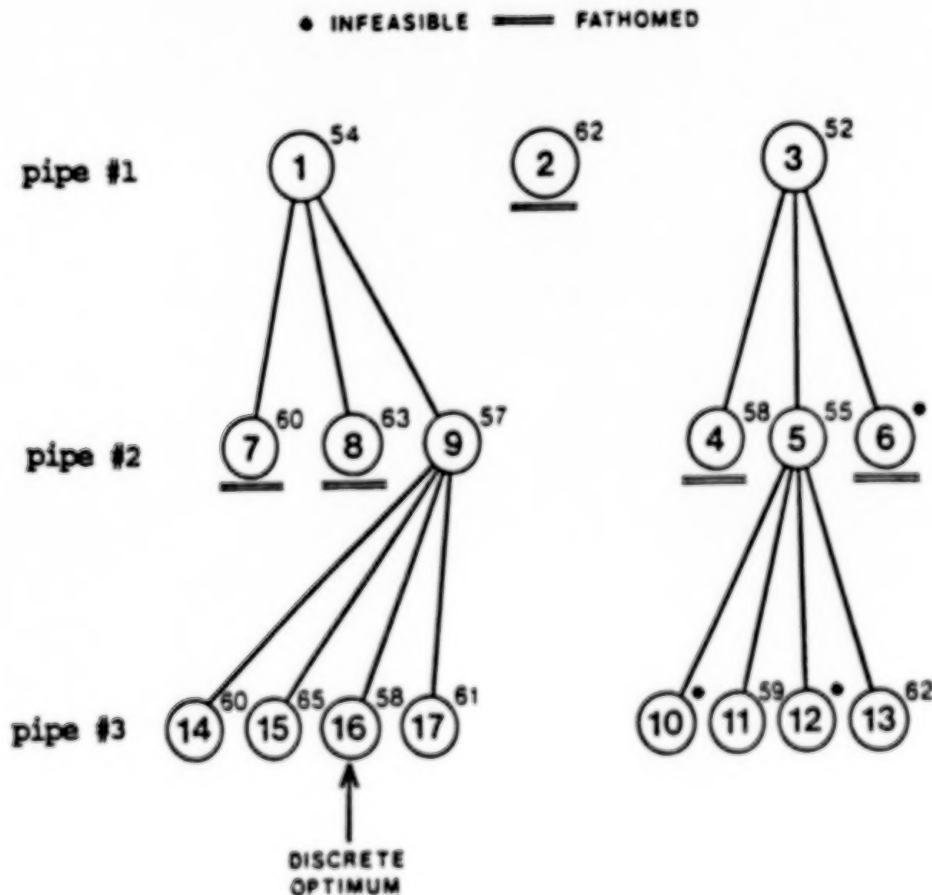
OPTIMIZATION WITH DISCRETE VARIABLES STEP 2: DISCRETE SEARCH

In the illustrative example, the neighborhoods included 3 dots for pipe #1, 3 dots for pipe #2, and 4 dots for pipe #3. The number of possible discrete designs are $3 \times 3 \times 4 = 36$. Exhaustive search would require 36 analyses. Not all these designs need be considered if a branch-and-bound strategy is used. The first step is to linearize the objective and constraints about the continuous optimum.

The figure shows a schematic of a branch-and-bound strategy. The circles represent "nodes" which are numbered in their order of generation. Nodes 1-3 represent designs where pipe #1 is fixed to the respective three dots within its neighborhood while pipes #2 and #3 remain continuous.

The small numbers beside each node represent the minimum costs for these designs. These values are found by optimizing continuous pipes #2 and #3 for minimum cost. These optimizations are solved as LP problems.

Nodes 4-6 are spawned from node 3 since it had the lowest minimum cost. In these nodes only pipe #3 remains continuous. Note that no feasible solution can be found for node 6, so it is "fathomed". After spawning nodes 10-13, node 11 represents a current best solution. Nonlinear analysis is performed at all current best solutions to check actual feasibility. Nodes 2, 7, and 8 are fathomed since their minimum costs are greater than that of the current best solution. The strategy continues until all possible branches are fathomed. The solution is found at node 16. Two nonlinear analyses and one gradient analysis were performed in the process.

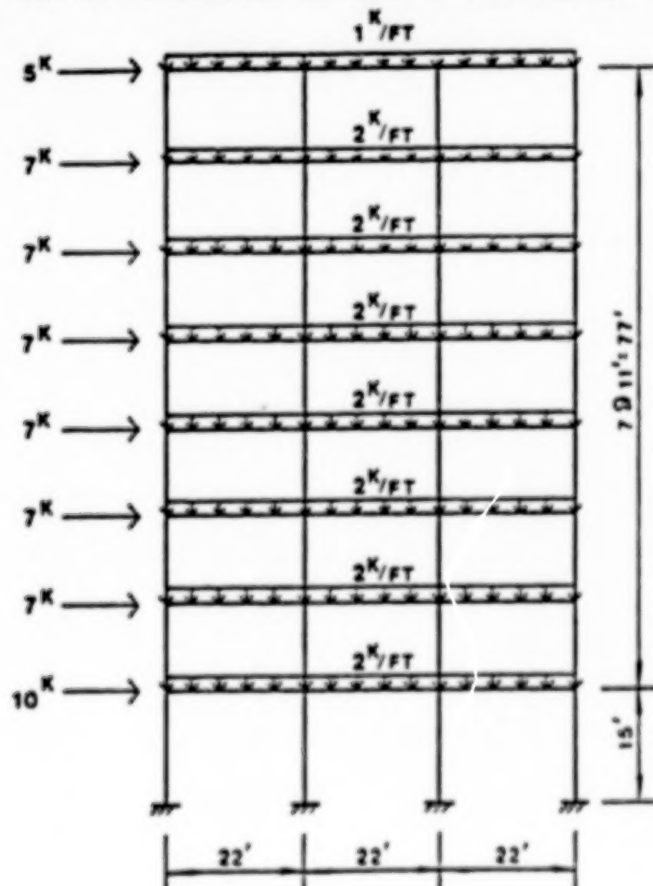


OPTIMIZATION WITH DISCRETE VARIABLES EXAMPLE: STEEL FRAME

The problem was to select from among the 194 standardized sections published by AISC the optimal 16 sections for the frame shown. The 16 sections to be selected included 8 girders (one continuous girder for each floor) and 8 columns (interior and exterior columns where each column was continuous for two stories). The AISC combined stress constraints were imposed for each of the 56 members, and total frame weight was minimized. Only in-plane deformation was considered, the K-factor for all members was taken as 2.5, and continuous lateral support was assumed.

There were three design variables for each of the 16 sections during continuous optimization, namely: area, moment of inertia, and section modulus. 74 enveloping constraints were generated about the 194 standardized sections in 3 dimensions. Since this would add $16 \times 74 = 1184$ constraints to the problem, only 24 enveloping constraints were retained accounting for 80% of the area of the convex hull. This added $24 \times 16 = 384$ to the problem. The continuous optimum was found, and it had a weight of 36,257 lbs.

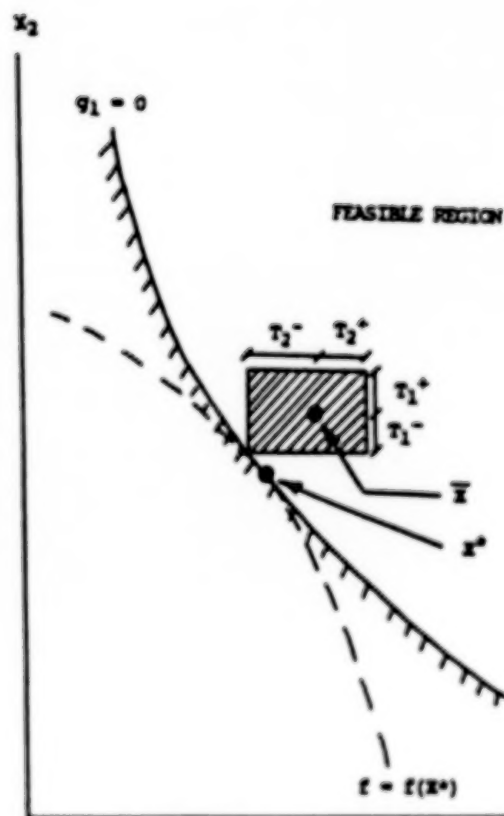
Neighborhoods about the continuous optimum were constructed such that 3 or 4 standardized sections were included for each of the 16 sections to be selected. An exhaustive search over the standardized sections in these neighborhoods would require 429,981,696 analyses. The linearized branch and bound strategy required one gradient analysis for linearization and 13 regular analyses to verify feasibility of current best solutions. The discrete optimum had a weight of 40,337 lbs. In going from the continuous optimum to the discrete optimum, all the areas increased, but 13 out of 16 moments of inertia decreased, and 6 out of 16 section moduli decreased.



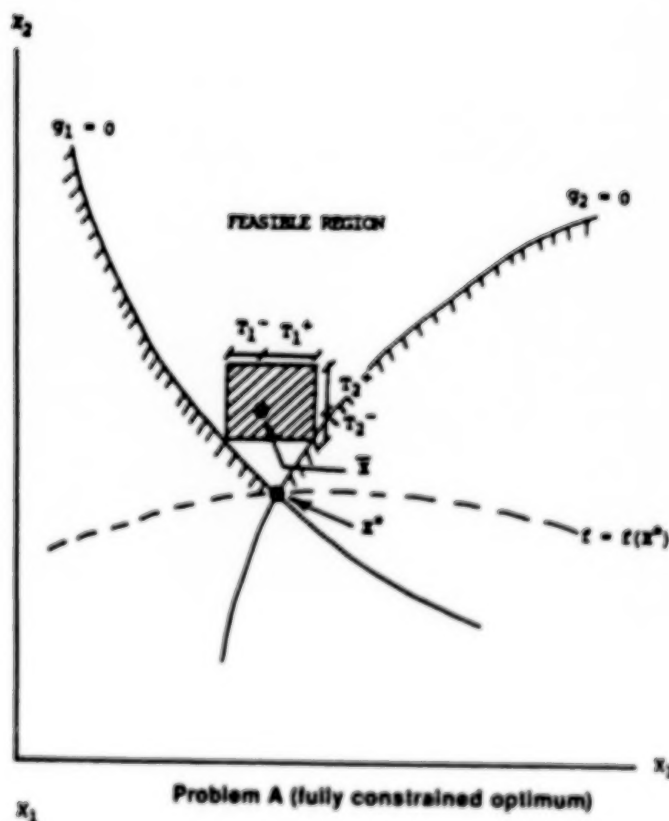
OPTIMIZATION WITH TOLERANCES PROBLEM A: TOLERANCES SPECIFIED

In this problem, one seeks a new design as close as possible to the optimal design such that constraints are not violated for any design within the specified tolerance ranges of this new design. This means that the shaded box in the figure must be entirely feasible, and centered as close as possible to the optimum.

The problem is solved by linearizing the constraints about the optimum. Examination of the signs of the terms in the constraint gradient vectors indicate which sides of the box control for each constraint. By minimizing the square of the distance from the box center to the optimum, the problem can be solved as a quadratic-programming problem.



Problem A (no-fully constrained optimum)



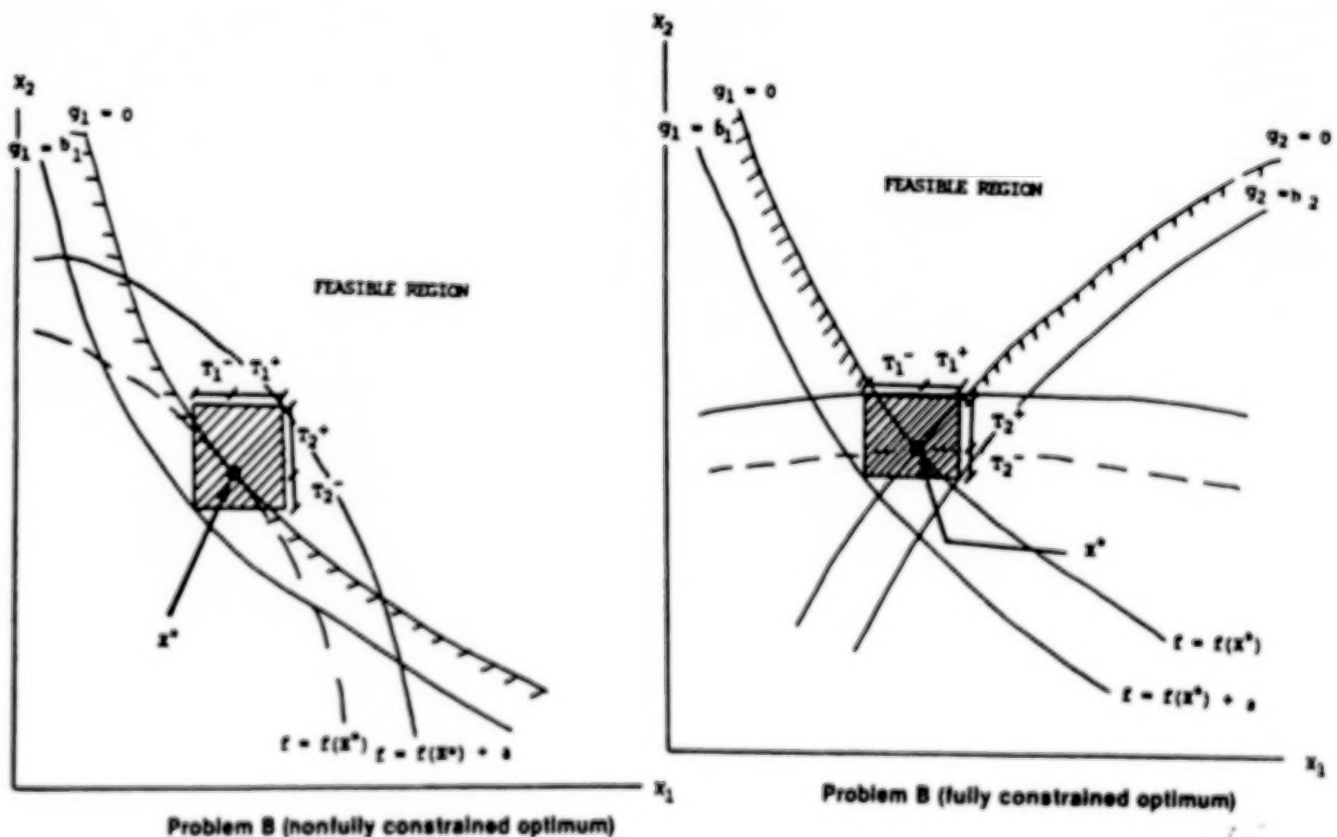
Problem A (fully constrained optimum)

OPTIMIZATION WITH TOLERANCES PROBLEM B: TOLERANCES COMPUTED

In this problem, one seeks the largest tolerance ranges according to some norm about the optimum design such that any design within these tolerance ranges does not exceed specified acceptance levels for the objective and constraints. Thus, the user "backs off" from the optimum values for the objective and constraints by specifying acceptance levels. The shaded box in the figure must be entirely contained within the region bound by these acceptance levels.

Again the objective and constraints are linearized, and the controlling sides of the box are identified for each constraint. Various norms of the tolerances could be maximized. If the L1 norm is used (tolerances simply added), the problem can be solved as a linear-programming problem.

To keep the problem well-posed, upper and lower bounds on the tolerances should be specified. Lower bounds represent the user's estimate of the tolerance that he must absolutely have as a minimum for each variable. Upper bounds represent his estimate of the tolerance that, if achieved, is all he needs for a variable (at this point the optimization should try to increase tolerances in other variables).



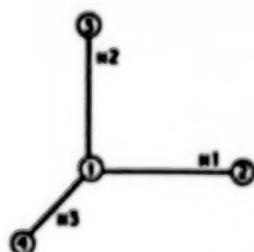
Approximation of Computationally Expensive and Noisy Functions

The approximation of design functions with first or second order polynomials for optimization has several advantages: 1) the polynomials smooth noisy functions, which can improve algorithm performance, 2) analysis and optimization can be decoupled so that optimization can be executed on one computer and the analysis on another, and 3) the number of analyses required to reach an optimum, particularly for noisy functions, can often be significantly reduced. Approximation is also an important aspect of several problem decomposition schemes.

The approach taken in this research is to use statistical test plans to determine where analysis should be run in order to make the approximation. The statistical test plans yield approximations that can be superior to approximations made from Taylor's series expansions because the analyses are spread throughout the range of the function being approximated, and, for each analysis, more than one variable is changed at a time (in contrast to finite difference derivative), making it possible to use several analyses to estimate a particular model coefficient.

This advantage is demonstrated in the figure below comparing the analyses evaluated with a "one at a time" test plan to the analyses evaluated with a saturated factorial test plan. For a problem with three variables, both strategies require a base point (variables set to -1) and three other analyses. In the "one-at-a-time" plan, each variable is perturbed in turn while the others are left at the base values. The effect of each variable can only be estimated from two analyses. In the saturated plan, however, two variables are perturbed for each analysis; as a result, twice as much information is available to estimate the model coefficient of each variable.

"one-at-a-time" or finite difference

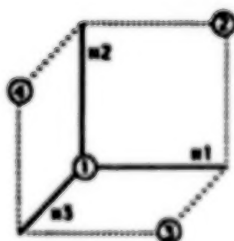


	n1	n2	n3
analysis 1	-1	-1	-1
analysis 2	+1	-1	-1
analysis 3	-1	+1	-1
analysis 4	-1	-1	+1

effect of n1 = 2 vs. 1 (2 analysis points)
 effect of n2 = 3 vs. 1 (2 analysis points)
 effect of n3 = 4 vs. 1 (2 analysis points)

The effect of each variable is estimated from only one other evaluation.

factorial design



	n1	n2	n3
analysis 1	-1	-1	-1
analysis 2	+1	+1	-1
analysis 3	+1	-1	+1
analysis 4	-1	+1	+1

effect of n1 = 1,4 vs. 2,3 (4 analysis points)
 effect of n2 = 1,3 vs. 2,4 (4 analysis points)
 effect of n3 = 1,2 vs. 3,4 (4 analysis points)

Twice as much information is available to estimate the effects of each variable for the same number of function evaluations.

The capability to approximate functions has been integrated fully into the OPTDES package. The user first specifies variable range limits for the approximation. OPTDES will then generate a test plan within those limits and write the analysis variable values in the proper file format for the user's analysis software. After the analysis is finished, OPTDES reads the analysis results and performs regression analysis to obtain the model, displaying the model goodness of fit. The user can then optimize directly on the model.

An example of this operation is shown below. For this example, which involved large scale thermal analysis, 57 analysis calls by OPTDES were required when direct optimization was used. Using model approximation with statistical test plans to determine where analysis should be performed, the number of analysis calls was reduced to 24.

Although very efficient test plans exist for estimating models with linear coefficients, statistical plans for second order models tend to be expensive, in that they require more analyses than the number of estimated coefficients. The popular Box-Behnken plan, for example, requires 25 analyses to estimate 15 second order coefficients for a problem with four variables. These extra analyses are used in part to determine the variance, or random error, of the analysis results. In a computer model, such variance does not usually exist. The statistics department at BYU has been testing efficient second order test plans that require the same number of analyses as coefficients for use in approximation for optimization. We feel that these test plans will be very useful for this application.

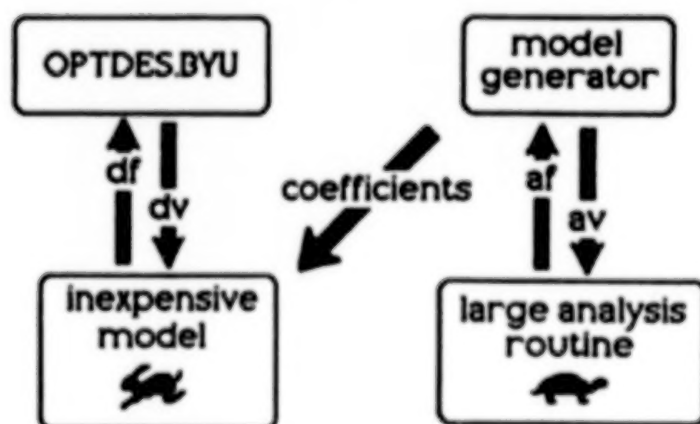
Without Approximation

57 calls



With Approximation

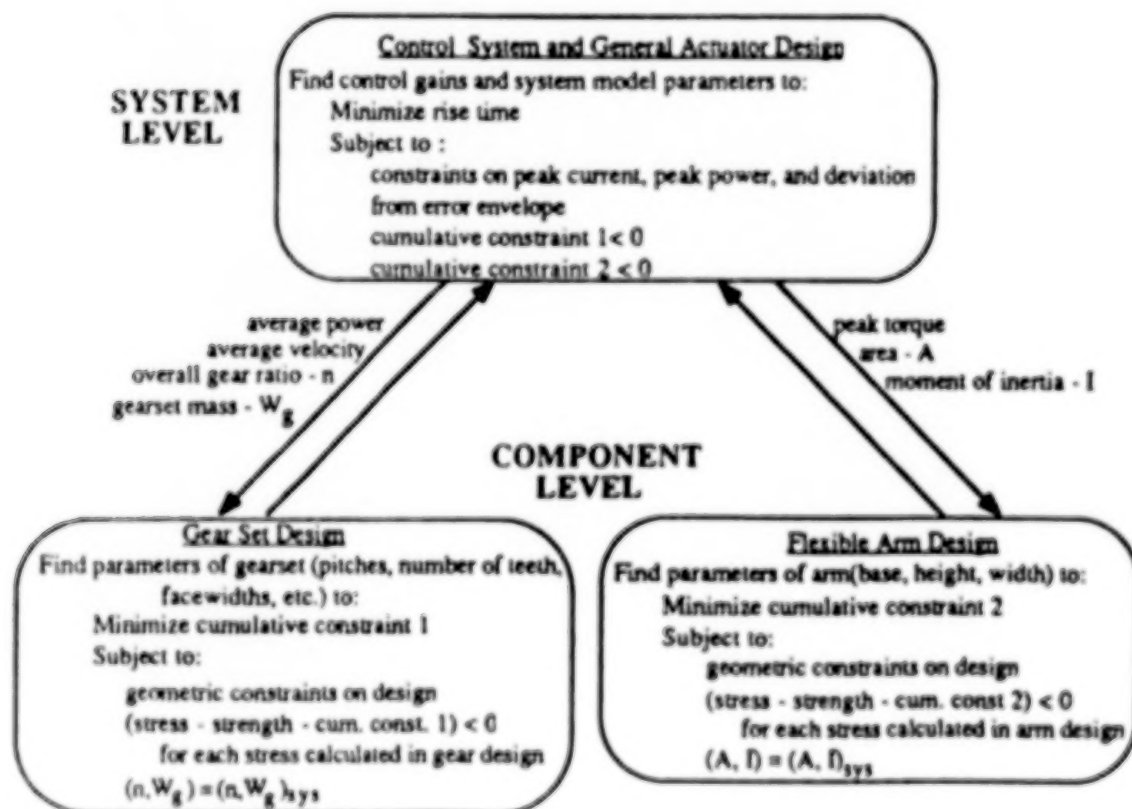
24 calls



Electromechanical Actuator/Control System Design Using Decomposition

Advancements in robotics and computer storage media require servomechanisms that are quick, precise, and powerful. The dynamic performance of a control system is ultimately limited by the actuator hardware. In addition, practical design considerations such as weight, volume, and power are dependent on actuator parameters. Normally the design of an actuator and its control system are approached sequentially: an actuator is selected or designed; the control system for the actuator is then determined. The objective of this research was to integrate the design of the actuator and control system in order to optimize the transient response. Because the design of such a system can be complex, decomposition methods were studied as a means of approaching the design problem. The discrete variable capabilities of OPTDES were also used to select an optimal motor from catalog values.

The electromechanical actuator considered consists of a permanent magnet dc motor coupled to a double reduction gear set with inline input and output shafts driving a flexible arm carrying an inertial load. The objective of the design problem was to minimize rise time of the actuator, subject to constraints on over/undershoot. The 22 design variables included six control gains, the resistance, inductance, time constant, torque constant, and rotor inertia of the motor, the detailed design of the gear set and the actuator arm. The problem was decomposed heuristically according to the physical makeup of the system, as given below.



Decomposition of Electromechanical Actuator.

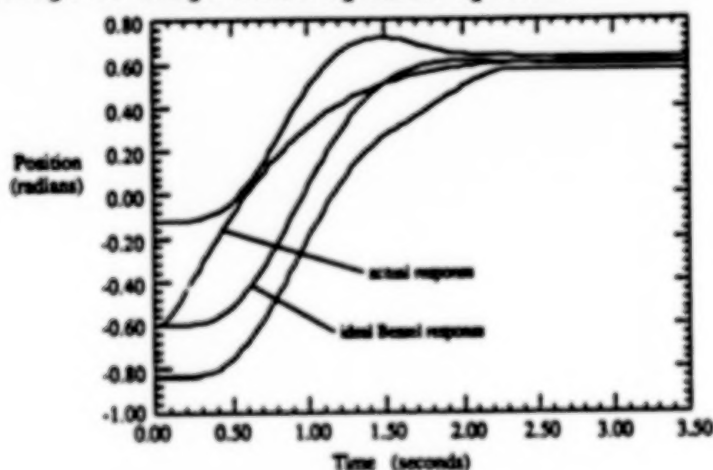
As the figure shows, the optimization of the system time response was assigned to be the overall objective of the system. The design of the gear set and actuator arm were designed at the component level. After decomposition, the system level problem contained 11 system variables; the gear component design problem had 8 design variables, and the arm design problem had 3 design variables. The strategy for solving the decomposed problem was that developed by Sobieski, using cumulative constraints. However, the cumulative constraint was not formulated using the Kresselmeier-Steinhauser function, but was formulated using the simple form,

$$\begin{aligned} &\text{Minimize } S \\ &\text{subject to } \text{Constraint}_i - S \leq 0 \text{ for all } i \end{aligned}$$

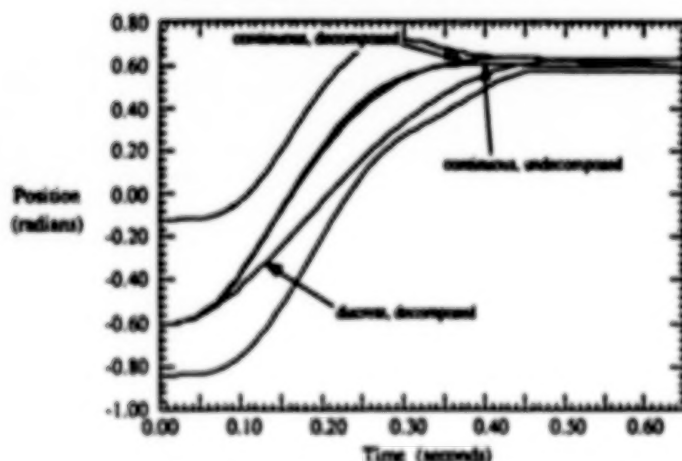
Minimizing S tends to maximize the feasibility of the design.

The step response of the system before optimization is shown below. The top and bottom response curves in the figure represent the error envelope the response must stay within. The optimal response is given in the second figure. The "continuous" response in the figure is the optimal response with the motor variables modeled as continuous variables. The "discrete" response is the response of the optimal actuator with the optimal discrete values of the motor as selected from a vendor's catalog.

The results from this sample problem show decomposition to be a potentially valuable tool in the design of large scale dynamic systems.



Electromechanical Actuator Response Before Optimization.

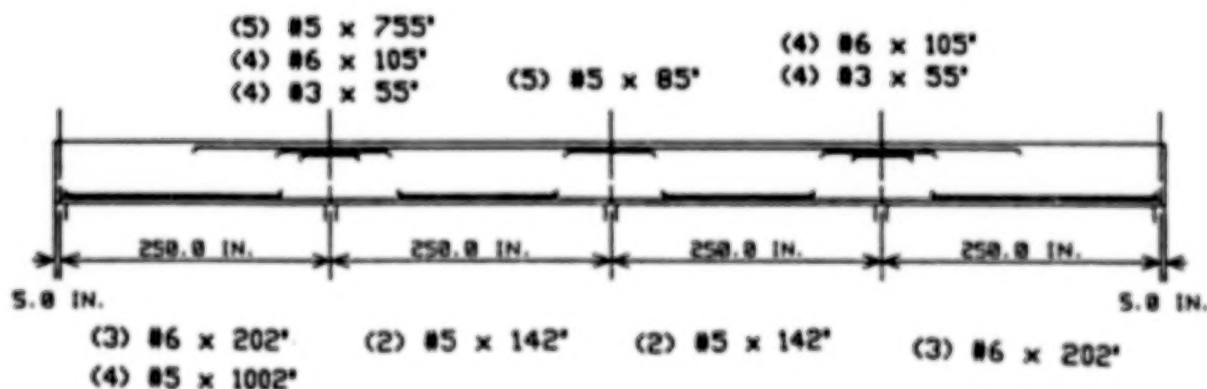
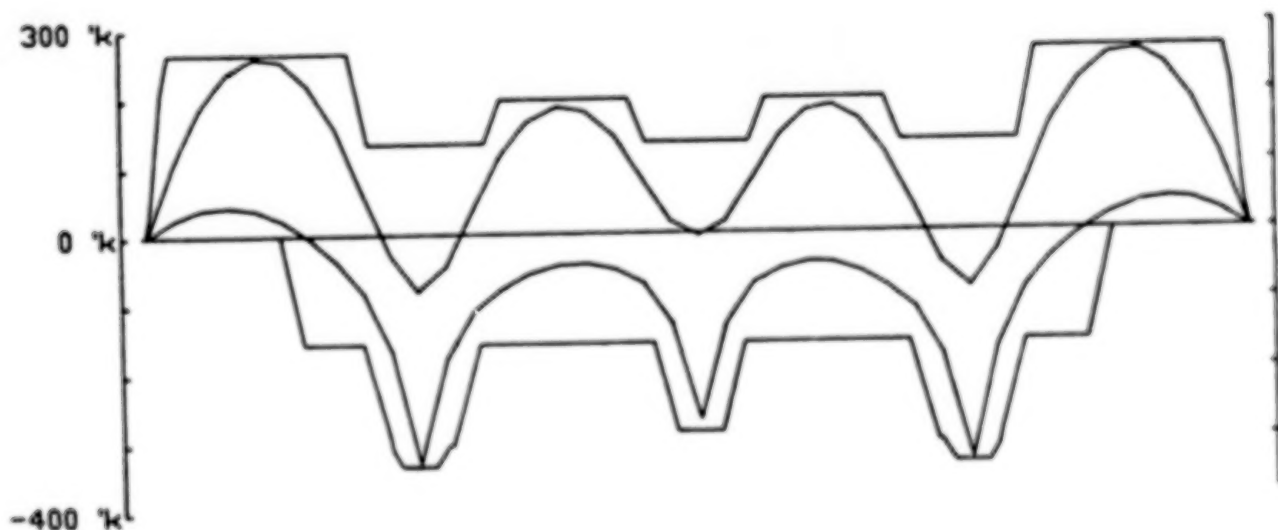


Optimal Response Plots for Electromechanical Actuator.

CONFIGURATION OR TOPOLOGICAL OPTIMIZATION EXAMPLE: REINFORCEMENT IN A CONCRETE BEAM

The problem here was to design the reinforcement in a concrete tee-beam over four equal 250-inch spans. The material properties and dimensions of the concrete beam were given. The moment envelopes under possible loading conditions are given in the figure. All constraints imposed by the ACI 318-83 Specification were applied. The reinforcement cost was minimized, which included material cost (\$.25/lb of steel) and placement cost (\$1.00 per bar).

The figure shows the optimum design. Note that the number of bars (given in parentheses), the discrete bar sizes (#5, #6, #3, etc.), the bar lengths (in inches), and the locations (top or bottom, over support or in the middle of the span, and layers) are given for each group of bars. The optimal moment capacity envelope is also shown in the figure.



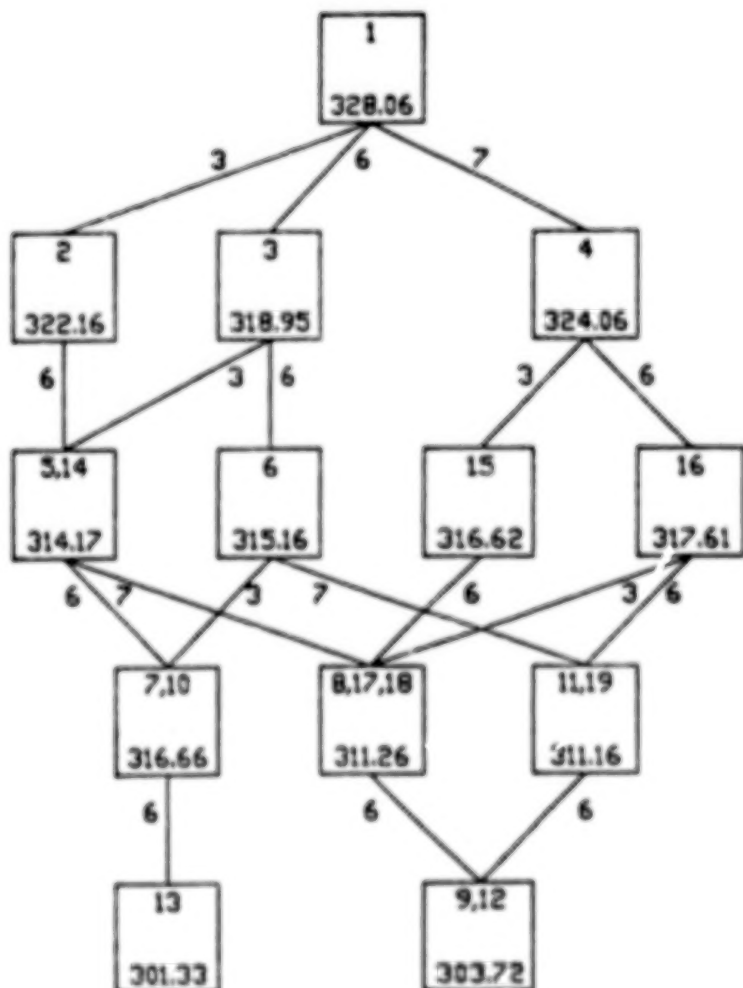
CONFIGURATION OR TOPOLOGICAL OPTIMIZATION RULE-BASED SEARCHING STRATEGY

The problem is solved by generating reinforcement configurations. The number of bar groups with the location and number of bars for each group are needed to specify a configuration. The configuration is then optimized via the linearized branch-and-bound method to determine the bar sizes, bar lengths, and total reinforcement cost. The figure shows boxes representing the various configurations. The boxes contain the configuration numbers according to the order in which they were generated, and the total reinforcement cost.

A rule-based algorithm is used to search through configurations. Configuration #1 contains both positive and negative "primary" groups extending all the way across the beam with enough steel to satisfy the minimum reinforcement requirements. "Secondary" groups are included over each support and in each span to provide necessary moment capacity.

"Child" configurations are spawned from the "parent" configurations as shown in the figure according to one of eight heuristic rules. These rules govern the deletion/addition of a bar within a group or the deletion/addition of an entire bar group. For example, rule #3 states that if the number of bars in a secondary group is more than twice as many as the number of bars in the primary group, divide the secondary group into two groups. The algorithm stops when no more rules apply to any children.

Note that the same child may be spawned from more than one parent. Note also that the cost of configuration 7,10 was greater than the cost of configurations 5,14 or 6 from whence it came. Nevertheless configuration 7,10 spawned configuration 13 which was the eventual optimum.



Application of Knowledge-Based Systems and Optimization for the Design of a Valve Anti-Cavitation Device

This research involves the design of a device to control cavitation for liquid valves. Cavitation can cause erosion of valve material and premature valve failure. An approach for preventing cavitation is to force the liquid through a series of expansion holes and contraction channels, machined into concentric cylinders, as shown in the figure below. The cylinders together comprise the "anti-cavitation retainer." A local valve company desired to develop software to automate the design of the retainer. Design of a good retainer can be complex and requires an experienced engineer.

Initially expert system technology was applied to capture the design rules of the expert. However, it became apparent as the expert described his design procedure, that many of his rules were associated with how to change variables to obtain a good design. These rules were replaced with an optimization algorithm.

The package that was developed consisted of a small expert system which applied the true heuristic rules to the problem, setup the optimization problem, called the algorithm, and interpreted the results. The optimization algorithm determined the values of variables. This strategy of combining heuristic search with numerical search could apply to a broad spectrum of engineering design problems. Knowledge-based systems and numerical optimization are complementary approaches that span both the qualitative and quantitative aspects of design.

When completed, the software was tested on ten actual design problems that had been previously solved by the expert. The expert verified the adequacy of the designs produced by the package. In five cases, the software developed satisfactory designs with a fewer number of cylinders—these designs would be cheaper to produce. In two cases, the package produced designs that violated a fewer number of customer requirements. The remaining three designs were equally satisfactory.

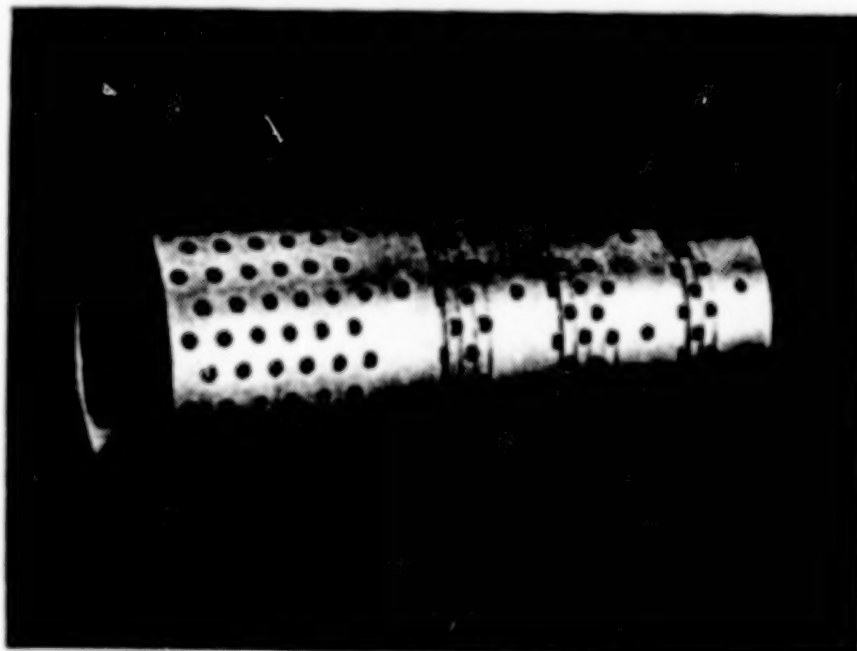


Photo courtesy of Valtek Incorporated.
Anti-Cavitation Retainer

REFERENCES

OPTDES.BYU

A.R.Parkinson, R.J.Balling, and J.C.Free, "Exploring Design Space: Optimization as Synthesizer of Design and Analysis", *COMPUTERS IN MECHANICAL ENGINEERING*, Vol. 3, No. 1, Pp. 28-36, 1985

A.R.Parkinson, R.J.Balling, and J.C.Free, "OPTDES.BYU: A Software System for Optimal Engineering Design", *ASME COMPUTERS IN MECHANICAL ENGINEERING CONFERENCE*, August 12-16, 1984, Las Vegas, NV

OPTIMIZATION WITH DISCRETE VARIABLES

K.Hager and R.J.Balling, "A New Approach for Discrete Structural Optimization", *ASCE JOURNAL OF STRUCTURAL ENGINEERING*, Vol. 114, No. 5, Pp. 1120-1134, May 1988

M.W.Brown and R.J.Balling, "Discrete Optimization of Water Networks", *ASCE 5TH CONFERENCE ON COMPUTING IN CIVIL ENGINEERING*, March 29-31, 1988, Alexandria, VA

OPTIMIZATION WITH TOLERANCES

R.J.Balling, J.C.Free, and A.R.Parkinson, "Consideration of Worst-Case Manufacturing Tolerances in Design Optimization", *ASME JOURNAL OF MECHANISMS, TRANSMISSIONS, AND AUTOMATION IN DESIGN*, Vol. 108, No. 4, Pp. 438-441, December, 1986

APPROXIMATIONS BASED ON STATISTICAL TEST PLANS

J.W.Free, A.R.Parkinson, G.R.Bryce, and R.J.Balling, "Approximation of Computationally Expensive and Noisy Functions for Constrained Nonlinear Optimization", *ASME JOURNAL OF MECHANISMS, TRANSMISSIONS, AND AUTOMATION IN DESIGN*, Vol. 109, No. 4, Pp. 528-532, December, 1987

DECOMPOSITION OF OPTIMIZATION

T.W.McLain, J.C.Free, and A.Teng, "Optimal Design of Complex Systems Using Decomposition Methods: Part II Example Application to Electromechanical Control", *ASME 14TH DESIGN AUTOMATION CONFERENCE*, September 24-28, 1988, Orlando, FL

A.R.Parkinson, R.J.Balling, A.Wu, and J.C.Free, "A General Strategy for Decomposing Large Design Problems Based on Optimization and Statistical Test Plans", *INTERNATIONAL CONFERENCE ON ENGINEERING DESIGN*, August 17-20, 1987, Boston, MA

TOPOLOGICAL OPTIMIZATION VIA ARTIFICIAL INTELLIGENCE

R.Ellsworth, A.R.Parkinson, and F.Cain, "The Complimentary Nature of Symbolic Computing and Numerical Optimization in Engineering Design Software", *ASME 13TH DESIGN AUTOMATION CONFERENCE*, September, 1987, Boston, MA

RECENT EXPERIENCES USING FINITE-ELEMENT-
BASED STRUCTURAL OPTIMIZATION

B. K. Paul, J. C. McConnell, M. H. Love
General Dynamics
Fort Worth Division
Fort Worth, Texas

OUTLINE

Structural optimization has been available to the structural analysis community as a tool for many years. The popular use of displacement method finite-element techniques to analyze linearly elastic structures has resulted in an ability to calculate the weight and constraint gradients inexpensively for numerical optimization of structures.

In this presentation, recent experiences in the investigation and use of structural optimization will be discussed. In particular, experience with the commercially available ADS/NASOPT (Reference 1) code is addressed. An overview of the ADS/NASOPT procedure and how it was implemented will be shown. Two example problems will also be discussed.

● BACKGROUND

● PROGRAM FORMAT

● TYPICAL INPUTS

● BUCKLING EXAMPLE

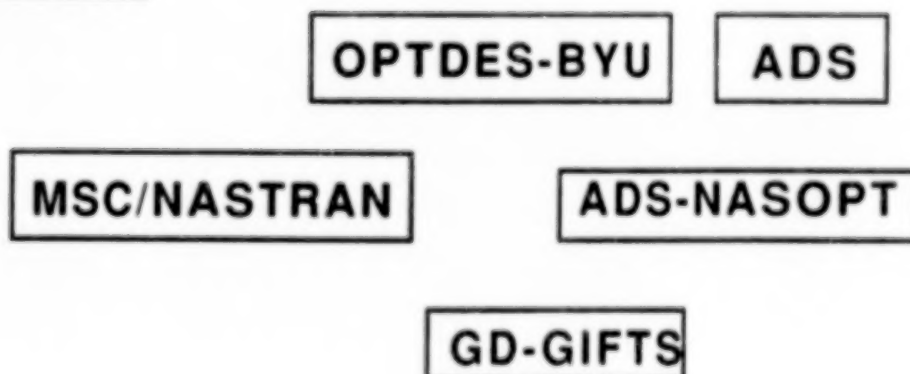
● CANOPY PROBLEM

SOFTWARE GOAL

The goal of our structural optimization software investigation was to develop a production level finite-element-based system for aircraft design and resizing. The tools available from vendors are diverse. Optimization methods range in mathematical programming techniques and optimality criteria with various types of sensitivity analyses, design variable linking options, materials capabilities and disciplines. The use of existing finite-element models was also an important consideration. The OPTDES-BYU (Reference 2) and GD-GIFTS, an in-house finite-element program, were combined into an application specific finite-element optimization package using the combined databases from each program. Difficulty arose in making this program generic enough in terms of sensitivity analysis and structural geometry. The ADS/NASOPT program was selected and used in the following applications with favorable results. Since our in-house pre and post finite-element processors communicate with MSC/NASTRAN (Reference 3), ADS/NASOPT minimizes changes to existing finite-element models. In addition, we had prior knowledge of ADS (reference 4).

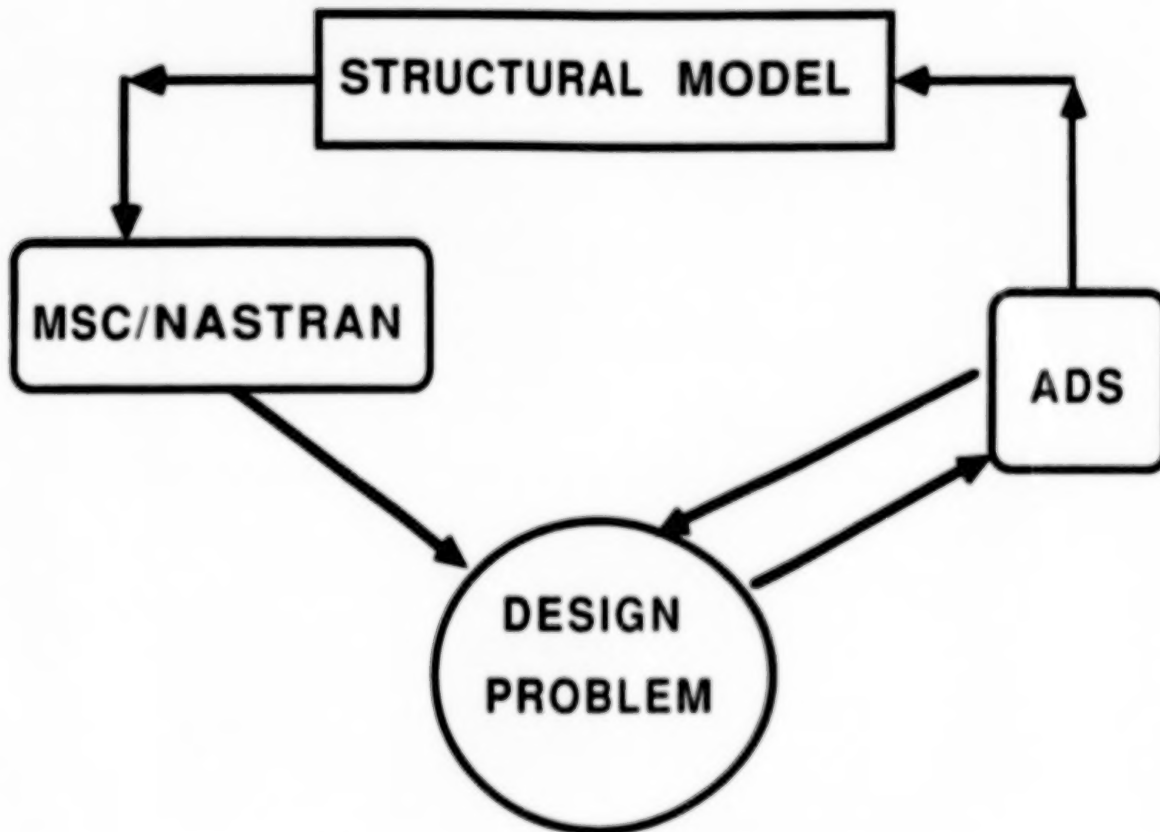
TO DEVELOP A PRODUCTION LEVEL FINITE ELEMENT BASED STRUCTURAL OPTIMIZATION SYSTEM FOR AIRCRAFT DESIGN AND RESIZING

TOOLS



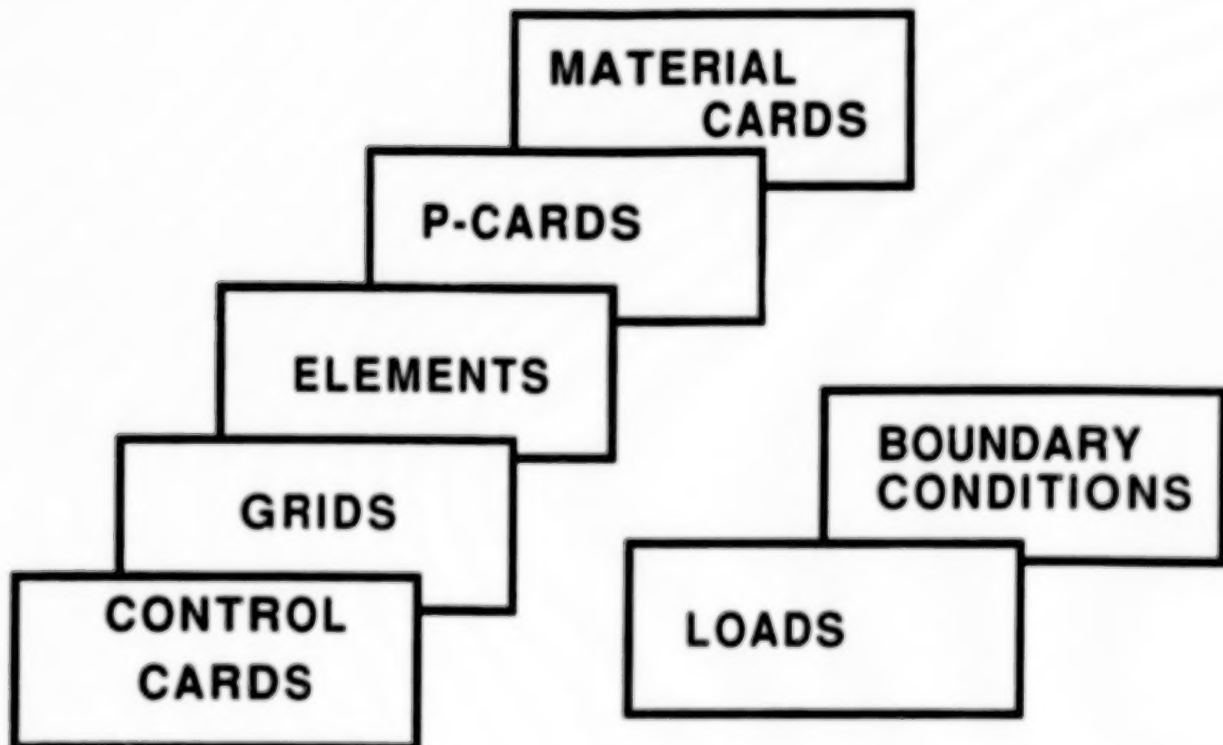
OUTLINE OF ADS/NASOPT

The ADS/NASOPT procedure uses a structural finite-element model as the starting point in an analysis cycle; then it translates this into a design model through NASOPT. The program then optimizes using the ADS optimization program and returns to the structural model to update the data if so chosen by the user. A combination of approximation techniques, sensitivity analysis and optimization algorithms allows the user to minimize his objective function (such as weight) subject to constraints (such as stress allowables, buckling load factors, or displacements).



TYPICAL MODEL REQUIREMENTS

The structural finite-element model includes the MSC/NASTRAN bulk data information such as control cards, grid points, elements, materials, properties, loads, and boundary conditions. ADS/NASOPT is limited in the variety of elements that can be resized as design variables; however, the finite-element model may contain unlimited types of elements available in the MSC/NASTRAN element library.



TYPICAL ADS/NASOPT INPUT

The ADS/NASOPT program requires some additional input in the form of NASTRAN data card images. These data include design variable, and constraint definitions, design variable upper, lower bounds, move limits, and method of optimization. A typical input sequence also requires NASOPT instructions or job control language. ADS/NASOPT is run in phases each performing a specific function in the optimization task. Phase 1 sets up the database by reading the NASTRAN and design data. Phase 2 prepares the NASTRAN sensitivity analysis data after screening the analysis results. Phase 3 reads sensitivity results, prepares the appropriate model and calls ADS to perform the optimization. Phases S and A call MSC/NASTRAN to execute the desired solution sensitivity solution sequences 51,53,55 (for phase S) and analysis solutions 24,61,63,65 (for phase A).

Generation of the extra data cards to convert a MSC/NASTRAN finite-element model to an ADS/NASOPT design model can be tedious for large models. Work station procedures included as a part of the finite-element pre-processors facilitate routine use of programs such as ADS/NASOPT.

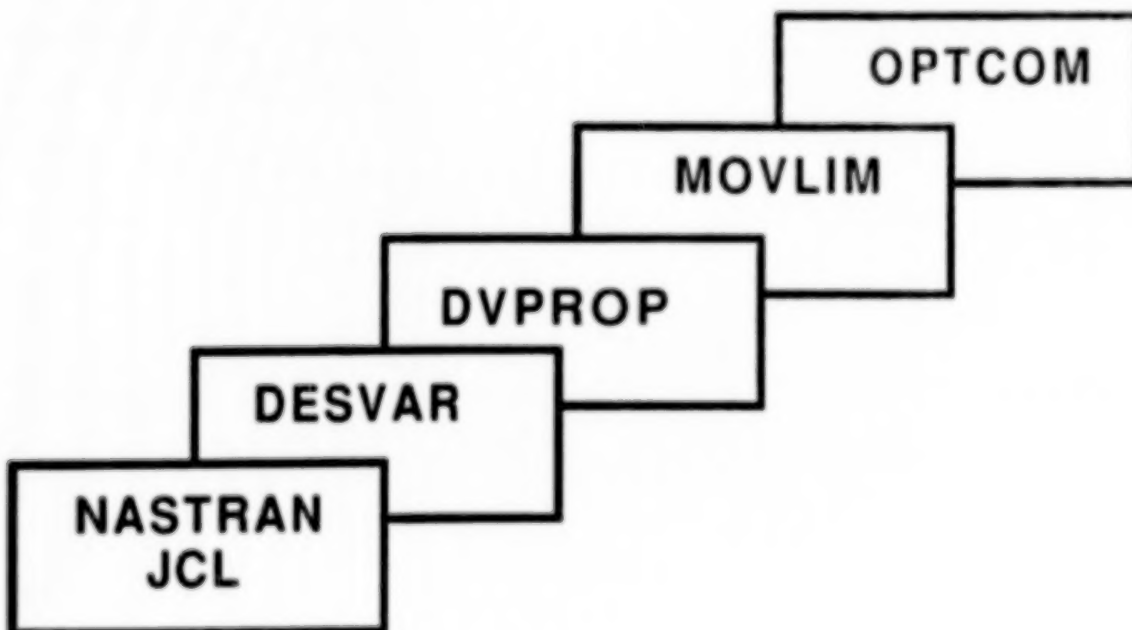


PLATE BUCKLING EXAMPLE - NASTRAN MODEL

The first example represents a typical section from an aircraft structure. This particular section was extracted from a fuselage keel beam and loaded with combined shear/biaxial displacements. The hole typifies routing requirements of plumbing, electrical, and fuel considerations.

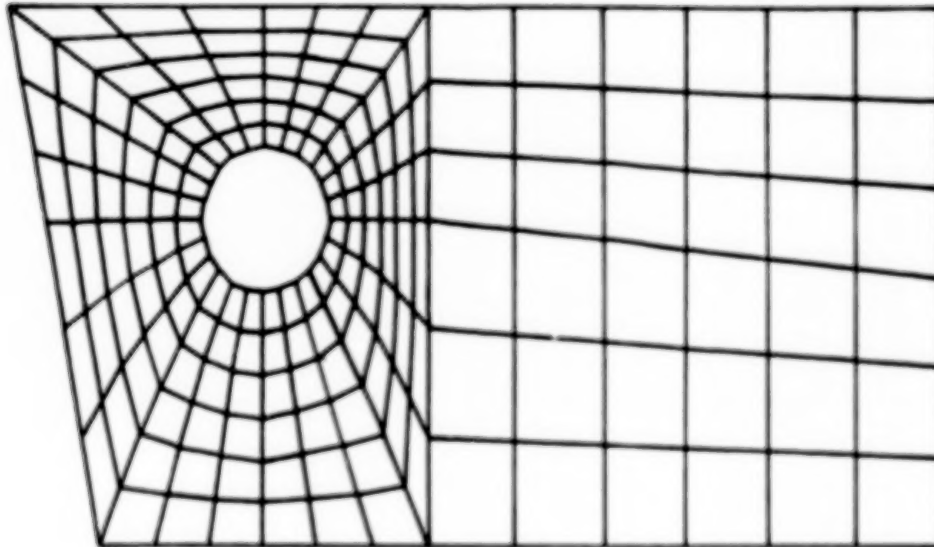


PLATE BUCKLING EXAMPLE - PROBLEM INPUTS

Material properties were selected for a typical aluminum alloy. In the case of this illustration, only two design variables were selected. Physical linking of the finite-element thicknesses was incorporated as shown in the figure. Although two design variables may be a crude definition of the design space, for manufacturing reasons, the design of such structure may often require this definition. And, the problem illustrates interesting results.

MATERIAL PROPERTIES

$E = 10.0 \text{ E}7$ POISSON'S RATIO = 0.3

DENSITY = 0.1 LB/CU INCH

DESIGN CONSTRAINTS

BUCKLING EIGENVALUE $\Rightarrow 1.5$

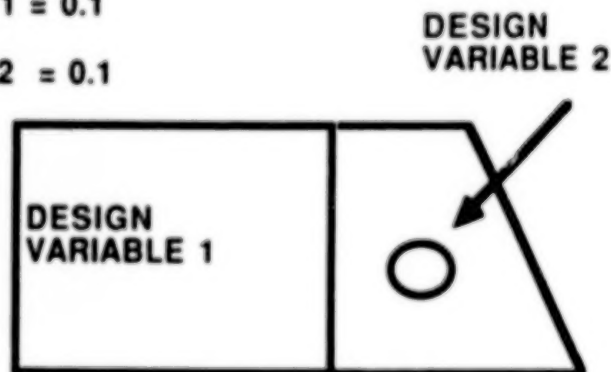
INITIAL DESIGN

THICKNESS VARIABLE 1 = 0.1

THICKNESS VARIABLE 2 = 0.1

OBJECTIVE FUNCTION

MINIMUM WEIGHT



DESIGN HISTORY OF PLATE BUCKLING EXAMPLE

The pertinent results from the ADS/NASOPT run are shown in both tabular form and graphically. The table displays weight, thickness (the two design variables), and the buckling load factor. The procedure was run for eight optimization iterations. The weight and buckling load factor are both displayed with respect to the vertical axis of the graph.

The first observation of note is that after eight iterations, the process failed to satisfy the buckling load factor constraint. The second observation is that the buckling load factor steadily increased along with the design thickness through iteration 3. At iteration 4, the thicknesses began to separate, and the buckling constraint attained its highest point. During the remaining iterations, the thicknesses flip/flop and the buckling constraint actually decreased.

As best as we could determine, the design process seemed to be confused. ADS/NASOPT incorporates linear approximations, and between the few number of design variables, nonlinearity of buckling, and the choice of move limits, satisfactory results were obtainable.

We attribute our lack of success in this example to problem complexity and user inexperience.

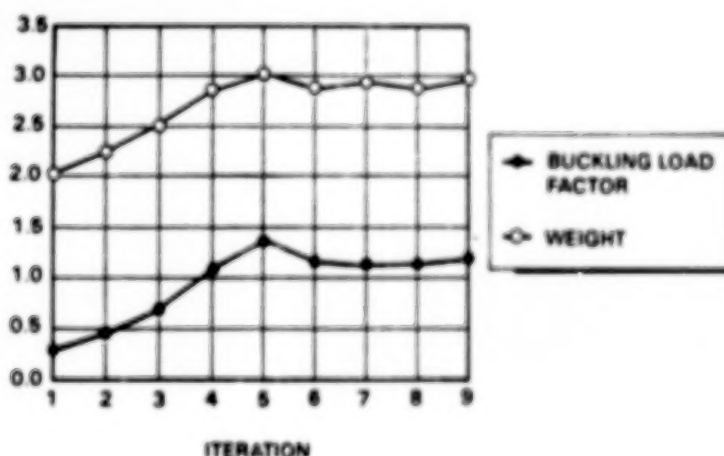


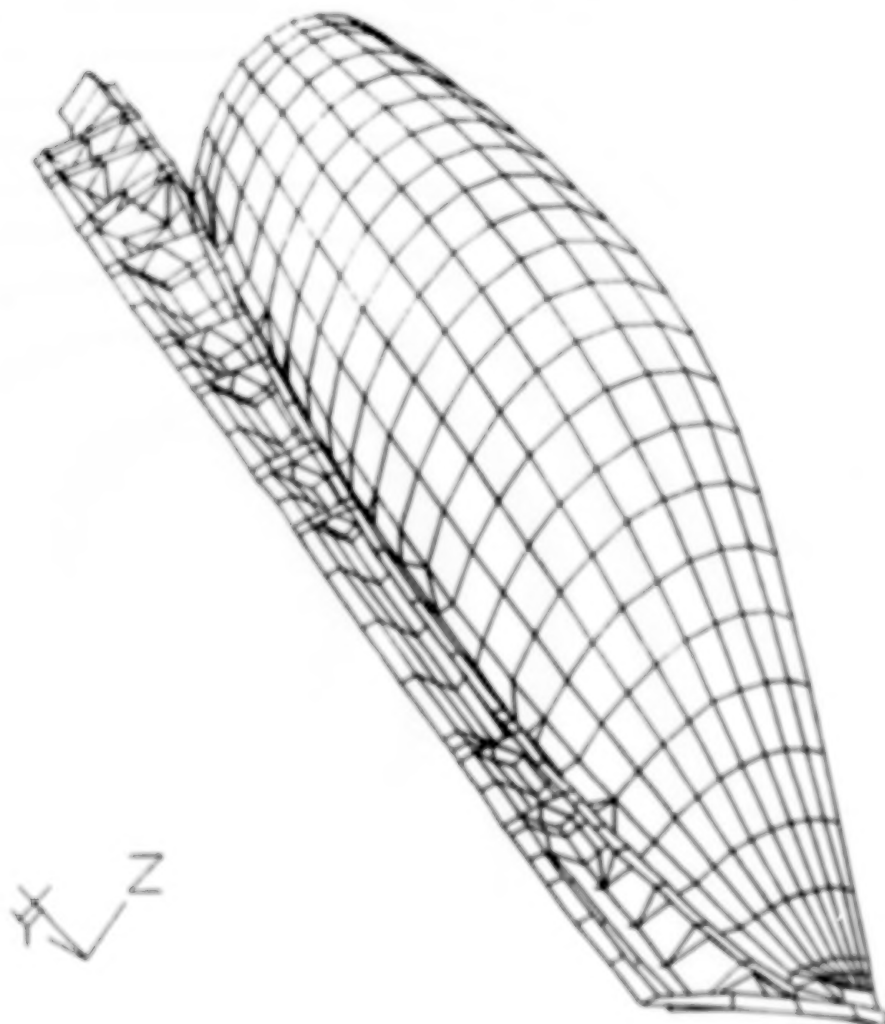
PLATE BUCKLING PROBLEM DESIGN VARIABLE VALUES

	INITIAL	1	2	3	4	5	6	7	8
WEIGHT	0.0000	0.0440	0.1170	0.2470	0.3100	0.3600	0.3900	0.4100	0.4100
THICKNESS UPPER	0.1000	0.1200	0.1400	0.1500	0.1500	0.1500	0.1500	0.1500	0.1500
THICKNESS LOWER	0.1000	0.1200	0.1400	0.1500	0.1500	0.1500	0.1500	0.1500	0.1500
BUCKLING LOAD FACTOR	0.2500	0.4000	0.7000	1.1000	1.4000	1.1000	1.1000	1.1000	1.1000

SINGLE PIECE CAST CANOPY FRAME - NASTRAN MODEL

A canopy bow frame model was optimized to test the functionality of the ADS/NASOPT software. A modern fighter aircraft canopy is primarily constructed of a polycarbonate transparency mounted in an aluminum frame. The frame is typically fabricated from various castings, extrusions, plate and sheet stock. This design is a labor intensive subcomponent to the canopy assembly. To replace the design with a single piece casting would represent a cost savings provided the additional tooling costs could be offset by the reduced labor costs.

The finite-element model of 1140 grid points and 588 bending elements was developed to represent the behavior of the structure. The NASTRAN model was adapted from the production finite-element model of the F-16 canopy frame with changes minimized to guarantee accurate comparisons in results.



C1

DESIGN AND ANALYSIS MODELS - INITIAL SIZING

Eighty-eight design variables representing the canopy frame were selected from the bending elements available with 84 given initial thickness of 0.2 gauge size. The remaining 4 design variables representing the bow hoops, external covers, transparency, and tension ties were given "fixed sizes" to maintain their assembly requirements. These design variables were used mainly to allow stress constraints related to these elements to be applied and influence the design process. It seemed that ADS/NASOPT allows the user to constrain element behavior only if the element is labeled as a design variable. Regardless, this incident highlighted the need to consider neighboring structure in an optimization design setting.

88 VARIABLES REPRESENTING GAUGE THICKNESS FOR VARIOUS PARTS OF THE CANOPY FRAME

SIZE CONSTRAINTS

<u>COMPONENT</u>	<u>SIZE CONSTRAINTS</u>
CANOPY FRAME	$0.080 < t < 0.500$ inch
EXTERNAL COVERS	$0.100 < t < 0.100$ inch
BOW HOOPS	$0.250 < t < 0.250$ inch
TRANSPARENCY	$0.700 < t < 0.700$ inch
TENSION TIE	$0.150 < t < 0.150$ inch ²

DESIGN AND ANALYSIS MODEL - LOADING CASES

Two symmetric loading cases were selected representing ultimate cabin pressure and a balanced ejection condition. The ejection condition was balanced by inertia loads at the latching mechanism location along the length of the frame. Boundary conditions of a plane of symmetry along the aircraft were accounted for with reaction points at the tension tie locations. These loading cases represent typical production loading configurations.

The candidate materials used were A357 alloy for the frame which is a high strength heat treatable Al-Si-Mg alloy that is relatively inexpensive to manufacture. Other materials were kept as the current design exists.

LOADING CONDITIONS

CASE 1 10.2 PSI CABIN PRESSURE

CASE 2 PILOT EJECTION

BOUNDARY CONDITIONS

3 HOOK LATCHES

1 PIVOT

CENTERLINE SYMMETRY

MATERIALS

FRAME, CAST A357

EXTERNAL COVERS, BOW HOOPS, AI 2024

TRANSPARENCY, POLYCARBONATE

PIVOT FITTING TENSION TIE, PH13-8 STAINLESS STEEL

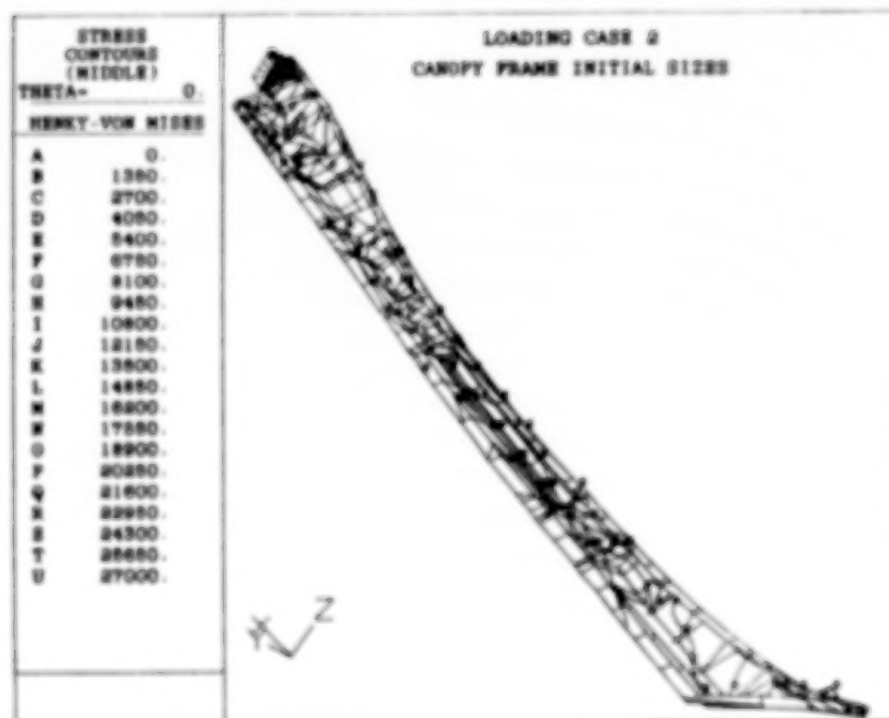
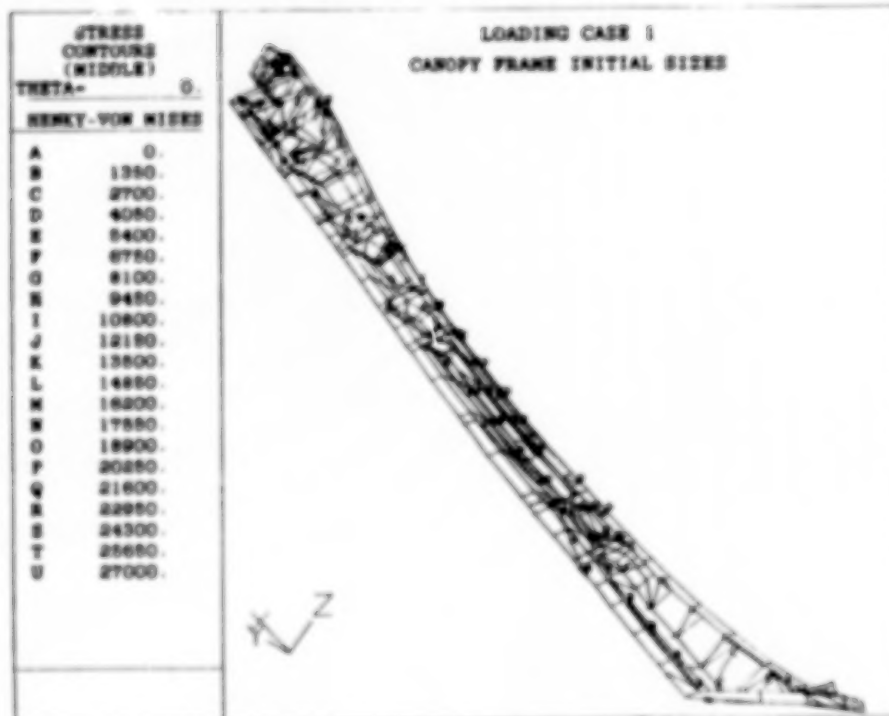
SINGLE PIECE CAST CANOPY FRAME - STRESS CONSTRAINTS

The canopy frame consists of bending elements representing flanges and webs. These elements were sized using a 26250 psi von Mises maximum stress. The bow hoops and external covers are loaded in tension with a required stress level between 40000 psi and 50000 psi for principal stresses. The polycarbonate transparency was held to a maximum 2000 psi von Mises stress. Finally the tension ties are loaded in tension, and the members were sized using 75000 psi as a maximum axial stress.

<u>COMPONENT</u>	<u>STRESS CONSTRAINTS</u>
CANOPY FRAME	VON MISES < 26250 PSI
BOW HOOPS, EXTERNAL COVERS	40000 < PRINCIPAL < 50000 PSI
TRANSPARENCY	VON MISES < 2000 PSI
TENSION TIE	AXIAL < 75000 PSI

SINGLE PIECE CAST CANOPY FRAME - INITIAL SIZING

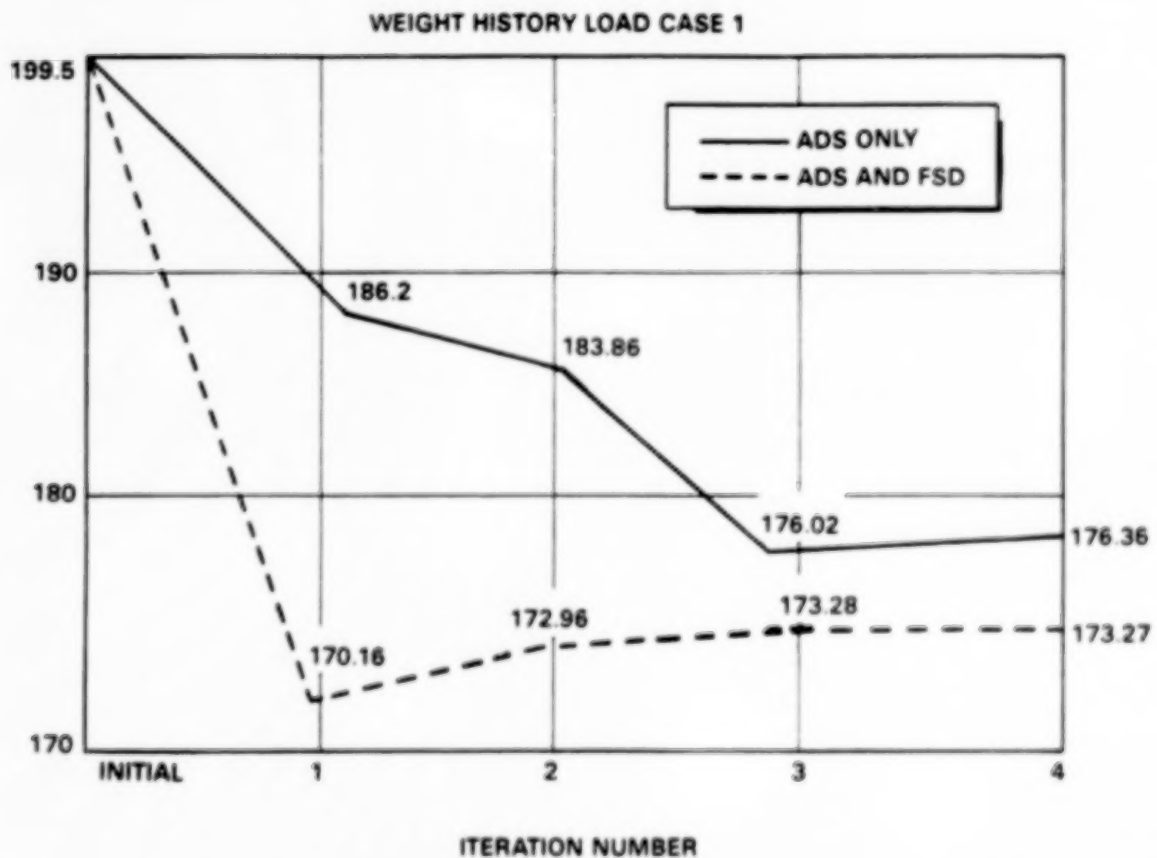
The finite-element results for the initial sizing show large regions of low stress as expected.



SINGLE PIECE CAST CANOPY FRAME - WEIGHT RESULTS

A comparison of two optimization methods was achieved for designs derived from load case 1, the ultimate cabin pressure case. Path 1 used 4 ADS steps using the Modified Method of Feasible Directions algorithm, while path 2 used 1 fully stressed design analysis and 3 ADS cycles. The FSD path also took less CPU time when run on the CRAY.

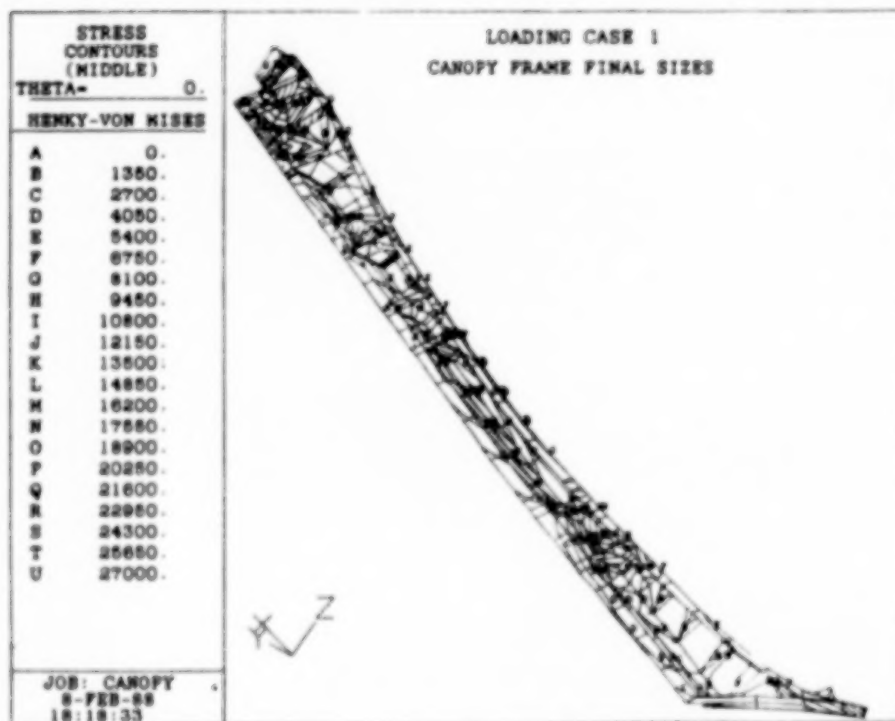
SINGLE-PIECE CANOPY FRAME

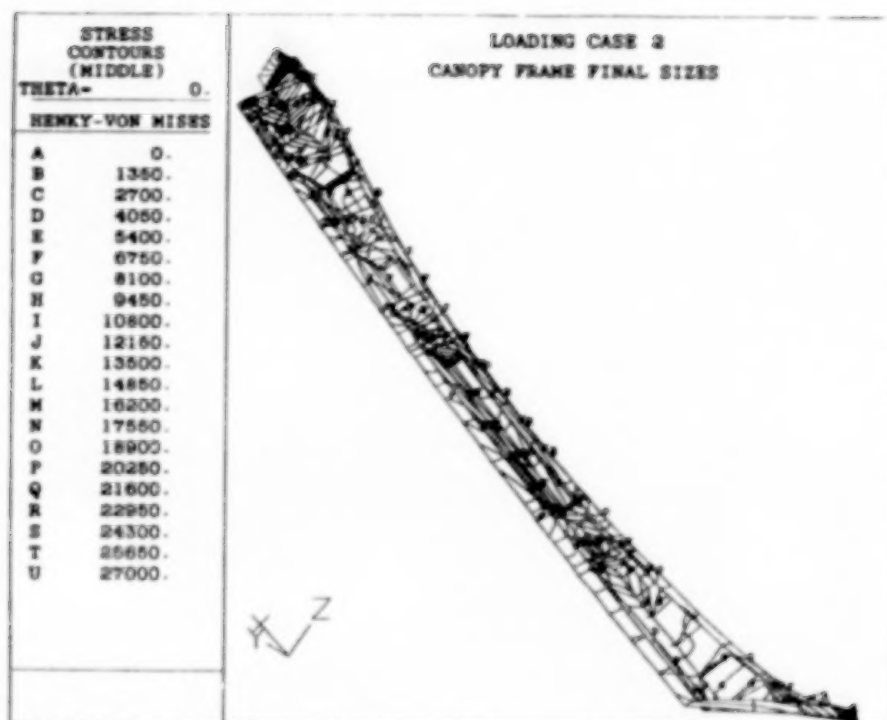


SINGLE PIECE CAST CANOPY FRAME - STRESS RESULTS

The final stress results for load case 1 the ultimate pressure case, show areas of high stress concentration near the tension ties. The optimized structure was sized predominantly to minimum gauge with the exception of the tension tie points and canopy latch hooks.

Although, it seems in hindsight that the problem was trivial as a built-up frame structure, the design was complex. This exercise demonstrated the functionality of ADS/NASOPT as a preliminary design tool because all aspects of the structure were included simultaneously in the structural sizing.





68

SUMMARY

In summary, our studies have provided four significant lessons learned. First it is evident that effective use of optimization techniques in design requires a robust-expert preprocessor as part of a basic finite-element preprocessor. Second, as in the example of the buckling problem, the design problem must be well posed both in a practical design sense and a numerical sense. The third observation to be made relates back to the problem definition. In particular, although neighboring elements to a design model may not be subject to resizing, their behavior may impose constraints on the design model. These constraints may be imposed through the use of larger models or formal decomposition methods. ADS/NASOPT provides functional use of MSC/NASTRAN as a preliminary design optimization tool.

- **LARGE DESIGN MODELS REQUIRE PREPROCESSORS**
- **ADS/NASOPT REQUIRES EXPERIENCED USAGE**
 - ✓ **DESIGN MODELS**
 - ✓ **ALGORITHM**
- **SENSITIVITY OF NEIGHBORHOOD STRUCTURE IS ESSENTIAL**
 - ✓ **DECOMPOSITION**
 - ✓ **LARGE MODELS**
- **ADS/NASOPT PROVIDES FUNCTIONAL USE OF MSC/NASTRAN**

REFERENCES

1. Gibson, W.C., Miura H., ADS/NASOPT User's Manual, version 1.00 Rev A. Palo Alto: CSA Engineering, Inc, Sept 1986.
2. OPTDES-BYU : A Software System for Optimal Engineering Design User's Manual version 3.1, Brigham Young University, Provo Utah, 1986.
3. MacNeal-Schwendler Corporation, MSC/NASTRAN Linear Static Analysis Manual version 65, Los Angeles: MacNeal Schwendler Corp., 1987.
4. Vanderplaats, G. N., ADS - a FORTRAN Program for Automated Design Synthesis, Version 1.10, Santa Barbara: EDO, Inc, 1985.

CRAY IS A REGISTERED TRADEMARK OF CRAY RESEARCH INC.

NASTRAN IS A REGISTERED TRADEMARK OF NASA. MSC/NASTRAN IS AN ENHANCED PROPRIETARY VERSION DEVELOPED AND MAINTAINED BY THE MACNEAL SCHWENDLER CORPORATION.

**The Sizing and Optimization Language (SOL)–
A Computer Language to Improve the
User/Optimizer Interface**

**S. H. Lucas
Vigyan Research, Inc.
Hampton, Virginia**

**S. J. Scotti
NASA Langley Research Center
Hampton, Virginia**

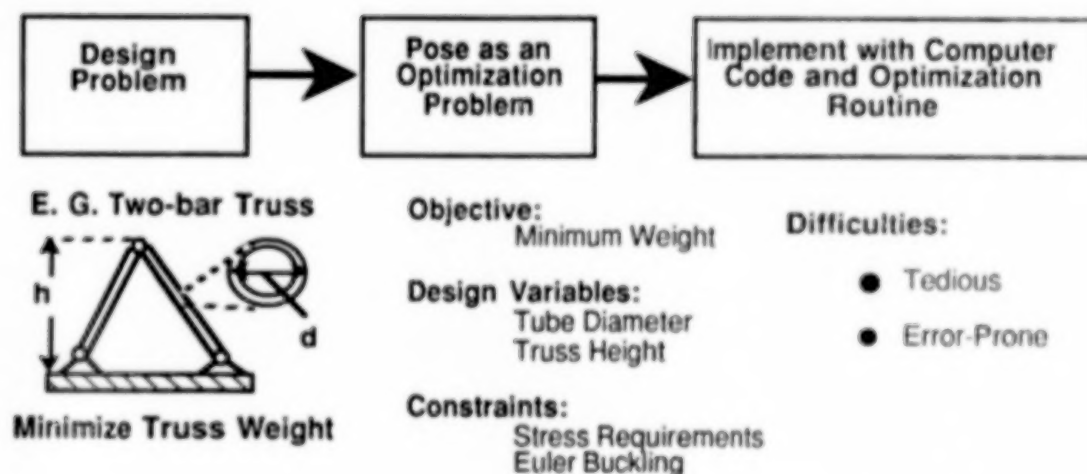
Optimization Techniques Applied to Design Problems

The nonlinear mathematical programming method (formal optimization) has had many applications in engineering design (refs. 1 and 2). This figure illustrates the use of optimization techniques in the design process. The design process begins with the design problem, such as the classic example of the two-bar truss designed for minimum weight as seen in the leftmost part of the figure.

If formal optimization is to be applied, the design problem must be recast in the form of an optimization problem consisting of an objective function, design variables, and constraint function relations. The middle part of the figure shows the two-bar truss design posed as an optimization problem. The total truss weight is the objective function, the tube diameter and truss height are design variables, with stress and Euler buckling considered as constraint function relations.

Lastly, the designer develops or obtains analysis software containing a mathematical model of the object being optimized, and then interfaces the analysis routine with existing optimization software such as CONMIN, ADS, or NPSOL (refs. 3, 4, and 5). This final stage of software development can be both tedious and error-prone.

This paper presents the Sizing and Optimization Language (SOL), a special-purpose computer language whose goal is to make the software implementation phase of optimum design easier and less error-prone.



SOL: A High-Level Computer Language

The use of a high-level computer language, as exemplified by SOL, meets the goals of making the optimum-design process easier and less error-prone, as seen in the figure below.

In terms of analysis, SOL provides statements which can either model a design mathematically or can model a design with subroutines and other code. In addition, a FORTRAN block feature permits the user to incorporate existing FORTRAN routines via subroutine calls and parameter-passing.

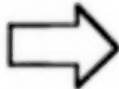
In terms of optimization, SOL provides an OPTIMIZE statement for describing an optimization problem. The OPTIMIZE description is concise and parallels the mathematical description of an optimization problem. Because the OPTIMIZE statement is a built-in language feature, like a DO or IF/THEN/ELSE statement, the language is the interface between optimization and analysis.

In terms of flexibility, SOL is quite general and can be used to code a variety of design problems.

In terms of error-checking, the SOL compiler provides a vehicle for error-checking specific to optimization problems. As the syntax of SOL statements is checked, semantic checks on the use of the statements can also be performed. Additionally, the compiler offers a listing which includes the SOL program indexed by line number; an optimization summary for each optimization which lists the objective, design variables, and constraints; and a cross-reference giving each variable and the lines on which the variable was used.

GOAL: Make Optimization Use **EASIER** and **LESS ERROR-PRONE**

Create or Incorporate
Analysis Software



- **Create** Analysis in SOL
- **Incorporate** existing FORTRAN codes via Subroutine calls

Interface Analysis and
Optimization Software



- Optimization a **built-in** Statement
- Language **Integrates** Optimization & Analysis

Method for a Variety
of Design Problems



- Language is **Flexible**

Error-Checking: Saves
Time and Face



- Compiler (Language Translator) provides **Error-Checking**
- Source Listing, Variable Cross Reference Options

SOL Statements

SOL is a simple but powerful language. A brief overview of the language elements of SOL is offered here, giving a representative list of available SOL statements. Further details can be found in NASA Technical Memorandum 100565 (ref. 6).

SOL offers many traditional language features found in "conventional languages," e.g. FORTRAN or Pascal. SOL provides declaration statements such as variable and subroutine declaration; control statements such as DO loops, IF/THEN/ELSE statements, and subroutine calls; calculation statements (i.e. assignments, math operators and built-in math functions); and output statements such as PRINT.

SOL has unique language features as well, such as an OPTIMIZE statement for describing an optimization problem and an ASSEMBLAGE statement (beyond the scope of this paper) to facilitate the hierarchical modeling of systems. As mentioned earlier, SOL's FORTRAN block allows existing FORTRAN code to appear within a SOL program. To make SOL programs easier to write and more readable, a MACRO feature allows the definition and use of text abbreviations within a SOL program. A single descriptive macro call can replace many lines of SOL code. For example, SOL has a pre-defined ?INCLUDE macro that allows entire text files to be included verbatim as part of a SOL program.

SOL's conventional features are combined with its unique features to solve design problems.

TRADITIONAL LANGUAGE FEATURES:

Declaration	Control	Calculation	Output
Variable Declaration	Conditional DO loops	Assignment	Print
Subroutine Declaration	IF/THEN/ELSE	Math Expressions	
	Iterative DO loops		
	Subroutine Call		

UNIQUE LANGUAGE FEATURES:

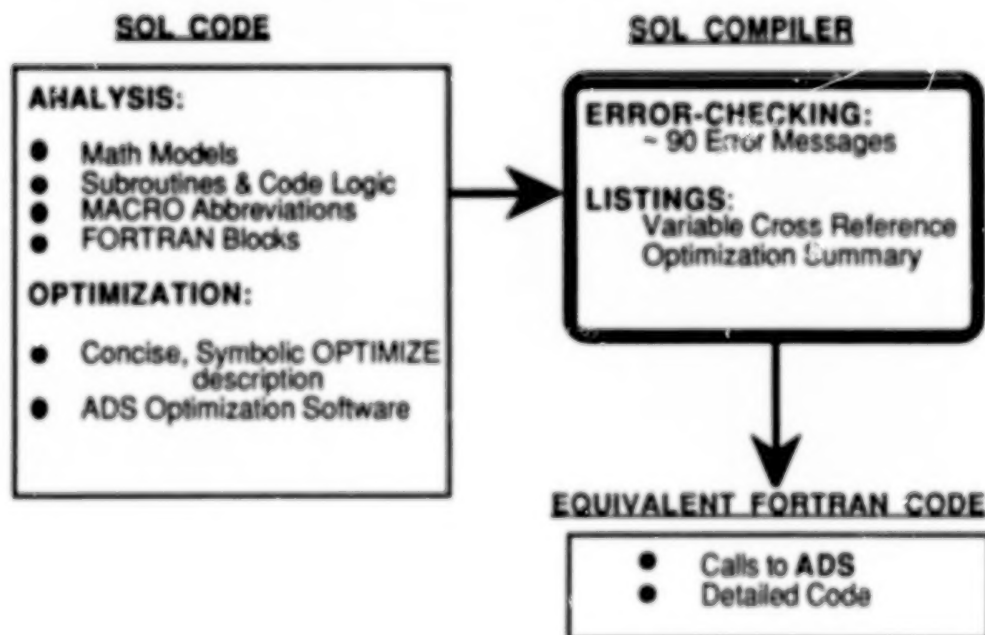
Description	Miscellaneous
OPTIMIZE Statement	FORTRAN block
ASSEMBLAGE Statement	Macro Definition
	Macro Call
	?INCLUDE macro

SOL Capabilities Used to Solve a Design Problem

Using SOL as a tool for engineering design involves writing a sequence of SOL statements that apply numerical optimization methods to a design problem. The process of solving a problem using SOL is shown in the figure below. A program composed of SOL statements is passed as input to the SOL compiler. Within the SOL program, the design can be modeled mathematically or with subroutines and other code. In addition, existing FORTRAN routines can be used via the FORTRAN block feature, and SOL's macro abbreviation feature can be used. SOL's OPTIMIZE statement describes the optimization problem, incorporating the methods of numerical optimization implemented in the ADS optimization routine (ref. 4).

The SOL compiler translates the SOL program into an equivalent FORTRAN program and does error-checking. The compiler offers approximately ninety different error messages, and can produce listings, a variable cross-reference, and an optimization summary which lists the objective, design variables, and constraints. However, SOL does not provide error-checking features for FORTRAN BLOCK code fragments; SOL's error-checking is limited to SOL statements only.

The FORTRAN program produced by the SOL compiler executes to solve the design problem. This resultant FORTRAN program includes subroutine calls to the ADS software and other detailed code.



Math and SOL Description of Two-Bar Truss

SOL's description of an optimization problem parallels the mathematical description of the problem as illustrated in the figure below which shows a minimum-weight, symmetric two-bar truss problem.

The mathematical description appears on the left of the figure. The truss weight is the objective function to be minimized as stated under the heading, "minimize." The design variables and constraint relations appear under the heading, "subject to." The tube diameter (d) and truss height (h) are design variables, with compressive stress and Euler buckling constraints to insure that the truss neither yields nor buckles. A mathematical model of the truss is given under the heading, "where," which includes the additional variables for truss length (L), half-span (B), tube wall thickness (t), load (P), compressive strength of material (σ^{\max}), modulus (E), and material density (ρ). The mathematical model defines the objective and constraint relations as functions of the design variables.

The SOL description on the right parallels the mathematics. The objective function is represented by a single variable (weight). Design variables and constraint function relations appear between the words **USE** and **END USE**. The lower and upper bounds on the design variables appear in brackets following the word, **IN**. In addition, the optimization software requires design variable initial values, which are given with each design variable after the "=" symbol. Compressive stress and Euler buckling constraints follow the design variables.

Finally, equations modeling the truss appear between the words **END USE** and **END OPTIMIZE**. Note that the single SOL variable (buckle), representing the Euler buckling constraint, acts identically to the constraint relation in the mathematical description.

Mathematical Description

Minimize: weight(d, h)

Subject to:

$$1 \leq d \leq 3$$

$$10 \leq h \leq 30$$

$$\sigma_{\text{stress}}(d, h) < \sigma^{\max}$$

$$\sigma_{\text{stress}}(d, h) - \sigma^{\theta}(d, h) < 0$$

Where:

$$\text{weight}(d, h) = 2\rho\pi d t L$$

$$\sigma_{\text{stress}}(d, h) = (P L) / (\pi t h d)$$

$$\sigma^{\theta}(d, h) = \pi^2 E (d^2 + t^2) / (8 L^2)$$

SOL Description

OPTIMIZE weight

USE

$$d = 1 \text{ IN } [1, 3]$$

$$h = 15 \text{ IN } [10, 30]$$

$$\text{stress} \text{ .lt. } \text{MaxStress}$$

$$\text{buckle} \text{ .lt. } 0$$

END USE

$$\text{weight} = 2 * \rho * \pi * d * t * L$$

$$\text{stress} = (P * L) / (\pi * t * h * d)$$

$$\text{Euler} = (\pi^2 * E * (d^2 + t^2)) / (8 * L^2)$$

$$\text{buckle} = \text{stress} - \text{Euler}$$

END OPTIMIZE

SOL Error-Checking Example

A SOL program is passed as input to the SOL compiler which translates the SOL code into an equivalent FORTRAN code, and provides the key feature of error checking for a variety of errors. The figure below illustrates the error-checking capability of the compiler.

An intentionally erroneous SOL program for the two-bar truss problem appears on the left of the figure. The program has been annotated with line numbers to aid the discussion. The inset box on the right lists the actual error messages given by the SOL compiler on receipt of this program. The first error occurs on line 11 where the word IN has been misspelled; the compiler can usually correct the spelling of reserved words when the word is misspelled by a single character. The next error is optimization specific, warning that the constraint variable stated on line 14 has not been assigned a value. The error message leads to the discovery that a typographical error on line 20 is the true culprit. Finally, an error appears for line 17 because the variable for material density, rho, was not initialized.

Either of the last two errors would have caused incorrect optimization results if left undetected. The last two errors are difficult to detect manually; a laborious examination of the optimization results could reveal that the results were incorrect, but would not provide the cause for the poor results.

It is important to note that the compiler is not clairvoyant; it cannot check the correctness of problem formulation nor infer one's intentions. However the example here, although not exhaustive, illustrates the general sorts of errors detected by the compiler.

Erroneous Program	Error Messages
<pre> 1 : PROGRAM TwoBar 2 : t = 0.1 3 : P = 3300 4 : B = 30 5 : E = 30000000 6 : pi = 3.141592554 7 : MaxStress = 10000 8 : 9 : OPTIMIZE weight 10 : USE 11 : d = 1 INN [1, 3] 12 : h = 15 IN [10, 30] 13 : stress .lt. MaxStress 14 : buckle .lt. 0 15 : END USE 16 : L = SQRT(B**2 + h**2) 17 : weight = rho*2*pi*d*t*L 18 : stress = (P*L)/(pi*t*h*d) 19 : E_stress = ((rho**2)*E*(o**2+t**2))/(8*L**2) 20 : buckl = stress - E_stress 21 : END OPTIMIZE 22 : END TwoBar </pre>	<pre> 11 : d = 1 INN [1, 3] *** ERROR * MISPELLED 'IN' CORRECTED 14 : buckle .lt. 0 ***ERROR *OPTIMIZATION VARIABLE HAS NOT BEEN SET 17 : weight = rho*2*pi*d*t*L ***ERROR *UNINITIALIZED IDENTIFIER </pre>

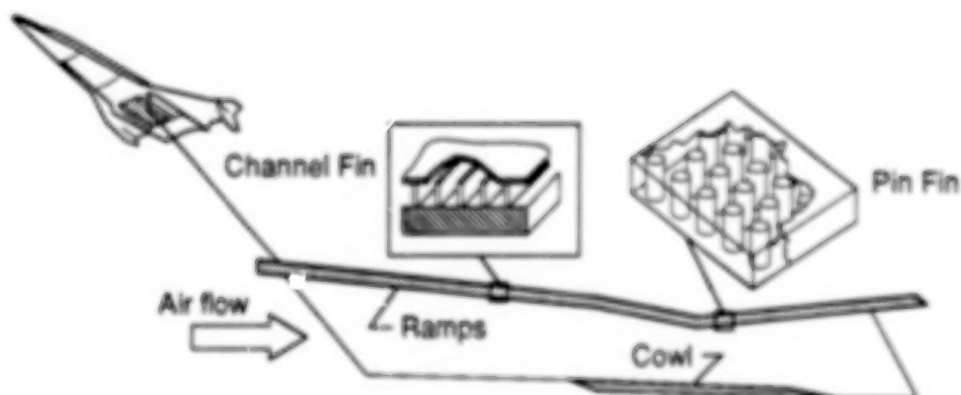
Scramjet Engine Cooling Jacket Application

The design of scramjet engine cooling jackets, in which numerical optimization is used as a design tool, illustrates SOL's use for an engineering application.

A scramjet engine resides on the lower surface of a hypersonic vehicle, as in the schematic below. A conceptual, two dimensional engine cross-section appears in the middle of the figure, showing the ramp and cowl portions of the engine. The heating of the engine surfaces wetted by the airstream is so extreme that an active cooling system is required to maintain a survivable temperature. Only the ramp and cowl portions of the engine are considered here, although other parts of the engine also require active cooling. A promising active cooling system for this application is a system of hydrogen-fuel-cooled, metallic, surface heat exchangers (cooling jackets) attached directly to the engine primary structure.

Both channel-fin and pin-fin cooling jackets were studied, but the example in this paper focuses on a channel-fin design. The design goal is to design cooling jackets which minimize the required coolant flow rate for specified heating rates. The design must also satisfy requirements such as material limits on cooling jacket temperature, fatigue life and stress.

The cooling jacket design problem was recast in the form of an optimization problem and implemented in SOL using SOL's OPTIMIZE statement. Existing FORTRAN routines were incorporated for the analysis of a single cooling jacket panel via SOL's FORTRAN block feature. Other SOL features were used to control the analysis and perform ancillary calculations.



Application Implemented with SOL

- Optimization problem posed in SOL.
- Single panel analysis with existing FORTRAN codes.
- SOL features used to control analysis routines.

Cooling Jacket Design Problem

The figure below illustrates the scramjet engine cooling jacket design problem in some detail. As seen in the top half of the figure, a coolant flows through cooling jacket panels to remove the incident heat flux (q). Only two panels of equal dimensions are shown in the figure, although many panels of varying sizes can be used. For more details of panel configurations see reference 7.

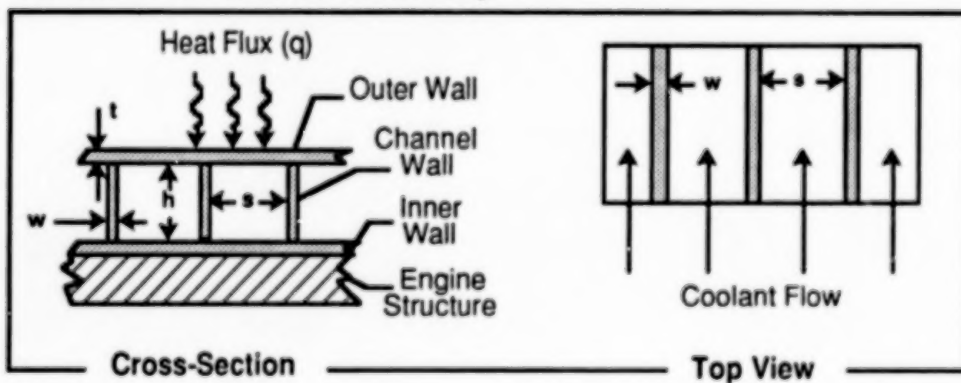
The lower half of the figure illustrates the geometry of a channel-fin cooling jacket. As seen on the left-hand side, a channel-fin geometry can be completely described by the channel width (s), the channel height (h), the channel wall thickness (w), and the outer wall thickness (t). The right-hand side of the figure shows a top view of a channel-fin cooling jacket, illustrating the coolant flow through the jacket channels.

When the design is recast in the form of an optimization problem, several design variables describe the coolant flow conditions and the remainder of the design variables describe the cooling jacket geometry.

Coolant Flow:



Channel Fin Jacket Geometry:



SOL's Use for Cooling Jacket Optimization

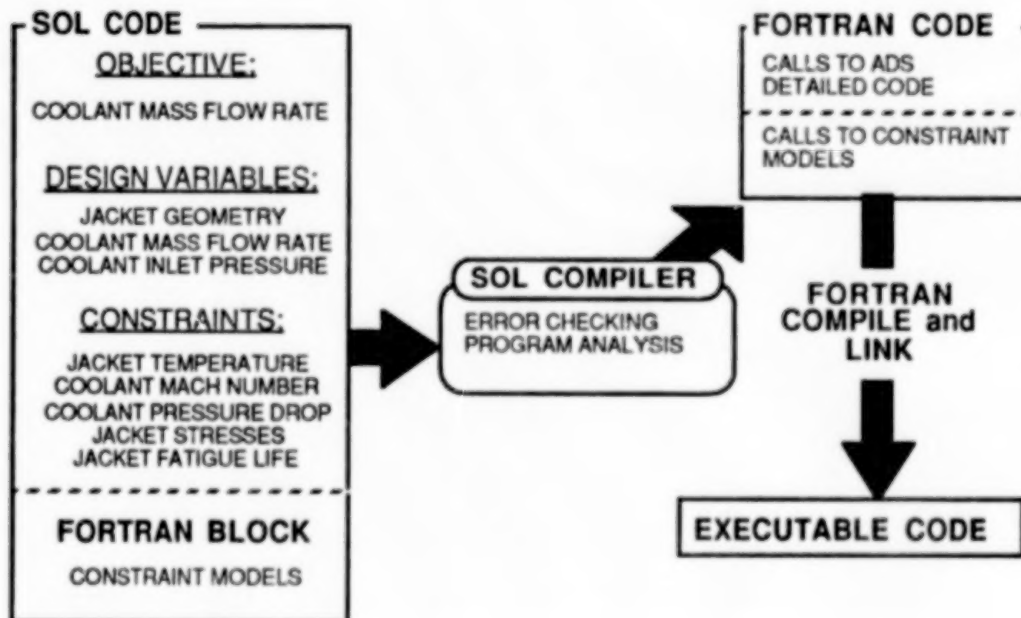
SOL's use in the cooling jacket optimization is shown in the schematic below. SOL code describes the optimization problem as in the left-hand part of the figure. The objective function to be minimized is the coolant mass flow rate. Weight is a more common objective function. But in this application minimizing the coolant mass flow rate can decrease the coolant needed, effectively reducing the total vehicle weight. The design variables consist of variables describing the coolant mass flow rate, the coolant inlet pressure, and several variables to describe cooling jacket geometry.

In addition, constraints on the coolant and jacket conditions are required. As stated earlier, existing FORTRAN routines calculate the constraint function relations. The constraint routines are called from the SOL program by subroutine calls. Design variable values are passed as parameters to the constraint routines, which return constraint function values, also via parameter-passing.

The SOL program for the cooling jacket application is passed as input to the SOL compiler, which produces an equivalent FORTRAN program as output. The compiler also performs program analysis and error-checking on the SOL code.

The output FORTRAN code contains calls to the ADS optimization software which provide's SOL's optimization capability, as well as calls to the constraint modeling routines. The output code also contains detailed code such as variable declarations and so forth.

The FORTRAN code output by the SOL compiler is compiled and linked using the FORTRAN compiler and linker. The resulting executable code is run to perform the cooling jacket optimization.



Cooling Jacket Optimization Description in SOL: An Overview

The figure below gives the SOL program for the cooling jacket optimization problem in outline form with all reserved words shown in boldface type. The program begins with the word **PROGRAM** followed by the name of the program. Before the optimization problem description begins, variables and subroutines are declared, and macro definitions appear. In the figure, the actual code has been replaced with comments, marked by exclamation point symbols, to simplify the discussion. Subsequent figures will discuss each of the comment sections in turn.

The optimization problem description is initiated by the word **OPTIMIZE** and terminated by the words **END OPTIMIZE**. A single variable given after the word **OPTIMIZE** states the objective function. Next, design variable, constraint relation and optimization software option declarations appear between the words **USE** and **END USE**. In the figure below, the three declarations have been replaced with comments. The SOL code for the cooling jacket analysis appears between the words **END USE** and **END OPTIMIZE**, as indicated by a SOL comment in the figure.

The main body of the SOL program terminates with the word, **END**, followed by the name of the program. In SOL, subroutines follow the end of the main program body. In the cooling jacket application, SOL's **?INCLUDE** macro is used to include the contents of the file "cool_jacket.sub," which contains the subroutines for cooling jacket analysis.

```
PROGRAM Cool_Jacket
  ! Variable and Subroutine Declarations
  ! Macro Definitions

OPTIMIZE total_panel_flowrate
USE
  ! Design Variable Declarations
  ! Constraint Function Relation Declarations
  ! Optimization Software Options
END USE
  ! Cooling Jacket Analysis
END OPTIMIZE

END Cool_Jacket

?INCLUDE Cool_Jacket.sub
```


Objective and Design Variable Description in SOL

The figure below details the SOL code for the design variable declaration section of the cooling jacket optimization as outlined previously. The objective function to be minimized, the coolant mass flow rate, follows the word **OPTIMIZE** and is represented by a single variable, "total_panel_flowrate."

Design variable declarations follow the word **USE**. For this application, six design variables are used. Two variables, "panel_flowrate" and "inlet_pressure," describe coolant conditions. Also, four design variables are needed to describe the geometry of each cooling jacket panel. The design variables for a single panel are shown in the figure; each of the panel geometry variables are suffixed with the panel name, "_panel_1." If a second panel were also considered, four additional design variables for the second panel's geometry would be required. Since design variables must have unique names, these variables could have the suffix "_panel_2." This naming convention provides a consistent way to handle multiple-panel optimizations.

The lower and upper bounds on the design variables appear to the right of each design variable enclosed by brackets; the actual numbers are unimportant for this discussion. In addition, initial values for design variables required by the optimization software appear with each design variable following the equals symbol.

```
OPTIMIZE total_panel_flowrate
USE
panel_flowrate      = 3.0      IN [1.000, 4.000]
inlet_pressure      = 1000.0   IN [1000., 1500.]
aspect_ratio_panel_1 = 0.5641  IN [0.400, 0.800]
spacing_panel_1     = 0.02     IN [0.020, 0.025]
outer_wall_panel_1  = 0.016    IN [0.010, 0.018]
channel_wall_panel_1 = 0.09     IN [0.060, 0.120]
! *** Constraint Relation Declarations ***
! *** Optimization Software Options ***
END USE
! *** Cooling Jacket Analysis ***
END OPTIMIZE
```

Constraint Function Relation Descriptions in SOL

The figure below details the SOL code for the constraint function relation declaration section of the cooling jacket optimization as outlined previously.

Six constraints are used for a single cooling jacket panel optimization. A single constraint on coolant pressure drop is represented by the variable, "pressure_drop." In SOL, the relation "less than" is represented by .lt. and the relation "greater than" is represented by .gt. In this case, the "pressure_drop" must be less than 100 psi. Five additional constraints are required for each panel, representing cooling jacket low cycle fatigue life, coolant Mach number at the panel exit, cooling jacket temperature, and cooling jacket stresses. As with the design variables, the cooling jacket panel constraints are suffixed with the panel name. In the figure, the name "_panel_1" is used as a suffix.

```
OPTIMIZE total_panel_flowrate
USE
! *** Design Variable Declarations ***
pressure_drop .lt. 100
fatigue_life_panel_1 .gt. 600
gas_mach_out_panel_1 .lt. max_coolant_mach
outer_temp_panel_1 .lt. 2000
wall_stress_panel_1 .lt. 1
web_stress_panel_1 .lt. 1
! *** Optimization Software Options ***
END USE
! *** Cooling Jacket Analysis ***
END OPTIMIZE
```

Optimizer Option Description in SOL

The figure below details the SOL code for the optimization software option declaration section of the cooling jacket optimization as outlined previously. The ADS optimization software used by SOL offers a variety of optimization algorithms and access to numerous internal parameters such as convergence criteria or maximum number of iterations. The software option declaration section provides access to these parameters from a SOL program.

The software option declaration section appears after the design variable and constraint function relation declarations. The software options section begins with the word **OPTIONS** and ends with the words **END USE**. In the figure below, a sequential quadratic programming strategy is selected along with a golden section method of one-dimensional search. The modified method of feasible directions for constrained minimization is used as the optimizer. SOL automatically supplies default option values for the new user, but the **OPTIONS** section permits a knowledgeable user to take full advantage of the options offered by the ADS software. Also, the **OPTIONS** section separates the description of the optimization problem, the objective; design variables; and constraints, from the details of the particular optimization software used to solve the problem.

The word **normalize** indicates that design variables are to be normalized between the values 0 and 1.0. Scaling variables often make an optimization problem better conditioned and hence easier to solve.

```
OPTIMIZE total_panel_flowrate
USE
  ! *** Design Variable Declarations ***
  ! *** Constraint function relation Declarations ***
OPTIONS
  strategy = sequential quadratic
  optimizer = modified feasible directions
  search    = golden section
  normalize
END USE
  ! *** Cooling Jacket Analysis ***
END OPTIMIZE
```

Cooling Jacket Analysis in SOL

The figure below details the SOL code for the cooling jacket analysis, as outlined previously. The analysis computes the values of the objective and constraints as functions of the design variables.

The analysis code appears between the words **END USE** and the words **END OPTIMIZE**. In the figure, the first two assignment statements define variables for the initial coolant pressure and coolant temperature. The next statement gives the location of the first cooling jacket panel.

A SOL macro, **?Channel_Panel**, analyzes a single cooling jacket panel as shown in the figure. The macro abbreviation hides the details of the analysis. The macro itself is shown in boldfaced type, whereas the macro parameters supplied by the user are shown in plain type. The first parameter, "panel_1" is the name of the panel being analyzed. The two parameters that follow "x=" define the length of the panel, and the two parameters for "q=" define the heat flux incident at the start of the panel and at the panel exit. The user simply calls the **?Channel_Panel** macro with the desired parameters to analyze a single cooling jacket panel. The macro defines the necessary variables and calls the external FORTRAN routines to perform the analysis. The user can conduct multiple panel analysis by calling the macro once for each panel analyzed. Although the actual code for the analysis is quite complex, the macro simplifies the complexity into a macro call with five parameters. This discussion focuses on the use of the **?Channel_Panel** macro, some details of how the macro was defined are presented subsequently.

Two assignment statements follow the macro call. The first assigns the objective function a value; the variable "panel_flowrate" is a design variable. The second assignment gives a value to the pressure drop constraint. Other constraint variables are defined by the macro call. The analysis and optimization ends with the words **END OPTIMIZE**.

```
OPTIMIZE total_panel_flowrate
USE
! *** Design Variables, Constraints and Options
END USE
gas_p_in = inlet_pressure ! a design variable
gas_t_in = 1000
Panelstart = 0
?Channel_Panel panel_1 begin x= 0 q= heatrate
                        end x= 75 q= heatrate
total_panel_flowrate = panel_flowrate
pressure_drop = inlet_pressure - gas_p_out
END OPTIMIZE
```

Cooling Jacket Analysis: ?Channel_Panel Macro Use

The figure below shows the creation of the ?Channel_Panel macro used to conduct cooling jacket analysis.

The box in the upper part of the figure shows how the Channel_Panel macro is defined. The definition begins with the word, ?DEF, followed by the name of the macro. The numbered items in plain text (#1, #2, ..., #5) are parameters to the macro. Also, SOL allows text (boldface in the figure) to be used to separate the macro parameters. Often the macro creator will use this delimiting text as a reminder for the parameters' use. For example the text, **begin**, was chosen to indicate that the second and third parameters are the location (**x=**) and heat flux (**q=**) at the panel START, whereas **end** is used to indicate that the fourth and fifth parameters are for the panel EXIT.

Macros are text abbreviations; the text that the macro abbreviates appears between the open and close curly braces in the definition. The ?Channel_Panel text initializes all the variables associated with a cooling jacket panel analysis. Only one initialization is shown in the figure with the remainder represented with ellipses. The text also calls an external FORTRAN routine which analyzes a panel, also only shown as a comment in the figure.

When the macro is called, the macro's text is executed with the user supplied parameters inserted. For example, the lower part of the figure shows a call to ?Channel_Panel. The effect is exactly as if the very bottom text box were typed instead of the call; the macro merely abbreviates text. Notice that the parameter, "panel_1," is inserted in the macro text in the place of "#1" when the macro is called.

A macro was used because the variable initializations and call to the external FORTRAN routine, which has 23 parameters, must be repeated for every panel analyzed; tedious typing if multiple panels are analyzed. The macro hides this complexity, replacing the tedious typing with one simple macro call per panel.

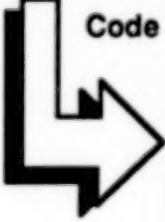
Macro Definition:

```
?DEF ?channel_Panel #1 begin x= #2 q= #3  
                        end x= #4 q= #5  
{  
  webheight = aspect_ratio_#1 * spacing_#1  
  .  
  .  
  .  
  ! Call external subroutine with FORTRAN block  
}
```

Macro Call:

```
?Channel_Panel panel_1 begin x= 0 q= 75 end x= 2000 q= 2500
```

Code SUBSTITUTED for Macro Call:



```
webheight = aspect_ratio_panel_1 * spacing_panel_1  
.  
.  
.  
! Call external subroutine with FORTRAN block
```

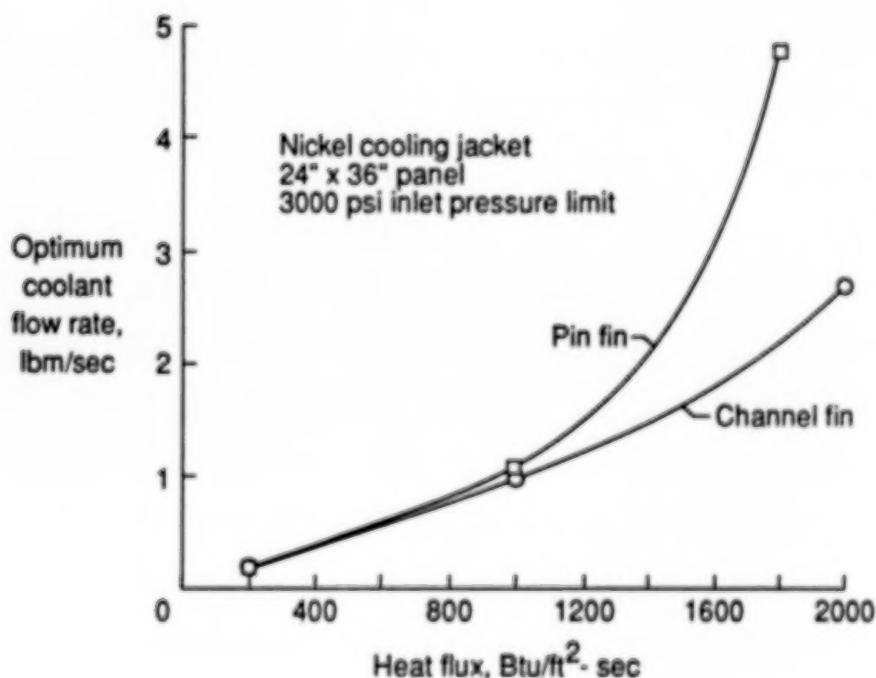
Some Results from Cooling Jacket Study: Channel Fin Versus Pin-fin Comparison

The cooling jacket study produced many results, some of which are illustrated in the figure below. The graph charts optimum coolant flow for channel-fin and pin-fin jackets as a function of heat flux. Results for a Nickel cooling jacket panel, 36 inches wide and 24 inches long with an inlet pressure limit of 3000 psi., are shown in the figure. The graph shows several significant results.

First, a simple energy-balance for determining coolant requirements predicts a linear relationship between coolant flow rate and heat flux. The results are clearly non-linear in the figure.

Second, at the lower heat-flux levels, there is little difference in the value of the optimum coolant flow rate for channel-fins and pin fins. But at high heat fluxes, the channel-fins have lower coolant flow requirements than the pin fins.

Finally, each point on the graph for channel-fins or pin-fins represents an optimum coolant flow rate. In this way, the graph can be interpreted as illustrating the optimum sensitivity of the coolant flow requirements to heat-flux for the given cooling jacket design. Note that smooth curves are faired through the calculated points of this figure, but the actual curves undoubtedly contain slope discontinuities whenever the set of active design constraints changes.



SUMMARY

A special-purpose programming language, SOL, has been developed to expedite implementation of optimization problems and to make the process less error-prone. A more detailed discussion of SOL can be found in reference 6. Currently SOL is only available for DEC VAX/VMS systems.

As a language, SOL provides a high-level interface to the ADS optimization software. SOL integrates optimization and analysis within a single OPTIMIZE description, which parallels the mathematical description of an optimization problem. In terms of analysis, SOL provides language statements which can be used to model a design mathematically, with subroutines and other code, or to model a design with existing FORTRAN routines and parameter-passing. SOL also provides error checking geared to optimization problems to make problem implementation less error-prone. Because optimization is a built-in language statement, the language is the interface.

SOL's use is illustrated in the design of scramjet engine cooling jackets. In this example, the cooling jacket optimization problem was posed in SOL. Existing FORTRAN routines for panel analysis were incorporated into the SOL program using SOL's FORTRAN block feature. Other SOL features were used to control the analysis routines, and provide a simple method of conducting multiple panel analysis. Reference 7 provides details of the scramjet engine cooling jacket application.

SOL, a computer language for optimization, developed.

- NASA TM 100565 details SOL
- Available for DEC VAX/VMS Systems

High-level Interface to Optimizer Software

- Simplifies Optimization Software use
- Reduces Errors with Error-Checking
- Language Integrates Optimization and Analysis

Cooling Jacket application illustrates SOL's use.

- Existing FORTRAN codes used for analysis
- NASA TM 100581 details Cooling Jacket application

References

- ¹Schmit, L.A.: Structural Synthesis -- Its Genesis and Development. *AiAA J.*, vol. 19, no. 10, Oct. 1981, pp. 1249 - 1263.
- ²Ashley, H.: On Making Things Best -- Aeronautical Uses of Optimization. *J. Aircr.*, vol. 19, no. 1, Jan. 1982d, pp. 5 - 28.
- ³Vanderplaats, G.N.: *CONMIN -- A FORTRAN Program for Constrained Function Minimization -- User's Manual*. NASA TM X-62282, 1973.
- ⁴Vanderplaats, G.N.: *ADS -- A FORTRAN Program for Automated Design Synthesis -- Version 1.10*. NASA Contractor Report 177985, Grant NAG1-567, 1985.
- ⁵Gill, P.E.; Murray, W.; Saunders, M.; and Wright, M.: User's Guide for NPSOL (Version 4.0): a FORTRAN Package for Nonlinear Programming. Systems Optimization Laboratory, Stanford University. January 1986. Available from the Stanford Office of Technology Licensing, 350 Cambridge Avenue, Suite 250, Palo Alto, California 94306, USA.
- ⁶Lucas, S.H. and Scotti, S.J.: *The Sizing and Optimization Language, SOL, -- A Computer Language for Design Problems*. NASA TM 100565, 1988.
- ⁷Scotti, S.J.; Martin, C.J.; and Lucas, S.H.: *Active Cooling Design for Scramjet Engines Using Optimization Methods*. NASA TM 100581, 1988.

ROBUST COMPUTER-AIDED SYNTHESIS AND OPTIMIZATION
OF LINEAR MULTIVARIABLE CONTROL SYSTEMS WITH
VARYING PLANT DYNAMICS VIA AUTOCON

C.P. LEFKOWITZ, J.A. TEKAWY, P.K. PUJARA
NORTHROP CORPORATION, AIRCRAFT DIVISION
HAWTHORNE, CALIFORNIA

and

M.G. SAFONOV
UNIVERSITY OF SOUTHERN CALIFORNIA
LOS ANGELES, CALIFORNIA

INTRODUCTION

AUTOCON is an automated computer-aided design tool for the synthesis and optimization of linear multivariable control systems based upon user-defined control parameter optimization. Violations in stability and performance requirements are computed from constraints on Single Input/Single Output (SISO) open- and closed-loop transfer function frequency responses, and from constraints on the singular-value frequency responses of Multiple Input/Multiple Output (MIMO) transfer functions, for all critical plant variations. Optimum nonlinear programming algorithms are used in the search for local constrained solutions in which violations in stability and performance are caused either to vanish or be minimized for a proper selection of the control parameters. Classical control system stability and performance design can, in this way, be combined with modern multivariable robustness methods to offer general frequency response loop-shaping via a computer-aided design tool. Complete Nichols, Nyquist, Bode, singular-value Bode magnitude and transient response plots are produced, including user-defined boundary responses. AUTOCON is used to synthesize and optimize the lateral/directional flight control system for a typical high-performance aircraft. (See figure 1.)

- Automated Computer-Aided Workbench Design Tool For Synthesis And Optimization Of Linear Multivariable Control Systems
 - Parameter Optimization Determines Local Constrained Optimal Solutions In Which Violations In User-Specified Stability/Performance Requirements Either Vanish Or Are Minimized
 - Frequency-Domain Loop Shaping Via Nonlinear Mathematical Programming
 - Synthesis/Optimization Considers Each Stability Loop And Constrained Transfer Function For All Plant Variations Simultaneously.
 - User-Defined Control System Architecture, Parameters, Stability Loops, Constrained Transfer Functions
 - Fixed and Varying Plant Dynamics
 - Classical Specs : Stability Margins, Bandwidth, Damping, Overshoot, etc.
 - Sensitivity Analysis

Figure 1

CLASSICAL CONTROL SYSTEM SYNTHESIS AND OPTIMIZATION

The "classical" version of AUTOCON (ref. 1) performs synthesis and optimization of linear control systems using nonlinear mathematical programming (NMP). Stability constraints (stability margins using Nyquist single-loop-at-a-time methods) and system performance constraints for scalar transfer functions are user-specified as are the system architecture and control parameters. Actual system open- and closed-loop frequency responses (airframe plus control system) are computed for the user-specified "initial system" for each stability-loop and constrained closed-loop transfer function, and for all selected plant variations. Similarly, desired and boundary responses are computed from the system requirements. Violations in the actual responses when compared with the desired and boundary responses at each frequency computed (considering all responses simultaneously) are caused either to vanish or are minimized by a proper selection (automated) of the control parameters (parameter optimization). A multivariable control system diagram and stability/performance constraints are depicted in figure 2 below.

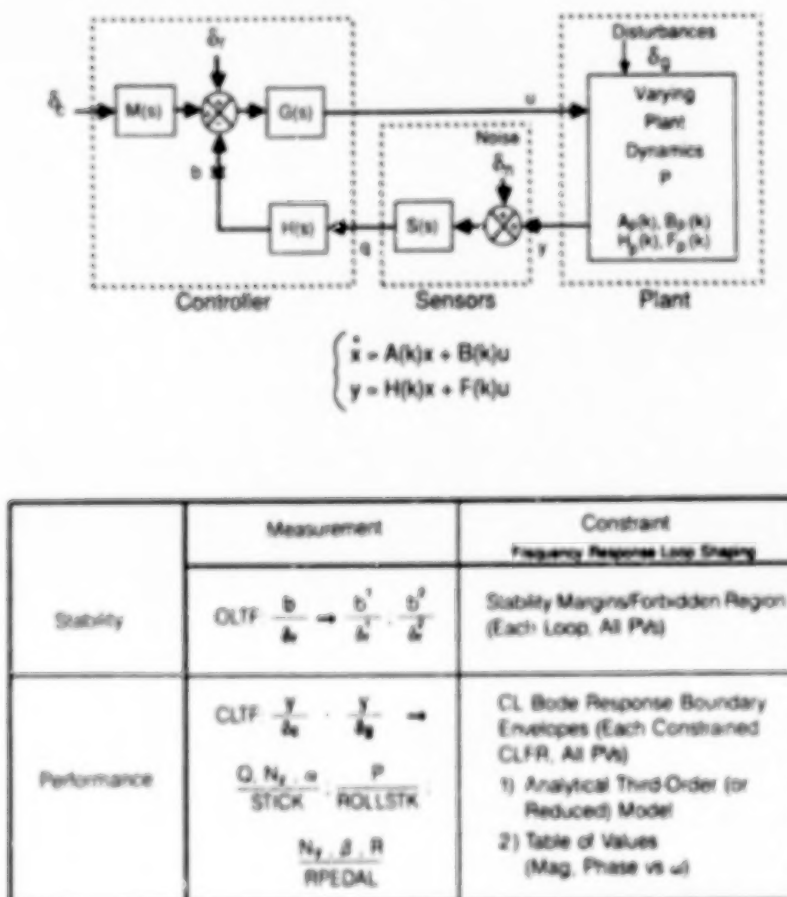


Figure 2

OBJECTIVE FUNCTION (CLASSICAL VERSION)

The objective function for the classical version of the program, shown in figure 3, combines violations in stability (open-loop frequency responses (OLFR)) for each stability loop with violations in the magnitude/phase frequency responses of selected closed-loop scalar transfer functions, for all plant variations. Classical gain and phase margins (GM, PM) are used to define a Forbidden Region in the Nyquist/Nichols plane. This region is an area of uncertainty centered at the Nyquist critical point $(-1, j0)$ or $(0\text{db}, -180^\circ)$ which the OLFR must avoid for adequate single input/single output (SISO) stability behavior. User-specified boundary constraints are imposed on the magnitude/phase closed-loop frequency responses (CLFR) which the actual CLFRs must be within to provide desirable performance.

$$J = J_{\text{Stability}}^{\text{OL}} + J_{\text{Performance}}^{\text{CL}}$$

$$J(p)_{\text{Stab}} = \sum_{\text{PVs}} \sum_{\text{OLTFs}} \sum_{\omega} f(\text{Stability Margins/Forbidden Region Violations})$$

$$J(p)_{\text{Perf}} = \sum_{\text{PVs}} \sum_{\text{CLTFs}} \sum_{\omega} f(\text{Magnitude/Phase Boundary Constraint Violations})$$



Figure 3

THE SEARCH ALGORITHM (NONLINEAR MATHEMATICAL PROGRAMMING)

A constrained local minimization procedure (Search Algorithm) is used to search for the active control parameters yielding minimum violation in all requirements considered collectively. The variable metric method of Davidson, Fletcher, and Powell (DFP Algorithm) (refs. 2,3) iteratively computes an approximation of the inverse Hessian matrix, H , which is used to deflect the gradient vector, $\nabla J(p) = \partial J / \partial p \approx \Delta J / \Delta p$, at a point in parameter hyperspace. The computation of this deflection matrix, η , ($\eta(p^i) \approx H^{-1}(p^i)$) hastens convergence since it is very effective in the vicinity of valleys in the hyperspace. The algorithm is also quite fast and not storage intensive since second partials need not be computed, nor must previous first or second derivatives be stored. The gradient is computed by a numerical perturbation procedure. A unidimensional search with quadratic interpolation is performed in the deflected gradient direction (search direction) to obtain the minimum in this direction. A gradient projection scheme is used to constrain the search within the feasible region. This is repeated for each search direction until the minimum is located. The iterative search algorithm is shown by the recursive equations and pictorially in figure 4.

• Constrained Local Minimization

- DFP Algorithm
- Unidimensional Search With Quadratic Interpolation
- Gradient Projection

$$p^{i+1} = p^i - \lambda^i \eta^i \nabla J(p^i),$$

$$p_{\min} \leq p \leq p_{\max}$$

$$\lambda^{*i} = J(p^i - \lambda^i \eta^i \nabla J(p^i))_{\min}$$

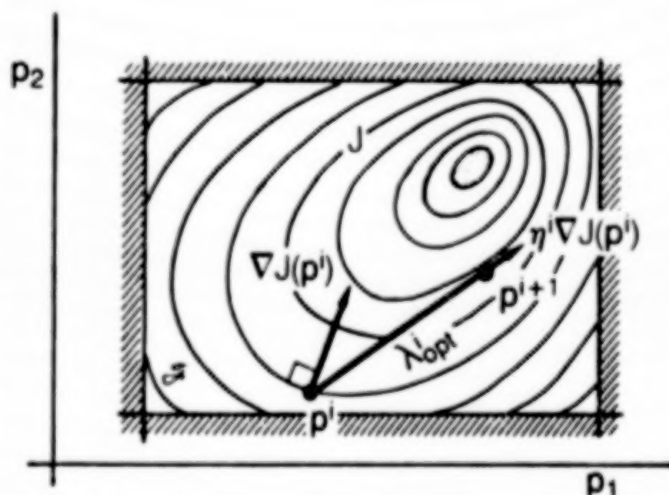
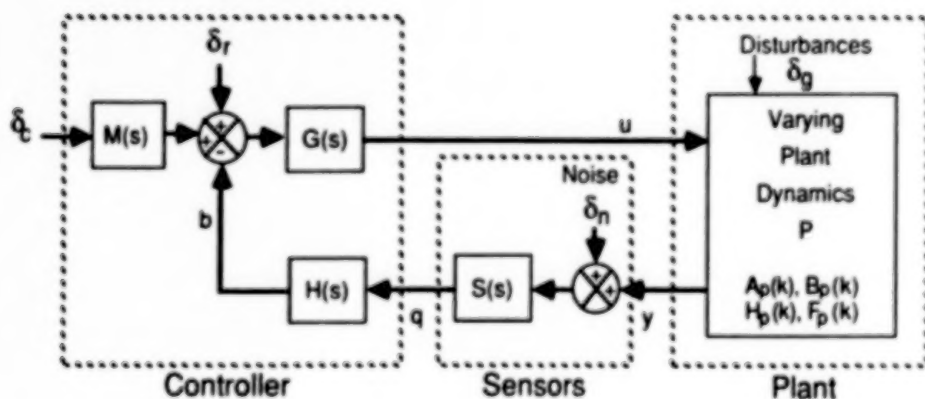


Figure 4

MIMO TRANSFER FUNCTION MATRICES DEFINITION

Shown below in figure 5 is a block diagram of a linear multivariable control system, subdivided into a controller, sensors and a plant. The representation here is of a plant with varying and uncertain plant dynamics given by the system matrices $A_p(k)$, $B_p(k)$, $H_p(k)$ and $F_p(k)$. The control system (controller and sensors) shown in Laplace transform notation can be combined with the plant state and output equations to form a total system state-space representation. It is convenient for multivariable systems to define certain matrix transfer functions. The loop transfer matrix, which depends upon the output node since matrix multiplication is not commutative, sensitivity matrix and complementary sensitivity matrix are defined in figure 5 (refs. 4,5).



$$\begin{cases} \dot{x} = A(k)x + B(k)u \\ y = H(k)x + F(k)u \end{cases} \quad P(k) = H(k) (I s - A(k))^{-1} B + F(k)$$

68-CSR-626-007

$$\text{Loop Transfer Matrix } L(s) = L(\omega, p) \triangleq P(s) G(s) H(s) S(s) \text{ at } y \text{ node} \\ \triangleq G(s) H(s) S(s) P(s) \text{ at } u \text{ node}$$

$$\text{Sensitivity Matrix } S(s) \triangleq (I + L(s))^{-1}$$

$$\text{Complementary Sensitivity Matrix } T(s) \triangleq I - S(s) = L(s) (I + L(s))^{-1}$$

Figure 5

SINGULAR-VALUES DEFINITION

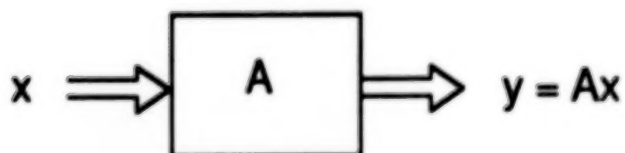
Nyquist stability theory, well founded and accepted for SISO systems, has been shown to be inadequate to describe robust MIMO system stability, because the determinant of the return difference matrix $(I + L(s))$ does not always provide a good indication of the proximity to singularity. Singular-values of a matrix A , $\sigma_i(A)$, however, provide a far better indication of system robustness since they provide a useful measure of the "size" of a matrix. Singular-values can be interpreted as the "gains" of a matrix for input vectors in various directions, as shown in figure 6 below. They also provide a natural extension to the familiar Bode frequency plots via the Bode sigma plot (Singular-values vs frequency). The singular-values of a matrix are defined as the nonnegative square roots of the eigenvalues $\lambda_i(A^H A)$, where A^H is the complex conjugate transpose of A . It is useful to define the maximum and minimum singular-values, $\bar{\sigma}(A)$ and $\underline{\sigma}(A)$, respectively. These will then form an upper and lower bound for $\sigma_i(A)$ on the Bode-sigma plot.

For Any Matrix A and Vector x

$$\sigma_i(A) \triangleq \sqrt{\lambda_i(A^H A)}$$

$$\bar{\sigma}(A) \triangleq \max_i \sigma_i(A)$$

$$\underline{\sigma}(A) \triangleq \min_i \sigma_i(A)$$



$$\bar{\sigma}(A) = \max_x \left(\frac{\|Ax\|}{\|x\|} \right) = \text{max gain of } A$$

$$\underline{\sigma}(A) = \min_x \left(\frac{\|Ax\|}{\|x\|} \right) = \text{min gain of } A$$

Figure 6

OBJECTIVE FUNCTION (MODERN ROBUSTNESS VERSION)

The objective function for the "modern" version of AUTOCON combines the MIMO robustness violation function $J_{\text{robustness}}$ with the "classical" version consisting of SISO stability and performance violation functions. The $J(p)_{\text{robust}}$ term considers violations in the user-defined singular-value constraints for each constrained matrix transfer function and for all plant variations. This is shown in figure 7 both with equations and graphically.

$$J = \left(J_{\text{Stability}}^{\text{OL}} + J_{\text{Performance}}^{\text{CL}} \right) + J_{\text{Robustness}}$$

$$J(p)_{\text{Stab}} = \sum_{\text{PVs}} \sum_{\text{OLTFs}} \sum_{\omega} f(\text{Stability Margins/Forbidden Region Violations})$$

$$J(p)_{\text{Perf}} = \sum_{\text{PVs}} \sum_{\text{CLTFs}} \sum_{\omega} f(\text{Magnitude/Phase Boundary Constraint Violations})$$

$$J(p)_{\text{Robust}} = \sum_{\text{PVs}} \sum_{\text{TFMs}} \sum_{\omega} f(\text{Singular-Value Constraint Violations})$$

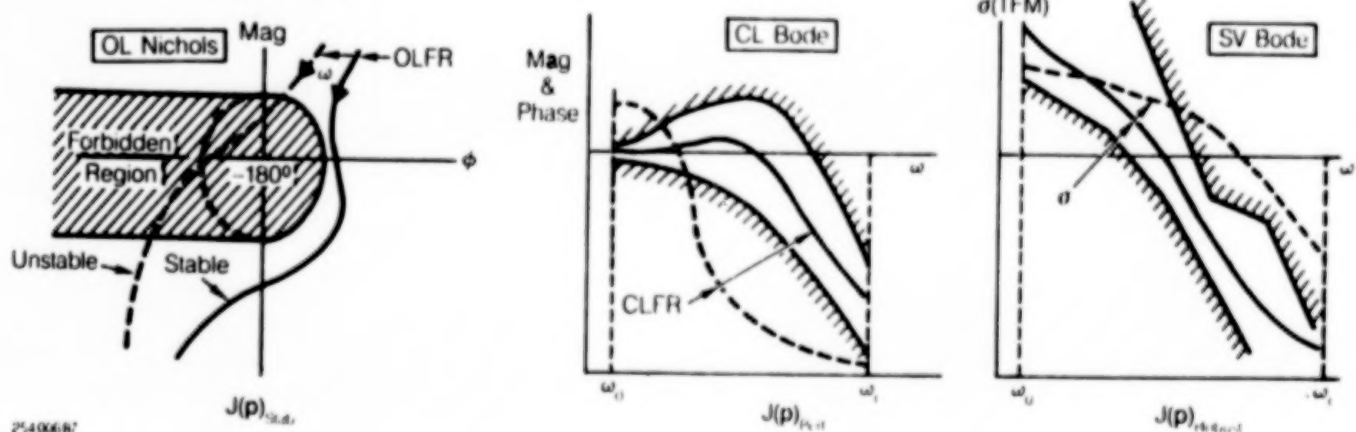
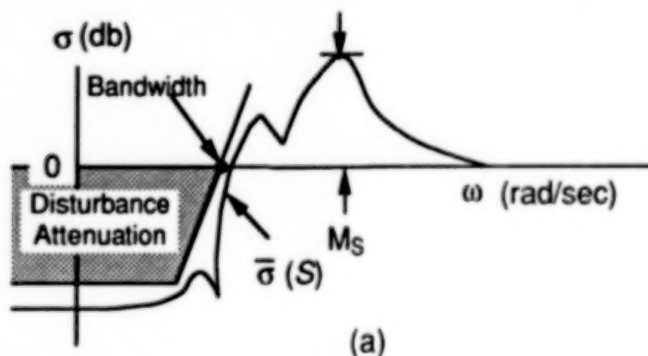


Figure 7

TYPICAL SINGULAR-VALUE BODE PLOTS AND SPECIFICATIONS

Typical singular-value frequency response (Bode) plots and constraints for a multivariable feedback control system are shown below in figure 8. The maximum singular-value plot of the sensitivity matrix $\bar{\sigma}(S)$ is constrained for disturbance attenuation and bandwidth in figure 8a, whereas, gain/phase margins (resonant peak) and unmodeled high frequency dynamics specifications are imposed on the maximum singular-value plot of the complementary sensitivity matrix $\bar{\sigma}(T)$ in figure 8b. Clearly, the singular-value frequency responses and specifications shown below are analogous to the usual SISO frequency responses and specifications. Connection between the resonant peaks M_T and M_S and classical gain/phase margins can be developed using the methods of references 6 and 7.

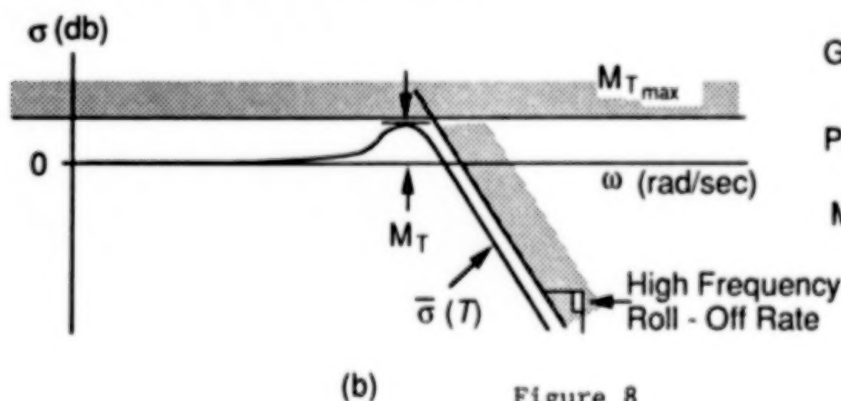
• Bandwidth & Disturbance Attenuation: $\bar{\sigma}(S)$



$$S \triangleq (I + L)^{-1}$$

$$T \triangleq L(I + L)^{-1}$$

• Gain / Phase Margin & Unmodeled High Frequency Dynamics : $\bar{\sigma}(T)$



$$GM \geq \max \left[\left(\frac{1}{1 - 1/M_S} \right), (1 + 1/M_T) \right]$$

$$PM \geq 2 \arcsin \left[\max \left(\frac{1}{2M_S}, \frac{1}{2M_T} \right) \right]$$

$$M_{T_{\max}} = \left[2 \sin \left(\frac{1}{2} PM_{\text{spec}} \right) \right]^{-1}$$

Figure 8

AUTOCON DESIGN EXAMPLE

A design problem is presented below in figure 9 in which program AUTOCON is asked to synthesize a typical aircraft lateral/directional flight control system in which control of roll rate, P , and lateral acceleration N_y using the roll-stick and rudder pedal is effected, subject to combined MIMO robustness constraints and classical SISO stability and performance constraints, for three different operating points or flight conditions (plant variations). The synthesis and optimization will involve each constrained open- and closed-loop scalar and matrix transfer function for all plant variations, simultaneously. It is necessary for both the modern robustness constraints and the classical constraints to be active: 1) to ensure that the individual stability loops remain stable (closed-loop eigenvalues do not migrate into the right-half plane) and 2) to provide desirable SISO frequency response loop-shaping (classical specifications). The active control parameters chosen for this example were K_1, K_2, \dots, K_9 . In this design, K_1, K_2, K_4 , and K_5 are scheduled (different gain value for each plant variation), while K_3, K_6, K_7, K_8, K_9 are nonscheduled (same value for each plant variation). This results in a total of 17 active control parameters.

A/F Dynamics (Plant)

- 5 States
- 3 Plant Variations

Controlled Outputs

- Roll Rate (P)
- Yaw Rate (R)
- Lateral Acceleration (N_y)

Inputs (Surface Deflections)

- ROLLSTK (δ_a)
- RPEDAL (δ_r)

Active Control Parameters (17)

$K_1, K_2, K_4, K_5 \rightarrow$ Scheduled
 $K_3, K_6, K_7, K_8, K_9 \rightarrow$ Nonscheduled

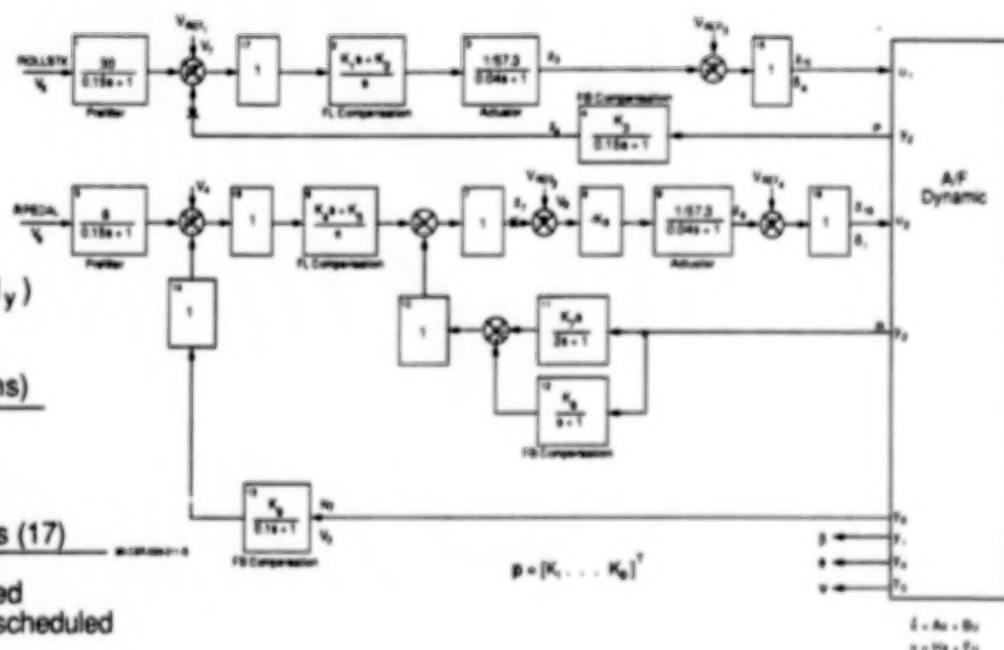


Figure 9

AUTOCON DESIGN EXAMPLE: SPECIFICATIONS

The classical SISO and modern MIMO robustness specifications for the AUTOCON design example are presented below in figure 10. Both the roll and yaw loops are desired to have at least 8 db of gain margin and 55 degrees of phase margin and each open-loop frequency response should not penetrate the Forbidden Region defined by the stability margins. It is also desired that the P/ROLLSTK response be within the performance bounds of an analytical 2nd-order model with parameters given below, with a steady-state value of 34 ± 0.4 db; and the Ny/RPEDAL response be within the performance bounds of a set of table values approximating a 2nd-order system with parameters given below, with a steady-state value of 11 ± 1.25 db. The robustness specifications include at least a 2 rad/sec system bandwidth, maximum disturbance attenuation and a $\bar{\sigma}(T)$ resonant peak less than or equal to 0.69 db (this provides at least 55 degrees phase margin and 8 db gain margin simultaneously in each loop).

SISO (Classical)

- Stability : Roll & Yaw Loops

$$\left. \begin{array}{l} \text{GM} \geq 8 \text{ db} \\ \text{PM} \geq 55 \text{ deg} \end{array} \right\} \text{Forbidden Region}$$

- Performance:

P/ROLLSTK - 2nd Order Model ($\zeta = 0.8$, $4.0 \leq \omega_n \leq 6.0$ rad/sec)
Steady-State : 34 ± 0.4 db

Ny /RPEDAL - Table Values ($\zeta = 0.8$, $2.5 \leq \omega_n \leq 3.5$ rad/sec)
Steady-State : 11 ± 1.25 db

MIMO (Robustness)

- Bandwidth ≥ 2 rad/sec
- Maximize Disturbance Attenuation
- Stability Margins

$$\left. \begin{array}{l} M_T \leq 0.69 \text{ db} \Rightarrow \text{PM} \geq 55 \text{ deg} \\ \text{GM} \geq 8 \text{ db} \end{array} \right\} \text{Simultaneously in each loop} \left\} \bar{\sigma}(T)$$

Figure 10

AUTOCON DESIGN EXAMPLE: PARAMETER CONSTRAINTS AND RESULTS

The admissible parameter range (linear inequality constraints) for the design problem is shown below in figure 11a. It is observed that the range for the forward-loop compensator parameters (scheduled) was selected as $.001 \leq p \leq 10.0$, whereas the remaining feedback parameter range (nonscheduled) was selected as $-10.0 \leq p \leq 10.0$. This was done to limit the forward-loop gains to positive values thereby preserving the sign convention, while allowing for possible feedback sign reversals from the nominal system shown in figure 9.

The results of the search, shown in figure 11b, indicate that a local minimum was found at a violation (J) of .0027. The effect of this violation is actually too small to be observed from the frequency responses presented in figures 12-15. The initial value chosen for all parameters was unity (no a priori information assumed). The final computer-generated scheduled and nonscheduled parameter values are also listed in figure 11b. It took 3.8 min on an IBM 3090 mainframe computer to synthesize this solution.

Active Parameter Constraints $P_{\min} \leq P \leq P_{\max}$

Parameter	K_1	K_2	K_3	K_4	K_5	K_6	K_7	K_8	K_9
P_{\min}	0.001	0.001	-10.0	0.001	0.001	-10.0	-10.0	-10.0	-10.0
P_{\max}	10.0								10.0

88 CSR 026-012

(a)

Results (J = .0027) CPU = 3.8 min (IBM 3090)

Scheduled Parameters

Parameter	K_1			K_2			K_4			K_5		
PV	1	2	3	1	2	3	1	2	3	1	2	3
Initial Value	1.0											1.0
Final Computer Generated Value	1.030	0.501	0.421	1.511	1.278	0.988	0.644	0.448	0.288	2.491	2.090	1.217

Nonscheduled Parameters

Parameter	K_3	K_6	K_7	K_8	K_9
Initial Value	1.0				1.0
Final Computer Generated Value	0.636	1.541	0.490	0.213	1.558

88 CSR 026-012a

(b)

Figure 11

AUTOCON DESIGN EXAMPLE: SISO NICHOLS PLOTS

The following pages contain the SISO and MIMO response plots of the airframe/control system with the unity initial control parameter values (before) and the system with the final computer-generated parameter values (after) for the three plant variations superimposed. The SISO open-loop frequency responses (Nichols plots) for the roll and yaw loops produced by AUTOCON are shown below in figure 12. The (8db, 55°) Forbidden Region (FR) is plotted as the closed broken contour (shaded). It is apparent from the initial roll loop responses in figure 12a that there is severe penetration into the FR for all three systems, violating the (8db, 55°)FR stability specification. As shown in figure 12c,d, SISO stability is adequate for the yaw loop. It is observed from figure 12b that AUTOCON has reshaped the roll loop Nichols responses around the FR by an adjustment of the active control parameters, the values of which are listed in Figure 11b.

AUTOCON MIMO LAT/DIR FCS 3PVS OPEN-LOOP FREQUENCY RESPONSE, NICHOLS PLOT

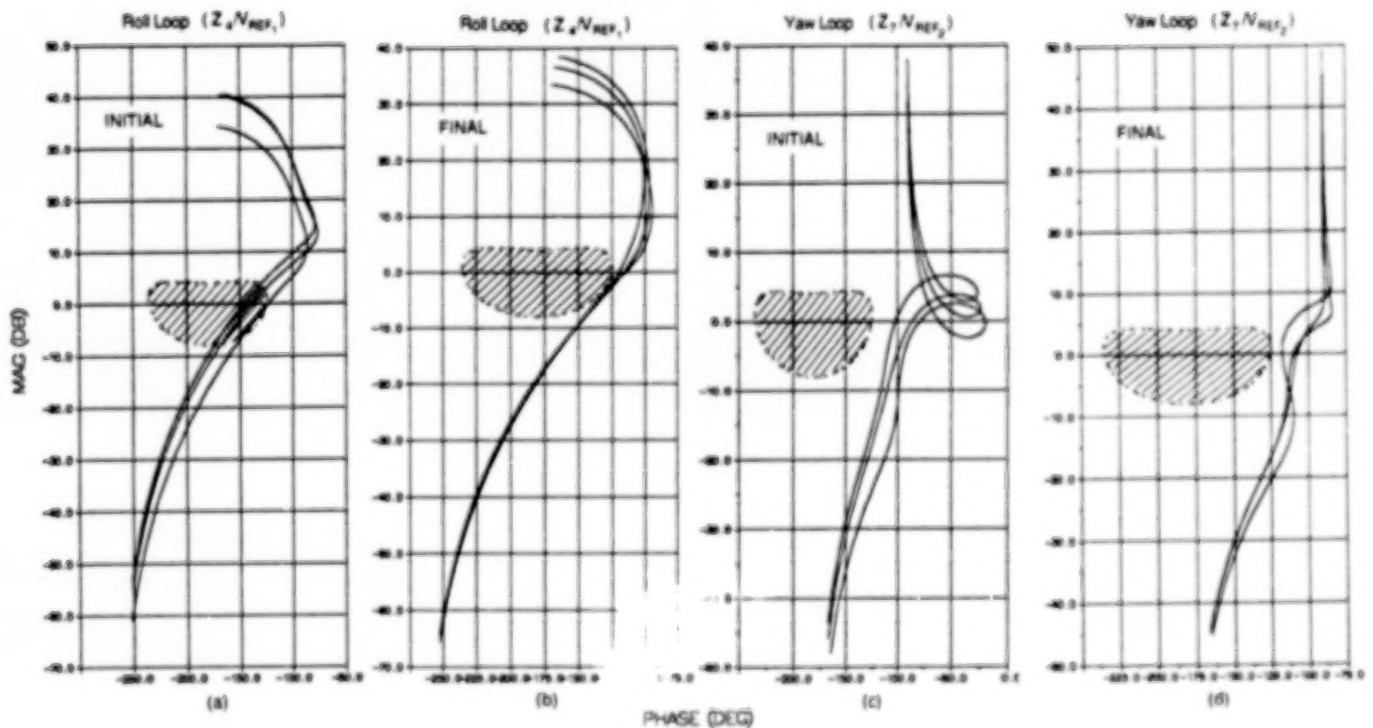


Figure 12

AUTOCON DESIGN EXAMPLE: SISO PERFORMANCE BODE RESPONSES

The SISO closed-loop Bode magnitude performance responses P/ROLLSTK and Ny/RPEDAL are presented below for the unity initial system in figure 13a,b and after the AUTOCON synthesis in figure 13c,d, respectively. The upper, lower and desired response boundary constraints consistent with the performance specifications given in figure 10 are shown as broken curves, with the unacceptable region shaded in figure 13. For this example, only the magnitude response was constrained. In general, magnitude and phase response constraints can be imposed. It is observed that there are severe violations for the unity initial parameter system both with respect to the steady-state values, shaping (notice the unacceptable resonance in the P/ROLLSTK response for two of the three plant variations), and sluggish Ny/RPEDAL responses. After the AUTOCON synthesis, the responses were forced into their respective boundaries, thereby satisfying the classical SISO specifications imposed on the system.

AUTOCON MMO LAT/DIR FCS 3PVS CLOSED-LOOP FREQUENCY RESPONSES

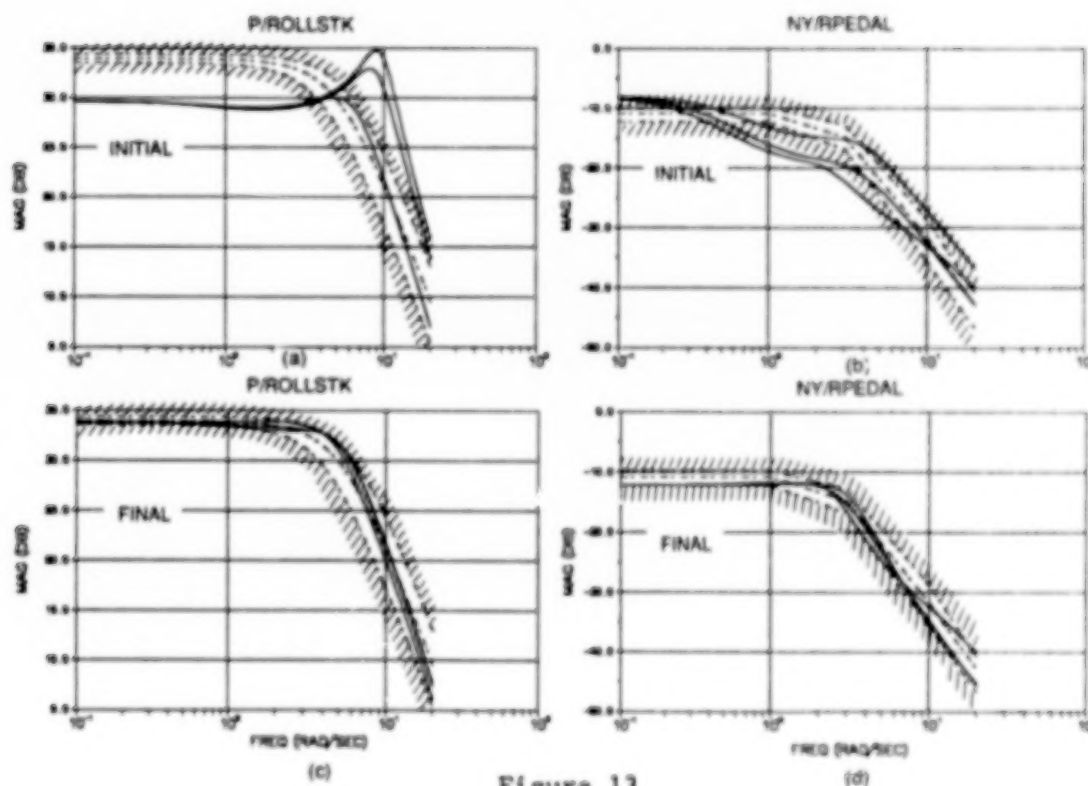


Figure 13

AUTOCON DESIGN EXAMPLE: MIMO SINGULAR-VALUE BODE RESPONSES

The singular-value sensitivity matrix and complementary sensitivity matrix Bode responses, $\sigma(S)$ and $\sigma(T)$, respectively, for the system with the unity initial parameter values and final computer-generated values are shown below in figure 14 for the three plant variations. Bandwidth, disturbance attenuation, gain/phase margin and unmodeled high-frequency roll-off specifications are drawn in figure 14 as broken boundary constraints with the unacceptable region shaded on the response plots. The $\sigma(S)$ and $\sigma(T)$ for this example are computed by AUTOCON from the MIMO matrix closed-loop transfer functions $(Z_{17}, Z_{18})/(V_{REF1}, V_{REF2})$ and $(Z_3, Z_4)/(V_{REF3}, V_{REF4})$ respectively. It is observed after comparing the initial and final sets of plots that AUTOCON successfully located a solution which satisfied the MIMO robustness specifications for all three plant variations, as given in figure 10. Note particularly the significant improvement in the disturbance attenuation for the $\sigma(S)$ responses and the resonant peak magnitude M_T attenuation for the $\sigma(T)$ responses. Satisfying the 0.69 db resonant peak magnitude constraint ensures at least 55 degrees phase margin in each loop even when the variations occur simultaneously in both loops. At least 8 db gain margin in each loop is also obtained by virtue of the equations shown in figure 8b.

AUTOCON
MIMO LAT/DR FCS 3PVS
SINGULAR-VALUE CLOSED-LOOP FREQUENCY RESPONSES

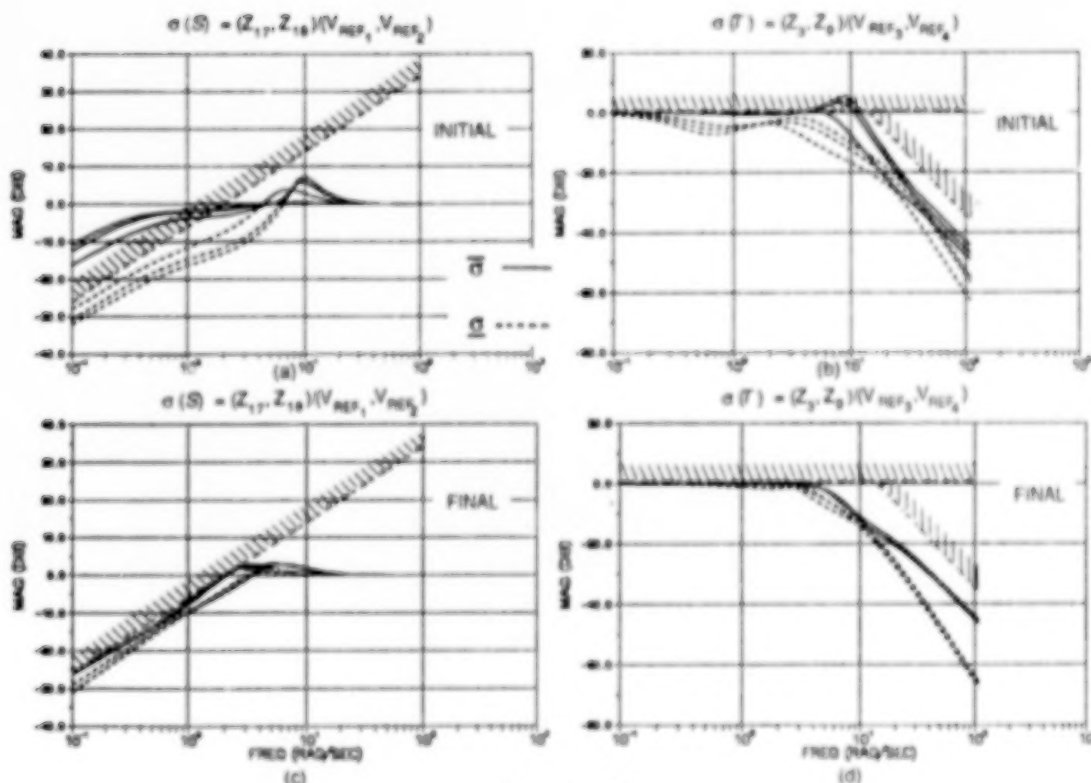


Figure 14

AUTOCON DESIGN EXAMPLE: TRANSIENT RESPONSES

Finally, transient responses of the constrained outputs roll rate, P , and lateral acceleration, N_y , to unit step ROLLSTK and RPEDAL input commands, respectively, are produced and shown below in figure 15 before and after the AUTOCON synthesis and optimization, for the systems with the three plant variations. Comparing the initial and final system P responses (figure 15a,b) shows that the poor initial responses (improper steady-state value and ringing) has been corrected by the optimization process and now satisfies the specifications. The upper, lower and desired transient boundary responses (broken curves) were computed from the second-order model parameters (specification) given in figure 10 and superimposed on the system transient responses. The shaded area indicates undesirable response regions. Objective function violations are measured in AUTOCON in the frequency-domain and not in the time-domain (transfer functions provide for a better more general measure for this application since they are not input dependent). Therefore, there may be some minor differences when comparing the two domains with respect to excursions from the desired response region. Since sets of table values were used to define the N_y /RPEDAL performance boundary constraints (note the sharp break-points in the broken boundary curves in figure 13b,d) exact 2nd order parameter values are unknown, and therefore, overlay boundary responses are not provided for the N_y transient response. Notice, however, how well the sluggish initial system N_y responses (figure 11c) were improved by the program (figure 15d). It is important to understand that all SISO "classical" and MIMO robustness specifications and constraints imposed for this AUTOCON design problem were active simultaneously in the search for an optimum solution and were satisfied by the final computer-generated values. The solution was obtained in only one computer run.

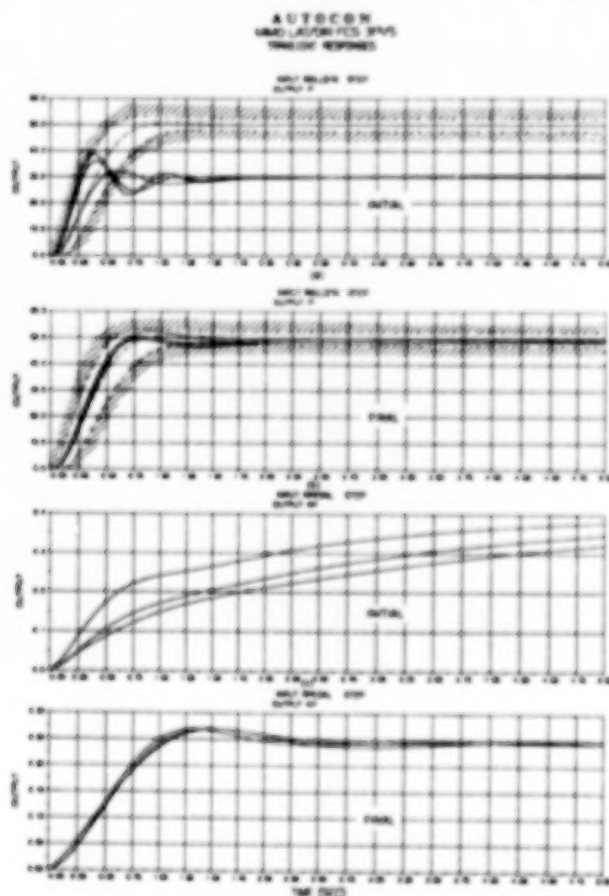


Figure 15

CONCLUSION

The automated computer-aided design tool, AUTOCON, used for the synthesis and optimization of linear control systems has been expanded to handle robust multivariable constraints in addition to the "classical" single-input/single-output stability and performance requirements. The synthesis and optimization can be performed on systems with fixed plant dynamics as well as those with varying dynamics. AUTOCON thereby enables the designer to combine classical SISO and modern MIMO control system stability/performance specifications within a highly flexible nonlinear programming design optimization environment.

The classical version of AUTOCON was first reviewed, followed by an introduction of the new multivariable robustness version of the program. Basic multivariable robustness concepts involving singular-values were discussed and an automated computer design example using AUTOCON was presented.

REFERENCES

1. Lefkowitz, C.P.: AUTOCON Version 3.0, User's Manual. Northrop Corp., March, 1987.
2. Davidon, W.C.: Variable Metric Method for Minimization. Argonne National Laboratory Report ANL-5990, November, 1959, revised February 1966.
3. Fletcher, R.; and Powell, M.J.D.: A Rapidly Convergent Descent Method for Minimization. Computer J. Vol. 6, pp. 163-168, 1963.
4. Safonov, M.G.; Laub, A.J.; and Hartmann, G.L.: Feedback Properties of Multivariable Systems: The Role and Use of the Return Difference Matrix. IEEE Trans. Auto. Contr., Vol. AC-26, pp. 47-65, February, 1981.
5. Doyle, J.C; and Stein, G.: Multivariable Feedback Design: Concepts for a Classical/Modern Synthesis. IEEE Trans. Auto. Contr., Vol. AC-26, pp. 4-16, February, 1981.
6. Safonov, M.G.; and Athans, M.: Gain and Phase Margin for Multiloop LQG Regulators. IEEE Trans. Auto. Contr., Vol. AC-22, pp. 173-179, April 1977.
7. Lehtomaki, N.A.; Sandell, N.R., Jr.; and Athans, M.: Robustness Results in Linear-Quadratic Gaussian Based Multivariable Control Designs. IEEE Trans Auto. Contr., Vol. AC-26, pp. 75-92, February 1981.

COMPUTERIZED DESIGN SYNTHESIS (CDS),
A DATABASE-DRIVEN MULTIDISCIPLINARY DESIGN TOOL

D. M. Anderson and A. O. Bolukbasi
McDonnell Douglas Helicopter Company
Mesa, Arizona

INTRODUCTION

Few mechanical systems are subject to as severe and as varied an aeromechanical environment as the helicopter. For instance, in each revolution of the rotor blade airflow can vary from stall to compressibility effects in unsteady flow. Designing control of the vehicle by applying twist at the base of the long narrow blades is an exercise in aeroelastic abstruseness. In no other aircraft is structural efficiency more essential, with the structure subject to such a severe fatigue environment. While design problems for rotorcraft are fully as complex as for fixed wing aircraft, the available resources and response time may be even more strictly limited.

Timely, responsive, and accurate concept studies are essential in rotorcraft development. It is difficult for highly specialized technical design support to be flexible and responsive enough to contribute significant influence early in the design process, when fast turnaround on multiple concepts is required. Supporting specialized studies requires time and effort which parallels the design development. Often the key analysis results for a conceptual design are obtained only near design task completion, in time to verify the concept but sometimes too late to significantly influence key design decisions. Computerizing the design trade-off process is necessary in order to enhance the availability and flow of technical information. Teaming the technical specialist with the designer and a shared data base will produce timely responses to customer inquiries and improve the efficiency of the design process.

The Computerized Design Synthesis (CDS) system under development at McDonnell Douglas Helicopter Company (MDHC) is targeted to make revolutionary improvements in both response time and resource efficiency in the conceptual and preliminary design of rotorcraft systems. It makes the accumulated design data base and supporting technology analysis results readily available to designers and analysts of technology, systems, and production, and makes powerful design synthesis software available in a user friendly format.

COMPUTERIZED DESIGN SYNTHESIS (CDS)

A SYSTEM TO PUT ACCUMULATED DESIGN DATA BASE AND
SUPPORTING TECHNOLOGY ANALYSIS RESULTS READY
AT THE HANDS OF DESIGNER AND ANALYST,
AND TO MAKE DESIGN SYNTHESIS SOFTWARE AVAILABLE
IN A USER-FRIENDLY FORMAT.

LESSONS LEARNED

Industry experience in similarly ambitious computerized design systems provides some lessons learned. Potential problems include: data incompatibility, the profusion of specialized languages and codes evolving continuously, and the not uncommon experience that global programs, (with globe-sized promises) can consume vast resources and take years to develop. Furthermore, when they are finally developed, they are sometimes somewhat incomprehensible to the ordinary aircraft designer--having become the brain-child of a team of computer systems specialists.

LESSONS LEARNED

- GLOBAL PROGRAMS ARE COSTLY
- DATA COMPATIBILITY
- PROFUSION OF LANGUAGES
- GROWTH OF SPECIALTIES

OVERALL APPROACH

In the light of observed experience, a careful development path was defined to avoid some of the costs and difficulties, and to provide early return on investment. The basic system was established for the conceptual design problem, and is being expanded to support more and more preliminary design tasks. Scope is carefully limited. User friendliness is essential, with tutorial aids and built-in constraints against misapplication. The system is data base driven, with a library of menu-controlled vehicle and subsystem synthesis programs. Wherever practical, existing software was adapted, using the resources of other McDonnell Douglas Corporation components. A key policy has been to bring each new capability on-line as soon as it is viable, and to support operational usage during development. This provides early feedback to influence the system toward practical utility, and brings the earliest cost savings.

OVERALL APPROACH

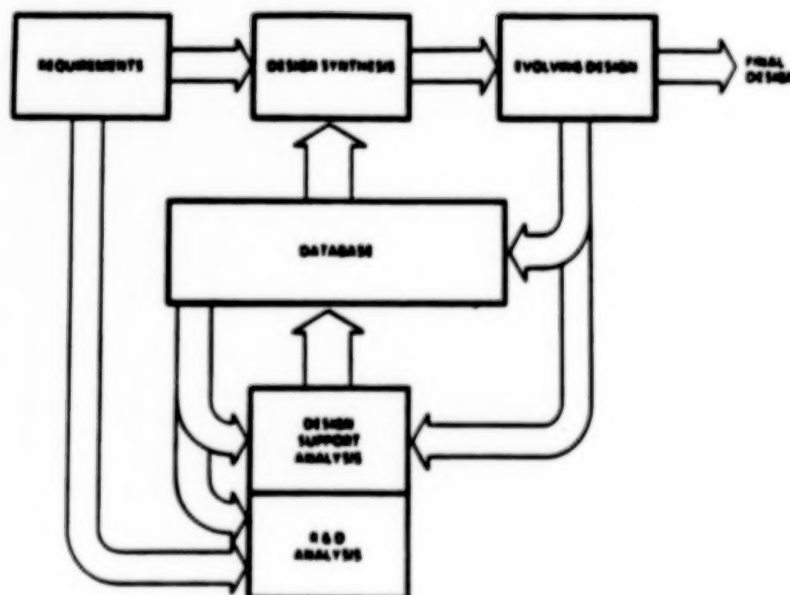
- TARGET: VEHICLE CONCEPTUAL DESIGN (RAPID VEHICLE SIZING),
CONCEPTUAL & PRELIMINARY DESIGN OF SUBSYSTEMS.
- LIMIT SCOPE, KEEP SYSTEM USER-FRIENDLY & TUTORIAL WITH
BUILT-IN CONSTRAINTS AGAINST MISAPPLICATION.
- DATA BASE-DRIVEN SYSTEM WITH LIBRARY OF MENU-CONTROLLED
VEHICLE & SUBSYSTEM SYNTHESIS PROGRAMS.
- ADAPT EXISTING SOFTWARE, PARTICIPATE IN MDC EXCHANGE
- SUPPORT OPERATIONAL USAGE DURING DEVELOPMENT

THE DATA BASE-DRIVEN SYSTEM

The CDS system was designed to be database-driven, as distinct from systems which are directly dependent on current customized applications of specialized analysis programs. Of course, such customized analyses are essential to the final refinement of preliminary and detail design. However, early and quick response efforts can use the data base for approximations, with parametric data developed from previous experience. The data base provides buffer storage between specialized design support analysis and the cyclic design process; making the analysis results available to the designer without the problems of language profusion and data incompatibility.

This is significantly different from many of the systems being developed for aerospace design support which are truly multidisciplinary, in that such analysis programs develop concurrent solutions from several separate disciplines. Those multi-disciplinary analysis programs remain specialized tools for the specialized analyst. Because familiarity with specialized theoretical mechanics is required, they are not suitable for direct use by the general aircraft designer--the one who is responsible for integrating the various specialized results.

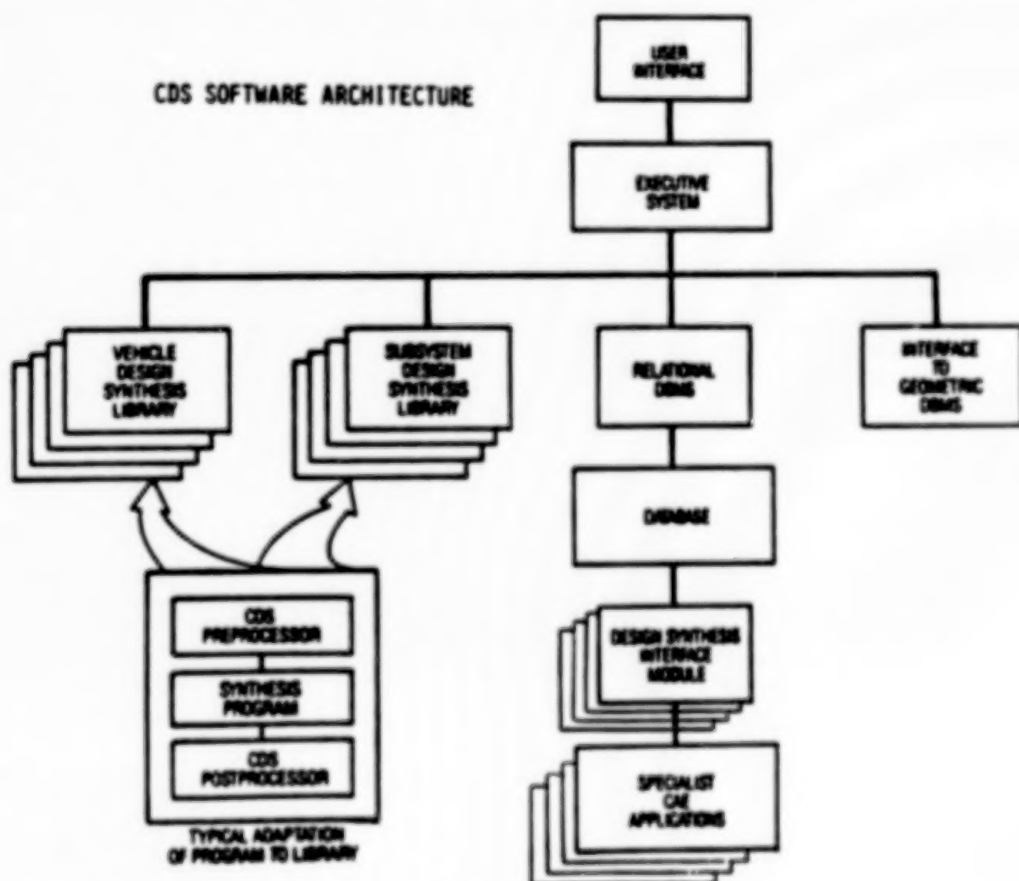
Data base-Driven Design Synthesis.



CDS SOFTWARE ARCHITECTURE

In the CDS system existing design synthesis software, for both vehicles and subsystems, is adapted by the addition of pre- and post-processors. These are managed through menu controls or commands, without the user being required to learn the intricacies of each program's jargon. This enables such programs as NASA's helicopter sizing and performance program "HESCOMP" (which contains over 14000 lines of code and requires over 4000 input parameters for operation) to be utilized in a highly simplified manner. The design synthesis library files include simulations of current vehicle designs. Through the menus of the executive system, these are easily used by designers and systems analysts to determine the effects on performance of variations in power, weight, fuel efficiency, and aerodynamics.

A commercially available relational database management system feeds data to the CDS executive system, which also interfaces with a geometric data base management system. The various specialized analyses are linked to the database through Design Synthesis Interface Modules (DSIM). These include programs from aerodynamics, acoustics, structures, thermodynamics, and other complex analytical disciplines; plus programs for evaluating process control, manufacturability, ballistic vulnerability, durability, etc. Each DSIM is, in effect, the data provider link for a highly technical supporting specialty. The DSIM also provides built-in constraints against misuse of the analytical data, informing the user if this difficulty should occur.



USER INTERFACE/MENU SUBROUTINES

The preprocessors which interface the programs in a design synthesis library assemble the program runstream, control parameters, and data deck according to the menu selections. The relevant choices are solicited and the user advised in the selections, and these are displayed in terms relating to the design mechanics (rather than relating to the program software). This process controls the program library and run options, component selections, missions, equipment, fuel, etc., for the model being exercised and the design requirements being served. It is also used to select output detail and format, plotting routines, and disposal of results, files, etc.

USER INTERFACE/MENU SUBROUTINES

OPTION CHOICES TO SET UP PRE- AND POST- PROCESSORS

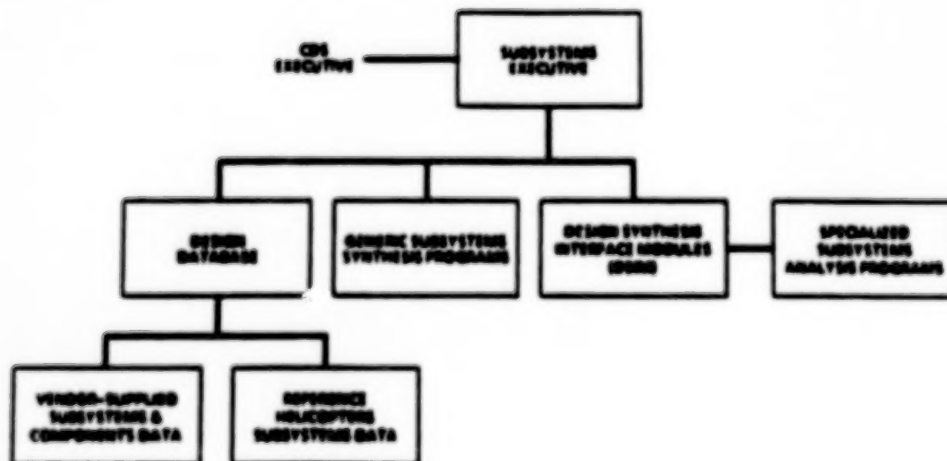
SOLICIT	}	PROGRAM LIBRARY OPTIONS
ADVISE		VEHICLE/COMPONENT SELECTIONS
DISPLAY		(ENGINES, CONFIGURATION, ETC.)
		MISSIONS, EQUIPMENT, FUEL
		SIZING AND/OR PERFORMANCE OPTIONS
		OUTPUT DETAIL
		PLOTTING ROUTINES
		BATCH/MULTIPLE RUN CONTROL
		FILE STORAGE AND CONTROL

SUBSYSTEMS DESIGN SYNTHESIS

All specialized analyses are treated autonomously by establishing an interface module (DSIM). This includes software providing graphic anthropometric modeling for cockpit layout and programs for design of drivetrains, engines, environmental control systems, and mission equipment packages. These provide the more advanced connection, to the analyses customized for the design task in progress.

The more ready-at-hand support is from reference data and generic simulation routines directly available through the subsystems executive. Such reference data include vendor-supplied information and published data collected in the data base.

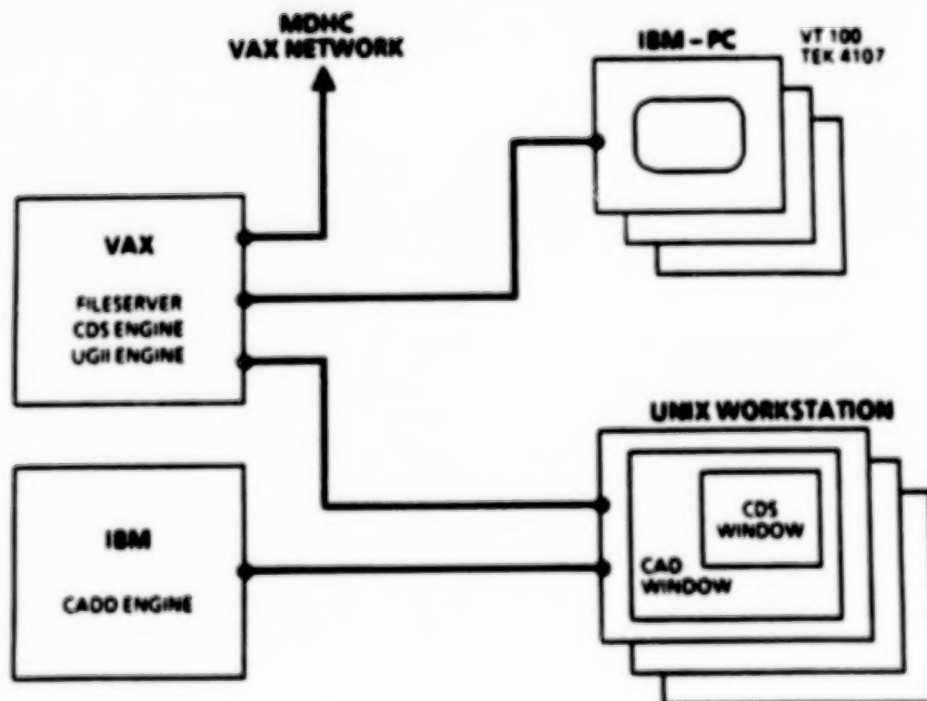
Computerized Design Subsystems Synthesis.



HARDWARE ARCHITECTURE

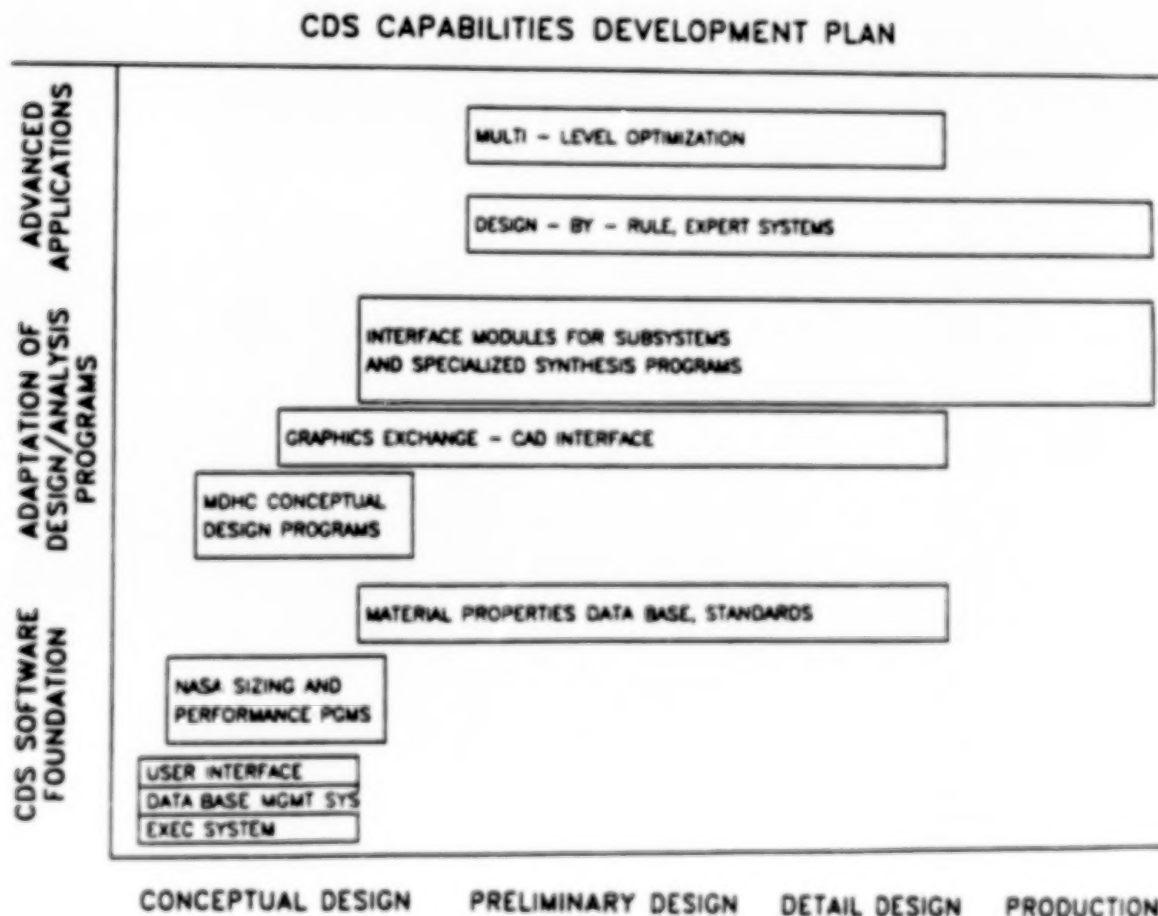
The CDS system is initially implemented on the VAX/VMS environment where the bulk of the specialized CAE application programs are installed. The CDS system will later be ported to a distributed computing environment that includes UNIX based workstations, file servers and compute servers all networked together.

CDS Hardware Architecture.



CAPABILITIES DEVELOPMENT PLAN

The adaptation of powerful conceptual design synthesis software such as NASA's HESCOMP helicopter sizing and performance program to the CDS executive system brings an immediate payoff in productivity, which in turn can fund further development of the system. As each new capability is developed and proven, it is added on-line to the CDS repertoire. The executive system, data base management system, and user interfaces have been developed for the conceptual design task. They are being expanded to incorporate the analytical support for the much more complex preliminary design task. This figure shows the capabilities being added, by category, with the abscissa representing both calendar time and design application category. Currently the basic system is in place for conceptual design, and improved in-house modules are being added which allow considerable choice in the level of detail to be used. The data base is being expanded to provide structural material data required for preliminary design, and Design Synthesis Interface Modules (DSIM) are being developed for drivetrain and structural component design synthesis. A graphics exchange interface will link graphic data from Unigraphics II and allow such exercises as putting the anthropometric model of program MACMAN in the cockpits being designed from the results of conceptual design trades.

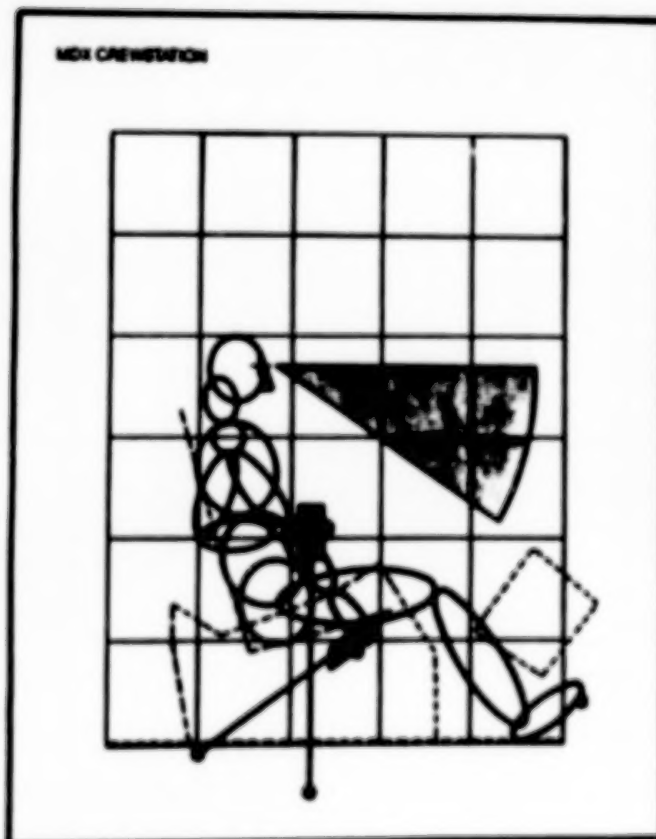


MACMAN: ANTHROPOMETRIC MODELING FOR CREW STATION DESIGN

Program MACMAN generates and manipulates a graphic depiction of a three-dimensional human body composed of linked ellipsoidal components. The default model is dimensioned to fit the 50th percentile Army man in overall size, with body components of standard proportion. Alternatively, size can be selected representing 25th or 5th percentile women, and 50th or 95th percentile men, based on NASA civilian data. Disproportionate figures can also be modeled. For example, a 50th percentile torso can be combined with 45th percentile legs and 52nd percentile arms. The program was used supporting conceptual design for the MDX light helicopter project, determining the following:

1. Seat position: height and limits of fore and aft adjustment.
2. Rudder pedal position and adjustments.
3. Seat back pan size and orientation.
4. Control locations for cyclic and collective.

The figure's limbs are animated. The entire graphical analysis is interactive, with 49 variables at the menu command of the operator.



PROGRAM MACMAN

DEVELOPED BY:
BUSHNELL DOUGLAS HELICOPTER COMPANY
COMPUTER AIDED TECHNOLOGY GROUP

OCCUPANT SIZE (P/100)	=	25		
TORSO AND HEAD ANGLES	=	10.0	0.0	0.0
BUTTOCK COMPRESSION FACTOR	=	7.0		
RIGHT UPPER ARM ANGLE	=	-23.0		
RIGHT LOWER ARM ANGLE (P/Y)	=	117.0	0.0	
LEFT UPPER ARM ANGLE	=	30.0		
LEFT LOWER ARM ANGLE (P/Y)	=	0.0	0.0	
FOOT ANGLE, LEG REACH INCH	=	30.0	0.0	
HISL POSITION (S/W)	=	40.0	0.0	
CYCLIC CENTER OF ROT (S.B.W)	=	22.0	0.0	-5.0
CYCLIC RAD. AND ANG. (P/R)	=	20.5	0.0	0.0
EYE REF. POSITION (S.W)	=	10.4	37.0	
SEAT REF. POSITION (S.W)	=	15.5	9.0	
SEAT PAN DIMENSIONS (S.W)	=	10.0	17.0	
SEAT BACK DIMENSIONS (S.W)	=	20.0	17.0	
SEAT PAN ANGLE	=	14.0		
SEAT BACK ANGLE	=	10.0		
RIGHT FOOT PEDAL POS (S.B.W)	=	52.0	4.0	4.0
LEFT FOOT PEDAL POS (S.B.W)	=	52.0	-4.0	4.0
COLLECT CENTER OF ROT (S.B.W)	=	10.0	10.0	-1.0
COLLECT RAD. AND ANG. (P/R)	=	30.0	30.0	

PLOT VIEW:	FRONT	SIDE	TOP
VISION PLOT:	YES	NO	
REVERSE VIDEO:	YES	NO	
INCREMENT:	1/16	1	5 10

PLOT	SAVE	HARDCOPY	EXIT
TITLE 25TH % WOMAN			

MACMAN Workstation Display, Side View.

STRUCTURAL COMPONENT DESIGN SYNTHESIS

Despite the fact that the technology of formal structural optimization has reached a state of practical applicability, the majority of structural component design tasks are still accomplished by the traditional draw-then-analyse procedure. If the component is not too complex, the designer can use handy stress formulae so that his first attempt is reasonable and then refined analysis can be used to tune the design. However, for most composite laminates the structural design task becomes complex, simply because of the increased number of design options opened up by the material and layup combinations. For such components there are also an increased number of failure modes to consider. A valuable step forward can be attained by putting user friendly analysis tools in the designers hands, and using the computer, with a small knowledge base associated with design practice, to illuminate design options and results. By providing information on selected bounds in design space, the designer can make optimal choices on a traditional heuristic basis. The software so developed forms a base for future expansion into applications of formal optimization.

A variety of stress analysis software is being inverted to provide solutions to the design problem instead of the stress analysis problem. (In the design problem stress is an allowable rather than a result.) Of course, when the problem is nonlinear, the relevant equations cannot be inverted directly, but a programmed series of forward runs can be used in mapping available design space.

COMPOSITE PANEL DESIGN TRADES

SANDWICH PANEL

BUCKLING, SHEAR, COMPRESSIVE FAILURE LIMITS PER:

- * FACING LAYUP, THICKNESS
- * CORE MATERIAL, THICKNESS
- * FACING HYBRID MATERIAL LAMINA

STIFFENED PANEL

BUCKLING, LOCAL CRIPPLING, JOINT FAILURE LIMITS PER:

- * PANEL LAYUP, THICKNESS
- * STIFFENER TYPE, SIZE, SPACING
- * HYBRID MATERIAL LAMINA

SESSION 6: SENSITIVITY ANALYSIS

Chairmen: R. T. Haftka and B. Prasad

**ON EQUIVALENCE OF DISCRETE-DISCRETE AND
CONTINUUM-DISCRETE DESIGN SENSITIVITY ANALYSIS†**

Kyung K. Choi
and
Sung-Ling Twu

Department of Mechanical Engineering
and
Center for Computer Aided Design
College of Engineering
The University of Iowa
Iowa City, Iowa

† Research supported by NSF Project No. MSM 83-19871.

Developments in design sensitivity analysis (DSA) method have been made using two fundamentally different approaches as shown in figure 1. In the first approach, a discretized structural finite element model is used to carry out DSA. There are three different methods in the discrete DSA approach: finite difference, semi-analytical, and analytical methods. The finite difference method is a popular one due to its simplicity, but a serious shortcoming of the method is the uncertainty in the choice of a perturbation step size of design variables (ref. 1). In the semi-analytical method, the derivatives of stiffness matrix is computed by finite differences (refs. 2-4) whereas in the analytical method, the derivatives are obtained analytically. For the shape design variable, computation of analytical derivative of stiffness matrix is quite costly (ref. 1). Because of this, the semi-analytical method is a popular choice in discrete shape DSA approach (refs. 3 and 4). However, recently, Barthelemy and Haftka (ref. 5) presented that the semi-analytical method can have serious accuracy problems for shape design variables in structures modeled by beam, plate, truss, frame, and solid elements. They found that accuracy problems occur even for a simple cantilever beam. In the second approach, a continuum model of the structure is used to carry out DSA. For shape design variable, the material derivative concept of continuum mechanics is used to relate variations in structural shape to measures of structural performance (refs. 6-10). Using continuum DSA approach, expressions for shape design sensitivity are obtained in the form of integrals with integrands written in terms of natural physical quantities such as displacements, stresses, strains, and domain shape changes. If exact solutions of the continuum equilibrium equations are used to evaluate these continuum design sensitivity expressions, the method is called continuum-continuum (C-C) method. On the other hand, if the analysis results of the finite element or boundary element methods are used to evaluate these terms, the method is called continuum-discrete (C-D) method. The analytical method of discrete design sensitivity analysis approach will be called discrete-discrete (D-D) method.

METHODS OF DESIGN SENSITIVITY ANALYSIS

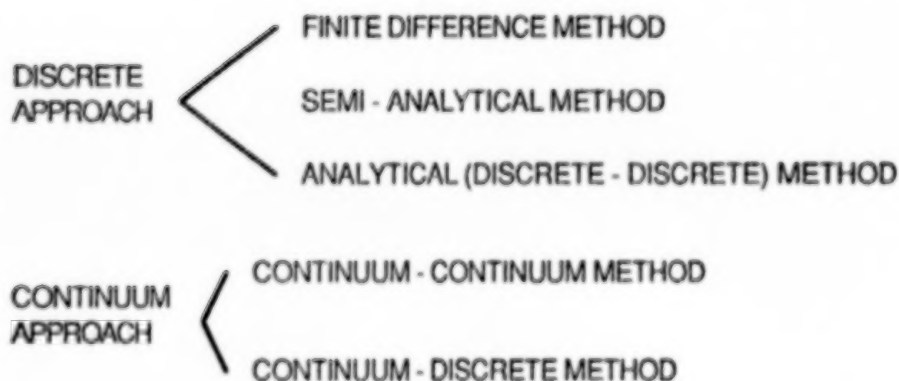


Figure 1

The D-D method starts with the finite element matrix equilibrium equation for linear structural system as shown in figure 2, where $K(b)$ is the reduced global stiffness matrix, z is the reduced displacement vector, $F(b)$ is the external load vector, and b is a design variable vector. Differentiating both sides of the matrix equilibrium equation with respect to b , a matrix equation for the derivative of displacement vector, dz/db , is obtained where the tilde (\sim) indicates a variable that is to be held constant for the process of partial differentiation. If the derivative dz/db is obtained by solving this equation, the method is called direct differentiation method. If derivatives of a general performance measure are needed, an adjoint variable method can be used (ref. 11). Even though the direct differentiation and adjoint variable methods are different in computational efficiency depending on situations, they are equivalent in accuracy as long as consistent computational procedure is used for both methods. For the D-D method, the derivative of stiffness matrix is obtained analytically, whereas it is obtained by finite differences for the semi-analytical method. The discrete DSA approach is applicable to both sizing and shape design variables. For the shape design case, the design variables are positions of the finite element grid points.

DISCRETE DSA APPROACH (DIRECT DIFFERENTIATION METHOD)

$$K(b)z = F(b)$$

$$K(b)\frac{dz}{db} = -\frac{\partial}{\partial b}(K(b)\tilde{z}) + \frac{\partial F(b)}{\partial b}$$

- **Semi-analytical and analytical (D-D) methods**
- For general performance measures, use the **adjoint variable method**.
- Accuracy of the **direct differentiation and adjoint variable methods** are equivalent.
- **Discrete approach** is applicable to both **sizing and shape design variables**.

For the continuum approach, using the principle of virtual work, the variational equilibrium equation of the structural system can be obtained (ref. 11) as shown in figure 3, where $a_{\Omega}(\cdot, \cdot)$ denotes energy bilinear form, $\ell_{\Omega}(\cdot)$ denotes load linear form, Ω

is the shape of the structure, z is the displacement, \bar{z} is the kinematically admissible virtual displacement, and Z is the space of kinematically admissible virtual displacements. Note that an approximate finite element matrix equilibrium equation can be obtained by applying the Galerkin method to the variational equilibrium equation for an approximate solution. For shape DSA, taking the material derivative of both sides of the variational equilibrium equation (refs. 10-12), a variational equation for the

material derivative \dot{z} of the displacement is obtained where V is the design velocity field.

Expressions for $a_V'(z, \bar{z})$ and $\ell_V'(\bar{z})$ can be obtained for various structural components (refs. 10-12). For the C-D method, an approximate finite element matrix equation is

used to obtain an approximate solution of the second variational equation for \dot{z} . On the other hand, for the C-C method, the analytical solution z of the first variational equation

is used in the second variational equation to obtain the analytical solution \dot{z} . As in the D-D method, if derivatives of a general performance measure are needed, an adjoint variable method can be used (refs. 10-12). The C-C method provides the exact design sensitivity of the exact model, whereas the C-D method provides an approximate design sensitivity of the exact model. On the other hand, D-D method yields the exact design sensitivity of an approximate finite element model, and both the finite difference and semi-analytical methods yield approximate design sensitivities of an approximate finite element model.

CONTINUUM SHAPE DSA APPROACH (DIRECT DIFFERENTIATION METHOD)

$$a_{\Omega}(z, \bar{z}) = \ell_{\Omega}(\bar{z}), \quad \text{for all } \bar{z} \in Z$$

$$a_{\Omega}(\dot{z}, \bar{z}) = \ell_V'(\bar{z}) - a_V'(z, \bar{z}), \quad \text{for all } \bar{z} \in Z$$

- **FEM equation** is an approximate equation of the **variational equation**.
- Use **material derivative** concept of the continuum mechanics for **shape DSA**.
- For general performance measures, use the **adjoint variable** method of DSA.
- **C-C** and **C-D** methods

Figure 3

One question often asked is; "Are the D-D and C-D methods equivalent?" For this question, certain conditions have to be given. First, the same discretization (shape function) used for the finite element analysis method must be used to evaluate the continuum design sensitivity results. Second, exact integrations (instead of numerical integrations) must be carried out for all integrations used for generation of stiffness matrix and evaluation of continuum design sensitivity expressions. The third condition to be met is that the exact solutions (not a numerical solution) of the finite element matrix equation and adjoint equation are used to compare two methods. The fourth condition is that movement of the finite element grid points for shape design change in the D-D method must be consistent with the parameterization method used for the design velocity field of the C-D method. For the sizing design variable, it is shown in reference 11 that the D-D and C-D methods are equivalent under the conditions given in figure 4 using a beam structural component. It has also been argued that the D-D and C-D methods are equivalent for shape design variable under the conditions given in figure 4 (refs. 13 and 14). One point to note is that these four conditions are not easy to satisfy; in many cases, numerical integrations are used and exact solutions of the finite element matrix equations cannot be obtained. In this paper, equivalence study of D-D and C-D methods for shape design variables is carried out under the conditions given in figure 4. To carry out equivalence study of the D-D and C-D method, two simple structural components, a truss and a cantilever beam, are used. The shape DSA results of the D-D and C-D methods derived in the published literature are cited and used here without being derived in this paper.

ARE THE D-D AND C-D METHODS EQUIVALENT?

Equivalence study under the following conditions:

- 1 The same shape function used for FEA must be used to evaluate the continuum DSA results.**
- 2 Exact integrations must be used to generate the stiffness matrix and evaluate the continuum DSA results.**
- 3 Exact solutions of the finite element and adjoint matrix equations are used to compare two DSA methods.**
- 4 Movement of FE grid points for the D-D method must be consistent with the parameterization of the design velocity field for the C-D method.**

Figure 4

In figure 5, the results of equivalence study of the D-D and C-D methods for shape design sensitivity are presented using a simple truss with one end fixed. The truss has a uniform cross-sectional area A and its length is ℓ which is the shape design variable. Three loading cases, a point load p at the tip, a uniformly distributed load f , and a linearly varying load qx/ℓ , are considered as shown in figure 5. For each loading case, linear and quadratic shape functions are used for finite element models. For the linear shape function, two element model is used whereas for the quadratic shape function, one element model is used. For the equivalence study, design sensitivities of the nodal displacements are considered using the adjoint variable method. In figure 5, 'same' denotes that the D-D and C-D methods yield the same result and 'not' denotes that the two methods do not yield the same result. Details of the equivalence study results are given in the following figures.

RESULTS OF EQUIVALENCE STUDY OF D-D AND C-D METHODS FOR TRUSS

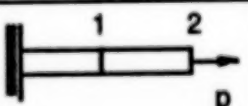
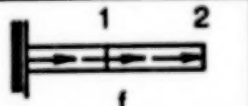

Loading Condition Design Velocity Field Shape Function						
	Linear	Quad	Linear	Quad	Linear	Quad
Linear	Same	Same	Same	Same	Same	Same
Quadratic	Same	Same	Not	Same	Not	Not
Cubic	Same	Same	Not	Not	Not	Not

Figure 5

For the design velocity $V(x)$ to be used in the C-D method, three parameterization methods; linear, quadratic, and cubic polynomials are used as shown in figure 6, where

$$\alpha_1 = \frac{4\epsilon_1 - \delta l}{l}, \quad \alpha_2 = \frac{2\delta l - 4\epsilon_1}{l^2}, \quad \beta_1 = \frac{18\epsilon_2 - 9\epsilon_3 + 2\delta l}{2l}$$

$$\beta_2 = \frac{-45\epsilon_2 + 36\epsilon_3 - 9\delta l}{2l^2}, \quad \beta_3 = \frac{27\epsilon_2 - 27\epsilon_3 + 9\delta l}{2l^3}$$

Note that for all three parameterizations of design velocity, the perturbation of length of the truss is δl at the tip. Moreover, for the quadratic and cubic design velocities, once $\epsilon_i, i=1,2,3$, are fixed, then the only one shape design variable is the length l . The movement of the finite element grid points for shape design changes in the D-D method must be consistent with these parameterization methods. For the D-D method, the shape design variables are the positions b_1 and b_2 of the nodal points. If the present design is $b_1=l/2$ and $b_2=l$, then $V(l/2)=\delta b_1=\delta l/2$ and $V(l)=\delta b_2=\delta l$ for the linear velocity, $V(l/2)=\delta b_1=\epsilon_1$ and $V(l)=\delta b_2=\delta l$ for the quadratic velocity, and $V(l/2)=\delta b_1=(9\epsilon_2+9\epsilon_3-\delta l)/16$ and $V(l)=\delta b_2=\delta l$ for the cubic velocity.

PARAMETERIZATIONS OF THE DESIGN VELOCITY $V(x)$

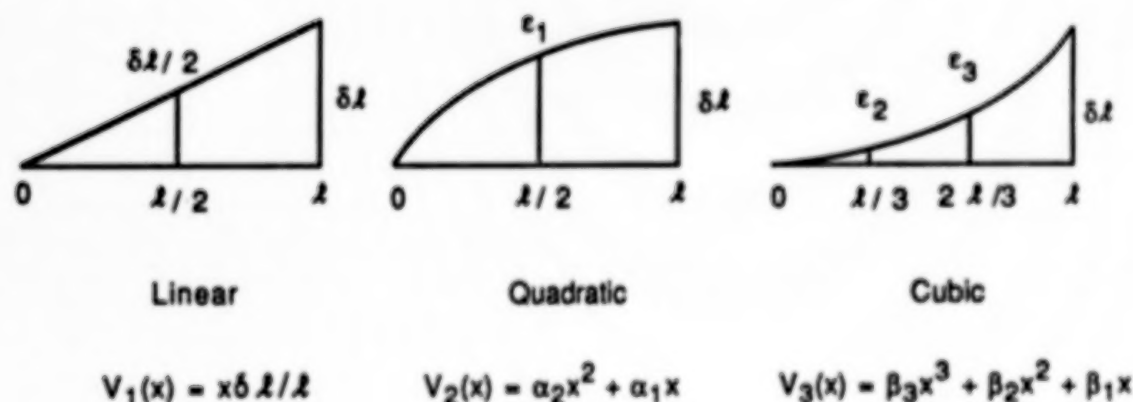


Figure 6

The first case of equivalence study is the truss with the point load p at the tip. For this, the finite element matrix equation, using linear shape function, is given in figure 7 where the stiffness matrix depends on the shape design variables b_i , $i=1,2$. The finite element matrix equation gives the solutions $z_1 = z(\ell/2) = p\ell/2EA$ and $z_2 = z(\ell) = p\ell/EA$ at the present design $b_1 = \ell/2$ and $b_2 = \ell$. Thus $z(x) = px/EA$ which is the exact solution of the truss with the point load p at the tip. If the design sensitivities of displacements at two nodal points, z_1 and z_2 , are desired, the adjoint equations are given in figure 7 with the adjoint solutions $\lambda^1(x) = x/EA$ for $0 \leq x \leq \ell/2$, $\lambda^1(x) = \ell/2EA$ for $\ell/2 \leq x \leq \ell$, and $\lambda^2(x) = x/EA$, respectively. These adjoint solutions are also exact.

FIRST CASE: TRUSS WITH THE POINT LOAD p AT THE TIP

(Linear Shape Function)

$$EA \begin{bmatrix} \frac{b_2}{b_1(b_2 - b_1)} & \frac{1}{b_1 - b_2} \\ \frac{1}{b_1 - b_2} & \frac{1}{b_2 - b_1} \end{bmatrix} \begin{bmatrix} z_1 \\ z_2 \end{bmatrix} = \begin{bmatrix} 0 \\ p \end{bmatrix} \quad z(x) = \frac{px}{EA} \text{ (exact)}$$

$$\frac{2EA}{\ell} \begin{bmatrix} 2 & -1 \\ -1 & 1 \end{bmatrix} \begin{bmatrix} \lambda_1^1 \\ \lambda_2^1 \end{bmatrix} = \begin{bmatrix} 1 \\ 0 \end{bmatrix} \quad \lambda^1(x) = \begin{cases} x/EA, & 0 \leq x \leq \ell/2 \\ \ell/2EA, & \ell/2 \leq x \leq \ell \end{cases} \text{ (exact)}$$

$$\frac{2EA}{\ell} \begin{bmatrix} 2 & -1 \\ -1 & 1 \end{bmatrix} \begin{bmatrix} \lambda_1^2 \\ \lambda_2^2 \end{bmatrix} = \begin{bmatrix} 0 \\ 1 \end{bmatrix} \quad \lambda^2(x) = \frac{x}{EA} \text{ (exact)}$$

Figure 7

Using the D-D method, design sensitivities for z_1 and z_2 are $z'_1 = p\delta l/2EA$ and $z'_2 = p\delta l/EA$, respectively, for the linear velocity as shown in figure 8. On the other hand, if the quadratic velocity is used, then $z'_1 = p\epsilon_1/EA$ and $z'_2 = p\delta l/EA$. Also for the cubic velocity, the D-D method yields $z'_1 = p(9\epsilon_2 + 9\epsilon_3 - \delta l)/16EA$ and $z'_2 = p\delta l/EA$. Now, using the C-D method, the design sensitivity expression is obtained as

$$z'_i = \int_0^l EA z_x \lambda_x^i V_x dx, \quad i = 1, 2$$

Using the finite element analyses results and the linear velocity in this design sensitivity expression, the C-D method gives $z'_1 = p\delta l/2EA$ and $z'_2 = p\delta l/EA$ which are the same as the results of the D-D method. Moreover, the design sensitivity expression yields $z'_1 = p\epsilon_1/EA$ and $z'_2 = p\delta l/EA$ for the quadratic velocity and $z'_1 = p(9\epsilon_2 + 9\epsilon_3 - \delta l)/16EA$ and $z'_2 = p\delta l/EA$ for the cubic velocity which are the same as the results of the D-D method. Thus, when the linear shape function is used for finite element model of the truss with the point load p , the D-D and C-D methods are equivalent for all parameterizations of velocity considered as indicated in the second column of figure 5. One point to emphasize in this case is that the original and adjoint responses of finite element models are the exact solutions of the truss with the point load. Note that the design sensitivity $z'_2 = p\delta l/EA$ is independent of the parameterizations of velocity for the C-D method.

DESIGN SENSITIVITY OF NODAL DISPLACEMENTS (First Case)

- D-D and C-D methods yield the same result for all parameterizations of velocity.

Linear Velocity	$z'_1 = p\delta l/2EA$	$z'_2 = p\delta l/EA$
Quadratic Velocity	$z'_1 = p\epsilon_1/EA$	$z'_2 = p\delta l/EA$
Cubic Velocity	$z'_1 = p(9\epsilon_2 + 9\epsilon_3 - \delta l)/16EA$	$z'_2 = p\delta l/EA$

Figure 8

The second case of study is the truss with the uniformly distributed load f along the truss. For this, using the quadratic shape function, the finite element matrix equation is obtained as given in figure 9. The solutions of the finite element matrix equation are $z_1 = z(\ell/2) = 3f\ell^2/8EA$ and $z_2 = z(\ell) = f\ell^2/2EA$ at the present design $b_1 = \ell/2$ and $b_2 = \ell$. Thus $z(x) = fx(-x+2\ell)/2EA$ which is the exact solution of the truss with the uniformly distributed load f . If the design sensitivities of z_1 and z_2 are desired, the adjoint equations are given in figure 9 with the adjoint solutions $\lambda^1(x) = (-3x^2/4\ell + 5x/4)/EA$ and $\lambda^2(x) = x/EA$, respectively. The adjoint solution $\lambda^2(x)$ is the same as in the linear shape function case which is the exact solution. On the other hand, the adjoint solution $\lambda^1(x)$ is different from the linear shape function case and not exact.

SECOND CASE: TRUSS WITH UNIFORMLY DISTRIBUTED LOAD f

(Quadratic Shape Function)

$$EA \begin{bmatrix} \frac{b_2^3}{3b_1^2(b_1 - b_2)^2} & -\frac{b_2^2}{3b_1(b_1 - b_2)^2} \\ -\frac{b_2^2}{3b_1(b_1 - b_2)^2} & \frac{4b_2^2 - 6b_1b_2 + 3b_1^2}{3b_2(b_1 - b_2)^2} \end{bmatrix} \begin{bmatrix} z_1 \\ z_2 \end{bmatrix} = \begin{bmatrix} \frac{f b_2^3}{6b_1(b_2 - b_1)} \\ \frac{f b_2(2b_2 - 3b_1)}{6(b_2 - b_1)} \end{bmatrix} \quad z(x) = \frac{fx(-x+2\ell)}{2EA} \text{ (exact)}$$

$$\frac{EA}{3\ell} \begin{bmatrix} 16 & -8 \\ -8 & 7 \end{bmatrix} \begin{bmatrix} \lambda_1^1 \\ \lambda_2^1 \end{bmatrix} = \begin{bmatrix} 1 \\ 0 \end{bmatrix} \quad \lambda^1(x) = \frac{-3x^2/4\ell + 5x/4}{EA} \text{ (approximate)}$$

$$\frac{EA}{3\ell} \begin{bmatrix} 16 & -8 \\ -8 & 7 \end{bmatrix} \begin{bmatrix} \lambda_1^2 \\ \lambda_2^2 \end{bmatrix} = \begin{bmatrix} 0 \\ 1 \end{bmatrix} \quad \lambda^2(x) = \frac{x}{EA} \text{ (exact)}$$

Figure 9

Using the D-D method, design sensitivities for z_1 and z_2 are $z_1' = 3f\ell\delta\ell/4EA$ and $z_2' = f\ell\delta\ell/EA$, respectively, for the linear velocity as shown in figure 10. On the other hand, if the quadratic velocity is used, then $z_1' = f\ell(\delta\ell + \epsilon_1)/2EA$ and $z_2' = f\ell\delta\ell/EA$. Also, for the cubic velocity, the D-D method yields $z_1' = f\ell(15\delta\ell + 9\epsilon_2 + 9\epsilon_3)/32EA$. Now, using the C-D method, the design sensitivity expression is obtained as

$$z_i' = \int_0^L (f\lambda^i + EA z_x \lambda_x^i) V_x dx, \quad i = 1, 2$$

Using the finite element analyses results and the linear velocity in this expression, the C-D method gives $z_1' = 3f\ell\delta\ell/4EA$ and $z_2' = f\ell\delta\ell/EA$ which are the same as the results of the D-D method. Also, using the finite element analyses results and the quadratic velocity in the design sensitivity expression, the C-D method gives $z_1' = f\ell(\delta\ell + \epsilon_1)/2EA$ and $z_2' = f\ell\delta\ell/EA$. These are the same as the results of the D-D method. However, the design sensitivity expression yields $z_1' = f\ell(42\delta\ell + 36\epsilon_2 + 9\epsilon_3)/80EA$ for the cubic velocity which is different from the result of the D-D method. Hence, it can be concluded that the D-D and C-D methods are not equivalent in the second case of study. Notice that the sensitivity results of the D-D method are the same as those of the C-D method up to the linear velocity when the linear shape function is used and up to the quadratic velocity when the quadratic shape function is used. Thus, the second case indicates the D-D and C-D methods might be equivalent under an additional condition that the shape function used in the finite element model is isoparametric with the discretization polynomial of the design velocity. However, this is not true as the results of the next case of study indicate.

DESIGN SENSITIVITY OF NODAL DISPLACEMENTS (Second Case)

	D - D	C - D
Linear Velocity	$\begin{aligned} z_1' &= 3f\ell\delta\ell/4EA \\ z_2' &= f\ell\delta\ell/EA \end{aligned}$	$\begin{aligned} z_1' &= 3f\ell\delta\ell/4EA \\ z_2' &= f\ell\delta\ell/EA \end{aligned}$
Quadratic Velocity	$\begin{aligned} z_1' &= f\ell(\delta\ell + \epsilon_1)/2EA \\ z_2' &= f\ell\delta\ell/EA \end{aligned}$	$\begin{aligned} z_1' &= f\ell(\delta\ell + \epsilon_1)/2EA \\ z_2' &= f\ell\delta\ell/EA \end{aligned}$
Cubic Velocity	$z_1' = f\ell(15\delta\ell + 9\epsilon_2 + 9\epsilon_3)/32EA$	$z_1' = f\ell(42\delta\ell + 36\epsilon_2 + 9\epsilon_3)/80EA$

Figure 10

The third case of study is the truss with the linearly varying load qx/l along the truss. Before carrying out design sensitivity computation, dependency of the external load on the shape design has to be defined as shown in figure 11. That is, as the length of the truss changes, the external load will maintain the form of qx/l . For this, using the quadratic shape function, the finite element matrix equation is given in figure 11. The matrix equation gives the solutions $z_1 = z(l/2) = 11ql^2/48EA$ and $z_2 = z(l) = ql^2/3EA$ at the present design $b_1 = l/2$ and $b_2 = l$. Thus $z(x) = qx(-3x+7l)/12EA$ which is not the exact solution of the truss with the linearly varying load. The same adjoint equations that are given in figure 9 are applicable in this case with the solutions $\lambda^1(x) = (-3x^2/4l + 5x/4)/EA$ and $\lambda^2(x) = x/EA$, respectively. As mentioned before, the adjoint solution $\lambda^1(x)$ is not exact, whereas $\lambda^2(x)$ is exact.

THIRD CASE: TRUSS WITH LINEARLY VARYING LOAD qx/l

(Quadratic Shape Function)

$$EA \begin{bmatrix} \frac{b_2^3}{3b_1^2(b_1 - b_2)^2} & -\frac{b_2^2}{3b_1(b_1 - b_2)^2} \\ -\frac{b_2^2}{3b_1(b_1 - b_2)^2} & \frac{4b_2^2 - 6b_1b_2 + 3b_1^2}{3b_2(b_1 - b_2)^2} \end{bmatrix} \begin{bmatrix} z_1 \\ z_2 \end{bmatrix} = \begin{bmatrix} \frac{qb_2^3}{12b_1(b_2 - b_1)} \\ \frac{qb_2(3b_2 - 4b_1)}{12(b_2 - b_1)} \end{bmatrix}$$

$$z(x) = \frac{qx(-3x+7l)}{12EA} \quad (\text{approximate})$$

Dependency of the External Load on Shape Design Variable

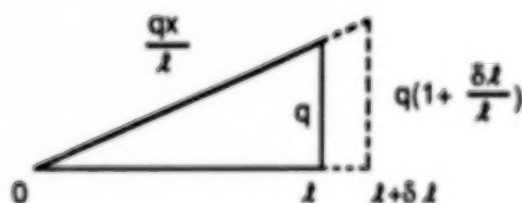


Figure 11

Using the D-D method, design sensitivities for z_1 and z_2 are $z'_1 = 11q\ell\delta\ell/16EA$ and $z'_2 = q\ell\delta\ell/EA$, respectively, for the linear velocity as shown in figure 12. On the other hand, if the quadratic velocity is used, then $z'_1 = q\ell(25\delta\ell + 16\epsilon_1)/48EA$. Also for the cubic velocity, the D-D method yields $z'_2 = q\ell\delta\ell/EA$. Now, using the C-D method, the design sensitivity expression is obtained as

$$z'_i = \int_0^{\ell} \left[\left(\frac{q}{\ell} \right) \lambda^i V + \left(\frac{qx}{\ell} \right) \lambda^i V_x + EA z_x \lambda^i_x V_x \right] dx, \quad i = 1, 2$$

Using the finite element analyses results and the linear velocity in this expression, the C-D method gives $z'_1 = 11q\ell\delta\ell/16EA$ and $z'_2 = q\ell\delta\ell/EA$ which are the same as the results of the D-D method. However, using the finite element analyses results and the quadratic velocity in the design sensitivity expression, the the C-D method gives

$z'_1 = q\ell(19\delta\ell + 292\epsilon_1)/240EA$, whereas it yields $z'_2 = q\ell(249\delta\ell + 27\epsilon_2 - 27\epsilon_3)/240EA$ for the cubic velocity. These are not the same as the results of the D-D method. Thus the D-D and C-D methods are not equivalent for the truss with a linearly varying load. Based on the equivalence study of truss problem, the D-D and C-D methods are possibly equivalent only for linear velocity. If this is the case, then both methods will give the exact design sensitivity information of the finite element analysis results that may not be acceptable at all. This is the situation for the fillet problem in reference 15 that the design sensitivity results of the C-D method agrees up to 5 to 6 digits with the finite difference even though the finite element model using constant stress triangular element does not provide accurate analysis result. On the other hand, when automatic regriding methods are employed for shape optimal design (refs. 16 and 17), parameterizations of the design velocity field cannot be limited to be only linear functions.

DESIGN SENSITIVITY OF NODAL DISPLACEMENTS (Third Case)


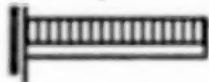

	D - D	C - D
Linear Velocity	$z'_1 = 11q\ell\delta\ell/16EA$ $z'_2 = q\ell\delta\ell/EA$	$z'_1 = 11q\ell\delta\ell/16EA$ $z'_2 = q\ell\delta\ell/EA$
Quadratic Velocity	$z'_1 = q\ell(25\delta\ell + 16\epsilon_1)/48EA$	$z'_1 = q\ell(19\delta\ell + 292\epsilon_1)/240EA$
Cubic Velocity	$z'_2 = q\ell\delta\ell/EA$	$z'_2 = q\ell(249\delta\ell + 27\epsilon_2 - 27\epsilon_3)/240EA$

Figure 12

The results of analytical equivalence study for a simple cantilever beam with moment of inertia I and length ℓ are given in figure 13. Like the truss problem, three lateral loading cases shown in figure 13 are considered. For all loading cases, Hermite cubic shape functions are used for the finite element model with one element. Also, for the design velocity $V(x)$, the same linear and quadratic parameterizations as in the truss problem are used. In addition to these, Hermitian parameterization of the velocity is used. That is, if the beam is fixed at $x=0$ and changes its length by $\delta \ell$ at $x=\ell$ and the slope of the velocity is zero at $x=0$ and θ at $x=\ell$, then the parameterization of the velocity is $V_4(x)$ as shown in figure 13 where γ_3 and γ_2 are given in terms of ℓ , $\delta \ell$, and

θ . For the equivalence study, design sensitivity of the tip displacement is considered. The results of equivalence study are summarized in figure 13. As in the truss case, the finite element model for the beam with the point load p at the tip yields the exact solutions of the original and adjoint structures. Hence the D-D and C-D methods give the same design sensitivity results for all parameterizations of velocity as shown in figure 13.

RESULTS OF EQUIVALENCE STUDY OF D-D AND C-D METHODS FOR BEAM

<div> <div>Loading Condition</div> <div>Design Velocity Field</div> </div>			
Linear	Same	Same	Same
Quadratic	Same	Not	Not
Hermitian	Same	Not	Not

Hermitian Velocity $V_4 = \gamma_3 x^3 + \gamma_2 x^2$ with $\gamma_3 = (\ell \theta - 2 \delta \ell) / \ell^3$, $\gamma_2 = (-\ell \theta + 3 \delta \ell) / \ell^2$

Figure 13

For the beam with the linearly varying load qx/ℓ along the beam, the finite element matrix equation is given in figure 14 with the solutions $z_1 = 11q\ell^4/120EI$ and $z_2 = q\ell^3/8EI$ at the present design $b = \ell$. Thus $z(x) = q\ell(18\ell x^2 - 7x^3)/120EI$ which is an approximate solution of the beam with linearly varying load. For the design sensitivity of z_1 , the solution of the adjoint equation given in figure 14 can be used. Using the D-D method, design sensitivity for z_1 is $z'_1 = 11q\ell^3\delta\ell/24EI$ for all parameterizations of velocity. For the C-D method, the design sensitivity expression is

$$z'_1 = \int_0^\ell \left\{ EI [3z_{xx}\lambda_{xx}V_x + (z_x\lambda_{xx} + z_{xx}\lambda_x) V_{xx}] + \left(\frac{q}{\ell}\right)\lambda V + \left(\frac{qx}{\ell}\right)\lambda V_x \right\} dx$$

Using the finite element analyses results in this design sensitivity expression, the C-D method yields $z'_1 = 11q\ell^3\delta\ell/24EI$ for the linear velocity which is the same as the result of the D-D method. However, the design sensitivity expression yields $z'_1 = q\ell^3(171\delta\ell - 12\epsilon_1)/360EI$ for the quadratic velocity and $z'_1 = q\ell^3(1194\delta\ell - 9\ell\theta)/2520EI$ for the Hermitian velocity which are not the same as the results of the D-D method. Thus the D-D method and C-D methods are not equivalent for the beam with linearly distributed load as indicated in figure 13. Based on the equivalence study of the beam problem, the D-D and C-D methods are possibly equivalent only for linear velocity.

DESIGN SENSITIVITY OF NODAL DISPLACEMENT FOR BEAM

(Linearly Varying Load qx/ℓ)

$$\frac{EI}{b^3} \begin{bmatrix} 12 & -6b \\ -6b & 4b^2 \end{bmatrix} \begin{bmatrix} z_1 \\ z_2 \end{bmatrix} = \begin{bmatrix} \frac{7qb}{20} \\ -\frac{qb^2}{20} \end{bmatrix}$$

$$z(x) = \frac{q\ell(18\ell x^2 - 7x^3)}{120EI} \quad (\text{approximate})$$

$$\frac{EI}{b^3} \begin{bmatrix} 12 & -6b \\ -6b & 4b^2 \end{bmatrix} \begin{bmatrix} \lambda_1 \\ \lambda_2 \end{bmatrix} = \begin{bmatrix} 1 \\ 0 \end{bmatrix}$$

$$\lambda(x) = \frac{x^2(3\ell - x)}{6EI} \quad (\text{exact})$$

D - D

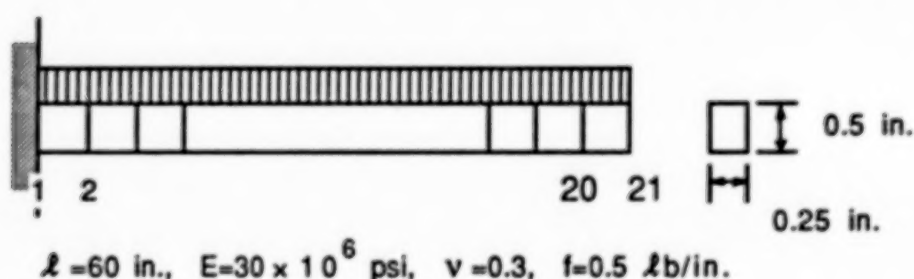
C - D

Linear Velocity	$z'_1 = 11q\ell^3\delta\ell/24EI$	$z'_1 = 11q\ell^3\delta\ell/24EI$
Quadratic Velocity	$z'_1 = 11q\ell^3\delta\ell/24EI$	$z'_1 = q\ell^3(171\delta\ell - 12\epsilon_1)/360EI$
Hermitian Velocity	$z'_1 = 11q\ell^3\delta\ell/24EI$	$z'_1 = q\ell^3(1194\delta\ell - 9\ell\theta)/2520EI$

Figure 14

Next, a numerical study is carried out for the C-D method using the cantilever beam with the uniformly distributed load to see effect of accuracy of the finite element analysis results on accuracy of the design sensitivity informations obtained. The finite element models with 1, 2, and 20 elements are considered for numerical study. Node numbering for all finite element models starts at the clamped end of the beam and the node number of free end of the beam is $(m+1)$ where m is the number of elements in the model. The beam is 60 in. long and has a uniform rectangular cross-section of 0.5 in. high and 0.25 in. wide. Young's modulus, Poisson's ratio, and uniformly distributed load are $E=30 \times 10^6$ psi, $\nu=0.3$, and $f=0.5$ lb/in., respectively. Finite element analysis is carried out using ANSYS finite element STIF4. Three parameterizations of velocity with 1% perturbation of the length $\ell=60$ in. of the beam are used for numerical study as shown in figure 15. Once the solutions of the original and adjoint structural system are obtained using ANSYS, the continuum design sensitivity expression is numerically integrated using three points Gauss quadrature.

CONTINUUM-DISCRETE METHOD FOR A CANTILEVER BEAM



ANSYS STIF4

Parameterizations of Velocity for Numerical Study of the C-D Method

Case	Design Velocity Type	Parameter Values
A	Linear	$\delta \ell = 0.6$ in.
B	Quadratic	$\delta \ell = 0.6$ in. and $\epsilon_1 = 10$ in.
C	Hermitian	$\delta \ell = 0.6$ in. and $\theta = -0.3$

Figure 15

To check accuracy of the design sensitivity obtained, the results are compared with the results obtained by finite difference as shown in figures 16 and 17. In these figures, $z(l-\delta l)$ and $z(l+\delta l)$ are the displacements of selected nodal points for perturbed backward and forward designs, respectively, $\Delta z = z(l+\delta l) - z(l-\delta l)$ is the finite difference, and z' is the difference predicted by the design sensitivity. The ratio of z' and Δz times 100 can be used as a measure of accuracy of the design sensitivity. In figures 16 and 17, for all finite element models, the case A with linear velocity yields excellent agreement between the design sensitivity z' and the finite difference Δz . This confirms with the results of analytic study that the D-D and C-D methods may be equivalent for linear velocity. On the other hand, for one element model, the design sensitivity z' and the finite difference Δz do not agree at all for other parameterizations (cases B and C) of velocity as can be seen in figure 16. For cases B and C, the agreements improve substantially for two elements model.

COMPARISON OF DESIGN SENSITIVITY OF THE C-D METHOD

One Element Model

Case	Node No.	$z(l-\delta l)$	$z(l+\delta l)$	Δz	z'	$(z'/\Delta z \times 100)\%$
A	2	0.99593E+00	0.10789E+01	0.41476E-01	0.41471E-01	100.0
B	2	0.99593E+00	0.10789E+01	0.41476E-01	-0.47926E-01	-115.6
C	2	0.99593E+00	0.10789E+01	0.41476E-01	0.64970E-01	156.6

Two Elements Model

Case	Node No.	$z(l-\delta l)$	$z(l+\delta l)$	Δz	z'	$(z'/\Delta z \times 100)\%$
A	2	0.35273E+00	0.38210E+00	0.14689E-01	0.14688E-01	100.0
	3	0.99593E+00	0.10789E+01	0.41476E-01	0.41471E-01	100.0
B	2	0.17939E+00	0.59469E+00	0.20765E+00	0.20744E+00	99.9
	3	0.99593E+00	0.10789E+01	0.41476E-01	0.35880E-01	86.5
C	2	0.30947E+00	0.42955E+00	0.60040E-01	0.61126E-01	101.8
	3	0.99593E+00	0.10789E+01	0.41476E-01	0.42939E-01	103.5

Figure 16

On the other hand, for twenty elements model, agreements become excellent as shown in figure 17. This confirms the fact that accurate design sensitivity informations can be obtained as long as accurate finite element analysis results are used for the C-D methods. This fact is not the case for the semi-analytic method, as demonstrated by Barthelemy and Haftka (ref. 5). They found that the design sensitivity error of the semi-analytic method is proportional to the square of the number of elements. This is completely opposite behavior from the C-D method since the design sensitivity error increases very rapidly as the finite element analysis results of the original structure become more accurate. As demonstrated in figures 16 and 17, an essential advantage that may accrue in the C-D method is associated with the ability to identify the effect of numerical error associated with finite element analysis results. That is, if disagreement arises between the design sensitivity of the C-D method and the finite difference, then error has crept into the finite element approximation. If the D-D method is used, in which the structure is discretized and the design variables are imbedded into the stiffness matrix, then any error inherent in the finite element model is consistently parameterized and will never be reported to the user. Therefore, precise design sensitivity coefficients of the matrix model of the structure are obtained without realizing that there may be substantial inherent error in the original model. On the other hand, the C-D method can be used to obtain a warning that approximation error is creeping into the finite element model.

COMPARISON OF DESIGN SENSITIVITY OF THE C-D METHOD (Cont)

Twenty Elements Model

Case	Node No.	$z(l-\delta l)$	$z(l+\delta l)$	Δz	z'	$(z'/\Delta z \times 100)\%$
A	2	0.48158E-02	0.52169E-02	0.20055E-03	0.20053E-03	100.0
	6	0.10504E+00	0.11379E+00	0.43744E-02	0.43739E-02	100.0
	11	0.35273E+00	0.38210E+00	0.14689E-01	0.14688E-01	100.0
	16	0.66525E+00	0.72066E+00	0.27704E-01	0.27701E-01	100.0
	21	0.99593E+00	0.10789E+01	0.41476E-01	0.41471E-01	100.0
B	2	0.70800E-03	0.13220E-01	0.62558E-02	0.62566E-02	100.0
	6	0.29727E-01	0.22933E+00	0.99800E-01	0.10127E+00	101.5
	11	0.17939E+00	0.59469E+00	0.20765E+00	0.21023E+00	101.2
	16	0.50771E+00	0.89205E+00	0.19217E+00	0.19269E+00	100.3
	21	0.99593E+00	0.10789E+01	0.41476E-01	0.41467E-01	100.0
C	2	0.47614E-02	0.52749E-02	0.25676E-03	0.25673E-03	100.0
	6	0.95061E-01	0.12480E+00	0.14869E-01	0.14863E-01	100.0
	11	0.30947E+00	0.42955E+00	0.60040E-01	0.60046E-01	100.0
	16	0.60858E+00	0.78134E+00	0.86383E-01	0.86384E-01	100.0
	21	0.99593E+00	0.10789E+01	0.41476E-01	0.41470E-01	100.0

Figure 17

00136

REFERENCES

1. Haftka, R. T. and Grandhi, R. V., "Structural Shape Optimization - A Survey," Computer Methods in Applied Mechanics and Engineering, Vol. 57, No. 1, 1986, pp. 91-106.
2. Carmarda, C. J. and Adelman, H. M., "Implementation of Static and dynamic Structure Sensitivity Derivative Calculations in the Finite-Element-Based Engineering Analysis Language System (EAL)," NASA TM-85743, 1984.
3. Nagendra, G. K. and Fleury, C., "Sensitivity and Optimization of Composite Structures Using MSC/NASTRAN," NASA Conference Publication, 2457, 1986, pp.147-159.
4. Fleury, C., "Computer Aided Optimal Design of Elastic Structures," Computer Aided Optimal Design: Structural and Mechanical Systems, (Ed. C. A. Mota Soares), Springer-Verlag, Heidelberg, 1987, pp. 831-900.
5. Barthelemy, B M. and Haftka, R. T., "Accuracy Analysis of the Semi-Analytical Method for Shape Sensitivity Calculation," AIAA Paper 88-2284-CP, 29th AIAA/ASME/ASCE/AHS Structures, Structural Dynamics and Materials Conf.,1988
6. Cea, J., "Problems of Shape Optimal design," Optimization of Distributed Parameter Structures, E. J. Haug and J. Cea (Eds.), Sijthoff & Noordhoff, Alphen aan den Rijn, The Netherlands, 1981, pp. 1005-1048.
7. Zolesio, J. P., "The Material Derivative (or Speed) Method for Shape Optimization," Optimization of Distributed Parameter Structures, E. J. Haug and J. Cea (Eds.), Sijthoff & Noordhoff, Alphen aan den Rijn, The Netherlands, 1981, pp. 1089-1151.
8. Choi, K. K. and Haug, E. J., "Shape Design Sensitivity Analysis of Elastic Structures," J. of Struct. Mechanics, Vol. 11, No. 2, 1983, pp.231-269.
9. Dems, K. and Mroz, Z., "Variational Approach by Means of Adjoint Systems to Structural Optimization and sensitivity Analysis -II, Structural Shape Variation," Int. J. Solids and Struct., Vol. 20, No. 6, 1984, pp. 527-552.
10. Choi, K. K. and Seong, H. G., "A Domain Method for Shape Design Sensitivity Analysis of Built-up Structures," Comp. Methods in Applied Mech. and Eng., Vol. 57, No. 1, 1986, pp. 1-15.
11. Haug, E. J., Choi, K. K., and Komkov, V., Design Sensitivity Analysis of Structural Systems, Academic Press, New York, 1986.
12. Choi, K. K. and Haug, E. J., "Shape Design Sensitivity Analysis of Elastic Structures," J. of Struct. Mechanics, Vol. 11, No. 2, 1983, pp.231-269.
13. Yang, R. J. and Botkin, M. E., "Accuracy of The Domain Method for The Material Derivative Approach to Shape Design Sensitivities," Sensitivity Analysis in Engineering, NASA Conference Publication 2457, 1987, pp. 347-353.

14. Cardoso, J. B. and Arora, J. S., "Design Sensitivity Analysis of Nonlinear Structural Response," Sensitivity Analysis in Engineering, NASA Conference Publication 2457, 1987, pp. 113-132.
15. Haber, R. B., "A New Variational Approach to Structural Shape Design Sensitivity Analysis," Computer Aided Optimal Design: Structural and Mechanical Systems, (Ed. C. A. Mota Soares), Springer-Verlag, Heidelberg, 1987, pp. 573-587.
16. Yao, T-M and Choi, K. K., "3-D Shape Optimal Design and Automatic Finite Element Regridding," IJNME, Jan., 1989.
17. Belegundu, A. D. and Rajan, S. D., "A Shape Optimization Approach Based on Natural Design Variables and Shape Functions," Computer Methods in Applied Mechanics and Engineering, No. 66, 1988, pp. 87-106.

An Investigation of Using an RQP Based Method to Calculate Parameter Sensitivity Derivatives

**Todd J. Beltracchi
Graduate Student**

**Gary A. Gabriele
Assistant Professor**

**Department of Mechanical Engineering,
Aeronautical Engineering & Mechanics**

**Rensselaer Polytechnic Institute
Troy, N.Y. 12180-3590**

Parameter Sensitivity Analysis

Estimation of the sensitivity of problem functions with respect to problem variables forms the basis for many of our modern day algorithms for engineering optimization. The most common application of problem sensitivities has been in the calculation of objective function and constraint partial derivatives for determining search directions and optimality conditions. A second form of sensitivity analysis, parameter sensitivity, has also become an important topic in recent years. By parameter sensitivity, we refer to the estimation of changes in the modeling functions and current design point due to small changes in the fixed parameters of the formulation. Methods for calculating these derivatives have been proposed by several authors (Armacost and Fiacco 1974, Sobieski et al 1981, Schmit and Chang 1984, and Vanderplaats and Yoshida 1985). Two drawbacks to estimating parameter sensitivities by current methods have been: (1) the need for second order information about the Lagrangian at the current point, and (2) the estimates assume no change in the active set of constraints. This paper addresses the first of these two problems and proposes a new algorithm that does not require explicit calculation of second order information.

The estimation of changes in the modeling functions and design point due to small changes in the fixed parameters of the formulation.

Standard Form of NLP Parameter Sensitivity Problem

To provide a framework about which to address the problem of parameter sensitivity analysis, we state the following standard form of the nonlinear programming problem which explicitly represents the problem parameters.

In the formulation given, we assume that the problem functions f , g , and h can be either linear or nonlinear functions of the design variables but we are concerned primarily with the nonlinear case. We assume that the problem parameters p , are held fixed during the course of the optimization, and the optimal solution point, x^* , satisfies the first order Kuhn-Tucker optimality conditions.

$$\begin{array}{ll}
 \text{Minimize} & f(x, p) \\
 \text{Subject to} & h_l(x, p) = 0 \quad l = 1, L \\
 & g_j(x, p) \geq 0 \quad j = 1, J \\
 & x_{\min} \leq x \leq x_{\max} \\
 & x = (x_1, x_2, \dots, x_n) \\
 & p = (p_1, p_2, \dots, p_k)
 \end{array}$$

OBJECTIVE: For a given p , find x^* , that satisfies the above problem. We are then interested in the effects of variations in p on the optimum.

$$\text{Given: } p_i' = p_i + \Delta p_i$$

$$\text{Find: } f(x^*, p'), x_{\text{new}}^*$$

Required Formulas

For any change in the parameter Δp_i , the new optimum value of the objective function or design variables can be estimated from the following linear extrapolations:

Extrapolations based on these equations are bounded by the assumption that the active set remains the same.

$$f(x^*, p') = f(x^*_{old}) + \Delta p_i \frac{df^*}{dp_i}$$

$$x^*_{new} = x^*_{old} + \Delta p_i \frac{\partial x^*}{\partial p_i}$$

where

$$\frac{df^*}{dp_i} = \frac{\partial f}{\partial p_i} + \sum_{l=1}^L v_l \frac{\partial h_l}{\partial p_i} - \sum_{j=1}^J u_j \frac{\partial g_j}{\partial p_i}$$

$$\frac{df^*}{dp_i} = \frac{\partial f}{\partial p_i} + \frac{\partial f^T}{\partial x} \frac{\partial x^*}{\partial p_i}$$

Derivatives to be determined:

$$\frac{\partial f}{\partial p_i}, \quad \frac{\partial x^*}{\partial p_i}, \quad \frac{\partial h_l}{\partial p_i}, \quad \frac{\partial g_j}{\partial p_i}$$

Methods for Calculating Parameter Sensitivities

The Brute Force Method

The brute force method is probably the most common method used to study the effect of problem parameters on solutions. The method is simply to change the parameter and then reoptimize the problem with the new value. This of course gives the truest indication of the effect of the parameter on the solution. A variation of the brute force method was proposed by Armacost and Fiacco (1974) and McKeown (1980) to calculate parameter sensitivities based on the central difference approximation given below.

Given the incremental change Δ in p_i , reoptimize the original problem at the new value of p . The sensitivity derivatives are given by the difference formulas.

$$\frac{df^*}{dp_i} = \frac{f(x^*, p_i + \Delta p_i) - f(x^*, p_i - \Delta p_i)}{2\Delta p_i}$$

$$\frac{\partial x^*}{\partial p_i} = \frac{x^*(p_i + \Delta p_i) - x^*(p_i - \Delta p_i)}{2\Delta p_i}$$

Methods for Calculating Parameter Sensitivities

Kuhn-Tucker Method

A more accurate estimate of the sensitivity derivatives can be found by differentiating the Kuhn-Tucker optimality conditions with respect to a parameter. We refer to this as the Kuhn-Tucker method. The set of Kuhn-Tucker sensitivity equations have been derived independently by several authors (Armstrong and Fiacco 1974, McKeown 1980, Sobieski et al. 1981) and result in the following linear system of equations.

Differentiate the Kuhn-Tucker conditions wrt to p_i and solve the resulting linear system for the desired derivatives.

$$\begin{bmatrix} \nabla_x^2 L & -\nabla_x(h,g) \\ \nabla_x(h,g)^T & 0 \end{bmatrix} \begin{bmatrix} \frac{\partial x^*}{\partial p_i} \\ \frac{\partial(v,u)}{\partial p_i} \end{bmatrix} + \begin{bmatrix} \frac{\partial \nabla_x L}{\partial p_i} \\ \frac{\partial(h,g)}{\partial p_i} \end{bmatrix} = 0$$

Methods for Calculating Parameter Sensitivities

Extended Design Space Method

The final category of parameter sensitivity methods has been proposed by Vanderplaats (1984,1987). The method, known as the extended design space (EDS) method, is based on using feasible directions for estimating parameter sensitivity derivatives. The method extends the design space and solves the following subproblem to obtain the sensitivity derivatives. Both first and second order estimates have been developed for the method (Vanderplaats and Yoshida 1985).

The fixed parameter p_i is added to the set of design variables,

$$x_{n+1} = p_i$$

Solve the following subproblem for s ,

$$\begin{array}{ll} \min & \nabla_x f^T s \\ \text{st.} & g_j + \nabla_x g_j^T s \geq 0 \quad j=1,J \end{array}$$

Calculate desired sensitivities from

$$\frac{\partial x}{\partial p_i} = (s_1, s_2, \dots, s_n) / s_{n+1}$$

$$\frac{df}{dp} = \frac{\partial f}{\partial p} + \frac{\partial f^T}{\partial x} \frac{\partial x}{\partial p}$$

Assessment of Current Methods for Calculating Parameter Sensitivities

As evidenced by their lack of extensive use, all the methods discussed above have some drawback associated with their use. Because the problem has to be reoptimized for several different values of the parameters, the efficiency of the Brute Force method is affected by the difficulty of the problem and the efficiency of the method used in the reoptimization. This approach is useful in studying large variations in parameters by plotting the response of the optimum versus the parameter, and has been used by Arbuckle and Sliwa (1984) and Robertson and Gabriele (1987).

The Kuhn-Tucker method is also computationally expensive because it requires second derivatives of the objective function and the active constraints. For most engineering design problems, this type of information may be difficult to obtain. This method requires that the strict complementarity and linear independence assumptions hold at the optimal design.

Finally, the first order ESD method is a very efficient, easy to implement method but it can provide inaccurate estimates of $\partial x^*/\partial p$ when the problem is not fully constrained and it does not provide $\partial u/\partial p_j$. The second order EDS method requires the calculation of second derivatives and also requires the solution of a quadratic approximating problem for each value of the parameter that is studied. However, the second order EDS method has the advantage of not being affected by changes in the active set.

Brute Force Method: Most commonly used method, provides accurate results, but inefficient.

Kuhn-Tucker Method: Sound mathematical basis, but assumes no changes in the active set and requires second order information.

Extended Design Space: Very efficient, easy to implement, but may not produce accurate estimates of $\partial x/\partial p$ and does not provide $\partial u/\partial p$

141

A Proposal for a New Method

From the previous discussion, we can deduce that what is needed to improve current methods for parameter sensitivity analysis is an algorithm that does not require second derivatives, is able to accurately predict the sensitivity derivatives, and can calculate sensitivities at degenerate points. In this paper, we propose using a new algorithm based on the Recursive Quadratic Programming (RQP) method for accomplishing these goals.

Our reasoning for such a method is based on the following virtues of the RQP method. In terms of number of function evaluations, the RQP method appears to be one of the most efficient methods available. This has been demonstrated in any of the published comparison studies in which codes for these methods were participants (Schittkowski, 1980 and Belegundu and Arora, 1985). Although the method is sensitive to variable and objective function scaling, it is not sensitive to constraint scaling. Finally, the RQP method provides an estimate of the Hessian of the Lagrangian, which can be useful for other purposes, and it is very efficient at locating an optimum, when the starting point is close to the true optimum. Both of these last advantages will be exploited in the development of our method for sensitivity estimation based on the RQP method.

Proposal:

Employ the Recursive Quadratic Programming Method (RQP) in conjunction with the Brute Force Method to estimate the required derivatives.

Reasoning:

The RQP method is very efficient when started near the optimum solution.

If the RQP method is used to solve the original problem, an approximation of the Hessian of the Lagrangian will be available.

Estimates of all derivatives, including $\partial u / \partial p$ can be developed.

The Recursive Quadratic Programming Method

All RQP methods use the same basic strategy of linearizing the constraints and approximating the Hessian of the Lagrangian to form a quadratic programming (QP) subproblem. The QP subproblem is then solved for the search direction s and a new estimate of the Lagrange multipliers of the constraints. The search direction s is then used to calculate a new estimate of the optimum.

The step length α is determined by minimizing a line search penalty function P of the general form given below, where Ω represents some combination of the constraints and the Lagrange multipliers. The penalty function attempts to assure that both the objective function and the violation of the constraints are reduced. As the method converges, the step length α which minimizes $P(x,u,v,R)$ approaches 1.

Form the following subproblem to determine a search direction s

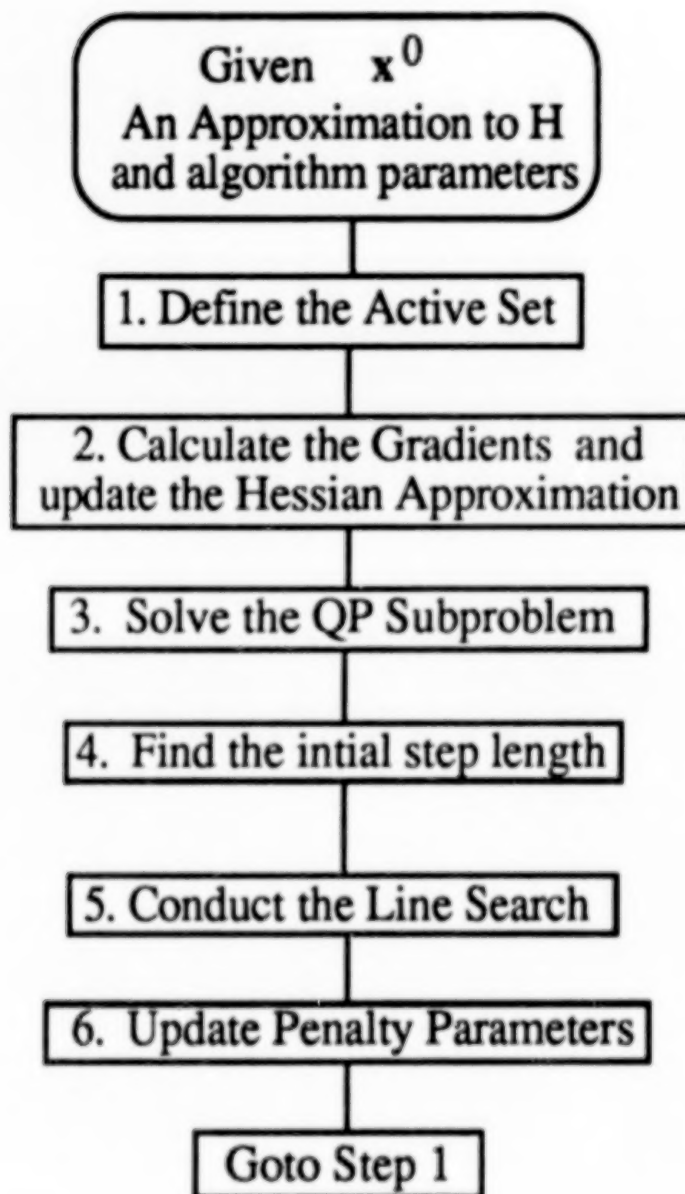
$$\begin{aligned} &\text{Minimize } 0.5 \ s^T B \ s + s^T \nabla f \\ &\text{subject to } \nabla h^T s + h = 0 \\ &\qquad \qquad \nabla g^T s + g \geq 0 \end{aligned}$$

Using s , perform a linear search to determine a new estimate of x^* by minimizing a penalty function of the following general form,

$$P(x,u,v,R) = f(x) + R * \Omega(h,g,u,v)$$

Basic Flowchart of RQP Method

The basic flowchart of the RQP method is given below. Several good implementations of the RQP method are available (Beltracchi and Gabriele 1987, Arora and Tseng 1987, Bartholomew-Biggs 1987, or Gill, et al. 1986). A more complete discussion of RQP methods can be found in (Beltracchi 1985 or Beltracchi and Gabriele 1988).



The RQP Sensitivity Algorithm

The new algorithm is based on combining the simplicity of the brute force method with the efficiency of the RQP method. The two characteristics of the RQP method that we feel can be exploited for determining parameter sensitivities are (1) an approximation to the Hessian of the Lagrangian is developed, and (2) if this approximation is exact (or close) then the RQP method will quickly and efficiently solve the perturbed problem. In other words, if we can develop good Hessian approximations, the RQP method is equivalent to applying Newton's method to solve the Kuhn-Tucker conditions for the perturbed problem, which may require only 1 or 2 iterations of RQP. The small number of iterations, coupled with the fact that the RQP method should require only a one step line search, should allow the reoptimizations to occur without the need for many function evaluations.

The end result of combining the differencing equations and the RQP method is a means to estimate the parameter sensitivities without the need to calculate higher order derivatives, and without an excessive number of function evaluations. Based on the above arguments, we propose the following procedure to calculate parameter sensitivity derivatives.

Step 0. Given an optimal solution x^* , f^* , u^* , an active set of constraints, and an approximation to the Hessian of the Lagrangian, all achieved by convergence of the RQP method (using the SR1/PD/BFS update).

Step 1. Perturb the fixed parameter p_i to $p_i^+ = p_i^* + \Delta p_i$ where Δp_i is some small perturbation to p_i .

Step 2. Perform two complete iterations of the RQP method. During the RQP iterations, update the Hessian approximation. From the results of the RQP iterations obtain f^+ , x^+ , u^+ , and g_j^+ $j \in$ active set.

Step 3. Perturb the fixed parameter p_i to $p_i^- = p_i^* - \Delta p_i$.

Step 4. Start from $x_0 = x^*(p_i^*) - \frac{\partial x}{\partial p_i} \Delta p_i$ where $\partial x / \partial p_i$ is calculated using forward differencing approximations and $x^*(p_i^*)$ and $x^*(p_i^* + \Delta p_i)$ from step 2. Perform one complete iteration of the RQP method to find f^- , x^- , u^- , and g_j^- $j \in$ active set.

Step 5. Obtain estimates for the sensitivity derivatives from the following central difference approximations

$$\frac{df^*}{dp} = \frac{f^+ - f^-}{2\Delta p}; \quad \frac{\partial x^*}{\partial p} = \frac{x^+ - x^-}{2\Delta p}$$

$$\frac{\partial u^*}{\partial p} = \frac{u^+ - u^-}{2\Delta p}$$

Equivalence to the Kuhn-Tucker Method

The major questions to be answered about the proposed algorithm are does it provide the desired sensitivities, and what are the possible sources of error. An investigation of the theoretical properties of the RQP based sensitivity algorithm reveals that in the limit, as Δp goes to zero, the new method provides an estimate to the solution of the equations given below. These equations are equivalent to the Kuhn-Tucker sensitivity equations with the Hessian of the Lagrangian replaced by an approximation **B** that is provided by the RQP method. The details of this derivation are too lengthy to be presented here but are included in (Beltracchi 1988). From the above, we can see that the new algorithm will provide accurate estimates of the parameter sensitivities if **B** is a good approximation of $\nabla_x^2 L$, and the differencing formula is a good approximation of the equations below.

It can be shown that the proposed method is equivalent to the following linear set of equations,

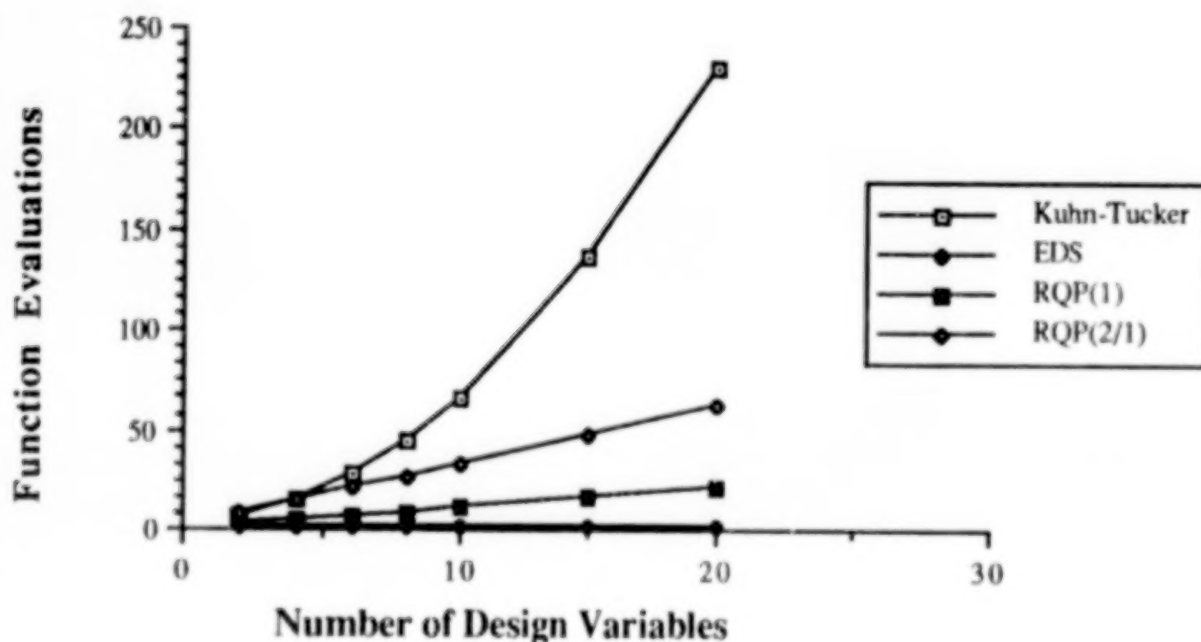
$$\begin{bmatrix} \mathbf{B} & -\nabla_x \mathbf{g} \\ \nabla_x \mathbf{g}^T & \mathbf{0} \end{bmatrix} \begin{bmatrix} \frac{\partial \mathbf{x}}{\partial \mathbf{p}} \\ \frac{\partial \mathbf{u}}{\partial \mathbf{p}} \end{bmatrix} + \begin{bmatrix} \frac{\partial \nabla_x L}{\partial \mathbf{p}} \\ \frac{\partial \mathbf{g}}{\partial \mathbf{p}} \end{bmatrix} = \mathbf{0}$$

These equations are the Kuhn-Tucker equations with the Hessian Approximation **B** replacing $\nabla_x^2 L$.

EFFICIENCY OF SENSITIVITY ALGORITHMS

As a measure of the efficiency of the new method, we present a comparison of the number of function evaluations required by the competing algorithms. The graph below represents the number of function evaluations required by various algorithms to find the sensitivity of the first parameter to be studied. The results are plotted for various problem sizes where n is the number of design variables.

Most of the work associated with the Kuhn-Tucker method is incurred when the Hessian matrix is calculated. For the first order EDS method, the work does not increase with problem size. However, as mentioned before, the method is not always accurate and $\partial u/\partial p$ is not determined. Each of the RQP methods is either more efficient or as efficient when compared to the Kuhn-Tucker method for small problems ($n < 5$), and considerably more efficient for larger problems ($n > 5$).



The SR1/PD/BFS Update

A major concern of the new algorithm is how well the Hessian approximation delivered from the RQP method agrees with the true Hessian. Toward this end, considerable research was conducted to find a variable metric update that provides good Hessian approximations without degrading the performance of the RQP algorithm. The two leading candidates were the Broyden-Fletcher-Shanno (BFS) method, and the Symmetric Rank One (SR1) method.

The SR1/PD/BFS (Symmetric Rank One/ Positive Definite/ Broyden Fletcher Shanno) is a hybrid variable metric update that combines the best features of the SR1 and BFS updates (Beltracchi 1988). The SR1 update has the advantage of not requiring exact line searches and producing good Hessian approximations, however it has the drawbacks of being undefined or producing indefinite Hessian approximations for some problems. The BFS update has the advantage of being self correcting; however, it has the drawback of requiring exact line searches, and the Hessian approximation does not converge unless fairly accurate line searches are performed. The SR1/PD/BFS update uses the BFS update when the SR1 update is undefined or likely to produce an indefinite Hessian approximation. The PD stands for a positive definite check (implemented in step 4), used to insure the new Hessian approximation is positive definite. Testing in Beltracchi (1988) found the SR1/PD/BFS update produced the best Hessian approximations.

(Symmetric Rank One / Positive Definite / Broyden Fletcher Shanno)

1. Calculate $y^T(By - z)$
2. If $\text{abs}(y^T(By - z)) \leq 10^{-10}$ goto step 7
3. Calculate ϕ^*, ϕ :

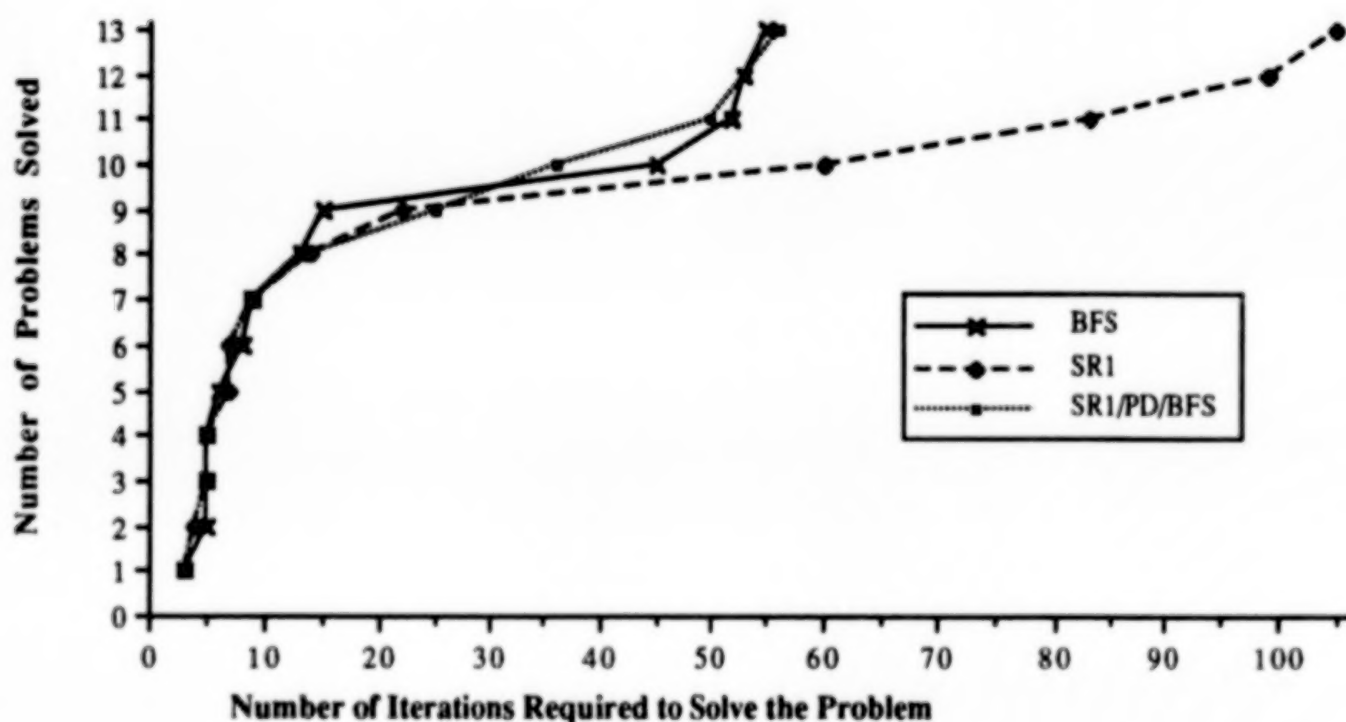
$$\phi^* = \frac{(y^T z)^2}{(y^T z)^2 - z^T B z \ y^T B^{-1} y}$$

$$\phi = \frac{y^T z}{y^T z - z^T B z}$$

4. If $\phi \leq \phi^*$ goto step 7.
5. If $y^T z \leq 0$ and $y^T(By - z) \leq 0$ goto step 7.
6. Update Hessian approximation using the SR1 update and return.
7. Update Hessian approximation using the BFS update and return.

PERFORMANCE OF NEW SR1/PD/BFS UPDATE

This slide shows the performance of the new SR1/PD/BFS variable metric update when implemented within the RQP method on a set of 13 commonly used test problems. The method is compared with the BFS and the SR1 method. We see from this plot that the new update provides the same level of robustness and efficiency as the BFS method and is generally more efficient than the SR1 method.



Convergence of the Hessian Approximation for Various Updates in Broyden's Family

This table shows the ability of the tested variable metric updates to approximate the Hessian of the Lagrangian on a set of test problems. Analytical Hessians were developed for each test problem and compared to the approximated Hessian returned from the RQP method. The entries in the table report the Frobenius norms of the difference between the known optimal Hessian, and the identity matrix, and with the final approximate Hessian. From this we see that the new SR1/PD/BFS update returned approximations that were as good or better than the BFS method in all cases, and better than the SR1 method in all but one case. In this instance (Woods), the scaling of the objective function affected the final result. The last two rows demonstrate that scaling the objective allowed the new update to improve the approximation considerably.

Problem	$\ H^*-I\ _F$	BFS	SR1	SR1/PD/BFS
RTS01	2.291	1.396	0.061	0.0008
RTS01/100	1.377	0.0183	0.974	0.00023
RTS01*100	369.12	206.7	0.243	0.243
RTS02 st pt 1	7.384	3.00	3.0	3.0
RTS02 st pt 2	7.384	5.430	0.0	0.0
RTS03	15.93	7.76	0.105	0.105
RTS04	23.28	3.623	9.307	3.356
Woods	1352.46	141.3	17.17	75.38
Woods/100	13.54	1.908	0.184	0.0944
Woods/1000	1.394	0.0283	0.974	0.113

TESTING OF RQP SENSITIVITY ALGORITHM

INITIAL TEST SET

Two phases were employed in testing the new algorithm. The first phase involved a test set of known characteristics, whose Hessians and sensitivity derivatives could be determined analytically. The initial test set involved 4 test problems with 3-4 parameters each. Various algorithm parameters were studied, such as the step size Δp , as well as the effectiveness of the SR1/PD/BFS update, the number of RQP iterations to allow for solving the perturbed problem, and the updating of the Hessian approximation during the sensitivity analysis. The table below provides a sample of the results obtained on this initial test set using the RQP based sensitivity algorithm. The entries represent the error in the sensitivity derivatives obtained from the new algorithm and the known sensitivities. The errors were calculated using the formulas established by Sandgren (1977).

The results shown here were fairly typical of the results obtained on all the test problems in the initial test set. In general, the results are very good and certainly usable for engineering purposes.

	PROBLEM 1			PROBLEM 2	
	p 1	p 2	p 3	p 1	p 2
$\frac{df}{dp}$.0002(10 ⁻⁹)	1.9(10 ⁻⁵)	0.126(10 ⁻⁶)	0.139(10 ⁻⁶)	0.00
ϵ_x	0.00	7.9(10 ⁻⁵)	3.11(10 ⁻⁷)	9.08(10 ⁻⁷)	2.00(10 ⁻⁷)
ϵ_u	0.00	2.66(10 ⁻³)	1.55(10 ⁻⁶)	9.79(10 ⁻⁷)	1.43(10 ⁻⁹)
ϵ_g				6.33(10 ⁻⁷)	0.00

TESTING OF RQP SENSITIVITY ALGORITHM ENGINEERING TEST PROBLEMS

The second phase of the testing consisted of applying the new algorithm to a set of engineering test problems where known sensitivities and Hessians could not be developed analytically. To determine the accuracy of the sensitivity derivatives returned by the new method, the actual sensitivities for each test problem were developed by reoptimizing the problem over a range of values for each parameter. The results were then fit with either a linear or quadratic curve, depending on the amount of nonlinearity present, and the resulting curve was used to estimate the derivatives. These were then compared with the derivatives obtained from the RQP based algorithm.

This slide describes the three engineering test problems that were used. Complete descriptions are available in Beltracchi (1988).

Four Bar Slider Crank Problem: Design a four bar slider crank mechanism to generate a desired coupler path. Four parameters were studied: a movability criteria parameter, two timing parameters, and the y position of a precision point.

Weld Beam Problem: Design a welded beam structure for minimum cost. Parameters studied: fixed length of beam, load on beam, yield stress in beam, and allowable shear in weld.

Corrugated Bulkhead: Design a ship bulkhead for minimum weight. Parameters studied: change in position of two stringers, and height of the free liquid.

ENGINEERING TEST PROBLEMS: RESULTS

The following tables report on the accuracy of the parameter sensitivity derivatives returned by the RQP based algorithm for the engineering test problems. The following general conclusions can be drawn from these results:

- The method produces results for df/dp , dx/dp , and dg/dp that are in the range of 3-4 significant digits of accuracy.
- The results for the four bar mechanism problem are generally worse than the other two problems. This is due to the highly nonlinear nature of this problem and the difficulty in locating accurate optimal points.

Four Bar Slider Crank

	p1	p2	p3	p4
$\frac{df}{dp}$	$2.0(10^{-5})$	$4.86(10^{-3})$	$2.25(10^{-5})$	$3.29(10^{-7})$
ϵ_x	$2.32(10^{-2})$	$6.38(10^{-3})$	$7.67(10^{-2})$	$2.65(10^{-2})$
ϵ_u	$3.62(10^{-1})$	$3.34(10^{-2})$	$6.14(10^{-2})$	$5.48(10^{-2})$
ϵ_g	$8.81(10^{-5})$	$1.94(10^{-3})$	$7.82(10^{-2})$	$9.36(10^{-3})$

Welded Beam

	p1	p2	p3	p4
$\frac{df}{dp}$	$1.26(10^{-5})$	$8.7(10^{-6})$	$8.62(10^{-6})$	$1.89(10^{-4})$
ϵ_x	$7.59(10^{-5})$	$4.28(10^{-5})$	$3.12(10^{-5})$	$1.26(10^{-4})$
ϵ_u	$2.45(10^{-4})$	$3.54(10^{-4})$	$1.80(10^{-4})$	$1.75(10^{-4})$
ϵ_g	$8.61(10^{-7})$	$1.05(10^{-4})$	$1.27(10^{-18})$	$1.45(10^{-4})$

Bulkhead Problem

	p1	p2	p3
$\frac{df}{dp}$	$3.21(10^{-5})$	$3.34(10^{-6})$	$3.51(10^{-5})$
ϵ_x	$5.21(10^{-5})$	$2.81(10^{-5})$	$1.92(10^{-4})$
ϵ_u	$7.74(10^{-5})$	$1.08(10^{-7})$	$8.11(10^{-5})$
ϵ_g	$5.12(10^{-5})$	$2.69(10^{-5})$	$3.23(10^{-5})$

CONCLUSIONS

In this paper, we have proposed an alternative to current methods for estimating parameter sensitivities. The new method is based on combining the use of an RQP algorithm with differencing formulas which provides a means to estimate the sensitivities without the need for calculating second order derivatives. The method has been tested against two different test sets, one with analytical derivatives available and one without, and in both cases the method was able to accurately determine the sensitivity derivatives. The two major issues in implementing the algorithm concern the ability to formulate an accurate approximation to the Hessian of the Lagrangian and the ability to accurately estimate the modified Kuhn-Tucker sensitivity equations using the differencing formulas. Based on the testing performed so far, we are led to the following conclusions:

1. In terms of efficiency, the method is competitive with existing methods.
2. Parameter sensitivity analysis can be performed using the RQP based method.
3. The Hessian approximation is improved if updating is allowed during the sensitivity calculations.
4. The SR1/PD/BFS update in general provided more accurate estimates of the Hessian of the Lagrangian than either the BFS or SR1 updates on our test set. The initial testing of this update was very encouraging in terms of the convergence of the Hessian approximation to the true Hessian.

1. The method is competitive with existing methods.
2. Parameter sensitivity analysis can be performed using the RQP based method.
3. The Hessian approximation is improved if updating is allowed during the sensitivity calculations.
4. The SR1/PD/BFS update in general provided more accurate estimates of the Hessian of the Lagrangian than either the BFS or SR1 methods.

REFERENCES

- Arbuckle, P. D., and Sliwa, S. M., 1984, "Experiences Performing Conceptual Design Optimization of Transport Aircraft" in *Recent Experiences in Multidisciplinary Analysis and Optimization, Part 1*, Compiled by J. Sobieski, NASA CP 2327, pp 87-101.
- Armacost, R. L., and Fiacco, A. V., 1974, "Computational Experience in Sensitivity Analysis for Nonlinear Programming", in *Mathematical Programming*, Vol. 6, pp 301-326.
- Arora, J. S., and Tseng, C. H., 1987, "Discussion on ASME Paper No. 86-DET-26," in *ASME Journal of Mechanisms, Transmissions and Automation in Design*, June, Vol 109 No. 2.
- Barthelemy, J. F., and Sobieszczanski-Sobieski, J., 1983 a, "Extrapolation of Optimum Designs Based of Sensitivity Derivatives," in *AIAA Journal*, Vol. 21, May , pp 797-799.
- Barthelemy, J. F., and Sobieszczanski-Sobieski, J., 1983 b, "Optimum Sensitivity Derivatives of Objective Functions in Nonlinear Programming" in *AIAA Journal*, Vol. 21, June pp 913-915.
- Bartholomew-Biggs, M. C., 1987, "Recursive Quadratic Programming Methods Based on the Augmented Lagrangian," in *Mathematical Programming Study 31, Computational Mathematical Programming*, edited by K. L. Hoffman, R. H. F. Jackson, and J. Telgen, North Holland - Amsterdam, pp 21-41.
- Beltracchi, T. J., 1985, *An Investigation of Pshenichnyi's Recursive Quadratic Programming Technique for Engineering Optimization*, MS Thesis Rensselaer Polytechnic Institute, Dec. 1985
- Beltracchi, T. J., and Gabriele, G. A., 1987, "An Investigation of Pshenichnyi's Recursive Quadratic Programming Technique for Engineering Optimization", in *ASME Journal of Mechanisms, Transmissions, and Automation in Design*, Vol 109 No. 2 pp 248-256 June 1987.
- Beltracchi, T. J., and Gabriele, G. A., "An Investigation of New Methods for Estimating Parameter Sensitivities," NASA CR 183195.
- Beltracchi, T. J., "An Investigation of Parameter Sensitivity Analysis by the Recursive Quadratic Programming Method," Ph.D. Thesis, Rensselaer Polytechnic Institute, 1988.
- Buys, J. D. and Gonin, R., 1977, "The use of Augmented Lagrangian Functions for Sensitivity Analysis in Nonlinear Programming." in *Mathematical Programming*, Vol. 12 No. 2, pp 281-284.
- Cha, J. Z., and Mayne R. W. 1987, "Optimization with Discrete Variables Via Recursive Quadratic Programming: Part II: Algorithm and Results," in *ASME DE Vol. 10-1, The Proceedings of the 1987 Design Automation Conference*, Boston Ma.
- Cullum, J. and Brayton, R. K., 1979 "Some Remarks on the Symmetric Rank-One Update," in *Journal of Optimization Theory and Applications*, Vol 29, No 4., pp 493-519 December
- Dantzig, G. B., 1963, *Linear Programming and Extensions*, Princeton University Press, Princeton New Jersey.
- Dennis, J. E., and Schnable, R. B., 1983, *Numerical Methods for Unconstrained Optimization and Nonlinear Equations*, Prentice Hall.

Falk, J. E., and Fiacco, A. V., 1982, "The use of Mathematical Programming: Who let the Man Out:", in *Computers and Operations Research*, Vol. 9, No. 1, pp. 3-5.

Fiacco, A. V., 1976, "Sensitivity Analysis For Nonlinear Programming Using Penalty Methods", in *Mathematical Programming*, Vol. 10, pp 287-311.

Fiacco, A. V., 1983, *Introduction to Sensitivity and Stability Analysis in Nonlinear Programming*, Academic Press, New York.

Fiacco, A. V., and Ghaemi, A., 1982, "Sensitivity Analysis of a Nonlinear Structural Design Problem", in *Computers and Operations Research*, Vol. 9, No. 1, pp 29-55.

Gal, T., 1984, "Linear Parametric Programming- A Brief Survey," in *Mathematical Programming Study* 21, North Holland, pp 43-68.

Gill, P. E., Murray, W., Saunders, M. A., and Wright, M. H., 1983 "Computing Forward-Difference Intervals for Numerical Optimization", in *SIAM Journal of Scientific and Statistical Computing*, Vol. 4, No. 2, June 1983, pp 310-321.

Gill, P. E., Murray, W., Saunders, M. A., and Wright, M. H., 1986, "Considerations of Numerical Analysis in a Sequential Quadratic Programming Method", in *Numerical Analysis Lecture Notes in Mathematics* No. 1230, Springer Verlag, New York 1986.

Haftka, R. T., Iott, J., and Adelman, H. M., 1985, "Selecting step sizes in sensitivity analysis by finite differences," Aug. 1985, NASA TM 86382.

Jittorntrum, K., 1984, "Solution Point Differentiability without Strict Complementarity in Nonlinear Programming," in *Mathematical Programming Study* 21, North Holland Amsterdam pp 127-138.

McKeown, J. J., 1980 , "Parametric Sensitivity Analysis of Nonlinear Programming Problems", In *Nonlinear Optimization Theory and Algorithms*, L. C. W. Dixon, E Spedicato and G. P. Szego editors, North Holland, Amsterdam, pp. 387-406

Robertson, W. D., and Gabriele, G. A., 1987, "The Optimal Design of a Rotary Type Actuator for Magnetic Disk Drives," in *Advances in Design Automation - 1987, Volume One: Design Methods, Computer Graphics, and Expert Systems*, ASME DE-Vol. 10-1, pp 107-114, to Appear in *ASME Journal of Mechanisms, Transmissions, and Automation in Design*.

Sandgren E., 1977, "The Utility of Nonlinear Programming Algorithms", Ph.D. dissertation Purdue University Dec. 1977, West Lafayette In.

Schmit, L. A., and Chang, K. J., 1984, "Optimum Design Sensitivity Based on Approximation Concepts and Dual Methods", in *International Journal for Numerical Methods in Engineering*, vol. 20, pp 39-75.

Sobieszczanski-Sobieski, J., Barthelemy, J. F., and Riley K. M., 1981, "Sensitivity of Optimum Solutions to Problem Parameters", *Proceedings of the AIAA/ASME/ASCE/AHS 22nd Structures, Structural Dynamics and Materials Conference*, Atlanta, Ga., April 1981, pp 184-205, also NASA TM 83134, May 1981, *AIAA Journal*, Vol 20., Sept. 1982, pp. 1291-1299.

Sobieszczanski-Sobieski, J., James, B. B., and Riley, M. F., 1987, "Structural Sizing by Generalized, Multilevel Optimization," in *AIAA Journal* Vol. 25, No. 1, January 1987, pp 139-145

Vanderplaats, G. N., 1984, "An Efficient Feasible Directions Algorithm for Design Synthesis", in AIAA Journal, Vol. 22, No. 11, Nov. , pp. 1633-1639

Vanderplaats, G. N., and Cai, H. D., 1987, "Alternative Methods for Calculating Sensitivity of Optimized Designs to Problem Parameters," in Sensitivity Analysis in Engineering, Edited by H. M. Alderman and R. T. Haftka, NASA CP-2457, pp 19-32.

Vanderplaats, G. N., and Yoshida, N., 1985, "Efficient Calculation of Optimum Design Sensitivity" in AIAA Journal, Nov. , pp 1798-1803.

GRID SENSITIVITY CAPABILITY FOR LARGE SCALE STRUCTURES

by

Gopal K. Nagendra*

and

David V. Wallerstein**

* Senior Engineer, The MacNeal-Schwendler Corporation, Los Angeles, California.

** Chief, Development, The MacNeal-Schwendler Corporation, Los Angeles, California.

ABSTRACT

This paper presents the considerations and the resultant approach used to implement design sensitivity capability for grids into a large scale, general purpose finite element system (MSC/NASTRAN). The design variables are grid perturbations with a rather general linking capability. Moreover, shape and sizing variables may be linked together. The design is general enough to facilitate geometric modeling techniques for generating design variable linking schemes in an easy and straightforward manner.

Test cases have been run and validated by comparison with the overall finite difference method. The linking of a design sensitivity capability for shape variables in MSC/NASTRAN with an optimizer would give designers a powerful, automated tool to carry out practical optimization design of real life, complicated structures.

INTRODUCTION

This paper presents the considerations and the resultant approach used to implement design sensitivity capability for grids into MSC/NASTRAN. MSC/NASTRAN is a large-scale, general purpose computer program which solves a wide variety of engineering problems by the finite element method. In 1983, the design sensitivity analysis (DSA) capability was installed in MSC/NASTRAN. This capability has recently been enhanced to include a fully integrated optimization capability for sizing variables. With the addition of shape sensitivity capability and with the increasing interest in aerospace and automotive industries, this general capability can be used in its own right for carrying out sensitivity analysis of complicated real life structures.

Shape optimization is still in a state where fundamental research is needed (Reference 1). The integration of shape optimization concepts within Finite Element Methods (FEM) and Computer Aided Designs (CAD) should help to bridge the gap between these two technologies. To be successful, the proposed integration of software should lead to a system easy to use. From a practical point of view, the computational tool should indeed be employed by design engineers with only a superficial knowledge of the theoretical basis of each technique.

The following sections will be devoted to the basic procedure for an efficient design variable linking scheme using reduced basis concepts. These are necessary to avoid generating unrealistic designs due to independent node movements.

The next section provides an overview of the design sensitivity capability in MSC/NASTRAN. The design constraints can be weight, volume, frequency, buckling loads, displacements, stresses, strains or forces. The design variables can be shape or sizing variables. The method chosen is a semianalytical approach based on a first variation (finite difference scheme) of the system's equilibrium equations with respect to the design variables.

A brief description follows of the program architecture and considerations that go into implementing such a capability into a large-scale, general-purpose computer program. The important considerations are ease of use, generality, compatibility with the existing architecture, data organization and management and, finally, a good restart capability for an active man/machine interaction.

Errors associated with shape sensitivity analysis using the semianalytical approach as shown in Reference 2 are examined. An iterative scheme and error index are employed to minimize the errors in the sensitivity calculations.

Two example problems were chosen to validate the capability and to highlight some of the salient features. The first example problem is a beam modeled by solid elements, with x-section as design variable. The second example problem is a cantilever beam with length as design variable.

BASIC PROCEDURE

When dealing with shape optimization problems, the design variables must be selected very carefully. The coordinates of the boundary nodes of the finite element model is a straightforward choice. This choice, however, exhibits many severe drawbacks. The set of design variables is very large and the cost and difficulty of the minimization process increase. It has a tendency to generate unrealistic designs due to the independent node movement and additional constraints avoiding such designs are difficult to cope with. Moreover, an automatic mesh generator is necessary to maintain the mesh integrity throughout the optimization process. One obvious remedy is to avoid a one-to-one correspondence between the finite element model and the design variables.

One way to achieve this goal is to use the concept of "design model" utilizing "reduced basis vectors". The general form of this relationship is (Reference 3)

$$\begin{array}{ccc} \{\Delta g\} & = & [T] \{x\} \\ nx1 & & nxm \quad mx1 \end{array} \quad (1)$$

The given design Δg define a system of n variables. We refer to columns of T as basis vectors. Clearly the method is most useful if $m \ll n$ and the method will produce a true optimum only if some combination of basis vectors can define that optimum.

From Equation 1, it is obvious that the reduced basis approach is simply a design variable linking scheme where the basis vectors are columns of the coefficient matrix T . Ideally, the basis vectors could most conveniently be generated using a graphics preprocessor.

To clarify ideas, consider the coordinate update equation given by

$$\begin{Bmatrix} x_{new} \\ y_{new} \\ z_{new} \end{Bmatrix} = \begin{Bmatrix} x_{old} \\ y_{old} \\ z_{old} \end{Bmatrix} + \sum x \cdot \begin{Bmatrix} D\text{-cosine-}x \\ D\text{-cosine-}y \\ D\text{-cosine-}z \end{Bmatrix} + \begin{Bmatrix} C_x \\ C_y \\ C_z \end{Bmatrix} \quad (2)$$

The constant term vector C_x, C_y, C_z are computed to make necessary adjustments so that $x_{new}, y_{new}, z_{new}$ are equal to $x_{old}, y_{old}, z_{old}$ for the initial values of the design variables x supplied by the user. Notice that in Equation 2, for the initial configuration, the values of the initial design variables x supplied by the user need not be zero. Equation 2 may be rewritten as

$$\begin{Bmatrix} x_{new} \\ y_{new} \\ z_{new} \end{Bmatrix} - \begin{Bmatrix} x_{old} \\ y_{old} \\ z_{old} \end{Bmatrix} - \begin{Bmatrix} C_x \\ C_y \\ C_z \end{Bmatrix} = \sum x \cdot \begin{Bmatrix} D\text{-cosine-}x \\ D\text{-cosine-}y \\ D\text{-cosine-}z \end{Bmatrix}$$

or

$$\{\Delta g\}_i = [T]_{ij} \{x\}_j$$

this is the same form as shown in Equation 1. The columns of the T matrix are then the basis vectors. The capability exists for the user to input the elements of the T matrix directly or in the future he may generate elements of the T matrix using a preprocessor. It should be clear from the above formulation that the design variables are the grid perturbations and not the grid coordinates.

DESIGN SENSITIVITY CAPABILITY IN MSC/NASTRAN

Design sensitivity analysis estimates the effects of interrelated design variables such as element properties and materials on the structural response quantities such as displacement, stress, natural frequency, buckling loads - and for composites lamina stresses and failure indices. Design sensitivity coefficients are defined as the gradients of the design constraints with respect to the design variables at the current design point. The method chosen for incorporation into MSC/NASTRAN is a semianalytical approach, based on a first variation (finite difference scheme) of the systems equilibrium equations with respect to the design variables.

Let $\psi_i(b_j, u)$ be a set of design constraints which are functions of b_j design variables and displacements u . The design constraints are expressed as

$$\psi_i(b_j, u) \leq 0$$

The first variation in ψ_i is given as

$$\delta\psi_i = \left[\frac{\partial\psi_i}{\partial b_j} \right]_{\substack{ixj \\ u\text{-fixed}}} \{ \delta b_j \}_{\substack{jx1 \\ b\text{-fixed}}} + \left[\frac{\partial\psi_i}{\partial u} \right]_{\substack{ixn \\ b\text{-fixed}}} \{ \delta u \}_{\substack{nx1 \\ b\text{-fixed}}}$$

consider u as a function of b_j , then

$$\{ \delta u \}_{\substack{nxj \\ b\text{-fixed}}} = \left[\frac{du}{db_j} \right]_{\substack{nxj \\ b\text{-fixed}}} \{ \delta b_j \}_{\substack{jx1 \\ b\text{-fixed}}}$$

and, therefore,

$$\{ \delta\psi_i \} = \left(\left[\frac{\partial\psi_i}{\partial b_j} \right] + \left[\frac{\partial\psi_i}{\partial u} \right] \left[\frac{du}{db_j} \right] \right) \{ \delta b_j \}$$

or

$$\frac{\delta\psi_i}{\delta b_j} \equiv \frac{\Delta\psi_i}{\Delta b_j} = \left[\frac{\partial\psi_i}{\partial b_j} \right] + \left[\frac{\partial\psi_i}{\partial u} \right] \left[\frac{du}{db_j} \right]$$

The matrix $\frac{du}{db_j}$ can be evaluated by taking the first variation of the systems equilibrium equation,

$$[K] \{u\} = \{P\}$$

which gives

$$[K] \{ \Delta u \} + [\Delta K] \{u\} = \{ \Delta P \}$$

solving for $\{ \Delta u \}$

$$\{ \Delta u \} = [K]^{-1} (\{ \Delta P \} - [\Delta K] \{u\})$$

or

$$[\Delta u] = [K]^{-1} (\{ \Delta P(\Delta b_1) \}, \{ \Delta P(\Delta b_2) \}, \dots, \{ \Delta P(\Delta b_i) \}) \\ - [K]^{-1} (\{ [\Delta K(\Delta b_1)] \{u\} \}, \{ [\Delta K(\Delta b_2)] \{u\} \}, \dots, \{ [\Delta K(\Delta b_i)] \{u\} \})$$

The elements of $\left[\frac{d\psi_i}{du} \right]$ matrix for an element constraint such as stress, force, or failure index can be expressed by the relationship

$$\{\psi_i\} = [S]_i \{u\}$$

or

$$\left[\frac{d\psi_i}{du} \right] = [S]_i$$

The design sensitivity coefficient matrices may thus be expressed as

$$[\Lambda_i] \equiv \left(\left\{ \frac{\Delta \psi_i}{\Delta b_1} \right\}, \left\{ \frac{\Delta \psi_i}{\Delta b_2} \right\}, \dots, \left\{ \frac{\Delta \psi_i}{\Delta b_j} \right\} \right) \Big|_{u_{fixed}} \\ + [S]_i \left(\left\{ \frac{\Delta U_1}{\Delta b_1} \right\}, \left\{ \frac{\Delta U_2}{\Delta b_2} \right\}, \dots, \left\{ \frac{\Delta U_i}{\Delta b_j} \right\} \right) \Big|_{b_{fixed}}$$

From this equation it is easy to see that the number of additional case control records (additional loading cases) required for design sensitivity analysis is equal to the number of design variables for each subcase (Design Space Technique).

A typical term of the coefficient matrix may be written as

$$\Lambda_{ij} = \left(\frac{S^{B+\Delta B} u^B}{\Delta B} - \frac{S^B u^B}{\Delta B} \right) + \left(\frac{S^B u^{B+\Delta B}}{\Delta B} - \frac{S^B u^B}{\Delta B} \right)$$

where B represents the base line or original state and B + ΔB represents the perturbed state. The first expression in parentheses on the right-hand side is thus the change in response quantity due to a change in design variable for the original solution vector. The second term represents the change in response quantity due to a change in displacement for the unperturbed design variable. For displacement constraints, the first term in parentheses on the right-hand side is identically zero.

The design constraints can be weight, volume, frequency, buckling loads, displacements, stresses, strains, forces, lamina stresses, lamina strains, failure indices or user supplied synthetic equations. The design variables can be grid movements or properties. The shape and sizing variables may be linked together.

PROGRAM ARCHITECTURE

In order to understand the reasons behind how a development is introduced into a large finite element program, a knowledge of the program architecture and technical purpose is necessary. A brief description of MSC/NASTRAN is presented as background (Reference 4)

The cornerstone of MSC/NASTRAN's architecture is its Executive System, whose essential functions are to establish and control the sequence of calculations, to allocate files, and to maintain a restart capability. Engineering calculations are performed by approximately 200 Functional Modules which communicate only with the Executive System and not with each other. Flexibility is maintained by a macro-instruction language called DMAP, which is under user control, but which also serves to establish preformatted calculation sequences for the major types of analysis, including linear analysis, buckling, vibration mode analysis, and design sensitivity.

The calculation of finite element data is concentrated exclusively in a few modules. The element matrices for stiffness, structural damping, and differential stiffness for elements of the structural model are generated in the Element Matrix Generator (EMG) module. These element matrices are subsequently assembled to form the elastic stiffness matrix, the structural damping matrix, the mass matrix, or the differential stiffness matrix.

The element contribution to the load vector is generated in the load generator module and the element stress and force are generated in the recovery module. In all these modules, the finite element descriptions are defined in the Element Summary Table (EST). The EST contains the element connection, material property and sectional property information.

Taking advantage of the table driven concept used by the element modules, much of the element dependent development can be avoided in implementing design sensitivity. The reason is that a procedure could be developed which only involves building EST tables that would cause existing modules to form the necessary element data.

How a given capability is introduced into a commercial general purpose finite element program is as important an issue to the user as its theoretical sophistication. If the user views a capability as hard to use, as having an insufficient capacity to solve his problem, or taking an inordinate time to comprehend its output, the product is of little practical use. In addition, the program developer, while heeding the user's needs, has to keep sight of the program as a whole when adding new capabilities. This involves interfacing well with existing capabilities, maintaining program reliability and generality, and producing software that makes effective use of computer resources.

The user interface is a major consideration in the design of a new capability. The following issues were considered when building up the design sensitivity analysis (DSA) capability.

1. DSA input should be straightforward, but allow flexibility to model complex structural design concepts.
2. DSA output should be concise and easily understood.
3. Avoid arbitrary program limits which restrict the allowable element types, constraint quantities, and problem size.
4. Provide an interface for external optimization postprocessors.

A brief discussion of the processes involved in a typical DSA STATIC analysis in MSC/NASTRAN will help bring into perspective the work involved in the various parts of the DSA solution.

DSA in a STATICS analysis is based on solving for $\{\Delta u\}$ the first order variation of the nodal equilibrium equation:

$$[K^0] \{\Delta u\} = \{\Delta P\} - [\Delta K] \{u^0\}$$

The DSA problem in this paper is considered to be the additional task required after the solution of primary analysis. By restarting from the primary STATIC analysis, the solution of the DSA system equation only involves the calculation of the right-hand side and the backward pass operation in the solution of Δu .

The work involved in solving the system equations (backward pass operation) is a function of the product of the number of design variables and loading conditions. The following DSA tasks are required in addition to solving the system equations:

1. DSA Data Organization
2. DSA Data Assembly
3. DSA Data Recovery

These tasks are functions of the triple product of the number of design variables, design constraints and loading conditions. For large DSA problems, the data organization, assembly and recovery tasks are the dominant users of computer resources.

Another major consideration was to support all structural finite element types in MSC/NASTRAN. Since a large number of the elements developed are semiempirical, the determination of consistent element derivative formulations cannot be practically accomplished. Therefore, a method was developed to calculate element derivatives by a differencing scheme about the current design point. This method involved the calculation of the element matrix at the design point plus or minus the user specified design

variable increment. This element data is differenced with the data at the design point to determine the corresponding element derivatives. For example, the following shows the change in element stiffness due to a change in the design variable.

$$[\Delta K] = [K_{B+\Delta B}] - [K^0]$$

An initial analysis is carried out to identify critical constraints and a data base is created. In the succeeding run, information about constraints, design variables, maximum and minimum side constraints is supplied. A special DMAP package was created which exploits the data base technology.

ERRORS ASSOCIATED WITH SEMI-ANALYTICAL APPROACH IN SHAPE SENSITIVITY

In Reference 2 it was shown that the semi-analytical approach can have serious accuracy problems for shape design variables in structures modeled by beam, plate, truss, frame and solid elements. An error index was developed to test the accuracy of the semi-analytical approach and some methods were proposed for improving the accuracy of the semi-analytical method. In the following section, the interactive scheme proposed in Reference 2 is examined in greater detail.

Consider the systems equilibrium equation

$$[k] \{u\} = \{P\}$$

Taking the first variation of the systems equilibrium equation gives

$$[k + \Delta k] \{u + \Delta u\} = \{P + \Delta P\}$$

Expanding the above equation and retaining the second order terms gives

$$[k] \{\Delta u\} = \{\Delta P\} - [\Delta k] \{u\} - [\Delta k] \{\Delta u\}$$

which can be cast as an iterative scheme

$$[k] \{\Delta u\}_i = \{\Delta P\} - [\Delta k] \{u\}_0 - [\Delta k] \{\Delta u\}_{i-1} \quad (3)$$

This iterative scheme can be used quite effectively with the error index as shown in Reference 3, i.e.,

$$E^{Imm} = \frac{[A]^I - [A]^m}{[A]^n} \quad (4)$$

An error index of the type described above is almost a must for a large scale system in the optimization context. If the sensitivity derivatives are significantly in error, the program needs to detect it and stop the execution to save time and resources of the user.

NUMERICAL EXAMPLES

Two example problems were chosen to validate the capability and to highlight some of the salient features.

Example 1 - Beam using solid elements

A cantilever beam is subjected to a tip loading. The model of the beam is shown in Figure 1. The beam is modeled using solid hexahedron elements. The analysis model consists of five HEXA elements and 24 grids.

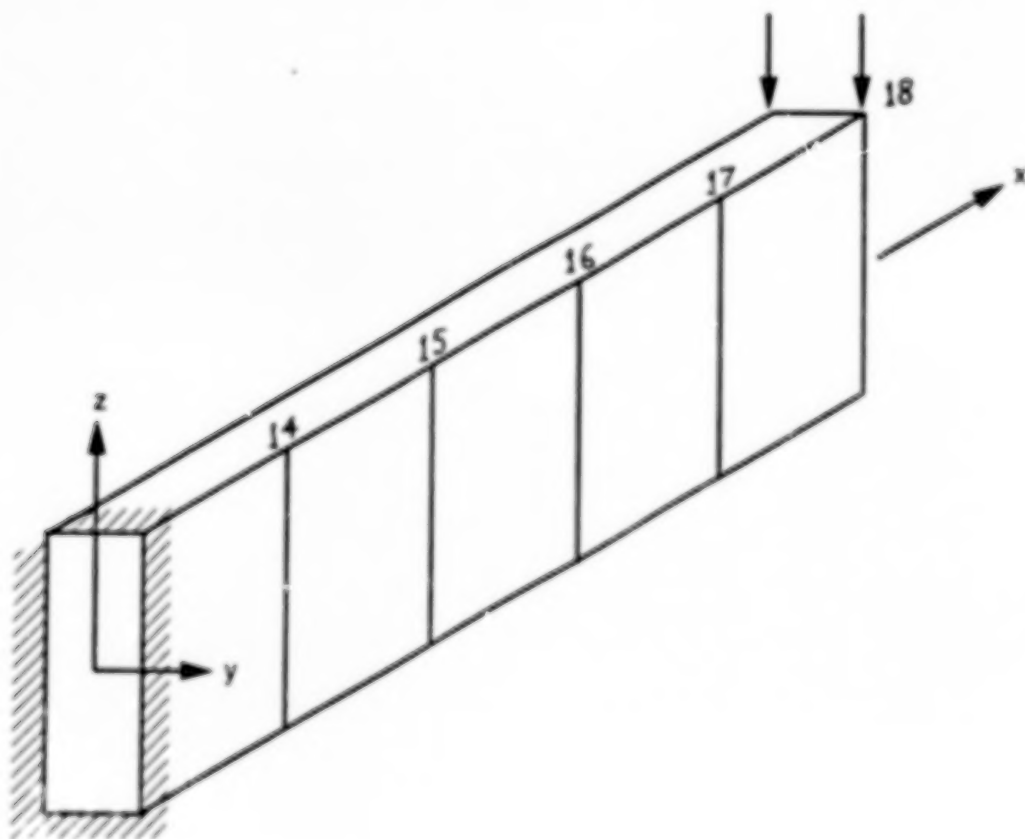


Figure 1. Beam using solid elements.

174

The design model consists of one design variable to perturb beam cross section to maximize the bending inertia about the y-axis. The cross-section is perturbed as shown in Figure 2 below.

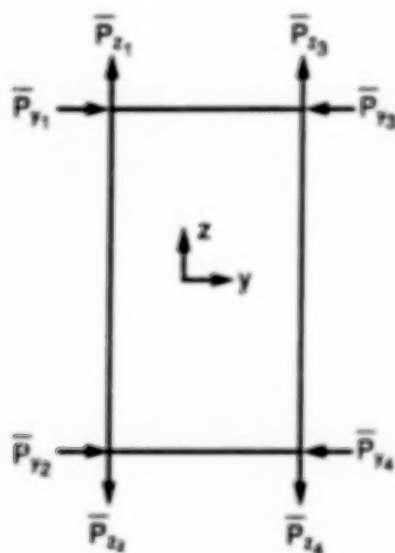


Figure 2. Design Variable Linking Scheme.

P_{y_i} and P_{z_i} are perturbation vectors in the y and z direction respectively.

The perturbation vectors are given by

$$P_{y_1} = P_{y_2} = 0.01(0\hat{i} + \hat{j} + 0\hat{k})$$

$$P_{y_3} = P_{y_4} = 0.01(0\hat{i} - \hat{j} + 0\hat{k})$$

$$P_{z_1} = P_{z_3} = 0.01(0\hat{i} + 0\hat{j} + \hat{k})$$

$$P_{z_2} = P_{z_4} = 0.01(0\hat{i} + 0\hat{j} - \hat{k})$$

The sensitivity coefficient results calculated using the semi-analytical approach are compared to the Overall Finite Difference (OFD) approach, wherein the entire problem is solved again for the perturbed configuration. The results are shown in Table 1. As can be seen, the correlation between the semi-analytical approach and the OFD is excellent for this particular example problem.

Grid-ID	Sensitivity OFD	Sensitivity SA	Error
14	-.0313	-.0307	1.92
15	-.0861	-.0845	1.86
16	-.0166	-.0163	1.81
17	-.0235	-.0231	1.7
18	-.0397	-.0389	2.0

Table 1. Vertical displacements along beam length..

Example 2 - Cantilever beam subjected to end moment

The same cantilever beam that was considered in Reference 2 is taken as an example here. The cantilever beam has uniform rigidity EI and length L under a tip moment M as shown in Figure 3.

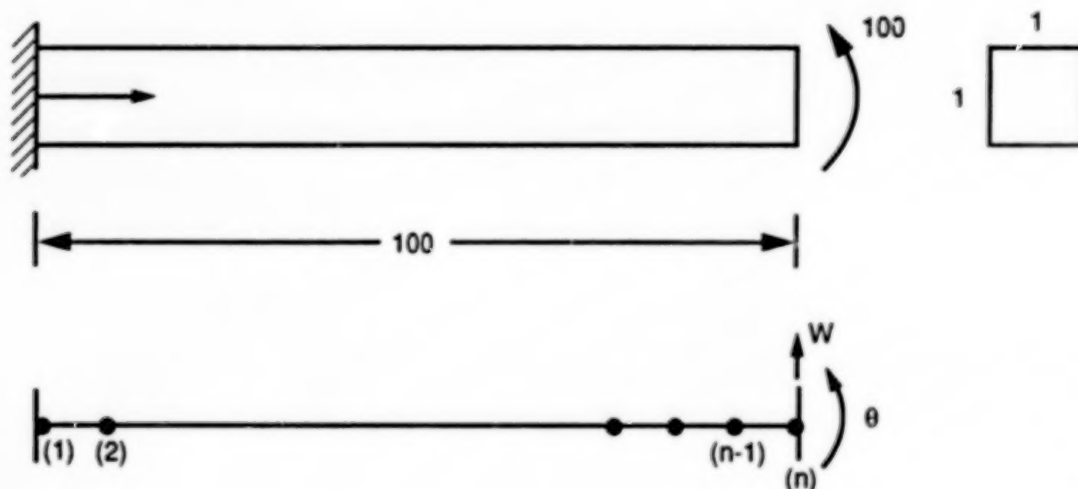


Figure 3. Cantilever beam subjected to end moment.

The modulus of elasticity is taken equal to $E = 10^7$. The theoretical tip deflection for the above configuration is

$$\delta = \frac{ML^2}{2EI} \quad (5)$$

The structure has been idealized into 20 beam elements. Sensitivity coefficients have been calculated for the tip displacement with respect to the length of the beam. The design model contains a single design variable, i.e., the length of the beam. The grid perturbations of all the grids have been linked together so that the perturbations vary linearly from root to tip of the beam.

170

Parametric studies have been carried out to determine the effect of the step size on the error. From Equation 5, the exact results are available.

First the sensitivity analysis is carried out using the Overall Finite Difference (OFD) and the semi-analytical (SA) method for step sizes of 1%, 0.5%, 0.1 % and 0.01%. The results, without using any iterative schemes are shown in Table 2. As can be seen, the results are quite accurate for a step size of 0.01%. Whereas they progressively degrade for increasing values of the step size and become quite unacceptable for a step size of 1%.

In Reference 2, the errors for the beam-type structure are associated with an incompatibility of the sensitivity field with the structural model. The error in the finite difference approximation consists of a truncation error because of neglecting higher order terms in the Taylor series expansion and a condition error because of the limited precision available for the computer. Thus, an optimum value of step-size would minimize the truncation error without the condition error becoming significant. As suggested in Reference 3, central difference scheme is an alternative to iterations.

Step-size (%)	Sensitivity Coefficient Λ
1.0	-10.459
0.5	-4.716
0.1	0.010
0.01	1.08
0.001	1.1885
0.0001	1.1874
0.00001	0.914*

* Degrades. (Theoretical value = 1.2)

Table 2. Variation of sensitivity coefficients with respect to step-size.

Next, we use the iterative scheme of Equation 3 to converge to the correct solution. As can be seen from Figure 4, the smaller the value of the step size, the lesser the number of iterations required to converge to the correct solution.

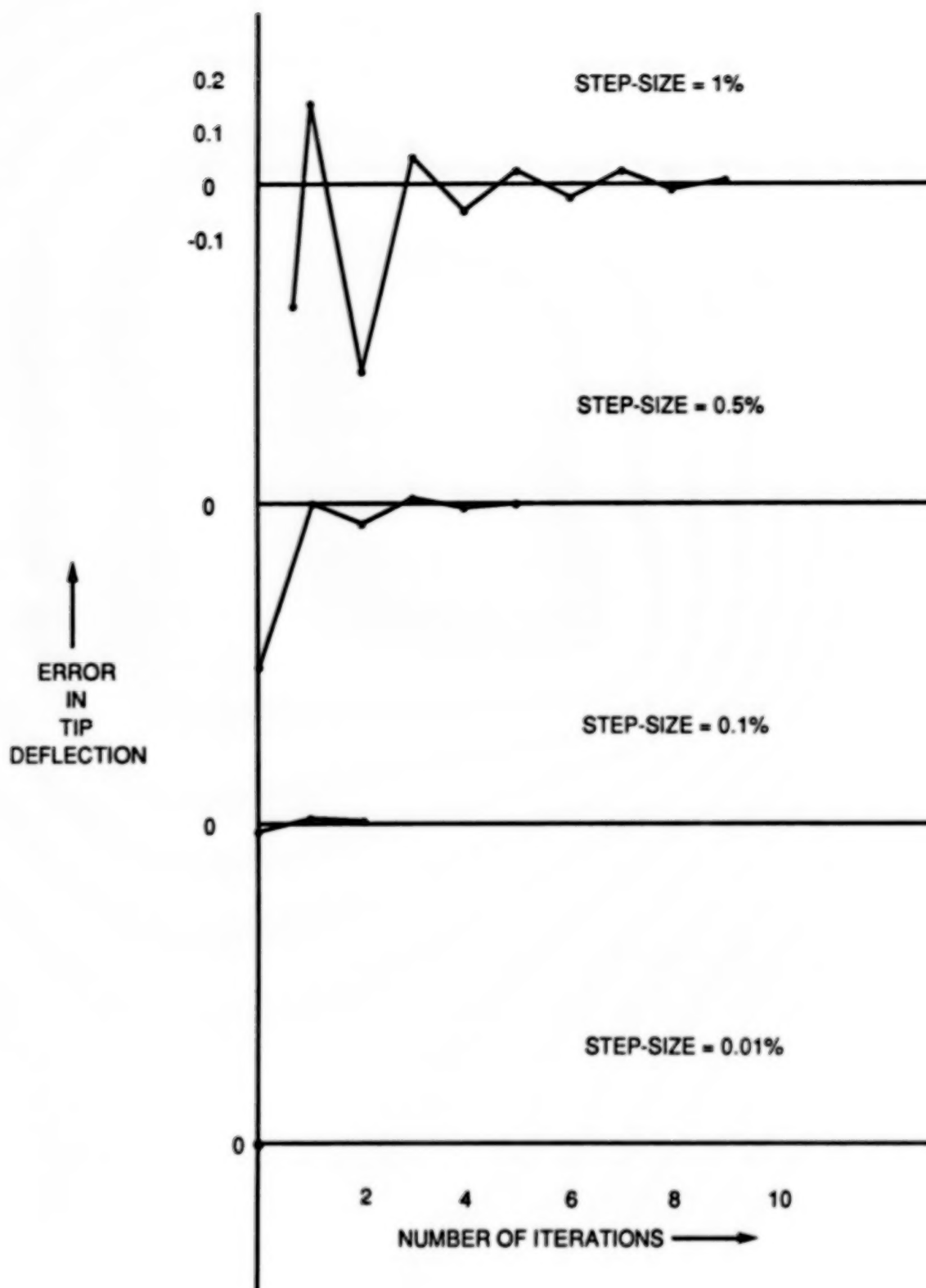


Figure 4. Plot of number of iterations versus error in tip-displacement using SA method.

CONCLUSIONS

This paper presented the considerations and the resultant approach used to implement design sensitivity capability for grids into a large scale, general purpose finite element system (MSC/NASTRAN). The design variables are grid perturbations with a rather general linking capability. Moreover shape and sizing variables may be linked together. The design is general enough to facilitate geometric modeling techniques for generating design variable linking schemes in an easy and straightforward manner.

The errors shown to be associated with the semianalytic method for shape variables for beam type structures can be mitigated by resorting to an iterative scheme. Examples have been presented highlighting the salient features of the approach.

REFERENCES

1. Fleury, C. and Braibant, V., *Toward a Reliable C.A.D. Tool*, computer aided optimal design, Troia, Portugal, July 1986
2. Barthelemy, B. and Haftka, R. T., *Accuracy Analysis of the Semi-Analytical Method for Shape Sensitivity Calculation*, 29th SDM Conference, April 18-20/Williamsburg, VA 572-581
3. Vanderplaats, G. N. *Numerical Optimization Techniques for Engineering Design: With Applications*, McGraw-Hill, 1984
4. Nagendra, G-K. and Fleury, C., *Sensitivity and Optimization of Composite Structures using MSC/NASTRAN*, NASA CP-2457, NASA Langley Research Centre, Hampton, Virginia, September 25-26, 1986

ITERATIVE METHODS FOR DESIGN SENSITIVITY ANALYSIS

A.D. Belegundu
Department of Mechanical Engineering
The Pennsylvania State University
University Park, PA 16802

and

B.G. Yoon
Graduate Student

ABSTRACT

A numerical approach is presented for design sensitivity analysis. The approach is based on perturbing the design variables and then using iterative schemes to obtain the response of the perturbed structure. A forward difference formula then yields the approximate sensitivity. Algorithms for displacement and stress sensitivity as well for eigenvalue and eigenvector sensitivity are developed. Results for the stress sensitivity problem are compared with the semi-analytical method. Examples are considered in structures and fluids.

INTRODUCTION

Iterative methods are presented for obtaining design sensitivity coefficients (or derivatives) of implicit functions. Design derivatives are important not only in gradient-based optimization codes, but also for examining trade-off's, system identification, and probabilistic design. Iterative methods are presented for both the algebraic and eigenvalue problems; stress, eigenvalue and eigenvector derivatives are considered. The iterative approaches provide approximate derivatives. They are very simple to implement in a program, especially for calculation of eigenvector derivatives. The idea of using iterative methods for a class of problems was suggested for one dimensional problems in (ref. 1). Here, this idea is developed to handle the matrix algebraic as well as the generalized eigenvalue problems.

The basic idea behind the approach is as follows. Let

$$g = g(\underline{b}, \underline{y}) \quad (1)$$

be a continuously differentiable function of a design variable vector \underline{b} of dimension $(k \times 1)$, and a state variable vector \underline{y} of dimension $(n \times 1)$. The state variables are implicitly dependent on design through the n state equations of the form

$$\phi(\underline{b}, \underline{y}) = 0 \quad (2)$$

Let \underline{b}^0 be the current design and \underline{y}^0 be the associated state variable vector. The problem of concern is to find the sensitivity, dg/db_i , at the current design. The iterative method is based on perturbing each design variable, in turn, as

$$b_i^E = b_i^0 + \epsilon \quad (3)$$

Equation (2) now becomes

$$\phi(\underline{b}^E, \underline{y}^E) = 0 \quad (4)$$

Now, a modified residual-correction or Newton-Raphson technique is applied to solve Eq. (4), treating \underline{y}^E as the vector of unknowns.

Then, the sensitivity vector is given approximately by

$$dg/db_i = [g(\underline{b}^E, \underline{y}^E) - g(\underline{b}^0, \underline{y}^0)]/\epsilon \quad (5)$$

For the eigenvalue problem, as discussed later, the system in Eq. (4) is augmented by a certain orthogonality relation. Note that certain coefficient matrices involving stiffness, mass, etc. have been decomposed at the current design while solving for y^0 . The iterative approach presented here can be viewed as re-analysis schemes used to solve Eq. (4), which uses the already decomposed matrices. Since the perturbation ϵ is very small, the iterative schemes converge very rapidly.

DISPLACEMENT AND STRESS SENSITIVITY

A finite element model of the structure is assumed. The problem of obtaining design derivatives of displacements and stresses is now considered. Consider a function

$$g = g(\underline{b}, \underline{z}) \quad (6)$$

which represents a stress constraint, with $\underline{b} = (k \times 1)$ design vector and $\underline{z} = (n \times 1)$ displacement vector which is obtained from the finite element equations

$$\underline{K}(\underline{b}) \underline{z} = \underline{F}(\underline{b}) \quad (7)$$

where \underline{K} is an $(n \times n)$ structural stiffness matrix, and \underline{F} is an $(n \times 1)$ nodal load vector. Let \underline{b}^0 be the current design. At this stage, the analysis has been completed. Thus, the decomposed $\underline{K}(\underline{b})^0$ and \underline{z}^0 are known.

The derivative of the function g with respect to the i th design variable is given by

$$dg/db_i = \partial g / \partial b_i + \partial g / \partial \underline{z} \cdot d\underline{z} / db_i \quad (8)$$

The partial derivatives $\partial g / \partial \underline{b}$ and $\partial g / \partial \underline{z}$ are readily available using the finite element relations. The problem, therefore, is to compute the displacement sensitivity, $d\underline{z} / db_i$. An iterative approach for computing this is now given.

Corresponding to the i th design variable, let the perturbed design vector, \underline{b}^ϵ , be defined as

$$\underline{b}^\epsilon = (b_1^0, b_2^0, \dots, b_i^0 + \epsilon, \dots, b_k^0)^T \quad (9)$$

The perturbation ϵ is relatively small, and a value of 1% of b_i has found to work well in practice. The choice of ϵ is based on balancing the truncation and cancellation errors. The problem is to find \underline{z}^ϵ , the solution of

$$\underline{K}(\underline{b}^\epsilon) \underline{z}^\epsilon = \underline{F}(\underline{b}^\epsilon) \quad (10)$$

using the decomposed $\underline{K}(\underline{b}^0)$ and \underline{z}^0 . A modified version of the residual-correction scheme given in (ref. 2) is given below.

Algorithm 1 (Displacement and Stress Sensitivity)

Step (0). Set $j=0$. Choose the perturbation ϵ and the error tolerance Δ .

Define \underline{b}^ϵ as in Eq. (9).

Step (i). Calculate the residual \underline{r}^j from

$$\underline{r}^j = \underline{K}(\underline{b}^\epsilon) \underline{z}^j - \underline{F}(\underline{b}^\epsilon) \quad (11)$$

Step (ii). Solve for the correction \underline{e}^j from

$$\underline{K}(\underline{b}^0) \underline{e}^j = -\underline{r}^j \quad (12)$$

Step (iii). Update

$$\underline{z}^{j+1} = \underline{z}^j + \underline{e}^j \quad (13)$$

Step (iv). Check the convergence criterion

$$|| \underline{z}^{j+1} - \underline{z}^j || \leq \Delta \quad (14)$$

If (14) is satisfied, then set $\underline{z}^\epsilon = \underline{z}^{j+1}$ and compute the displacement sensitivity as

$$d\underline{z} / d\mathbf{b}_i = (\underline{z}^\epsilon - \underline{z}^0) / \epsilon \quad (15)$$

The stress sensitivity can be recovered from Eq. (8). If Eq. (14) is not satisfied, set $j = j+1$ and re-execute steps (i)-(iv) above.

Numerical results and comparison with the exact and semi-analytical methods discussed in the literature are presented subsequently. Theoretically, it can be shown that the above scheme will converge provided [2]:

$$r_\sigma [\underline{I} - \underline{K}^{-1}(\underline{b}^0) \underline{K}(\underline{b}^\epsilon)] < 1 \quad (16)$$

where $r_\sigma(\underline{A})$ = spectral radius of the matrix \underline{A} , which is the maximum size of the eigenvalues of \underline{A} . In the problem considered here, $\underline{K}(\underline{b}^0)$ and $\underline{K}(\underline{b}^\epsilon)$ are roughly equal owing to ϵ being small, and (16) can generally be expected to hold.

EIGENVALUE AND EIGENVECTOR SENSITIVITY

Eigenvalue sensitivity is useful when resonant frequencies or critical buckling loads need to be restricted. Exact analytical expressions for eigenvalue sensitivity can be readily derived for the case of non-repeated roots [3]. The problem of obtaining eigenvector sensitivity, on the other hand, is more complicated and is an area of current interest [4-7]. Eigenvector sensitivity is useful in obtaining the design derivatives of

forced dynamic response. Here, an iterative approach is presented for approximate derivatives of eigenvalues and eigenvectors. The approach is particularly easy to implement in a program and provides both eigenvalue and eigenvector derivatives simultaneously. Further, the derivative of a particular eigenvector does not require knowledge of all eigenvectors of the problem, as with certain analytical methods.

Consider the generalized eigenvalue problem

$$\underline{K}(\underline{b})\underline{y} = \lambda \underline{M}(\underline{b})\underline{y} \quad (17)$$

where λ is a particular non-repeated eigenvalue and \underline{y} is the associated eigenvector. For the frequency problem, \underline{K} and \underline{M} represent the structural stiffness and mass matrices, respectively. For the buckling problem, \underline{K} and \underline{M} represent the structural stiffness and geometric stiffness matrices, respectively. It is desired to find the sensitivities $d\lambda/db$ and $d\underline{y}/db$. Let \underline{b}^0 be the current design vector and $(\lambda_0, \underline{y}^0)$ be a given

eigenvalue-eigenvector pair at the current design. Let \underline{b}^ϵ be a perturbed design vector as given in Eq. (9). The residual is given by

$$\underline{R} = \underline{K}(\underline{b}^\epsilon)\underline{y}^\epsilon - \lambda_\epsilon \underline{M}(\underline{b}^\epsilon)\underline{y}^\epsilon \quad (18)$$

The object is to solve the nonlinear equations $\underline{R} = \underline{0}$ for the unknowns λ_ϵ and \underline{y}^ϵ ; the Newton-Raphson technique is used for this purpose. The Jacobian \underline{J}

of the system in Eq. (18) is $[\partial \underline{R} / \partial \underline{y}^\epsilon, \partial \underline{R} / \partial \lambda_\epsilon]$. The Newton-Raphson equations are consequently:

$$[\underline{K}(\underline{b}^\epsilon) - \lambda_\epsilon \underline{M}(\underline{b}^\epsilon) \quad -\underline{M}(\underline{b}^\epsilon)\underline{y}^\epsilon] \begin{pmatrix} \delta \underline{y} \\ \delta \lambda \end{pmatrix} = -\underline{R} \quad (19)$$

Note, however, that Eq. (19) represents a system with n equations and $(n+1)$ unknowns; an additional equation is needed. This additional equation is obtained by introducing the normalization condition

$$-\underline{y}^T \underline{M} \delta \underline{y} = 0 \quad (20)$$

which states that the change in the eigenvector is orthogonal to the original eigenvector with respect to the mass matrix. In fact, the above scheme has been used as a re-analysis approach in (ref. 8). Here, an additional modification is made: the Jacobian matrix in Eq. (19) is

modified by replacing $\underline{K}(\underline{b}^\epsilon)$ by $\underline{K}(\underline{b}^0)$, \underline{y}^ϵ by \underline{y}^0 and λ_ϵ by λ_0 . The

motivation for this, as in the previous section, is to preserve a constant coefficient matrix in the iterative scheme. The resulting efficiency has not been found to affect the convergence of the procedure owing to the relatively small size of ϵ . The above modifications lead to an iterative scheme based on solving the system.

$$[\underline{C}] \begin{pmatrix} \delta \underline{y} \\ \delta \lambda \end{pmatrix} = \begin{pmatrix} -\underline{R} \\ 0 \end{pmatrix} \quad (21)$$

where

$$\underline{C} = \begin{pmatrix} \underline{K}(\underline{b}^0) - \lambda_0 \underline{M}(\underline{b}^0) & -\underline{M}(\underline{b}^0) \underline{y}^0 \\ -\underline{y}^{0T} \underline{M}(\underline{b}^0) & 0 \end{pmatrix} \quad (22)$$

The coefficient matrix is symmetric and nonsingular for the case of non-repeated roots [8]. Gaussian elimination can be used to solve Eq. (21). The algorithm for eigenvalue-eigenvector sensitivity is now given.

Algorithm 2 (Eigenvalue-Eigenvector Sensitivity)

Step (0). Set $j=0$. Choose the perturbation ϵ and the error tolerances Δ_1 and Δ_2 .

Define \underline{b}^ϵ as in Eq. (9). Decompose the matrix \underline{C} given in Eq. (22).

Step (i). Define the residual

$$\underline{R}^j = \underline{K}(\underline{b}^\epsilon) \underline{y}^j - \lambda_j \underline{M}(\underline{b}^\epsilon) \underline{y}^j \quad (23)$$

Step (ii). Solve the algebraic equations

$$[\underline{C}] \begin{pmatrix} \delta \underline{y} \\ \delta \lambda \end{pmatrix} = \begin{pmatrix} -\underline{R}^j \\ 0 \end{pmatrix} \quad (24)$$

for $\delta \underline{y}$ and $\delta \lambda$.

Step (iii). Update

$$\begin{aligned} \underline{y}^{j+1} &= \underline{y}^j + \delta \underline{y} \\ \lambda_{j+1} &= \lambda_j + \delta \lambda \end{aligned} \quad (25)$$

Step (iv). Check the convergence criterion

$$\| \delta \underline{y} \| \leq \Delta_1, \quad | \delta \lambda | \leq \Delta_2 \quad (26)$$

If (26) is satisfied, then set $\underline{y}^\epsilon = \underline{y}^{j+1}$, $\lambda_\epsilon = \lambda_{j+1}$ and compute the sensitivity as

$$\begin{aligned} d\underline{y}/db_i &= (\underline{y}^\epsilon - \underline{y}^0)/\epsilon \\ d\lambda/db_i &= (\lambda_\epsilon - \lambda_0)/\epsilon \end{aligned} \quad (27)$$

If (26) is not satisfied, set $j = j+1$ and re-execute steps (i)-(iv) above.

Numerical results are presented in the following section.

NUMERICAL RESULTS

Thin plate problem

Consider the plane stress problem in Fig. 1, where inverse thicknesses are the design variables. That is, the reciprocal of the plate thickness is chosen as a design variable. Inverse design variables are used in optimal design literature because they linearize the stress function and lead to improved convergence. The stress constraint function is the von Mises failure criterion in element j , given by

$$g_j = \sigma_{VM}/\sigma_a - 1 \quad (28)$$

where $\sigma_{VM}^2 = \sigma_x^2 + \sigma_y^2 - \sigma_x\sigma_y + 3\tau_{xy}^2$ and σ_a = constant allowable stress limit. Constant strain triangular elements are used. For brevity, only the design sensitivity coefficients, dg_{19}/db_{19} and dg_{24}/db_{24} , are presented in Table 1. The sensitivity vectors have been obtained using Algorithm 1 discussed earlier. In Table 1, the results obtained by the iterative method are compared with the semi-analytical method used widely in the literature, based on the formula in Eq. (8) with dz/db_i obtained from

$$K \frac{dz}{db_i} = - \frac{K(b^E) - K(b^0)}{\epsilon} \frac{z}{\epsilon} + \frac{[F(b^E) - F(b^0)]}{\epsilon} \quad (29)$$

The results are also compared with the exact sensitivity obtained using analytical derivatives. It is interesting to note that the semi-analytical method yields the same result as the first iteration of the iterative method. However, the iterative method further improves upon this and approaches the exact sensitivity (Table 1). While all methods yield values of acceptable accuracy, the comparison serves to illustrate the nature of the iterative process. This aspect is shown graphically in Fig. 2. It is noted that when using direct variables (as opposed to reciprocal variables), the semi-analytical method yields essentially exact sensitivity owing to the fact that stiffness is a linear function of design variables.

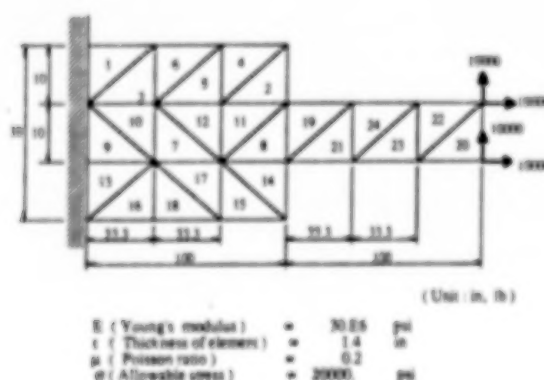


Figure 1.

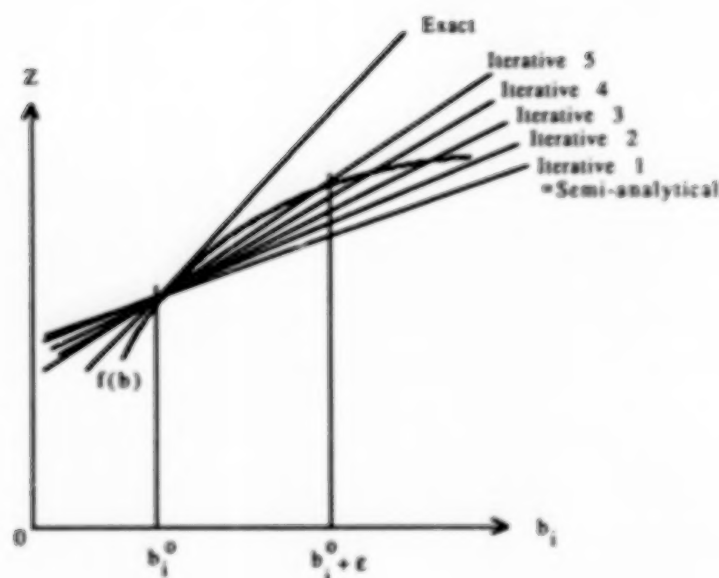


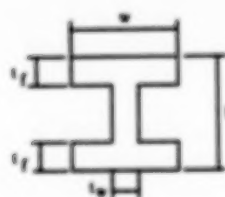
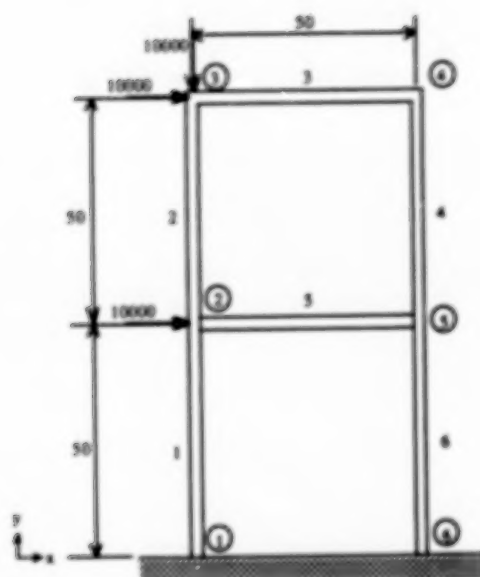
Figure 2.

Table 1.

Method		dg19/db19	dg24/db24
Iterative	1	8.7098	5.6437
	2	8.7949	5.6980
	3	8.7957	5.6986
Semi-analytical		8.7098	5.6437
Exact		8.7969	5.7002

Plane Frame Problem

Consider the frame structure in Fig. 3. The design variables associated with the I-section are $\mathbf{b} = (h, w, t_w, t_f)$ as shown in Fig. 3. The current design is $\mathbf{b} = (3.0, 3.0, 0.3, 0.5)$ for each element. The sensitivity of the lowest eigenvalues and corresponding eigenvector obtained using Algorithm 2 given earlier is presented in Tables 2 and 3, respectively. For the eigenvector, only selected sensitivity coefficients are presented for brevity. The maximum number of iterations required for an error tolerance of 10^{-7} is five. Thus, we see that convergence of the algorithm is very rapid and simple to implement. Also, the algorithm does not require computation of all eigenvectors to find the sensitivity of a few specific eigenvectors. However, if the sensitivity of all eigenvectors is required, then alternative approaches may be preferable.



Section

figure 3.

Table 2.

No. of design variable	Eigenvalue sensitivity
1	4359.6
2	1746.9
3	1418.1
4	10481.0
5	807.7
6	-1077.6
7	-4369.5
8	-6465.5
9	803.2
10	-2058.8
11	-7315.0
12	-12353.0
13	807.7
14	-1077.6
15	-4369.5
16	-6465.5
17	9957.6
18	1964.0
19	540.4
20	11784.0
21	4359.6
22	1746.9
23	1418.1
24	10481.0

Table 3.

No. of degree of freedom	dy/db ₅	dy/db ₁₇
4	0.036758	0.021438
5	0.000370	0.002413
6	-0.000868	0.003890
7	-0.028554	-0.007628
8	0.000378	0.002547
9	-0.002667	-0.000389
10	-0.028327	-0.007628
11	-0.000653	-0.002547
12	0.001614	-0.000389
13	0.036339	0.021438
14	-0.000407	-0.002413
15	0.000147	0.003890

Fluid Mechanics Problem

The objective of this problem in Fig. 4 is to obtain the sensitivities of the maximum absolute eigenvalue and eigenvector of the amplification matrix G of the incompressible Euler equations in fluid mechanics (ref. 9). This problem is motivated from a study of the stability of the computational algorithm. The Euler equations are

$$\begin{aligned}
 & \left[\underline{I} - \Delta t \underline{D} + \frac{\epsilon_1}{4} (1 - \cos \theta_x) \underline{I} + i \frac{\Delta t}{\Delta x} \underline{A} \sin \theta_x \right] (\underline{I} - \Delta t \underline{D})^{-1} \\
 & + \left[\underline{I} - \Delta t \underline{D} + \frac{\epsilon_1}{4} (1 - \cos \theta_y) \underline{I} + i \frac{\Delta t}{\Delta y} \underline{B} \sin \theta_y \right] (\underline{I} - \Delta t \underline{D})^{-1} \\
 & + \left[\underline{I} - \Delta t \underline{D} + \frac{\epsilon_1}{4} (1 - \cos \theta_z) \underline{I} + i \frac{\Delta t}{\Delta z} \underline{C} \sin \theta_z \right] (\underline{G} - \underline{I}) \\
 & = \Delta t \underline{D} \frac{\epsilon_e}{2} [(1 - \cos \theta_x)^2 + (1 - \cos \theta_y)^2 + (1 - \cos \theta_z)^2] \underline{I} \\
 & \quad - i \left[\frac{\Delta t}{\Delta x} \underline{A} \sin \theta_x + \frac{\Delta t}{\Delta y} \underline{B} \sin \theta_y + \frac{\Delta t}{\Delta z} \underline{C} \sin \theta_z \right]
 \end{aligned}$$

where, \underline{I} is a (4x4) identity matrix.
The source Jacobian Matrix is

$$[D] = \begin{Bmatrix} 0 & 0 & 0 & 0 \\ 1/r & 0 & 2\omega + 2u_y/r & 0 \\ 0 & -2\omega - u_y/r & -u_x/r & 0 \\ 0 & 0 & 0 & 0 \end{Bmatrix}$$

and the flux Jacobian matrices are

$$[A] = \begin{Bmatrix} 0 & \beta & 0 & 0 \\ 1 & 2u_x & 0 & 0 \\ 0 & u_y & u_x & 0 \\ 0 & u_z & 0 & u_x \end{Bmatrix}$$

$$[B] = \begin{Bmatrix} 0 & 0 & \beta & 0 \\ 0 & u_y & u_x & 0 \\ 1 & 0 & 2u_y & 0 \\ 0 & 0 & u_z & u_y \end{Bmatrix}$$

$$[C] = \begin{Bmatrix} 0 & 0 & 0 & \beta \\ 0 & u_z & 0 & u_x \\ 0 & 0 & u_z & u_y \\ 1 & 0 & 0 & 2u_z \end{Bmatrix}$$

The time step is

$$\Delta t = \frac{CFL}{\sqrt{\lambda_x^2 + \lambda_y^2 + \lambda_z^2}}$$

The maximum eigenvalue of matrices [A], [B], [C] are

$$\begin{aligned} \lambda_x &= \frac{1}{\Delta x} \left[|u_x| + \sqrt{u_x^2 + \beta} \right] \\ \lambda_y &= \frac{1}{\Delta y} \left[|u_y| + \sqrt{u_y^2 + \beta} \right] \\ \lambda_z &= \frac{1}{\Delta z} \left[|u_z| + \sqrt{u_z^2 + \beta} \right] \end{aligned}$$

Data

Grid sizes in x, y and z directions are $\Delta x = 1/16$, $\Delta y = \pi/32$, $\Delta z = 1/32$.
Parameter of time-derivative term is $\beta = 1$.
Radius is $r=2$, angular velocity of propeller is $\omega=2$.
Parameter CFL (Courant-Friedrichs-Lewy Number) is $= 5$.
Fluid velocities in x, y, z directions are $u_x = 0.5$, $u_y = 1$, $u_z = 1$.
The implicit second-order artificial viscosity is $\epsilon_i = 0$.
The explicit fourth-order artificial viscosity is $\epsilon_e = 0$.
The lower boundaries of wavenumbers θ_x , θ_y , θ_z are $= 0$, and the upper boundaries are $= \pi$.

Results

The optimum values of wavenumbers θ_x , θ_y , θ_z at which the absolute value of maximum eigenvalue are maximum, are obtained by using the optimization program LINRM [10]. The results are $\theta_x = \theta_y = \theta_z = \pi/2$. All sensitivity calculations are now done at these values of θ_x , θ_y and θ_z . The sensitivity of the maximum eigenvalue, absolute maximum eigenvalue and corresponding eigenvector are shown in Tables 4 and 5.

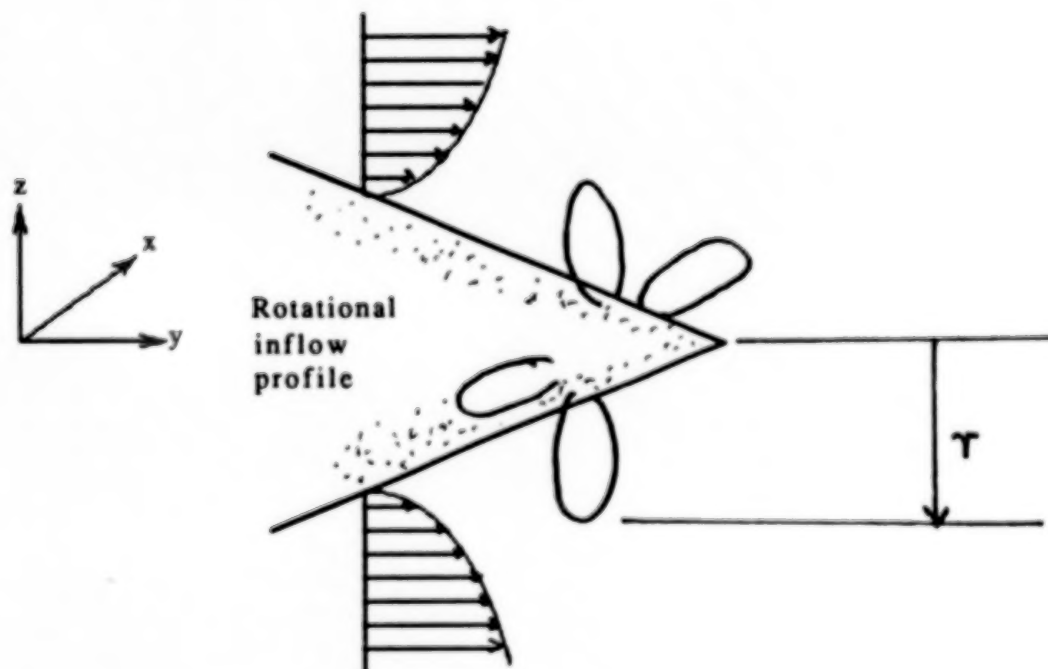


Figure 4.

Table 4. Eigenvalue Sensitivity for Fluid Mechanics Problem

$$\Delta = 1 \times 10^{-8}, \epsilon = 0.01$$

Design Variable	Eigenvalue Sensitivity	
	$d\lambda/db$	$d \lambda /db$
u_x	-0.03928 -0.11272 i	-0.08543
u_y	0.25361 -0.02037 i	0.21790
u_z	-0.23827 -0.36236 i	-0.37489
CFL	0.13254 +0.06004 i	0.14541
ϵ_i	-0.12951 -0.29317 i	-0.24668
ϵ_e	-0.84451 -0.46701 i	-0.54753
ω	-0.01807 +0.02823 i	-0.00358
θ_x	-0.00138 -0.00002 i	-0.00125
θ_y	-0.00182 -0.00010 i	-0.00167
θ_z	-0.00204 -0.00189 i	-0.00267

$$b^0 = (0.5, 1, 1, 5, 0, 0, 2, \pi/2, \pi/2, \pi/2)$$

$$\lambda^0 = 0.94882 + 0.47287 i$$

$$|\lambda^0| = 1.0601$$

Table 5. Eigenvector Sensitivity for Fluid Mechanics Problem

$$\Delta = 1 \times 10^{-8}, \epsilon = 0.01$$

Degree of Freedom	$dy/d \text{ CFL}$	$dy/d\omega$
1	-0.22740 -0.27610 i	0.03483 +0.01911 i
2	-0.34796 -0.03808 i	0.00969 -0.00969 i
3	-0.20260 -0.10825 i	0.07636 +0.00170 i
4	-0.19075 -0.10196 i	0.03520 -0.01693 i

192

SUMMARY AND CONCLUSIONS

A numerical method has been presented for design sensitivity analysis. The idea is based on using iterative methods for re-analysis of the structure due to a small perturbation in the design variable. A forward difference scheme then yields the approximate sensitivity. Algorithms for displacement and stress sensitivity as well as for eigenvalues and eigenvector sensitivity are developed. The iterative schemes have been modified so that the coefficient matrices are constant and hence decomposed only once. The convergence is found to be very rapid. Further, implementation of the algorithms is simple.

REFERENCES

1. Adelman, H.M., Haftka, R.T., Camarda, C.J. and Walsh, J.L.: Structural Sensitivity Analysis: Methods, Applications and Needs. Proc. Symposium on Recent Experiences in Multidisciplinary Analysis and Optimization, NASA Langley Research Center, Hampton, VA, April 1984, pp. 367-384.
2. Atkinson, K.E.: An Introduction to Numerical Analysis. John Wiley, New York, 1978.
3. Haug, E.J. and Arora, J.S.: Applied Optimal Design. John Wiley, New York, 1979.
4. Reiss, R.: Design Derivatives of Eigenvalues and Eigenfunctions for Self-Adjoint Distributed Parameter Systems. AIAA Journal, Vol. 24, No. 7, July 1986, pp. 1169-1172.
5. Hou, J.W. and Yuan, J.Z.: Calculation of Eigenvalue and Eigenvector Derivatives for Nonlinear Beam Vibrations. Submitted to AIAA Journal, Feb. 1986.
6. Ojalvo, I.U.: Efficient Computation of Mode-Shape Derivatives for Large Dynamic Systems. AIAA Journal, Vol. 25, No. 10, 1987, pp. 1386-1390.
7. Cardani, C. and Mantegazza, P., "Calculation of Eigenvalue and Eigenvector Derivatives for Algebraic Flutter and Divergence Eigenproblems. AIAA Journal, Vol. 17, No. 4, April 1979, pp. 408-412.
8. Robinson, A.R. and Harris, J.F.: Improving Approximate Eigenvalues and Eigenvectors. Journal of the Engineering Mechanics Division, Vol. 97, No. EM2, April 1971, pp. 457-475.
9. Merkle, C.L., Tsai, Y.P. and Huang, T.T.: Euler Equation Analysis of Rotational Flow Through Propellers. Presented at the 17th Symposium of Naval Hydrodynamics, Belgium, 1988.
10. Belegundu, A.D. and Arora, J.S.: A Recursive Quadratic Programming Method with Active Set Strategy for Optimal Design. Int'l. Journal for Numerical Methods in Engineering, Vol. 20, 1984, pp. 803-816.

RESULTS OF AN INTEGRATED STRUCTURE/CONTROL LAW DESIGN SENSITIVITY ANALYSIS

**Michael G. Gilbert
Structural Dynamics Division
Aeroservoelasticity Branch
NASA Langley Research Center
Hampton VA**

ABSTRACT

Next generation air and space vehicle designs are being driven by increased performance requirements, demanding a high level of design integration between traditionally separate design disciplines. Interdisciplinary analysis capabilities have been developed, for aeroservoelastic aircraft and large flexible spacecraft control for instance, but the requisite integrated design methods are only beginning to be developed. One integrated design method which has received attention is based on hierarchical problem decompositions, optimization, and design sensitivity analyses. This paper highlights a design sensitivity analysis method for Linear, Quadratic Cost, Gaussian (LQG) optimal control laws, which predicts the change in the optimal control law due to changes in fixed problem parameters using analytical sensitivity equations. Numerical results of a design sensitivity analysis for a realistic aeroservoelastic aircraft example are presented. In this example, the sensitivity of the optimally controlled aircraft's response to various problem formulation and physical aircraft parameters is determined. These results are used to predict the aircraft's new optimally controlled response if the parameter was to have some other nominal value during the control law design process. The sensitivity results are validated by recomputing the optimal control law for discrete variations in parameters, computing the new actual aircraft response, and comparing with the predicted response. These results show an improvement in sensitivity accuracy for integrated design purposes over methods which do not include changes in the optimal control law. Use of the analytical LQG sensitivity expressions is also shown to be more efficient than finite difference methods for the computation of the equivalent sensitivity information.

INTRODUCTION

The design of new generation air and space vehicles is increasingly becoming subject to extensive requirements for design integration, that is, close coordination in the design of the various systems of the vehicle. For example, many modern fighter aircraft require integration of the flight control system and the propulsion system so that sufficient power is available at all flight conditions possible with the flight control system. To meet the challenge of the integrated system design requirements, design methods which tie together existing system design methods are needed.

One such integrated design methodology currently under development at NASA Langley Research Center is based on hierarchical problem decompositions, multilevel optimization methods, and design sensitivity analyses [1]. This methodology depends on the decomposition of the integrated design problem into vehicle requirements, system requirements, and subsystem requirements. Optimization methods are used to satisfy all levels of the design requirements, subject to the constraints that any previously satisfied design requirements remain satisfied. The continued satisfaction of previous design requirements is achieved through the use of design sensitivity information which relates the change in the previous design to the current design variables. This sensitivity information is used as gradient information in the current optimization to make sure the constraints are satisfied.

One application of the multilevel integrated design methodology is to the aeroservoelastic design of aircraft, which is the simultaneous consideration of aircraft aerodynamics, control laws, and structural dynamics. This application requires the incorporation of dynamic response design requirements and a control law design method which uses the available feedback signals, both of which required development and validation of appropriate design sensitivity information. Linear Quadratic Gaussian (LQG) control law design methods were selected. The sensitivity developments have recently been completed [2] and the application and validation of the sensitivity expressions is described here. Initially, aerodynamic design would not be attempted, although aerodynamic effects must be included in the calculation of dynamic responses.

Integrated Interdisciplinary Methods Are Needed for Advanced Air and Space Vehicle Design

One Approach Is Hierarchically Decomposed, Optimization and Sensitivity Analysis Based Methods

Criteria for Initial Aeroservoelastic Design Method:

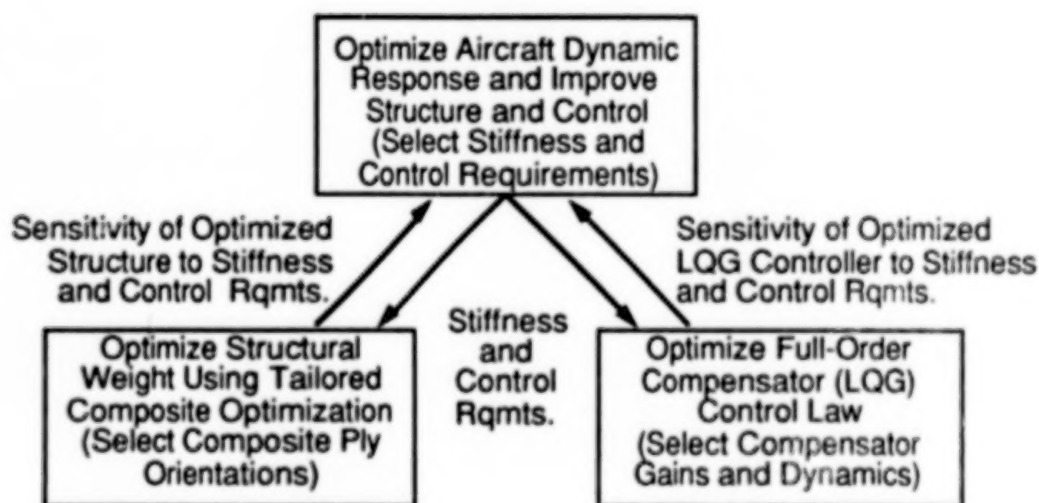
- Include Dynamic Response, Stability, and Robustness Requirements In Problem Formulation
- Control Law Design Method Must Use Measured Feedback Signals
- Use Existing Multilevel Structural Optimization Methods

Emphasis Here is on Sensitivity Analysis and Validation Results

MULTILEVEL STRUCTURE/CONTROL LAW DESIGN

A multilevel, integrated structure/control law design problem for an aeroelastic aircraft can be formulated conceptually as shown. In this formulation, the structural design problem is to minimize the weight of the structure subject to stiffness and stress requirements, and also to control law design requirements. Since the aircraft is aeroelastic, steady-state control actions (control surface deflections) can change structural deflections under given loads, and so must be considered in the structural design. The control law design problem is to minimize a quadratic performance index in aircraft responses and control inputs. Since the structural design defines the structural dynamic properties of the aircraft, the control law design problem is also dependent on the structural design requirements. The multilevel optimization approach to integrated design then treats the structural and control law design requirements as design variables, selecting those requirements so that the dynamic response of the vehicle is improved, and so that the structural design and the control law design are also improved. It requires the sensitivity of the optimized structure and control law designs to stiffness and control design requirements as gradient information at the upper level.

Analytical expressions for the sensitivity of optimized LQG control laws have previously been developed directly from the necessary conditions of optimality for the LQG problem. These results will be described following a statement of the LQG problem formulation.



Analytical Expressions for the Sensitivity of the Optimized LQG Control Law Have Previously Been Developed

Sensitivity Expressions Were Derived Directly From the Necessary Conditions of Optimality for the LQG Problem

LQG CONTROL LAW FORMULATION

The Linear, Quadratic Cost, Gaussian (LQG) optimal control law problem formulation is shown below, where x is the system state vector, u is the vector of control inputs, y is the vector of pertinent system responses, z is the vector of measured outputs to be used for feedback, and w and v are uncorrelated, zero mean, Gaussian distributed "white" noise disturbance vectors. The matrices A , B , C , D , and M are appropriately dimensioned coefficient matrices, and W and V are intensity matrices of the white noise disturbance vectors. It is assumed that each of these matrices is a known continuous differentiable function of one or more scalar parameters p which have some known nominal value. The LQG problem is to find the control $u(t)$ such that the cost function J is a minimum, where the weighting matrices Q and R are also assumed to be known continuous differentiable functions of p . The solution of this problem is well known and is the interconnection of the optimal Linear Quadratic Regulator (LQR) and the optimal Kalman Filter (KF) state estimator as shown below, where the matrices G and F are the regulator and state estimator gain matrices respectively [3]. Clearly the gain matrices G and F are functions of the parameter p , and it is desired to know the change in G and F due to variations in the nominal value of the parameter p . Analytical expressions for the change (sensitivity) of G and F with respect to p have been derived from the LQG necessary conditions of optimality, and are summarized on the next page.

$$\begin{aligned}\dot{x} &= A(p)x + B(p)u + D(p)w & E(w) &= 0; E(w(t)w^T(\tau)) = W(p)\delta(t-\tau) \\ y &= C(p)x & E(w(t)v^T(\tau)) &= 0 \\ z &= M(p)x + v & E(v) &= 0; E(v(t)v^T(\tau)) = V(p)\delta(t-\tau)\end{aligned}$$

Problem is to find $u(t)$ such that J is minimized for a given p :

$$J = \lim_{T \rightarrow \infty} E \left\{ \frac{1}{T} \int_0^T (y^T Q(p) y + u^T R(p) u) dt \right\}$$

Solution is the Interconnection of the Optimal Regulator and Kalman Filter

$$u = -G\hat{x}$$

$$\dot{\hat{x}} = A\hat{x} + Bu - F(z - M\hat{x})$$

Want Analytical Expressions for the Sensitivity of the Solution to Changes in Fixed Parameter p

LQG CONTROL LAW SENSITIVITY

The optimal LQR and KF gain matrices G and F are computed as shown below, where S and T are the steady-state solutions of the appropriate nonlinear matrix Riccati equations. Also shown are expressions for the partial derivatives of G and F with respect to p . Under the assumptions regarding the functional dependence of B , M , R , and V on p , the only unknowns in these expressions are the partial derivatives of the Riccati equation solutions S and T with respect to p . Analytical expressions for these partial derivatives can be derived from the necessary conditions of optimality [2] and the final results are shown below. These expressions are valid only when the necessary conditions of optimality are satisfied, that is when G and F are the gain matrices which make the cost function J be a minimum. They are themselves linear Lyapunov equations in the unknown derivatives (sensitivities) S_p and T_p , and have coefficient matrices which are asymptotically stable by the properties of the LQR and KF solutions. The asymptotic stability properties of the coefficient matrices guarantees that the Lyapunov equations have solutions which exist and are unique. Additionally, the coefficient matrices are the same for every parameter p , with only the known term in the $\{\}$ brackets changing. This affords considerable computational savings, since the coefficient matrices need only be decomposed once for the initial solution of the Lyapunov equations, stored, and reused for the remaining parameter sensitivity calculations.

(Note: Subscript p denotes partial derivative w.r.t. parameter p)

LQG Solution Given by:

$$G = R^{-1} B^T S \quad ; \quad 0 = A^T S + SA - SBR^{-1} B^T S + C^T QC$$

$$F = TM^T V^{-1} \quad ; \quad 0 = AT + TA^T - TM^T V^{-1} MT + DWD^T$$

Sensitivity of G and F with Respect to p is:

$$G_p = -R^{-1} R_p R^{-1} B^T S + R^{-1} B_p^T S + R^{-1} B^T S_p$$

$$0 = S_p(A-BG) + (A-BG)^T S_p + \{SA_p + A_p^T S + (C^T QC)_p - S(BR^{-1} B^T)_p S\}$$

$$F_p = T_p M^T V^{-1} + TM_p^T V^{-1} - TM^T V^{-1} V_p V^{-1}$$

$$0 = (A-FM)T_p + T_p(A-FM)^T + \{A_p T + TA_p^T + (DWD^T)_p - T(M^T V^{-1} M)_p T\}$$

OPTIMAL COST SENSITIVITY

Several equivalent expressions for the optimized value of the LQG cost function in terms of the LQR and KF gain matrices G and F and the Riccati equation solutions S and T are shown below, where J^* denotes the optimized cost function value and $\text{tr}\{\}$ denotes the trace of a matrix. By the chain rule of differentiation, the partial derivative of the optimized cost is the derivative of the optimized cost with respect to the gain matrix (G or F) times the derivative of the gain matrix with respect to p , plus the partial derivative products of all the other matrices in the cost function expressions. However, since the cost function J has been optimized with respect to the gain matrices (i.e. G and F satisfy the necessary conditions of optimality), the derivatives J_G^* and J_F^* are identically equal to zero, which means that the sensitivity of the optimized cost J_p^* is independent of changes in the optimal gain matrices G and F [2]. This makes the optimized value of the cost function J^* unattractive for use in the integrated structure/control law design algorithm as a measure of control law performance, since the sensitivity J_p^* does not reflect the actual changes in the optimal control law. For this reason, other measures of the optimally controlled systems performance, such as time and frequency responses, system eigenvalues, and covariance responses must be used in the integrated design methodology even though these responses have not been optimized with respect to G and F . The sensitivities of these other performance measures do reflect the effects of the change in the optimal gain matrices G and F due to changes in the parameter p . Analytical expressions for the sensitivities of these other controlled system performance measures also exist and are summarized on the next pages.

Optimized Cost Function Value

$$J^* = \text{tr}\{SFVF^T + TC^TQC\} = \text{tr}\{SDWD^T + TG^TRG\}$$

Consider That

$$J_p^* = J_F^* F_p + J_S^* S_p + \dots = J_G^* G_p + J_T^* T_p + \dots$$

But J is Optimal With Respect to F and G , i.e.

$$J_F^* = J_G^* = 0$$

So the Sensitivity of the Optimized Cost is Independent of the Sensitivity (Changes) in the Optimal Gain Matrices

DYNAMIC RESPONSE SENSITIVITY

Once the optimal LQG control law is computed, the regulator and Kalman Filter equations can be interconnected to form a set of state-space equations which represent the controlled system. This is represented below where the vector x is the controlled system state vector, y is the controlled system outputs, and w is the combined vector of disturbance inputs. Taking the partial derivative of the state equations with respect to the parameter p and interchanging the order of differentiation leads to the system sensitivity equations shown. When integrated over time for a known input time history $w(t)$ these equations give the sensitivity of the controlled system state vector and output vector time histories as a function of both the input and state vector time histories. These equations can also be used to determine the sensitivity of the frequency response of a single input/output pair by transformation of the system and sensitivity equations into the Laplace domain and replacing the Laplace transform variable s by the complex frequency $j\omega$ for zero initial conditions. Denoting the complex response of one input/output pair at a given frequency ω by h and the corresponding complex sensitivity result by h_p , the sensitivity of magnitude and phase of the response are computed as shown. If the interest is in more than one input/output pair, the singular values of the complex transfer function matrix H relating the input vector w and the output vector y are often calculated at discrete frequencies ω as a means of determining the response magnitude in all loops simultaneously. Assuming that none of the singular values is repeated, the sensitivity of the singular values at a given frequency is calculated from the complex transfer function sensitivity matrix using the same unitary transformation pair as determined in the singular value calculation [4].

$$\dot{x} = Ax + Dw$$

$$\dot{x}_p = A_p x + A x_p + D_p w$$

$$y = Cx$$

$$y_p = C_p x + C x_p$$

Sensitivity Equations Depend on System Response - Can Be Solved in Either Time or Frequency Domain

Frequency Response Sensitivities -

For a Complex Response $h = a + jb$ and Sensitivity $h_p = a_p + jb_p$

$$|h| = \sqrt{a^2 + b^2} \quad ; \quad |h|_p = \frac{1}{|h|} (aa_p + bb_p)$$

$$\phi = \tan^{-1} \frac{b}{a} \quad ; \quad \phi_p = \frac{1}{|h|^2} (ab_p - ba_p)$$

Singular Values of Complex Transfer Function Matrix H :

$$\Sigma = U^* H V \quad ; \quad \Sigma_p = U^* H_p V$$

(* here denotes complex conjugate transpose)

DYNAMIC RESPONSE SENSITIVITY (CONC.)

The eigenvalues of the system dynamics matrix A of a linear state-space system are often used as a measure of stability and performance. If the change in the matrix A with respect to a parameter p is known and there are no repeated eigenvalues, then the sensitivity of the eigenvalues due to a change in the parameter p can be calculated in terms of the derivative matrix A_p and the matrix E , whose columns are the right eigenvectors of the matrix A [5].

The response of a linear system to Gaussian distributed, "white" noise random inputs is measured in terms of covariance or mean square quantities. These are computed using the (steady-state) covariance equations shown below, where the matrix W is the intensity matrix of the random noise input and X is the state vector covariance to be calculated. Once X is known, other response quantities of interest are easily computed. Differentiation of the covariance equation with respect to the parameter p results in an equation for the sensitivity of the state vector covariance X_p in terms of the state vector covariance X [6]. The sensitivity of the other response quantities of interest are also easily computed.

System Eigenvalue Sensitivity

$$\Lambda = E^{-1}AE \quad ; \quad \text{diag}(\Lambda_p) = \text{diag}(E^{-1}A_pE)$$

Covariance Response Sensitivity

$$0 = AX + XA^T + DWD^T \quad ; \quad Y = CXC^T \quad ; \quad U = GXG^T$$

$$0 = AX_p + X_pA^T + A_pX + XA_p^T + (DWD^T)_p \quad ; \quad Y_p = (CXC^T)_p \quad ; \quad U_p = (GXG^T)_p$$

NUMERICAL SENSITIVITY STUDY

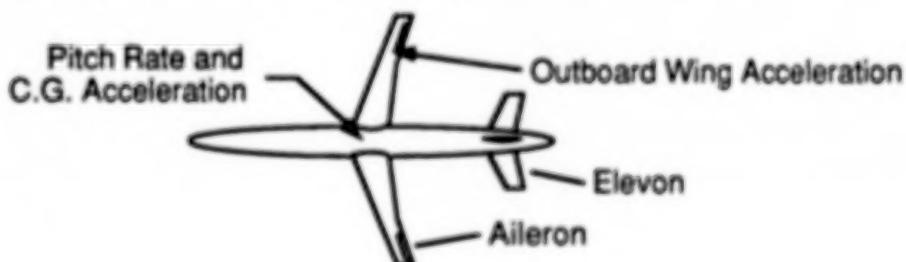
The previously described analytical sensitivity expressions for the change in optimal LQG control law designs and the optimally controlled linear system responses have been exercised on a real aeroservoelastic aircraft example. This problem considered the DAST ARW-II (Drones for Aerodynamic and Structural Testing, Advanced Research Wing II) aircraft, which was a Firebee drone vehicle modified for high risk aeroelastic and aeroservoelastic stability testing [7]. A mathematical model of the longitudinal dynamics of this vehicle including rigid-body pitch and plunge motions, three symmetric vibration modes, and elevon and symmetric aileron control surfaces was used. This model included unsteady aerodynamic effects for each mode. Vehicle pitch rate and vertical acceleration at the center-of-gravity, and outboard vertical wing acceleration measurements were available as feedback signals. An LQG optimal control law problem was formulated for this example to stabilize a nominally unstable short period mode. The sensitivity of the optimal control law and the dynamic responses of the controlled aircraft were computed for twelve different problem formulation and physical parameters. The response sensitivities computed included the sensitivity of the covariance response of the vehicle subjected to Dryden random vertical gust environment, the sensitivity of the vehicle time response to a discrete 1-Cosine vertical gust, and the sensitivity of the frequency response in the elevon loop of the aircraft.

25th Order State-Space Model of DAST ARW-II

- Rigid Body Plunge, Pitch, 3 Symmetric Elastic Modes, Unsteady GA's
- Elevon and Symmetric Aileron Control Surfaces
- Pitch Rate and Acceleration at C.G., Outboard Wing Acceleration Sensors

Sensitivity Information Calculated For Twelve Design Parameters:

- Response to Random Gust Environment (Covariance)
- Time Response to Discrete 1-Cos Gust
- Frequency Response of Open Elevon Loop (Aileron Loop Closed)



SENSITIVITY PARAMETERS

Shown below are the nominal values and descriptions of the twelve parameters for which the sensitivity of the DAST ARW-II control law and dynamic responses were computed. All twelve parameters influence the dynamic responses of the controlled system. The first four parameters are elements in the weighting matrices of the cost function for the LQG problem and directly affect the LQR regulator gain matrix G discussed previously. Parameters 5 through 8 are elements of the noise intensity matrices in the LQG formulation and directly affect the KF gain matrix F . The final four parameters represent physical quantities or characteristics of the vehicle and affect the LQR gain G , the KF gain F , and the basic dynamics of the vehicle. Parameter 9 is a wing bending stiffness related parameter which was used to uniformly increase or decrease the natural frequencies of the two wing bending modes. Parameter 10 is a wing torsion stiffness parameter similar to parameter 9 that was used to scale the wing torsion mode natural frequency. Parameters 11 and 12 were used to locate the wing accelerometer used for feedback longitudinally and laterally on the wing. The results to be presented in the next several figures emphasize the sensitivity of the aircraft responses to the four physical related parameters 9 through 12.

Parameter	Nominal Value	Description
1	0.01	Q Matrix Weight on Pitch Rate
2	0.01	Q Matrix Weight on Fwd. Wing. Acc.
3	1.00	R Matrix Weight on Elevon Com.
4	1.00	R Matrix Weight on Aileron Com.
5	2.00×10^{-3}	Pitch Rate Sensor Noise Intensity
6	6.00×10^{-3}	Aft Wing Acc. Sensor Noise Intensity
7	1.00×10^{-6}	Injected Elevon Noise Intensity
8	1.00×10^{-6}	Injected Aileron Noise Intensity
9	1.00	Wing Bending Stiffness Parameter
10	1.00	Wing Torsion Stiffness Parameter
11	7.58	Aft Wing Acc. Longitudinal Location
12	2.00	Aft Wing Acc. Lateral Location

OPTIMAL COST SENSITIVITY

The optimal LQG control law for the DAST ARW-II example problem was computed and analyzed for sensitivity to the twelve sensitivity parameters. Shown below are the value of the optimized cost function (J^*) and the semi-relative sensitivities of the cost function value to the sensitivity parameters. (Semi-relative sensitivity results are normalized such that the results are directly comparable for equal percent changes in the nominal parameter values.) Two sets of results are shown. Under the heading Design Sensitivity is the sensitivity of the optimized cost function to the twelve parameters computed using the analytical LQG sensitivity expressions discussed earlier. Under the heading Alternate Sensitivity is the sensitivity of the optimized cost to the four physical parameters 9 through 12 when the change in the optimized control law (gain matrices G and F) is ignored. These sensitivity results show only the effect of a change in basic system dynamics and do not include the effects of a change in the control law. The results are identical, verifying the previous assertion that the cost function sensitivity does not reflect changes in the optimized control law. Furthermore, the current method provides sensitivity information for a wider range of parameters than the alternate sensitivity information, since the first eight parameters affect only the gain matrices G and F .

(Optimal Cost = 1.222, Semi-Relative Sensitivity)

Parameter	Design Sensitivity	Alternate Sensitivity
1	5.17×10^{-4}	
2	2.35×10^{-1}	
3	7.58×10^{-3}	
4	4.90×10^{-1}	
5	1.35×10^{-3}	
6	2.53×10^{-2}	
7	5.90×10^{-6}	
8	1.48×10^{-10}	
9	-1.57×10^1	-1.57×10^1
10	-4.44×10^1	-4.44×10^1
11	9.84×10^{-3}	9.84×10^{-3}
12	-2.14×10^{-3}	-2.14×10^{-3}

COVARIANCE RESPONSE SENSITIVITY

The covariance response of the optimally controlled DAST ARW-II aircraft was computed for a 12 ft./sec. RMS vertical gust input using a Dryden gust spectrum. The sensitivity of the RMS vehicle pitch rate and center-of-gravity acceleration and vertical wing acceleration were computed for the twelve sensitivity parameters as shown. The wing acceleration result was measured at a constant point independent of the wing acceleration feedback signal so that the sensitivity results for parameters 11 and 12, which actually locate the feedback sensor, are consistent with the results for all the other parameters.

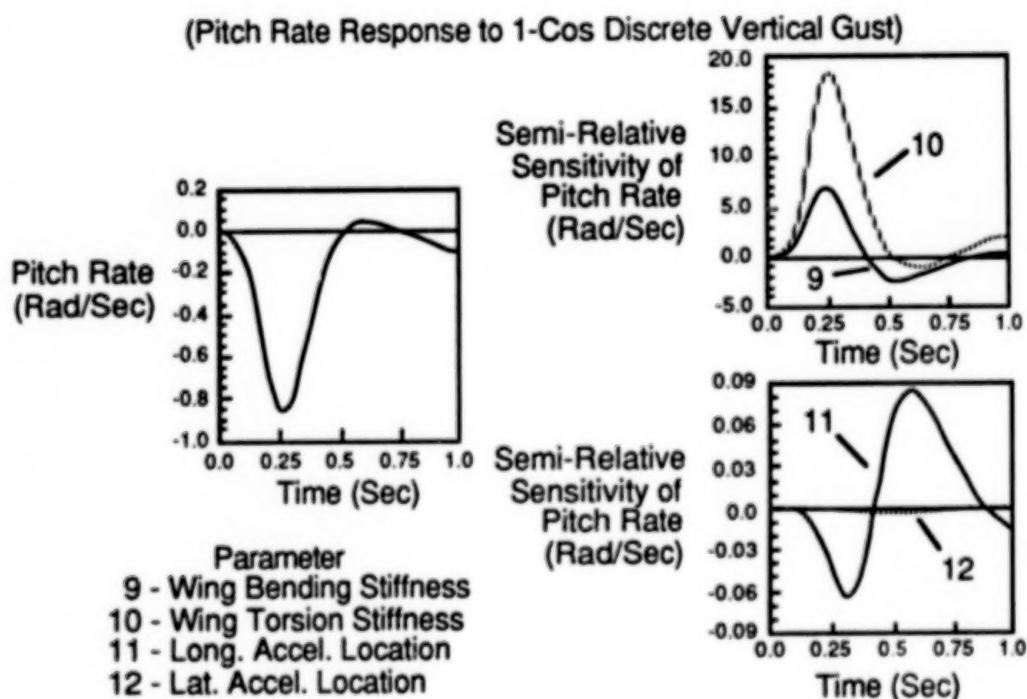
The results shown are best interpreted in terms of their sign and the magnitude of the exponents. For example the sensitivities of the three responses to parameter 9, the wing bending stiffness parameter, are all negative with the largest effect on wing acceleration. This means an increase in the wing bending stiffness would largely decrease the wing acceleration while also decreasing the pitch rate and c.g. acceleration. A positive change in parameter 10, the wing torsional stiffness parameter, would yield a larger decrease in the wing acceleration than the bending stiffness but would increase the pitch rate and c.g. acceleration results. A negative change in parameter 11, which locates the wing acceleration feedback sensor longitudinally on the wing, would decrease all three responses, while a change in parameter 12, the lateral wing feedback sensor locating parameter, would have a negligible effect compared to parameter 11.

(12 ft/sec RMS Vertical Gust Input, Semi-Relative Sensitivity)

Parameter	Pitch Rate (5.15×10^{-2} deg/sec)	C. G. Acceleration (2.65×10^{-2} g)	Wing Acceleration (2.35×10^{-1} g)
1	-6.18×10^{-3}	2.24×10^{-4}	6.24×10^{-5}
2	6.18×10^{-5}	-6.62×10^{-4}	-2.69×10^0
3	-1.60×10^{-2}	2.08×10^{-3}	1.00×10^{-1}
4	4.04×10^{-4}	1.93×10^{-3}	8.21×10^0
5	5.91×10^{-3}	9.91×10^{-4}	5.21×10^{-3}
6	1.22×10^{-3}	9.04×10^{-4}	7.98×10^{-1}
7	-1.77×10^{-4}	-4.77×10^{-6}	3.75×10^{-6}
8	-1.74×10^{-9}	1.55×10^{-8}	4.36×10^{-5}
9	-9.84×10^{-2}	-3.38×10^{-3}	-5.32×10^1
10	7.00×10^{-2}	4.04×10^{-2}	-1.22×10^2
11	1.35×10^{-3}	1.16×10^{-3}	2.94×10^{-1}
12	-3.43×10^{-5}	-6.64×10^{-5}	-6.80×10^{-2}

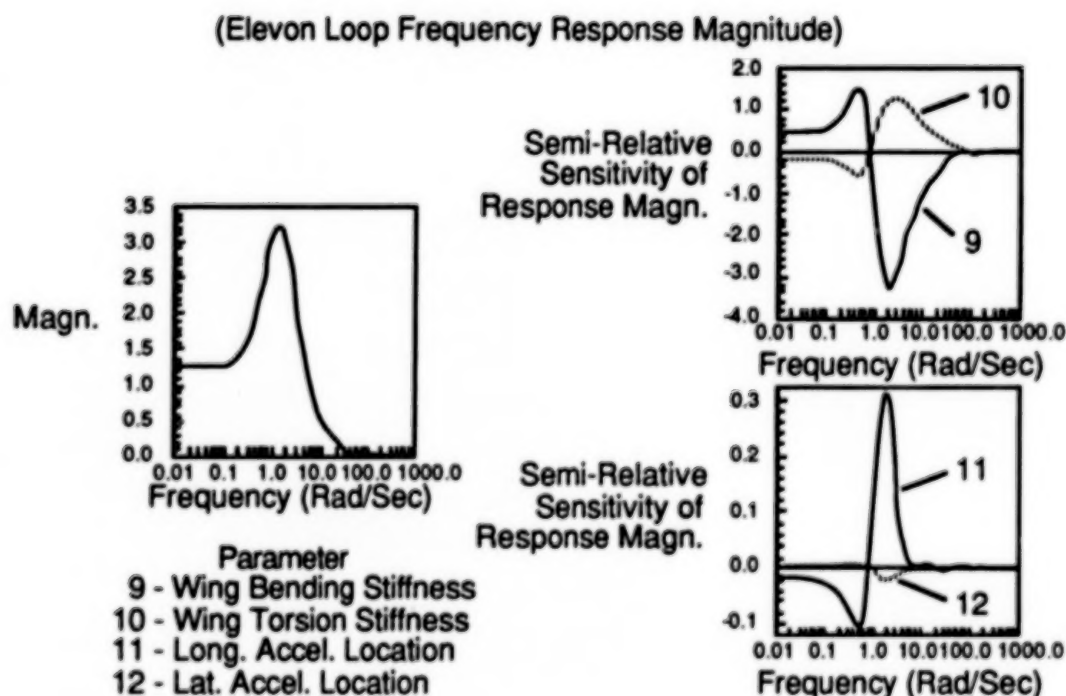
TIME RESPONSE SENSITIVITY

The time response of the optimally controlled DAST ARW-II aircraft was computed for a 1-cosine discrete vertical gust input with a maximum amplitude of 5 ft./sec. and a duration of 0.25 seconds. Shown below is the pitch rate response of the vehicle over one second and the sensitivity of that pitch rate response to the four physical parameters 9 through 12. The pitch rate response is more sensitive to the wing bending and torsion stiffness parameters than the wing acceleration feedback sensor location parameters. Increasing either the wing bending or torsion stiffness would tend to alleviate the peak negative pitch rate response at about 0.25 seconds. A negative change in the wing acceleration longitudinal position would also tend to reduce the peak negative pitch rate response at 0.25 seconds, but would increase oscillation in the response by adding an additional peak at about 0.65 seconds. The lateral location of the wing acceleration sensor would have a negligible effect on the pitch rate response.



FREQUENCY RESPONSE SENSITIVITY

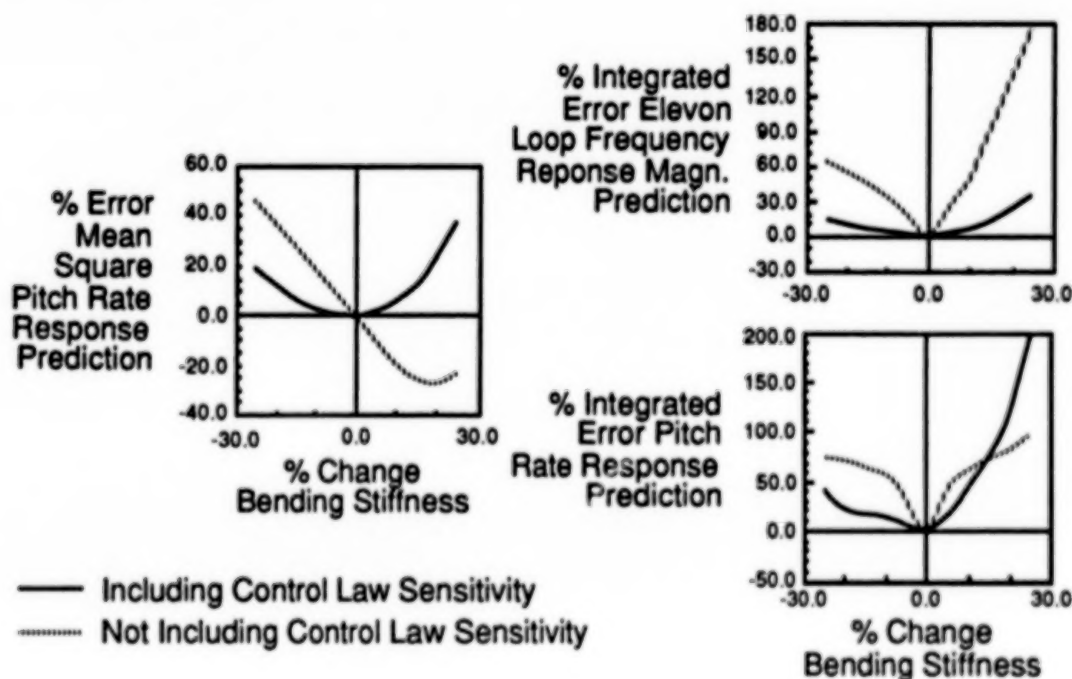
The magnitude of the elevon loop frequency response, computed with the aileron loop closed, is shown below as is the sensitivity of frequency response magnitude to the four physical parameters 9 through 12. Any one of the three parameters 9 through 11 could be used to reduce the peak magnitude of the response at about 2.0 rad./sec., or to decrease the bandwidth of the control loop by reducing the response magnitude above 2.0 rad./sec. Both actions could not be achieved using a single parameter, since the sensitivity results show that any parameter change used to decrease the peak response at 2.0 rad./sec. would tend to increase the bandwidth by increasing the response magnitude at higher frequencies.



SENSITIVITY VALIDATION

The covariance, time, and frequency response sensitivity results presented in the previous figures were validated against actual response changes, including the optimal LQG control law change effects, due to variations in various nominal parameter values. This was accomplished by computing the new optimal LQG control law for up to $\pm 25\%$ changes in nominal parameter values in $\pm 5\%$ increments, and then computing the actual covariance, time, or frequency response for that parameter value. These results were then compared with predictions of the new responses obtained by a first-order Taylor series expansion about the nominal response using the available sensitivity data and the magnitude of the parameter change. In addition, a second set of sensitivity data for the four physical parameters 9 through 12 was generated which ignored the changes in the optimal LQG control law (changes in the G and F matrices). This second set of sensitivity data was also used to predict changes in the optimally controlled response of the system due to changes in the nominal parameter values. Percent error comparisons for the two sets of response predictions are shown below for variations in the wing bending stiffness parameter (parameter 9).

For the covariance response predictions, the percent error in prediction of the mean square pitch rate response to the random gust environment is shown on the left. For the current design sensitivity method, which includes the effects of the optimal control law change, the percent error passes through zero with no slope, indicating an exact derivative result. The alternate sensitivity method, which does not include the control law change effects, has a nonzero slope in the error at the nominal parameter value. For variations in the wing bending stiffness of up to $+15\%$, the design sensitivity method gives more accurate predictions (smaller errors) of the actual pitch rate response. Similar types of results are shown on the right for elevon loop frequency response magnitude predictions and the pitch rate time response predictions for the discrete vertical gust input. In the case of these results, the percent error calculations were integrated over the frequency range or time interval to obtain a single error number for each varied value of wing bending stiffness parameter. As was the case for the covariance response predictions, the design sensitivity method gives more accurate results about the nominal parameter value, up to $+15\%$ variation in the wing bending stiffness parameter.



COMPARISON OF COMPUTATIONAL TIMES

The analytical expressions for the sensitivity of the optimal LQG control law involve the solution of two linear Lyapunov equations for each parameter of interest. In order to assess the computational burden associated with these calculations, a comparison of computational times to compute the derivative information using the analytical expressions and by finite difference methods was made. Four results are shown. The first is the CPU time required for the original LQG optimal control law solution using a DEC MicroVax II computer and a commercially available control analysis and design software package. The second result is the CPU time required for the original LQG solution and the solution of the two Lyapunov equations for the sensitivity of the gain matrices G and F and the Riccati matrices S and T for a single parameter. The third result is the CPU time required for the original LQG solution and a second LQG solution for a perturbed parameter value, as would be required for a one-step finite difference calculation of the change in the gain matrices G and F . The actual finite difference calculation is not included in the CPU time. The final result is similar to the third except two perturbed LQG solutions are computed, as would be required for a two-step finite difference calculation. Again the actual finite difference calculation is not included in the CPU time result. These results show that it is significantly faster to use the analytical expressions rather than finite difference calculations for the equivalent derivative information for a single parameter. As discussed earlier, the coefficients of the Lyapunov equations for the Riccati sensitivities are the same for every parameter, which can lead to additional computational savings by eliminating expensive decomposition of the coefficient matrices for each parameter. This means the computational efficiency of the analytical approach will be even better than shown here for the multiple parameter case.

Calculation	CPU Time (Sec.)
Original LQG Solution	100.68
LQG and Analytical Sensitivity of G, F, S, T	133.55
LQG and One Perturbed LQG For Numerical Sensitivity of G, F (Not Including Difference Calculation)	196.44
LQG and Two Perturbed LQG For Numerical Sensitivity of G, F (Not Including Difference Calculation)	287.39

CONCLUDING REMARKS

This paper has highlighted a method for computing the sensitivity of optimal LQG control laws to various problem parameters using analytical sensitivity expressions. The LQG sensitivity results are used in conjunction with the sensitivity of dynamic systems responses, also calculated using analytical expressions, to predict the changes in optimally controlled system responses due to changes in the nominal values of the problem parameters of interest. These sensitivity results are shown to be useful for integrated structure/control law design problems through a large aeroservoelastic aircraft example. Sensitivities of covariance, time, and frequency responses of the aircraft to twelve parameters were computed, and the results for four physical parameters were emphasized. The sensitivity results were validated against actual response changes due to changes in the nominal values of various parameters and found to be more accurate than alternate sensitivity calculations. It was also found that it is cheaper to evaluate the analytical expressions than to calculate the equivalent sensitivity derivatives by finite difference means.

A Control Law and Dynamic Response Sensitivity Analysis Capability Has
Been Developed

Exercised on a Large Aeroservoelastic Mathematical Model Example

- Sensitivities to Twelve Control Law and Physical Design Parameters
Calculated
- Validated Against Actual Response Changes Due to Changes in
Design Parameters
- More Accurate For Integrated Design Purposes Than Standard
Sensitivity Analysis Methods
- Analytical Expressions Cheaper To Evaluate Than Equivalent Finite
Difference Calculations

211

REFERENCES

- [1] Sobieszczanski-Sobieski, J., Barthelemy, J., and Giles, G., "Aerospace Engineering Design by Systematic Decomposition and Multilevel Optimization", ICAS-84-4.7.3, Sept. 1984.
- [2] Gilbert, M. G., "Design Parameter Sensitivity of Optimum LQG Control Laws for Application to an Integrated Interdisciplinary Design Methodology", PhD Dissertation, Purdue University, W. Lafayette IN, Dec. 1988.
- [3] Kwakernaak, H., and Sivan, R., *Linear Optimal Control Systems*, Wiley-Interscience, 1972.
- [4] Newsom, J., and Mukhopadhyay, V., "The Use of Singular Value Gradients and Optimization Techniques to Design Robust Controllers for Multiloop Systems", AIAA 83-2191, Guidance and Control Conference, Aug. 1983.
- [5] Crossley, T., and Porter, B., "Eigenvalue and Eigenvector Sensitivities in Linear Systems Theory", *Int. Journal of Control*, Vol. 10, No. 2, pg. 163-170, 1969.
- [6] Schaechter, D., "Closed-Loop Control Performance Sensitivity to Parameter Variations", *Journal of Guidance, Control, and Dynamics*, Vol. 6, No. 5, pg 399-402, Sept./Oct. 1983.
- [7] Murrow, H. N., and Eckstrom, C. V., "Drones for Aerodynamic and Structural Testing (DAST) - A Status Report", *Journal of Aircraft*, Vol. 16, No. 8, August 1979, pg. 521-526.

**ON THE CALCULATION OF
DERIVATIVES OF EIGENVALUES AND EIGENVECTORS
IN THE SIMULTANEOUS DESIGN AND CONTROL OF STRUCTURES**

**Luis Mesquita
Department of Engineering Mechanics
University of Nebraska at Lincoln
Lincoln, Nebraska**

and

**Manohar P. Kamat
School of Aerospace Engineering
Georgia Institute of Technology
Atlanta, Georgia**

ABSTRACT

Independent Modal Space Control (IMSC) is a technique that is often used for the control of large order structural systems. The pertinent optimization problem in the simultaneous design and control of structures is a min - min problem that minimizes with respect to the structural design variables, the minimum value of the performance index with respect to the control forces obtained using the IMSC technique. The minimization process requires derivatives of eigenvalues and eigenvectors with respect to the design variables. These derivatives can be computed by a rather involved analytical procedure or a relatively simple finite difference procedure. This paper examines the computer cost effectiveness of these two procedures for the derivative calculations.

INTRODUCTION

One of the objectives of structural control is to suppress undesirable motion resulting from some unavoidable excitation such as onboard machinery or docking maneuvers. In active control the motion of structure is sensed and suitable forces are applied to reduce and ultimately eliminate the undesirable motion. In optimal control the forces are applied such that a preselected performance index is minimized. The solution of the optimal control problem requires the solution of the matrix Ricatti equation. Because of the difficulties encountered in numerical computations, the solution of the matrix Ricatti equation is not feasible for large order systems. For large order systems, an alternate method known as the Independent Modal Space Control (IMSC) [1] is more suitable.

In the IMSC method, the control forces are specified in the modal space instead of in the physical space. Also by suitably choosing the modal control forces, each mode of vibration is controlled independently of the other modes. The performance index is assumed to be of the form

$$J = \sum_{r=1}^{\ell} J_r \quad (1)$$

where ℓ is the number of modes controlled and J_r is the performance index associated with the r -th mode and has the definition

$$J_r = \int_0^{t_f} (\omega_r^2 \xi_r^2 + \omega_r^2 \eta_r^2 + R_r z_{cr}^2) dt \quad (2)$$

where

$$\eta_r = \dot{\xi}_r / \omega_r \quad (3)$$

□

ω_r is the frequency of the r th mode and $R_r > 0$ is the penalty parameter imposed on the control effort. A higher value of R_r will result in a smaller control force in the modal space and vice versa.

The modal coordinates ξ_r , $r = 1, \dots, l$ are related to the displacement vector u , by the relation

$$u = X\xi \quad (4)$$

where X is the modal matrix, having as its columns the eigenvectors, obtained by the solution of the eigenvalue problem

$$KX = \omega^2 MX \quad (5)$$

ξ_r and η_r satisfy the constraint equations

$$\ddot{\xi}_r(t) + \omega_r^2 \xi_r(t) = z_{cr}(t) \quad (6.a)$$

$$\xi_r(0) = \xi_{r0} \quad (6.b)$$

$$\dot{\xi}_r(0) = \eta_r(0) \omega_r \quad (6.c)$$

where $Z_c = X^T F \quad (7)$

is the modal control vector. Minimization of J_r in Eq. (2) with the differential constraint equations given by Eqs. (6) leads to a 2×2 matrix Riccati equation that can be solved analytically for $t_f = \infty$.

For this case, the control force is given by [2]

$$\begin{aligned} z_{cr}(t) = & \omega_r \left(\omega_r - \left(\omega_r^2 + R_r^{-1} \right)^{1/2} \right) \xi_r(t) \\ & - \left[2 \omega_r \left(-\omega_r + \left(\omega_r^2 + R_r^{-1} \right)^{1/2} \right) + R_r^{-1} \right]^{1/2} \dot{\xi}_r(t) \end{aligned} \quad (8)$$

and the solution of the closed loop modal equations (6) for the controlled modes gives

$$\xi_r(t) = e^{-a_1 t} (\alpha_1 \cos \theta t + \beta_1 \sin \theta t) \quad (9)$$

with

$$a_1 = \lambda_r \omega_r \quad (10)$$

$$\theta = (\omega_d)_r \quad (11)$$

$$\alpha_1 = \xi_{r0} \quad (12)$$

$$\beta_1 = \frac{\omega_r}{(\omega_d)_r} (\xi_{r0} \lambda_r + \eta_r(0)) \quad (13)$$

$$\lambda_r = - \frac{f_{22}}{2\omega_r} \quad (14)$$

$$(\omega_d)_r = (\omega_r^2 - \omega_r f_{21} - \frac{f_{22}^2}{4})^{1/2} \quad (15)$$

$$f_{21} = - R_r^{-1} k_{21}, \quad f_{22} = - R_r^{-1} k_{22} \quad (16)$$

$$k_{21} = k_{12} = - \omega_r R_r + (\omega_r^2 R_r^2 + R_r)^{1/2} \quad (17)$$

$$k_{22} = (R_r - 2\omega_r^2 R_r^2 + 2\omega_r R_r (\omega_r^2 R_r^2 + R_r)^{1/2})^{1/2} \quad (18)$$

Substitution of Eqs. (9) through (18) into Eq. (2) followed by its integration with $t_f = \infty$ yields

$$J_r = \frac{\omega_r^2}{2} (E I_{11} + F I_{22} + G I_{22}) \quad (19)$$

with

$$J_{11} = 1 + \frac{k_{12}^2}{\omega_r^2 R_r}, \quad J_{12} = \frac{2 k_{12} k_{22}}{\omega_r^2 R_r}, \quad J_{22} = 1 + \frac{k_{22}^2}{\omega_r^2 R_r} \quad (20)$$

$$K_{11} = \left[\frac{1}{\omega_r^2} + \frac{2}{\omega_r R_r} (\omega_r^2 \eta_r^2 + R_r)^{3/2} - 2 R_r^2 \omega_r^2 - R_r \right]^{1/2} \quad (21)$$

$$\alpha_2 = \eta_r(0) \quad (22)$$

$$\beta_2 = \frac{1}{(\omega_d)_r} [\epsilon_{ro} (f_{21} - \omega_r) - \eta_r(0) \omega_r \lambda_r] \quad (23)$$

$$E = J_{11} \alpha_1^2 + J_{22} \alpha_2^2 + J_{12} \alpha_1 \alpha_2 \quad (24)$$

$$F = J_{11} \beta_1^2 + J_{22} \beta_2^2 + J_{12} \beta_1 \beta_2 \quad (25)$$

$$G = 2 J_{11} \alpha_1 \beta_1 + 2 J_{22} \alpha_2 \beta_2 + J_{12} (\alpha_1 \beta_2 + \alpha_2 \beta_1) \quad (26)$$

$$I_{11} = \frac{1}{4 a_1} + \frac{a_1}{4 a_1^2 + \theta^2} \quad (27)$$

$$I_{22} = - \frac{a_1}{4 a_1^2 + \theta^2} + \frac{1}{4 a_1} \quad (28)$$

$$I_{12} = \frac{1}{4} \left(\frac{\theta}{a_1^2 + \theta^2} \right) \quad (29)$$

Simultaneous Design and Control

The process of simultaneous design and control of structures is a min - min problem that minimizes with respect to the structural design variables the minimum value of the performance index with respect to the control forces.

The minimum value of the performance index with respect to control forces is given by Eq. (1) wherein J_r can be evaluated from Eqs. (8) through (29). In the process of minimization of this minimum value of the performance index, its derivatives with respect to the design variables are required. These derivatives can be evaluated explicitly by a laborious, even though straightforward differentiation of Eqs. (8) through (29) with respect to the design variables provided the derivatives of the eigenvalues ω_r and the eigenvectors x_r , $r = 1, 2 \dots \ell$ are available. The other alternative is to calculate the derivatives of J with respect to the design variables by using say the forward difference scheme. The latter is easily programmable since no explicit derivatives of the eigenvalues and eigenvectors with respect to the design variables are then required. The thrust of this paper is a comparison of the computational cost and the efficiency of the two procedures for calculating the derivatives of the performance index.

Before we elaborate on this comparison however, we will digress and discuss the calculation of the derivatives of the eigenvalues and eigenvectors using the well known Nelson's method [3].

Derivatives of Eigenvalues and Eigenvectors with Respect to the Design Variables

Purely from a computer programming point of view the simplest and the most straightforward though not necessarily the most efficient way to compute the derivatives of eigenvalues and eigenvectors is by using finite differences in particular the forward difference scheme with an appropriate step size [4]. The main disadvantage of the forward difference scheme is that it requires the solution of an eigenvalue problem once for each design variable. This could be a computationally expensive process. Furthermore, to obtain an accurate value of the computed derivatives, the eigenvalue problems need to be solved with a high degree of precision.

The eigenvalue ω_r^2 , and the eigenvector x_r , of the previous section are obtained by the solution of the eigenvalue problem.

$$\omega_r^2 M x_r = K x_r, \quad r = 1, 2 \dots \ell \quad (30)$$

where M and K are the assembled mass and stiffness matrices respectively of the finite-element model of the structure. The mode shape x_r is normalized with respect to the mass matrix M as

$$x_r^T M x_s = \delta_{rs} \quad (31)$$

wherein δ_{rs} is the Kronecker delta. Differentiating Eqs. (30) and (31) with respect to a design variable p_j for a particular eigenpair (ω_r^2, x_r) with distinct eigenvalues one obtains

$$(K - \omega_r^2 M) \left(\frac{dx_r}{dp_j} \right) - \left(\frac{d\omega_r^2}{dp_j} \right) M x_r = - \left(\frac{dK}{dp_j} - \omega_r^2 \frac{dM}{dp_j} \right) x_r \quad (32)$$

$$x_r^T M \frac{dx_r}{dp_j} = - \frac{1}{2} x_r^T \left(\frac{dM}{dp_j} \right) x_r \quad (33)$$

where use has been made of the symmetry of the mass matrix M .

To obtain the derivatives of eigenvalues, Eq. (32) is premultiplied by x_r^T followed by the use of Eq. (31) to yield

$$\frac{d\omega_r^2}{dp_j} = x_r^T \left(\frac{dK}{dp_j} - \omega_r^2 \frac{dM}{dp_j} \right) x_r \quad (34)$$

To obtain the derivatives of the eigenvector x_r , Eqs. (32) and (33) are combined as

$$\begin{bmatrix} K - \omega_r^2 M & - M x_r \\ - x_r^T M & 0 \end{bmatrix} \begin{Bmatrix} dx_r/dp_j \\ d\omega_r^2/dp_j \end{Bmatrix} = \begin{Bmatrix} - \left(\frac{dK}{dp_j} - \omega_r^2 \frac{dM}{dp_j} \right) x_r \\ - \frac{1}{2} x_r^T \left(\frac{dM}{dp_j} \right) x_r \end{Bmatrix} \quad (35)$$

Equations (35) could be solved for both the eigenvalue and the eigenvector derivatives except that the principal minor $K - \omega_r^2 M$ is singular. To circumvent this apparent difficulty, Nelson [5] proposed a method that temporarily imposes the normalization equation (31) by the requirement that the largest component of the eigenvector be equal to one. If the re-normalized eigenvector is denoted by \bar{x}_r and it is assumed that its largest component is the m -th one, then Eq. (31) is replaced by

$$\bar{x}_{rm} = 1 \quad (36)$$

and Eq. (33) is replaced by

$$\frac{d\bar{x}_{rm}}{dp_j} = 0 \quad (37)$$

For \bar{x}_r , Eq. (32) reduces to

$$\left(K - \omega_r^2 M \right) \left(\frac{d\bar{x}_r}{dp_j} \right) = \left(\frac{d\omega_r^2}{dp_j} \right) M \bar{x}_r - \left(\frac{dK}{dp_j} - \omega_r^2 \frac{dM}{dp_j} \right) \bar{x}_r \quad (38)$$

Equation (37) is now used to reduce the order of Eqs. (38) by deleting the m -th row and m -th column. When the eigenvalue ω_r^2 is distinct, the reduced system is not singular and can be solved by a standard technique for the derivative vector $d\bar{x}_r/dp_j$. The required vectors x_r and dx_r/dp_j are then obtained from \bar{x}_r and $d\bar{x}_r/dp_j$ by the following easily verified relations

$$x_r = \bar{x}_r \left(\bar{x}_r^T M \bar{x}_r \right)^{1/2} \quad (39)$$

and

$$\frac{dx_r}{dp_j} = \frac{\left(\frac{d\bar{x}_r}{dp_j} \right)}{\left(\bar{x}_r^T M \bar{x}_r \right)^{1/2}} - \frac{\bar{x}_r \left[\bar{x}_r^T \frac{dM}{dp_j} \bar{x}_r + 2 \bar{x}_r^T M \frac{d\bar{x}_r}{dp_j} \right]}{2 \left(\bar{x}_r^T M \bar{x}_r \right)^{3/2}} \quad (40)$$

In finite element computer codes that exploit the sparsity structure of the K and M matrices, it may be inconvenient to obtain the re-normalized vector, x_r , by setting the largest component to unity. Such a scheme necessitates the recalculation of the sparsity structure. Instead, it is more convenient to obtain the re-normalized eigenvector, \bar{x}_r by setting

$$\bar{x}_{rn} = 1 \quad (41)$$

where n is the order of the matrices K and M .

As mentioned previously, the derivative of the eigenvector x_r with respect to the design variable p_j can also be calculated by the forward difference scheme

$$\frac{dx_r}{dp_j} = \frac{(x_r)_{p_j+h} - (x_r)_{p_j}}{h} \quad (42)$$

where $(x_r)_{p_{j+h}}$ is the eigenvector calculated at p_{j+h} . In order to assess the accuracy of the forward difference scheme relative to Nelson's analytical method, an error measure is defined as

$$\epsilon(h) = \sum_j \sum_r \sum_i \left(\left(\frac{\partial x_{ri}}{\partial p_j} \right)_A - \left(\frac{\partial x_{ri}}{\partial p_j} \right)_F \right)^2 \quad (43)$$

where $\left(\frac{\partial x_{ri}}{\partial p_j} \right)_A$ and $\left(\frac{\partial x_{ri}}{\partial p_j} \right)_F$ are the eigenvector derivatives by the analytical and the forward difference scheme respectively. The error ϵ is summed over all the components of the eigenvector, over the mode shapes controlled and over all the design variables.

Application to a Stiffened Composite Plate

A laminated composite square plate reinforced by two stiffeners placed symmetrically with respect to the laminate midplane along the two centerlines of the plate is considered. As in reference [6] the plate is discretized using a mesh of 8 noded isoparametric, shear deformable plate bending elements. Assuming the plate is simply-supported along all its four edges, the resulting finite-element model has a respectable (from control engineer's point of view) 127 degrees of freedom and thirteen design variables consisting of five discrete fiber orientations and eight continuous stiffener cross-sectional areas.

Table 1 provides an assessment of the error ϵ as a function of the step size h for the finite difference derivative calculations. As expected, the error decreases with a decrease in h and then begins to increase as a result of machine roundoff.

A comparison was made of the computational cost for the calculation of the eigenvector derivatives using Nelson's method and the finite difference scheme. Using Nelson's method to compute the gradient of the three eigenvectors with respect to the thirteen design variables the required CPU time was 17.2 seconds. To compute the eigenvector gradients using forward differences several eigenvalue problems need to be solved. Using subspace iteration in conjunction with the Jacobi method [7] for the solution of the eigenvalue problem, the total time for the required gradient calculations was 39.5 seconds. Note that the design vector has thirteen variables, and it was necessary to solve the perturbed eigenvalue problem thirteen times. Since the solution of the unperturbed eigenvalue problem provides an excellent guess for the eigenvalue of the perturbed system, an inverse iteration scheme [7] in conjunction with shifting of the stiffness matrix K can be used to accelerate the solution process. Using such a strategy, the CPU time required for the calculation of the eigenvector gradients using forward differences was down to 27.6 seconds.

Thus, in relation to the analytical method the computational cost of the finite difference calculation of the eigenvector gradients is not at all prohibitive. On the other hand, in spite of this modestly higher computational cost, the simplicity of the calculation of the eigenvector gradients using forward difference scheme is overwhelming. However some caution must be exercised when using inverse iteration in conjunction with shifting of the stiffness matrix. It should be noted that the normalization scheme $x_r^T M x_r = 1$ fixes only the magnitude of the eigenvector and if x_r is an eigenvector, then $-x_r$ is also an eigenvector of the system. Hence, when eigenvectors of the perturbed system are computed, care must be taken to choose the eigenvector $(x_r)_{p_j+h}$ such that

$$(x_r)_{p_j+h}^T (x_r)_{p_j} > 0$$

This can be done very easily in practice by simply calculating the above dot product and changing the sign of the vector x_r if the dot product is negative.

Table 1. Error ϵ as a Function of the Step Size h

h	ϵ
0.156×10^{-1}	0.79×10^{-6}
0.781×10^{-2}	0.21×10^{-6}
0.390×10^{-2}	0.54×10^{-7}
0.195×10^{-2}	0.13×10^{-7}
0.976×10^{-3}	0.34×10^{-8}
0.488×10^{-3}	0.98×10^{-9}
0.244×10^{-3}	0.80×10^{-9}
0.122×10^{-3}	0.25×10^{-8}
0.610×10^{-4}	0.101×10^{-7}
0.305×10^{-4}	0.404×10^{-7}
0.152×10^{-4}	0.162×10^{-6}

Table 2 provides a comparison of the computational effectiveness of the two approaches for the control of the stiffened laminated composite plate problem for cases involving different number of design variables and different number of frequencies being controlled.

Table 2. Finite Difference Versus Nelson's Approach - Normalized CPU Time

Type of Design	Finite Difference Approach	Nelson's Approach
13 design variable, 3 frequencies	1.598	1.0
13 design variables, 8 frequencies	1.939	1.0
5 design variables, 8 frequencies	1.700	1.0

It is clear from Table 2 that in all the cases considered the finite difference approach requires more CPU time as compared to the Nelson's Analytic approach. The percentage increase in CPU time increases with the number of frequencies considered. In the finite difference approach an eigenvalue problem needs to be solved for each design variable considered. If shifting the K matrix in conjunction with inverse iteration is used to calculate the eigenvalues/eigenvectors, the finite difference approach is quite competitive with the Nelson's analytic approach. Even though the approach may require about twice the time of Nelson's method, the coding effort is far less. In the case of the finite difference approach. Secondly, calculation of $\frac{\partial K}{\partial p}$, $\frac{\partial M}{\partial p}$ (derivatives of stiffness and mass matrices respectively) required in the case of Nelson's approach can be quite difficult in some cases. In the case where the design variables are element frame areas, calculation of $\frac{\partial K}{\partial p}$, $\frac{\partial M}{\partial p}$ is fairly straightforward. However, if p, corresponds to the number of plies with a given orientation then the calculation of $\frac{\partial K}{\partial p}$, $\frac{\partial M}{\partial p}$ is fairly involved.

In conclusion, it needs to be emphasized that the finite difference scheme for the calculation of the eigenvalue and eigenvector derivatives does not appear to be costly enough to warrant the use of the analytical method. With the former scheme one does not have to "tinker" with the "black box" that generates the eigenvalues and eigenvectors for a given design variable vector. The analytical method on the other hand needs an intimate knowledge of this "black box".

REFERENCES

- [1] Meirovitch, L., and Oz, H., "Active Control of Structures by Modal Synthesis," Structural Control, H.H.E. Leipholz (ed.), North Holland Publishing Co. & SM Publications, Iutam, 1980.
- [2] Kalman, R.E., and Bucy, R.S., "New Results in Linear Filtering and Prediction Theory," Journal of Basic Engineering, Transactions ASME, Vol. 83, 1961.
- [3] Haftka, R.T., and Kamat, M.P., "Elements of Structural Optimization," Martinus Nijhoff Publishers, 1985.
- [4] Iott, A.J., Haftka, R.T., and Adelman, H., "Selecting Step Sizes in Sensitivity Analysis by Finite Differences," NASA TM-86382, 1985.
- [5] Nelson, R.B., "Simplified Calculation of Eigenvector Derivatives," AIAA Journal, Vol. 14, pp. 1201-1205, 1976.
- [6] Mesquita, L., and Kamat, M.P., "Optimization of Stiffened Laminated Composite Structures with Frequency Constraints," Engineering Optimization, Vol. 11, pp. 77-88, 1987.
- [7] Bathe, K.J., "Finite Element Procedures in Engineering Analysis", Prentice-Hall, Englewood-Cliffs, N.J., 1982.

**TREATMENT OF BODY FORCES IN
BOUNDARY ELEMENT DESIGN SENSITIVITY ANALYSIS***

**Sunil Saigal, R. Aithal and Jizu Cheng
Mechanical Engineering Department
Worcester Polytechnic Institute
Worcester, Massachusetts**

***Sponsor: NSF grant MSM - 870742**

INTRODUCTION

The inclusion of body forces has received a good deal of attention in boundary element research. The consideration of such forces is essential in the design of high performance components such as fan and turbine disks in a gas turbine engine. Due to their critical performance requirements, optimal shapes are often desired for these components. The boundary element method (BEM) offers the possibility of being an efficient method for such iterative analysis as shape optimization.

A survey of efforts in the area of sensitivity analysis in BEM was given by Mota, Soares and Choi [1]. The shape sensitivity using a finite-difference formulation was given by Wu [2] and using the implicit-differentiation formulation by Barone and Yang [3], Saigal et al. [4-6], and Rice and Mukherjee.* Mukherjee and Chandra [7] presented a BEM sensitivity formulation for materially nonlinear problems. The treatment of body forces for sensitivity analysis has not received much attention.

In this paper, the implicit-differentiation of the boundary integral equations [8] is performed to obtain the sensitivity equations. The body forces are accounted for by either the particular integrals [9,10] for uniform body forces or by a surface integration [11] for non-uniform body forces. The corresponding sensitivity equations for both these cases are presented. The validity of present formulations is established through a close agreement with exact analytical results.

*Rice, J.S. and Mukherjee, S., "Design Sensitivity Coefficients for Axisymmetric Elasticity Problems by Boundary Element Methods", private communication.

BOUNDARY ELEMENT ANALYSIS EQUATIONS

Including the effect of temperature variation ϕ , the stress tensor σ_{ij} is given in equation (1), and the equation of equilibrium is given in equation (2). Starting with a weak statement of equation (2) and using the divergence theorem twice the integral equation (3) is obtained. Assuming steady state condition, using the divergence theorem, and applying Green's second function leads to equation (4) where the thermal effects have been reduced to a boundary integral form.

$$\sigma_{ij} = \frac{E}{(1+\nu)} e_{ij} + \frac{\nu E}{(1+\nu)(1-2\nu)} \delta_{ik} e_{kk} - \frac{E}{(1-2\nu)} \delta_{ij} \alpha \phi \quad (1)$$

$$\sigma_{ij,j} + F_i = 0 \quad (2)$$

$$u_i(p) = - \int_{\Gamma} T_{ij}(p,q) u_j(q) d\Gamma + \int_{\Gamma} U_{ij}(p,q) t_j(q) d\Gamma + \int_{\Omega} U_{ij}(p,q) F_i(q) d\Omega - \frac{\alpha E}{(1-2\nu)} \int_{\Omega} U_{ij}(p,q) \phi d\Omega \quad (3)$$

$$u_i(p) = - \int_{\Gamma} T_{ij}(p,q) u_j(q) d\Gamma + \int_{\Gamma} U_{ij}(p,q) t_j(q) d\Gamma + \frac{\alpha(1+\nu)}{8\pi(1-\nu)} \int_{\Gamma} \left\{ \frac{\phi}{R} \left(n_i - R_{,i} \frac{\partial R}{\partial n} \right) - R_{,i} \frac{\partial \phi}{\partial n} \right\} d\Gamma + \int_{\Omega} U_{ij}(p,q) F_i(q) d\Omega \quad (4)$$

E , ν , and α are the modulus of elasticity, Poisson's ratio, and coefficient of thermal expansion, respectively. T_{ij} and U_{ij} are the fundamental (Kelvin) solutions for traction and displacement, respectively. p and q are the load point and the field point, respectively, and R is the distance between these points. u_i , t_i , and F_i are the components of displacement, traction and body force, respectively.

GRAVITATIONAL AND CENTRIFUGAL FORCE SENSITIVITY

If the total displacement is written as a sum of a complementary and a particular integral component

as in equation (5), then in the absence of temperature variation, the last two terms in equation (4) drop out giving equation (6). Discretizing the boundary using boundary elements with displacements and tractions interpolated as shown in equation (7), we get the matrix relationship (8). Substituting from equation (5) into equation (8), we obtained a relationship in equation (9) including the effect of particular solutions due to body forces. Particular solutions $\{u^p\}$ and $\{t^p\}$ were given by Banerjee and co-workers [9-10] at SUNY - Buffalo. Implicit differentiation of equation (9) with respect to the design variable X_L results in the sensitivity equation (10). The contribution of the body forces is included in the vector $\{f^p\}$ given in equation (11).

$$u_i = u_i^c + u_i^p \quad (5)$$

$$u_i^c(p) = - \int_{\Gamma} T_{ij}(p,q) u_j^c(q) d\Gamma + \int_{\Gamma} U_{ij}(p,q) t_j^c(q) d\Gamma \quad (6)$$

Discretizing equation (6) using interpolation functions for displacements and tractions

$$u = [H]\{u\} ; t = [H]\{t\} \quad (7)$$

The matrix form of equation (6) is obtained as

$$[F]\{u^c\} = [G]\{t^c\} \quad (8)$$

Substituting equation (5) in equation (8)

$$[F]\{u\} = [G]\{t\} + [F]\{u^p\} - [G]\{t^p\} \quad (9)$$

Differentiating with respect to the design variable, X_L

$$[F]\{u\}_{,L} = [G]_{,L}\{t\} + [G]\{t\}_{,L} - [F]_{,L}\{u\} + \{f^p\} \quad (10)$$

Where

$$\{f^p\} = [F]\{u^p\}_{,L} + [F]_{,L}\{u^p\} - [G]\{t^p\}_{,L} - [G]_{,L}\{t^p\} \quad (11)$$

The superscripts c and p refer to the complementary and particular solutions, respectively. $[H]$ is a matrix of interpolation functions. $()_{,L}$ denotes the derivative of $()$ with respect to the design variable X_L .

THERMOELASTIC SENSITIVITY

For the case of temperature variation ϕ and temperature gradient $\phi_{,n}$, the term with volume integral in equation (4) drops out. Then using the interpolation given in equation (7), we get the matrix relationship given in the equation (12). Implicit differentiation of equation (12) leads to an equation similar to equation (10) but with a different definition for vector $\{f^p\}$. This relationship is given in equations (13) and (14). The matrix $[V]$ involves thermoelastic kernels which include elliptic integrals of the first and the second kind. The present sensitivity analysis requires derivatives of these elliptic integrals which are easily determined through chain rule of differentiation.

$$[F]\{u\} = [G]\{t\} + [V]\{T\} \quad (12)$$

$$[F]\{u\}_{,L} = [G]_{,L}\{t\} + [G]\{t\}_{,L} - [F]_{,L}\{u\} + \{f^p\} \quad (13)$$

$$\{f^p\} = [V]_{,L}\{T\} + [V]\{T\}_{,L} \quad (14)$$

$\{T\}$ is the vector of nodal temperatures.

SEMI-ANALYTICAL SENSITIVITY FORMULATION

The sensitivities can now be obtained using equations (10) and (11) for centrifugal and gravitational body forces, and using equations (13) and (14) for thermal body forces. We, however, need to determine sensitivity matrices such as $[F]_{,L}$ and $[G]_{,L}$; and sensitivity vectors such as $\{u^p\}_{,L}$ and $\{t^p\}_{,L}$. In the semi-analytical approach, the design variable X_L is first perturbed by an amount ΔX_L . The system matrices $[F(X_L + \Delta X_L)]$, $[G(X_L + \Delta X_L)]$, etc., are generated based on the new geometry. The sensitivities are then simply obtained using forward-difference relationships shown in equations (15) and (16). It is noted that the sensitivity results will depend on the perturbation step size ΔX_L . However, this step will result in substantial simplification of the implementation of the sensitivity algorithm.

$$[F]_{,L} = \frac{[F(X_L + \Delta X_L)] - [F(X_L)]}{\Delta X_L}, \text{ etc} \quad (15)$$

$$\{u^p\}_{,L} = \frac{[u^p(X_L + \Delta X_L)] - [u^p(X_L)]}{\Delta X_L}, \text{ etc} \quad (16)$$

FULL ANALYTICAL SENSITIVITY FORMULATION

For the full-analytical approach, the sensitivity matrices and vectors are directly calculated from their analytical expressions given in equations (17) and (18). These expressions, however, need the sensitivities of geometry quantities such as $x_{,L}$, $y_{,L}$, $n_{,L}$, etc. The initial geometry is first used for solution of vectors $\{u\}$ and $\{t\}$ in equations (8) or (12). This geometry is then changed through a

perturbation ΔX_L of the design variable. Only the geometry sensitivities are then calculated using forward-difference approximation. These geometry sensitivities are needed for evaluating terms in equations (17) and (18).

$$\begin{aligned} [F]_{,L} &= \sum_{j=1}^N \int_0^1 \{ [t^*]_{,L}^T [H] J + [t^*]^T [H] J_{,L} \} d\xi \\ [G]_{,L} &= \sum_{j=1}^N \int_0^1 \{ [u^*]_{,L}^T [H] J + [u^*]^T [H] J_{,L} \} d\xi \end{aligned} \quad (17)$$

The superscripts T and * refer to the transpose of the matrix and the fundamental solutions, respectively.

3-D Centrifugal Loading Particular Integral Sensitivities:

$$\begin{aligned} u1_{,L} &= (2c_1(xx_{,L} + yy_{,L}) + 2c_2zz_{,L})x + (c_1(xx + yy) + c_2zz)x_{,L} \\ u2_{,L} &= (2c_1(xx_{,L} + yy_{,L}) + 2c_2zz_{,L})y + (c_1(xx + yy) + c_2zz)y_{,L} \\ u3_{,L} &= 2c_3(xx_{,L} + yy_{,L})z + c_3(xx + yy)z_{,L} \\ c_1 &= -\rho\omega^2(5\lambda + 4\mu)/4(\lambda + \mu) \\ c_2 &= -\rho\omega^2\mu/8(\lambda + 2\mu)/(\lambda + \mu) \\ c_3 &= \rho\omega^2/8/(\lambda + 2\mu) \end{aligned} \quad (18)$$

λ, μ are the Lamé's constants. x_L denotes the derivative of coordinate x with respect to the design variable X_L and y_L and z_L have similar definitions. The corresponding traction sensitivities can be found using the constitutive relation.

SINGULAR TERMS IN SYSTEM SENSITIVITY MATRIX

For determining terms in $[F]_{,L}$ an extension of rigid body technique used for singular terms in $[F]$ is used. This extension is based on the fact that the sensitivities corresponding to rigid body displacements and tractions are zero leading to a row-sum type property for $[F]_{,L}$. Thus from equation (10), the singular terms for 3-D can be obtained as given in equation (21). For 2-D, these terms are similarly obtained. For axisymmetric case, a rigid body motion in Z - direction and an inflation mode in the radial direction are used.

$$\{u_{\text{rigid}}\}_{x_1} = \begin{Bmatrix} 1 \\ 0 \\ 1 \\ 0 \\ \vdots \\ 1 \\ 0 \end{Bmatrix} ; \quad \{u_{\text{rigid}}\}_{x_2} = \begin{Bmatrix} 0 \\ 1 \\ 0 \\ 1 \\ \vdots \\ 0 \\ 1 \end{Bmatrix} \quad (19)$$

$$\{t\}_{\text{rigid}} = \{0\} \quad (20)$$

$$\sum_{j=1,3,\dots}^{n-1} F_{ij,L} = 0 ; \quad \sum_{j=2,4,\dots}^n F_{ij,L} = 0 ; \quad \text{for each } i \quad (21)$$

STRESS SENSITIVITY RECOVERY

The solution of sensitivity equations yields the boundary traction sensitivities only. The stress sensitivities at other locations can be obtained directly using differentiated elasticity equations describing stress-strain relationships. These relations are given in equation (22) for the axisymmetric case.

$$\begin{Bmatrix} \sigma_{rr} \\ \sigma_{zz} \\ \sigma_{rz} \end{Bmatrix} = \begin{bmatrix} n_r^2 & n_z^2 & -2n_r n_z \\ n_z^2 & n_r^2 & 2n_r n_z \\ n_r n_z & -n_r n_z & (n_r^2 - n_z^2) \end{bmatrix} \begin{Bmatrix} \sigma_{11} \\ \sigma_{22} \\ \sigma_{12} \end{Bmatrix}_{,L}$$

n_r, n_z are the components of the outward normal in the r and z directions, respectively.

$$\sigma_{22,L} = \frac{\nu}{(1-\nu)} \sigma_{11,L} + \frac{E}{(1-\nu^2)} (e_{22,L} + \nu e_{\theta\theta,L})$$

$$e_{22,L} = -\frac{J_{,L}}{J^2} u_{2,\xi} + \frac{1}{J} u_{2,\xi L}$$

$$e_{\theta\theta,L} = \frac{1}{r^2} (u_{r,L} r - u_r r_{,L}) \quad (22)$$

$u_{2,\xi L}$ denotes the mixed derivative with respect to the dimensionless coordinates ξ and the design variable X_L .

NUMERICAL EXAMPLES

The above formulations were applied to a series of selected examples to determine the design sensitivities for displacements and tractions. These examples include: (a) a rotating circular disk of constant thickness with a central hole shown in Figure 1 analyzed using two-dimensional elements, (b) a rotating circular disk with hyperbolic varying thickness and with a central hole shown in Figure 2 analyzed using axisymmetric elements, (c) a hollow cylinder under plane strain shown in Figure 3 subjected to pressure and temperature change and analyzed using axisymmetric elements, (d) a pressurized hollow cylinder under temperature variation shown in Figure 4 and analyzed using axisymmetric elements, (e) a solid circular bar (Figure 5) under self-weight analyzed using three-dimensional elements, and (f) a rotating circular disk (Figure 6) analyzed using three-dimensional elements. For examples without temperature variation the material data used were $E=30 \times 10^7$ psi, $\nu=0.3$; and for examples with temperature variation the material data used were $E=1$ psi, $\nu=0.3$, and $\alpha=0.02/^{\circ}\text{F}$. The results obtained from the present formulations were compared with the exact solutions to check these formulations. For exact sensitivities the elasticity solutions were first expressed in terms of the design variable and then differentiated with respect to this design variable. A good comparison of the present results was seen from the results presented in the following pages.

Design Sensitivity Analysis of a Rotating Circular Disk.

Sensitivity				
Location*	Radial Displacement $\times (10^{-3})$		Traction $(\times 10^{-3})$	
	Analytical	This Study	Analytical	This Study
A	6.7678	6.7677	4.8061	4.7625
B	6.5929	6.5929	8.7301	8.6993
C	2.8329	2.8330	3.6905	3.6923
D	2.6684	2.6685	3.8066	3.8103
E	6.7678	6.7678		
F	6.7678	6.7676		

* Location coordinates (r, z) in inches are: A(4.333, 0.), B(5.061, 0.), C(17.061, 0.), D(19.0, 0.), E(3.864, 1.035), F(3.967, 0.522)

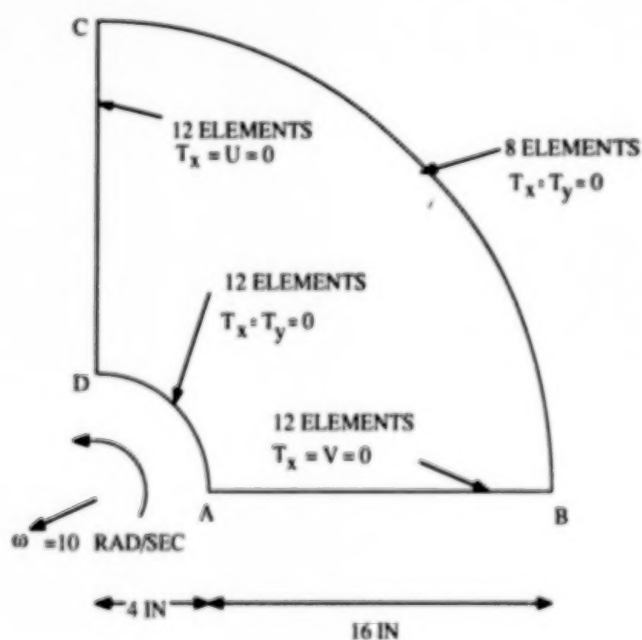


FIGURE 1

Design Sensitivity Analysis of a Rotating Disk with Hyperbolic Varying Thickness

RADIUS (inch)	SENSITIVITY				
	DISPLACEMENT X 10 ³			HOOP STR. X 10 ⁻³	
	Exact	Mesh A	Mesh B	Exact	Mesh B
4.00	2.05931	1.9987	1.9986	5.07485	3.9470
4.25	2.05819	--	1.9887	5.66207	5.4810
4.50	2.04760	1.9725	1.9725	5.99760	5.6433
4.75	2.02989	--	1.9522	6.16066	5.8450
5.00	2.00685	1.9296	1.9294	6.20577	5.8609
5.25	1.97984	--	1.9046	6.17095	5.8355
5.50	1.94995	1.8789	1.8785	6.08307	5.7574
5.75	1.91803	--	1.8512	5.96129	5.6542
6.00	1.88478	1.8236	1.8229	5.81938	5.5318
6.25	1.85078	--	1.7940	5.66731	5.4024
6.50	1.81653	1.7653	1.7645	5.51231	5.2668
6.75	1.78246	--	1.7348	5.35968	5.1372
7.00	1.74893	1.7060	1.7052	5.21325	5.0076
7.25	1.71628	--	1.6759	5.07583	4.8915
7.50	1.68481	1.6482	1.6474	4.94945	4.7787
7.75	1.65480	--	1.6198	4.83557	4.6831
8.00	1.62650	1.5945	1.5937	4.73521	4.5934
8.25	1.60016	--	1.5692	4.64908	4.5222
8.50	1.57602	1.5474	1.5466	4.57767	4.4589
8.75	1.55428	--	1.5261	4.52126	4.4141
9.00	1.53517	1.5089	1.5081	4.48003	4.3782
9.25	1.51889	--	1.4928	4.45403	4.3596
9.50	1.50565	1.4811	1.4803	4.44327	4.3511
9.75	1.49564	--	1.4710	4.44769	4.3540
10.00	1.48906	1.4660	1.4652	4.46718	4.4120

Note: Exact solution is for the assumption of plane stress.
Mesh A: 15 element model; Mesh B: 30 element model

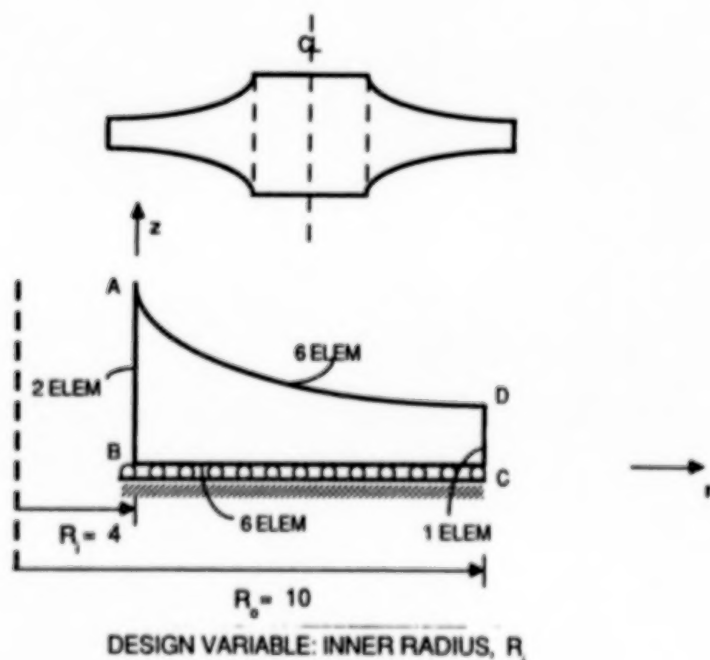


FIGURE 2

Design Sensitivity Analysis of a Plane Strain Hollow Cylinder Under Pressure and Temperature Variation

RADIUS (inch)	SENSITIVITY					
	RADIAL DISPLACEMENT		RADIAL STRESS		CIRCUMFERENTIAL STRESS	
	Exact	This Study	Exact	This Study	Exact	This Study
3.0	3.6305	3.6315	0.000	0.000	0.5955	0.5956
3.5	3.6694	3.6712	-0.1058	-0.1074	0.6995	0.6993
4.0	3.6168	3.6174	-0.1181	-0.1186	0.7112	0.7110
4.5	3.5302	3.5309	-0.0971	-0.0975	0.6903	0.6902
5.0	3.4341	3.4350	-0.0653	-0.0654	0.6591	0.6594
5.5	3.3396	3.3402	-0.0318	-0.0318	0.6264	0.6265
6.0	3.2513	3.2523	0.000	0.000	0.5955	0.5956

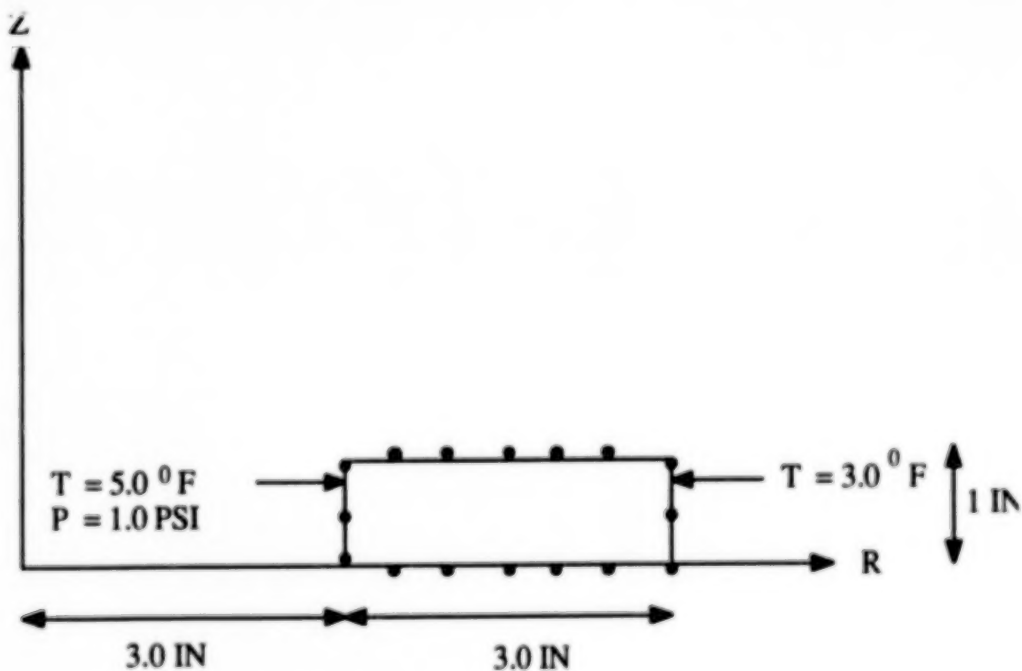


FIGURE 3

Pressurized Hollow Sphere Under Temperature Variation

RADIUS (inch)	SENSITIVITY					
	RADIAL DISPLACEMENT		RADIAL STRESS		CIRCUMFERENTIAL STRESS	
	Exact	This Study	Exact	This Study	Exact	This Study
1.00	1.5126	1.4992	0.000	0.0003	1.500	1.495
1.125	1.758	1.7448	-0.754	-0.618	1.857	1.886
1.25	1.8563	1.8436	-0.901	-0.927	1.923	1.910
1.375	1.8985	1.887	-0.815	-0.791	1.879	1.876
1.50	1.9247	1.9144	-0.653	-0.642	1.801	1.796
1.625	1.9526	1.9433	-0.471	-0.466	1.715	1.709
1.75	1.9896	1.9813	-0.297	-0.290	1.634	1.630
1.875	2.0384	2.0311	-0.139	-0.128	1.562	1.561
2.00	2.0996	2.0952	0.000	0.0003	1.500	1.496

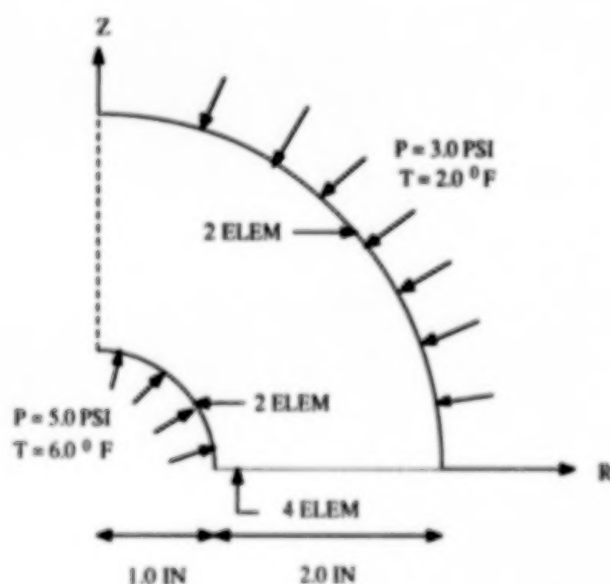


FIGURE 4

Solid Circular Bar under Self-weight

Location	Sensitivity of displacements in Z direction (10^3)			Sensitivity of Stress in Z direction		
	Exact	Full-Analytical	Semi-Analytical	Exact	Full-Analytical	Semi-Analytical
x = 3.536 y = 3.536						
A(z=0.0)	0.0	0.0	0.0	2318.4	2320.4	2351.6
B(z=5.0)	6.7620	6.7613	6.7614	1738.8	1747.6	1758.3
C(z=10.0)	11.592	11.589	11.589	1159.2	1188.7	1189.8
D(z=15.0)	14.490	14.488	14.488	579.6	587.6	589.4
E(z=20.0)	15.456	15.448	15.448	0.0	0.0	0.0

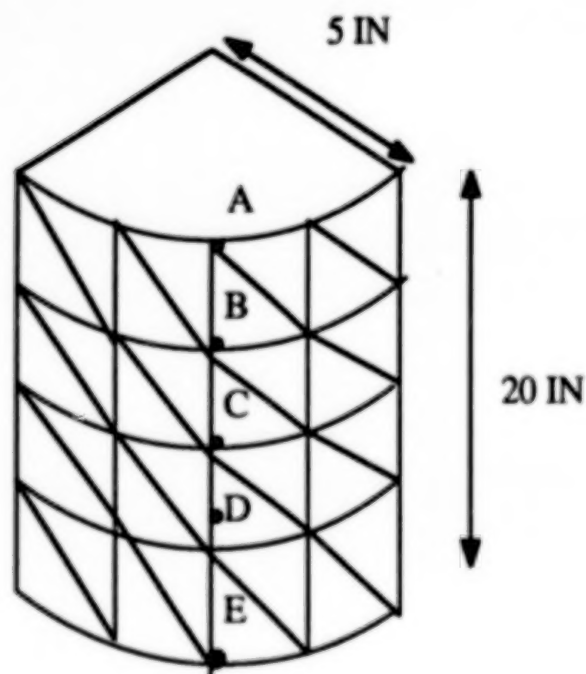


FIGURE 5

Three Dimensional Rotating Circular Disk

Location $y=0.0$ $z=1.5$	Displacement Sensitivity $u_{r,L}(10^{-3})$			Radial Stress Sensitivity (10^4)		
	Exact	Full-Analytical	Semi-Analytical	Exact	Full-Analytical	Semi-Analytical
$x=4.0$	0.6768	0.6775	0.6735	0.0840	0.1907	0.2023
$x=5.0$	0.6613	0.6610	0.6571	0.8564	0.8413	0.8511
$x=6.0$	0.6216	0.6212	0.6179	0.9650	0.9674	0.9644
$x=7.0$	0.5768	0.5765	0.5737	0.9018	0.8966	0.8945
$x=8.0$	0.5329	0.5326	0.5302	0.8004	0.8061	0.8032
$x=16.0$	0.2981	0.2978	0.2969	0.3740	0.3814	0.3800
$x=17.0$	0.2840	0.2838	0.2829	0.3691	0.3649	0.3635
$x=18.0$	0.2736	0.2733	0.2725	0.3715	0.3782	0.3770
$x=19.0$	0.2668	0.2667	0.2660	0.3807	0.3752	0.3740
$x=20.0$	0.2640	0.2639	0.2631	0.3960	0.4083	0.4083

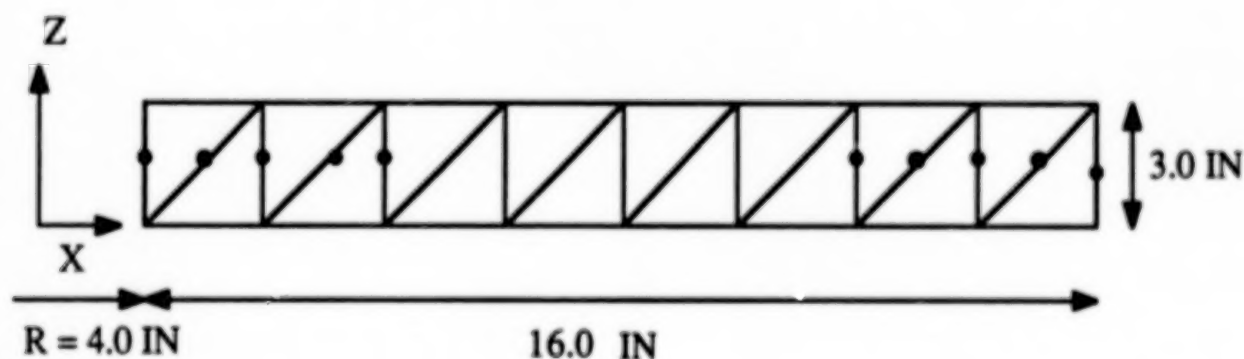


FIGURE 6

CONCLUSIONS

The treatment of body forces of the centrifugal, gravitational, and thermal types in the implicit-differentiation formulation for the design sensitivity analysis of two-dimensional, axisymmetric, and three-dimensional problems is presented. The particular integral sensitivity expressions for the gravitational and centrifugal type body forces are developed. The thermoelastic sensitivity kernels are given for the thermal type body forces. A semi-analytical and a full-analytical approach for determining the sensitivity system matrices are used. A wide range of problems are solved for design sensitivities due to body forces and the results are validated through comparisons with exact analytical solutions.

REFERENCES

1. Mota, Soares, C.A., and Choi, K.K., "Boundary Elements in Shape Optimal Design of Structures", The Optimum Shape, International Symposium, General Motors Research Labs, Warren, Michigan (J.A. Bennett and M.E. Botkin, eds.), Plenum Press, New York, 1986, pp. 199-231.
2. Wu, S.J., "Application of the Boundary Element Method for Structural Shape Optimization", Ph.D. Thesis, The University of Missouri, Columbia, 1986.
3. Barone, M.R. and Yang, R.-J., "Boundary Integral Equations for Recovery of Design Sensitivities in Shape Optimization", AIAA Journal, Vol. 26, No. 5, May 1988, pp. 589-594.
4. Kane, J.H. and Saigal, S., "Design Sensitivity Analysis of Solids Using BEM", Journal of Engineering Mechanics, Vol. 114, No. 10, October 1988, pp. 1703-1721.
5. Saigal, S., Borggard, J.T., and Kane, J.H., "Boundary Element Implicit Differentiation Equations for Design Sensitivities of Axisymmetric Structures", International Journal of Solids and Structures, June 1989.
6. Aithal, R., Saigal, S., and S. Mukherjee, "On the Three-Dimensional Boundary Element Implicit-Differentiation Formulation for Structural Design Sensitivity Analysis", Computers and Mathematics With Applications, 1989.

7. Mukherjee, S. and Chandra, A., "A Boundary Element Formulation for Design Sensitivities in Materially Nonlinear Problems", Acta Mechanica, 1989.
8. Banerjee, P.K. and Butterfield, R., Boundary Element Methods in Engineering Science, McGraw-Hill, 1981.
9. Pape, D.A., and Banerjee, P.K., "Treatment of Body Forces in 2D Elastostatic BEM using Particular Integrals", Journal of Applied Mechanics, Vol. 54, 1987, pp. 866-871.
10. Henry, D.P., Jr., Pape, D.A., and Banerjee, P.K., "New Axisymmetric BEM Formulation for Body Forces using Particular Integrals", Journal of Engineering Mechanics, Vol. 113, No. 5, 1987, pp. 671-688.
11. Rizzo, F.J., and Shippy, D.J., "An Advanced Boundary Integral Equation Method for Three-Dimensional Thermoelasticity", International Journal for Numerical Methods in Engineering, Vol. 11, 1977, pp. 1753-1768.

**DESIGN SENSITIVITY ANALYSIS OF
BOUNDARY ELEMENT SUBSTRUCTURES**

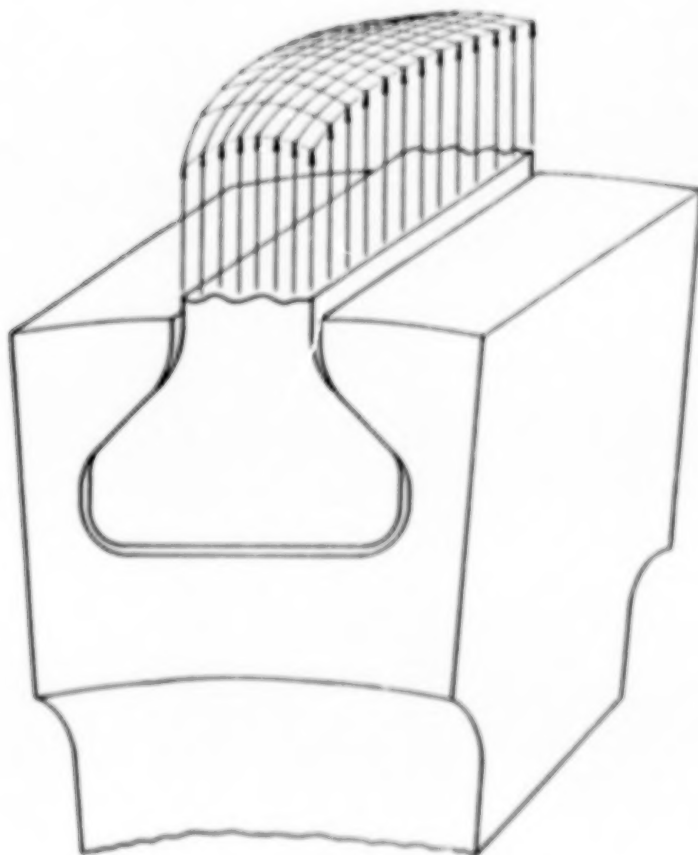
James H. Kane¹, Sunil Saigal², and Richard H. Gallagher¹

**1 - Clarkson University
Potsdam, New York 13676**

**2 - Computer Aided Engineering Center
Worcester Polytechnic Institute
Worcester Massachusetts 01609**

OUTLINE OF PRESENTATION

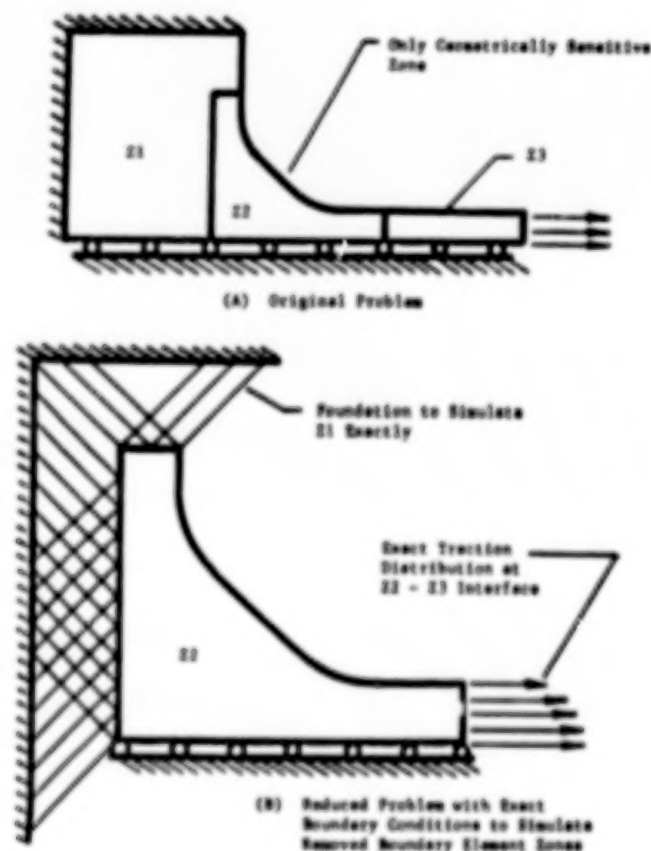
This presentation comments on the ability to reduce or condense a three dimensional model exactly, and then iterate on this reduced size model representing the parts of the design that are allowed to change in an optimization loop. The discussion presents the results obtained from an ongoing research effort to exploit the concept of substructuring within the structural shape optimization context using a Boundary Element Analysis (BEA) formulation. The first part of the talk contains a formulation for the exact condensation of portions of the overall boundary element model designated as substructures. The use of reduced boundary element models in shape optimization requires that structural sensitivity analysis can be performed. A reduced sensitivity analysis formulation is then presented that allows for the calculation of structural response sensitivities of both the substructured (reduced) and unsubstructured parts of the model. It is shown that this approach produces significant computational economy in the design sensitivity analysis and reanalysis process by facilitating the block triangular factorization and forward reduction and backward substitution of smaller matrices. The implementation of this formulation is discussed and timings and accuracies of representative test cases presented.



Model of the Attachment of a Compressor or Turbine Blade to its Disk.
The Top of the Blade Has Been Substructured.

THE CONCEPT OF REDUCED MODELS IN SHAPE OPTIMIZATION

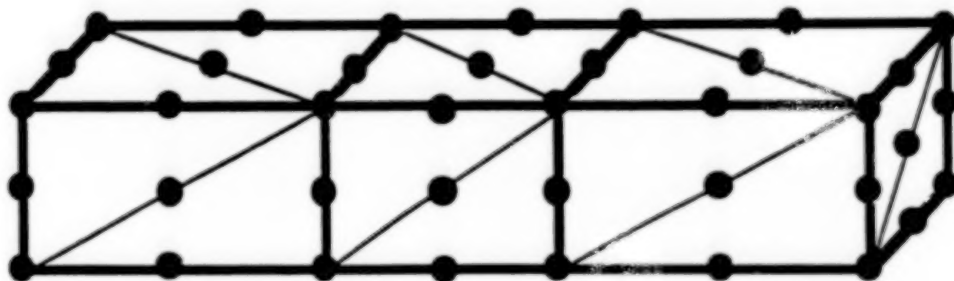
Kane, Saigal, et al.¹⁻⁹ have shown that a multi-zone approach significantly impacts the ability to exploit the additional matrix sparsity present in the design sensitivity analysis step occurring during shape optimization of objects with partial geometric sensitivity. They have also shown how the multi-zone capability facilitates the effective utilization of reanalysis techniques in the shape optimization context. In other publications¹⁰⁻¹¹ they describe a sparse blocked equation solver that incorporates a multi-zone boundary element analysis (BEA) capability and boundary element substructuring in a completely arbitrary fashion. The overall algorithm is described that allows for the assembly and solution of arbitrarily connected boundary element zones that may also be arbitrarily either condensed or maintained at their original size. The approach thus allows for both condensed and uncondensed boundary element zones to consistently coexist in the same multi-zone problem. The development of this capability was motivated by an application in shape optimization, where a portion of the design remains geometrically insensitive to the design variables that control the shape. This discussion presents the results obtained from an ongoing research effort to exploit this powerful concept of substructuring within the structural shape optimization context using a boundary element formulation.



Physical Interpretation of the Condensation of Insensitive Zone Matrices

MULTI-ZONE BOUNDARY ELEMENT ANALYSIS

Multi-zone boundary element analysis¹²⁻¹⁹ is accomplished by first breaking up an entire boundary element model into zones as illustrated by the three zone model shown. The governing boundary integral relationship can then be written for each zone. In elastostatics, for example, Somigliana's identity¹²⁻¹⁴ is the appropriate relationship. Substituting for the actual surface response an approximate surface response interpolated from the node point values of traction and displacement using boundary element interpolation functions, one obtains the discretized boundary integral equations¹²⁻¹⁴. By evaluating this expression at a set of locations of the load point of the fundamental solutions occurring in the boundary integral equation corresponding to the node point locations for the zone in question, one can generate a matrix system of equations for each zone. The matrix relations written for each of the individual zones can be put together for use in an overall analysis¹²⁻¹⁴ by considering the conditions of displacement compatibility and equilibrium of the traction components at all zone interfaces. In these compatibility and equilibrium relations, the double subscript notation is used to convey that the vector in question is a column vector of components entirely on the interface between zone-i and zone-j.



Multi-zone boundary element analysis^{10,11} is accomplished by writing

- 1.) individual zone BIE's

$$[F^i] \{u^i\} = [G^i] \{t^i\}$$

- 2.) coupling them together using compatibility and equilibrium conditions

$$\{u_{ij}^i\} = \{u_{ij}^j\}; \{t_{ij}^i\} = -\{t_{ij}^j\}$$

- 3.) This involves

- 3.1 **Expanding** the size of each zone matrix to the overall system size.
- 3.2 Renumbering, partitioning, and **accounting** for degrees of freedom in blocks.

- 4.) The result - **Speed, Sparsity, Accuracy**, but programs are more complex

MULTI-ZONE BOUNDARY ELEMENT ANALYSIS - Continued

Expanding the size of the boundary element zone matrix equations to the size of the overall problem, bringing the unknown tractions at zone interfaces to the left hand side of the equation, and using the compatibility and equilibrium relations, one can form the boundary element system equations for the overall multi-zone BEA problem. For example, the equations for the three zone problem shown are given below. It should be noted that this model has no interface between zone-1 and zone-3. In this instance, the final multi-zone BEA system of equations can be produced by simply removing the blocks associated with this 1-3 interface shown in the equation below.

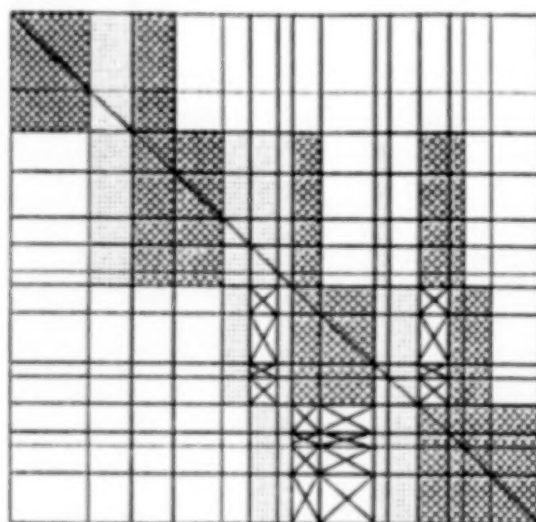
Formal sparse blocked hypermatrix structure associated with three zone model

$$\begin{bmatrix} [F_{11}^1] & [F_{12}^1] & [0] & -[G_{12}^1] & [0] & [0] & [0] & [0] & [0] \\ [0] & [F_{12}^2] & [0] & [G_{12}^2] & [F_{22}^2] & [F_{23}^2] & [0] & -[G_{23}^2] & [0] \\ [0] & [0] & [0] & [0] & [0] & [F_{23}^3] & [0] & [G_{23}^3] & [F_{33}^3] \end{bmatrix} \begin{Bmatrix} \{u_{11}^1\} \\ \{u_{12}^1\} \\ \{u_{13}^1\} \\ \{t_{21}^1\} \\ \{u_{22}^2\} \\ \{u_{23}^2\} \\ \{t_{31}^1\} \\ \{t_{22}^2\} \\ \{t_{32}^2\} \\ \{u_{33}^3\} \end{Bmatrix} \\
 = \begin{bmatrix} [G_{11}^1] & [0] & [0] & [0] & [0] & [0] & [0] & [0] & [0] \\ [0] & [0] & [0] & [0] & [G_{22}^2] & [0] & [0] & [0] & [0] \\ [0] & [0] & [0] & [0] & [0] & [0] & [0] & [0] & [G_{33}^3] \end{bmatrix} \begin{Bmatrix} \{t_{11}^1\} \\ \{0\} \\ \{0\} \\ \{0\} \\ \{t_{22}^2\} \\ \{0\} \\ \{0\} \\ \{0\} \\ \{0\} \\ \{t_{33}^3\} \end{Bmatrix}$$

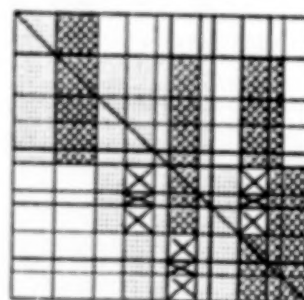
Actual matrix population results by removing all '13' partitions because they are empty

MULTI-ZONE BOUNDARY ELEMENT MATRIX POPULATIONS

The previous example points out the basic features of multi-zone boundary element matrix equations. The matrix equation shown above is actually a hypermatrix with matrices as its entries. Generally these matrix entries are called blocks or partitions. Likewise, the overall vectors shown have vectors for their entries and these entries are also referred to as blocks or partitions. The blocked sparsity characteristic of the matrices that result from the multi-zone BEA approach is clearly evident from the zero blocks present in the previous equation. A typical boundary element system matrix left hand side population is shown below. This matrix population is for a slightly different model and the smaller of the two matrix population shown results when the individual zones are condensed into boundary element substructures as described in subsequent parts of this presentation.



a) MATRIX POPULATION WHEN NO CONDENSATION IS PERFORMED



b) MATRIX POPULATION WHEN ALL ZONES ARE CONDENSED



= BLOCK CONTAINING INFORMATION FROM $[F]$ OR $[M_1]$ MATRIX



= BLOCK CONTAINING INFORMATION FROM $[G]$ OR $[M_2]$ MATRIX



= BLOCK THAT IS INITIALLY EMPTY BUT EXPERIENCES FILL IN DURING THE BLOCK TRIANGULAR FACTORIZATION STEP

Left hand side boundary element system matrix populations for a four zone mesh.

SPARSE BLOCKED SOLUTION PROCEDURES

The blocked matrix triangular factorization procedure used in this study is shown below. The procedure starts with the triangular factorization of the first diagonal block. This is performed using a Gauss elimination algorithm with partial pivoting. The triangular factors of this diagonal block are stored in the same location that the original diagonal block was located. This matrix factorization is then used to alter the second block column. This is accomplished by forward reduction and backward substitution of the columns of the matrix block A_{12} to form the matrix D_{12} (in the figure this matrix is symbolized by D). This matrix is then used to alter all the blocks below A_{12} in block column two by the matrix multiplication and subtraction step shown below. All blocks below block A_{13} in column three are then processed in a similar fashion and then the fourth column and so forth until the entire matrix has been altered. This entire process is then repeated using the submatrix consisting of all blocks except those in block row and column one. The second major phase in the algorithm causes the alteration of the submatrix consisting of all blocks except those in block rows and columns one and two. At every stage of this process, checks are made concerning the sparsity of the matrix. Any block operation that can be avoided due to the block sparsity present in the matrix, is avoided. A fundamental characteristic of the block triangular factorization algorithm described above is that it is sequential in nature.

```

START_PROC.  Start block triangular factorization procedure
              I = 0
TOP_DIAG_LOOP.  I = I + 1
                IF ( I > N-1 ) GO TO LAST_BLOCK
                Factor  $A_{II} = L_{II} U_{II}$  using Gauss elimination with partial
                pivoting
                J = 0
TOP_COL_LOOP.  J = J + 1
                IF ( J > N ) GO TO TOP_DIAG_LOOP
                IF (  $A_{JI} = 0$  ) GO TO TOP_COL_LOOP
                Solve  $A_{II} D = A_{JI}$  For  $D$  by forward reduction and
                backward substitution of the columns of  $D$  using the
                factorization of  $A_{II}$ 
                K = 1
TOP_ROW_LOOP.  K = K + 1
                IF ( K > N ) GO TO TOP_COL_LOOP
                IF (  $A_{KI} = 0$  ) GO TO TOP_ROW_LOOP
                Form  $A_{KJ} = A_{KJ} - A_{KI} D$ 
                GO TO TOP_ROW_LOOP
LAST_BLOCK.  Factor  $A_{II} = L_{II} U_{II}$ 
END_PROC.  Return

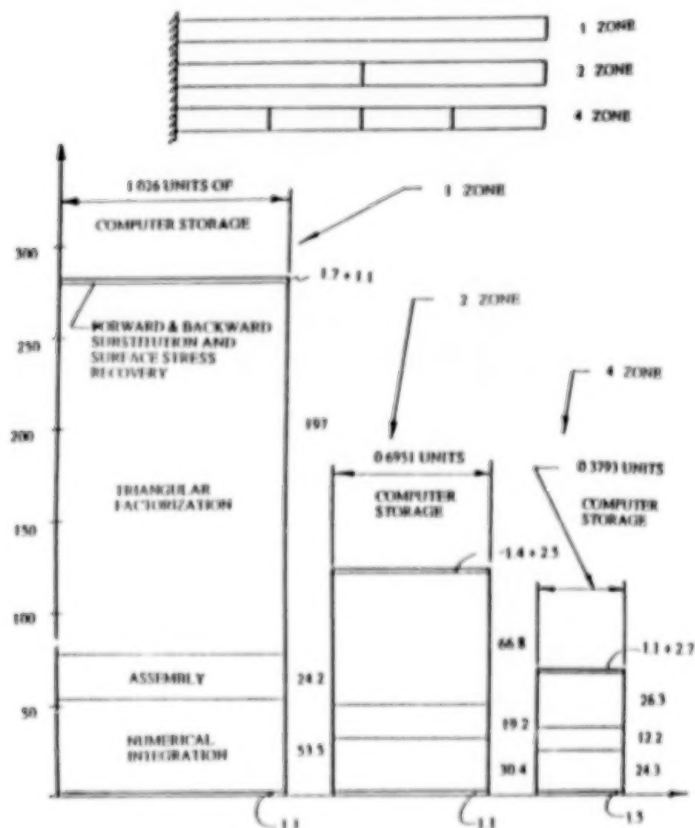
```

Sparse blocked matrix triangular factorization algorithm.

PERFORMANCE OF MULTI-ZONE ANALYSIS

In order to illustrate the advantages associated with multi-zone analysis relative to single-zone boundary element analysis, an example geometry has been selected for study and modeled as both a single zone and as a multi-zone model. Corresponding storage space and CPU times required for the single and multi-zone analyses are shown in the figure below. Comparison of the resources consumed during the equation solving step for both the single zone and the multi-zone analyses shows the dramatic improvements that can be obtained by employing the multi-zone approach in this class of problems. The accuracy of the boundary element method when applied to model such slender objects is also dramatically improved when multi-zone techniques are utilized. Numerical integration times tend to also be less for multi-zone models because only load points corresponding to nodes in the particular zone being integrated are used in the sequence of integrations used to form coefficient matrices. Although this particular problem was chosen to present the multi-zone approach in the most favorable light, it is representative of the much larger class of problems that becomes tractable for boundary element analysis when a multi-zone strategy is included.

TIMING AND STORAGE EXAMPLE



BOUNDARY ELEMENT SUBSTRUCTURES

Reordering the degrees of freedom and partitioning the boundary element system equation for an individual zone into blocks that correspond to master degrees of freedom and also into blocks that correspond to degrees of freedom that could be condensed, one can arrive at the matrix equation shown below. In this equation, the additional right hand side vector is included to consistently account for any body force type of loading that might be present in the analysis, such as gravity, centrifugal, or thermal loading. In these equations the symbolism for $\{u\}$ and $\{t\}$ will be generalized to imply that $\{u\}$ contains the unknown values of the boundary response while $\{t\}$ contains the specified values of the boundary response, regardless of whether they are displacement or traction components. When the specified values are displacement components, then appropriate column exchanges and negations must be performed as explained in References [12-14]. Therefore, whenever $\{t_C\}$ appears in the equations presented below, it is implied to be a column vector of known values of the specified boundary conditions for the particular zone in question. At first inspection, the substructuring process seems to require the inversion of the matrix block $[F_{CC}]$. A closer examination of the formulation, however, reveals that this is not the case. Whenever the matrix $[F_{CC}]^{-1}$ appears in these equations, it always premultiplies either a column vector or a rectangular matrix. As shown below, the use of the matrix inversion notation is purely symbolic, and in the computer implementation of this substructuring approach, no matrix inversion is ever actually performed. Instead, the triangular factorization of the matrix block $[F_{CC}]$ is performed once, and subsequently these factors are reused to solve the matrix equations shown below by forward reduction and backward substitution of the right hand side vector or group of vectors shown below.

Substructuring^{10,11}, in BEA can be accomplished by renumbering d.o.f., partitioning into **master** and **condensed** blocks, and solving for $\{u_C\}$ in the second block row.

$$\begin{bmatrix} [F_{MM}] & [F_{MC}] \\ [F_{CM}] & [F_{CC}] \end{bmatrix} \begin{Bmatrix} \{u_M\} \\ \{u_C\} \end{Bmatrix} = \begin{bmatrix} [G_{MM}] & [G_{MC}] \\ [G_{CM}] & [G_{CC}] \end{bmatrix} \begin{Bmatrix} \{t_M\} \\ \{t_C\} \end{Bmatrix} + \begin{Bmatrix} \{f_M\} \\ \{f_C\} \end{Bmatrix}$$

$$\{u_C\} = [F_{CC}]^{-1}[G_{CM}]\{t_M\} + [F_{CC}]^{-1}[G_{CC}]\{t_C\} - [F_{CC}]^{-1}[F_{CM}]\{u_M\} + [F_{CC}]^{-1}\{f_C\}$$

Substitute this **expansion equation** into the first block row and solve for $\{u_M\}$ to obtain the **exactly condensed equation** for the boundary element model.

$$[M_1]\{u_M\} = [M_2]\{t_M\} + [M_3]\{t_C\} + [M_4]\{f_C\} + \{f_M\}$$

$$[M_1] = [F_{MM}] - [F_{MC}][F_{CC}]^{-1}[F_{CM}]; \quad [M_3] = [G_{MC}] - [F_{MC}][F_{CC}]^{-1}[G_{CC}]$$

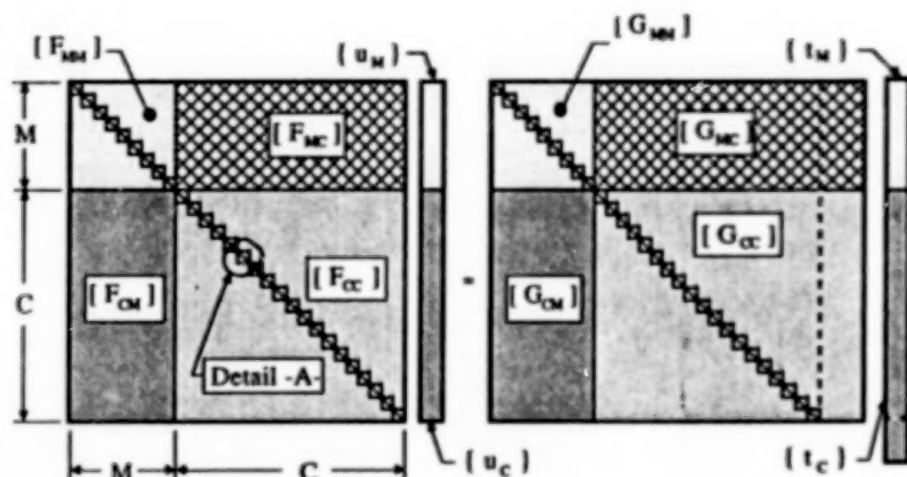
$$[M_2] = [G_{MM}] - [F_{MC}][F_{CC}]^{-1}[G_{CM}]; \quad [M_4] = -[F_{MC}][F_{CC}]^{-1}$$

Inversion shown is symbolic. Major computational step involves the triangular factorization of the square block $[F_{CC}]$. Note this can be reused in expansion step.

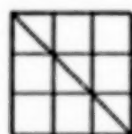
$$[D] = [F_{CC}]^{-1}[V] \text{ or } [F_{CC}]\{D\} = [V] \text{ where } [D] = [\{d_1\}, \{d_2\}, \dots, \{d_N\}]$$

PARTITIONS IN BOUNDARY ELEMENT ZONE CONDENSATION

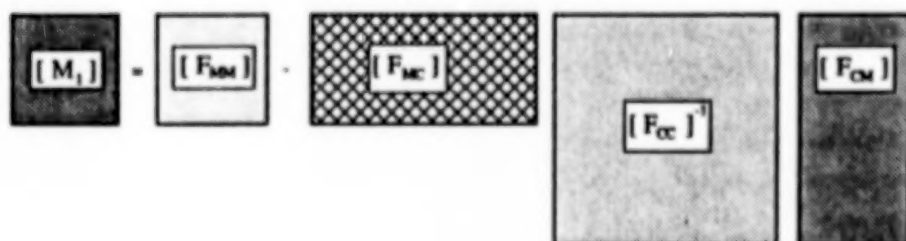
The typical sizes and locations of the partitions present in boundary element zone condensation are shown below. This figure also helps to illustrate the first assembly procedure required to form zone partitions prior to the condensation process. It should also be noted that the condensation procedure embodied in the equations presented above is an exact formulation, in that, no terms have been neglected, nor has any approximation been made.



Assembled zone matrix showing master and condensed partitions



Detail - A- ; The 3 x 3 block of the zone matrices corresponding to singular integration



Typical matrix condensation operation with corresponding matrix sizes

Details associated with the assembly, reordering, partitioning, and condensation of a boundary element zone matrix

MULTI-ZONE ANALYSIS WITH SUBSTRUCTURES

Kane and Saigal¹¹ have shown that a very natural way to combine substructuring with multi-zone boundary element analysis capability is to allow for the possible condensation of degrees of freedom that appear exclusively in a particular boundary element zone. In this case the partitions to be eliminated by the condensation process coincide exactly with certain partitions already present in the multi-zone boundary element analysis procedure. This approach is also very natural from a modeling perspective, since entire boundary element zones can be easily and arbitrarily identified for either condensation or no condensation, and also for subsequent expansion if they are to be condensed. Utilization of this strategy requires that a second level assembly procedure for the formation of the overall sparse blocked system of equations must be able to assemble condensed or uncondensed zone contributions to the overall matrix. The algorithm for the second assembly step is very similar to the assembly procedures described in References [15-19], except for the additional complication of dealing with both condensed and uncondensed zone contributions. This procedure takes each column of a zone matrix partition, determines its block destination and column destination within the block, and proceeds to assemble this column. The entire overall matrix is stored in a one dimensional array with appropriate accounting arrays used to indicate the locations and sizes of the individual blocks, along with indicators regarding whether each block is full, empty, or to-be-filled-in in the subsequent block triangular factorization step.

Arbitrary condensing, noncondensing sparse blocked equation solver^{10,11}

- 1.) Natural way to combine both **multi-zone** and **substructuring** in same analysis
- 2.) Master and condensed d.o.f. are chosen to exactly coincide with the blocks used in the multi-zone scheme.
 - 2.1 **condensed blocks** correspond to all d.o.f. **exclusively** in a single zone.
 - 2.2 **master blocks** correspond to all zone **interface** d.o.f.
- 3.) **Condensation** and subsequent expansion is **optional**, thus allowing **full and condensed** boundary element zones to consistently **coexist** in the same analysis.
- 4.) Essentially forms an **out of core** solver with reduced sensitivity to zone numbering.
- 5.) Has reduced sensitivity to **zone numbering**.
- 6.) Facilitates the **extension of partial pivoting** outside of diagonal blocks
- 7.) **Key ingredient** in the effective treatment of optimization problems for **partially insensitive** three dimensional shapes via **reanalysis** techniques.

BOUNDARY ELEMENT FORMULATION FOR DSA

A very concise summary of the boundary element sensitivity analysis formulation follows to establish notation and terminology and to serve as a starting point for the discussion of the reduced Design Sensitivity Analysis (DSA) algorithm presented below. In this discussion the concept can first be considered in the single zone context, and then generalized to include multi-zone models. The superscript notation for multi-zone problems is again not explicitly written but rather implied. The implicit differentiation formulation for the boundary displacement- and traction-sensitivities, requires that a partial derivative be taken of the already discretized boundary integral equations, with respect to the design variable, X_L . The vectors $\{u\}$ and $\{t\}$ will be known in the resulting equation, subsequent to the performance of an analysis, and the equation can then be used for the solution of the sensitivity vectors $\{u\}_{,L}$ and $\{t\}_{,L}$. It is noted here that $u_{i,L} = 0$ when u_i is specified and, likewise, $t_{i,L} = 0$ when t_i is specified for any i . The $[L][U]$ decomposition of matrix $[A]$, done for the solution of the analysis equations, can be saved and reused for the solution of this new equation, resulting in considerable economy in computational effort. This is a significant advantage of the implicit differentiation technique. However, the method relies on the ability to determine the fictitious right hand side vector in this equation that includes contributions from the terms $[F]_{,L} \{u\}$ and $[G]_{,L} \{t\}$. In the fully analytical sensitivity analysis approach^{2,4,6-8} the matrices, $[F]_{,L}$ and $[G]_{,L}$, are formed by numerical integration of derivatives of quantities found in the formation of $[F]$ and $[G]$. It has also been shown⁵ that it is possible to obtain the matrices $[F]_{,L}$ and $[G]_{,L}$ by a semi-analytical finite difference procedure.

Implicit differentiation approach¹⁻⁹ to design sensitivity analysis (DSA)

$$\frac{\partial}{\partial X_L} \{ [F] \{u\} = [G] \{t\} \} \Rightarrow [F]_{,L} \{u\} + [F] \{u\}_{,L} = [G]_{,L} \{t\} + [G] \{t\}_{,L}$$

$$\text{or} \quad [F] \{u\}_{,L} = [G]_{,L} \{t\} + [G] \{t\}_{,L} - [F]_{,L} \{u\}$$

When symbolism is generalized, this matrix equation has the **same left hand side** matrix as the analysis. Therefore this **obviates** the need for repeated **triangular factorizations** of perturbed matrices.

Analytical approach^{1-3,5-6,8,10,12,15} for computing the required right hand side vectors.

$$\frac{\partial}{\partial X_L} \left([F] \Leftarrow \sum [F]^E = \sum \left\{ \int_{-1}^{+1} [T]^T [h] J da \right\}^E \right) = \sum [F]_{,L}^E$$

$$[F]_{,L}^E = \int_{-1}^{+1} [T]_{,L}^T [h] J da + \int_{-1}^{+1} [T]^T [h] J_{,L} da; \quad [G]_{,L}^E = \int_{-1}^{+1} [U]_{,L}^T [h] J da + \int_{-1}^{+1} [U]^T [h] J_{,L} da$$

Requires numerical integration of **new kernels** containing some familiar terms.
Many elements may be **insensitive**, thereby yielding **sparse sensitivity matrices**.

DSA WITH SUBSTRUCTURES

When boundary element substructuring has been used, as described previously, to condense certain zones in a multi-zone analysis, the design sensitivity analysis matrix equations shown in the previous figure can still be used to symbolize the overall multi-zone system matrix equations. In this instance, the block entries in this equation, contributed by the condensed zones, are assembled from the matrices $[M_1]$ and $[M_2]$ shown in the discussion on boundary element zone condensation. It is also possible to have boundary element zones that have not been condensed to coexist consistently with zones that have been condensed in the same analysis¹⁴. For the uncondensed zones, the appropriate zone $[F]$ and $[G]$ matrices are assembled in the appropriate places in the overall matrix equations. Implicit differentiation of this equation has the same symbolic outcome except that the block entries in this matrix equation for the condensed zones require the formation of $[M_1]_{,L}$, $[M_2]_{,L}$, and $[M_3]_{,L}$, as shown below. In a completely analogous fashion to the implicit differentiation DSA approach described¹⁻⁹ for multi-zone models without substructuring, the terms in the condensed matrix equation can be manipulated to produce the same left hand side matrix as that used in the analysis.

Design sensitivity analysis of substructures¹¹ starts with the implicit differentiation of the condensation and expansion equations.

$$\frac{\partial}{\partial X_L} ([M_1]\{u_M\} = [M_2]\{t_M\} + [M_3]\{t_C\} + [M_4]\{f_C\} + \{f_M\})$$

$$\frac{\partial}{\partial X_L} (\{u_C\} = [F_{CC}]^{-1}[G_{CM}]\{t_M\} + [F_{CC}]^{-1}[G_{CC}]\{t_C\} - [F_{CC}]^{-1}[F_{CM}]\{u_M\} + [F_{CC}]^{-1}\{f_C\})$$

or

$$[M_1]\{u_M\}_{,L} = [M_2]\{t_M\}_{,L} + b_1 \Leftrightarrow \text{Same l.h.s. matrix as in the analysis}$$

where

$$b_1 = -[M_1]_{,L}\{u_M\} + [M_2]_{,L}\{t_M\} + [M_3]_{,L}\{t_C\} + [M_4]_{,L}\{f_C\} + [M_4]\{f_C\}_{,L} + \{f_M\}_{,L}$$

and

$$\{u_C\}_{,L} = ([F_{CC}]^{-1}[G_{CM}])_{,L}\{t_M\} + ([F_{CC}]^{-1}[G_{CM}])\{t_M\}_{,L} + ([F_{CC}]^{-1}[G_{CC}])_{,L}\{t_C\}$$

$$- ([F_{CC}]^{-1}[F_{CM}])_{,L}\{u_M\} - ([F_{CC}]^{-1}[F_{CM}])\{u_M\}_{,L} + ([F_{CC}]^{-1}\{f_C\})_{,L}$$

and

DSA WITH SUBSTRUCTURES - Continued

This, in turn, requires what looks like the computation of the sensitivity of the inverse of the matrix $[F_{CC}]$. This apparent requirement at first inhibited the authors from using the substructuring concept in concert with DSA.

$$[M_1]_{,L} = [F_{MM}]_{,L} - \{ [F_{MC}]_{,L} ([F_{CC}]^{-1} [F_{CM}]) + [F_{MC}] ([F_{CC}]^{-1} [F_{CM}])_{,L} \}$$

$$[M_2]_{,L} = [G_{MM}]_{,L} - \{ [F_{MC}]_{,L} ([F_{CC}]^{-1} [G_{CM}]) + [F_{MC}] ([F_{CC}]^{-1} [G_{CM}])_{,L} \}$$

$$[M_3]_{,L} = [G_{MC}]_{,L} - \{ [F_{MC}]_{,L} ([F_{CC}]^{-1} [G_{CC}]) + [F_{MC}] ([F_{CC}]^{-1} [G_{CC}])_{,L} \}$$

The r.h.s. vectors seem to need the **sensitivity of the matrix inverse** $[F_{CC}]^{-1} ???$

This apparent requirement has delayed the implementation of substructuring techniques in design sensitivity analysis for shape optimization.

OBVIATING THE NEED FOR SENSITIVITIES OF MATRIX INVERSES

The derivation shown below, however, obviates the need to compute the sensitivity of any matrix inverse. The reason that this can be done is because the matrix $[F_{CC}]^{-1}$, appearing in the reduced DSA formulation, is always postmultiplied by another matrix. When the product of the two matrices is considered together, an approach to the computation of the sensitivity of the matrix product becomes clear. This shows that the required term $[D]_{,L}$ can be obtained by 'solving' the resulting equation shown below. Thus, the formation of the matrix term $[D]_{,L}$ can be obtained by forward reduction and backward substitution of the columns of the right hand side matrix shown. This is extremely efficient if the triangular factors of the matrix block $[F_{CC}]$, computed during the condensation step of the analysis, are saved and reused. The sensitivities of the other matrix products shown in the design sensitivity analysis formulation with substructures can be obtained in an analogous fashion. The sensitivity of the matrix $[M_4]$ is not found by itself, but rather, the product of $[M_4] (f_C)$ is treated in a manner similar to that discussed above.

Obviating the requirement of computing sensitivities of matrix inverses in DSA of substructures is accomplished by exploiting the fundamental observation that $[F_{CC}]^{-1}$ always premultiplies a vector or rectangular matrix. Notice

$$[F_{CC}]^{-1} [F_{CM}] = [D] \Rightarrow \text{premultiplying by } [F_{CC}] \Rightarrow [F_{CM}] = [F_{CC}] [D]$$

and differentiating

$$[F_{CM}]_{,L} = [F_{CC}]_{,L} [D] + [F_{CC}] [D]_{,L} \text{ or } [F_{CC}] [D]_{,L} = [F_{CM}]_{,L} - [F_{CC}]_{,L} [D]$$

Which was what was wanted !!! $[D]_{,L}$ can be obtained from a forward reduction and backward substitution procedure using the (already computed) triangular factors of the $[F_{CC}]$ block and the right hand side vector shown.

This formulation has been successfully implemented in an overall package for design sensitivity analysis.

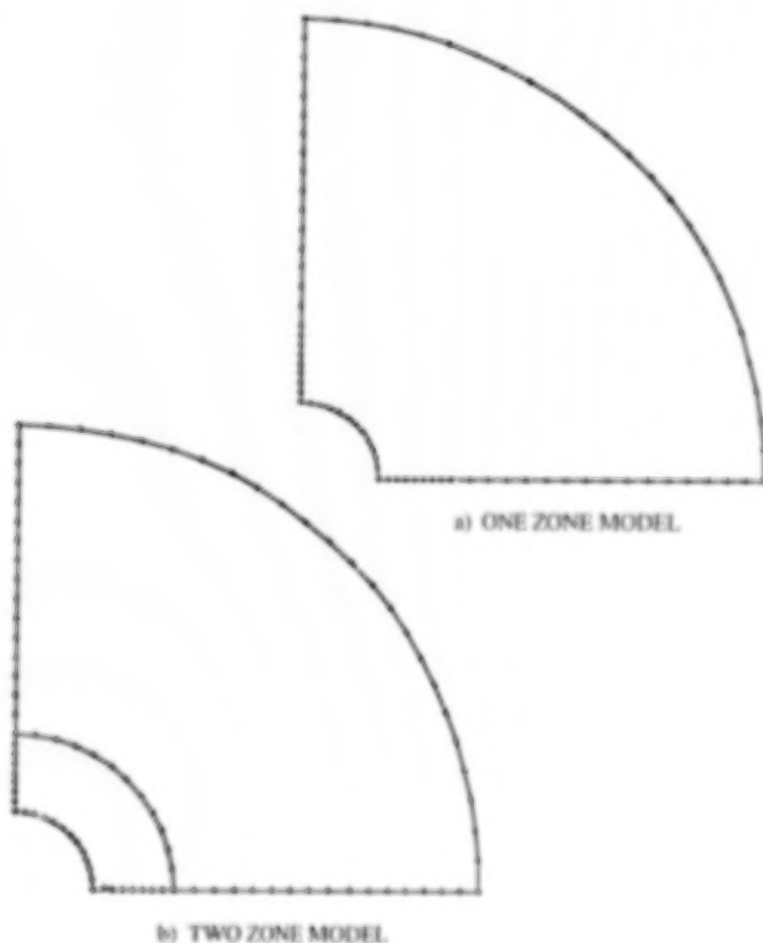
SENSITIVITIES AT CONDENSED DEGREES OF FREEDOM

Once traction and displacement sensitivities are known at master degrees of freedom, the differentiated substructure expansion equation, shown above, can be used to optionally recover sensitivities of displacement and tractions at condensed degrees of freedom in a similar fashion without recourse to the computation of sensitivities of matrix inverses. It is thus possible to obtain complete sensitivity information for the boundary element substructures. Again one sees that the approach for expanding sensitivities relies on the ability to compute the sensitivities of matrix products involving $[F_{CC}]^{-1}$. As discussed above, this computation can be done economically using the factorization of $[F_{CC}]$ which has already been computed in the reduction process.

$$\begin{aligned} \{u_C\}_{,L} = & ([F_{CC}]^{-1} [G_{CM}])_{,L} \{t_M\} + ([F_{CC}]^{-1} [G_{CM}]) \{t_M\}_{,L} + ([F_{CC}]^{-1} [G_{CC}])_{,L} \{t_C\} \\ & - ([F_{CC}]^{-1} [F_{CM}])_{,L} \{u_M\} - ([F_{CC}]^{-1} [F_{CM}]) \{u_M\}_{,L} + ([F_{CC}]^{-1} \{f_C\})_{,L} \end{aligned}$$

NUMERICAL RESULTS

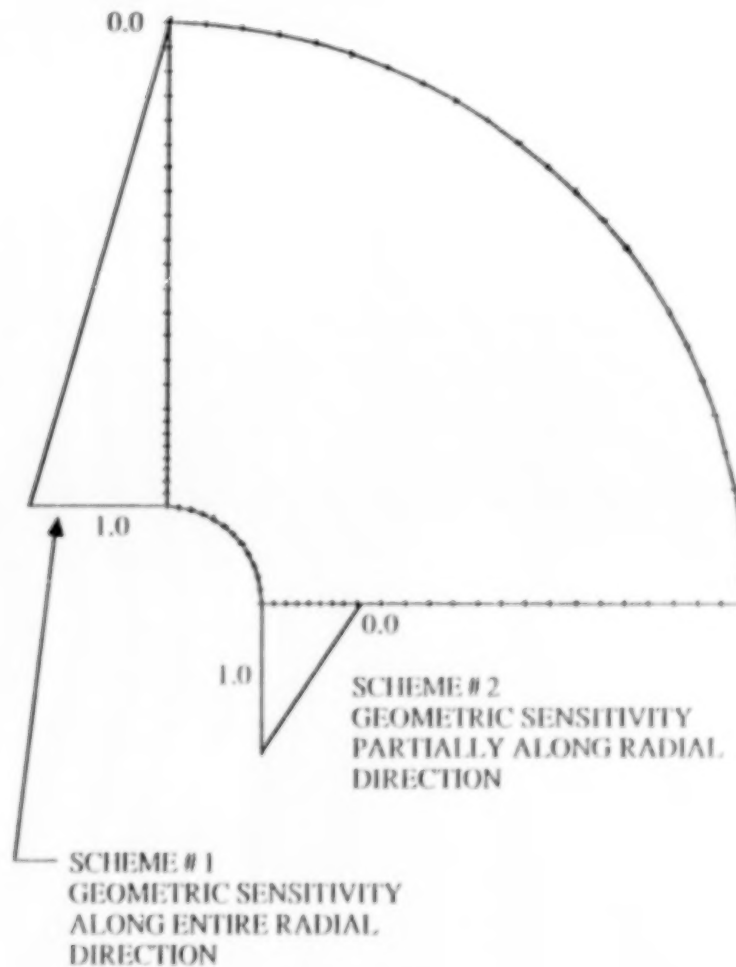
The problem considered was that of a hollow circular cylinder, subjected to an external normal traction. The inner radius was selected as the design variable. This problem was chosen partly because a closed form elasticity solution for its response is known. Using the elasticity solution, it is possible to determine a closed form solution for the sensitivity of the response with respect to the design variable. This is accomplished by parameterizing the sample point location and taking a material derivative of the resulting expression. Also, this problem can be thought of as a specific manifestation of the generic situation of a design with partial geometric sensitivity. It is therefore a candidate for the substructuring techniques described in this paper. Two quarter symmetry models of the hollow cylinder, shown below, were used in this study of the accuracy and computational requirements associated with design sensitivity analysis of full size, partially condensed, and fully condensed models. The first model is a single zone model for which no substructuring is performed.



One Zone and Two Zone Boundary Element Models Used as Test Cases.

NUMERICAL RESULTS - Continued

Both this single zone boundary element mesh and the two zone mesh had the geometry of its nodes controlled according to the two schemes shown. These two sets of geometric sensitivities are considered to illustrate how a certain geometric feature of a boundary element mesh, (i.e. the inner radius of the hollow cylinder), can be controlled by one design variable and yet several mesh control strategies may be possible. These different mesh control strategies will be shown to have quite different consequences in terms of the computational requirements of the resulting design sensitivity analysis. In this example, the second set of geometric sensitivities cause significant sparsity in the matrices $[F]_L$ and $[G]_L$. For the two zone models, this second set of geometric sensitivities will cause entire blocks in the multi-zone DSA formulation to be completely empty, thus producing substantial reductions in the resources required to perform DSA.

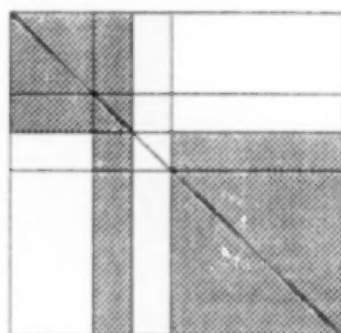


Two different Geometric Sensitivity Schemes Used in this Study.

MATRIX POPULATIONS

The first comparison to be presented in this study concerns the storage required to perform an analysis and a sensitivity analysis of the hollow cylinder employing the various options discussed in this paper. The cases considered are listed below. Case 1.1 is a single zone model with no condensation and its associated left hand side boundary element system matrix is fully populated and therefore not shown. Case 1.2 is a two zone model and its left hand side boundary element system matrix is populated as shown below in Part a. It is seen to require marginally the same amount of computer memory as the single zone model. The Case 1.3 is a two zone model with the largest zone condensed. The left hand side matrix population for this case is depicted in Part c. Case 1.4 has both of its boundary element zones condensed and the resulting matrix population for the left hand side system matrix is illustrated in Part b. From this example one can see that the condensation technique discussed in this paper allows for the analysis and design sensitivity analysis to be performed in much less computer memory. The condensation technique effectively functions as an out of core solver reducing memory requirements to almost one third for case 1.3 and to more than one seventh for case 1.4.

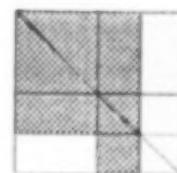
case	zones	zone1	zone2	storage (kwords)
1.1	1	full	-----	261.
1.2	2	full	full	260.
1.3	2	full	condensed	94.
1.4	2	condensed	condensed	37.





a) MATRIX POPULATION WHEN NO CONDENSATION IS PERFORMED



b) MATRIX POPULATION WHEN ALL ZONES ARE CONDENSED



c) MATRIX POPULATION WHEN ZONE TWO IS CONDENSED AND ZONE ONE IS LEFT FULL SIZE

-  = BLOCK CONTAINING INFORMATION FROM $[F]$ OR $[M_1]$ MATRIX
 = BLOCK CONTAINING INFORMATION FROM $[G]$ OR $[M_2]$ MATRIX

Left hand side boundary element system matrix populations for the two zone mesh shown previously for various combinations of zone condensation options.

CAPITALIZING ON GEOMETRIC INSENSITIVITY

There are frequent occasions when portions of a design are geometrically insensitive to the design variables that control its shape. It is also possible in many instances to enhance the amount of geometric insensitivity that a model possesses through modeling techniques such as the one shown above. Here the inner radius is the design variable and yet two schemes for controlling the boundary element node point geometric sensitivity along the radial edges of the model are shown. Listed below are a series of test cases that help to quantify the ability of the various analysis and sensitivity analysis options discussed in this paper to exploit geometric insensitivity for computational performance improvement. The cases 2.1 through 2.4 reveal that the single zone boundary element method is unable to exploit the additional geometric insensitivity present in the partially geometrically sensitive model, while the multi-zone model (case 2.4) yielded analysis and sensitivity analysis results in less than 75 % of the time used for the fully sensitive model. If one compares the time for the DSA alone, the two zone partially sensitive model (case 2.4) can be used for sensitivity calculation in about 35 % of the time taken by the fully sensitive two zone model (case 2.3), and in less than 45 % of the time spent using either of the single zone models. Cases 2.4 through 2.8 demonstrate that the condensation and expansion procedures discussed in this paper are competitive with the straightforward multi-zone analysis and sensitivity analysis techniques that do not involve substructuring (i.e. case 2.4). These cases also demonstrate that the cost of performing the expansion step in DSA of substructures is not significant. Case 2.9 points out that for designs with total geometric sensitivity the substructuring technique requires more computer time than procedures that do not involve condensation and expansion.

case	zones	geometric sensitivity	condensation option		expansion option		Analysis	DSA	Total
			zone1	zone2	zone1	zone2			
2.1	1	full	full	full	no	no	30.9	16.4	47.3
2.2	1	partial	full	full	no	no	30.9	16.3	47.2
2.3	2	full	no	no	no	no	26.6	19.6	46.2
2.4	2	partial	no	no	no	no	26.6	7.0	33.6
2.5	2	partial	no	yes	no	no	25.5	7.8	33.3
2.6	2	partial	no	yes	no	yes	25.5	8.4	33.9
2.7	2	partial	yes	yes	no	no	25.6	9.4	35.0
2.8	2	partial	yes	yes	yes	yes	25.6	10.9	36.5
2.9	2	full	yes	yes	yes	yes	25.6	31.7	57.3

ACCURACY

In both the analysis and the design sensitivity analysis, there was absolutely no discernable difference in the accuracy of the computed results that was dependent on whether condensation or expansion was performed.

CONCLUSIONS

- 1.) Substructuring technique can dramatically economize shape optimization for partially sensitive models
- 2.) Requires
 - Arbitrary condensing / noncondensing assembly and equation solving procedures
 - Design sensitivity analysis of substructures
- 3.) Formulation presented for DSA of substructures that is efficient because it obviates the need for the computation of sensitivities of matrix inverses
- 4.) Accuracy is exactly the same as when no substructuring is done
- 5.) Procedure can be done in parallel mode
- 6.) Implementation currently being incorporated in the Computer Aided Engineering Center's shape optimization system

Acknowledgments

Research discussed in this paper has been supported by grants from the U. S. National Science Foundation DMC-8708254 and MSM-8707842 to Worcester Polytechnic Institute's Computer Aided Engineering Center and also from the Electric Boat Division of General Dynamics Corp. and United Technologies Corp.

REFERENCES

1. J. H. Kane, "Optimization of Continuum Structures Utilizing a Boundary Element Formulation," Ph.D. Dissertation, University of Connecticut, Storrs Connecticut, 1986.
2. J. H. Kane, "Shape Optimization Utilizing a Boundary Element Formulation," BETECH 86, Proceedings, 1986 Boundary Element Technology Conference, MIT.
3. J. H. Kane and S. Saigal, "Design Sensitivity Analysis of Solids Using BEM," Journal of Engineering Mechanics, ASCE, vol. 114, no. 10, Oct. 1988.
4. S. Saigal and J. H. Kane, "A Boundary Element Shape Optimization System for Aircraft Components," AIAA Journal, to appear, also Worcester Polytechnic Institute paper CAE88-1.
5. S. Saigal, J. H. Kane and R. Aithal, "Semi-Analytical Structural Sensitivity Formulation using a Boundary Elements," AIAA Journal, to appear, also Worcester Polytechnic Institute paper CAE88-2.
6. S. Saigal, J.T. Borggaard and J.H. Kane, "Boundary Element Implicit Differentiation Equations for Design Sensitivities of Axisymmetric Structures," International Journal of Solids and Structures, to appear, also Worcester Polytechnic Institute paper CAE88-3.
7. J. H. Kane, "A Second Generation Structural Shape Optimization Capability Employing a Boundary Element Formulation," Proceedings, NUMETA 87.
8. S. Saigal and J. H. Kane, "Design Sensitivity Analysis of Aircraft Engine Components Subject to Body Forces Using a Boundary Element Formulation," Second NASA / Airforce Symposium on Recent Experiences in Multi Disciplinary Analysis and Optimization, September, 1988, Accepted for presentation.
9. J. H. Kane and M. Stabinsky, "Simultaneous Computation of Multiple Sensitivities by a Boundary Element Structural Analysis Formulation," Proceedings, Third International Conference on CAD / CAM Robotics and Factories of the Future, August 1988, Springer-Verlag, 1989.
10. S. Saigal and J. H. Kane, "Numerical Integration and Sparse Blocked Equation Solution Techniques for Large Scale Boundary Element Analysis," Proceedings, Two-Day Symposium on the Solution of Super Large Problems in Computational Mechanics, Sponsored jointly by: Office of Naval Research, Naval Underwater Systems Center, and Worcester Polytechnic Institute, Connecticut, October 18-19, 1988, (J. H. Kane and A. D. Carlson, Editors, Plenum Press Publishers, 1989)
11. J. H. Kane and S. Saigal, "An Arbitrary Condensing, Noncondensing Solution Strategy for Large Scale, Multi Zone Boundary Element Analysis," International Journal for Numerical Methods in Engineering, submitted for review, also Worcester Polytechnic Institute paper CAE88-4.
12. P. K. Banerjee and R. Butterfield, Boundary Element Methods In Engr. Sci., McGraw Hill Book Co. UK. London, 1981

13. C. A. Brebbia and S. Walker, Boundary Element Techniques in Engineering, Newnes Butterworths, London and Boston, 1980
14. C. A. Brebbia, J. C. F. Telles, and L. C. Wrobel, Boundary Element Techniques, Springer Verlag, Berlin and New York, 1984
15. J. C. Lachat, and J. O. Watson, "A Second Generation Boundary Integral Program for Three Dimensional Elastic Analysis," Chapter in, Boundary Integral Equation Method: Computational Applications in Applied Mechanics (Eds. T.A. Cruse and F. J. Rizzo) Appl. Mech. Div., ASME Vol 11, New York, 1975.
16. J. C. Lachat, "Further Developements of the Boundary Integral Technique for Elasto-statics," Ph.D. Thesis, Southampton Univ., 1975.
17. J. C. Lachat and J. O. Watson, "Progress in The Use of Boundary Integral Equations, Illustrated by Examples," Computational Methodes in Applied Mechanical Engineering, 10, 273-289.
18. J. M. Crotty, "A Block Equation Solver for Large Unsymmetric Matrices Arizing in the Boundary Element Method," International Journal for Numerical Methods in Engineering, Vol 18, pp 997-1017, 1982
19. P. C. Das, "A Disc Based Block Elimination Technique Used for the Solution of Non-Symmetrical Fully Populated Matrix Systems Encountered in the Boundary Element Method," Proc. Int. Symp. On Recent. Dev. In Boundary Element Meth., Southampton Univ. pp 391-404, 1978

SESSION 7: CONTROL OF AEROELASTIC STRUCTURES

Chairmen: I. Abel and N. A. Radovcich

**AEROSERVOELASTIC TAILORING
for
LATERAL CONTROL
ENHANCEMENT**

Terrence A. Weisshaar
and
Changho Nam
Purdue University
West Lafayette, Indiana

237

THE PURPOSE - AIRCRAFT ROLL EFFECTIVENESS AT REDUCED COST

The need for effective aileron power for aircraft lateral control and turning maneuvers dates back to the Wright Brothers and their wing warping concept for active stabilization of their aircraft. Early researchers in Great Britain, Japan, Germany and the U.S. explored ways to increase the effectiveness of control aileron to generate a roll moment. Figure 1 illustrates the basic problem of aileron effectiveness and the interrelationship between structural distortion and the loads applied by the control surface. A rigid wing/aileron surface will develop the capability to generate increased roll rates as airspeed increases. A flexible surface will become less effective as airspeed increases because of the twisting distortion created by the aft-mounted control surface. This tendency is further worsened by bending distortion of an aft swept wing. This study focuses its attention on the ability of a combined effort between structural redesign of a wing and sizing and placement of a control surface to create specified roll performance with a minimum hinge moment.

Control Effectiveness

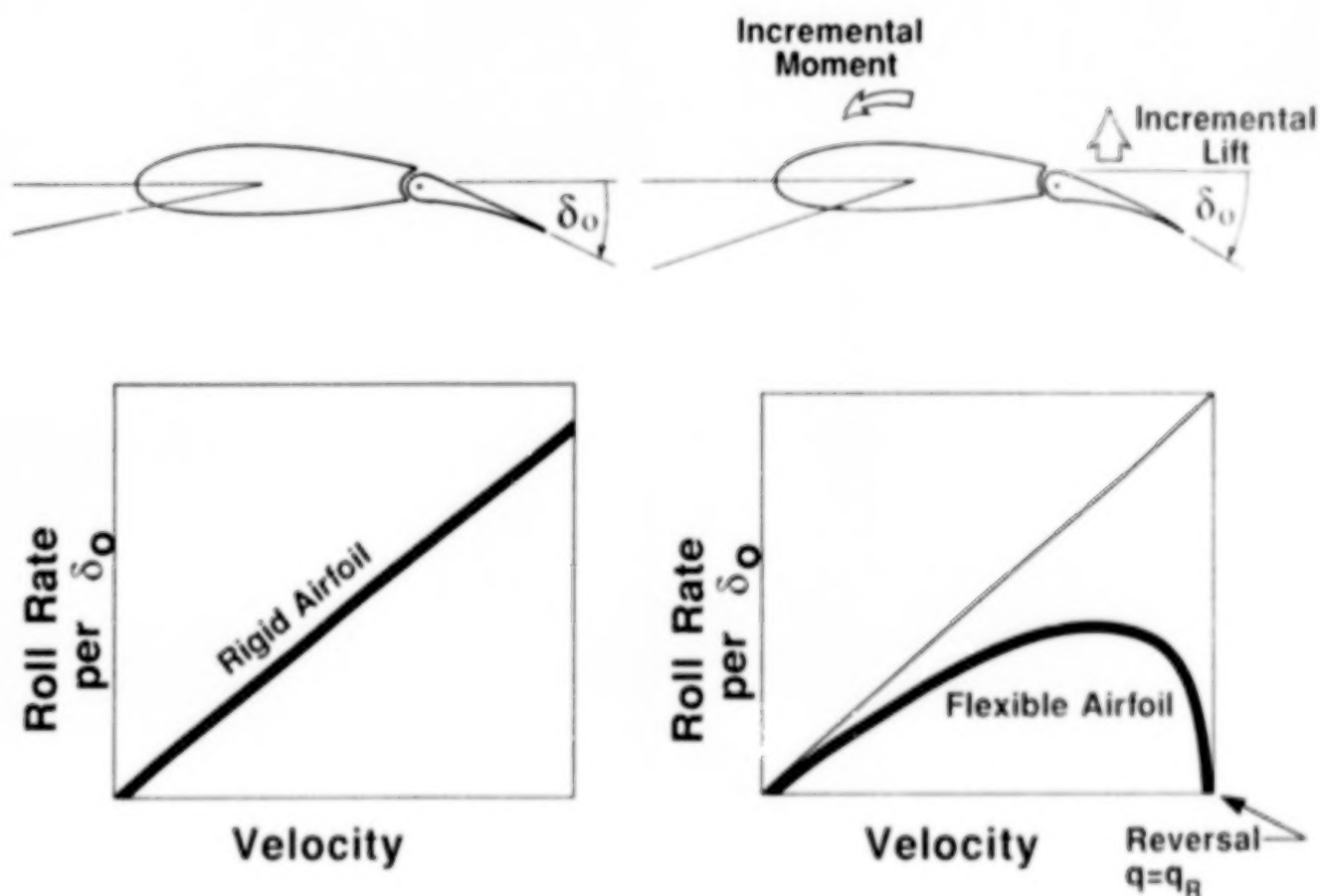


Figure 1

THE OPTIMIZATION PROBLEM AND DESIGN VARIABLES

The wing planform used for this study is shown in Figure 2. The wing is composed of 10 layers of Graphite/epoxy composite material. Three of the upper surface plies are treated as design variables so that cross-sectional stiffness and stiffness cross-coupling can be changed to decrease the aileron hinge moment while still maintaining the same roll-rate at a specified design airspeed. Because the laminate must be symmetric through the thickness so as to disallow warping during the manufacturing process, the three lower plies must also follow the reorientation of their upper surface counterparts. The sign convention for the ply orientation is shown on the planform diagram. The aileron surface is shown located at a distance N_a outboard of the wing root. This distance is also a design variable. The spanwise size of the aileron is fixed at 30% of the span; however, the chordwise size is allowed to change. The combination of 3 ply orientations and the spanwise position and chordwise size of the aileron defines the set of design variables.

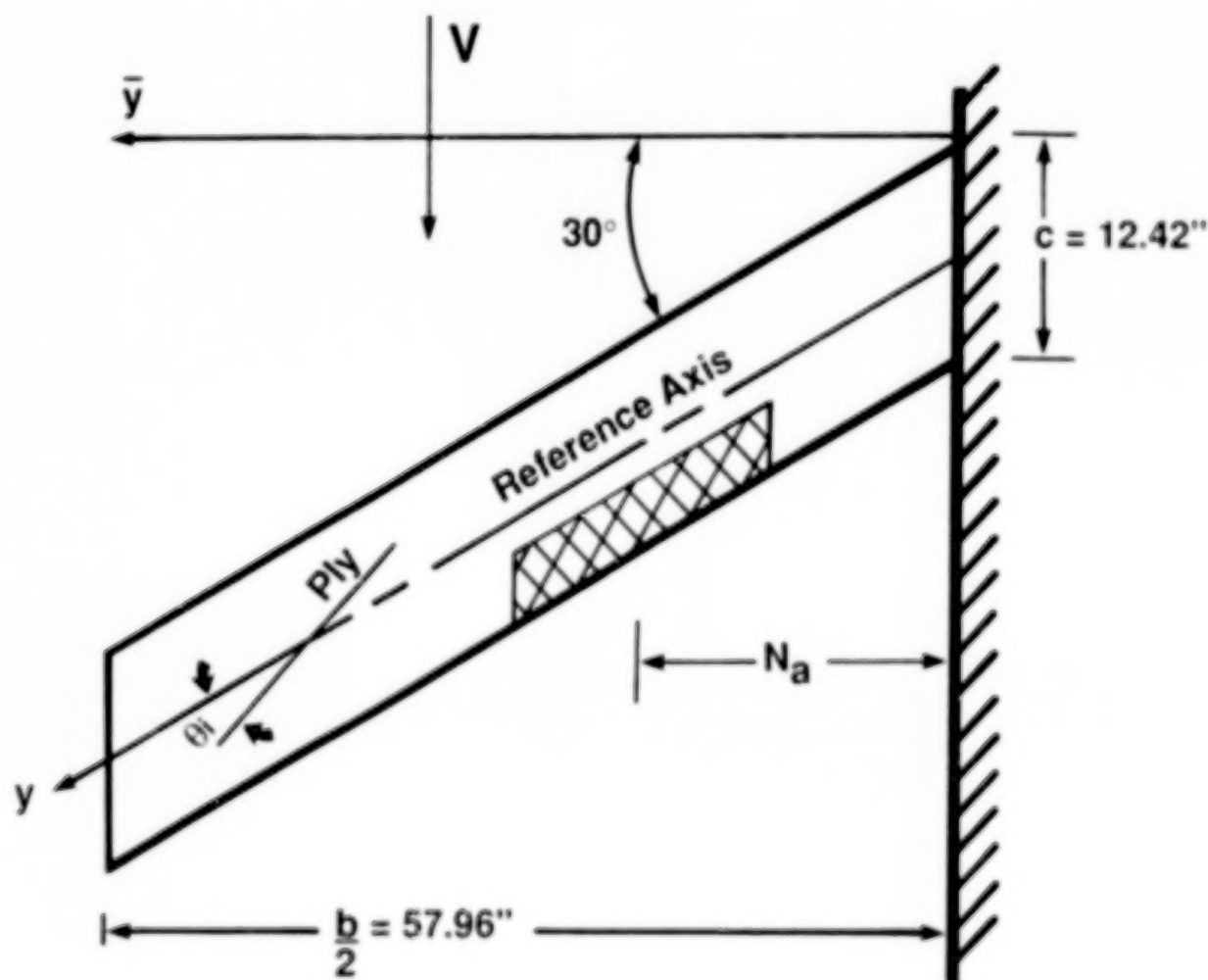


Figure 2

THE EFFECT OF PLY ORIENTATION AND AILERON POSITION ON HINGE MOMENT

Aileron hinge moment was chosen as the cost function for optimization because the actuator size necessary to move the aileron is a function of the power required. As a result, aircraft weight is buried within this cost function. A matrix method representation of the wing structural stiffness and the aerodynamic loads was used to provide the analytical representation of the wing in Figure 2. A computer code that had been used in previous FSW work was used as the basis of the optimization code developed at Purdue. This code has the acronym CWINGSM. Expressions for hinge moment and aerodynamic derivatives necessary to run the code were taken from DATCOM and classical references. The effect of aileron spanwise position and wing laminate orientation on the magnitude of the aileron hinge moment is indicated in Figure 3. Two local minima are observed on this diagram. One local minimum is associated with the inboard aileron position, while the other is associated with the outboard position. While the inboard position is predictable given the experience of the last 40 years, the outboard position is unusual. This diagram also indicates that the final outcome of any optimization procedure that minimizes aileron hinge moment will depend upon the initial conditions given to the program.

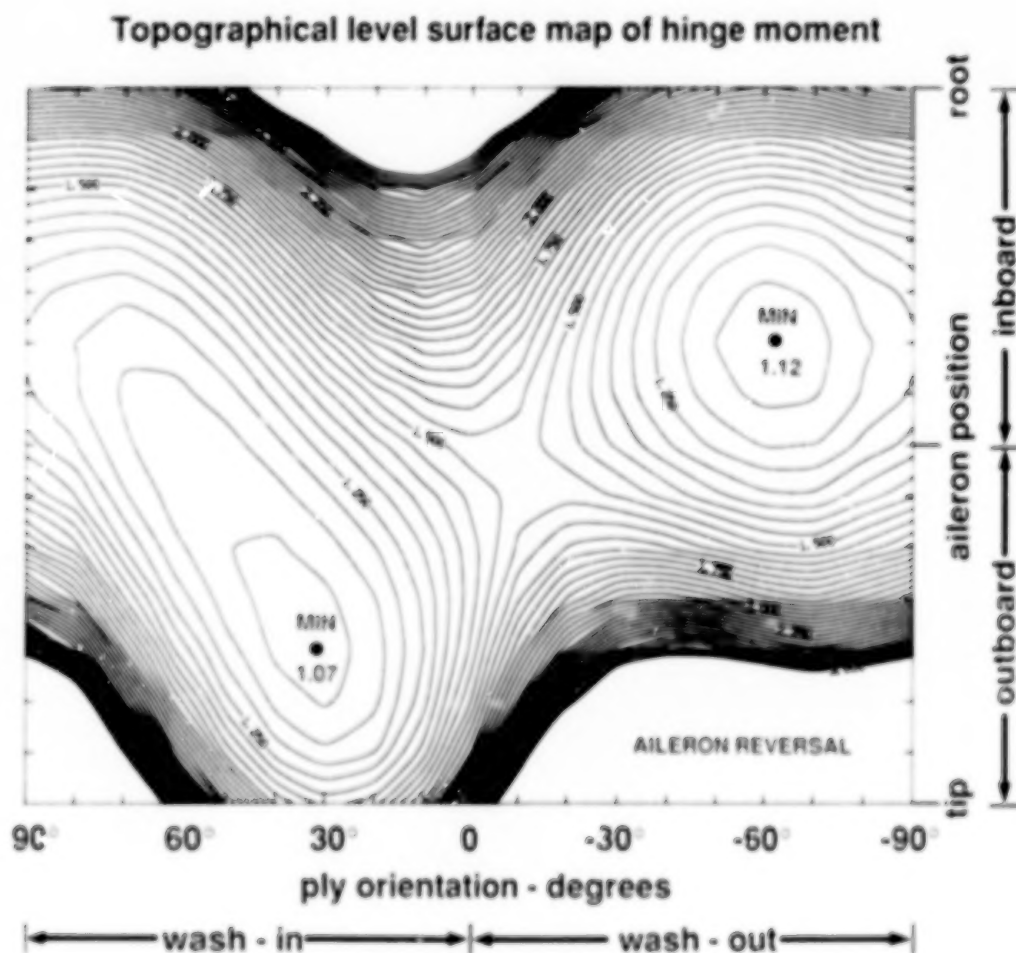


Figure 3

DESIGN CONFLICT AND COMPROMISE - ROLLING MOMENT versus DAMPING-IN-ROLL

The aileron hinge moment depends upon the orientation of the aileron with respect to the flow. This orientation depends upon the amount of mechanical rotation of the aileron and the wing surface distortion due to aeroelastic effects. For a certain size aircraft operating at a specified design airspeed, the roll rate is found by computing the ratio between the aileron rolling power and the wing damping-in-roll. The behavior of these two parameters as a function of aileron position and laminate orientation is shown in Figure 4. To generate this figure, all three laminate ply angles were constrained to be equal. Large values of aileron rolling power are generated when the aileron is outboard and ply angles are oriented in an aft swept position with respect to the swept wing center span line. Unfortunately, Figure 4(b) indicates that this wash-in laminate orientation leads to a situation for which damping-in-roll is also magnified.

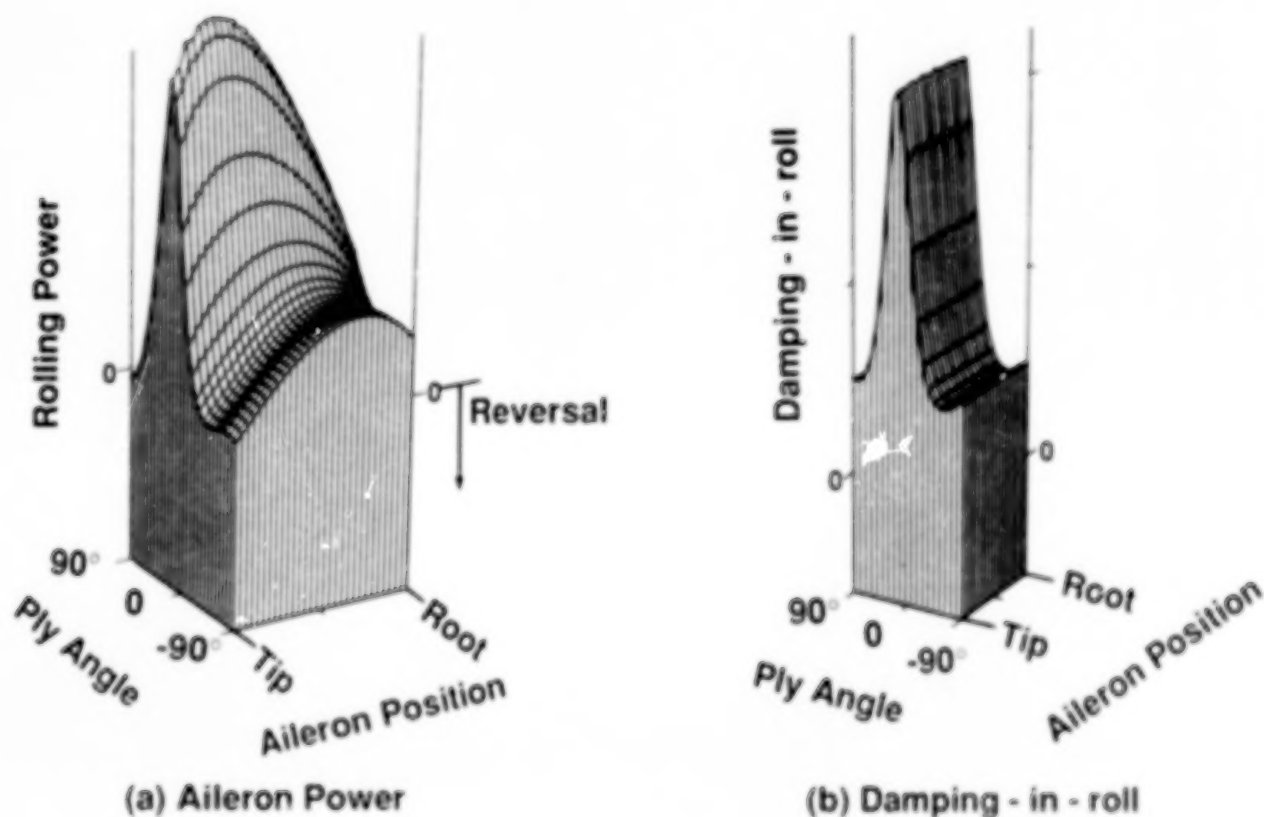


Figure 4

AN OPTIMIZATION EXAMPLE PROBLEM-AILERON CHORD SIZE FIXED

To study the optimal design process itself, an example problem was developed. A series of optimization problems were solved in which the aileron chord dimension and the position of the aileron on the wing were held fixed. An unconstrained minimization problem was posed in which the three laminate ply angles were design variables and the roll rate was a constraint used to remove one of these variables. For the example cases chosen, convergence to the optimum design was rapid, as indicated in Figure 5. The inset to this figure shows a typical design cycle history for a case in which the aileron is in the outboard position. As anticipated, there are two local minima to be found by the procedure, depending upon the initial design condition chosen. Figure 5 also shows a comparison between the optimum design performance and the hinge moment for a similar, unoptimized, orthotropic laminate. Note that in this case all 3 final laminate ply angles are nearly equal.

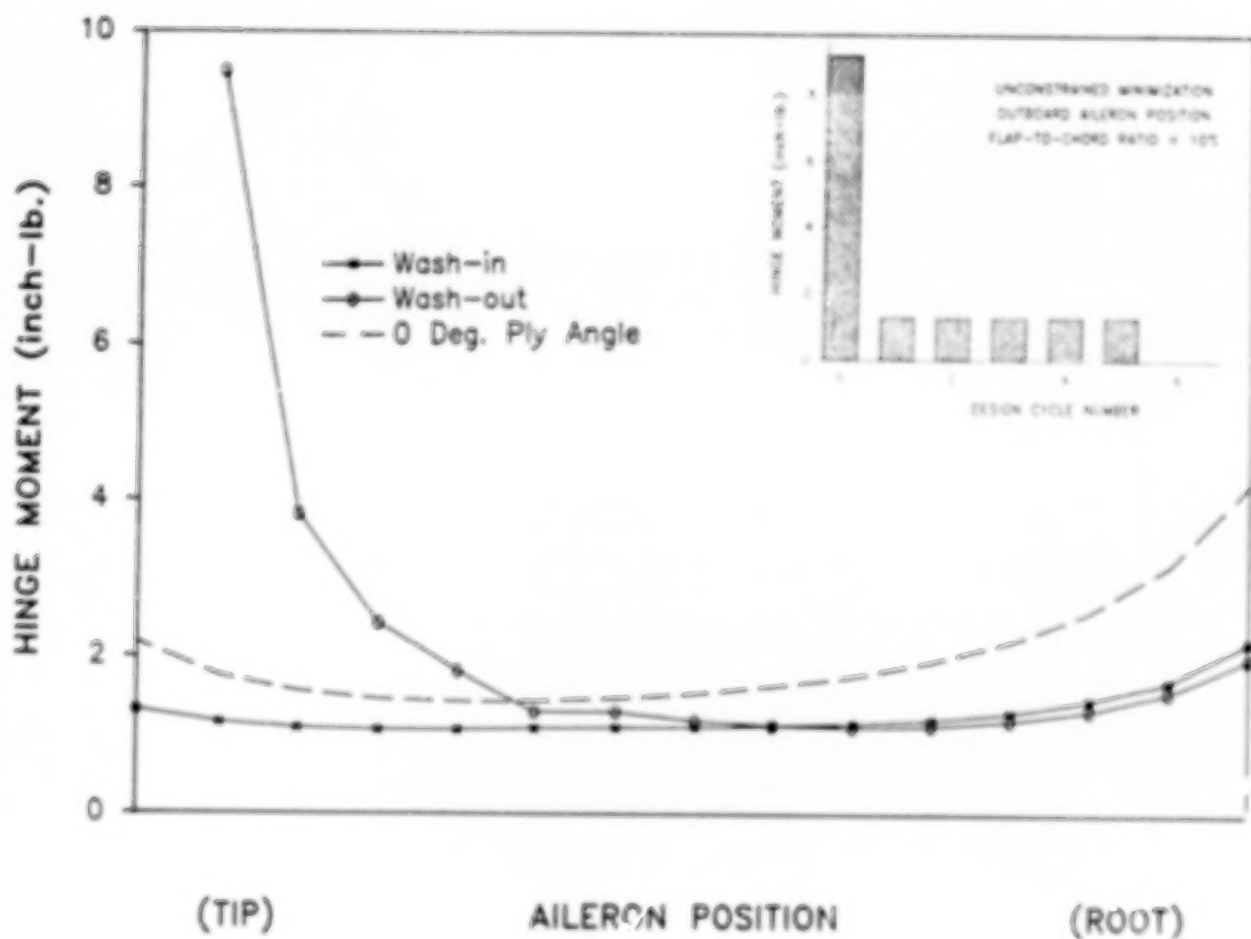


Figure 5

OPTIMAL PLY ORIENTATION FOR MINIMUM HINGE MOMENT

The ply orientations found to create minimum hinge moment while still allowing the specified roll rate are shown in Figure 6. While not constrained to be equal, in this case their values are indistinguishable from each other. The wash-in design orientation is created by sweeping the 3 plies aft to create a bending-shear coupling effect that causes the wing sections to rotate upward as they bend upward. This promotes aileron effectiveness and damping-in-roll (DIR), but the increase in rolling power outweighs the increase in DIR. The wash-out design is created by sweeping the plies forward. This couples nose-up twist with downward bending to create a less effective aileron surface. However, the damping-in-roll is also minimized so that the trade-off is favorable.

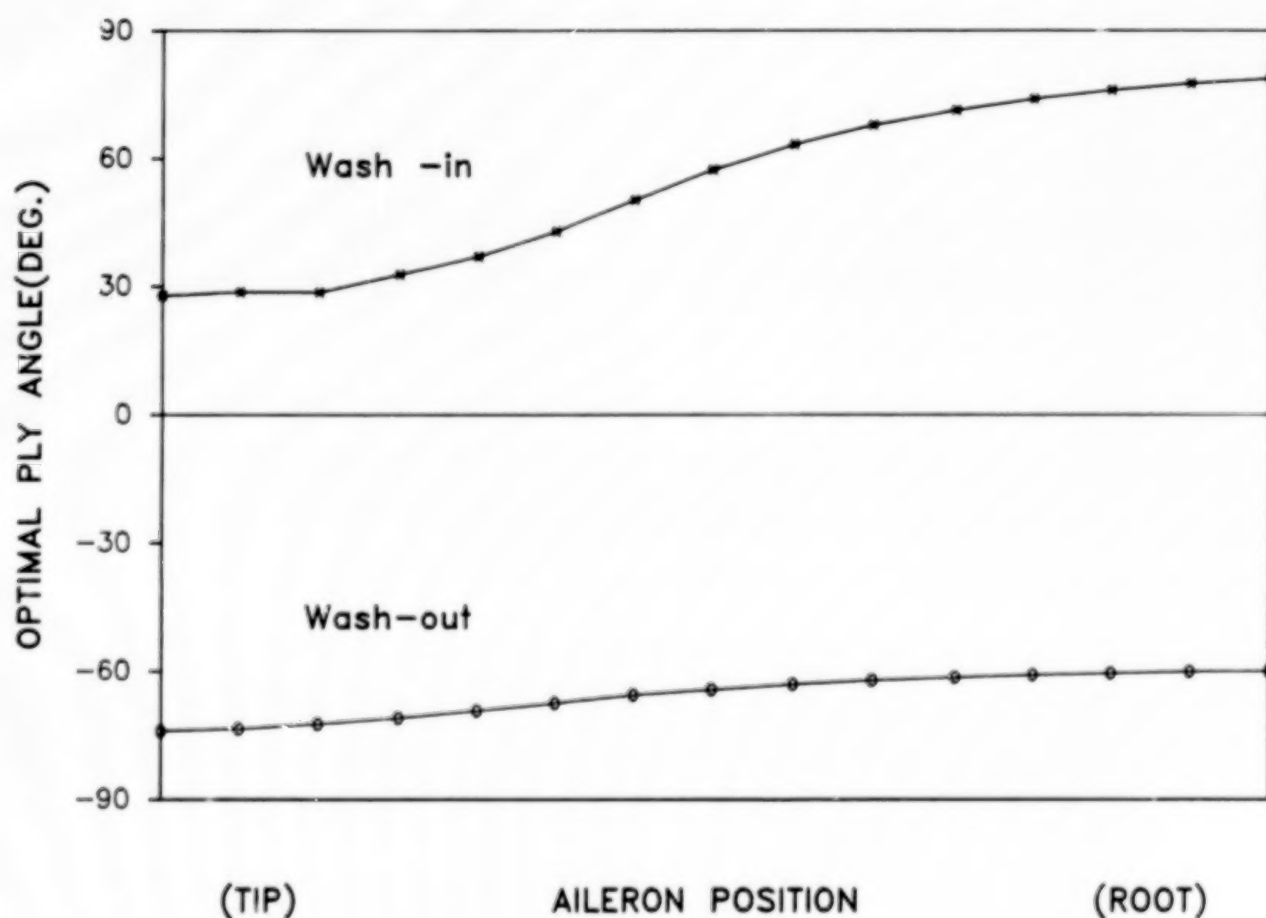


Figure 6

THE AEROSERVOELASTIC OPTIMAL DESIGN PROBLEM

When the aileron spanwise position and its chordwise dimension were included in the optimal design problem, the optimization technique chosen was an interior penalty function method. A pseudo-objective function was defined as the sum of the actual hinge moment and penalty functions representing; the aileron flap-to-chord ratio (which is free to take on any values above 0.075); the aileron spanwise position (which must lie between the wing root and tip); and the roll rate (which must be a specified rate). Figure 7 shows the values of this performance index as a function of design cycle history, plotted together with the value of the actual hinge moment. The Davidon-Fletcher-Powell method, in conjunction with a cubic interpolation method was programmed to generate these results.

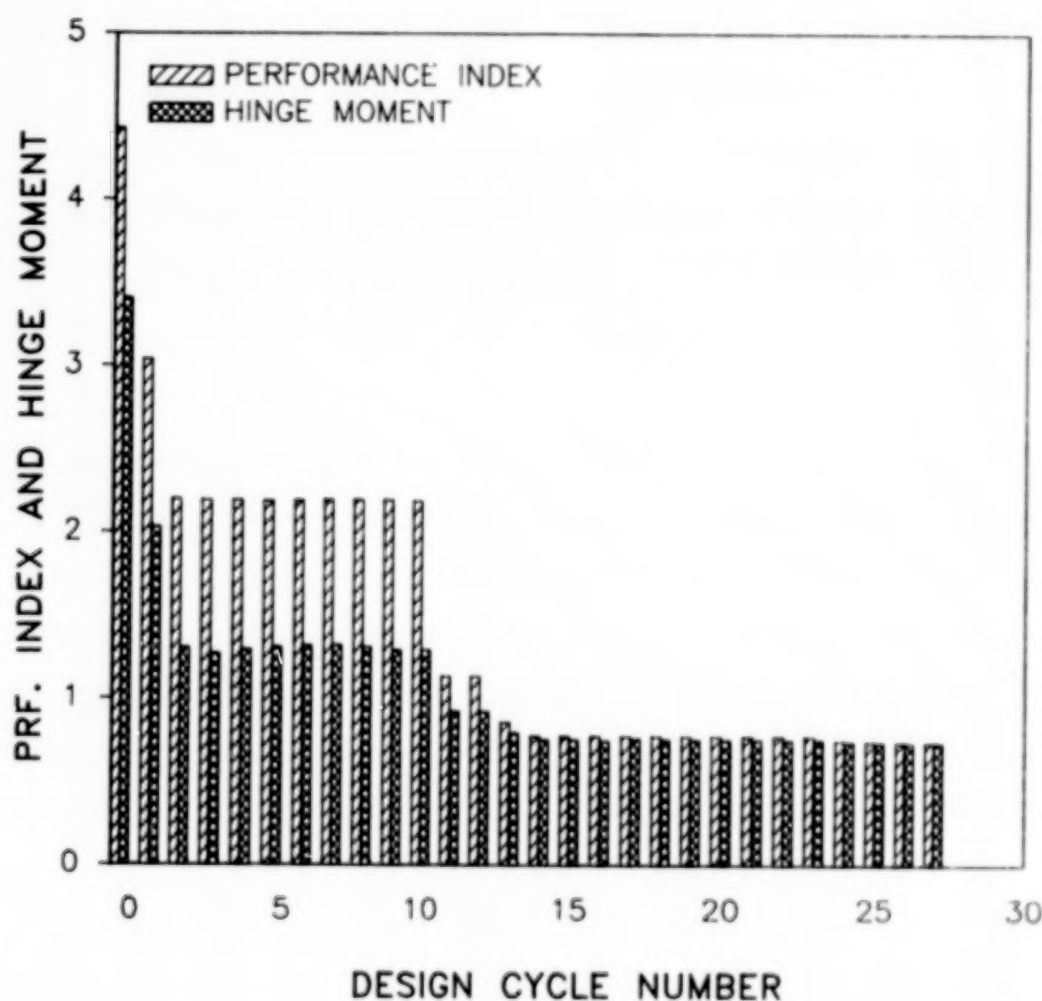


Figure 7

LAMINATE PLY ANGLE BEHAVIOR DURING OPTIMIZATION

All 3 plies began the optimization search oriented 20 degrees forward of the swept span reference line. During the design process they acquired different orientations, but finally became nearly equal as more design cycles occurred. The final design was a wash-in design with the design plies at about 30 degrees aft of the reference axis (Figure 8).

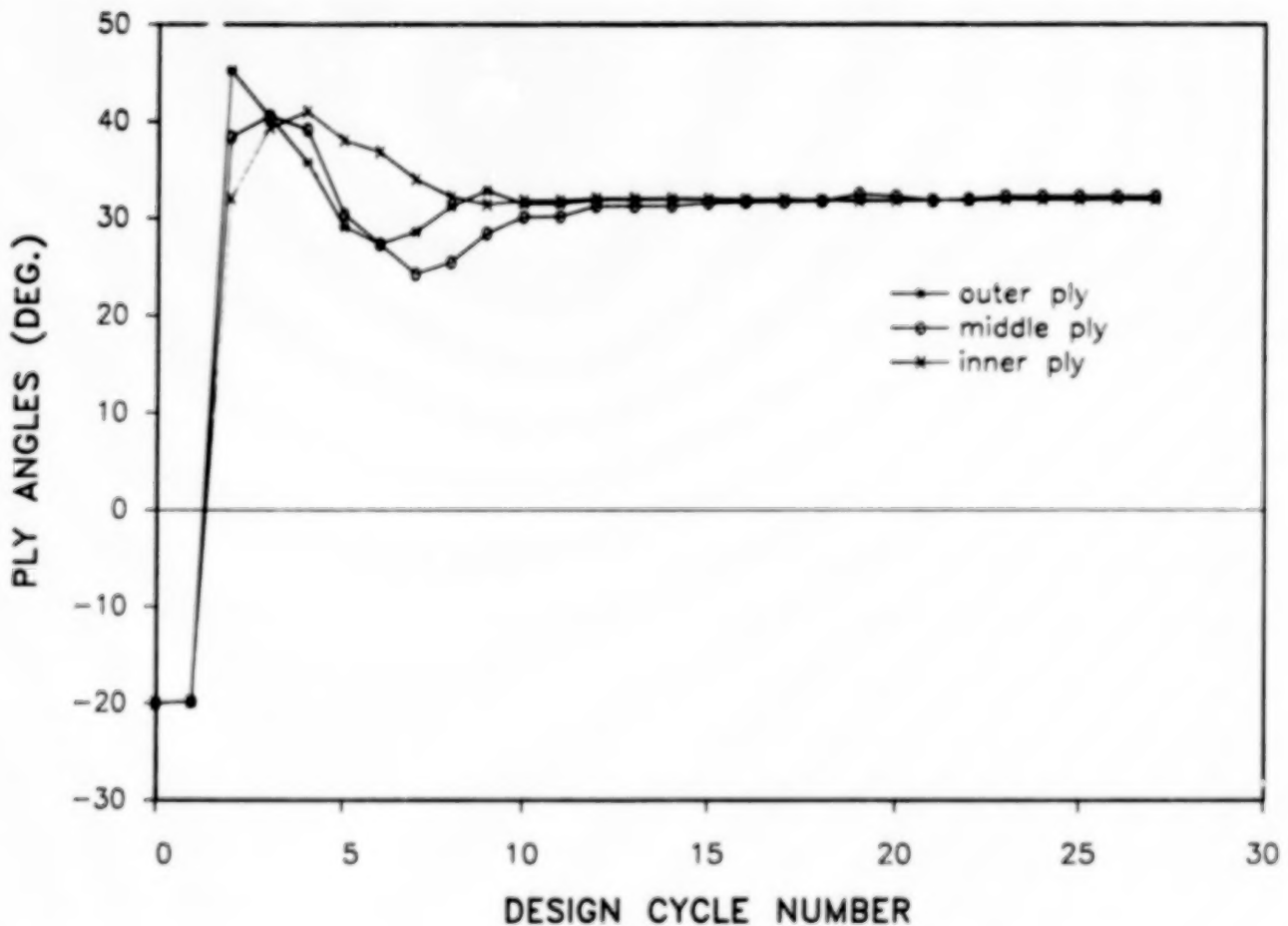


Figure 8

OPTIMAL SPANWISE AILERON POSITION

While the laminate plies are re-orienting themselves, the aileron is moving along the span to try to relieve the load on the hinge, while at the same time maintaining performance. Figure 9 shows the design history of this movement. The aileron begins near the 3/4 span position, moves inward slightly, and then proceeds to move outward to the 8/10 span position.

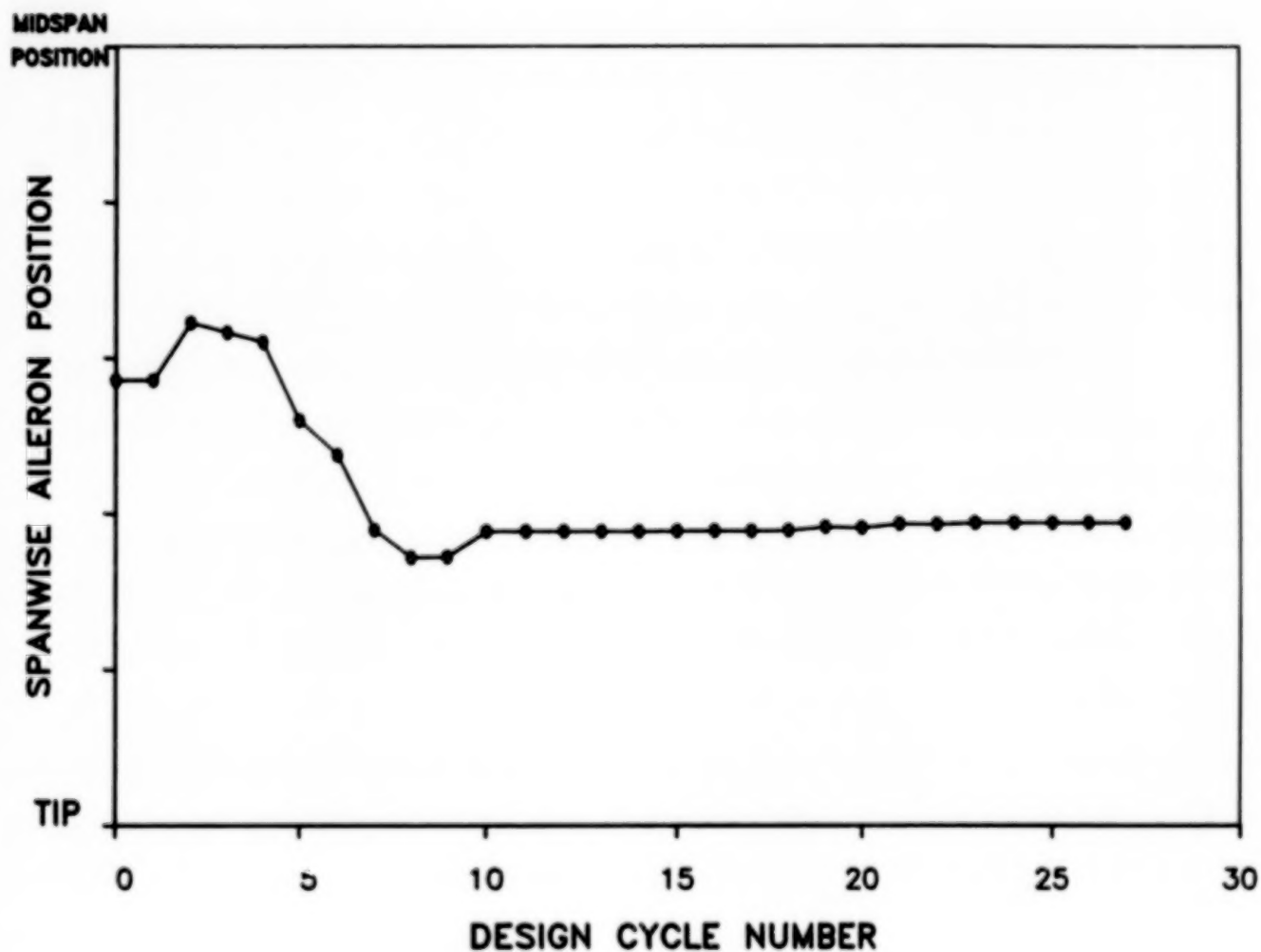


Figure 9

FLAP-TO-CHORD RATIO DESIGN HISTORY

The history of the value of aileron flap-to-chord ratio is shown in Figure 10. Because of the model used, this ratio tries to become as small as possible, but is not allowed to become less than 0.075. When other initial starting point designs were input to the procedure, the final result was essentially the same.

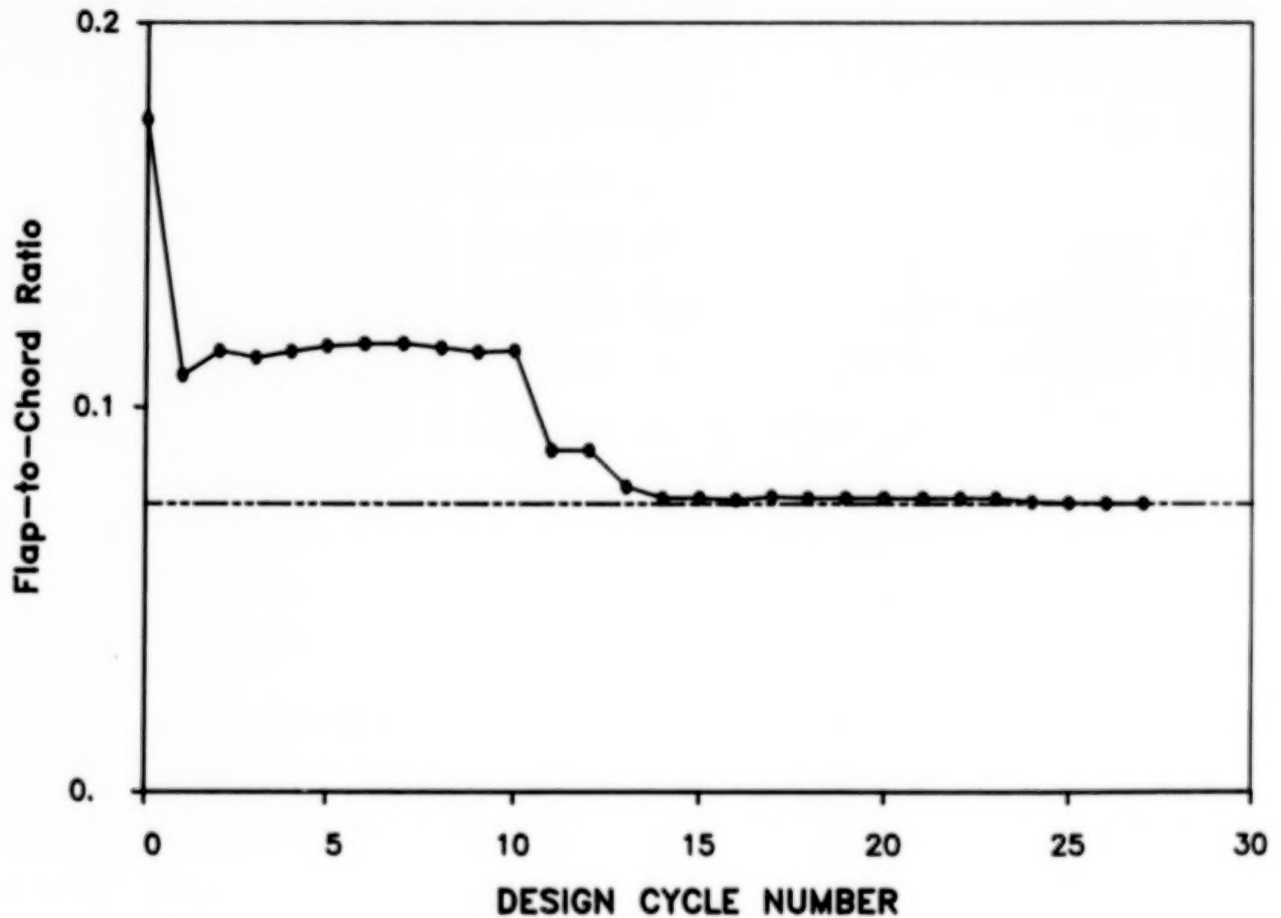


Figure 10

SUMMARY OF RESULTS AND OUTLOOK FOR THE FUTURE

This design optimization problem indicates the advantages of simultaneous consideration of structural design and control design. The performance index, the aileron hinge moment, has appeal to both groups, and because of the actuator weight associated with it, appeal to all. Besides the numbers generated, the interesting aspect of the problem is that it indicates that there is a trade-off between large values of rolling power and low damping-in-roll of the wing surface itself. The method used was made efficient by using subroutines that computed design sensitivity derivatives directly from analytical expressions obtained by algebraic manipulation. Present efforts have been directed towards including wing taper ratio as a design variable to further control damping-in-roll and including wing sweep angle itself to control aileron effectiveness and damping-in-roll.

**RESULTS OF INCLUDING GEOMETRIC NONLINEARITIES
IN AN AEROELASTIC MODEL OF AN F/A-18**

Carey S. Buttrill
NASA Langley Research Center
Hampton, Virginia

Why the Effort?

The trend in design indicates that future airplanes will be statically unstable in pitch, be more flexible than current aircraft, and require highly integrated, interdisciplinary, design methodologies [1]. Fighter aircraft will be more maneuverable and will use active flutter suppression. One application of active flutter suppression is to provide the required margin between the maximum attainable speed in a dive and the speed at which flutter occurs while also requiring open-loop flutter to be at or above the maximum dive speed. A more ambitious application of flutter suppression would be to allow the normal operating envelope to exceed the open-loop flutter speed. If active flutter suppression is to become part of the integrated flight control system, then an integrated modeling and simulation capability is required. This modeling and simulation capability would embrace traditional non-linear, rigid-body mechanics for aircraft and traditional linear aeroservoelastic dynamic models. In particular, a unified set of equations and notation should arise.

A variety of programmatic responses arose from the concern that current modeling practices needed to be reexamined in light of anticipated applications to future aircraft. At the Langley Research Center a Functional Integration Technology (FIT) team was established to perform dynamics integration research using the F/A-18 as a focus vehicle. A central part of this effort has been the reexamination of the aeroelastic equations of motion for fixed-wing aircraft [2,3] and the development of a comprehensive simulation modeling capability [4]. At the Wright Research and Development Center, a 30-month contract was awarded to Lockheed to develop an aeroservoelastic analysis and design software package wherein the equations of motion are developed from first principles [5]. At the Air Force Office of Scientific Research a contract was let to Professor Luigi Morino to develop the equations of motion of a maneuvering, flexible airplane with minimal simplifying assumptions [6]. The Lockheed effort [5] adapts the method of hybrid coordinates used by Likens for space-craft applications [7] to the aircraft problem. Morino's approach [6] is very similar to the FIT effort [2,3] and does a nice job of incorporating the total vehicle rotational degrees-of-freedom in a Lagrangian framework by taking partial derivatives of kinetic and potential energy with respect to the entire direction cosine matrix.

• OBSERVED TRENDS IN AIRPLANE DESIGN (FIGHTERS)

- STATIC INSTABILITY IN PITCH
- MORE FLEXIBLE
- MORE MANEUVERABLE
- HIGHLY INTEGRATED DESIGN
- ACTIVE FLUTTER SUPPRESSION TO PROVIDE MARGIN

• URGE TO "UNIFY" AND GENERALIZE NOTATION AND EQUATIONS

- TRADITIONAL, RIGID-BODY AEROMECHANICS
- TRADITIONAL, LINEAR ASE ANALYSIS

• PROGRAMATIC RESPONSE - (1986-88)

- LARC - FIT (Functional Integration Technology)
- AFWAL - LOCKHEED ASE CONTRACT
- USAF OFFICE OF SCIENTIFIC RESEARCH - L. MORINO

The Path Followed by FIT

When the FIT team began its investigations, no references in the aircraft literature could be found wherein equations of motion for elastic airplanes were developed with what seemed to be sufficient generality. The usual developments made assumptions that resulted in the absence of any inertial coupling between angular rates and elastic deformation. Occasionally questions were raised as to the conditions under which these simplifying assumptions might not be justified [8]. The literature for spacecraft and rotorcraft was not examined initially.

In the FIT team development, a Lagrangian approach was used to derive the equations of motion of an elastic airplane flexing about a rotating reference frame. As a result of retaining the coupling terms in the kinetic energy expression, non-linear terms representing inertial coupling between angular and elastic degrees-of-freedom were identified. Equations including these terms were implemented in a simulation model of an F/A-18 and a number of trajectories calculated to determine the effects of these coupling terms [2]. At the same time, a number of articles were appearing in the literature that examined the errors that can arise in predicting centrifugal stiffening when all the nonlinear terms are retained in the kinetic energy expression but not in the potential energy expression [9,10]. The result was that either zero stiffening or negative stiffening is predicted in cases where positive stiffening should result. This error was common to most of the multi-flexible body simulation codes then available and to the initial developments of the FIT team and Lockheed [2,5]. The approach adopted by the FIT team to correct the error in centrifugal effects was to augment the existing simulation structure with terms resulting from retaining non-linear strain/displacement terms in the potential energy expression and mapping their effect into the existing simulation structure. The FIT approach and its application to an example problem are described in detail in reference [3].

- **PERFORMED LITERATURE SEARCH**

- VERY LITTLE IN AIRCRAFT LITERATURE ON MANEUVERING, FLEXIBLE STRUCTURES
- SPACECRAFT AND ROTORCRAFT LITERATURE IGNORED

- **REDERIVED EQUATIONS OF MOTION**

- AIRPLANE FLEXING ABOUT A ROTATING FRAME
- INERTIAL COUPLING BETWEEN ANGULAR MOTION AND ELASTIC MODES IDENTIFIED
- APPLIED TO MODEL OF F18 TO DETERMINE EFFECTS - AIAA 87-2501-CP

- **THEORETICAL WEAKNESS ADDRESSED**

- CENTRIFUGAL EFFECTS - [Kane], [Eke]
- APPROACH CHOSEN: NONLINEAR STRAIN/DISPLACEMENT - GEOMETRIC STIFFENING
- APPLIED TO SIMPLE ROTATING STRUCTURE - AIAA 88-2232-CP

The Issues

One is left with with two questions at this point: (1), Is geometrically-exact flexible body modeling theory required for the dynamic analysis of fixed-wing aircraft, even highly-augmented, unstable ones; and (2), how is such modeling best accomplished? Previous work [2] indicates that for most fixed-wing aircraft in a clean-wing configuration, geometrically exact theory is probably unnecessary. Exceptions may occur in cases of underwing-store and T-tail configurations. Nonlinear terms due to the complex geometry can assert themselves in the form of parametrically excited oscillations. The most compelling reason for geometrically-exact modeling theory may be just the urge to have a comprehensive theory that works for all cases. The difficulty is establishing a non-linear theory that is sufficiently correct for the airplane problem without resorting to full-blown computational structural dynamics. An example of the computational structural mechanics approach is the Large Angle Transient DYNamics (LATDYN) code [11] developed at Langley and the work of Belytschko and Hsieh on which LATDYN was based [12]. These methods [11,12] assign a separate reference frame to each finite element that translates and rotates ("convects") with each finite-element. This "convected" coordinate method has been applied to large deformation problems such as car collisions and antenna deployment and would accommodate the nonlinear rotational/elastic coupling of a typical airplane structure with ease. However, a theory based on assumed modes and correct to second order may be sufficient for airplane applications and would require less computer resources than an approach similar to that of [11] and [12].

(1) ARE GEOMETRICALLY-EXACT MODELING THEORIES REQUIRED FOR AIRPLANE DYNAMIC ANALYSIS?

- SPACECRAFT AND HELICOPTERS - YES
- MOST AIRPLANES - NO
- REASONS FOR / POSSIBLE EXCEPTIONS:
 - INERTIAL FORCES APPROACH AERODYNAMIC FORCES
 - COMPLEX GEOMETRIES - STORES
 - THEORETICAL PURITY

(2) IF SO, WHAT IS THE BEST WAY TO IMPLEMENT SUCH THEORY?

- MUST PROPERLY MODEL CENTRIFUGAL EFFECTS OR LEAVE THEM OUT
- MANY POSSIBLE APPROACHES

Outline

The remainder of this paper is organized as follows. First the equations of motion are briefly described. Since an energy approach was taken in the development of the equations of motion [2,3], expressions for kinetic and potential energy are defined. The differences between the FIT model and the more typical aircraft aeroelastic equations [8,13] are explained. Prior to defining the the potential energy, a simple example [10] is presented to illustrate the notion of "geometric" stiffness. The higher order terms in the FIT potential energy expression are explained in light of the simple example. Once the equations are established, the effects of the including the nonlinear inertial coupling terms in the simulation model of an F/A-18 are presented. Time responses due to a high-authority roll command are compared for the following cases: (1), additional terms included; and (2), additional terms ignored. Finally, conclusions and recommendations are offered.

- **EQUATIONS OF MOTION**

- KINETIC ENERGY
- EXAMPLE OF GEOMETRIC STIFFNESS
- POTENTIAL ENERGY

- **EFFECT OF INERTIAL LOADING - F/A-18**

- **CONCLUSIONS**

Modeling Assumptions

The operating assumptions in the equations of motion are listed below. Assumptions (2) through (4) are typical for airplane applications [8,13]. Assumptions (5) through (7) are atypical and lead to the differences between the FIT model and the more typical aeroelastic equations of motion [8,13].

The structural finite-element model obtained for the F/A-18 was a lumped mass model, which provided the principal motivation for assumption (1). For a continuum model, summations over the lumped masses are replaced with integrations over the entire airplane. The finite-element model had both lumped masses and lumped inertial quantities and both were utilized in the calculations. Assumption (2) and (3) are consistent with each other. Assumption (2) leads to a generalized Hooke's law and assumption (3) allows the superposition of deformation modes. Assumption (4) reflects the fact that gravity gradients are only of concern in spacecraft dynamics.

Assumption (5) acknowledges that while deformation is assumed to be small, total vehicle angular rate may not be small. The result is that products of total angular rate and deformation rates are retained in the kinetic energy expression. The effect of assumption (6) is that the term resulting from summing (integrating) the cross product of deformation with deformation rates over the total vehicle is retained in the kinetic energy expression. Assumption (7) recognizes that a transverse deformation of a beam will result in axial strain. This effect becomes critical in correctly predicting centrifugal effects and is best explained in the simple example that appears later. Apart from assumptions (5), (6), and (7), the following development closely parallels other developments of the aeroelastic equations [8,13].

(1) LUMPED MASS APPROXIMATION

(2) LINEAR STRESS/STRAIN

(3) DEFORMATION IS SMALL - SUPERPOSITION

(4) GRAVITY CONSTANT OVER THE AIRPLANE

FOLLOWING ATYPICAL AEROELASTIC ASSUMPTIONS WERE MADE

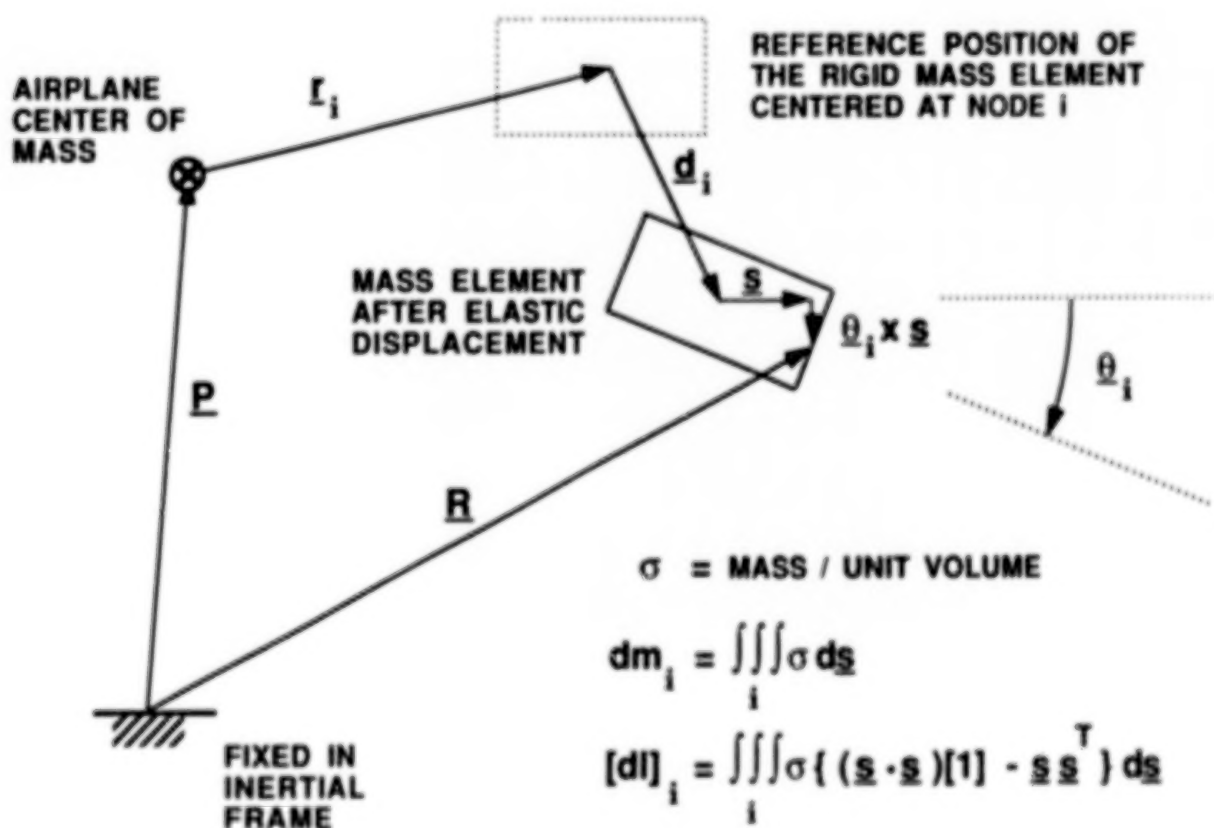
**(5) PRODUCTS OF ROTATION RATE AND DEFORMATION
ARE NOT NEGLIGIBLE**

**(6) ELASTIC DISPLACEMENT AND ELASTIC VELOCITIES
MAY NOT BE PARALLEL**

(7) NON LINEAR STRAIN / DISPLACEMENT

Symbols and Definitions

For the purposes of calculating kinetic energy, the total vehicle is viewed as a collection of small rigid bodies centered at the finite-element node locations. The lumped mass $(dm)_i$ and the lumped inertia $[dI]_i$ associated with the i^{th} node can be interpreted as the result of performing integrations over the volume of the i^{th} rigid body using \underline{s} as a variable of integration and the mass density, σ , as a weighting function. The i^{th} rigid body undergoes a translational deformation \underline{d}_i and a rotational deformation $\underline{\theta}_i$. The assumption of small deformations allows the rotation to be described as a vector and implemented as a cross product. The vector \underline{r}_i locates the undeformed position of the i^{th} rigid body in the vehicle body frame. The origin of the body frame is at the center of mass of the total vehicle when the vehicle is in the undeformed configuration. The vector \underline{R} locates an arbitrary point of the i^{th} rigid body in the inertial frame.



Total Kinetic Energy

The total kinetic energy is calculated in two steps. First the kinetic energy of the i^{th} rigid body (lumped mass) is found by performing the volume integration indicated in the brackets. The inertial velocity of an interior point is squared, multiplied by the mass density, σ , and integrated over the small rigid body. All volume integral expressions involving the variable of integration \underline{s} can be resolved into the "known" parameters, $(dm)_i$ and $[dI]_i$, that are defined in the previous figure. A summation is then performed over the small rigid bodies indexed by i . If the deformations are described as a sum of spatial functions (mode shapes) and time-dependent generalized coordinates, a separation of variables is achieved. The kinetic energy becomes a summation of terms where each term is a product involving time varying coordinates and constant mass or length terms resulting from the summation (integration) over the total vehicle.

- INTEGRATE OVER THE IDEALIZED LUMPED MASS TO GET KINETIC ENERGY FOR EACH LUMPED MASS
- SUM THE KINETIC ENERGIES ASSOCIATED WITH EACH LUMPED MASS

$$T = \frac{1}{2} \sum_i \left\{ \iiint_{\text{OVER } i} \sigma \left(\frac{d\underline{R}}{dt_I} \right) \cdot \left(\frac{d\underline{R}}{dt_I} \right) d\underline{s} \right\}$$

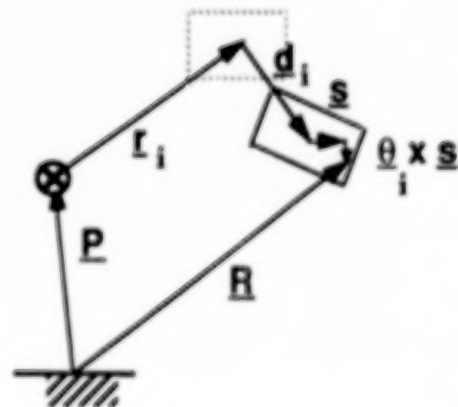
WHERE

$$\underline{R} = \underline{P} + \underline{r}_i + \underline{d}_i + \underline{s} + \underline{\theta}_i \times \underline{s}$$

$$\underline{d}_i = \underline{\Phi}_i \eta^j \quad \text{TRANSLATIONAL DEFORMATION IN MODAL COMPONENTS}$$

$$\underline{\theta}_i = \underline{\Psi}_i \eta^j \quad \text{ROTATIONAL DEFORMATION IN MODAL COMPONENTS}$$

$$\frac{d}{dt_I} \quad \text{TIME RATE OF CHANGE WITH RESPECT TO THE INERTIAL FRAME}$$



Kinetic Energy in Modal Components

The first three terms of the expression defining kinetic energy, shown below, are found in the standard aeroelastic equations of motion developments [8,13] and represent "rigid" translational energy, "rigid" rotational energy, and elastic kinetic energy, respectively. The term $[J_0]$ is the inertia dyadic of the total undeformed airplane expressed in body-frame components and has units of mass-length². The fourth line describes coupling between translational, rotational, and elastic momenta. If the assumed mode shapes are the modes of free vibration of an unrestrained structure, they satisfy the first-order mean axis conditions [8,13] and the terms, \underline{a}_j and \underline{h}_j are zero. The term \underline{a}_j is simply the location of the center of mass of the j^{th} mode shape in the body frame and has units of length. The term \underline{h}_j is the first moment of the j^{th} mode shape in the body frame using mass as the weighting function and has units of mass-length². The terms in the dashed-line box result from assumptions (5) and (6). The terms $[J]_j$ and $[J]_{jk}$ are the first and second partial derivatives of the inertia dyadic matrix with respect to elastic modes j and k . The term \underline{h}_{jk} results from summing (integrating) the cross product of mode shape j with mode k over the vehicle and has units of mass-length². For a more complete explanation, see reference 2.

$$\begin{aligned}
 T = & \frac{1}{2} m \underline{V} \cdot \underline{V} && \bullet \text{ RIGID BODY TRANSLATIONAL KINETIC ENERGY} \\
 & + \frac{1}{2} \underline{\omega} \cdot [J_0] \cdot \underline{\omega} && \bullet \text{ RIGID BODY ROTATIONAL KINETIC ENERGY} \\
 & + \frac{1}{2} M_{jk} \dot{\eta}^j \dot{\eta}^k && \bullet \text{ MODAL ELASTIC KINETIC ENERGY} \\
 & + m \underline{V} \cdot \underline{a}_j \dot{\eta}^j + \underline{\omega} \cdot \underline{h}_j \dot{\eta}^j + m \underline{V} \cdot \underline{\omega} \times \underline{a}_j \dot{\eta}^j && \bullet \text{ ZERO FOR UNRESTRAINED MODES} \\
 & + \frac{1}{2} \underline{\omega} \cdot \{ [J]_j \eta^j + \frac{1}{2} [J]_{jk} \eta^j \eta^k \} \cdot \underline{\omega} && \bullet \text{ NONLINEARITIES RESULTING FROM ASSUMPTIONS (5), (6)} \\
 & + \underline{\omega} \cdot \underline{h}_{jk} \eta^j \dot{\eta}^k
 \end{aligned}$$

Illustration of Geometric Stiffness

The example shown below is taken from reference [10] and provides a simple paradigm of the beam problem. Pictured is a simple 3 degree-of-freedom, planar system. A mass, m , is located at the outermost point and is the only mass in the system. The structure rotates freely about the point P . The angle between rod a and an inertial reference is given by ψ . There is a torsional spring, k_θ , and a linear spring, k_d . The deflection of the torsional spring is given by θ and the linear spring by $d = r\delta$, where δ is a nondimensional deflection. Another coordinate system (x,y) is given by an axis system located at the zero-strain position of the mass, m . The (x,y) coordinates are analogous to those typically used in the beam problem. The coordinates (ξ,η) are the non-dimensional forms of (x,y) . Both the (ψ,δ,θ) and the (ψ,ξ,η) coordinate systems are equally valid for describing this system. The (ψ,δ,θ) system leads to a particularly simple expression for strain energy. The reason is that a change in δ produces only a linear distortion in the spring, k_δ , and similarly for θ . Thus the strain energy, U , is given by,

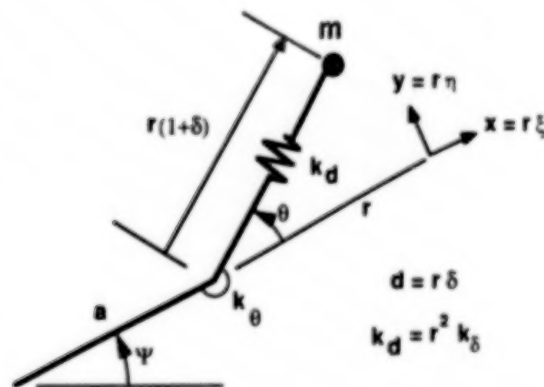
$$U = (1/2) \{ k_\theta \theta^2 + k_\delta \delta^2 \}$$

where $k_\delta = k_d r^2$. The (ψ,ξ,η) system produces a complex expression for strain energy. A change in η produces nonlinear changes in both springs and similarly for ξ if there is some deflection in η . Using the relations,

$$\delta = -1 + (\eta^2 + (1+\xi)^2)^{1/2} \quad \text{and} \quad \theta = \tan^{-1}[\eta/(1+\xi)],$$

one gets for the strain energy, U , in terms of ξ and η ,

$$U = (1/2) \{ k_\delta \{ -1 + [\eta^2 + (1+\xi)^2]^{1/2} \}^2 + k_\theta \{ \tan^{-1}[\eta/(1+\xi)] \}^2 \}.$$



- TWO CHOICES FOR COORDINATES: (ψ, δ, θ) OR (ψ, ξ, η)
- $(\delta, \theta) \rightarrow$ SIMPLE EXPRESSION FOR STRAIN ENERGY
- $(\xi, \eta) \rightarrow$ COMPLEX STRAIN ENERGY EXPRESSION
- PARADIGM OF BEAM PROBLEM

Comparison of Resulting Linear Models

If the full nonlinear equations are derived using the (ψ, δ, θ) coordinates, the ψ equation removed, and the quantities $\dot{\psi}$ and $\ddot{\psi}$ are treated as parameters, the remaining two equations can be linearized in θ and δ and the resulting **correct** linear equations are given in case 1 below. Suppose the procedure is repeated for the (ψ, ξ, η) coordinates except that a linear approximation for strain energy given by,

$$U \sim (1/2) \{ k_{\theta} \eta^2 + k_{\delta} \xi^2 \},$$

is used, then the resulting equations are given as case 2 below [10]. The only differences occur in the stiffness matrix. The foremost difference is that a de-stiffening result is predicted in case 2 for the η degree-of-freedom due to the spin rate when a stiffening effect should be predicted.

CASE 1: $\ddot{\psi}$ AND $\dot{\psi}$ GIVEN; ψ EQUATION REMOVED; LINEARIZED IN δ AND θ

$$\begin{bmatrix} I_r & 0 \\ 0 & I_r \end{bmatrix} \begin{bmatrix} \ddot{\theta} \\ \ddot{\delta} \end{bmatrix} + 2 \begin{bmatrix} 0 & I_r \dot{\psi} \\ -I_r \dot{\psi} & 0 \end{bmatrix} \begin{bmatrix} \dot{\theta} \\ \dot{\delta} \end{bmatrix} + \begin{bmatrix} k_{\theta} + I_{ar} \dot{\psi}^2 & (I_{ar} + 2I_r) \ddot{\psi} \\ I_{ar} \ddot{\psi} & k_{\delta} - I_r \dot{\psi}^2 \end{bmatrix} \begin{bmatrix} \theta \\ \delta \end{bmatrix} = \begin{bmatrix} -(I_{ar} + I_r) \ddot{\psi} \\ (I_{ar} + I_r) \dot{\psi}^2 \end{bmatrix}$$

CASE 2: (ξ, η) COORDINATES; LINEAR STRAIN / DISPLACEMENT, $U = (1/2) \{ k_{\theta} \eta^2 + k_{\delta} \xi^2 \}$

$$\begin{bmatrix} \text{SAME} \\ \text{AS} \\ \text{ABOVE} \end{bmatrix} \begin{bmatrix} \ddot{\eta} \\ \ddot{\xi} \end{bmatrix} + 2 \begin{bmatrix} \text{SAME} \\ \text{AS} \\ \text{ABOVE} \end{bmatrix} \begin{bmatrix} \dot{\eta} \\ \dot{\xi} \end{bmatrix} + \begin{bmatrix} k_{\theta} - I_{ar} \dot{\psi}^2 & I_r \ddot{\psi} \\ -I_{ar} \ddot{\psi} & k_{\delta} - I_r \dot{\psi}^2 \end{bmatrix} \begin{bmatrix} \eta \\ \xi \end{bmatrix} = \begin{bmatrix} \text{SAME} \\ \text{AS} \\ \text{ABOVE} \end{bmatrix}$$

$$I_r = m r^2$$

$$I_{ar} = m a r$$

Potential Energy

Returning to the equations of motion development for an airplane, the total potential energy is composed of a component due to the work performed by strain and a component due to the work performed against gravity. The gravity component is straightforward since gravity is assumed constant over the airplane. If a second order expression is used for describing strain as a function of displacement and a linear stress / strain relationship exists, then a fourth-order strain energy expression results [3]. The strain energy expression, however, is accurate only to third order, so the fourth-order term is dropped. A third-order term in the strain energy expression, shown in modal components below, would lead to second-order stiffness terms in the final equations. If the third-order strain-energy term is left in this form, then modes with significant axial displacement need to be included in the dynamic model. As seen from the simple example, coupling occurs between axial and transverse displacement in the strain energy expression when beam-like coordinates are used. Since, for airplanes, axial modes are typically much higher frequency than transverse modes, the effects of the axial modes can be residualized. This residualization is accomplished in the FIT framework by solving for the elastic displacements that result from combinations of unit values of rotational velocity about the airplane body-frame axes. Thus for a unit roll rate, p , the steady state deflections are calculated for the full finite-element model. These "static" deflections are combined with the third order stiffness tensor to produce an increment to the basic stiffness matrix that is appropriate for unit roll rate. Thus the j,k^{th} element of an incremental stiffness matrix, $[\Delta K]$, is given by,

$$\Delta K_{jk} = \Delta K_{jkp} \eta_{ss}^p.$$

The j,k^{th} element of $[\Delta K]$ becomes one entry into the 3×3 matrix $[J]_{jk}^g$. Because of symmetry, the matrix, $[J]_{jk}^g$, has 6 free parameters, and each is calculated by repeating this process for different combinations of unit roll rate, p , pitch rate, q , and yaw rate, r . This process is discussed in greater detail in reference [3].

POTENTIAL ENERGY = STRAIN + GRAVITY CONTRIBUTION

$$U = U_s + U_g$$

STRAIN ENERGY IN TERMS OF MODAL STIFFNESS MATRICES

$$\begin{aligned} U_s &= (1/2) [K_{jk} + \Delta K_{jkp}^g \eta^p + \Delta^2 K_{jkpq}^g \eta^p \eta^q] \eta^j \eta^k \\ &\cong (1/2) [K_{jk} - \omega \cdot \{ \frac{1}{2} [J]_{jk}^g \} \cdot \omega] \eta^j \eta^k \end{aligned}$$

HIGHER ORDER TERMS RESULT FROM NONLINEAR STRAIN / DISPLACEMENT EQUATIONS

Final Equations - Unrestrained Modes

The final equations in modal form are shown below. These equations apply to the case where the assumed modes satisfy the first-order mean axis conditions, otherwise additional coupling is present. The terms that are inside the dashed boxes result from assumptions (5), (6), and (7). The terms outside the boxes are equivalent to the equations seen in the more traditional approaches [8,13].

TRANSLATIONAL MOMENTUM

$$m \dot{\underline{V}} + m \underline{\omega} \times \underline{V} = \underline{F} + m \underline{g}$$

ROTATIONAL MOMENTUM

$$[\underline{J}] \dot{\underline{\omega}} + \boxed{h_{jk} \eta^j \dot{\eta}^k} + \underline{\omega} \times [\underline{J}] \underline{\omega} + \boxed{[\underline{J}] \underline{\omega} + h_{jk} \dot{\eta}^j \eta^k + \underline{\omega} \times h_{jk} \eta^j \dot{\eta}^k} = \underline{L}$$

ELASTIC MODE j

$$M_{jk} \ddot{\eta}^k - \boxed{\underline{\omega} \cdot h_{jk} \eta^k} + K_{jk} \eta^k - \boxed{2 \underline{\omega} \cdot h_{jk} \dot{\eta}^k - \frac{1}{2} \underline{\omega}^T \{ [\underline{J}]_j + [\underline{J}]_{jk} \eta^k + [\underline{J}]_{jk}^g \eta^k \} \underline{\omega}} = Q_j$$

TOTAL INERTIA MATRIX IN THE BODY FRAME

$$[\underline{J}] = [\underline{J}_0] + [\underline{J}]_j \eta^j + \boxed{\frac{1}{2} \{ [\underline{J}] + [\underline{J}]_{jk}^g \} \eta^j \eta^k}$$

Inertial Effects - Time History Responses

In assessing the effects of the additional terms in the FIT equations of motion on a predicted response, a variety of cases were calculated. While all three axes were examined, the most interesting responses involved roll rate. The responses shown here were presented at the 1987 Flight Simulation Technologies Conference [2] and were generated prior to the incorporation of the geometric stiffness terms, $[J]_{jk}^g$, in the simulation model. Preliminary runs made subsequently, but not presented in this paper, suggest that the effect of the additional stiffness terms is small for the angular rates considered and that qualitative conclusions drawn from the data presented in reference [2] are still valid.

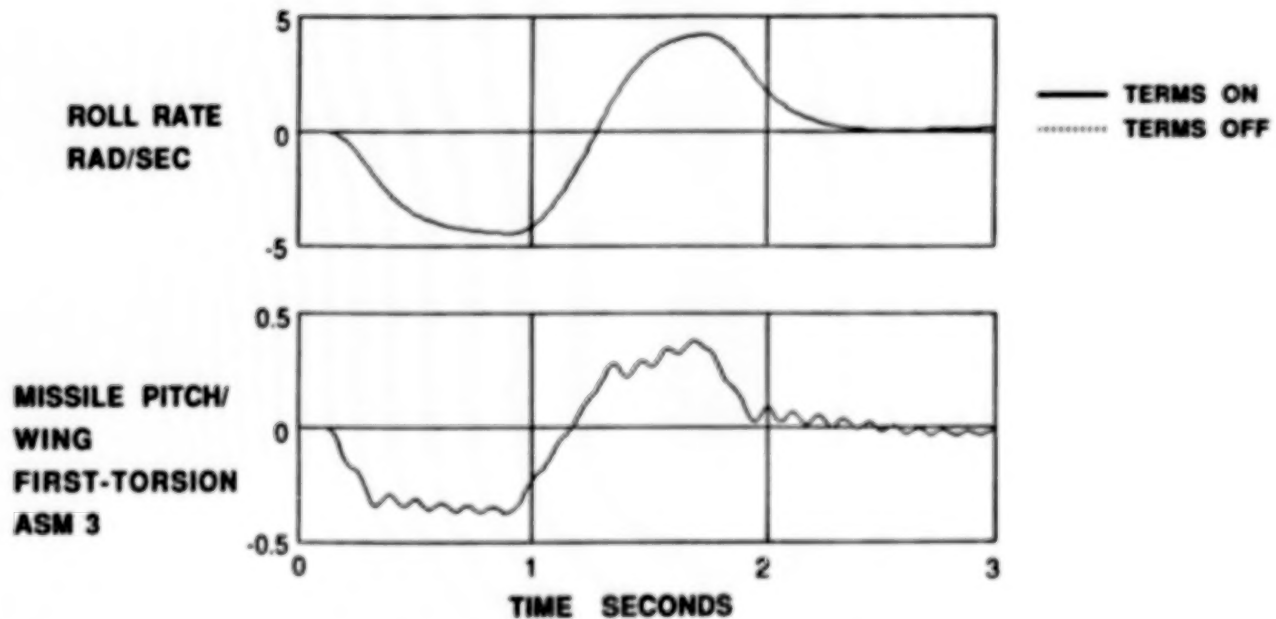
The time responses were generated by injecting a roll command doublet at the actuator input. A combination of aileron and stabilator was used. The initial conditions were straight and level flight at Mach .7 at sea level. Responses were generated with ("terms on") and without ("terms off") the additional angular/elastic coupling terms that are part of the FIT equations of motion.

- **GOAL: ACHIEVE SUFFICIENT ANGULAR RATE TO EXCITE INERTIAL RESPONSE**
- **ROLL DOUBLET - 1 SECOND EACH SIDE**
- **20 DEG AILERON / 10 DEG DIFFERENTIAL STABILATOR**
- **INITIAL CONDITIONS**
 - **MACH = .7**
 - **SEA LEVEL**
 - **STRAIGHT AND LEVEL 1 G TRIM**
- **COMPARE RESPONSE WITH AND WITHOUT ANGULAR/ELASTIC INERTIAL COUPLING**
 - **"TERMS ON" - FIT MODEL**
 - **"TERMS OFF" - TYPICAL ASE MODEL**

289

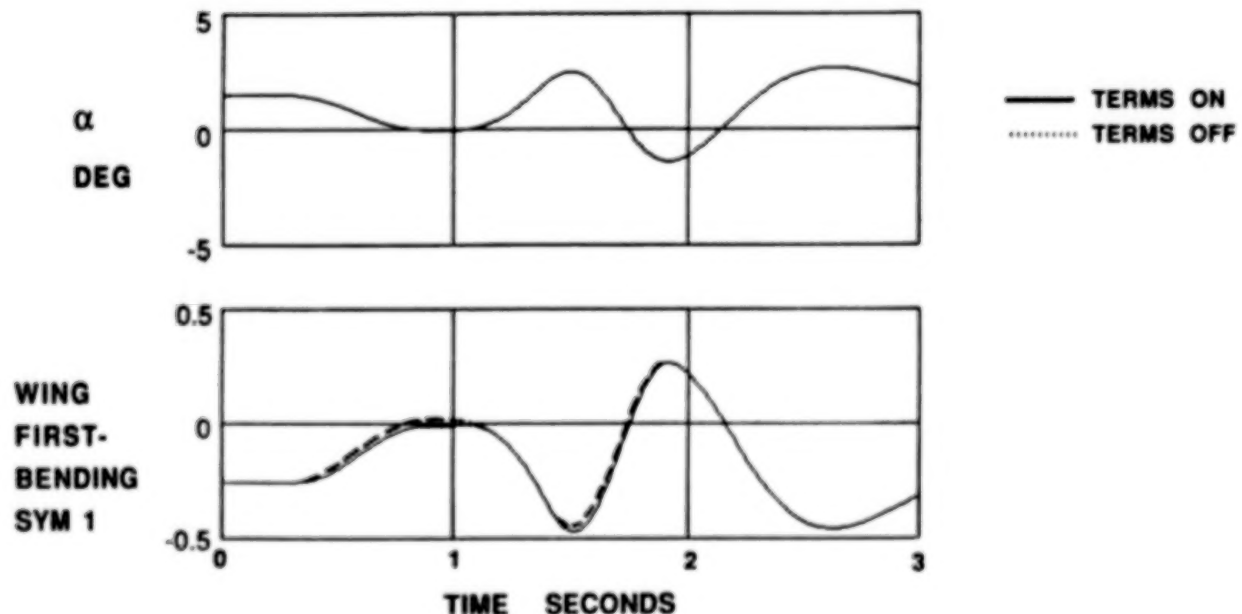
Lateral / Anti-Symmetric Response

For the anti-symmetric responses to the roll command, there was no discernable difference between "terms on" and "terms off" responses. The responses shown below, roll rate and the third anti-symmetric mode, are typical. The third anti-symmetric mode is characterized as a wing first-torsion mode with significant missile pitch. The finite-element model had tip missiles. The reason that no difference occurred is that for anti-symmetric modes, the elastic modes are excited by the terms pq , pr , and qr in the angular/elastic coupling terms. Since the roll maneuver remained well-coordinated, the pitch rate, q , and the yaw rate, r , remained small. Thus the coupling terms, pq , pr , and qr , remained small.



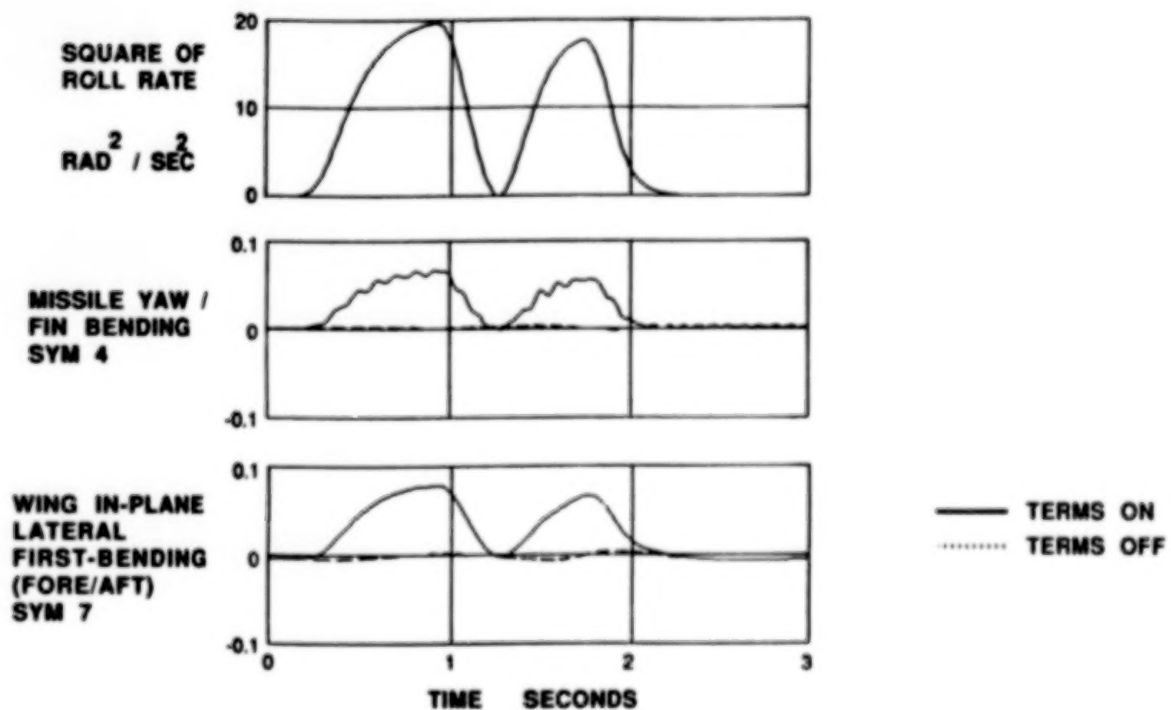
Symmetric Response - Set 1

The inertial coupling terms made no effect on rigid body symmetric responses. The angle-of-attack response is shown below. The angle-of-attack at time equal zero is due to the 1-g trim. The second response shown below is the first symmetric mode, wing first-bending. The y-axis indicates the deflection of the mode in feet measured at the point of maximum deflection, presumably at the wing tip. The mode is positive for tip-down deflection, so the mode is displaced about .25 feet tip-up at time zero. While the angle-of-attack is clearly the principal driver of symmetric wing first-bending in this maneuver, a discernable difference has occurred between the "terms on" and the "terms off" responses. Only two symmetric modes showed more difference in "terms on/off" responses than the first symmetric mode and these two modes are shown in the figure on the next page.



Symmetric Response - Set 2

Symmetric modes 4 and 7 were the only modes to show significant inertially induced response. Symmetric mode 4 is characterized by tip-missile yawing together with fin-bending and symmetric mode 7 is a wing first-bending in the fore/aft plane. The fact that roll rate squared is the principal driver is seen clearly in the figure. The y-axis for the elastic mode responses shown below represents strain energy absorbed normalized by that of the first symmetric mode. In other words, a unit deflection in modes 4 or 7 represents the same strain energy absorbed as would occur with a deflection of one foot in the first symmetric mode. Since the wing is swept backwards, a forward deflection in the the wing results in outboard movement of mass and is therefore excited by roll rate. A natural question to ask is if these sort of responses can be predicted from merely examining the parameters of the simulation model.



Modal Sensitivity Parameter

As part of determining when inertial coupling might be important in an analysis, the following simple parameter can be calculated. The parameter $R_j(\omega)$ defined below is simply a first order approximation to the steady-state response of elastic mode j to a constant angular rate represented by the angular velocity vector, ω . The γ constant is used to scale the responses so that for different modes j , identical R_j 's represent the same strain energy.

$$R_j(\omega) = \gamma \frac{\frac{1}{2} \{ \omega^T [J]_j \omega \}}{K_j}$$

- MODAL DISPLACEMENT NORMALIZED BY STRAIN ENERGY
- APPROXIMATES RESPONSE OF MODE "j" TO CENTRIFUGAL LOADING FOR A GIVEN ROTATIONAL VELOCITY
- MAX DESIGN ROTATIONAL RATES ARE LIKELY INPUTS

$$\gamma = \left[\frac{M_j}{M_{11}^{xy}} \right]^{\frac{1}{2}} \left[\frac{\omega_j}{\omega_1^{xy}} \right]$$

Modal Sensitivity at Max Roll

The parameter $R_j(\underline{\omega})$ is shown below for each of the 20 elastic modes included in the simulation model. The input angular rates correspond to the max roll rate achieved at about .9 second into the maneuver. The angular velocity vector $\underline{\omega} = [p, q, r]^T$ in body-frame components. The fourth and seventh symmetric modes are clearly singled out by the $R_j(\underline{\omega})$ parameter. Again, the units of $R_j(\underline{\omega})$ are strain energy normalized to the first symmetric elastic mode.

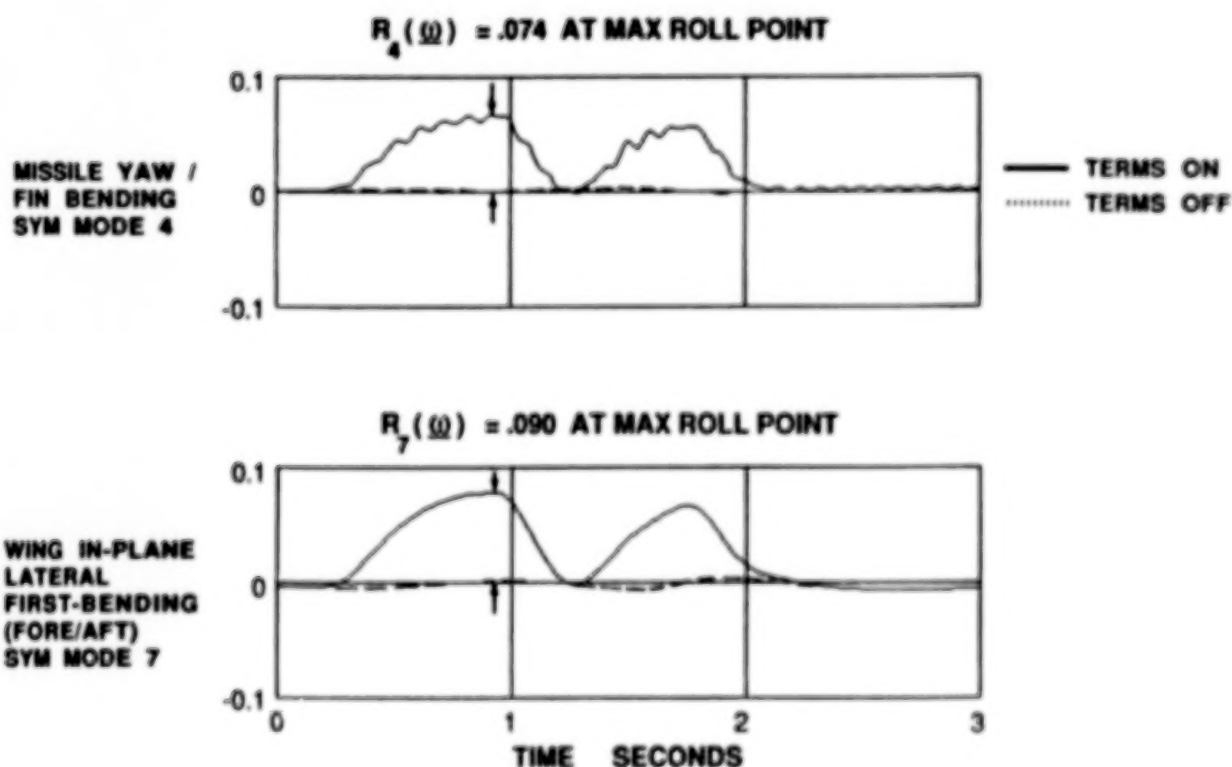
$R_j(\underline{\omega})$		
MODE	SYMMETRIC	ANTISYMMETRIC
1	-.0283	.0008
2	.0048	-.0120
3	.0064	.0004
4	.0739	.0039
5	.0075	-.0001
6	-.0028	-.0090
7	.0899	-.0016
8	-.0115	-.0006
9	-.0043	.0018
10	-.0027	-.0012

$$\underline{\omega} = [4.7, .17, .03]^T \quad (\text{RAD/SEC})$$

Illustration of R Parameter

The amplitudes of the response of symmetric modes 4 and 7 are essentially equal to the values of the R parameter calculated in the previous figure. This parameter, which is a linear approximation to steady-state response, is far from the end of the story. In the case of the FIT simulation model, even though symmetric modes 4 and 7 were excited by inertial effects, these modes are essentially decoupled from the rest of the dynamic model. This occurred because both modes 4 and 7 are dominated by in-plane bending of the wing lifting surface. A doublet-lattice code was used to calculate the generalized aerodynamic forces and in-plane motions produce no change in the normal washes induced at the 3/4 chord points of the aerodynamic boxes. Thus none of the other modes are significantly affected by symmetric modes 4 and 7.

One can imagine other cases where inertially affected modes are more coupled to the rest of the system dynamics. One case is if such a mode contributes to a feedback signal. Another case might occur in an underwing store configuration. As the underwing stores were slung outboard by centrifugal forces, they would induce out-of-plane bending in the wings, the primary lifting surfaces.



Conclusion

An integrated, nonlinear simulation model suitable for aeroelastic modeling of fixed-wing aircraft has been developed. While the author realizes that the subject of modeling rotating, elastic structures is not closed, it is believed that the equations of motion developed and applied herein are correct to second order and are suitable for use with typical aircraft structures. The equations are not suitable for large elastic deformation. In addition, the modeling framework generalizes both the methods and terminology of non-linear rigid-body airplane simulation and traditional linear aeroelastic modeling.

Concerning the importance of angular/elastic inertial coupling in the dynamic analysis of fixed-wing aircraft, the following may be said. The rigorous inclusion of said coupling is not without peril and must be approached with care. In keeping with the same engineering judgment that guided the development of the traditional aeroelastic equations, the effect of non-linear inertial effects for most airplane applications is expected to be small. A parameter has been presented to help in the determination of when such effects are significant. The parameter does not tell the whole story, however, and modes flagged by the parameter as significant also need to be checked to see if the coupling is not a one-way path, i.e. the inertially affected modes can influence other modes. Classically, configurations where nonlinear inertial effects can come into play are characterized by complex geometries such as stores mounted under the wings or the presence of a T-tail.

- **INTEGRATED NONLINEAR MODEL DEVELOPED**
 - CORRECT TO SECOND ORDER
 - SUITABLE FOR AIRPLANE STRUCTURES
 - **GENERALIZES CONVENTIONAL ASE MODELS AND NONLINEAR RIGID-BODY MODELS**
 - **ANGULAR / ELASTIC INERTIAL COUPLING**
 - RIGOROUS INCLUSION PROBLEMATIC
 - EFFECT NORMALLY SMALL FOR AIRPLANES
 - EXCEPTIONS CHARACTERIZED BY
 - $R(\omega)$ PARAMETER IS SIGNIFICANT FOR SOME MODE
- AND**
- AFFECTED MODE IS COUPLED TO THE REST OF THE MODEL.

REFERENCES

1. Hood, R.V.; Dollyhigh, S.M.; and Newsom, J.R.: Impact of Flight Systems Integration on Future Aircraft Design. AIAA Paper 85-1855, August 1985.
2. Buttrill, C.S.; Zeiler, T.A.; and Arbuckle, P.D.: Nonlinear Simulation of a Flexible Aircraft in Maneuvering Flight. AIAA Paper 87-2501-CP. AIAA Flight Simulation Technologies Conference (Monterey, CA), August 1987.
3. Zeiler, T.A.; and Buttrill, C.S.: Dynamic Analysis of an Unrestrained, Rotating Structure Through Nonlinear Simulation. AIAA Paper 88-2232-CP. AIAA/ASME/ASCE/AHS 29th Structures, Structural Dynamics and Materials Conference (Williamsburg, VA), April 1988.
4. Arbuckle, P.D.; Buttrill, C.S.; and Zeiler, T.A.: A New Simulation Model Building Technique For Use In Dynamic Systems Integration Research. AIAA Paper 87-2498-CP. AIAA Flight Simulation Technologies Conference (Monterey, CA), August 1987.
5. Youssef, H.M.; Nayak, A.P.; and Gousman, K.G.: Integrated Total Flexible Body Dynamics of Fixed Wing Aircraft. AIAA Paper 88-2364-CP. AIAA/ASME/ASCE/AHS 29th Structures, Structural Dynamics and Materials Conference (Williamsburg, VA), April 1988.
6. Morino, L.; and Baillieul, J.: A Geometrically-Exact Non-Linear Lagrangian Formulation for the Dynamic Analysis of a Flexible Maneuvering Airplane. Prepared for the USAF Office of Scientific Research, Contract F49620-86-C-0040. Center for Computational and Applied Dynamics, Boston University, CCAD-TR-87-02.
7. Likens, P.W.: Dynamics and Control of Flexible Space Vehicles. NASA Technical Report 32-1329. Jet Propulsion Laboratory, Pasadena, CA. February 15, 1969.
8. Cavin, R.K.; and Dusto, A.R.: Hamilton's Principle: Finite-Element Methods and Flexible Body Dynamics. AIAA Journal, vol. 15, no. 12, December 1977, pp. 1684-1690.
9. Kane, T.R.; Ryan, R.R.; and Bannerjee: Dynamics of a Cantilever Beam Attached to a Moving Base. AIAA Journal of Guidance, Control, and Dynamics, vol. 10, no. 2, Mar-Apr 1987, pp. 139-151.
10. Eke, F.O.; and Laskin, R.A.: On the Inadequacies of Current Multi-Flexible Body Simulation Codes. AIAA Paper 87-2248-CP. AIAA Guidance, Navigation and Control Conference (Monterey, CA), August 1987.
11. Housner, J.M.; McGowan, P.E.; Abrahamson, A.L.; and Powell, M.G.: The LATDYN User's Manual. NASA TM 87635, 1986.
12. Belytschko, T.; and Hsieh, B.J.: Non-Linear Transient Finite Element Analysis With Convected Coordinates. International Journal for Numerical Methods in Engineering, vol. 7, 1973, pp. 255-272.
13. Waszak, M.; and Schmidt, D.K.: Flight Dynamics of Aeroelastic Vehicles. AIAA Journal of Aircraft, vol. 25, no. 6, June 1988, pp 563-571.

FLUTTER SUPPRESSION USING EIGENSPACE FREEDOMS TO MEET REQUIREMENTS

William M. Adams, Jr.
NASA Langley Research Center
Hampton, Virginia

Robert E. Fennell
Clemson University
Clemson, South Carolina

and

David M. Christhilf
Planning Research Corporation
Hampton, Virginia

INTRODUCTION

This paper, although much more tersely written, is similar in content to reference 1; however, additional results are presented herein.

Since the early works (refs. 2 and 3) describing the freedoms in multivariable systems beyond eigenvalue assignment, a number of researchers have expanded and applied the eigenspace design approach (e.g. refs. 1, and 4-9). The contribution of reference 1 and this paper is to provide a systematic procedure for solving for eigenspace variables such that design requirements are met. The design requirements are expressed as inequality constraints which must be satisfied by a constrained optimization procedure.

Results are presented which show an application of the procedure to the design of a control law to suppress symmetric flutter on an aeroelastic vehicle. In this example, the stability of the flutter mode is sensitive to change in dynamic pressure and eigenspace methods are used to enhance the performance properties of a "minimum energy" linear quadratic regulator (LQR) designed controller. Results indicate that the eigenspace methods coupled with order reduction can provide a low-order controller such that the closed-loop system stability is relatively insensitive to changes in dynamic pressure. However, some sacrifice of robustness with respect to error at the input occurred; this design example thus illustrates the necessity for tradeoff of conflicting requirements.

An outline of the material presented in the paper follows.

- **EIGENSPACE FREEDOMS**
- **DESIGN APPROACH**
- **PLANT DESCRIPTION**
- **STATE FEEDBACK**
- **FULL ORDER OBSERVER**
- **REDUCED ORDER CONTROLLER**

EIGENSPACE DESIGN FREEDOMS

Consider a linear time invariant system with m inputs u . For the case of a full-state controller, one can place all controllable poles, λ_i ; all eigenvectors, v_i , can be modified, including those associated with uncontrollable poles (refs. 2, 3, and 7). Each closed-loop eigenvector, v_i , must, however, lie in the subspace, W_i , that is spanned by

$$(\lambda_i I - A)^{-1} B$$

It has been assumed here that the eigenvalues are all distinct. The basis for W_i is computed using singular value decomposition techniques (refs. 10 and 11). Thus, as shown below, a designer is free to choose m variables c_i for each real eigenvalue ($2m$ variables for each complex conjugate pair of eigenvalues). When the constraint that $v_i^* v_i = 1$ is imposed, the number of free variables becomes $m-1$ for real eigenvalues ($2(m-1)$ for each complex conjugate pair of eigenvalues). Here v_i^* is the conjugate transpose of v_i .

SYSTEM

$$dx/dt = Ax + Bu$$

u is m by 1

STATE FEEDBACK

$$u = -Kx$$

FREEDOMS

$$\lambda_i$$

PLACE ALL CONTROLLABLE POLES

$$v_i$$

MODIFY ALL EIGENVECTORS

$$v_i = W_i c_i$$

c_i IS $m \times 1$ AND W_i IS BASIS FOR
 $(\lambda_i I - A)^{-1} B$

DESIGN APPROACH

Given a linear model, the design process for development of a control law to suppress symmetric flutter begins with the assumption of the availability of full-state feedback. A minimum energy stabilizing feedback design is obtained using linear quadratic regulator (LQR) theory (ref. 12). The minimum energy stabilizing solution is the solution which occurs when the performance of the controller is measured solely by the control deflection requirements (i.e., the state weighting matrix is zero)(ref 12).

The second step is to utilize a subset of the eigenvector freedoms to modify the full-state feedback design to minimize the sensitivity of the critical closed-loop pole to variation in a system parameter. This minimization is performed subject to design constraints.

The third step is to relax the full-state feedback assumption and develop a full-order observer which approximately recovers the robustness characteristics of the reduced sensitivity full-state feedback design (ref. 13). Eigenspace techniques are employed in developing the observer (refs. 6 and 7).

The eigenspace approach to observer design (refs. 6 and 7) is an alternate approach to that of reference 13. The two are equivalent in the limit in that each recovers the full-state robustness characteristics for plants with no right half plane transmission zeros. The eigenspace approach is more flexible in the sense that one can individually approach the limit for selected observer poles as opposed to the simultaneous approach of reference 13.

The final step is to reduce the full-order controller to an order that is low enough to be implementable.

- **LQR DESIGN (MINIMUM ENERGY STABILIZING FEEDBACK)**

- **EIGENVECTOR MODIFICATION FOR REDUCED SENSITIVITY (FULL-STATE FEEDBACK)**

- **OBSERVER DESIGN FOR LOOP TRANSFER RECOVERY (FULL-ORDER OBSERVER)**

- **CONTROLLER ORDER REDUCTION**

EIGENSPACE TECHNIQUES TO MEET REQUIREMENTS

The method is to choose a subset of the closed-loop eigenvectors to be modified and then to determine values for each selected vector c_j such that a function of these variables is minimized. In this study the magnitude of the sensitivity of the flutter mode eigenvalue to variations in dynamic pressure is minimized subject to n_g constraints. In the equations below g_{uj} and g_{lj} are upper and lower bounds, respectively, on the j th constrained

variable g_j (e.g. control saturation). The scalar variable, $\bar{g}_j \geq 0$, is the violation of the j th constraint. The vector u_i is a left eigenvector of the system matrix A .

The constrained optimization process appends a weighted square of each constraint violation, \bar{g}_j , to the function to be minimized (P is a positive definite diagonal weighting matrix). In the limit as each weight P_{jj} approaches infinity, $|S|^2$ is minimized subject to the constraints provided that the number of constraints on a constraint boundary in this limit is less than the number of design variables (ref. 14). A nongradient optimizer was employed in this study (ref. 15).

The constraints to be employed in this study are on root mean square (rms) values for control deflections, control rates, and incremental wing root bending moment, shear, and torque due to random gust inputs. In addition a constraint was imposed upon robustness of the control law with respect to error at the plant input.

— PARAMETERIZATION OF ATTAINABLE EIGENVECTORS

$$v_j = W_j c_j, j = 1, n$$

— SENSITIVITY

$$S = d\lambda_i / dq = \frac{u_i^* (dA/dq) v_i}{u_i^* v_i}$$

— CONSTRAINTS

$$\bar{g}_j = \max(0, g_j - g_{uj}, g_{lj} - g_j), j = 1, n_g$$

— AUGMENTED PERFORMANCE INDEX

$$J_P = |S|^2 + \bar{g}^T P \bar{g}$$

— NONGRADIENT OPTIMIZATION

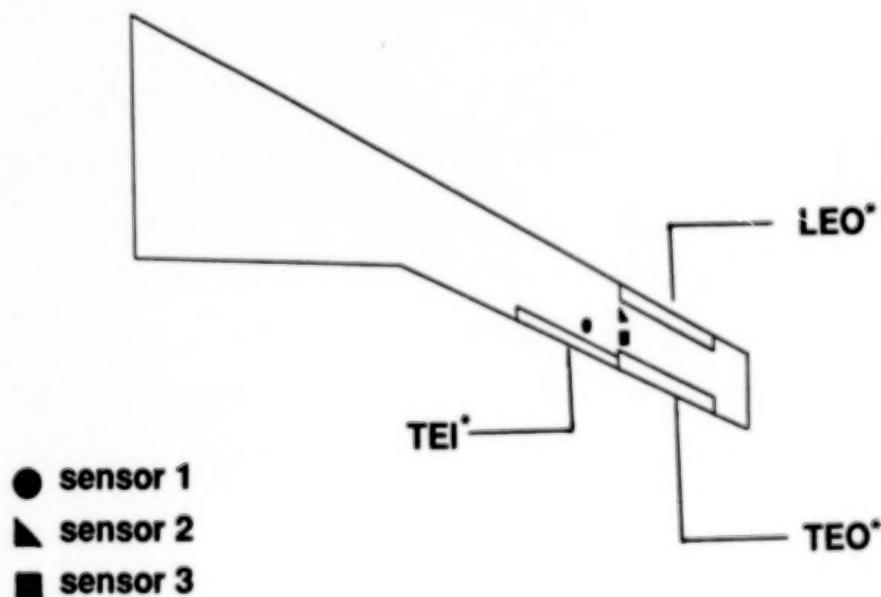
CONTROL SURFACE AND SENSOR LOCATIONS (Symmetric Full Span)

The mathematical model is based upon one that represents an actual aeroelastic drone vehicle (ref. 16). The actual vehicle has only one effective control surface for flutter suppression (the trailing-edge outboard surface shown in the planform view). For this study fictitious leading-edge and inboard trailing-edge controls have been added per semispan to provide three effective symmetric and antisymmetric flutter suppression surfaces. The surfaces are driven by high bandwidth actuators each having transfer functions

$$\delta_1 = \frac{180 (314)^2}{(s + 180) (s^2 + 251s + (314)^2)} \delta_{c1}$$

where δ_{c1} is commanded deflection and δ_1 is actual. The poles for each actuator are separated slightly in the mathematical representation to improve numerical conditioning.

Three vertical accelerometers are located as indicated. These high bandwidth devices have virtually no dynamics in the frequency range of interest and are, therefore, modeled as unity gains. The sensor locations correspond to three of the four sensors on the actual wing. The locations were chosen early in the wing design cycle as desirable for flutter suppression sensors based upon analytical studies (ref. 17).



*Trailing-edge inboard (TEI); leading-edge inboard (LEI); trailing-edge outboard (TEO).

DESIGN MODEL (Symmetric Modes)

The aircraft is designed to be symmetric about a plane perpendicular to the wings and to intersect them at the centerline. Consequently, to a good approximation for small perturbations from rectilinear flight, the symmetric and antisymmetric degrees of freedom are uncoupled. Thus, symmetric and antisymmetric designs can be obtained separately. This study considers symmetric modes only.

The underlying symmetric evaluation model contains 2 rigid body and 11 elastic modes. A lower-order linear time invariant state space design model was extracted from the evaluation model. The design model was chosen by a trial and error truncation of modes. The effect of a candidate truncation upon frequency responses of interest and upon the loci of eigenvalues with dynamic pressure was observed. Modes having little impact were deleted. The modes deleted included the rigid-body modes, predominantly fuselage and tail modes and higher-order wing modes. If they are troublesome, rigid-body contributions to the actual sensor (accelerometer) outputs can be removed either by employing a high pass filter or by making use of measured linear and angular accelerations at the center of mass.

The resulting design model is twenty-sixth order. The uncontrollable gust states correspond to a Dryden filter representation with a gust scale length of 2500 ft. The rational function approximation (ref. 18) made to the unsteady aerodynamic forces included one lag term having a reduced frequency of 0.13. The B matrix is independent of the dynamic pressure, q . The u vector contains the three commanded control deflections and a white noise input into the Dryden filter.

$$\frac{dx}{dt} = A(q)x + Bu$$

$$y = C(q)x$$

5 MODES (SECOND ORDER)	10
1 AERO LAG PER MODE	5
3 THIRD-ORDER ACTUATORS	9
2ND ORDER GUST	2

26 STATES

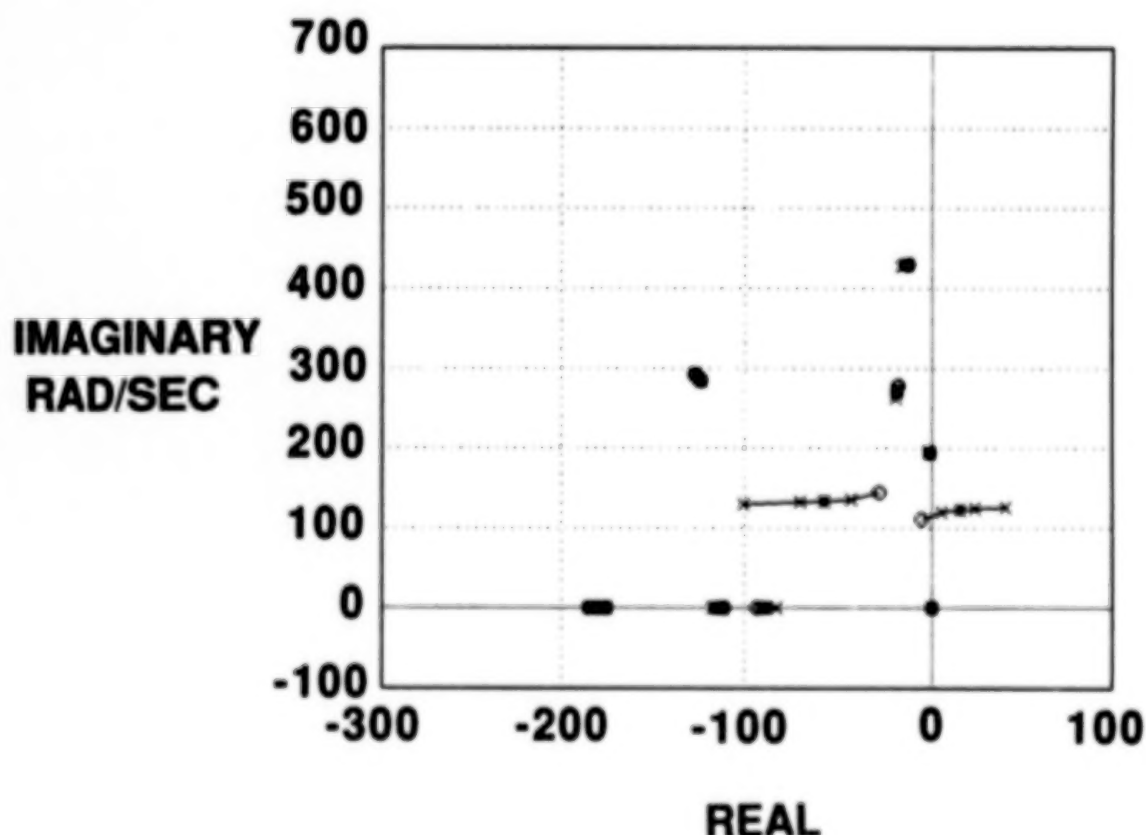
DYNAMIC PRESSURE ROOT LOCUS
(Uncontrolled Plant)

A variation of the uncontrolled design model roots with dynamic pressure is shown. The variation corresponds to an altitude variation at a fixed Mach number of 0.775. With no feedback, the actuator poles are stationary near $(-180, 0)$ and $(-120, \pm 280)$.

The circle symbol corresponds to the lowest dynamic pressure. The highest dynamic pressure point corresponds to a dynamic pressure 44 percent above that at flutter. The 44 percent increase in flutter dynamic pressure corresponds to what would be required if active controls were to provide the full 20 percent margin above the design dive speed for a transport aircraft.

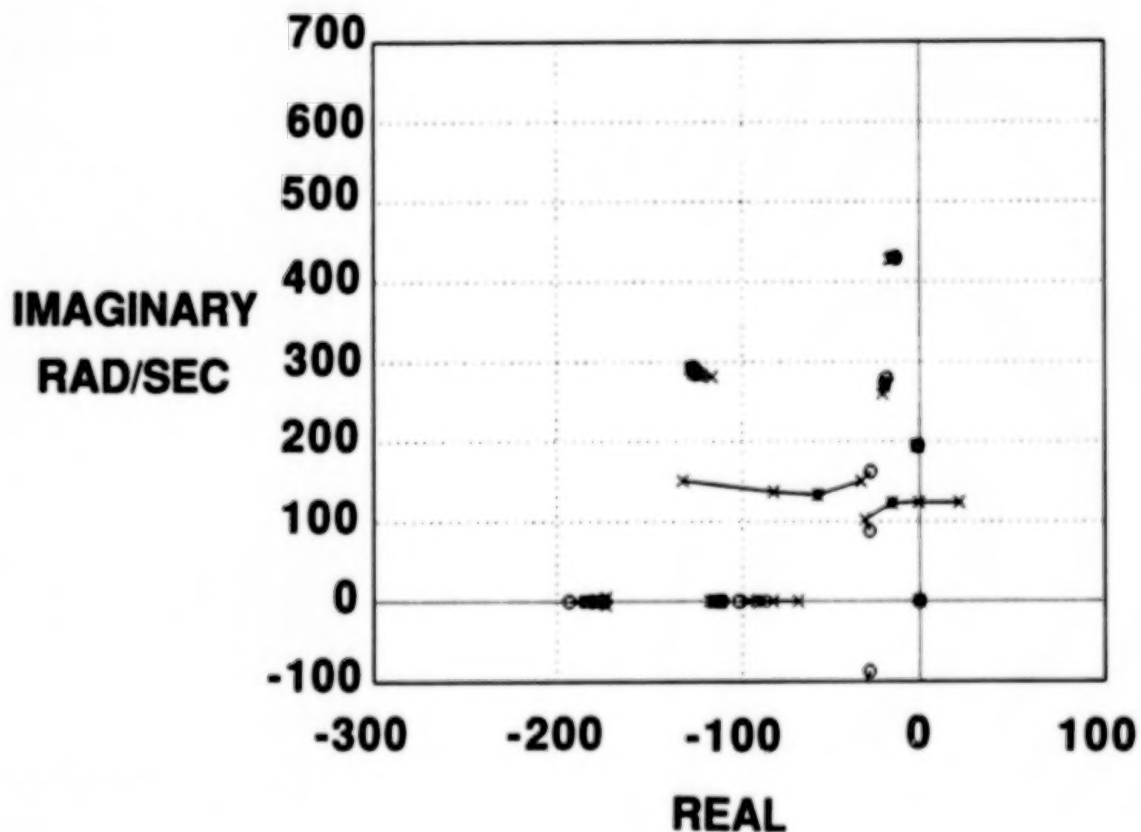
The flutter is explosive (i.e., the time to double amplitude decreases rapidly with increasing dynamic pressure). The interacting modes exhibit classical frequency coalescence. The zero dynamic pressure characteristics of the retained elastic modes in ascending frequency order are 1) wing bending, 2) second wing bending with some torsion, 3) wing fore and aft bending with a torsional normal component, 4) wing torsion, and 5) a higher order wing mode exhibiting bending and torsion.

The * on the figure depicts the point for which the controller was designed. This design point is approximately 11.5 percent above the uncontrolled flutter dynamic pressure.



DYNAMIC PRESSURE ROOT LOCUS
(Min Energy LQR Controller)

The locus of closed-loop roots with dynamic pressure for the minimum energy Linear Quadratic Regulator (LQR) full-state feedback controller shows that the closed-loop system remains stable only up to a point 20 percent above that of open-loop flutter (7.7 percent above the design point). One could maximize robustness with respect to error at the input by repeating the LQR design at each dynamic pressure and scheduling the controller as a function of dynamic pressure; however, it is of interest here to see what tradeoffs are required to minimize the effect of dynamic pressure on the closed-loop stability characteristics.



DESIGN CONSTRAINTS

The constraints to be imposed on the reduced sensitivity full-state feedback design will now be enumerated. The first two sets of constraints were that the rms control deflections and rates not exceed 5 deg and 372 deg/sec, respectively, when the system was forced by a vertical gust field having a 12 ft/sec rms gust velocity. The physical control limits were ± 15 deg and ± 740 deg/sec. Bending moment, shear, and torque rms incremental loads at the wing root were also constrained to remain near their values at a stable point (lowest dynamic pressure point on the previous root locus). Finally, the minimum singular value of the return difference matrix was constrained to be

$$\sigma_{\min} = \min_{\omega} \sigma(I + K(j\omega)G(j\omega)) > 0.6$$

where $G(s)$ is the plant transfer matrix and $K(s)$ is the controller transfer matrix. This singular value is a measure of robustness due to multiplicative error at the input. Error occurrences at other points are important but are not addressed herein. The choice of $\sigma_{\min} > 0.6$ allows an appreciable tradeoff to occur between σ_{\min} and the sensitivity reduction objective. It is also representative of robustness levels that have been achieved in implementable designs (e.g. ref. 19).

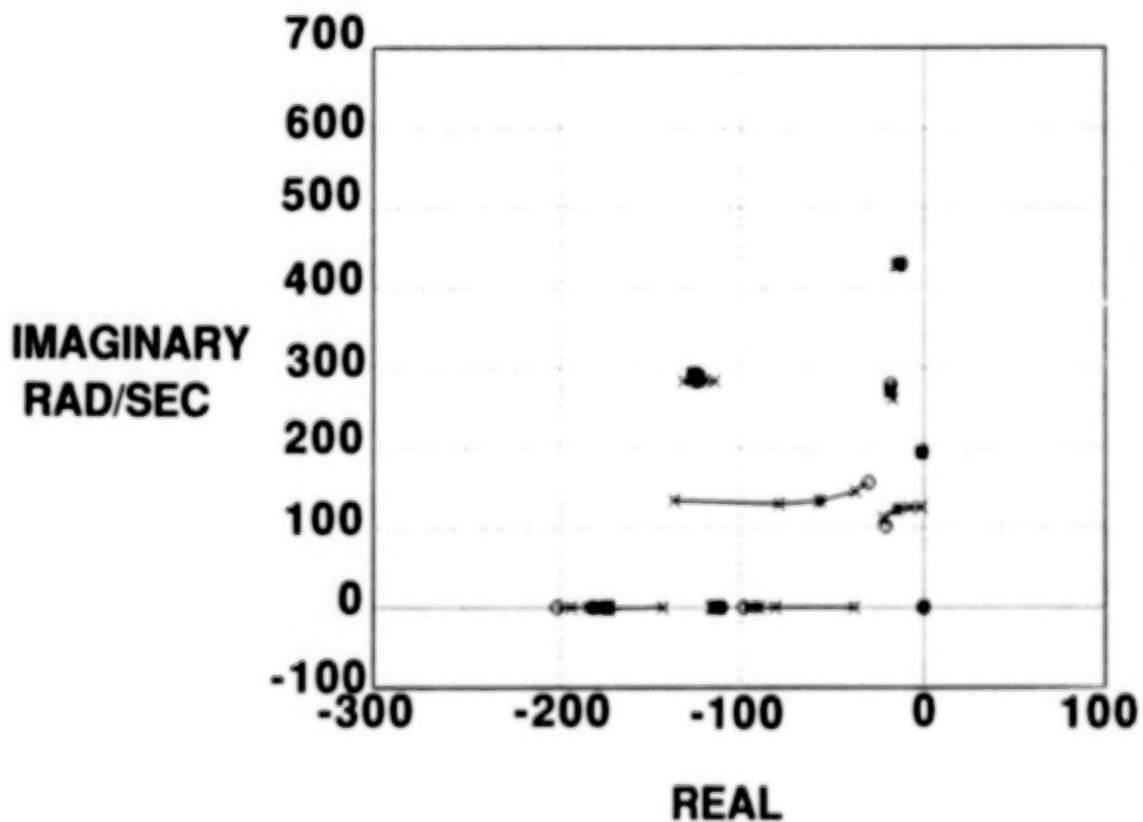
A value for $\sigma(j\omega)$, the minimum singular value at the frequency ω , near zero means that the nominal closed-loop system is near instability at that frequency. Thus, even a small difference between the true plant and its nominal representation can cause instability. For the minimum energy linear quadratic regulator (LQR) full-state feedback design of this paper $\sigma(j\omega) = \bar{\sigma}(j\omega) = \sigma_{\min} = 1$ at all frequencies. (Here $\bar{\sigma}(j\omega)$ is the maximum singular value at the frequency ω .) This fact can be seen by examining the development of the Kalman inequality (e.g. ref. 20, p. 7-3). When the state weightings are null (minimum energy controller) and the control weightings are unity, the equality holds.

	RMS CONTROL DEFLECTION DEGREES	RMS CONTROL RATE DEGREES/SEC	RMS BENDING MOMENT In-lb	RMS SHEAR lb	RMS TORQUE In-lb	MINIMUM SING. VALUE
UPPER BOUND	5	372	30,000	1,000	2,000	1.
LOWER BOUND	0	0	0	0	0	.6

RMS GUST VELOCITY 12 FT/SEC

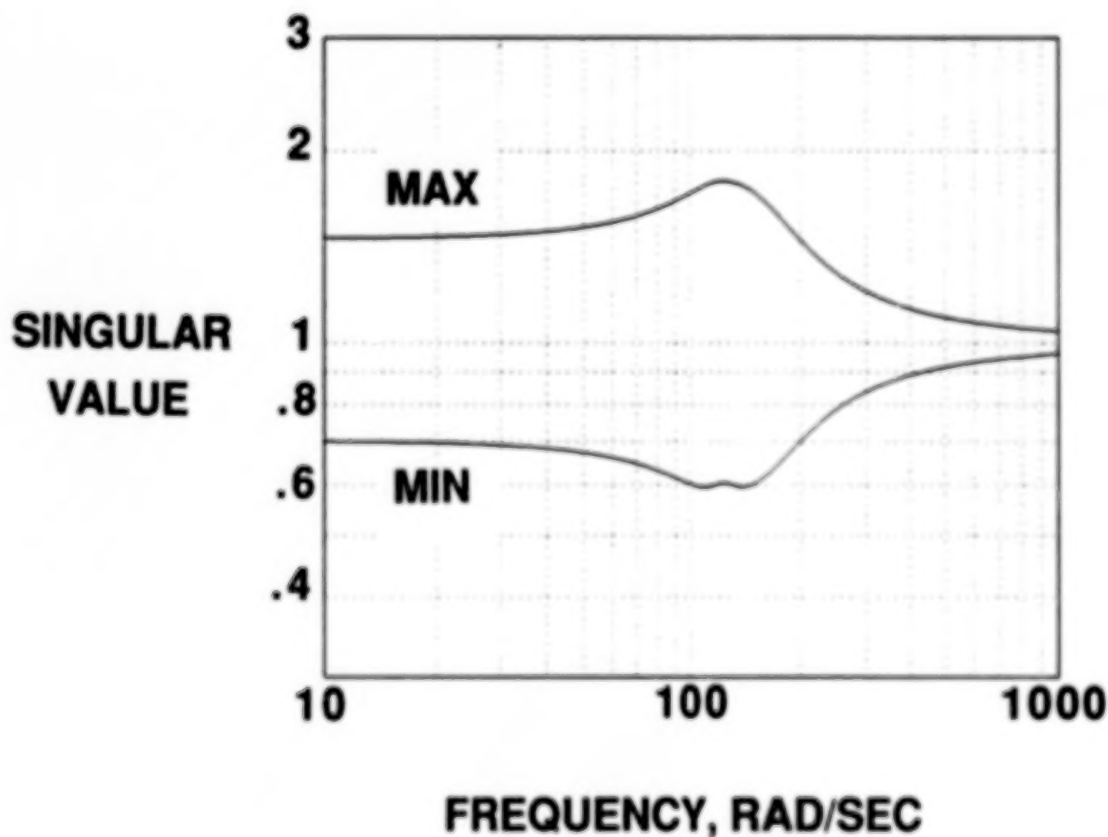
(Reduced-Sensitivity Full-State Feedback)

A full-state feedback design was obtained for which the critical eigenvalue had reduced sensitivity to dynamic pressure variation. This design satisfied the constraints at the design point. The design was achieved by utilizing the eigenvector freedoms associated with the two coalescent modes. Thus, there were 12 free variables (eight after mode normalization constraints). The resulting control law stabilizes the system over the full range of dynamic pressures.



SINGULAR VALUES OF $(I + K(s)G(s))$
(Reduced-Sensitivity Full-State Feedback)

The locus of maximum and minimum singular values of the return difference for the reduced sensitivity state feedback controller shows the constraint of 0.6 was met as prescribed. The figure illustrates the tradeoff that has occurred. (for comparison, as discussed earlier, the minimum energy LQR controller with unity control weightings has a minimum (and maximum) singular value of one at all frequencies). Further analysis is required to assess how conservative the unstructured singular values are; nevertheless, a minimum value of 0.6 indicates a substantial capability for rejection of input disturbances.



OBSERVER DESIGN

Eigenspace techniques were also employed to obtain a full-order observer. The approach was to place observer poles near the finite plant transmission zeros and the corresponding observer eigenvectors at plant left zero directions (refs. 6 and 7). Poles in excess of the transmission zeros were placed far into the left half plane with arbitrary eigenvectors. The observer poles corresponding to the six transmission zeros at zero (from the three sensors being accelerometers) were displaced an arbitrary five units into the left half plane to avoid problems associated with implementation of pure integrators. In the equations H is the observer gain matrix. K_m is the reduced-sensitivity full-state feedback gain matrix and the subscript "o" emphasizes that the controller is developed for the design point but then evaluated at off-design points.

SYSTEM MODEL

$$\dot{x} = Ax + Bu$$

$$y = Cx$$

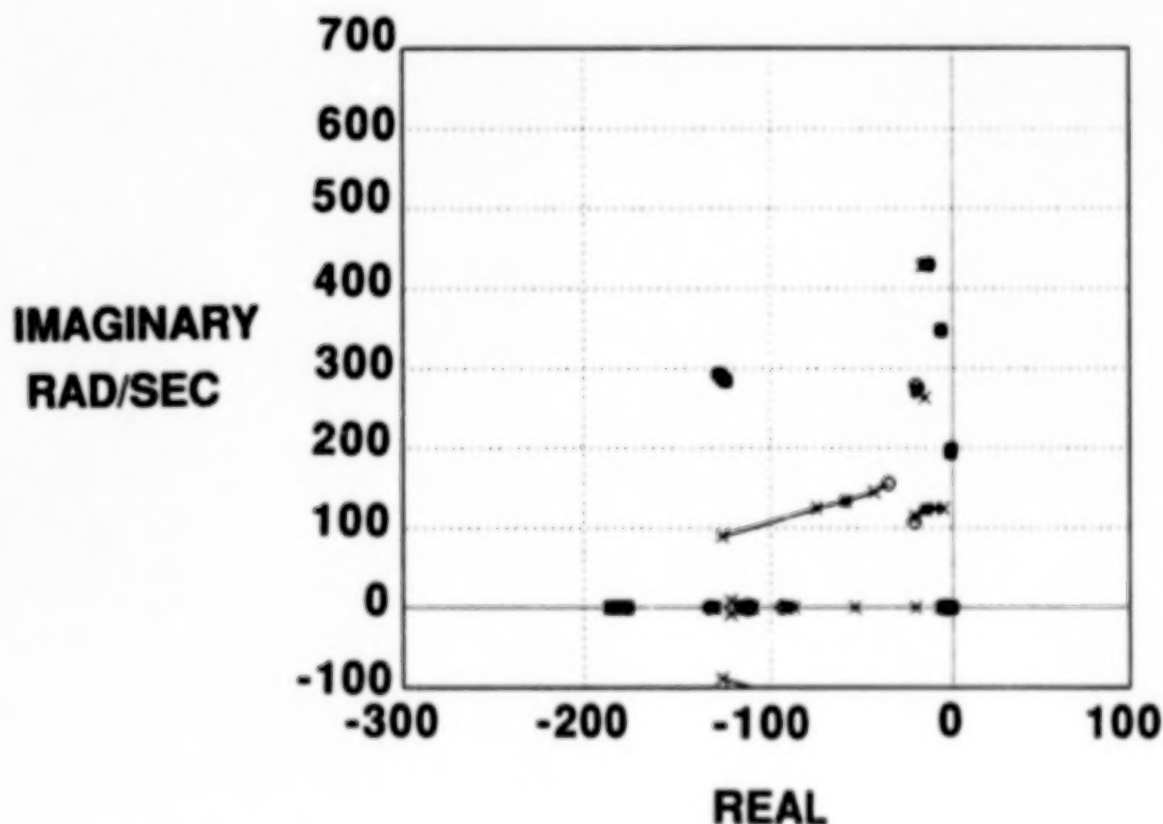
CONTROLLER

$$\dot{z} = Hy + (A_o - B_o K_M - H C_o) z$$

$$u = -K_M z$$

DYNAMIC PRESSURE ROOT LOCUS
(Reduced-Sensitivity Feedback Plus Full-Order Observer)

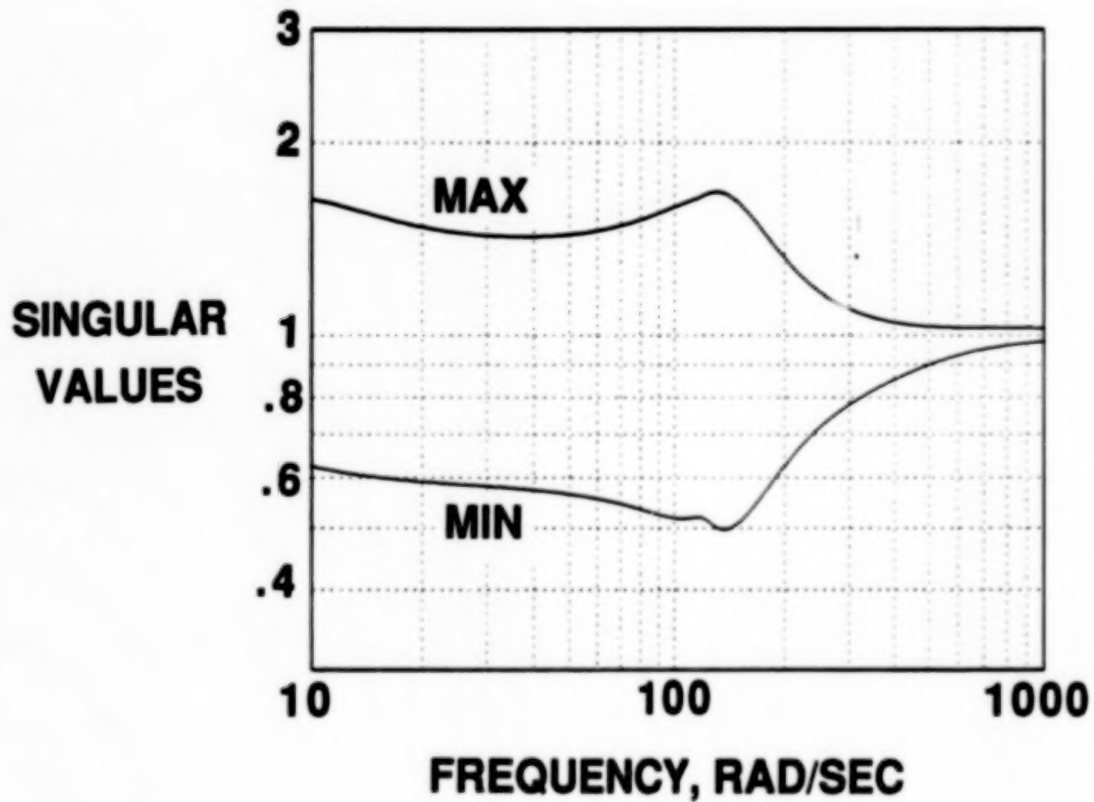
The locus of poles with dynamic pressure for reduced-sensitivity full-state feedback plus a full-order observer to estimate the states given only three accelerometer outputs shows that stability was also achieved for this case over the full dynamic pressure range. One can see by comparing this figure with the corresponding one for reduced-sensitivity full-state feedback that controller poles are located near $(-5, 0)$ rad/sec, $(-150, 0)$ rad/sec, a lightly damped complex conjugate pair near a frequency of 200 rad/sec and a complex conjugate pair near a frequency of 340 rad/sec. If the true plant pole/zero pair near 200 rad/sec is different than that of the design model, the closed-loop performance in this frequency region may be substantially degraded. Further discussion of this point is given below in the section describing the reduced-order controller performance with respect to the evaluation model of the plant. Other poles not shown here are further in the left half plane than the limits of the figure. A compilation of the full set of observer poles at the design point and a locus of all closed-loop poles with dynamic pressure are given in reference 1.



C14

SINGULAR VALUES OF $(I + K(s)G(s))$
(Reduced-Sensitivity Feedback Plus Full-Order Observer)

A small degradation in minimum singular value resulted from adding the observer to estimate the states. The minimum singular value in this case is about 0.5 as compared with 0.6 in the reduced-sensitivity full-state feedback case.



CONTROLLER ORDER REDUCTION

The full-order controller was then reduced from 26th order down to eighth order. The process employed in the reduction was to determine which controller states had little impact upon controller performance. The controller was transformed to modal form, modes were truncated based upon small residues and/or large separation from the flutter frequency, and the resulting closed-loop root locus and minimum singular value of the return difference matrix were examined; this allowed determination of the highest frequency controller mode that should be retained. Relatively unimportant modes having eigenvalues with amplitudes greater than the highest frequency mode to be retained were temporarily included in the controller representation. The input and output controller matrices were balanced and a second modal decomposition was performed. The temporarily included modes were then removed by residualization. For this case nine states were removed by truncation and nine states were removed by residualization.

The resulting eighth-order controller has six poles clustered near $(-5, 0)$ rad/sec and one complex conjugate pair near a frequency of 200 rad/sec.

TRUNCATION

MODAL DECOMPOSITION

TRUNCATE MODES WITH SMALL EFFECT ON CONTROL

RESIDUALIZATION

BALANCED REALIZATION

RESIDUALIZED FAST MODES

REDUCED ORDER CONTROLLER

EIGHTH ORDER

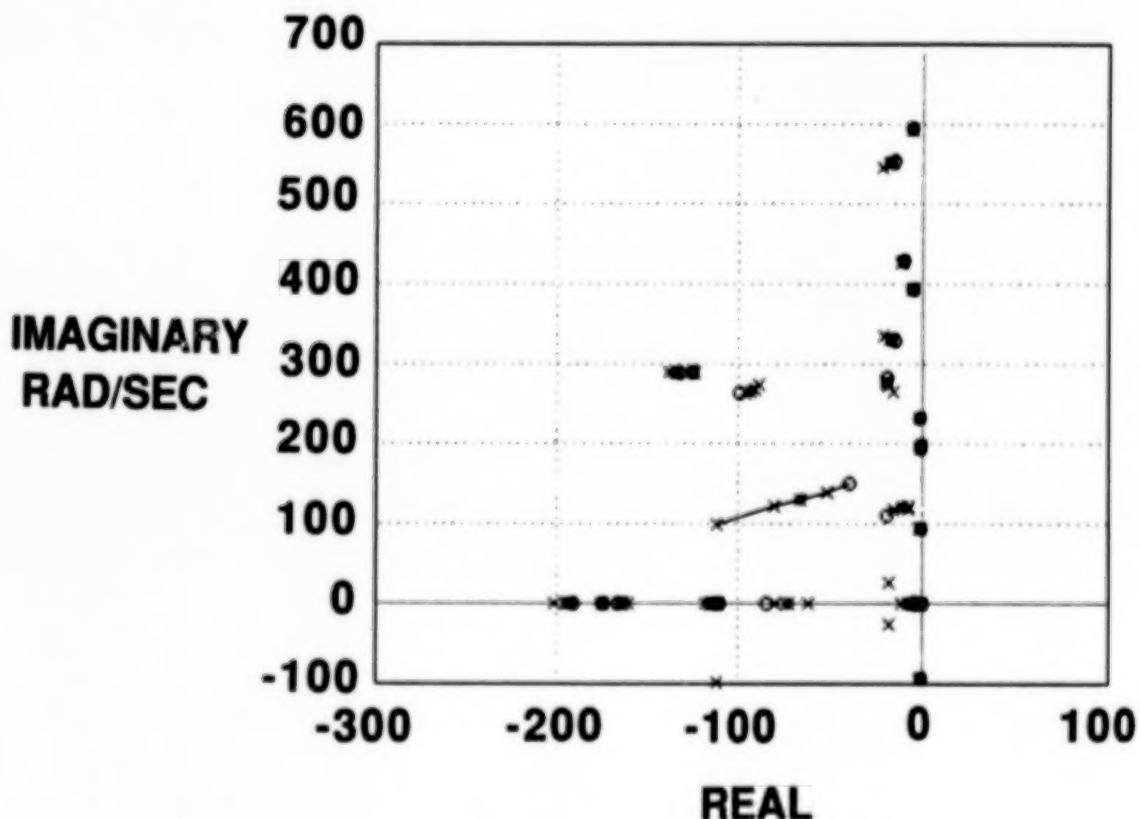
645

DYNAMIC PRESSURE ROOT LOCUS
(Evaluation Plant with Reduced Order Controller)

This figure shows that stability is achieved over the full dynamic pressure range with an eighth-order controller. In fact, the sensitivity of the critical closed-loop pole to dynamic pressure is lower for this controller and the evaluation model of the plant than was found for the design model with reduced sensitivity full-state feedback. The retained controller poles were the six poles near $(-5, 0)$ rad/sec, and a very lightly damped complex conjugate pair of poles at a frequency near 200 rad/sec.

The latter controller poles which have associated zeros near but to the left of them in the left half plane are troublesome since they and the corresponding plant poles are severely underdamped. From a stability standpoint these controller poles can be removed for the nominal system; however, the singular value measure of robustness is then degraded substantially at this frequency. For this particular vehicle, one can argue for two reasons that the problem is not real but arises only due to a plant modeling deficiency.

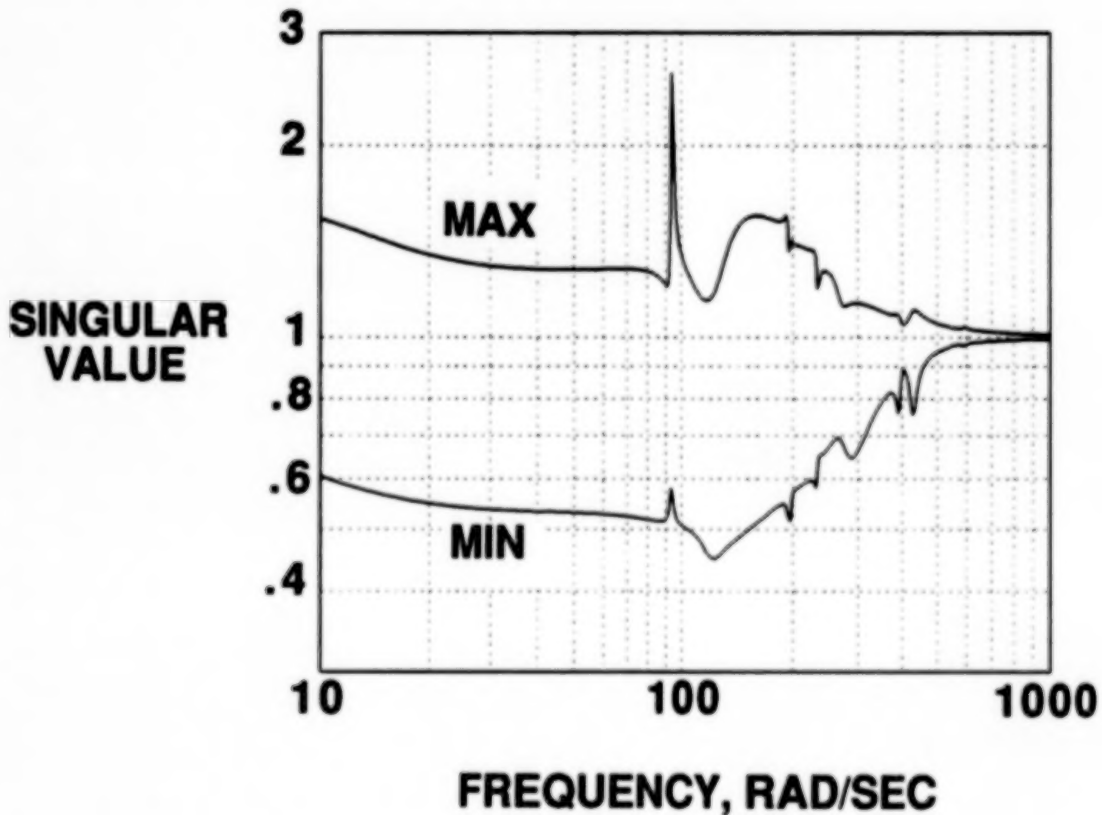
The first reason is that the vehicle has been wind tunnel tested with no problems occurring in this frequency range. The second reason is that the plant mode at this frequency is predominantly fore and aft bending with a small amplitude torsional component. The doublet lattice aerodynamic computation produces no aerodynamic damping due to the fore and aft motion. Thus, the mode should probably be further in the left half plane than is the case for the mathematical model. In general, however, one would prefer to gain stabilize or perhaps notch out a high-frequency underdamped pole that remains essentially stationary.



00 317

SINGULAR VALUES OF $(I + K(s)G(s))$
(Evaluation Plant Model with Reduced Order Controller)

The minimum singular value of the return difference matrix for the eighth-order controller and the evaluation model of the plant is about 0.44 as compared with 0.5 for the full-order controller and the design model. This is a guaranteed margin and may be quite conservative. The spike seen at a frequency of 92 rad/sec is due to a mode in the evaluation model that was not accounted for in the design. The mode is a predominantly fuselage mode that remains unchanged in frequency over the dynamic pressure range. It could be dealt with effectively with a notch filter.



010

RMS PERFORMANCE
(LQR and RSFSF)

All of these results are for a Dryden gust spectrum with rms gust input of 12 ft/sec. The rms control power performances for LQR at the design point are on the order of 10 to 25 percent of the constraint.

For the reduced-sensitivity full-state feedback (RSFSF) design, i.e., the eigenspace reduced sensitivity design, the rms control effort at the design point varies from approximately 100 to 225 percent larger than for LQR for each of the outboard surfaces. Lower usage is made of the smaller, less effective, inboard trailing-edge control surface. An increase in rms output with increasing dynamic pressure is evident; the sharper increase between the last two points is due to the larger dynamic pressure difference here than for other pairs of points and, more importantly, to the low damping in the critical pole at the highest dynamic pressure condition. Small constraint violations occur at the highest dynamic pressure.

			Dynamic Pressure, lb/in ²					design point
RMS			4.417	4.768	5.141	5.537	6.639	
LQR	δ , deg	TEO	.480	.475	.571	2.07	---	
		TEI	.542	.460	.494	1.62		
		LEO	.899	.768	.831	2.74		
	$\dot{\delta}$, deg/sec	TEO	49.9	56.6	71.3	248.3		
		TEI	41.5	46.5	57.8	199	---	
		LEO	70.1	78.5	97.7	336		
	M, in-lb	Moment	24,337	25,727	27,146	29,969		
	S, lb	Shear	455.5	479.8	505.1	582.4	---	
	T, in-lb	Torque	464.8	576	823.4	3,470.8		
RSFSF	δ , deg	TEO	1.45	1.20	1.11	1.47	6.11	
		TEI	.220	.205	.215	.261	.689	
		LEO	1.98	1.60	1.42	1.72	6.28	
	$\dot{\delta}$, deg/sec	TEO	158.5	164.1	174.5	196.6	438.8	
		TEI	22.7	24.5	27.4	32.5	72.3	
		LEO	163.5	165.5	171.2	186.9	400.5	
	M, in-lb	Moment	24,158	25,479	27,042	29,010	39,587	
	S, lb	Shear	440.2	468.3	501.1	541.6	748.3	
	T, in-lb	Torque	352.5	414.9	542.7	779.0	2,647	

CONSTRAINTS: $\delta_{rms} < 5$ deg, $\dot{\delta}_{rms} < 372$ deg/sec

$M_{rms} < 30K$ in-lb

$S_{rms} < 1000$ lb, $T_{rms} < 2000$ in-lb

RMS PERFORMANCE (FOC and FOM/ROC)

For the full-order controller (FOC) the utilization of the TEI control is further reduced as compared to the RSFSF results on the previous page. The TEO rms deflection is approximately quadrupled as compared with RSFSF except at the highest dynamic pressure; the LEO control deflection is also increased except at the highest dynamic pressure where it is reduced by over 30 percent. The rms rates are somewhat reduced as compared to RSFSF for the LEO surface. Wing root torque is higher at lower dynamic pressure and lower at the highest dynamic pressure as compared to the RSFSF results. No constraint violation occurs for control rate but the TEO deflection constraint is violated at the two higher dynamic pressures.

More violations occur when the eighth-order controller is coupled with the evaluation model of the plant (FOM/ROC). Little of the increased activity is due to controller reduction; this was found by comparing the design model full-order controller results (FOC) with the design model reduced order control results (not shown here). The increased activity of the FOM/ROC as compared with the FOC is primarily a result of contributions to the output from the modes in the evaluation model that were absent in the design model. For the FOM/ROC case, rate violation occurs only for the TEO control at the highest dynamic pressure. The rms deflection violations are small except for TEO at the highest dynamic pressure.

Load rms violations are also small except at the highest dynamic pressure. The loads computations are only approximate for the FOM case because modal load coefficients were only available for the five modes retained in the design model.

			Dynamic Pressure, lb/in ²				
			4.417	4.768	5.141	5.537	5.939
LOC	RMS						
	δ , deg	TEO	4.04	4.38	4.78	5.29	7.41
		TEI	.141	.156	.176	.202	.269
		LEO	2.37	2.54	2.75	3.01	4.07
	$\dot{\delta}$, deg/sec	TEO	144.5	160.1	181.2	208.4	302.8
		TEI	17.1	18.9	21.2	24.1	28.9
		LEO	96.0	104.9	116.7	132.7	286.5
	M, in-lb	Moment	25,129	26,259	27,475	28,648	32,277
	S, lb	Shear	465	488.7	513.6	540.1	619.5
	T, in-lb	Torque	827.3	970.9	1,150	1,375	2,300
FOM/ROC	δ , deg	TEO	4.72	5.21	5.84	6.66	11.05
		TEI	.162	.183	.210	.243	.343
		LEO	2.66	2.91	3.21	3.62	5.74
	$\dot{\delta}$, deg/sec	TEO	181.3	203	231.9	270.3	416.1
		TEI	19.8	22	24.6	27.44	28.35
		LEO	106.4	118	133.8	154.8	225.29
	M, in-lb	Moment	27,363	28,774	30,277	31,924	38,013
	S, lb	Shear	503.8	533	564.4	599.2	728.9
	T, in-lb	Torque	962	1,155	1,398	1,718.9	3,423.3

CONSTRAINTS: $\delta_{rms} < 5$ deg, $\dot{\delta}_{rms} < 372$ deg/sec

$M_{rms} < 30K$ in-lb

$S_{rms} < 1000$ lb, $T_{rms} < 2000$ in-lb

SUMMARY

A constrained optimization methodology has been developed which allows specific use of eigensystem freedoms to meet design requirements. A subset of the available eigenvector freedoms was employed. The eigenvector freedoms associated with a particular closed-loop eigenvalue are coefficients of basis vectors which span the subspace in which that closed-loop vector must lie. Design requirements are included as a vector of inequality constraints.

The procedure was successfully applied to develop an unscheduled controller which stabilizes symmetric flutter of an aeroelastic vehicle to a dynamic pressure 44 percent above the open-loop flutter point. Eigenvector freedoms, for fixed eigenvalue locations, of the two coalescent modes were employed to minimize the sensitivity of the critical closed-loop eigenvalue to dynamic pressure variation subject to control power, loads, and robustness constraints. The reduced sensitivity was achieved at the expense of reduced robustness to errors at the input.

The design process proceeded from full-state feedback to the inclusion of a full-order observer to the selection of an eighth-order controller which preserved the full-state sensitivity characteristics.

Only a subset of the design freedoms was utilized (i.e., assuming full-state feedback only four out of 26 eigenvectors were used, and no variations were made in the closed-loop eigenvalues). Utilization of additional eigensystem freedoms could further improve the controller.

- **CONSTRAINED OPTIMIZATION METHODOLOGY DEVELOPED TO USE EIGENSYSTEM FREEDOMS TO MEET REQUIREMENTS**
- **SUCCESSFULLY USED EIGENVECTOR FREEDOMS TO LOWER SENSITIVITY TO DYNAMIC PRESSURE VARIATION**
- **REDUCED SENSITIVITY TO DYNAMIC PRESSURE ACHIEVED AT EXPENSE OF ROBUSTNESS AS MEASURED BY MINIMUM SINGULAR VALUE OF RETURN DIFFERENCE MATRIX**
- **EIGHTH ORDER CONTROLLER FOUND WHICH PRESERVED REDUCED SENSITIVITY CHARACTERISTICS**
- **UNUSED EIGENSPACE FREEDOMS COULD FURTHER IMPROVE CONTROLLER**

REFERENCES

1. Fennell, Robert E.; Adams, William M., Jr.; and Christhilf, David M.: An Application of Eigenspace Methods to Symmetric Flutter Suppression. AIAA Paper No. 88-4099-CP.
2. Moore, B. C.: On the Flexibility Offered by State Feedback in Multivariable Systems Beyond Closed-Loop Eigenvalue Assignment. IEEE Trans. Automatic Control, vol. AC-21, 1976, pp. 689-692.
3. Srinathkumar, S.: Eigenvalue/Eigenvector Assignment Using Output Feedback. IEEE Trans. Automatic Control, vol. AC-23, 1978, pp. 79-81.
4. Andry, A. N.; Shapiro, E. Y.; and Chung, J. C.: Eigenstructure Assignment for Linear Systems. IEEE Trans. Aerospace and Electronic Systems, vol. AES-19, 1983, pp. 711-729.
5. Kautsky, J.; Nichols, N. K.; and Van Dooren, P.: Robust Pole Assignment in Linear State Feedback. Int. Journal of Control, vol. 5, 1985, pp. 1129-1155.
6. Kazerooni, H.; and Houpt, P. K.: On the Loop Transfer Recovery. Int. Journal of Control, vol. 43, 1986, pp. 981-996.
7. Garrard, W. L.; Liebst, B. S.; and Farm, J. A.: Eigenspace Techniques for Active Flutter Suppression. NASA CR-4071, 1987.
8. Sobel, K. M.; and Shapiro, E. Y.: Application of Eigenstructure Assignment to Flight Control Design: Some Extensions. Journal of Guidance, Control, and Dynamics, vol. 10, 1987, pp. 73-81.
9. Klema, V.; and Laub, A. J.: The Singular Value Decomposition: Its Computation and Some Applications. IEEE Trans. Automatic Control, vol. AC-25, 1980, pp. 164-176.
10. Porter, B.; and D'Azzo, J. J.: Algorithm for Closed-Loop Eigenstructure Assignment by State Feedback in Multivariable Linear Systems. Int. Journal of Control, vol. 27, 1978, pp. 943-947.
11. Golub, G. H.; and Van Loan, C. F.: Matrix Computations. The Johns Hopkins University Press, Baltimore, Maryland, 1983.
12. Kwakernaak, H.; and Sivan, R.: Linear Optimal Control Systems. Wiley Interscience, New York, 1972.
13. Doyle, J. C.; and Stein, G.: Multivariable Feedback Design: Concepts for a Classical/Modern Synthesis. IEEE Trans. on Automatic Control, vol. AC-26, 1981, pp. 4-16.
14. Courant, R.: Variational Methods for the Solution of Problems of Equilibrium and Vibrations. Bull. American Math Society, vol. 49, January 1943, pp. 1-23.
15. Olsson, D. M.; and Nelson, L. S.: The Nelder-Mead Simplex Procedure for Function Minimization. Technometrics, vol. 17, 1975.
16. Murrow, H. N.; and Eckstrom, C. V.: Drones for Aerodynamic and Structural Testing (DAST) - A Status Report. AIAA Paper No. 78-1485. Presented at the 1978 Atmospheric Flight Mechanics Conference, August 1978.

17. Boeing Wichita Company: Integrated Design of a High Aspect Ratio Research Wing with an Active Control System for Flight Tests on a BQM-34E/C Drone Vehicle. NASA CR-166108, 1979.
18. Rodger, Kenneth L.: Airplane Math Modeling Methods for Active Control Design. AGARD CR-228, August 1977.
19. Adams, William M., Jr.; and Tiffany, Sherwood H.: Design of a Candidate Flutter Suppression Control Law for the DAST ARW-2. NASA TM-86257, July 1984.
20. Ridgely, D. Brett; and Banda, Siva S.: Introduction to Robust Multivariable Control. AFWAL-TR-85-3102, February 1986.

Aeroelastic Modeling for the FIT* Team
F/A - 18 Simulation

Thomas A. Zeiler
Planning Research Corporation
Aerospace Technologies Division
Hampton, Virginia

and

Carol D. Wieseman
National Aeronautics and Space Administration
Langley Research Center
Hampton, Virginia

*Functional Integration Technology

624

Abstract

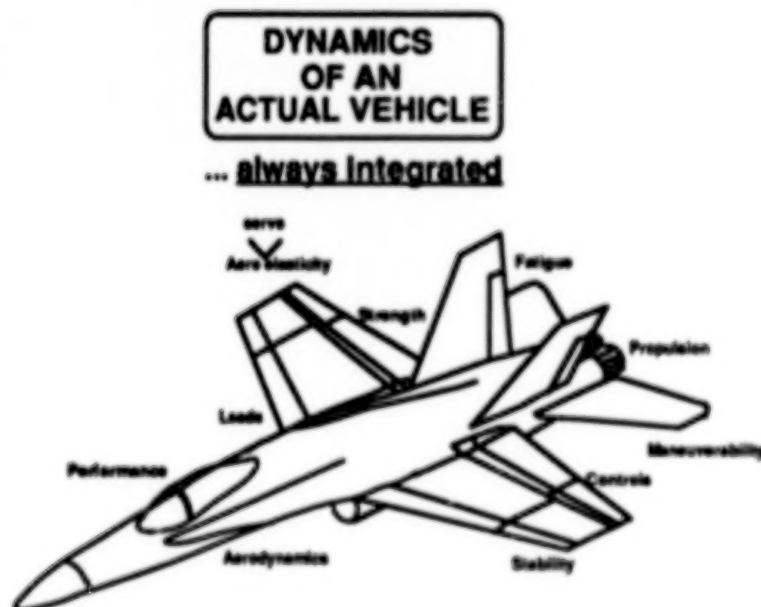
As part of Langley Research Center's commitment to developing multidisciplinary integration methods to improve aerospace systems, the Functional Integration Technology (FIT) team was established to perform dynamics integration research using an existing aircraft configuration, the F/A - 18. An essential part of this effort has been the development of a comprehensive simulation modeling capability that includes structural, control, and propulsion dynamics as well as steady and unsteady aerodynamics. The structural and unsteady aerodynamics contributions come from an aeroelastic model. Some details of the aeroelastic modeling done for the FIT team research is presented in this paper. Particular attention is given to work done in the area of correction factors to unsteady aerodynamics data.

Dynamics of an Actual Vehicle

The dynamics of an actual flight vehicle are always integrated. For better or worse, all the physical elements of the vehicle and its operating environment interact to varying degrees continually and without exception. It is only when we desire to analyze or design a complex physical system that nature's continuum becomes discretized into specialties and segregated into disciplines. It's recognized, of course, that real systems are not so discretized and some "multidisciplines" have emerged and are given due consideration in analysis and design. Aeroelasticity and its descendent, aeroservoelasticity, are examples.

Even where "multidisciplines" have not emerged to deal with complex physical interactions, interdisciplinary communication is still established to analyze and design the vehicle. A structures group will obtain force and pressure data from the aerodynamics, propulsion, and guidance and control groups to define the operating environment and, particularly, loads to which the structure is subjected [1]. In turn, the structures group might provide the guidance and control group with modal dynamics and, more likely, flexible stability derivatives and maneuver constraints.

However, the cross - disciplinary data flow is not always smooth. Each group uses models, methods, theories, and assumptions peculiar to its own discipline. This state of affairs makes one discipline seem remote and even incomprehensible to another discipline even though they are all subject to the same laws of physics and may be involved in designing parts of the same airplane. So, there is still a need for more in-depth integration of multiple disciplinary techniques [2].



FIT Background

In its statement of mission and goals [3], NASA's Langley Research Center lists that one of its major goals is to "develop multidisciplinary integration methods to improve aerospace systems." In pursuit of this goal two working groups were formed in January of 1985. One group, known as ACIG (for Aircraft Configuration Integration Group), was to concentrate on structural and aerodynamic configuration parameters. The other, known as the FIT (for Functional Integration Technology) Team, would work on the integration of vehicle dynamics.

Using an existing configuration, specifically the F/A - 18, the FIT Team has been working toward two major objectives: improving the effectiveness of piloted simulation in the preliminary and conceptual design phases, and removing unfavorable or exploiting favorable dynamic systems interactions. The plan is to eventually merge the activities of the two groups to produce comprehensive, integrated analysis and design methodologies.

- A NASA/LaRC Major Goal - - "Develop multidisciplinary integration methods to improve aerospace systems"

- Two Working Groups Formed:

- Aircraft Configuration Integration Group (ACIG) - Aero & Structures

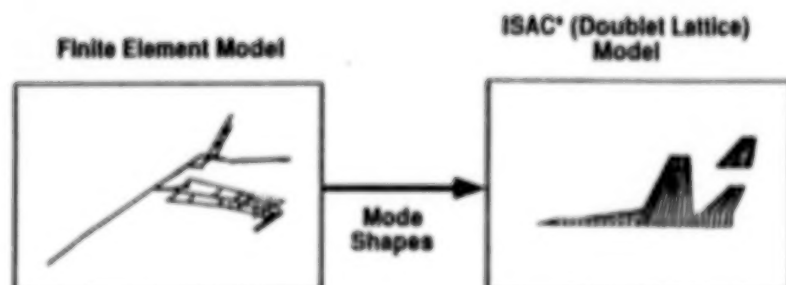
- Functional Integration Technology (FIT) - Dynamics Integration

- Improve Effectiveness of Piloted Simulation in Preliminary and Conceptual Design Phases

- { Remove Unfavorable
Exploit Favorable } Dynamic Systems Interactions

FIT Aeroelastic Model

An essential part of the FIT effort has been the development of a comprehensive simulation modeling capability that includes structural, control, and propulsion dynamics as well as steady and unsteady aerodynamics [4]. The structural and unsteady aerodynamic contributions come from the aeroelastic model. The aeroelastic model of the F/A - 18 used in the FIT studies consists of a finite element beam model obtained from the manufacturer, and a doublet lattice model constructed using ISAC (Interaction of Structures, Aerodynamics, and Controls, Ref. 5). Mode shapes are determined from the structural model and used with the doublet lattice model for the computation of generalized oscillatory aerodynamic loads. A discussion of some modeling details follows.



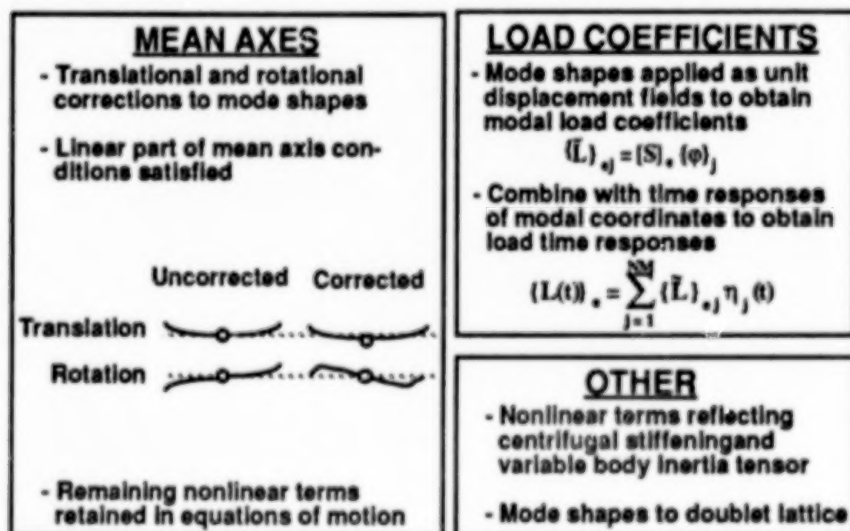
* Interaction of Structures, Aerodynamics, and Controls

Structural Modeling

In the general nonlinear equations of motion of a free-flying aeroelastic aircraft, a great deal of coupling between the body and elastic momenta can occur unless the body reference axes are chosen to be "mean axes" [6, 7, 8]. So, it is advantageous to use vibration modes that satisfy the mean axis conditions. Free vibration modes theoretically satisfy these conditions exactly and the mode shapes for this model were determined for the unrestrained structure. However, computations showed that the conditions were not satisfied exactly [6], likely as the result of computational error. Since the mean axis conditions are known, the mode shapes could, in principle, be modified so as to satisfy the conditions. But the mean axis conditions themselves are nonlinear, making it difficult to determine the modifications. Therefore, only the linear portions of the conditions were satisfied by applying small translational and rotational corrections to the mode shapes. This leaves small nonlinear terms coupling the body and elastic angular momenta. These terms are retained in the nonlinear equations of motion [6, 7]. If the structure were undergoing free vibration in a gravity-free vacuum, a true mean axis system would be observed to be perfectly stationary with respect to an inertial reference. However, since the body frame in the present model is only approximately a mean axis system, it would be seen to undergo small angular oscillations.

Modal load coefficients were determined by applying the mode shapes to the structural model as unit displacement fields [6]. The internal loads within each element resulting from the application of one mode become the load coefficients for that mode. The internal loads are comprised of the six stress resultants: two bending moments; one torsion moment; two shears; and one axial force. The coefficients are combined with time histories of the modal coordinates (which are the generalized coordinates representing the structure in the integrated model) to produce time histories of the internal loads.

As the structure deforms, the inertia tensor of the body changes since mass is being redistributed in space. The structural model is used to compute terms reflecting this effect as well as terms representing centrifugal stiffening, frequencies, and generalized modal masses - all of which are supplied to the integrated simulation model. [6, 7]. Finally, as mentioned previously, the corrected mode shapes are supplied to the doublet lattice model for computation of generalized, unsteady aerodynamic loads.



Unsteady Aerodynamics Modeling

In order to obtain a representation of the unsteady aerodynamic loads in state-space form for the simulation model, a rational function approximation (RFA) is used. The form of RFA used is known generally as Roger's approximation and is shown in the figure. The coefficient A matrices are determined by a least-squares fit of the approximation to oscillatory loads tabulated over a range of reduced frequencies [9, 10]. The approximations are only valid for a given Mach number, so sets of coefficient matrices must be calculated to cover the Mach number range of interest. The aerodynamic loads provide the simulation model with incremental loads resulting from elastic and control deflections and from unsteady motion. A total of four (4) lags (the β 's) were used in the FIT F/A - 18 model.

- Unsteady aerodynamic loads in the Laplace domain :

$$F_s(s) = q [Q(s)] X(s)$$

- Roger's Rational Function Approximation (RFA) :

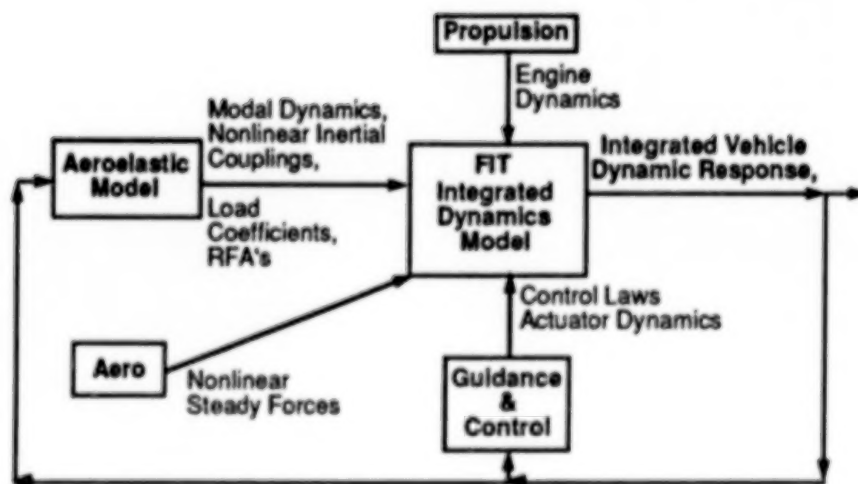
$$\hat{Q}(s) = \hat{\lambda}_0 + \hat{\lambda}_1 s + \hat{\lambda}_2 s^2 + \sum_{i=1}^N \frac{\hat{\lambda}_{i+2} s}{s + \beta_i}$$

- Least-Squares fit of $\hat{Q}_{ij}(k)$ to tabulated $Q_{ij}(k)$ over a range of k values for given Mach number
- Incremental loads from elastic and control deflections and from unsteady motion

FIT Integrated Dynamics Model

The general, nonlinear equations of motion [6, 7] are implemented in a batch simulation model written in ACSL (Advanced Continuous Simulation Language, Ref. 11). The model incorporates elements from an engine dynamics model, control laws and actuator dynamics, nonlinear steady aerodynamic data, which for the present F/A - 18 model comes from the LaRC Real-Time Simulation Facility's own F/A-18 simulation, and data from the aeroelastic model. As described earlier, this data includes generalized masses and frequencies, nonlinear momentum coupling terms, nonlinear terms representing centrifugal stiffening and the effects of deformation on the body's inertia tensor, and the rational function coefficients for the unsteady aerodynamic loads. Modal load coefficients may also be supplied to the simulation for immediate calculation of load time histories. But since this places an additional computational burden on the simulation, it is more efficient to send the modal coordinate time histories back to the aeroelastic model for a comprehensive evaluation of the loads.

A time history of internal loads for the F/A - 18 model resulting from a roll doublet maneuver was animated using colors to represent various internal load levels. A videotape of the display was prepared and shown as part of the oral presentation of the paper. As it turns out, the nonlinear inertial terms are not a major factor for the F/A - 18 loads and would not likely be important for any conventional aircraft configuration. For rotorcraft, aircraft with stores or high T - tails, or for flexible spacecraft they may become more important [6, 7].



Needs

A future concern for FIT team efforts is improvement in the representation of the unsteady aerodynamic loads. The present form of RFA being used, Roger's approximation, introduces a large number of states into the model [6]. For a formulation including six rigid body modes, twenty elastic modes, and four aerodynamic lags, the number of aerodynamic states alone is 104 [4]. Add to this the rigid body and elastic modes, altitude, quaternion, actuator, and engine states, and the size of the simulation model becomes very large. This substantially affects the run time of the batch simulation limiting its utility. Work is underway to incorporate an updated form of Karpel's Minimum State Method [9, 12] into the options available in the ISAC programs being used for the unsteady aerodynamics. Another concern is the quality of the unsteady aerodynamic data being approximated, particularly for rigid-body motions at low reduced frequencies and near the transonic regime. Work being done in this area with correction factors will occupy the latter part of this paper.

Unsteady Aerodynamics

- **Simpler approximation
(Minimum State Method - Karpel)**
- **Improved quality of unsteady aerodynamics
data near zero reduced frequency and
transonic regime (Correction Factors)**

Correction Factor Methodologies

The Doublet Lattice Method is one method used to calculate unsteady aerodynamics for a wide variety of applications, but it has limitations. It is a linear, subsonic, and small perturbation method [13]. One method to expand the usefulness and the accuracy of the Doublet Lattice Method is the use of correction factors. Correction factors are modifiers of either the pressures or the downwashes calculated with the doublet lattice method. Correction factors can be calculated to match pressure distributions, section properties, or total loads (force and moment derivatives) that are obtained from experiment or CFD calculation [14]. Matching total forces requires solving an optimization problem that can be formulated in one of several ways. One way is to minimize the difference between the experimental and analytical loads with side constraints on the changes in the pressure or downwash distribution. Alternatively, the change in the original pressure or downwash distribution can be minimized subject to constraints on the differences between the experimental and analytical loads [15].

WHY - Doublet Lattice has limitations: linear, subsonic, small perturbation

WHAT - Correction Factors are modifications to pressures and / or downwashes in order to match experimental or CFD data

HOW-

Match Pressure Distributions

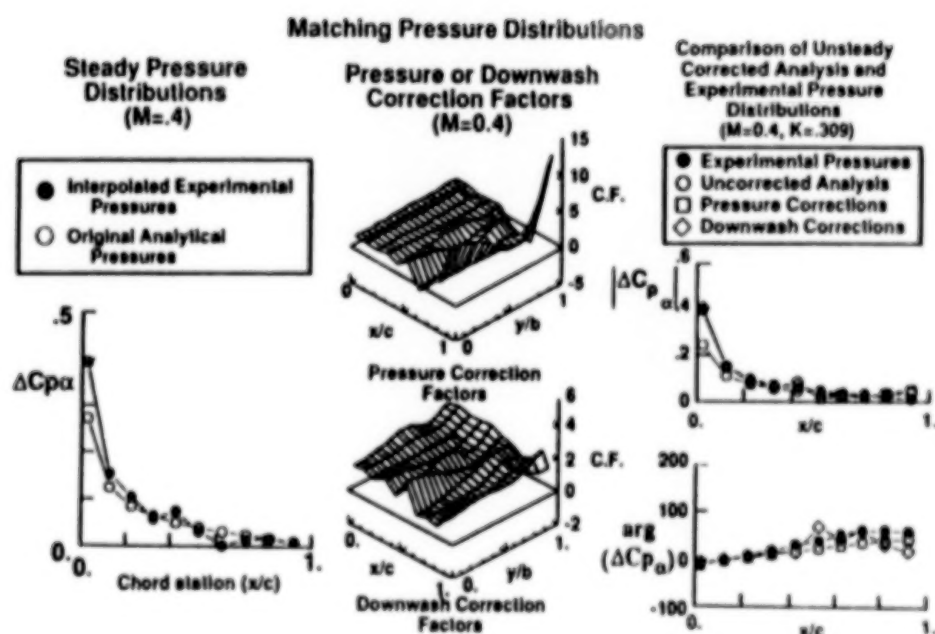
Match Section Properties

Match Total Loads - Force and Moment Derivatives by Optimization

$$\min_{\{\Delta w, \Delta p\}} \left\{ \text{Load error} \right\}, \text{ subject to } \left\{ \Delta w, \Delta p \right\}$$

Correction Factor Methodologies - Methodology and Results

A brief description of the methodology of matching pressure distributions is presented here. For the purpose of explanation and example, the methodology was exercised on a Rectangular Supercritical Wing that was tested in the NASA Langley Transonic Dynamics Tunnel [16,17]. The steps to calculating these correction factors are as follows. First, experimental pressures are interpolated to analytical locations, which in the case of Doublet Lattice correspond to the quarter-chord and mid-span location of each of the doublet lattice boxes. This is accomplished using one-dimensional spline interpolation in the chordwise direction followed by the spanwise direction. The pressures at each of the analytical locations are then interpolated using splines as a function of angle-of-attack. The analytical first derivative of the spline interpolation curve is evaluated at an angle-of-attack of zero degrees to obtain the quantity which will be matched using correction factors. Correction factors are calculated to modify either the analytical pressures or the downwashes such that the steady pressure distributions are matched. Typical distributions of pressure and downwash correction factors are shown in the center of the slide. These correction factors were then applied to the calculation of the unsteady pressures. The methodology was validated by comparing corrected unsteady analytical aerodynamic data and unsteady experimental aerodynamic data.



Doublet Lattice Modeling of F/A - 18

An aerodynamic model of the F-18 was needed to calculate Doublet Lattice aerodynamics for the FIT integrated dynamics model. In the original aerodynamic model of the F-18, the fuselage was modeled as a flat plate, the horizontal tail and the wing had no dihedral, and the tip missile was not modeled. An initial attempt at calculating correction factors for this model was unsatisfactory, primarily because the pitching moment derivative of the doublet lattice model was of the wrong sign. The method concentrated on improving the pitching moment derivative at the expense of the other stability derivatives, resulting in a poor overall "corrected" model, and unrealistic values for the correction factors. Because of this problem, a parametric study was conducted to evaluate the sensitivities of the stability derivatives to different models of the fuselage and tip missile, the inclusion of wing dihedral, and wing panelling. The fuselage was modeled several different ways as a flat plate or as a slender body with interference panels. The models investigated are shown in the figure. Several tip missile models having different sizes of slender bodies as well as cross sections of interference panels were evaluated as shown. Dihedral was also included in the wing and horizontal tail.

- Original model

Flat plate fuselage, no tip missile, no wing dihedral and no horizontal tail dihedral

- Sign of $C_{M_{\alpha}}$ - wrong

- Parametric study of doublet lattice model features

- 1) Fuselage



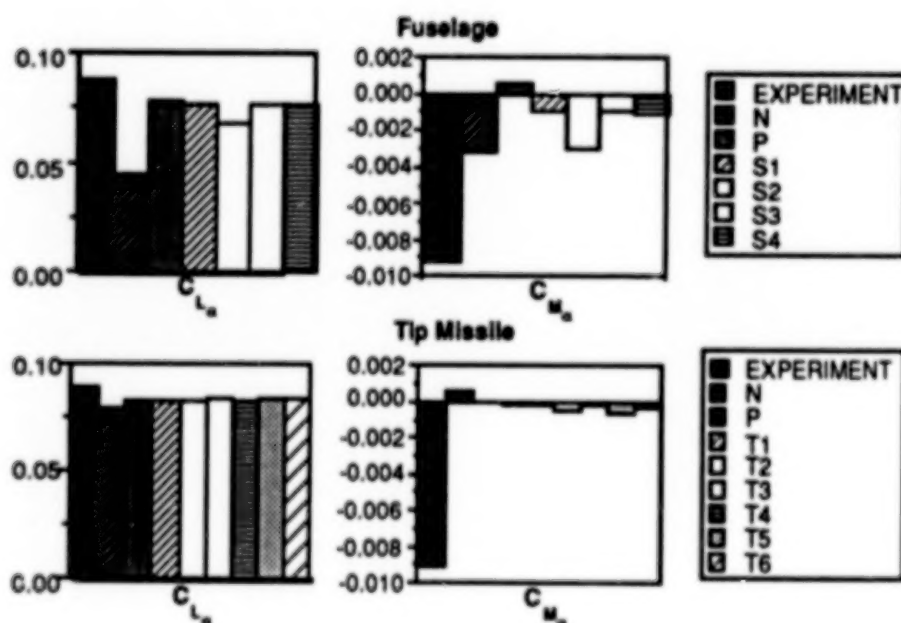
- 2) Tip missile



- 3) Dihedral - Wing (-3 degrees) and horizontal tail (-2 degrees)

Sensitivities of Stability Derivatives to Modeling

Shown here are some typical comparisons of the effect of modeling the fuselage and the tip missile on the several stability derivatives. The top half of the figure shows the effect of modeling the fuselage. N signifies no fuselage, P signifies a flat plate fuselage, S# identifies the slender body and interference panel model used, shown on the previous figure. Modeling the fuselage as a slender body changes the sign of the pitching moment. Incorporating the slender body fuselage model, however, does not greatly change the lift due to angle of attack. The bottom of the figure shows the effect of different tip missile models. N signifies none, P signifies a flat plate, and T# refers to the tip missile models as shown on the previous figure. The tip missile comparison also shows that the adding a tip missile improves the pitching moment with negligible effect on the lift coefficient due to angle of attack.



Sensitivities of Stability Derivatives to Modeling (cont.)

Summarized here are the results of the parametric study of the effect of modeling on the analytical stability derivatives. Results showed that the modeling the fuselage as a slender body resulted in improving the analytical calculation of the pitching moment due to angle-of-attack and lift coefficient due to pitch rate. There was a small effect on the antisymmetric loads. The tip missile modeling improved the pitching moment due to angle-of-attack and the rolling moment coefficients with respect to the wing trailing edge control surfaces. Implementing dihedral on the wing and the tail affected the antisymmetric derivatives and had a small beneficial effect on the pitching moment due to angle-of-attack. Based on this parametric study, the best starting model for calculating correction factors is one in which the fuselage is modeled as a slender body with interference panels and the tip missile is modeled in the simplest manner. Though the tip missile does not have a great effect on the stability aerodynamic forces for this application, it has been shown that how the tip missile is modeled does affect local loads and flutter [18].

Fuselage modeling	Modeling fuselage as slender body improves C_{M_α} , C_{L_q} Negligible effect on antisymmetric forces and moments
Tip Missile	Negligible effect except for C_{M_α} and rolling moment coefficients with respect to trailing edge flap and aileron
Dihedral	Negligible effect on symmetric derivatives except for C_{M_α}
Wing (-3 deg)	Small beneficial effect on C_{Y_β}
Tail (-2 deg)	Small detrimental effect on C_{N_β} and C_{L_β}

Concluding Remarks

This paper has presented some details of an aeroelastic model of the F/A - 18 created for NASA LaRC's Functional Integration Technology team's research in dynamics integration. This model was used to directly incorporate aeroelastic effects, including modal structural dynamics, unsteady aerodynamics, and structural loads, into a comprehensive nonlinear simulation model that combines aeroelasticity, propulsion dynamics, control dynamics, and a nonlinear steady aerodynamics data base. Data passed to the simulation model include modal generalized mass, frequencies, nonlinear inertial coupling terms, nonlinear terms accounting for centrifugal stiffening and variation of the body inertia tensor resulting from deformation, rational function approximation coefficients for generalized unsteady aerodynamic forces, and a limited number of modal load coefficients. The structural model can also be used for a broader loads analysis using output time histories of the elastic modal coordinates from the simulation model.

As a result of experiences with the simulation model, several aeroelastic modeling needs have been identified. These deal with the representation of unsteady aerodynamics. First, it is felt that the Minimum State Method will provide a lower order approximation. Second, correction factor methodologies are being developed to improve the quality of the doublet lattice data being approximated, extending its usefulness. As part of this work, some issues related to fuselage and tip missile modeling and its effects upon efforts to calculate correction factors have been resolved.

- **Aeroelasticity included directly in an integrated dynamics model**
 - Structural modal dynamics
 - RFA's of modal generalized aerodynamic forces
- **Have need for improvements in unsteady aerodynamics**
 - Lower order RFA's needed
 - Correction Factor Methodologies developed and tested on Rectangular Supercritical Wing
 - Fuselage and tip missile modeling issues resolved

References

1. Stauffer, Warren A., Lewolt, John G., and Hoblit, Frederic M., "Application of Advanced Methods to Design Loads Determination for the L-1011 Transport," *AIAA Journal of Aircraft*, Vol.10, No. 8, August 1973, pp. 449 - 458.
2. Rommel, Bruce A., and Dodd, Alan J., "Practical Considerations in Aeroelastic Design," *Proceedings of a Symposium on Recent Experiences in Multidisciplinary Analysis and Optimization*, NASA CP 2327, April 24 - 26, 1984.
3. "Mission and Goals," National Aeronautics and Space Administration, Langley Research Center Brochure, July 1988.
4. Arbuckle, P. Douglas, Buttrill, Carey S., and Zeiler, Thomas A., "A New Simulation Model Building Process For Use in Dynamic Systems Integration Research," AIAA Paper No. 87-2498-CP, *1987 AIAA Flight Simulation Technologies Conference Proceedings*, Monterey, CA, August 17 - 19, 1987.
5. Peele, E. L., and Adams, W. M., Jr., "A Digital Program for Calculating the Interaction Between Flexible Structures, Unsteady Aerodynamics, and Active Controls," NASA TM-80040, 1979.
6. Buttrill, Carey S., Zeiler, Thomas A., and Arbuckle P. Douglas, "Nonlinear Simulation of a Flexible Aircraft in Maneuvering Flight," AIAA Paper No. 87-2501-CP, *1987 AIAA Flight Simulation Technologies Conference Proceedings*, Monterey, CA, August 17 - 19, 1987.
7. Zeiler, Thomas A., and Buttrill, Carey S., "Dynamic Analysis of an Unrestrained, Rotating Structure Through Nonlinear Simulation," AIAA Paper No. 88-2232-CP, *29th SDM Conference Proceedings*, Williamsburg, VA, April 18 - 20, 1988.
8. Cavin, R. K., and Dusto, A. R., "Hamilton's Principle: Finite Element Methods and Flexible Body Dynamics," *AIAA Journal*, Vol. 15, No. 12, December 1977, pp 1684 - 1690.
9. Tiffany, S. H., and Adams, W. M., Jr., "Nonlinear Programming Extensions to Rational Function Approximations of Unsteady Aerodynamics," AIAA Paper No. 87-0854-CP, *28th SDM Conference Proceedings*, Monterey, CA, April 6 - 8, 1987.
10. Adams, W. M., Jr., Tiffany, S. H., Newsom, J. R., and Peele, E. L., "STABCAR - A Program for Finding Characteristic Roots of Systems Having Transcendental Stability Matrices," NASA TP-2165, June 1984.
11. *Advanced Continuous Simulation Language (ACSL), Reference Manual, Fourth Edition*, Mitchell and Gauthier Associates, Concord, MA, 1986.
12. Karpel, Mordechai, "Design for Active and Passive Flutter Suppression and Gust Alleviation," NASA CR 3482, 1981.
13. Giesing, J.P., Kalman, T.P., and Rodden, W.P.; *Subsonic Unsteady Aerodynamics for General Configurations*, AFFDL-TR-71-5.

14. Wieseman, Carol D., "Methodology for Matching Experimental and Analytical Aerodynamic Data," AIAA Paper No. 88-2392-CP, 29th SDM Conference Proceedings, Williamsburg, VA, April 18 - 20, 1988.
15. Giesing, J. P., Kalman, T.P., and Rodden, W.P., "Correction Factor Techniques for Improving Aerodynamic Prediction Methods", NASA CR 144967, May, 1976.
16. Ricketts, R. H., Watson, J.J., Sandford, M.C., and Seidel, D.A., "Geometric and Structural Properties of a Rectangular Supercritical Wing Oscillated in Pitch for Measurement of Unsteady Transonic Pressure Distributions." NASA TM 85763, Nov. 1983.
17. Ricketts, R. H., Sandford, M.C., Watson, J.J., and Seidel, D.A., "Subsonic and Transonic Unsteady- and Steady-Pressure Measurements on a Rectangular Supercritical Wing Oscillated in Pitch", NASA TM 85765. August 1984.
18. Triplett, W.E., "Wind Tunnel Correlation Study of Aerodynamic Modeling for F/A-18 Wing-Store Tip-Missile Flutter", *Journal of Aircraft*, Vol. 21, no. 5, May 1984, p 329-334.

**DIGITAL ROBUST CONTROL LAW SYNTHESIS
USING CONSTRAINED OPTIMIZATION**

**Vivekananda Mukhopadhyay
Planning Research Corporation
MS 243, NASA Langley Research Center
Aeroservoelasticity Branch
Hampton, Virginia 23665-5225**

ABSTRACT

Development of digital robust control laws for active control of high performance flexible aircraft and large space structures is a research area of significant practical importance. The flexible system is typically modeled by a large order state space system of equations in order to accurately represent the dynamics. The active control law must satisfy multiple conflicting design requirements and maintain certain stability margins, yet should be simple enough to be implementable on an onboard digital computer. This paper describes an application of a generic digital control law synthesis procedure for such a system, using optimal control theory and constrained optimization technique. A linear quadratic Gaussian type cost function is minimized by updating the free parameters of the digital control law, while trying to satisfy a set of constraints on the design loads, responses and stability margins. Analytical expressions for the gradients of the cost function and the constraints with respect to the control law design variables are used to facilitate rapid numerical convergence. These gradients can be used for sensitivity study and may be integrated into a simultaneous structure and control optimization scheme. An existing control law as well as an estimator based full or reduced order control laws can be optimized in order to meet the multiple design requirements. Low order, robust digital control laws were synthesized for gust load alleviation and flutter suppression of a flexible aircraft.

INTRODUCTION

The small perturbation dynamics of a flexible aircraft or space structure with active control is typically modeled by a large order state space system of equations in order to accurately represent the rigid and flexible body modes, unsteady aerodynamic forces, actuator dynamics, antialiasing filters, computational delays and gust spectra (Ref. 1). The control law of this multi-input multi-output (MIMO) system is expected to satisfy multiple conflicting design requirements on the dynamic loads, root-mean-square (RMS) responses, actuator surface deflection and rate limitations, as well as maintain certain guaranteed stability margins based in the system singular values. Robust control laws for the linear MIMO system with modeling uncertainty can be developed using optimal control theory, which is also known as linear quadratic Gaussian (LQG) technique. This control law is usually of the same or higher order than the plant and is difficult to implement on an onboard digital microprocessor. There are several model reduction techniques to reduce the control law to a lower order but the reduced order control law may not satisfy the design requirements. This paper describes an application of a generic control law synthesis procedure (Ref. 2) for such a system, using optimal control theory and constrained optimization technique. The basic multivariable system and the design problem is schematically described in Fig. 1. The formulation and synthesis procedure is briefly described first. Application to a gust load alleviation (GLA) of a remotely piloted flexible drone is presented. Some recent results of a flutter suppression system (FSS) design are also presented.

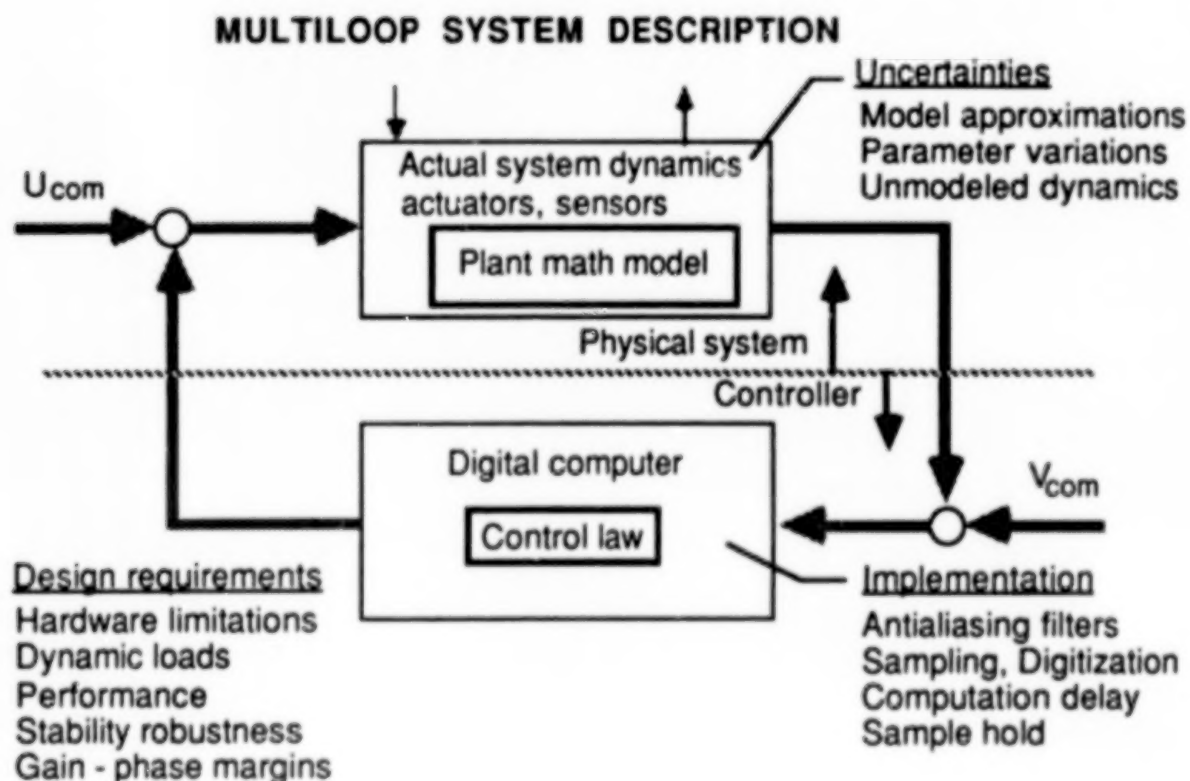


FIGURE 1

SYSTEM STATE SPACE EQUATIONS

The typical state space system of equations for a discrete system is shown in Fig. 2. These equations represent discrete time, linear equations of motion, due to a small perturbation from a steady state equilibrium flight condition of a flexible system. The plant equations are usually of large order and include the effects of antialiasing filters and computational delays at each measurement output channel. The antialiasing filters attenuate unmodeled high frequency signals but introduce significant phase lags which must be included in the control law synthesis. The plant and sensor measurement models also contain discrete white noise inputs w_k and v_k , respectively. The design outputs are the quantities on which design constraints are imposed. The control law is also expressed in state space form and is required to be of lower order than the plant. The discrete control law can be obtained from a full order LQG design after suitable stable order reduction and discretization at a specified sampling rate.

SYSTEM STATE SPACE EQUATIONS

$$\text{PLANT} \quad X_{k+1} = F X_k + G_u u_k + G_w w_k$$

$$\text{SENSOR} \quad y_k = H X_k + v_k$$

$$\text{DESIGN} \quad y_{dk} = H_d X_k + E_d u_k$$

$$\begin{aligned} \text{CONTROL} \quad Z_{k+1} &= A Z_k + B y_k \\ \text{LAW} \quad u_k &= C Z_k + D y_k \end{aligned}$$

FIGURE 2

AUGMENTED SYSTEM EQUATIONS

The closed loop system equations can be written in an augmented form as shown in Fig. 3. The new term η can be considered as an input command or a fictitious input noise. Using the 'hat' overscript to denote each of the augmented matrices, the closed loop dynamic system looks like a simple output gain feedback system. This type of representation simplifies the derivation of the analytical gradient expressions. Other variations of the augmented system formulation are possible depending upon the controller structure. The design variables are selected parameters of the control law quadruple matrix \hat{C} .

CLOSED LOOP AUGMENTED SYSTEM

$$\begin{aligned} \begin{Bmatrix} X \\ Z \end{Bmatrix}_{k+1} &= \begin{bmatrix} F & 0 \\ 0 & 0 \end{bmatrix} \begin{Bmatrix} X \\ Z \end{Bmatrix}_k + \begin{bmatrix} G_u & 0 \\ 0 & I \end{bmatrix} \begin{Bmatrix} u_k \\ z_{k+1} \end{Bmatrix} + \begin{bmatrix} G_u & G_w & 0 \\ 0 & 0 & 0 \end{bmatrix} \begin{Bmatrix} \eta \\ w \\ v \end{Bmatrix}_k \\ &\quad \hat{F} \quad \hat{X}_K \quad \hat{G} \quad \hat{u}_K \quad \hat{G}_w \quad \eta_K \\ \begin{Bmatrix} y \\ Z \end{Bmatrix}_k &= \begin{bmatrix} H & 0 \\ 0 & I \end{bmatrix} \begin{Bmatrix} X \\ Z \end{Bmatrix}_k + \begin{bmatrix} 0 & 0 & I \\ 0 & 0 & 0 \end{bmatrix} \begin{Bmatrix} \eta \\ w \\ v \end{Bmatrix}_k \\ &\quad \hat{H} \quad \hat{I} \\ \begin{Bmatrix} u_k \\ z_{k+1} \end{Bmatrix} &= \begin{bmatrix} D & C \\ B & A \end{bmatrix} \begin{Bmatrix} y \\ Z \end{Bmatrix}_k \\ &\quad \hat{C} \quad \hat{y}_K \end{aligned}$$

FIGURE 3

GRADIENTS

The analytical expressions for the gradients of the cost function and the constraints with respect to the control law design variables are used for computation. The typical expressions for the gradients are shown in Fig. 4. The underlined matrices are specified for each constraint and cost function. The derivation is quite general in nature. The gradients with respect to other parameters can also be derived in a similar manner. The use of analytical expressions for the gradients in the optimization scheme facilitates rapid convergence of the optimization process. The gradients can also be used for sensitivity study and can be integrated into a simultaneous structure and control optimization scheme. The minimum singular value of the return difference matrix at the plant input and output is also used as additional inequality constraint, in order to improve robustness properties in the frequency domain. These constraints are usually applied at a later stage of the synthesis process.

GRADIENTS OF COST FUNCTION AND CONSTRAINTS

$dJ/d\hat{C}$ and $dg_n/d\hat{C}$ are known from steady state solution of discrete Lyapunov equations

$$X_{K+1} = F_a X_K F_a^T + G_a R_a G_a^T$$

$$\Lambda_K = F_a^T \Lambda_{K+1} F_a + \underline{Q}_a$$

where

$$F_a = \hat{F} + \hat{G}\hat{C}\hat{H}$$

$$G_a = \hat{G}_w + \hat{G}\hat{C}\hat{I}$$

$$\underline{Q}_a = \underline{\hat{Q}}_1 + (\hat{C}\hat{H})^T \underline{\hat{Q}}_2 (\hat{C}\hat{H}) + \underline{(\hat{M}\hat{C}\hat{H})} + \underline{(\hat{M}\hat{C}\hat{H})}$$

FIGURE 4

PROBLEM DEFINITION

The constrained optimization problem is defined as shown in Fig. 5. The control law synthesis procedure minimizes a linear quadratic Gaussian type cost function, subject to a set of constraints on the design loads, RMS responses and stability margins. The stability margin requirement is imposed as constraints on the minimum singular value of the system return difference matrices at the plant input and output (Ref. 3). In a LQG design one has to find a set of weighting matrices and noise intensity matrices in order to satisfy all the RMS response and stability margin requirements. If this trial and error process fails to achieve the desired result, the designer can impose the violated design requirements as RMS response constraints and singular value constraints instead of searching for the weighting matrices.

CONSTRAINED OPTIMIZATION PROBLEM

Equations $\hat{x}_{k+1} = \hat{F} \hat{x}_k + \hat{G} \hat{u}_k + \hat{G}_w \hat{w}_k$

$$\hat{y}_k = \hat{H} \hat{x}_k + \hat{I} \hat{w}_k$$

$$\hat{u}_k = \hat{C} \hat{y}_k$$

Minimize $J = E \left[\begin{bmatrix} \hat{x}_k \\ \hat{u}_k \end{bmatrix}^T \begin{bmatrix} Q & M \\ M^T & R \end{bmatrix} \begin{bmatrix} \hat{x}_k \\ \hat{u}_k \end{bmatrix} \right]_{SS}$ By Changing $S(\hat{C})$

Subject to inequality constraints on

a) RMS responses and loads

b) Min. singular value

FIGURE 5

OPTIMIZATION SCHEME

The constrained optimization problem is solved by using the method of feasible directions (Ref. 4). The optimization scheme block diagram is shown in Fig. 6. This procedure is the discrete time equivalent of those presented in Refs 1,3,5 for a continuous system. Similar procedures without the inequality constraints were also presented in Refs 6-9 in the continuous time domain. The development of the initial stable control law required to start the optimization cycle needs some effort and experience. This is usually done by first designing a full order optimal control law using a continuous plant model, which includes the effects of antialiasing filters and computational delays. The order of the control law is then reduced by block diagonalization and truncation. Advanced methods of order reduction have recently been developed by Sofanov (Ref. 10), Meyer (Ref. 11) and Lenz, et al (Ref. 12). The reduced order control law is then optimized in the continuous domain and tested for performance and stability characteristics. This control law is then discretized in a stable manner and is reoptimized in the discrete domain using the analytical gradient expressions which facilitate fast numerical convergence.

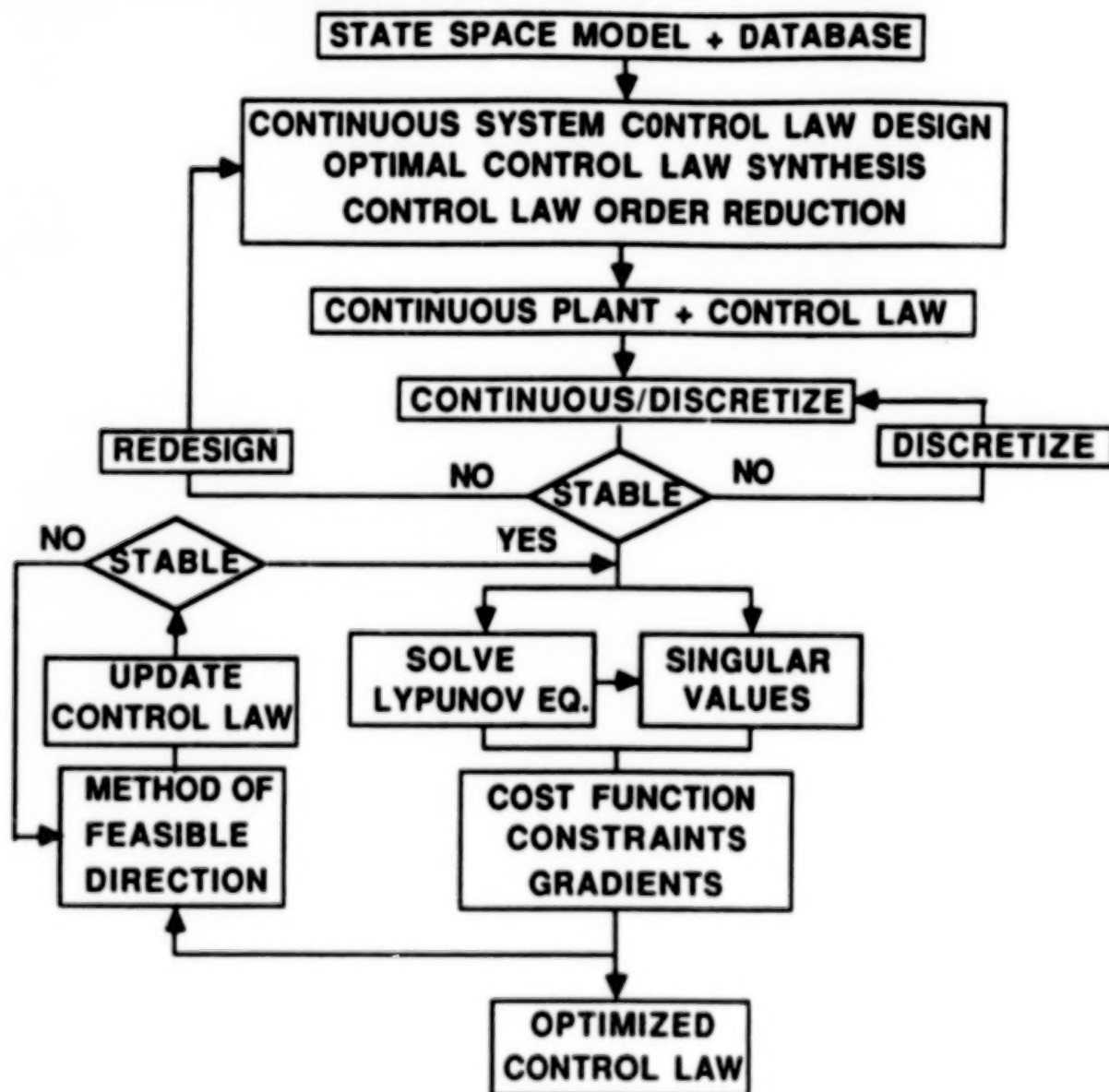


FIGURE 6

530

GUST LOAD ALLEVIATION PROBLEM

A gust load alleviation scheme of a remotely piloted drone aircraft is shown in Fig. 7. The drone is in symmetric longitudinal flight. The random vertical gust is represented by Dryden Spectrum, (Ref. 1). The accelerations are sensed by the fuselage and wing mounted accelerometers and are fed back through a set of antialiasing filters to a digital controller. The sampling rate is 100 Hz. The processed signal activates symmetric deflection command to the elevator and aileron. The primary dynamic loads are generated by the wing flexing due to short period motion. A simple gust load alleviation control law is needed to reduce the open loop RMS bending moment and shear force at the wing root by 50% without increasing the outboard bending moment and torsion.

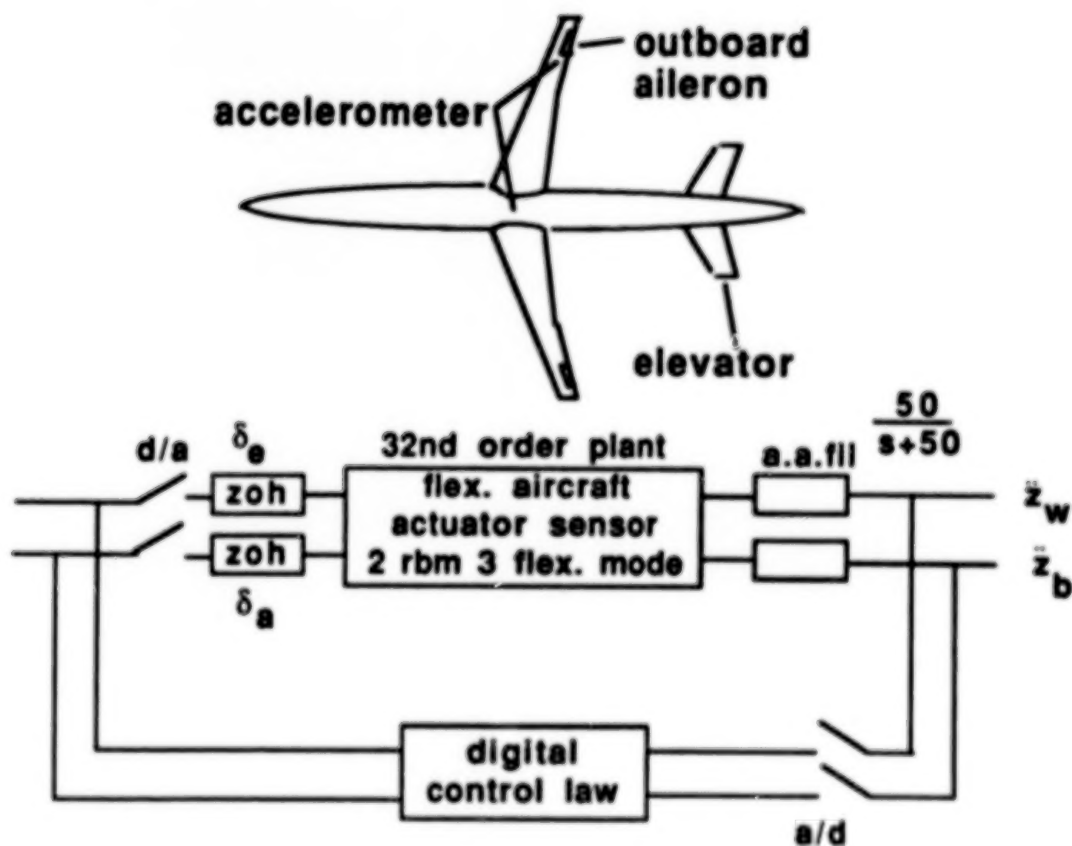
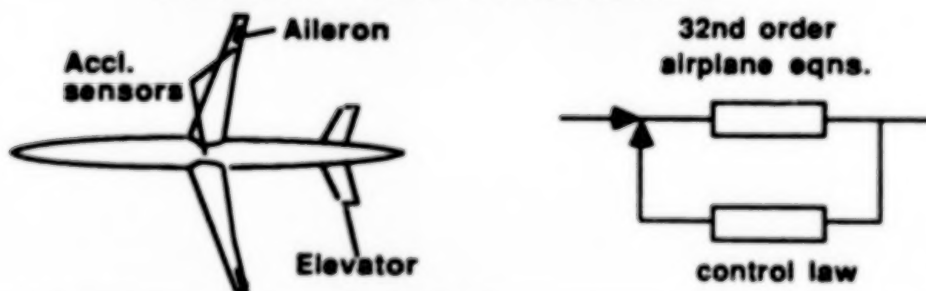


FIGURE 7

GLA DESIGN OBJECTIVES

The gust load alleviation (GLA) control law design objectives and synthesis procedure is shown in Fig. 8. The objective is to obtain a low order robust digital GLA control law which would reduce the open loop root-mean-square values of the wing root bending moment and shear by 50% without increasing the wing outboard bending moment and torsion. The control law should maintain certain guaranteed stability margins based on minimum singular value of 0.6 at both the plant input and output (Ref. 3). The control surface deflections and rates should be within the allowable limits. First a full order LQG control law is synthesized to satisfy the design requirements. This 32nd order control law is then reduced to a second order control law and then discretized. This control law does not satisfy the design requirements. After unconstrained optimization most of the requirements are satisfied except the wing outboard bending moment and the singular values. Using constraints on the RMS wing loads and on the minimum singular values of the return difference matrix at the plant input and output, the control law parameters are reoptimized (Ref.2).

GUST LOAD ALLEVIATION DESIGN REQUIREMENTS



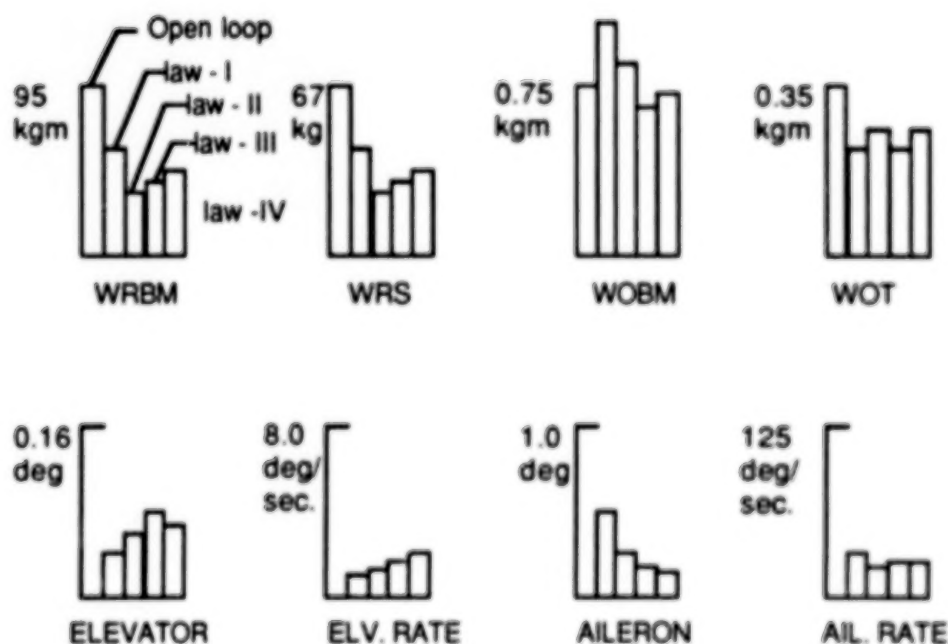
Physical quantities	Design objectives	How we do it
Root bending moment	50% reduction	1. LQG design 2. Control law order reduction 3. Discretize 4. Optimization 5. Apply constraints a) on rms loads b) on singular val.
Root shear	50% reduction	
Outboard bending mom.	No increase	
Outboard torsion	No increase	
Elevator deflection	Within max limit	
Elevator rate	Within max limit	
Aileron deflection	Within max limit	
Aileron rate	Within max limit	

FIGURE 8

COMPARISON OF RMS RESPONSES

The Fig. 9 shows a comparison of RMS responses and control surface deflections for a sequence of second order GLA control laws. The RMS values of wing root bending moment (WRBM), wing root shear (WRS), wing outboard bending moment (WOBM) and wing outboard torsion (WOT) are normalized to their open loop values and control surface deflection and rates are normalized to their maximum allowable values. The control law-I is obtained by digitization of a continuous control law obtained via reduction of a full order LQG design. This control law does not satisfy any of the design requirements. After an unconstrained optimization the control law-II is obtained which satisfies all the RMS response requirements except that on the WOBM. This is satisfied by a constrained optimization sequence to obtain law-III. After imposing the stability margin constraints, the control law -IV is obtained. The stability margins are improved at the cost of increased RMS responses.

COMPARISON OF NORMALIZED RMS RESPONSES DUE TO 1 M/S RMS DRYDEN GUST



law - I Initial 2nd order digital
law - II After Optimization

law - III After Opt. with RMS Constraints
law - IV After Opt. with SV Constraints

FIGURE 9

UNCONSTRAINED AND CONSTRAINED OPTIMIZATION

The cost function consists of weighted sum of the wing RMS loads and control surface RMS deflections using Bryson's inverse square weighting rule. The plot of normalized cost function versus iteration for the unconstrained optimization process used to obtain law-II is shown in Figure 10. The convergence is obtained in one iteration starting from the initial control law-I. In order to prevent the small increase in the wing outboard bending moment (WOBM), the control law-II is reoptimized by treating WOBM as a constraint instead of lumping it in the cost function. The result of this constrained optimization is also shown in Figure 10. The constraint is satisfied in one iteration, at the expense of increased cost function, which is subsequently reduced along with the wing outboard bending moment.

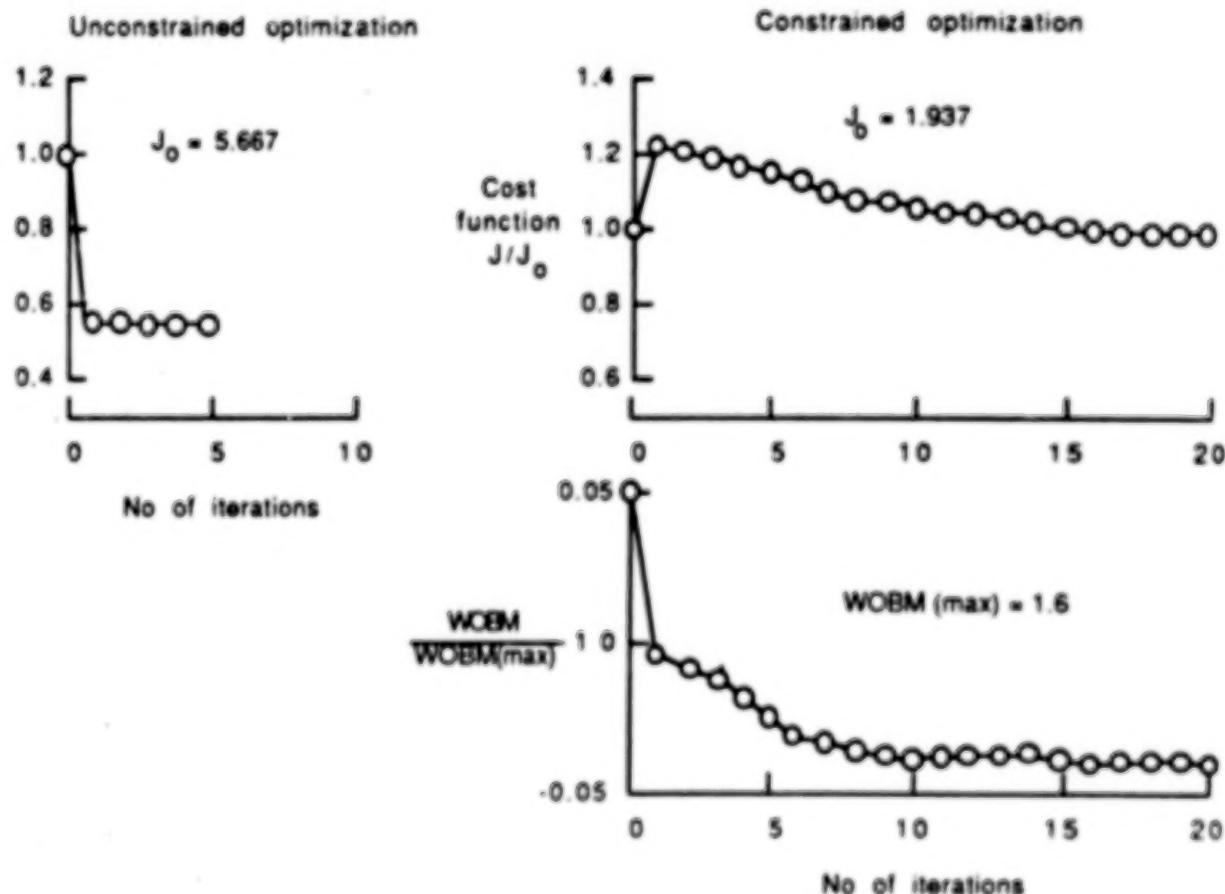


FIGURE 10

STABILITY ROBUSTNESS

In obtaining control laws I, II and III, no constraints were applied to the minimum singular value of the return difference matrix at the plant input and output which is a measure of the system's stability robustness properties (Ref. 3). The minimum singular value plot of the control laws II and III are shown in Fig. 11 at the plant input and output. In order to maintain a guaranteed phase and gain margins of ± 35 degrees and ± 8.0 dB, ± 4.0 dB respectively in each channel, the minimum singular value plots should be above the horizontal dotted line at -4.43 dB which corresponds to a minimum singular value of 0.60 . Figure 1 indicates that none of the control laws satisfy these criteria although the control law-III is fairly robust compared to control law -II. Additional constrained optimization is required to improve the stability robustness at the plant input and output. These results are shown next.

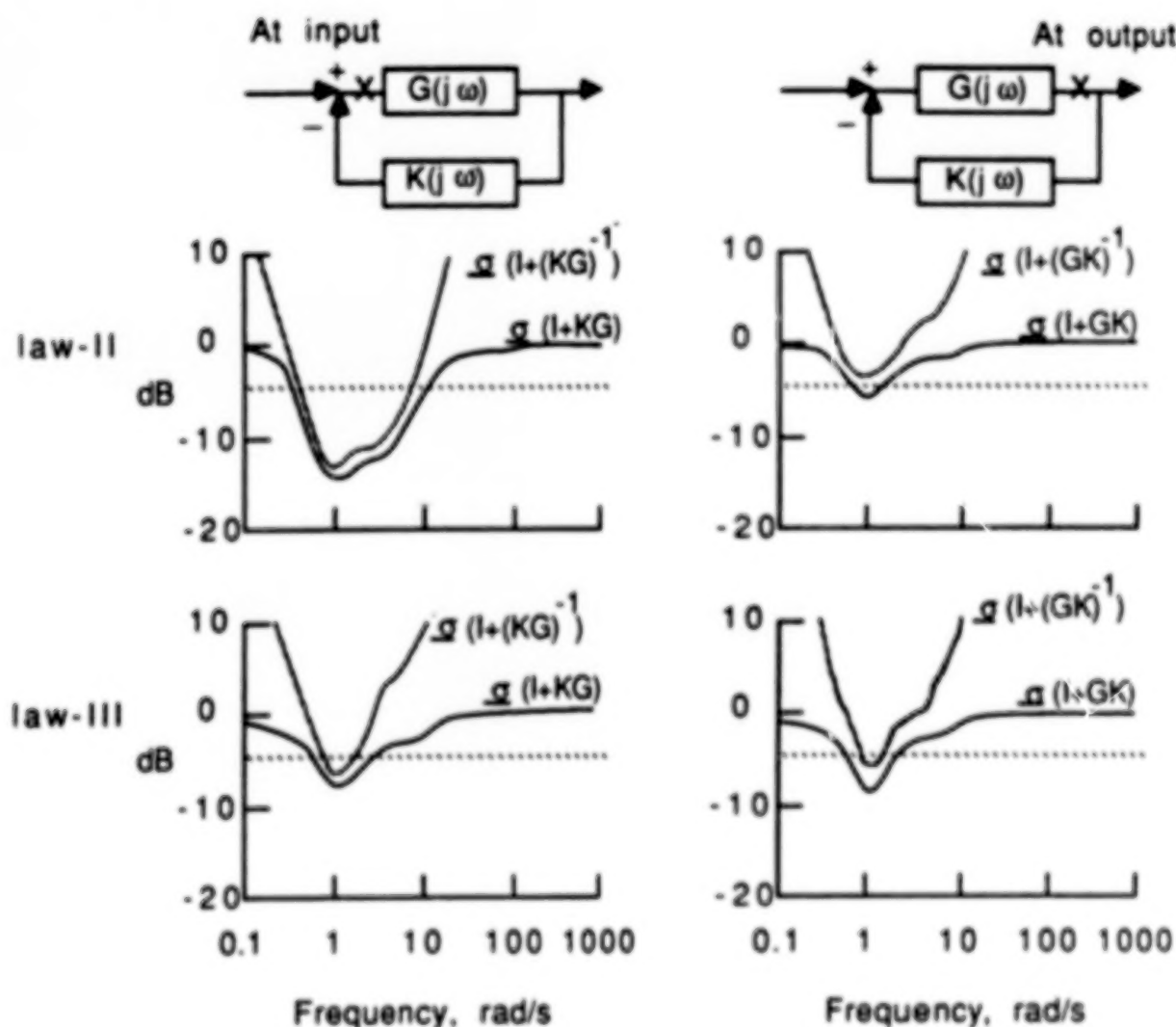


FIGURE 11

STABILITY ROBUSTNESS IMPROVEMENT

In order to improve the stability margins at both the plant input and output, the control law-III was reoptimized using two additional constraints corresponding to the required minimum singular value of $(I+KG)$ and $(I+GK)$ not less than 0.60 or -4.43 dB. Other constraints were also retained. The resulting control law-IV obtained after 7 iterations satisfies all the constraints. The increased robustness is at the cost of higher RMS responses compared to law-III. The minimum singular value plot is shown in Fig. 12. With control law-IV, the system has guaranteed simultaneous gain margins of +5.7 dB, -17.0 dB and phase margins of +53 and -53 degrees at each channel. Thus substantial improvement in stability robustness was obtained by using constrained optimization.

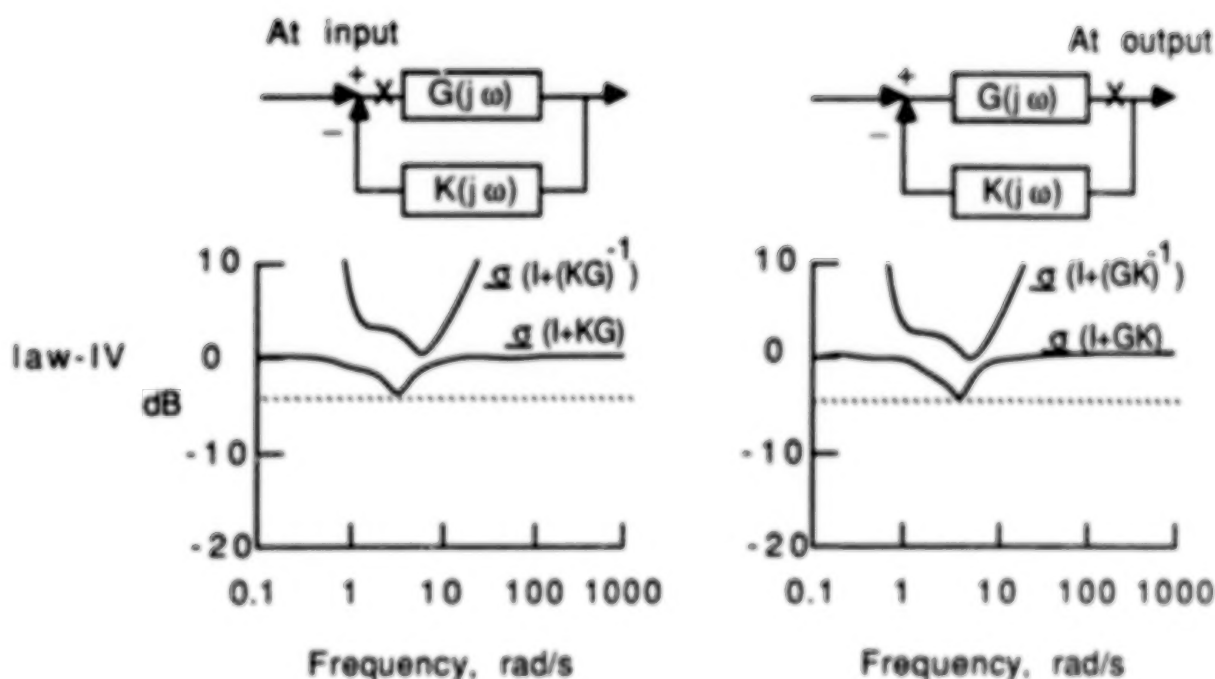


FIGURE 12

AFW SYMMETRIC FLUTTER SUPPRESSION

Digital robust control law synthesis for the Active Flexible Wing (AFW) wind tunnel model is presently being carried out in collaboration with Rockwell International. The basic block diagram for a two input two output symmetric flutter suppression system is shown in Fig.13 for a sting mounted model using leading edge outboard (LEO) and trailing edge outboard (TEO) symmetric actuators and colocated accelerometer sensors. The sampling rate is 200 Hz. The design takes into account the effects of actuator dynamics, 4th order 100 Hz Butterworth filters and one cycle computational delay at each channel. Full order and reduced order analog and discrete robust control laws were synthesized based on an approximate 38th order system at 300 psf design dynamic pressure. The discrete 8th order control law was able to stabilize the system over the range 300 to 150 psf. The more detailed 80th order model was also stable at 300 and 200 psf. Starting with these preliminary control laws, detailed analysis will be carried out using the discrete system optimization procedure.

SYMMETRIC FLUTTER SUPPRESSION SYSTEM

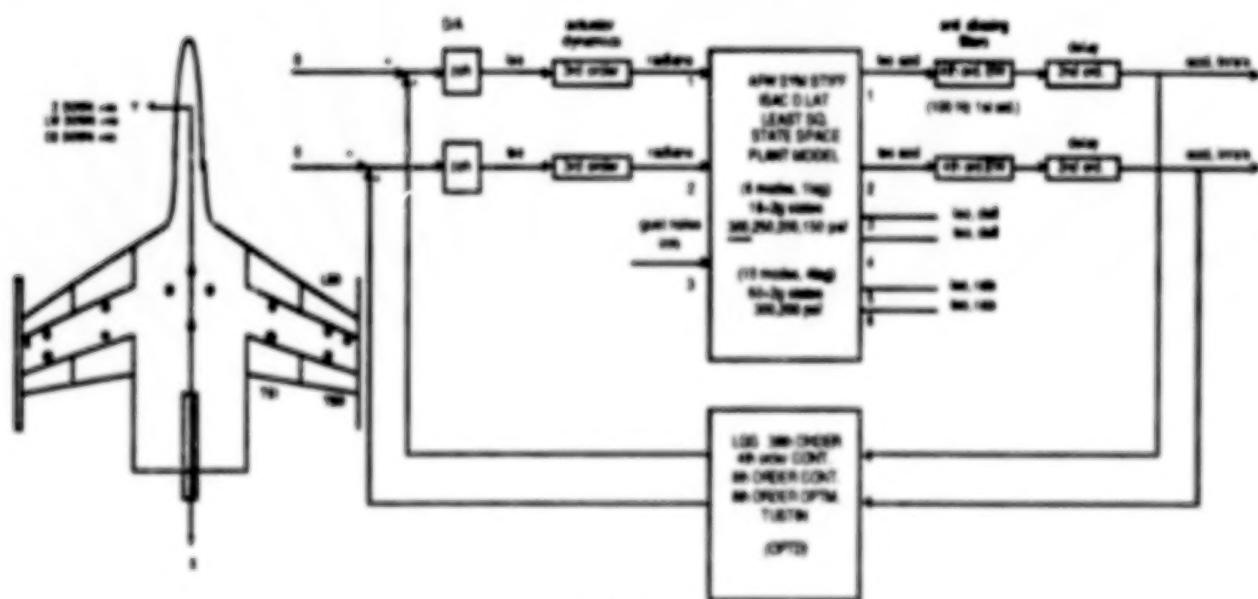


FIGURE 13

CONCLUSIONS

Constrained optimization technique was used to synthesize low order robust digital control law for large order flexible systems. The methodology provides a systematic design tool for control system synthesis where a large number of conflicting design requirements on the performance and stability robustness must be satisfied to arrive at a compromise solution. Both continuous and discrete control system can be synthesized and optimized. The procedure can be used to update a classical control law as well as a Kalman estimator based full or reduced order control law. The effects of digitization, antialiasing filters and computational delays can be included in the synthesis process. The synthesis procedure has been successfully applied to a gust load alleviation problem of a drone aircraft and a flutter suppression problem of the AFW wind tunnel aeroelastic model. Future applications include a rapid roll maneuver load control system design for the AFW wind tunnel model. A block diagram of the control scheme is shown in Figure 14. Control and vibration suppression of large space structures is another potential application area. The gradient expressions derived to facilitate rapid convergence of the optimization process can also be used for sensitivity study and integrated structure-control optimization formulation.

AFW RAPID ROLL CONTROL

Active Flexible Wing Rapid Roll Mechanization Wind Tunnel Model Digital Control

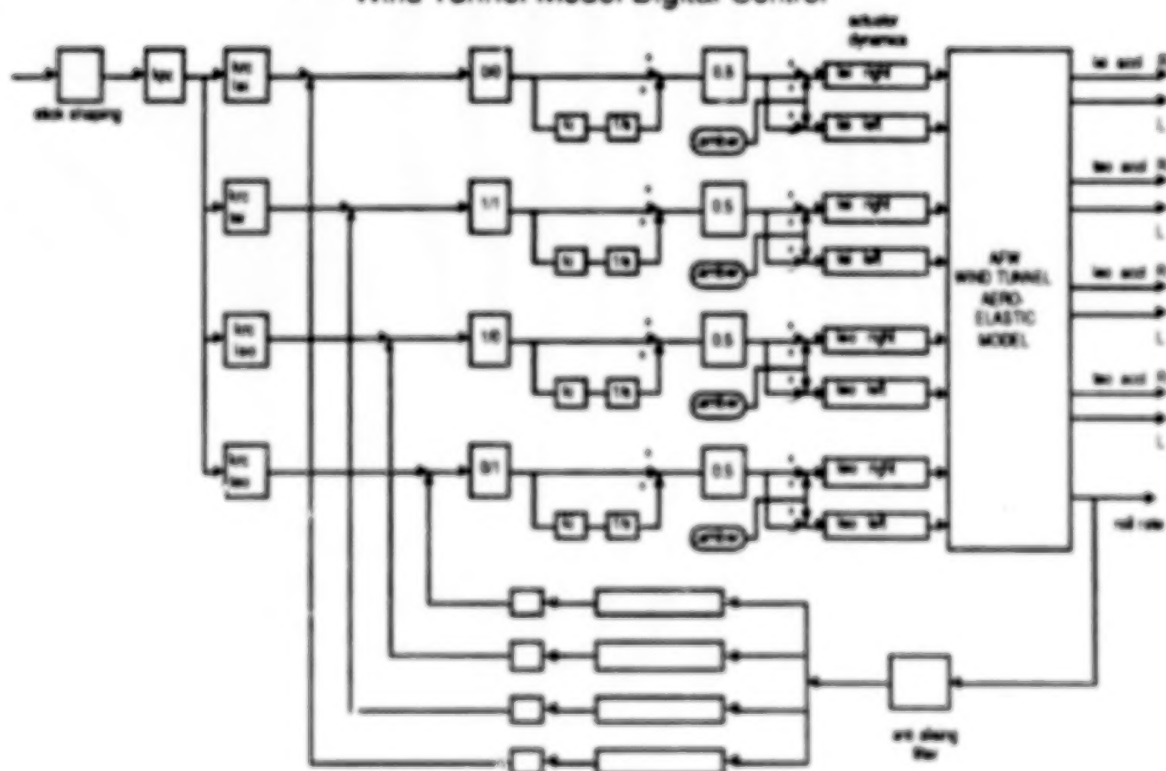


FIGURE 14

ACKNOWLEDGMENT

The research support through NASA Langley Contract NAS-18000 and technical discussion with Irving Abel, Tom Noll, Mike Gilbert and Boyd Perry of Structural Dynamics Division and Aeroservoelasticity Branch are gratefully acknowledged.

REFERENCES

1. Mukhopadhyay, V., Newsom, J. R. and Abel, I., "A Method for Obtaining Reduced Order Control Laws for High Order Systems Using Optimization Technique," NASA TP 1876, August 1981.
2. Mukhopadhyay, V., "Digital Robust Active Control Law Synthesis For Large Order Systems Using Constrained Optimization," AIAA Paper No. 87-2588, August, 1987.
3. Mukhopadhyay, V., "Stability Robustness Improvement Using Constrained Optimization Techniques," Journal of Guidance, Control and Dynamics, Vol. 10, No. 2, March-April 1987, pp. 172-177.
4. Vanderplatts, G. N., "CONMIN - A Fortran Program for Constrained Function Minimization - User Manual," NASA TM X 62282, August 1973.
5. Newsom, J. R. and Mukhopadhyay, V., "Application of Constrained Optimization to Active Control of Aeroelastic Response," NASA TM-83150, June 1981.
6. Martin, G. D. and Bryson, A. E. Jr., "Attitude Control of Flexible Spacecraft," Journal of Guidance, Control, and Dynamics, Vol. 3, pp. 37-41.
7. Gangsaas, D. and Ly, Uy-Loi, "Practical Gust Load Alleviation and Flutter Suppression Control Laws Based on LQG Methodology," AIAA Paper 81-0021, January 1981.
8. Mukhopadhyay, V., Newsom, J. R. and Abel, I., "Reduced Order Optimal Feedback Control Law Synthesis for Flutter Suppression," Journal of Guidance, Control, and Dynamics, Vol. 5, July-Aug. 1982, pp. 389-395.
9. Uy, Uy-Loi, "A Design Algorithm for Robust Low Order Controllers," Department of Aeronautics and Astronautics, Stanford University, SUDAAR Report No. 536, Nov. 1982.
10. Safonov, M. G. and Chiang, Y. A., "A Schur Method for Balanced Model Reduction," Proc. of 1988 American Control Conference, Atlanta, Ga., June, 1988, pp. 1036-1040.
11. Meyer, D. G., "A fractional Approach to Model Reduction," Proc. of 1988 American Control Conference, Atlanta, Ga., June, 1988, pp. 1041-1047.
12. Lenz, K. E., P. Khargonekar and Doyle, J. C., "Controller Order Reduction with Guaranteed Stability and Performance," Proc. of 1988 ACC, June 1988, pp. 1697-1698.

AN INTEGRATED APPROACH TO THE OPTIMUM DESIGN OF
ACTIVELY CONTROLLED COMPOSITE WINGS #

E. Livne⁺
Mechanical, Aerospace and Nuclear Engineering Department
University of California, Los Angeles
Los Angeles, California

+ Graduate Student

This research is supported by AFOSR Contract F 49620-87-K-0003.

670

INTRODUCTION AND OUTLINE OF THE PRESENTATION

The importance of interactions among the various disciplines in airplane wing design has been recognized for quite some time. With the introduction of high gain, high authority control systems and the design of thin, flexible, lightweight composite wings, the integrated treatment of control systems, flight mechanics and dynamic aeroelasticity became a necessity. A research program is underway now aimed at extending structural synthesis (Ref. 1) concepts and methods to the integrated synthesis of lifting surfaces, spanning the disciplines of structures, aerodynamics and control for both analysis and design. Mathematical modeling techniques are carefully selected to be accurate enough for preliminary design purposes of the "complicated, built-up lifting surfaces of real aircraft with their multiple design criteria and tight constraints" (Ref. 2, p.17). The presentation opens with some observations on the multidisciplinary nature of wing design. A brief review of some available state of the art practical wing optimization programs and a brief review of current research effort in the field serve to illuminate the motivation and support the direction taken in our research. (These reviews are not exhaustive, and the interested reader is referred to the review papers, Refs. 3-8.) The goals of this research effort will be presented next, followed by a description of the analysis and behavior sensitivity techniques used. The presentation will conclude with a status report and some forecast of upcoming progress (Figure 1.).

- BRIEF REVIEW OF CURRENT WING OPTIMIZATION CAPABILITIES AND RESEARCH ACTIVITY, SOME OBSERVATIONS
- GOALS FOR MULTIDISCIPLINARY WING SYNTHESIS RESEARCH AT UCLA
- DESCRIPTION OF ANALYSIS TECHNIQUES CHOSEN
- STATUS REPORT ON THE SYNTHESIS CAPABILITY UNDER DEVELOPMENT

Figure 1

THE MULTIDISCIPLINARY NATURE OF WING DESIGN

Figure 2 describes the multidisciplinary nature of wing design. Discussion is limited to wings operating in the subsonic to low supersonic flight speeds, so that thermal effects can be neglected. It is instructive to unite the sets of Preassigned Parameters and Design Variables (Ref. 1) into the set of "Design Parameters", whose elements define a particular wing design. Which of the parameters will be preassigned and which will be used as design variables depends on the level of application for optimization techniques in the hierarchy described in Ref. 1, namely, whether the design space includes sizing, configuration (geometry) or topological design variables. The set of behavior functions, from which constraints and objectives will be selected, can be divided into two categories. Primary (system level) Behavior Functions are those performance measures which determine the overall quality and competitiveness of the wing. Secondary (sub-system level) Behavior Functions are the behavior functions which must be taken into account during the design to guarantee the prevention of failure in all possible failure modes and introduce known constraints on subsystem performance. They are usually not the real design objectives although sometimes there is high correlation between a secondary behavior and a primary behavior function (e.g. mass and airplane performance).

<u>DISCIPLINE</u>	<u>STRUCTURES/ STRUCTURAL DYNAMICS</u>	<u>AERODYNAMICS</u>	<u>CONTROL</u>
<u>SIZING DESIGN PARAMETERS:</u> (DESIGN VARIABLES OR PREASSIGNED) PARAMETERS	ELEMENT SIZE (AREA, THICKNESS)	CAMBER, LE/TE CONTROL SURFACE DEFLECTION	GAINS, TRANSFER FUNCTION COEFFICIENTS
<u>CONFIGURATION DESIGN PARAMETERS</u>	PLANFORM SHAPE (SWEEP AR, TAPER RATIO) AIRFOIL CROSS SECTION, PLY ANGLE	PLANFORM SHAPE (SWEEP AR, TAPER RATIO) AIRFOIL CROSS SECTION	ORDER OF TRANSFER FUNCTIONS
<u>TOPOLOGICAL DESIGN PARAMETERS:</u>	NUMBER OF RIBS, SPARS, PLIES	NUMBER OF LE, TE CONTROL DEVICES	CONTROL SYSTEM STRUCTURE AND CONNECTIVITY
<u>SECONDARY BEHAVIOR FUNCTIONS:</u>	DEFLECTION/SLOPE, STRESS, BUCKLING, NATURAL FREQ'S, FATIGUE, LOAD FACTOR, MASS, CONTROL EFFECTIVENESS	DRAG, LIFT, CL MAX, DRAG POLAR, CONTROL EFFECTIVENESS	DYNAMIC STABILITY (INCLUDING FLUTTER, BODY FREEDOM FLUTTER), HINGE MOMENTS, CONTROL ACTIVITY
<u>PRIMARY BEHAVIOR FUNCTIONS:</u>	AIRPLANE PERFORMANCE : (ROLL RATE, TURN RATE, ENDURANCE, RANGE, COST...)		

Figure 2

SOME EXISTING PROGRAMS FOR PRACTICAL WING OPTIMIZATION

Several approaches, with a varying degree of multidisciplinary capability, aimed at the synthesis of practical composite wings were developed during the seventies (Refs. 3-8). In addition to the constraints on stress, displacement and aeroelastic stability, performance constraints in terms of induced drag or drag polar specification were added in the TSO computer code (Refs. 9,10) and to WIDOWAC (Refs. 11-13). It was reported recently that a rudimentary servoaeroelastic analysis capability was about to be inserted into the ASTROS computer code (Ref. 14). It should be noticed that except for the TSO code, the design space in the programs contains only structural design variables, thus they are really multidisciplinary in analysis only. The TSO code makes it possible to include some configuration design variables (the fiber orientation of cover skin layers) and some aerodynamic constraints in the form of wing twist or camber distribution under load (Figure 3).

PROGRAMS SURVEYED :

- TSO, FASTOP, WIDOWAC, ELFINI, ASTROS

ANALYSIS PROBLEM

DISCIPLINES :

- STRUCTURES, AERODYNAMICS, AEROELASTICITY.

MODELING :

STRUCTURAL :

- EQUIVALENT PLATE (TSO)
- FINITE ELEMENTS (FASTOP, WIDOWAC, ELFINI, ASTROS)

AERODYNAMIC :

STEADY AERODYNAMICS :

- LINEAR POTENTIAL PANEL METHODS (e.g. Woodward in TSO)

UNSTEADY AERODYNAMICS :

- DOUBLET LATTICE ($M < 1$) (TSO, FASTOP, ASTROS)
- KERNEL FUNCTION ($M < 1$) (WIDOWAC)
- MACHBOX ($M > 1$) (FASTOP)
- POTENTIAL GRADIENT METHOD ($M > 1$) (ASTROS)
- PISTON THEORY ($M > 1$) (WIDOWAC)

BEHAVIOR SENSITIVITY

- ANALYTIC (FASTOP, WIDOWAC, ELFINI, ASTROS)
- FINITE DIFFERENCES (TSO)

SYNTHESIS PROBLEM

PREASSIGNED PARAMETERS :

- PLANFORM SHAPE, CROSS SECTION, STRUCTURAL TOPOLOGY, MATERIALS

DESIGN VARIABLES :

- STRUCTURAL SIZING (TSO - ALSO FIBER ORIENTATION)

CONSTRAINTS :

- DEFLECTION, STRESS, FLUTTER, DIVERGENCE, CONTROL EFFECTIVENESS
- DRAG (TSO, WIDOWAC)
- BUCKLING (ELFINI, ADDED TO WIDOWAC IN A SIMPLIFIED FORM)

OBJECTIVE FUNCTIONS :

- MASS, DRAG, CONTROL EFFECTIVENESS

OPTIMIZATION

- MATH PROGRAMMING (TSO)
- MATH PROGRAMMING + APPROXIMATION CONCEPTS (WIDOWAC, ELFINI, ASTROS)
- OPTIMALITY CRITERIA (FASTOP)

Figure 3

THE NEED FOR MULTIDISCIPLINARY WING OPTIMIZATION

During the last decade structural synthesis has matured. Realistic designs described by a large number of design variables and subject to a variety of load conditions can now be efficiently treated. However, it is still quite common to find fixes and modifications being introduced late in the development stage of fighter aircraft, when aeroservoelastic effects, rigid body- elastic mode coupling or static aeroelastic effects have not been properly accounted for in the design process (Refs. 15-20). At the same time, following almost twenty years of progress in active flutter suppression and gust alleviation (Refs. 22-26), there is a growing recognition that multidisciplinary interactions might be harnessed to benefit modern, complex wing designs. However, a review of the literature reveals that the application of modern optimization methods to wing design problems involving multiple objective functions and a diverse mix of constraints based on analyses from several discipline areas (e.g. structures, structural dynamics, controls, aerodynamics and performance) has not yet been treated in a comprehensive and realistic manner. To overcome the inherent complexity and address the computationally intensive nature of this problem two approaches have been suggested in the literature. The first approach is based on the application of multi-level decomposition techniques combined with existing tools for detailed analysis and sensitivity analysis for each of the disciplines (Refs. 27,28). The second approach attempts to gain some insight into the nature of the problem by using highly simplified mathematical models or simple airplane configurations for structural, aerodynamic and control system analysis (Refs. 29-35). Research is now under way in several research centers and universities in two main directions :

- a) the addition of control system sizing type design variables to a design space spanning design variables for structures and control (control augmented aeroelastic optimization) (Refs. 31,36)
- b) expanding the wing design space by adding configuration design variables (structural and aerodynamic shape) (Refs. 37-39) (Figure 4.).

MOTIVATION :

PROBLEMS :

- * SERVOAERELASTIC INTERACTIONS
- * INSUFFICIENT CONTROL EFFECTIVENESS
- * BODY FREEDOM FLUTTER

HARNESS MULTIDISCIPLINARY INTERACTIONS FOR ACHIEVING BETTER DESIGNS

CURRENT DIRECTIONS IN RESEARCH :

OPENING UP A SIZING DESIGN SPACE TO INCLUDE SIZING TYPE CONTROL SYSTEM DESIGN VARIABLES

OPENING UP THE DESIGN SPACE TO INCLUDE STRUCTURAL AND AERODYNAMIC SHAPE DESIGN VARIABLES

PROBLEMS :

- * HEAVY COMPUTATIONAL COST OF ANALYSIS
- * LACK OF INTUITION AND EXPERIENCE TO GUIDE IN CONSTRUCTING ROBUST APPROXIMATIONS
- * ABSENCE OF STANDARD TERMINOLOGY, CRITERIA, MODELING AND ANALYSIS METHODS WIDELY ACCEPTED IN ALL DISCIPLINES

APPROACHES TO THE PROBLEM :

- * SIMPLIFIED MODELING (BEAM,STRIP THEORY) OR STUDIES INVOLVING SIMPLE CONFIGURATIONS (SAILPLANES) -
ONE LEVEL OPTIMIZATION
GAIN INSIGHT
- * MULTILEVEL DECOMPOSITION BASED ON DETAILED MODELING AND SENSITIVITY ANALYSIS

Figure 4

RESEARCH GOALS

In Ref. 2 Ashley writes : " In the absence of experience when new technology is being tried for the first time, the search for *extremas* can produce unanticipated, surprising and often very satisfactory discoveries". But he adds a word of caution : "Yet the counterintuitive may also be counterproductive and even ridiculous. Very undesirable consequences can result from omission or careless handling of constraints".

It is one of the major goals of the present research to begin to bridge the gap between over idealized modeling and detailed structural and aerodynamic modeling by introducing balanced design and analysis models that capture the essential behavior characteristics, without making the integrated multidisciplinary design optimization task intractable. This balanced approach combines high quality, approximate, but computationally efficient analyses for the structural, aerodynamic and aeroservoelastic behavior of realistic composite wings. Thus, the entire optimization problem may be treated at one level without the need for multilevel decomposition. A rich variety of constraints makes it possible to study the effect of multidisciplinary interactions on synthesis as well as on analysis (Figure 5).

OBJECTIVES :

DEVELOP MULTIDISCIPLINARY WING SYNTHESIS CAPABILITY WITH AN
EMPHASIS ON STRUCTURE/CONTROL/UNSTEADY AERODYNAMICS
INTERACTION

BRIDGE THE GAP IN MODELING DETAIL BETWEEN THE VERY SIMPLE AND
DETAILED ANALYSIS TECHNIQUES SO AS TO ENABLE MULTIDISCIPLINARY
SYNTHESIS OF REAL WINGS FOR PRELIMINARY DESIGN

STUDY THE CONSTRUCTION OF ROBUST APPROXIMATIONS TO BEHAVIOR
FUNCTIONS

PROVIDE A TEST CASE FOR ASSESSING DECOMPOSITION TECHNIQUES

SELECTED APPROACH

ANALYSIS :

CAREFUL SELECTION OF ANALYSIS TECHNIQUES -
GOOD ACCURACY
HIGH COMPUTATIONAL SPEED
BALANCED APPROACH

BEHAVIOR SENSITIVITY :

ANALYTIC

SYNTHESIS PROBLEM :

SIZING :
STRUCTURAL/AERODYNAMIC AND CONTROL D.V.'s PLUS θ , $\dot{\theta}$

PREASSIGNED : SHAPE, TOPOLOGY

CONSTRAINTS : δ , ω , SERVOAEROELASTIC STABILITY, CONTROL POWER

ALTERNATIVE OBJECTIVE FUNCTIONS : MASS, PERFORMANCE MEASURES

OPTIMIZATION STRATEGY :

MATH PROGRAMMING + APPROXIMATION CONCEPTS
(10 ANALYSES PER OPTIMIZATION - GOAL)

Figure 5

ANALYSIS METHODS SELECTED

The integrated optimum design capability outlined here is based on approximate analysis techniques for the required disciplines, which are consistent with each other in terms of accuracy and efficiency and lead to a balanced treatment. In the structures area, an equivalent plate analysis, as incorporated in the TSO computer code (Ref. 10) and further generalized by Giles (Refs. 37-39), is used. Although the equivalent plate approach for structural modeling of low aspect ratio wings has been known for many years, it was Giles who recently showed that, using present day computers, a single high order power series can be used for approximating displacements over wing planforms made of several trapezoidal segments to obtain accurate stress as well as displacement information. The simplicity of manipulating simple power series leads to analytic rather than numerical integration for the mass and stiffness expressions. With the careful organization of computer storage space and ordering of calculations, major savings can be achieved in terms of computation times and core storage requirements. The extended equivalent plate approach is integrated with the PCKFM (Piecewise Continuous Kernel Function Method) of Nissim and Lottati for lifting surface unsteady aerodynamics (Refs. 40-43). This method combines the power of the doublet lattice method in dealing with pressure singularities with the accuracy and speed of the kernel function method. Extensive numerical experimentation has demonstrated (Ref. 40) that the PCKFM method is highly accurate and converges rapidly. For configurations involving control surfaces, it is faster and considerably more accurate than the doublet lattice method. Thus, it is especially suited for calculating the generalized unsteady air loads (on lifting surfaces made up of wing and control surface elements) that are needed for active flutter suppression and gust alleviation studies.

For the finite state modeling of the unsteady air loads, the Minimum State Method of Karpel (Ref. 44) is used to generate accurate approximations to unsteady generalized aerodynamic forces with addition of only a small number of augmented states to the mathematical model of the aeroservoelastic system. In comparison with other finite state modeling techniques, the number of added states needed in the minimum state method can be smaller for the same overall accuracy of approximation (Ref. 45). This leads to a state space model of lower order, thus reducing memory requirements and computation times considerably. The integrated servoaeroelastic system is modeled as a Linear Time Invariant (LTI) system and its stability is examined by computing the eigenvalues of a generalized eigenvalue problem (Figure 6).

STRUCTURE:

EQUIVALENT PLATE

AERODYNAMICS:

SUBSONIC/SUPERSONIC LIFTING SURFACE PIECEWISE CONTINUOUS KERNEL
FUNCTION METHOD (PCKFM) (NISSIM/LOTTATI)

UNSTEADY AERODYNAMIC FINITE STATE MODELING:

MINIMUM STATE APPROXIMATION

CONTROL:

STATE SPACE LTI SYSTEM MODELING

Figure 6

EQUIVALENT PLATE MODELLING OF AIRPLANE/ WING/ CONTROL SURFACE ASSEMBLIES BY THE PRESENT CAPABILITY

Figure 7 shows an airplane modeled as an assembly of flexible lifting surfaces. Each lifting surface is modeled as an equivalent plate whose stiffness is controlled by contribution from thin cover skins (fiber composite laminates) and the internal structure (spar and rib caps). Plate sections are connected to each other via stiff springs (to impose displacement compatibility at attach points) and flexible springs (representing the stiffness of actuators and their backup structure). Each wing section can be made of several trapezoidal parts continuously connected to each other. Concentrated masses are used to model nonstructural items and balance masses.

The present equivalent plate modeling capability makes it possible to efficiently analyze combined wing box/control surface configurations. A wing assembly and a canard or horizontal tail may be attached to a fuselage (modeled as a flexible beam or a flexible plate) to simulate complete airplane configurations. Modeling detail of all plate sections can be identical. Thus the degree of detail in modeling control surfaces for analysis and synthesis is not limited, as is the case in the TSO code.

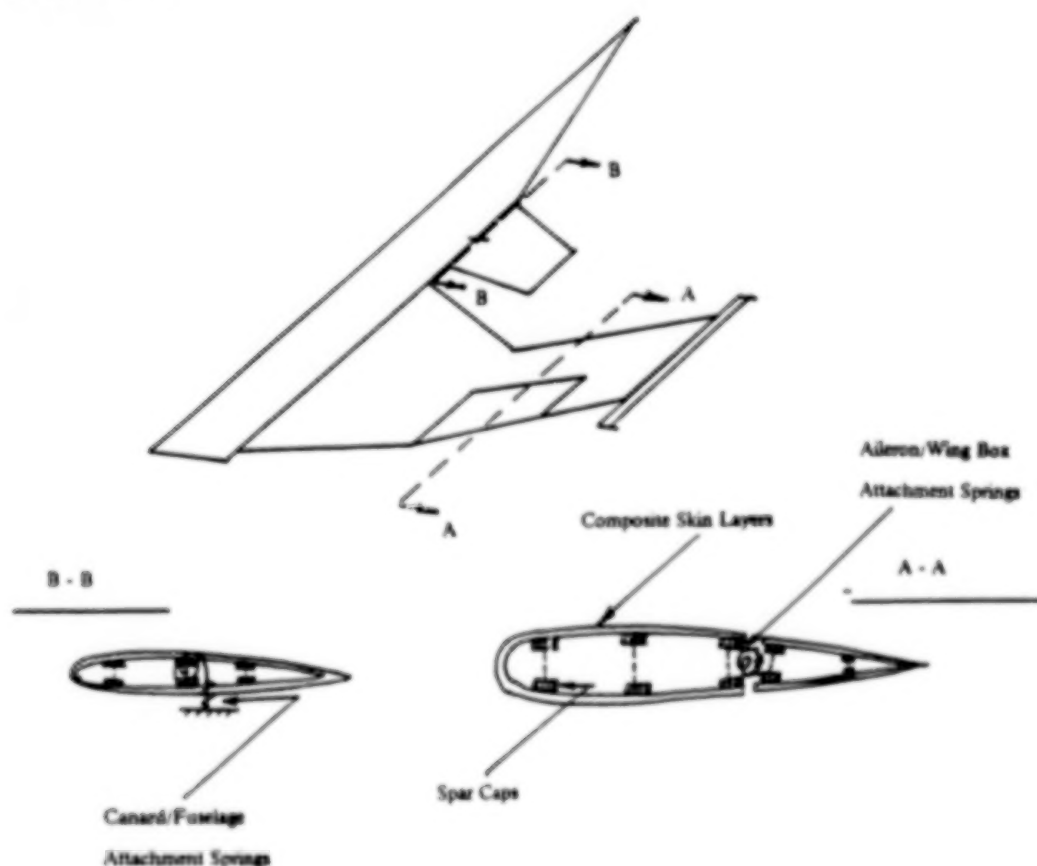


Figure 7

SOME ANALYTICAL ASPECTS OF THE EQUIVALENT PLATE APPROACH

It is a well known fact in the numerical solution of partial differential equations that the use of a simple polynomial series to approximate the solution in a Ritz or Galerkin analysis leads to ill conditioning of the problem matrices when it is of an order higher than a certain degree. However, Giles (Refs. 37,38) has shown that when a simple polynomial series is used in a Ritz solution of anisotropic plate static and dynamic problems, accurate displacements, stresses and natural frequencies can be obtained for practical wings before ill conditioning appear. His results were obtained on a CDC Cyber 173 (60 bit words). Our results obtained on an IBM 3090 computer in extended precision and on a SUN 3/280 computer using double precision support his findings. When the depth of the wing and the thickness distribution of skin layers are also expressed as power series, it can be shown that the stiffness and mass matrices are expressed as linear combinations of certain area and line integrals and polynomial terms calculated at points where wing section are connected or where concentrated masses are placed. These integrals and polynomial tables are fixed once a planform shape is given. Thus they are evaluated only once at the beginning of an optimization task. This leads to major computation time savings along with the fact that the relatively small number of generalized coordinates needed to accurately approximate displacement and stresses in a wing section (about 21-30) result in small mass and stiffness matrices(although fully populated) compared with finite element analysis (Figure 8.).

POLYNOMIAL FUNCTIONS:

THE SHAPE FUNCTIONS : $f(x,y) = x^m y^n$ ($m = m(i)$, $n = n(i)$)

A TYPICAL SKIN LAYER THICKNESS DISTRIBUTION : $t(x,y) = \sum_{i=1}^{m_0} T_i x^m y^n$
(k_i DEPEND ON i)

WING DEPTH : $h(x,y) = \sum_{i=1}^{m_0} H_i x^m y^n$ ($r_{i,j}$ DEPEND ON i)

SPAR/RIB CROSS SECTIONAL AREA : $A(x) = A_0 + A_1 x$

FUNDAMENTAL INTEGRALS:

AREA INTEGRAL OVER A SKIN TRAPEZOIDAL SECTION : $I_{mn} = \iint x^m y^n dx dy$

LINE INTEGRAL OVER THE LENGTH OF A RIB : $I_{2n}^R = \int_{y_1}^{y_2} x^n dx$

LINE INTEGRAL OVER THE LENGTH OF A SPAR : $I_{2m}^S = \int_{x_1}^{x_2} x^m y^n dx$

ASSEMBLY:

MASS AND STIFFNESS MATRICES ARE LINEAR COMBINATIONS OF THESE INTEGRAL TERMS WITH VARYING INDICES : (m,n)

DISPLACEMENT RITZ SERIES FOR TWO WING SECTIONS CONNECTED TO EACH OTHER VIA SPRINGS:

$w_1 = [\dots (x_1)^{m_1} (y_1)^{n_1} \dots] \{ q_i \}$ $w_2 = [\dots (x_2)^{m_2} (y_2)^{n_2} \dots] \{ q_i \}$

FUNDAMENTAL POLYNOMIAL TERM TABLES:

$x_1^m y_1^n$, $x_2^m y_2^n$, $x_1^m y_2^n$, $x_2^m y_1^n$

ASSEMBLY:

ATTACHMENT CONTRIBUTION TO STIFFNESS MATRIX IS A LINEAR COMBINATION OF POLYNOMIAL TERMS TAKEN FROM THE FUNDAMENTAL TABLES.

Figure 8

FEATURES OF THE PRESENT EQUIVALENT PLATE MODELLING

In order to structurally analyze (statics and dynamics) wing/control surface/ canard or tail configurations and to accelerate the generation of approximate problems for synthesis, the equivalent plate approach of Giles was further extended to include multi-element wing box/control surfaces plus analytic behavior sensitivity derivatives with respect to structural design variables. Stiffness and mass matrices can now be generated using analytic integration for wing structures made of composite skins, spars and ribs, concentrated masses and equivalent springs which connect plate sections to each other (Figure 9).

CONFIGURATIONS MODELLED INCLUDE :

WING/ CONTROL SURFACE/ CANARD/ FUSELAGE ASSEMBLIES

FUSELAGE AND MISSILES CAN BE MODELLED AS EQUIVALENT BEAMS

DESIGN VARIABLES INCLUDE :

SKIN LAYER THICKNESS DISTRIBUTION POLYNOMIAL COEFFICIENTS,

SPAR/ RIB CAP AREA DISTRIBUTION (LINEAR ALONG SPAR/RIB LINE)

CONCENTRATED MASSES

LINEAR AND ROTATIONAL SPRING STIFFNESSES

ANALYSIS CAPABILITY :

FAST STIFFNESS,MASS MATRIX GENERATION

STATIC SOLUTION FOR DISPLACEMENTS AND STRESSES UNDER GIVEN LOADS

CALCULATION OF NATURAL FREQUENCIES AND MODE SHAPES

SENSITIVITY :

ANALYTIC BEHAVIOR SENSITIVITY ANALYSIS FOR DISPLACEMENTS, SLOPE, QUADRATIC FAILURE CRITERIA FOR STRESSES IN SKINS, STRESSES IN SPAR RIB CAPS

ADJOINT OR DIRECT METHOD - OPTIONAL

Figure 9

NUMERICAL TESTING

Extensive numerical tests were carried out to study the accuracy of the present equivalent plate modeling and assess its computational efficiency. Several wings of different construction, aspect ratio and thickness were used. Displacements, stresses in skins and spar caps as well as natural frequencies and mode shapes were compared to finite element results and to test results where available. As an example, Figure 10 includes a comparison between YF16 wing natural frequencies calculated using a detailed finite element analysis, the TSO program and our present structural module. The YF16 wing configuration includes a wing box plus a leading edge flap and a flaperon. The results demonstrate the accuracy of the new multi-element equivalent plate modeling capability in analyzing wing/ control surface configurations. Some ground vibration test results available in Ref. 46 made it possible to check the accuracy of the present code when a fuselage, wing, control surfaces and tip missile configuration is analyzed. Although the first bending frequency of the cantilevered wing as calculated here is 6.5% below the reference result, it is somewhat sensitive to the modeling of root structure and a better correlation can be achieved by tuning the springs representing root and wing-fuselage attachment flexibility. Overall the correlation is good, and further refinement of the model seems unnecessary at this stage.

EQUIVALENT PLATE CAPABILITY TESTING

NATURAL FREQUENCIES (HZ) OF THE YF16

CANTILEVERED WING/LE FLAP/

FLAPERON ASSEMBLY

F-F A/C WITH WING TIP

MISSILES (ANTI-SYMMETRIC)

No.	F.E.M (REF.10)	TSO (REF.10)	PRESENT CODE	No.	GVT (REF.46)	PRESENT CODE
1	10.67	10.74	9.98	1	6.5	6.30
2	33.92	35.05	34.98	(Missile		
3	35.78	42.75	36.48	Pitch)		
4	56.45	64.24	54.02	2	8.0	7.99
5	62.47	73.43	65.28	(Wing 1st		
6	67.96	95.31	73.57	Bending)		

Figure 10

208

NUMERICAL TESTING (CONCLUDED)

The first six mode shapes for the cantilevered YF16 example (without tip missile), generated by the new multi-element equivalent plate analysis, are shown in Fig. 11. These mode shapes correlate well with finite element results reported in Ref. 10. The quality of this correlation can be attributed to the high order of control surface displacement representation and better modeling of elastic point attachment of the control surfaces to the wing box.

A typical computation time for the static analysis of the wing of Ref. 37 (including the calculation of 384 displacement, slope and stress constraints and their sensitivities with respect to inner and outer panel skin thicknesses at an array of points over the wing) is 12.6 cpu seconds on the UCLA IBM 3090. Analysis and constraint generation for YF16 six static load cases and natural modes take 18.9 seconds. These relatively short computation times are essential to the construction of an efficient multidisciplinary synthesis capability.

MODE SHAPES OF THE YF16 CANTILEVERED WING

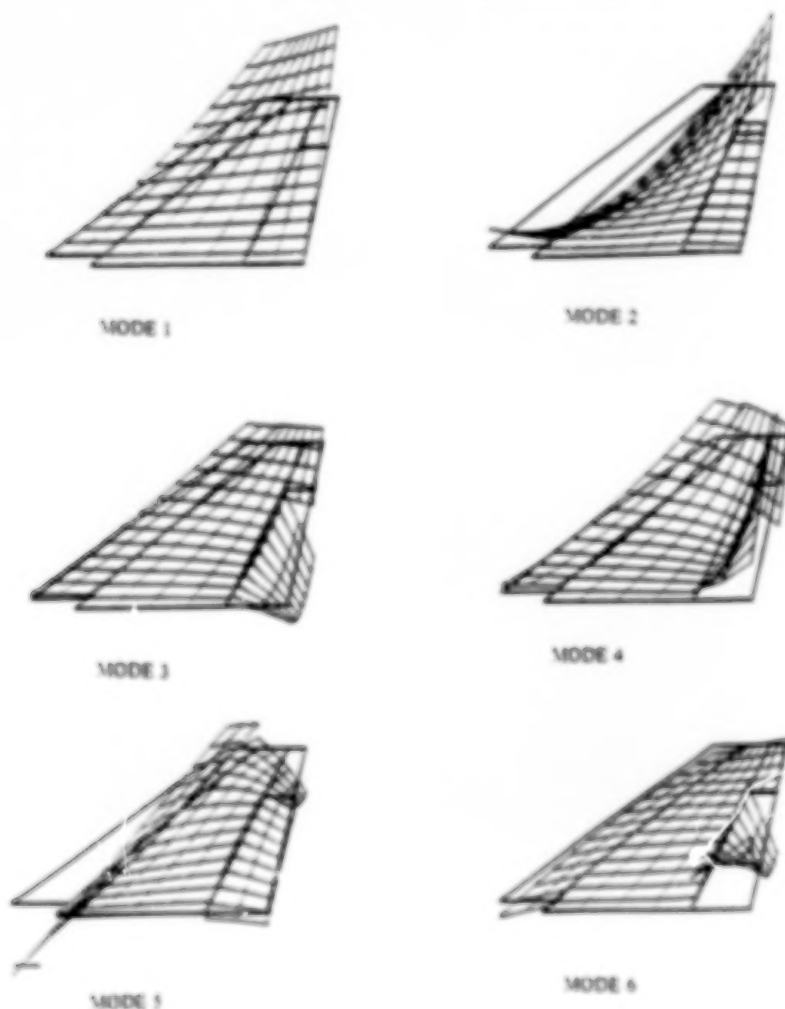


Figure 11

369

LIFTING SURFACE UNSTEADY AERODYNAMICS :THE PCKF METHOD

Along the line of improving the mathematical modeling of the servoaeroelastic wing dynamic system, the use of lifting surface theory (Refs. 47,48) for the calculation of the unsteady aerodynamic loads is considered a definite step forward compared with strip theories. Lifting surface aerodynamics are still widely accepted in the aerospace industry for the flutter and gust response analysis of airplanes in the subsonic and supersonic speed regimes. Thus including lifting surface modeling in the analysis part of a multidisciplinary wing synthesis is important if the synthesis of real wings is sought.

In the PCKF method for the solution of the integral equation relating downwash and pressure distribution over a lifting surface (Refs. 40-43) an assembly of lifting surfaces is divided into a group of trapezoidal boxes, as shown in Fig. 12 for a subsonic case.

MODELING A CONFIGURATION BY AN ASSEMBLY OF TRAPEZOIDAL BOXES : (SUBSONIC)

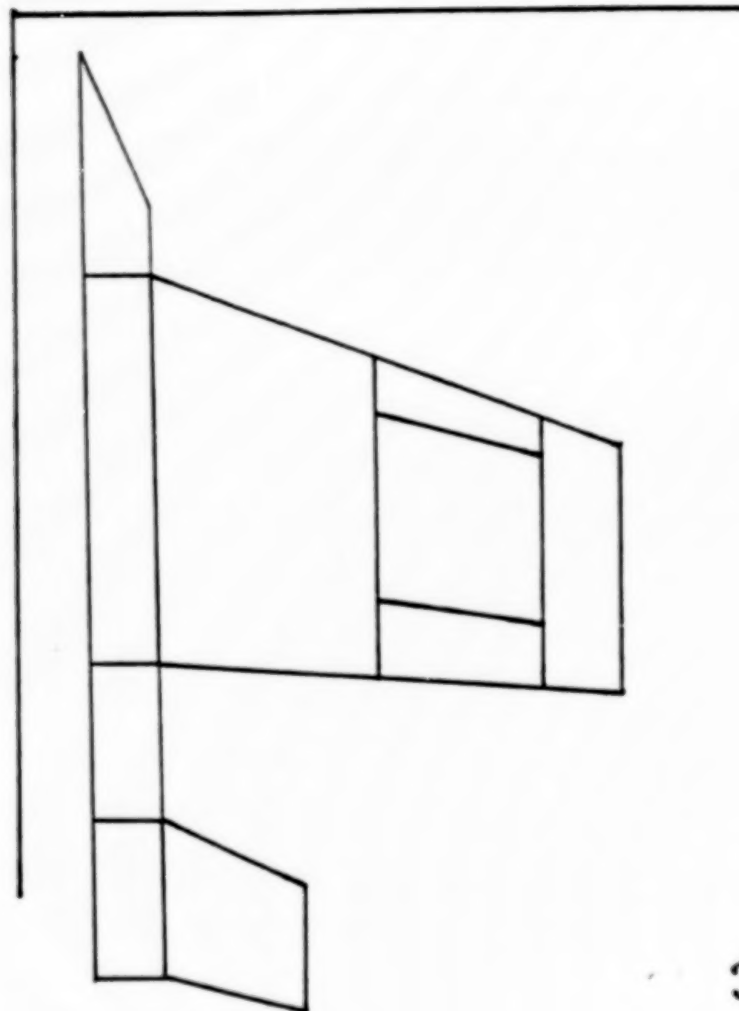


Figure 12

THE PCKF METHOD : SOME ANALYTICAL ASPECTS

The pressure distribution on each box is approximated by weighting functions representing the known pressure singularities along the box edges multiplied by a series of polynomials orthogonal to these weighting functions. Collocation points over the planform are chosen so as to minimize the error in the pressure integrals needed to calculate generalized aerodynamic forces. The PCKF method is fast, accurate and especially suited to handle wing/control surface configurations. It is more accurate than the vortex lattice method especially when leading edge flaps or controls with gaps around them are considered (Ref. 40). This is due to the inability of lattice methods to impose the pressure singularities along the different boundaries of the wing. In the present application it is integrated with the equivalent plate structural analysis to generate a set of generalized loads for the same generalized polynomial coordinates used for structural analysis. The number of collocation points per box and the number of integration points used are carefully selected to be compatible with the order of displacement polynomials used (Figure 13).

POLYNOMIAL SERIES APPROXIMATION FOR PRESSURE OVER A BOX :

$$\frac{\Delta p(\xi, \eta)}{q_D} = \sum_{j=1}^{n_{span}} \sum_{i=1}^{n_{chord}} A_m W(\eta) p(\eta) w(\xi) p(\xi)$$

where $m = (j - 1)n_{chord} + i$

$W(\eta), w(\xi)$:

WEIGHT FUNCTIONS REPRESENTING KNOWN PRESSURE SINGULARITY ALONG BOX EDGES

COLLOCATION POINT PLACEMENT : OPTIMAL SO AS TO MINIMIZE ERROR IN PRESSURE INTEGRALS (GENERALIZED AERODYNAMIC FORCES)

ADVANTAGES :

SUBSONIC / SUPERSONIC

GENERAL NON PLANAR WING/CONTROL SURFACE CONFIGURATIONS

FAST CONVERGENCE OF GENERALIZED LOADS WITH INCREASED NUMBER OF POLYNOMIALS - HIGH COMPUTATIONAL SPEED

GOOD ACCURACY OF CONTROL SURFACE HINGE MOMENT AND CONTROL SURFACE DERIVATIVES (VORTEX LATTICE METHOD OVERPREDICTS HINGE MOMENTS) - IMPORTANT FOR SERVOAEROELASTIC MODELING

EXTENSIVE NUMERICAL TESTING BY THE DEVELOPERS FOLLOWED BY ACCURATE RESULTS IN THE FLUTTER AND SERVOAEROELASTIC ANALYSIS OF THE F16 IN AN INDUSTRY ENVIRONMENT

A DEFINITE IMPROVEMENT OVER STRIP THEORIES

Figure 13

371

UNSTEADY AERODYNAMICS FINITE STATE MODELING

The generalized aerodynamic loads in the Laplace transformed small perturbation equations of motion (for a steady level flight) given below are transcendental functions of the Laplace variable s . The flight dynamic pressure and flight speed are q_D, U_∞ respectively; M, C, K are the mass, damping and stiffness matrices; $Q(s, Mach)$ is the matrix of generalized aerodynamic forces in the Laplace domain; $w_d(s)$ is the Laplace transformed vertical gust velocity; S is a reference area and $\{q(s)\}$ is the vector of Laplace transformed generalized displacements.

To use modern control system analysis and design techniques, it is necessary to cast them in Linear Time Invariant (LTI) state space form. The common practice is to match rational function approximations to generalized aerodynamic loads calculated for harmonic motion at a set of reduced frequencies (Ref. 45). There is a resulting increase in the order of the LTI state space model due to the addition of aerodynamic states. This increase in size can be quite significant. With n generalized displacements, each lag term in the commonly used Roger approximation (see Ref. 45 for further detail) adds n states to the model order. Since four lag terms are usually needed for a reasonable approximation in this method, $4n$ states are added to the system. This makes it computationally expensive to carry out any control system analysis and behavior sensitivity analysis using state space techniques. In the Minimum State Method of Karpel (Ref. 44), the functional dependence of the generalized aerodynamic force matrix on the Laplace variable, is approximated by a rational expression of a special form so as to reduce the number of added states needed to achieve given quality of fit.

Given the generalized aero forces in simple harmonic motion for a number of reduced frequencies, it is possible to match the approximation exactly to the data for $k=0$ and one other reduced frequency. This determines the matrices P_1, P_2, P_3 . Choosing R to be a diagonal matrix with negative elements, the matrices D and E are determined in an iterative process so that the approximation fits the rest of the data in a least-squares manner (Figure 14.).

THE SMALL PERTURBATIONS LAPLACE TRANSFORMED EQ. OF MOTION OF AN ELASTIC AIRPLANE IN LEVEL FLIGHT :

$$s[M]s^2 + [C]s + [K]\{q(s)\} = q_D S [Q(s, Mach)]\{q(s)\} = q_D S [Q_0(s, Mach)] \frac{w_d(s)}{U_\infty}$$

PURPOSE OF FINITE STATE MODELING : CAST EQ. OF MOTION IN LINEAR TIME INVARIANT STATE SPACE FORM

PRINCIPLE : RATIONAL FUNCTION APPROXIMATIONS OF UNSTEADY AIRLOADS IN TERMS OF LAPLACE VARIABLE

PRICE : ADDED STATES

MINIMUM STATE APPROXIMATION FORM :

$$[Q_0] = \{P_1\}s^2 + \{P_2\}s + \{P_3\} + [D](sI - R)^{-1}[E]s$$

MATCHING PROCESS :

- * GENERALIZED AERO FORCES ARE GIVEN FOR HARMONIC MOTION AT A SET OF REDUCED FREQUENCIES
- * A SET OF AERODYNAMIC LAG TERMS IS CHOSEN : R_k
- * P_3 IS EQUATED TO $Q(k=0)$
- * P_1, P_2 ARE EXPRESSED IN TERMS OF D.E SO AS TO ENSURE PERFECT FIT AT A SELECTED REDUCED FREQUENCY k_f
- * D.E ARE DETERMINED IN AN ITERATIVE LEAST-SQUARES PROCESS TO FIT THE REST OF THE DATA

ADVANTAGE :
MINIMAL INCREASE IN MODEL ORDER

PROBLEMS :

ITERATIVE PROCESS IS TIME CONSUMING

RELATIVELY LITTLE EXPERIENCE WITH REAL CONFIGURATIONS

Figure 14

SOME PRELIMINARY MINIMUM STATE FITS TO A LARGE MATRIX OF UNSTEADY AERODYNAMIC GENERALIZED FORCES

Order reduction of the state space model used for servoacoustic stability and control analysis is essential for synthesis purposes in order to make the analysis cycle as computationally fast as possible. This motivates the choice of the Minimum State Approximation for finite state unsteady aerodynamic modeling in the current research. Preliminary tests of the quality of approximation achieved when applied to a large matrix of generalized aerodynamic forces show promising results. A 44×44 matrix of generalized aero forces for the YF16 airplane with tip missiles is approximated using only 22 lag terms. Comparison with a one lag term Roger approximation (which will add 44 aerodynamic states to the model) shows an advantage of the minimum state approach (Figure 15.).

SOME RECENT EXAMPLES OF QUALITY OF FIT FOR A YF16 COMPLETE A/C CONFIGURATION :

(44 POLYNOMIAL GENERALIZED COORDINATES)

SOME LOW ORDER SHAPE FUNCTIONS FOR THE WING BOX
 $f_1(x,y) = 1$, $f_2(x,y) = x$, $f_3(x,y) = x^2$

A HIGHER ORDER SHAPE FUNCTION : $f_{11}(x,y) = x^4$

ROGER APPROXIMATION BASED ON 1 LAG (44 ADDED STATES)

MINIMUM STATE BASED ON 22 LAGS (22 ADDED STATES)

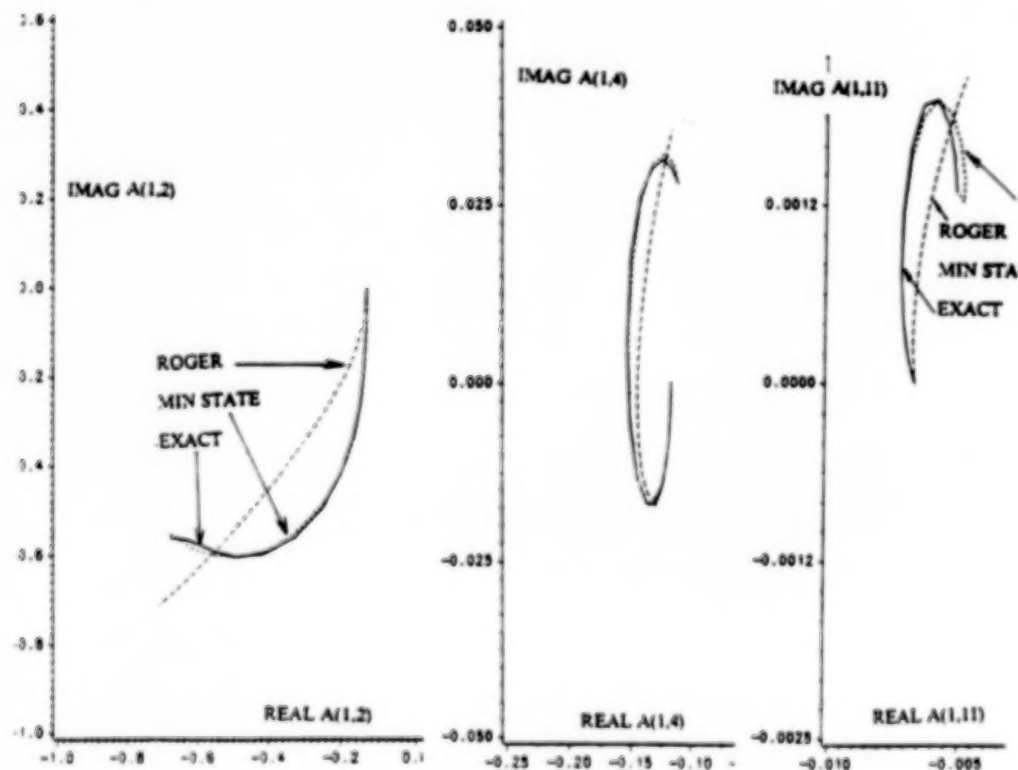


Figure 15

CONTROL SYSTEM MODELING

A block diagram of the actively controlled servoaeroelastic system is shown in figure 16. Airplane motions (acceleration and angular rates) are sensed by a set of sensors placed at different points on the structure. The resulting signals are used as inputs to the control law block which commands control surface actuators. The control surface motions guarantee stability and desirable dynamic response of the complete system.

For the control system, only sizing type design variables are considered at present to keep the balance in our approach, and these are the coefficients of numerator and denominator polynomials in the control law transfer functions. Control surface locations, sensor locations, the structure of the control system and order of transfer functions are preassigned. It is assumed that sensor and actuator transfer function are given, although the formulation is general enough to allow treating their elements as design variables as well.

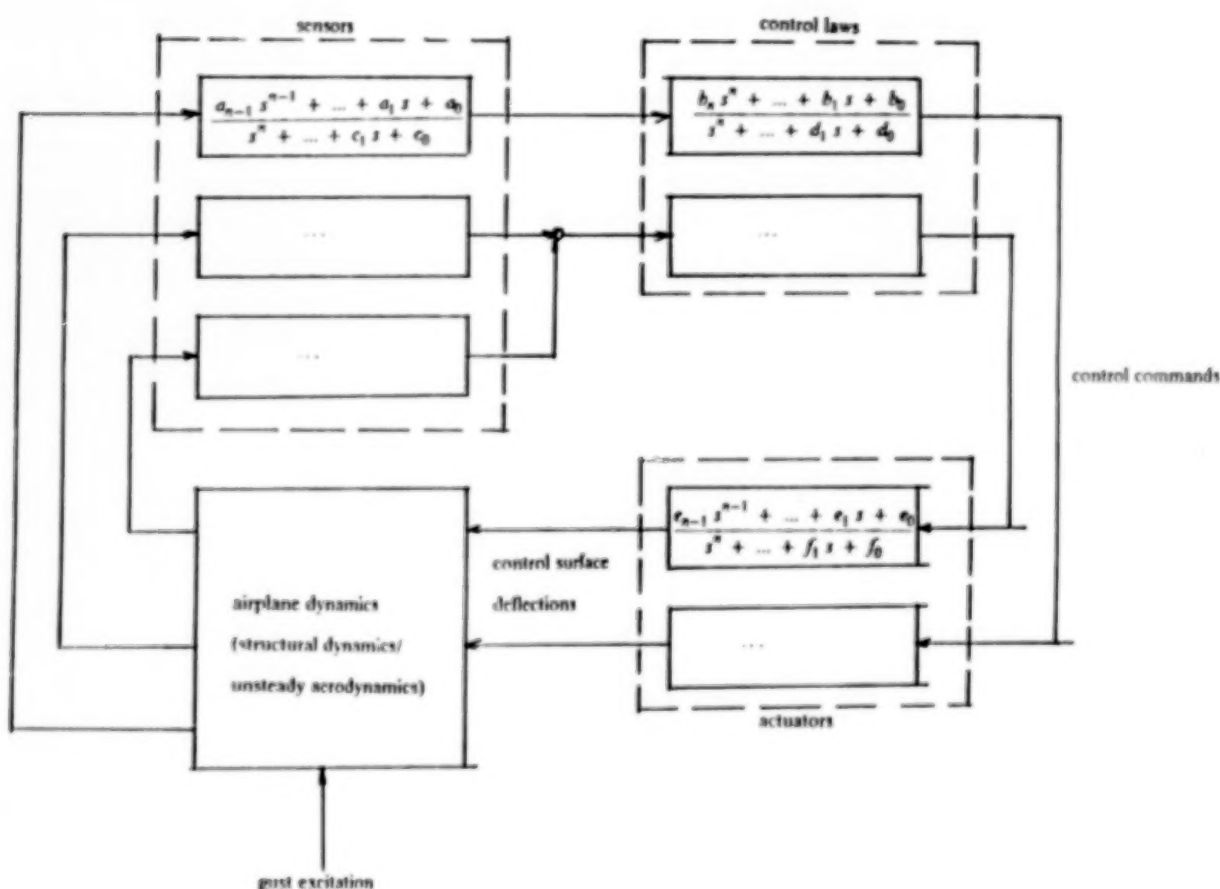


Figure 16

LTI STATE SPACE MODEL AND STABILITY ANALYSIS

Formulations of the state space control augmented servoacoustic equations of motions can be found in many works on active flutter suppression (e.g. Ref. 49). A transfer function model of an element of the control system (whether sensor, actuator or a control law) can be transformed into a state space model, where the A, B, C and D matrices are explicitly expressed in terms of the transfer function numerator and denominator polynomial coefficients. Assembly of the sensor, actuator, control law, structural dynamics, gust and unsteady aerodynamics state space models leads to the system matrices U, V and W in a LTI state space model of the whole system. These matrices are functions of the structural design variables through their dependence on the stiffness and mass matrices. They depend on the control system design variables through their dependence on the state space models of the control elements.

For given flight conditions (Mach number and altitude) the stability of the system is determined by the real part of the eigenvalues of a generalized eigenvalue problem. Sensitivity of a critical eigenvalue with respect to any design variable, p , is calculated using standard eigenvalue sensitivity analysis based on the derivatives: $\partial U/\partial p$, $\partial V/\partial p$ and the left and right corresponding eigenvectors $\{\psi\}$, $\{\phi\}$. It is planned to use the original Ritz functions directly as generalized coordinates. This approach leads to an increased order model but avoids natural mode calculation and aerodynamic force updates associated with natural mode reduced models. Computation times and accuracy will determine whether there is a need to resort to natural modes. Alternative approximations to system eigenvalues in terms of structural and control system design variables will be studied (Figure 17.).

STATE SPACE MODELS OF ACTUATORS, SENSORS AND GUST FILTER :

$$\dot{x}_i(x_i) = [A_i](x_i) + [B_i](u_i)$$

$$y_i = [C_i](x_i)$$

$i = ACT$ FOR ACTUATORS
 $i = SEN$ FOR SENSORS
 $i = G$ FOR GUST

STATE SPACE MODEL OF THE CONTROL BLOCK :

$$\dot{x}_{LAW} = [A_{LAW}](x_{LAW}) + [B_{LAW}](u_{LAW})$$

$$y_{LAW} = [C_{LAW}](x_{LAW}) + [D_{LAW}](u_{LAW})$$

THE A,B,C,D MATRICES ARE EXPLICITLY EXPRESSED AS A FUNCTION OF THE CONTROL SYSTEM DESIGN VARIABLES.

SYSTEM STATE VECTOR $\{x\} = \{x_1, x_2, \dots, x_n\}$ CONTAINS :

STRUCTURAL STATES ; ACTUATOR STATES ; SENSOR STATES ; CONTROL LAW STATES ; GUST STATES ; AERODYNAMIC STATES ASSOCIATED WITH GENERALIZED AERO MATRIX ; AERODYNAMIC STATES ASSOCIATED WITH GUST VECTOR .

THE CLOSED LOOP STATE SPACE EQUATIONS OF THE COMPLETE SYSTEM :

$$\dot{x}[U](x(t)) = [V](x(t)) + [W]u_d(t)$$

STABILITY BY EIGENVALUE ANALYSIS :

$$\lambda[U(p)](\phi) = [V(p)](\phi)$$

EIGENVALUE SENSITIVITY WITH RESPECT TO DESIGN VARIABLE p :

$$\frac{\partial \lambda}{\partial p} = \frac{\psi^T \left[\lambda \frac{\partial U}{\partial p} - \frac{\partial V}{\partial p} \right] \phi}{\psi^T U \phi}$$

Figure 17

STATUS OF MULTIDISCIPLINARY ANALYSIS AND BEHAVIOR SENSITIVITY

Figure 18 presents status of research activities associated with the development of the analysis and sensitivity capabilities for the multidisciplinary synthesis of wings. It is expected that based on these capabilities, it will be practical to synthesize on a preliminary design level realistic representations of control augmented wings. The generality of the approximation concepts based mathematical programming approach to synthesis and the realism in modeling are expected to be of major importance in coping with complicated multidisciplinary interaction, where little experience exists and intuition is often misleading.

ANALYSIS AND BEHAVIOR SENSITIVITY STATUS

	STRUCTURE	AERODYNAMICS *	CONTROL
FORMULATION : ANALYSIS	+	+	+
SENSITIVITY	+	+	+
ANALYSIS IMPLEMENTATION :	+	+	+
ANALYSIS TESTING :	+	+	in progress
SENSITIVITY IMPLEMENTATION :	+	in progress	in progress
SENSITIVITY TESTING :	+	-	-
APPROXIMATION CONCEPTS PERFORMANCE ASSESSED :	+	-	-

AERODYNAMICS INCLUDE :

- UNSTEADY AERODYNAMICS FOR SERVOAEROELASTIC ANALYSIS
- STEADY TRIM AND DRAG CALCULATIONS

Figure 18

REFERENCES

1. Schmit, L.A., "Structural Optimization - Some Key Ideas and Insights," in New Directions in Optimum Structural Design, edited by Atrek, E., Gallagher, R.H., Ragsdell, K.M., and Zienkiewicz, O.C., John Wiley and Sons, 1984.
2. Ashley, H., "On making things the best - The aeronautical uses of optimization," Journal of Aircraft, Vol.19, No.1, January 1982, pp. 5-28.
3. Lansing, W., Lerner, E. and Taylor, R.F., "Applications of Structural Optimization for Strength and Aeroelastic Design Requirements," AGARD-R-664, 1978.
4. McCullers, L.A., "Automated Design of Advanced Composite Structures," Mechanics of Composite Materials, Zvi Hashin(ed.), Pergamon Press, 1983.
5. Triplett, W.E., "Flutter Optimization in Fighter Aircraft Design," in NASA CP-2327 Recent Experiences in Multidisciplinary Analysis and Optimization, 1984, pp.47-63.
6. Shirk, M.H., Hertz, T.J. and Weisshaar, T.A., "Aeroelastic Tailoring - Theory, Practice, Promise," Journal of Aircraft, Vol. 23, No. 1, January 1986, pp. 6-18.
7. Haftka, R.T., "Structural Optimization with Aeroelastic Constraints : A Survey of US Applications," International Journal of Vehicle Design, Vol.7, No.3-4, 1986, pp. 381-392.
8. Weisshaar, T.A., "Aeroelastic Tailoring - Creative Uses of Unusual Materials," AIAA Paper 87-0976-CP, AIAA/ASME/ASCE/AHS 28th Structures, Structural Dynamics and Materials Conference, Monterey, California, April 6-8, 1987.
9. Lynch, R.W., and Rogers, W.A., "Aeroelastic Tailoring of Composite Materials to improve Performance," Proceedings of the 16th Structures, Structural Dynamics and Materials Conference, 1975.
10. Lynch, R.W., Rogers, W.A., and Braymen, W.W., "Aeroelastic Tailoring of Advanced Composite Structures for Military Aircraft," AFFDL-TR-76-100, Volume 1, April 1977.
11. Haftka, R.T., "Automated Procedure For Design of Wing Structures to Satisfy Strength and Flutter Requirements," NASA TN D-7264, 1973.
12. Starnes Jr., J.H., and Haftka, R.T., "Preliminary Design of Composite Wings for Buckling, Strength and Displacement Constraints," Journal of Aircraft, Vol.16, No.2, August 1979, pp.564-570.
13. Haftka, R.T., "Optimization of Flexible Wing Structures Subject to Strength and Induced Drag Constraints," AIAA Journal, Vol. 15, pp. 1101-1106, 1977.
14. Neill, D.J., Johnson, E.H. and Canfield, R., "ASTROS - A Multidisciplinary Automated Structural Design Tool," AIAA Paper no. 87-0713 presented at the 28th AIAA/ASME/ASCE/AHS Structures, Structural Dynamics and Materials Conference, Monterey, California, April 1987.
15. Peloubet, R.P., "YF16 Active Control System/Structural Dynamics Interaction Instability," AIAA Paper 75-823, AIAA/ASME/SAE 16th Structures, Structural Dynamics and Materials Conference, Denver, Colorado, May 1975.
16. Felt, L.R., Huttsett, J. et al. "Aeroservoelastic Encounters," Journal of Aircraft, Vol. 16 No. 7, July 1979, pp.477-483.
17. Swaim, R.L., "Aeroelastic Interactions with Flight Control," AIAA Paper 83-2219, in AIAA Conference on Guidance and Control, 1983.
18. Miller, G.D., Wykes, J.H., and Bronsan, M.J., "Rigid Body/Structural Mode Coupling on a Forward Swept Wing Aircraft," Journal of Aircraft, Vol. 20, Aug.1983, pp.696-702.
19. Weisshaar, T.A., and Zeiler, T.A., "Dynamic Stability of Flexible Forward Swept Wing Aircraft," Journal of Aircraft, Vol. 20, 1983, pp. 1014-1020.
20. Yurkovich, R., "Flutter of Wings with Leading Edge Control Surfaces," AIAA Paper 86-0897, Proceedings of the AIAA/ASME/SAE 27th Structures, Structural Dynamics and Materials Conference, San Antonio, Texas, 1986.
21. Brinks, W.H., "F/A-18 Full Scale Development Test," The Society of Experimental Test Pilots 24th Symposium Proceedings, December 1980, p. 38.
22. Newsom, J.R., Adams, W.M., Mukhopadhyay, V., Tiffany, S.H., and Abel, I., "Active Controls : A look at Analytical Methods and Associated Tools," ICAS paper ICAS-84-4.2.3, Proceedings of the 14th Congress of the International Council of the Aeronautical Sciences, Toulouse, France, 1984.
23. Nissim, E., and Abel, I., "Development and Application of an Optimization Procedure for Flutter Suppression using the Aerodynamic Energy Concept," NASA TP 1137, February, 1978.
24. Nissim, E., and Lottati, I., "Active External Store Flutter Suppression in the YF-17 Flutter Model," Journal of Guidance and Control, Vol.2, No.5, Sept-Oct. 1979, pp. 395-401.

25. Liebst, B.S., Garrard, W.L., and Adams, W.M., "Design of an Active Flutter Suppression System," Journal of Guidance, Control and Dynamics, Vol. 9, No. 1, Jan. - Feb. 1986, pp. 64-71.
26. Rimer, M., Chipman, R., and Muniz, B., "Control of a Forward Swept Wing Configuration Dominated by Flight Dynamics/Aeroelastic Interactions," Journal of Guidance, Control and Dynamics, Vol. 9, No. 1, January-February 1986, pp. 72-79.
27. Tolson, R.H., and Sobieszczanski-Sobieski, J., "Multidisciplinary Analysis and Synthesis: Needs and Opportunities," AIAA Paper 85-0584.
28. Sobieszczanski-Sobieski, J., and Haftka, R.T., "Interdisciplinary and Multilevel Optimum Design," in Computer Aided Optimal Design: Structural and Mechanical Systems, Mota Soares, C. A., (ed.), Springer Verlag 1987.
29. McGeer, T., "Wing Design for Minimum Drag with Practical Constraints," Journal of Aircraft, Vol. 21, No. 11, November 1984, pp. 879-886.
30. Gilbert, M.G., Schmidt, D.K., and Weisshaar, T.A., "Quadratic Synthesis of Integrated Active Controls for an Aeroelastic Forward Swept Wing Aircraft," AIAA Paper 82-1544, Proceedings of the 1982 AIAA Guidance and Control Conference, 1982.
31. Zeiler, T.A., and Weisshaar, T.A., "Integrated Aeroservoelastic Tailoring of Lifting Surfaces," Journal of Aircraft, Vol. 25, No. 1, January 1988, pp. 76-83.
32. Weisshaar, T.A., Newsom, J.R., Zeiler, T.A., and Gilbert, M.G., "Integrated Structure/Control Design - Present Methodology and Future Opportunities," ICAS Paper ICAS-86-4.8.1, presented at the 1986 Conference of the International Council of the Aeronautical Sciences, London, England.
33. Grossman, B., Strauch, G.J., Eppard, W.M., Gurdal, Z., and Haftka, R.T., "Integrated Aerodynamic/Structural Design of a Sailplane Wing," AIAA Paper 86-2623, AIAA Aircraft Systems, Design & Technology Meeting, October, 1986.
34. Haftka, R.T., Grossman, B., Eppard, W.M., and Kao, P.J., "Efficient Optimization of Integrated Aerodynamic-Structural Design," Proceedings of the International Conference on Inverse Design Concepts and Optimization in Engineering Sciences - II, October 26-28, 1987, University Park, Pennsylvania.
35. Barthelemy, J.F.M., and Bergen, F.D., "Shape Sensitivity Analysis of Wing Static Aeroelastic Characteristics," paper AIAA 88-2301, presented at the AIAA/ASME/ASCE/AHS 29th Structures, Structural Dynamics and Materials Conference, Williamsburg, Virginia, 1988.
36. Gilbert, M.G., "Sensitivity Method for Integrated Structure/Active Control Law Design," in NASA CP 2457, Sensitivity Analysis in Engineering, 1987.
37. Giles, G.L., "Equivalent Plate Analysis of Aircraft Wing Box Structures with General Planform Geometry," Journal of Aircraft, Vol. 23, No. 11, November 1986, pp. 859-864.
38. Giles, G.L., "Further Generalization of the Equivalent Plate Representation for Aircraft Structural Analysis," AIAA Paper No. 87-0721-CP, AIAA/ASME/ASCE/AHS Structures, Structural Dynamics and Materials Conference, Monterey, California, April 1987.
39. Pittman, J.L., and Giles, G.L., "Combined Nonlinear Aerodynamic and Structural Method for the Aeroelastic Design of Three Dimensional Wing in Supersonic Flow," AIAA paper No. 86-1769, AIAA 4th Applied Aerodynamics Conference, San Diego, California, 1986.
40. Lottati, I., and Nissim, E., "Three Dimensional Oscillatory Piecewise Continuous Kernel Function Method", (in three parts), Journal of Aircraft, Vol. 18, No. 5, May 1981, pp. 346-363.
41. Lottati, I. and Nissim, E., "Nonplanar, Subsonic, Three Dimensional Oscillatory Piecewise Continuous Kernel Function Method", Journal of Aircraft, Vol. 22, No. 12, December 1985, pp. 1043-1048.
42. Lottati, I., "Induced Drag and Lift of Wing by the Piecewise Continuous Kernel Function Method", Journal of Aircraft, Vol. 21, No. 11, pp. 833-834.
43. Nissim, E., and Lottati, I., "Supersonic Three Dimensional Oscillatory Piecewise Continuous Kernel Function Method," Journal of Aircraft, Vol. 20, No. 8, August 1983, pp. 674-681.
44. Karpel, M., "Design for Active Flutter Suppression and Gust Alleviation using State Space Aeroelastic Modeling," Journal of Aircraft, Vol. 19, No. 3, March 1982, pp. 221-227.
45. Tiffany, S.H., and Adams, W.M., "Nonlinear Programming Extensions to Rational Function Approximations of Unsteady Aerodynamics," Proceedings of the 28th Structures, Structural Dynamics and Materials Conference, Monterey, California, 1987.
46. Moore, R.L., "Aeroservoelastic Stability Analysis of an Airplane with a Control Augmentation System", Phd Thesis, The Ohio State University, 1978 (Available from University Microfilms International, No. 7902191)

47. Watkins, C.E., Runyan, H.L., and Woolston, D.S., "On the Kernel Function of the Integral Equation Relating the Lift and Downwash of Oscillating Finite Wings in Subsonic Flow," NACA Report 1234, 1955.
48. Rowe, W.S., "Comparison of Analysis Methods used in Lifting Surface Theory," in Computational Methods in Potential Aerodynamics, edited by L. Morino, Springer Verlag, 1985.
49. Mukhopadhyay, V., Newsom, J.R., and Abel, I., "A Method for Obtaining Reduced Order Control Laws for High Order Systems Using Optimization Techniques", NASA Technical Paper 1876, 1981.

BIBLIOGRAPHY

1. Rogers, W.A., Brayman, W.W., and Shirk, M.H., "Design, Analysis, and Model Tests of an Aeroelastically Tailored Lifting Surface," Journal of Aircraft, Vol. 20, No. 3, March 1983, pp. 208-215.
2. Wilkinson, K., Markowitz, J., Lerner, E., George, D., and Batill, S.M., "FASTOP - A Flutter and Strength Optimization Program for Lifting Surface Structures," Journal of Aircraft, Vol. 14, No. 6, June 1977.
3. Markowitz, J., and Isakson, G., "FASTOP3 - A Strength, Deflection and Flutter Optimization Program for Metallic and Composite Structures," AFFDL - TR - 78 - 50, May 1978.
4. Isakson G., Pardo H., Lerner E. and Venkayya V.B.
ASOP3 - A Program for Optimum Structural Design to Satisfy Strength and Deflection Constraints. Journal of Aircraft, Vol. 15, No. 7, July 1978, pp. 422-428.
5. Lerner, E., "The Application of Practical Optimization Techniques in the Preliminary Structural Design of a Forward - Swept Wing," The Second International Symposium on Aeroelasticity and Structural Dynamics, Aachen, W. Germany, April 1-3, 1985, DGLR-Bericht 85-02.
6. Lecina, G. and Petiau, C., "Advances in Optimal Design with Composite Materials," in : Computer Aided Optimal Design : Structural and Mechanical Systems, C.A. Mota Soares (ed.), Springer-Verlag, 1987.

Control Surface Spanwise Placement In Active Flutter Suppression Systems

E.Nissim¹

NRC-NASA Research Associate
NASA Ames-Dryden Flight Research Facility

J.J.Burken

NASA-Ames-Dryden Flight Research Facility

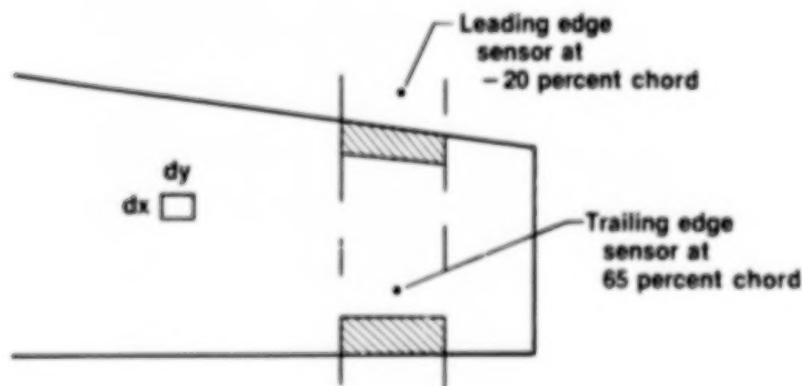
¹On leave from Technion-I.I.T.;Haifa,Israel

1 INTRODUCTION

All flutter suppression systems require sensors to detect the movement of the lifting surface and to activate a control surface according to a synthesized control law. Most of the work performed to date (refs. 1 through 5) relate to the development of control laws based on predetermined locations of sensors and control surfaces. These locations of sensors and control surfaces are determined either arbitrarily, or by means of a trial and error procedure (ref. 5)

The aerodynamic energy concept (ref. 6) indicates that the sensors should be located within the activated strip. Furthermore, the best chordwise location of a sensor activating a T.E. control surface, is around the 65-percent chord location (ref. 7). The best chordwise location for a sensor activating a L.E. surface is shown to lie upstream of the wing (around 20-percent upstream of the leading edge), or alternatively, two sensors located along the same chord should be used.

Plan View of a Wing with Active Control Surfaces and Recommended Sensor Locations



The present work describes a method which enables one to determine the best spanwise placement of an activated control surface without resorting to any specific control law. The method is based on the aerodynamic energy concept whereby the activated control surface is placed at the location where most energy is fed into the unstable structure.

2 APPROACH

Let the pressure $p(x, y)$ be given by eq.(1) and let the displacement $z(x, y)$ be given by eq.(2), where the q 's denote the generalized coordinates of the system. The generalized aerodynamic forces per unit area are given by eq.(3), or in a more condensed form by eq.(4).

$$p(x, y) = \begin{bmatrix} p_1(x, y) & p_2(x, y) & \cdots & p_n(x, y) \end{bmatrix} \begin{Bmatrix} q_1 \\ q_2 \\ \vdots \\ q_n \end{Bmatrix} \quad (1)$$

$$z(x, y) = \begin{bmatrix} z_1(x, y) & z_2(x, y) & \cdots & z_n(x, y) \end{bmatrix} \begin{Bmatrix} q_1 \\ q_2 \\ \vdots \\ q_n \end{Bmatrix} \quad (2)$$

$$\{Q\}_{x,y} = \begin{bmatrix} z_1(x, y) \\ z_2(x, y) \\ \vdots \\ z_n(x, y) \end{bmatrix} \begin{bmatrix} p_1(x, y) & p_2(x, y) & \cdots & p_n(x, y) \end{bmatrix} \begin{Bmatrix} q_1 \\ q_2 \\ \vdots \\ q_n \end{Bmatrix} \quad (3)$$

$$\{Q\}_{x,y} = [A]_{x,y} \{q\} \quad (4)$$

The work per unit area $W_{x,y}$ done by the system on its surroundings per cycle of oscillation is given by (ref. 6) eq.(5), where eq.(6) provides a definition for some of the parameters in eq.(5). If $W_{x,y} > 0$, energy is dissipated by the system. If $W_{x,y} < 0$, energy is fed into the system. Eq.(8) is obtained by integrating eq.(5) along the chord, and it yields the work W_y per unit span done by the system on its surroundings per cycle of oscillation. The total work W is obtained by integrating eq.(8) along the span, as shown in eqs.(10),(11).

$$W_{x,y} = \frac{\pi}{2} [q_0^*] \left(-[A_I + A_I^T]_{x,y} + i[A_R - A_R^T]_{x,y} \right) \{q_0\} \quad (5)$$

$$[A]_{x,y} = [A_R]_{x,y} + i[A_I]_{x,y} \quad (6)$$

$$W_y = \int_{L.E.}^{T.E.} W_{x,y} dx \quad (7)$$

$$W_y = \frac{\pi}{2} [q_0^*] \left(-[A_I + A_I^T]_y + i[A_R - A_R^T]_y \right) \{q_0\} \quad (8)$$

$$[A]_y = \int_{L.E.}^{T.E.} [A]_{x,y} dx \quad (9)$$

$$W = \int_{-s}^s W_y dy \quad (10)$$

$$W = \frac{\pi}{2} [q_0^*] \left(-[A_I + A_I^T] + i[A_R - A_R^T] \right) \{q_0\} \quad (11)$$

$$[A] = \int_{-s}^s [A]_y dy \quad (12)$$

Define the specific energy ratio by $\overline{\overline{W}}_A$, as given by eq.(13), and note that its integral along the span must have a unit absolute value (see eq.(14)).

$$\overline{\overline{W}}_A = \frac{W_y}{|W|} \quad (13)$$

$$\int_{-s}^s \overline{\overline{W}}_A dy = \pm 1 \quad (14)$$

It is argued that the best spanwise placement of an active control surface for flutter suppression is around the location where $\overline{\overline{W}}_A$ is negative and assumes the largest numerical values.

3 DETAILED PROCEDURE

1. Determine the flutter dynamic pressure Q_F of the system
2. Increase Q_D , so as to lie within the unstable region, and obtain the eigenvector $\{q_0\}$ of the unstable mode. The amount by which Q_D is increased is immaterial since only energy ratios are used.
3. Compute W (which must be negative), and $\overline{\overline{W}}_A$ for the different spanwise locations.
4. Plot the specific energy ratio $\overline{\overline{W}}_A$ versus the span and determine the strip where $\overline{\overline{W}}_A$ assumes the largest negative value. This strip absorbs most energy per unit span and therefore would present the location where an active control surface would be most effective in suppressing flutter.

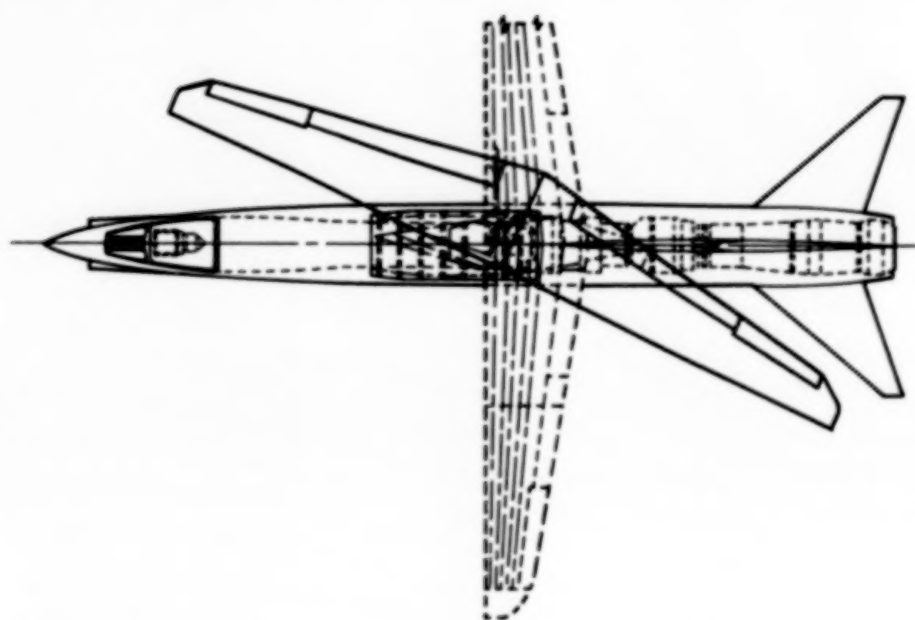
4 NUMERICAL EXAMPLES

Three numerical examples are used. These examples relate to

1. DAST-ARW2, 12 modes (2 rigid body modes), see ref. 8.
2. OBLIQUE WING, 20 modes (5 rigid body modes), see ref. 9.
3. MODIFIED OBLIQUE WING (with one torsional modal frequency reduced so as to cause wing flutter)

The relevant aerodynamic matrices were computed using Langley's doublet lattice ISAC program. The results obtained are shown in the following figures.

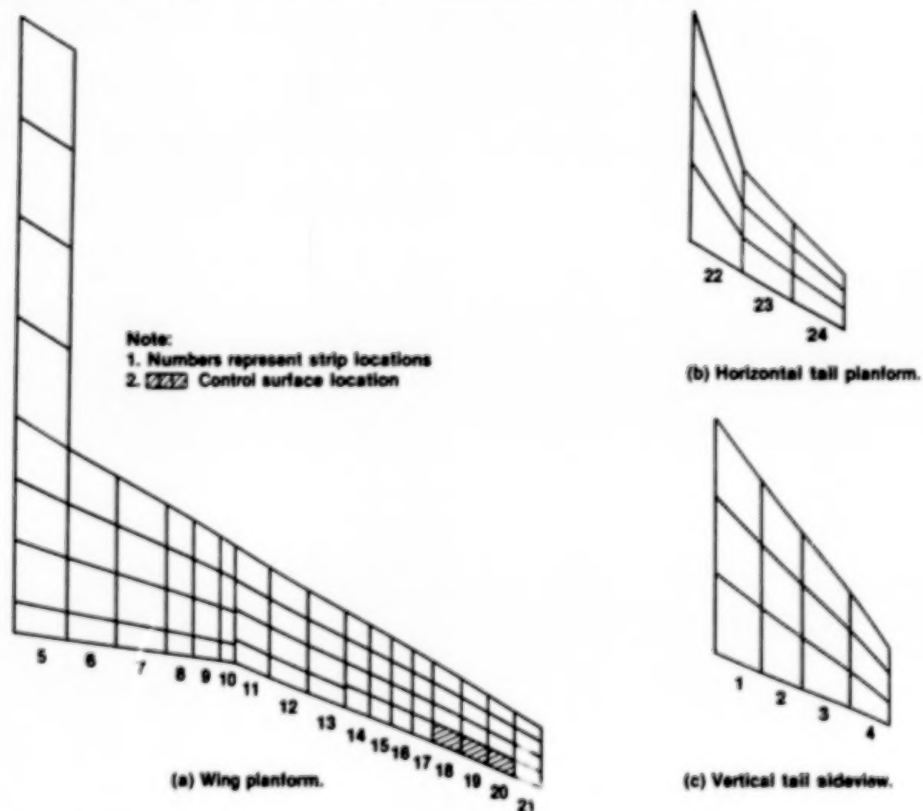
Oblique Wing Model Planform View with Wing Skewed 65°



5 Results for the DAST-ARW2 Mathematical Model

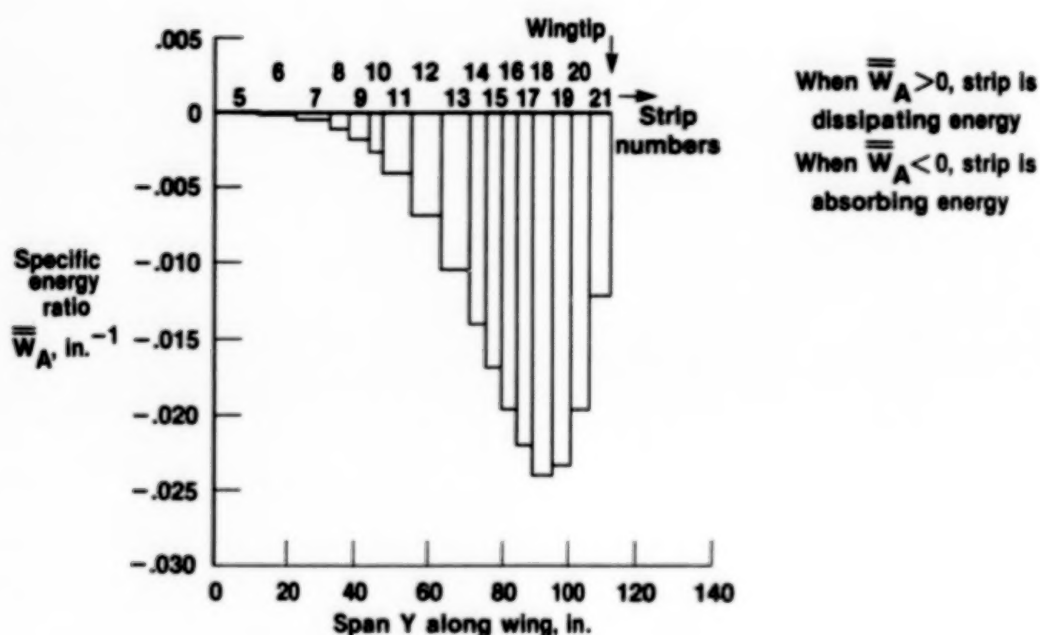
The geometrical layout of the DAST-ARW2 model is shown below. It can be seen that out of the 24 strips allowed for the model, 17 strips lie along the wing, 4 strips lie along vertical tail and 3 strips lie along the horizontal tail. This model yields a flutter dynamic pressure $Q_F = 490 \text{ psf}$ (at $M=0.85$) and a flutter frequency $\omega_F = 117 \text{ rad/s}$. The unstable eigenvector was computed for $Q = 550 \text{ psf}$ and the matrices $[A]$ and $[A]_y$ were computed for all the 24 strips at the reduced frequency $k = 0.132$ associated with the unstable mode.

ARW2 Geometric Layout, Together with Doublet Lattice Paneling and Strip Number Allocations



The figure below shows a plot of the specific energy ratios $\overline{\overline{W}}_A$ for only those 17 strips that lie along the wing. The values of $\overline{\overline{W}}_A$ are negligible for all the other strips and therefore will not be shown herein. As can be seen, the specific energy ratio is negative for all wing strips, except for the root strip (strip 5) where $\overline{\overline{W}}_A$ is very small and positive. The largest negative numerical value of $\overline{\overline{W}}_A$ relates to strip 18, which coincides with the inboard portion of the aileron. Following the method described herein, this is the location around which the aileron should be placed for best effects regarding flutter suppression (i.e. around the 80-percent span location).

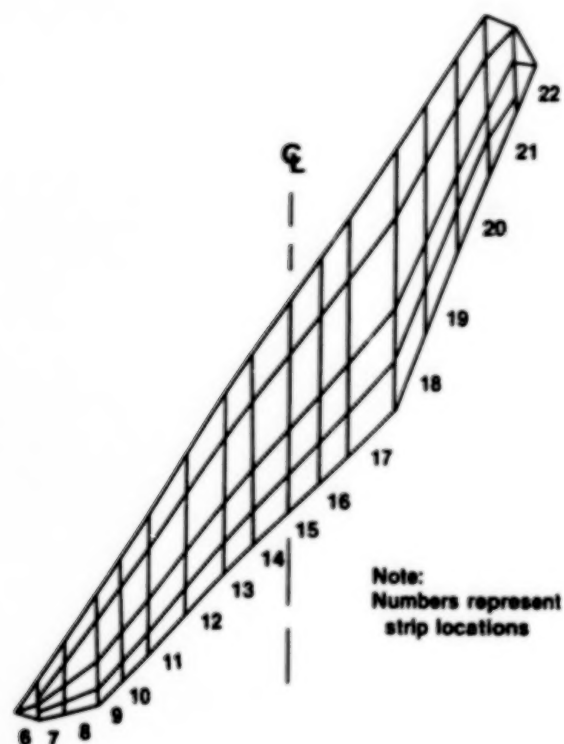
DAST - ARW2 Model - Variation of Specific Energy Ratio $\overline{\overline{W}}_A$ with Strip Locations Along the Wing



6 Results for the Oblique Wing

The geometrical layout of the wing in a 65-degrees skew position (with right wing forward) is shown. Note that the wing has again 17 strips along its span, with strip 6 at the tip of the left wing and strip 22 at the tip of the right wing.

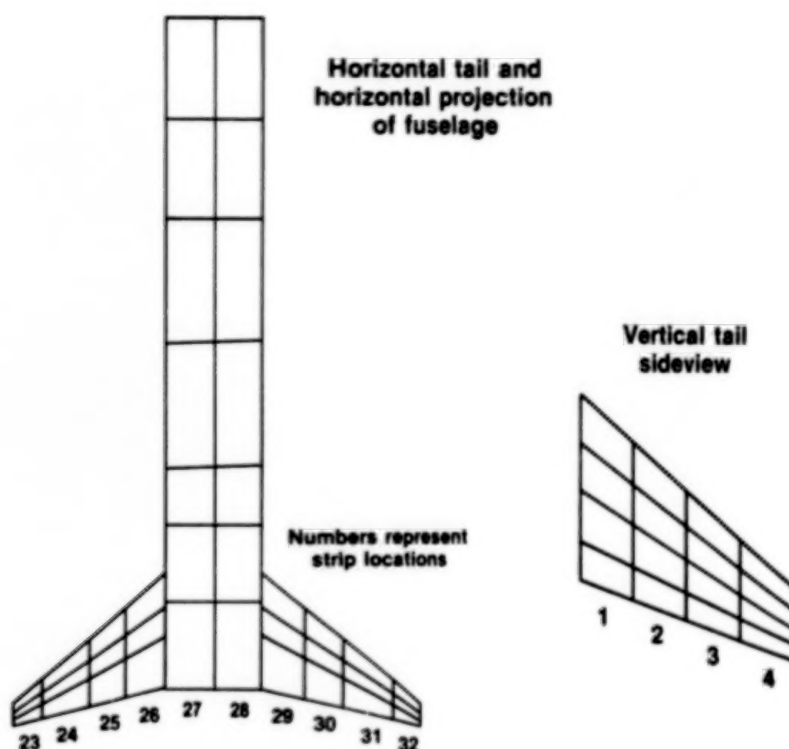
Oblique Wing Model – Geometric Layout Together with Doublet Lattice Paneling and Strip Numbers Planeform 65° Skew



The horizontal tail, the horizontal projection of the fuselage, and the side view of the vertical tail are both shown in the figure below. There are 4 strips on each of the horizontal tails (left and right surfaces), 2 strips on the horizontal projection of the fuselage, and 4 strips on the vertical tail.

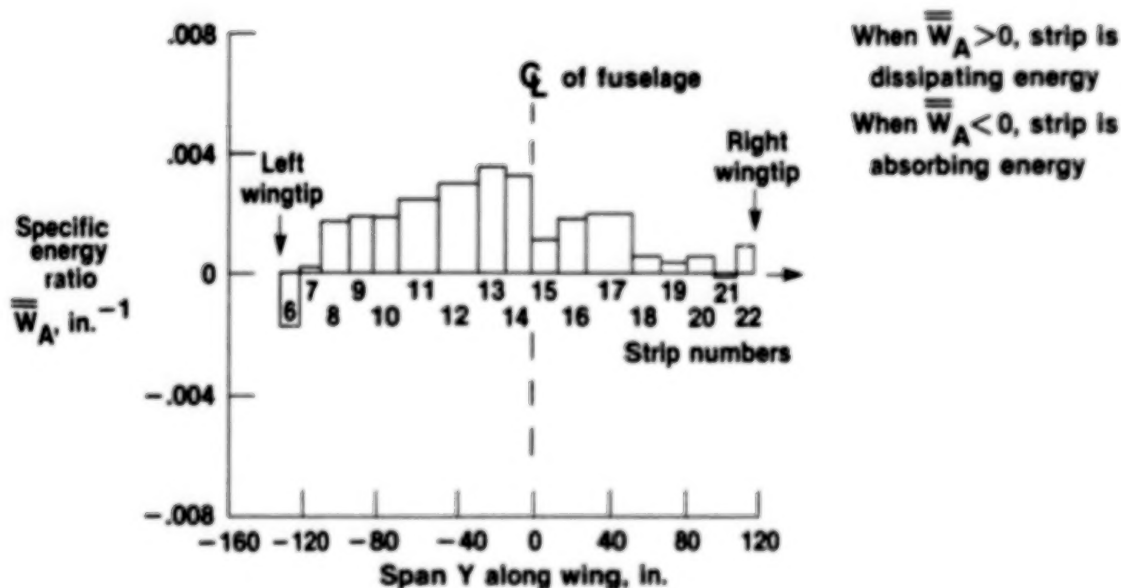
A flutter computation at Mach 0.95 shows that a mild, 78 rad/s, vertical tail flutter instability develops around $Q_F = 780 \text{ psf}$.

Oblique Wing Model – Geometric Layout Together with Doublet Lattice Paneling and Strip Numbers



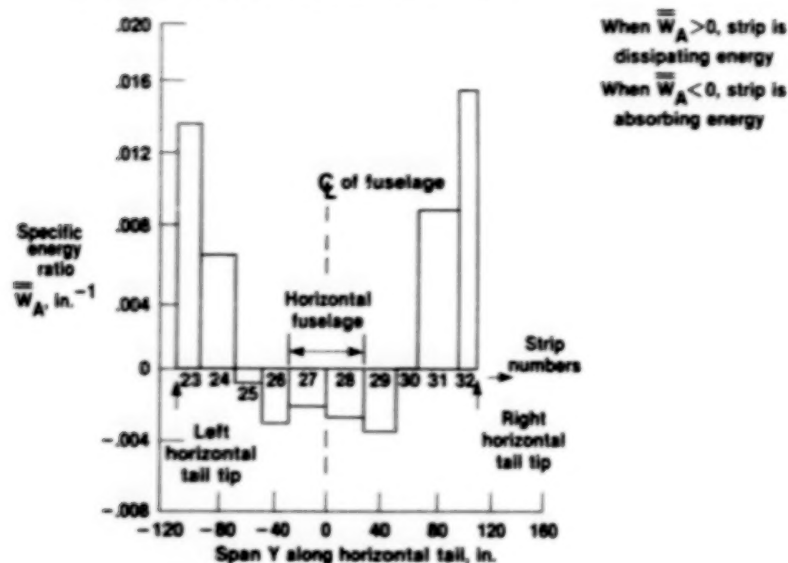
The specific energy ratio distribution was computed for $Q=1600$ psf. It can be seen that most of the energy input into this fluttering system takes place through the vertical tail and the tips of the horizontal tail. The inboard parts of the horizontal tail, the horizontal fuselage, and practically all of the wing, all dissipate energy and thus contribute to the mildness of the flutter obtained. The following figures indicate that for the suppression of this flutter mode, the active control surface should be placed around the center of strip 3 of the vertical tail (i.e. around its 60-percent span location).

Oblique Wing Model – Variation of Specific Energy Ratio \bar{W}_A with Strip Locations



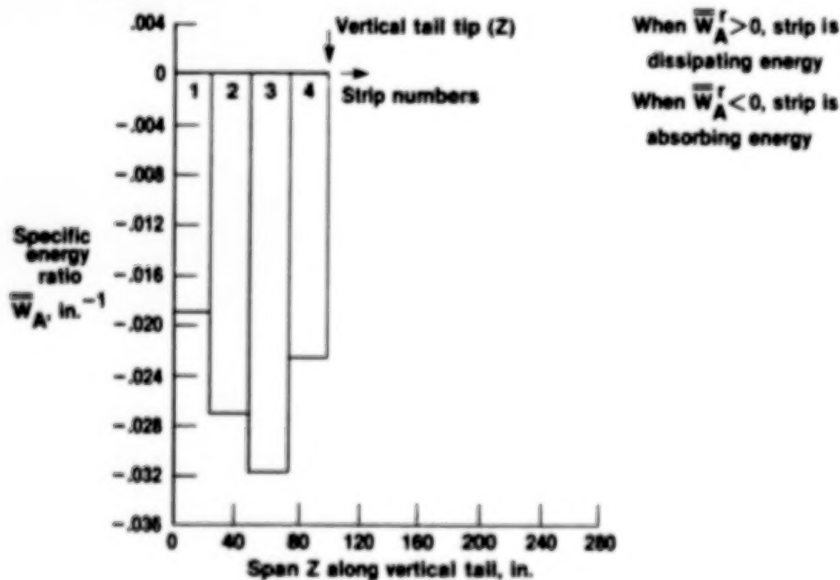
Oblique Wing Model - Variation of Specific Energy Ratio \bar{W}_A with Strip Locations

Horizontal Tail and Horizontal Fuselage



Oblique Wing Model - Variation of Specific Energy Ratio \bar{W}_A with Strip Locations

Vertical Tail

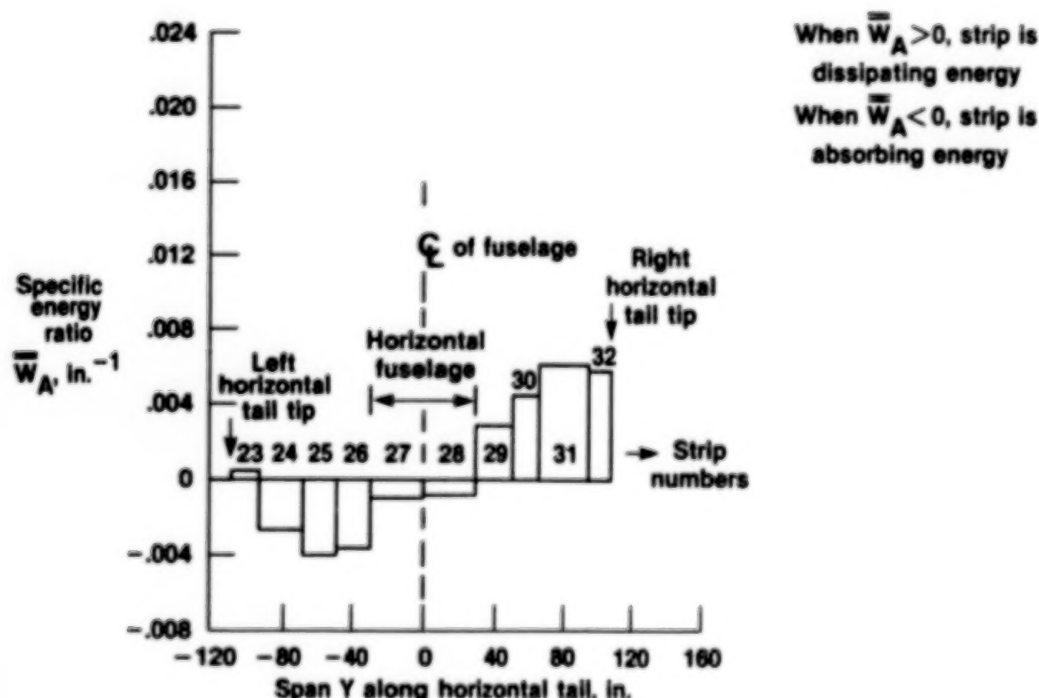


7 Results for the Modified Oblique Wing

The oblique wing is unique from the point of view of asymmetry. The best placement of an activated strip along its span could present an interesting challenge. The mathematical model of the wing was therefore modified so as to 'force' the wing to flutter. This was done by lowering one of the torsional frequencies of the wing from 45 HZ to 12 HZ. Therefore, the following results do not relate to the actual wing but to a synthetically modified wing. This modified model yields, in addition to the already seen vertical tail flutter, a wing flutter mode with $Q_F = 1050 \text{ psf}$ and $\omega_F = 70 \text{ rad/s}$. The following results relate to this wing flutter mode, with specific energy ratios computed at $Q=1300 \text{ psf}$.

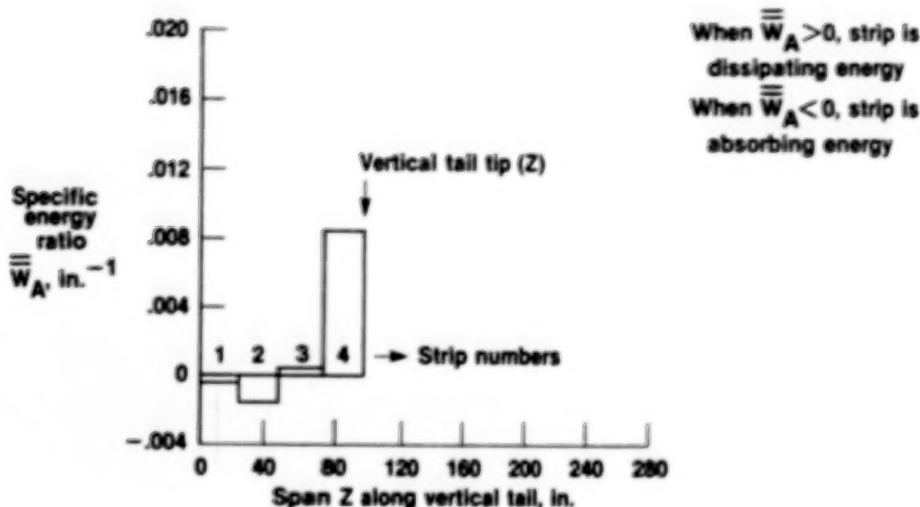
Modified Oblique Wing Model – Variation of Specific Energy Ratio \bar{W}_A with Strip Locations

Horizontal Tail and Horizontal Fuselage

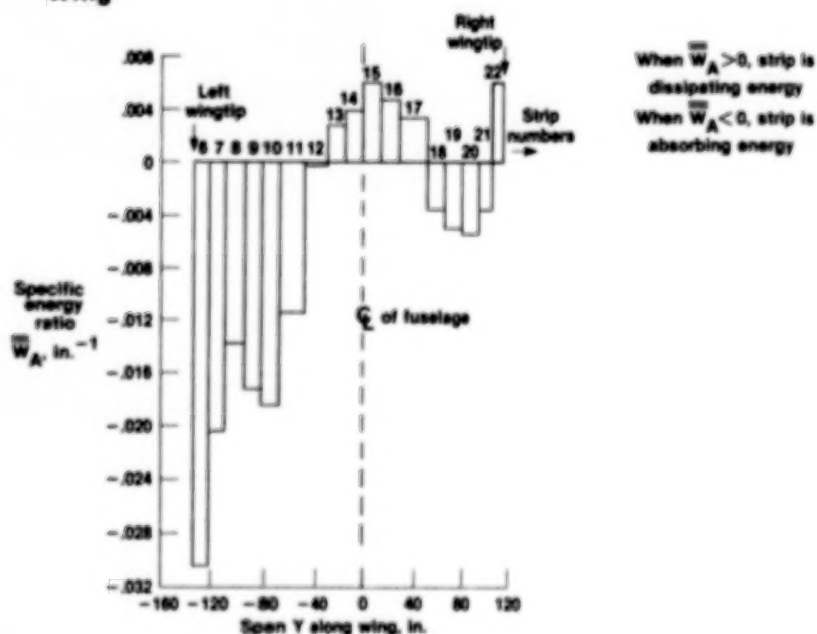


332

Modified Oblique Wing Model – Variation of Specific Energy Ratio \overline{W}_A with Strip Locations Vertical Tail



Modified Oblique Wing Model – Variation of Specific Energy Ratio \overline{W}_A with Strip Locations Wing



003

As seen from the above 3 figures, most of the energy input into the system takes place through the left wing. The vertical tail essentially dissipates energy, and the horizontal tail absorbs energy through its left surface and dissipates around the same amount of energy through its right surface. The largest negative numerical value for \overline{W}_A is obtained in strip 6 which represents the tip of the left (aft) wing. Hence, for the suppression of this flutter mode, the activated control surface should be placed as close to the left tip of the wing as is structurally possible. Strips 9 and 10 can also form a reasonable alternative to the above extreme tip placement of the activated control surface, i.e., around the 65-percent span location of the left wing.

8 REFERENCES

1. Newsom, J.R.: A Method For Obtaining Practical Flutter Suppression Control Laws Using Results of Optimal Control Theory. NASA TP-1471,1979.
2. Mukhopadhyay, V.;Newsom,J.R.;and Abel,I.: A Method For Obtaining Reduced Order Control Laws For High Order Systems Using Optimization Techniques. NASA TP-1876,1981.
3. Nissim,E.;and Abel,I.: Development and Application Of An Optimization Procedure For Flutter Suppression Using The Aerodynamic Energy Concept. NASA TP-1137,1978.
4. Mahesh,J.K.;Stone,C.R.;Garrard,W.L.;and Dunn,H.J.:Control Law Synthesis For Flutter Suppression Using Linear Quadratic Gaussian Theory. AIAA J. Guidance and Control, vol.4, no.4, July-August 1981,pp.415-422.
5. Nissim,E.;Caspi,A.;and Lottati,I.: Application of the Aerodynamic Energy Concept To Flutter Suppression And Gust Alleviation By Use Of Active Controls. NASA TN D-8212,1976.
6. Nissim,E.: Flutter Suppression Using Active Controls Based On The Concept Of Aerodynamic Energy.NASA TN D-6199.
7. Nissim,E.: Recent Advances In Aerodynamic Energy Concept For Flutter Suppression And Gust Alleviation Using Active Controls.NASA TN D-8519,1977.
8. Adams,W.;and Tiffany,S.: Development Of A Flutter Suppression Control Law By Use Of Linear Quadratic Gaussian And Constrained Optimization Design Techniques. 2nd International Symposium On Aeroelasticity And Structural Dynamics, April 1985,Germany.
9. Burken,J.J.;Alag,G.S.;and Gilyard,G.B.: Aeroelastic Control Of Oblique Wing Aircraft. NASA TM-86808.

SESSION 8: STRUCTURES

Chairmen: R. Levy and P. Papalambros

**An Approximation Function for Frequency Constrained
Structural Optimization**

R. A. Canfield

Flight Dynamics Laboratory
Air Force Wright Aeronautical Laboratories *
Wright-Patterson AFB, Ohio

* Now the Wright Research Development Center

00 037

Introduction

The purpose of this study is to examine a function for approximating natural frequency constraints during structural optimization. The nonlinearity of frequencies has posed a barrier to constructing approximations for frequency constraints of high enough quality to facilitate efficient solutions. A new function to represent frequency constraints, called the Rayleigh Quotient Approximation (RQA), is presented. Its ability to represent the actual frequency constraint results in stable convergence with effectively no move limits.

The objective of the optimization problem is to minimize structural weight subject to some minimum (or maximum) allowable frequency and perhaps subject to other constraints such as stress, displacement, and gage size, as well. A reason for constraining natural frequencies during design might be to avoid potential resonant frequencies due to machinery or actuators on the structure. Another reason might be to satisfy requirements of an aircraft or spacecraft's control law. Whatever the structure supports may be sensitive to a frequency band that must be avoided. Any of these situations or others may require the designer to insure the satisfaction of frequency constraints. A further motivation for considering accurate approximations of natural frequencies is that they are fundamental to dynamic response constraints. Techniques for natural frequency constraints may have application to transient response and frequency response problems.

Problem

Minimize Weight of Structure

Subject to Constraints on Structural Response (Natural Frequencies)

For a Finite Element Model (Cross-Sectional Properties as Design Variables)

With a Given Geometric Configuration.

Obstacle

Highly Nonlinear Frequency Constraints

Difficult to Approximate

Solution

Better Approximation Using Modal Energies

"Best" Choice of Intermediate Design Variables

Engineers have long used the Taylor Series Approximation (TSA) as a tool to simplify problems. In 1974 Schmit and Farshi exploited the use of TSAs to form approximate problems to the actual design problem.¹ Since then much attention has been focused on finding the most appropriate intermediate design variables to use for the best TSA. Schmit and Miura originally championed the use of reciprocal variables.² Starnes and Haftka³ and Fleury and Braibant⁴ have shown that a hybrid constraint using mixed variables (*i.e.*, a combination of direct and reciprocal variables) yields a more conservative approximation. Woo generalized the concept in his Generalized Hybrid Constraint (GHC) Approximation where a variable exponent controls how conservative is the convex approximation.⁵ Fleury devised a means of selecting an "optimal" intermediate variable based on second order information.⁶ Vanderplaats and Salajegheh demonstrated improved quality for frequency constraint approximations in the element property space of frame elements when the optimization design variables are cross-sectional dimensions.⁷ All of these approaches have sought improvement through the "best" choice of intermediate variables. Yet all of them have used a Taylor series of some sort for the eigenvalue.

- **Taylor Series Approximation (TSA)—Reciprocal Variables**
 - Schmit & Farshi, 1974
 - Schmit & Miura, 1976
- **Hybrid Constraint—Mixed Variables**
 - Starnes & Haftka, 1979
 - Fleury & Braibant, 1984
- **Generalized Hybrid Constraint (GHC)**
 - Woo, 1986 (Frequencies)
- **Cross-Sectional Property Space for Frames**
 - Mills-Curran, Lust & Schmit, 1983
 - Vanderplaats & Salajegheh, 1988 (Frequencies)

Alternatives to Conventional TSA

The nonlinearity of frequencies is readily observed through the appearance of cross-sectional variables in both the numerator and denominator of Rayleigh's quotient. Venkayya has pointed out that in practical structures, the denominator (kinetic energy) is typically dominated by the non-structural mass.⁸ In this case, frequency eigenvalues are more nearly linear in the cross-sectional property (direct design variable) space. Based on this assumption some researchers have preferred a Taylor series constructed in the direct design variable space.⁷ On the other hand, Miura and Schmit presented results that were better in the reciprocal design space than in the direct design space.⁹ Nevertheless, their studies revealed that the eigenvalues are highly nonlinear in both direct and reciprocal design variable space, requiring strict move limits. As a result, they used a second order Taylor series. Although the second order approximation provided stable convergence without strict move limits, they reported the total computational time was "comparable with that required using first order approximations with move limits."

In 1987 Vanderplaats and Salajegheh demonstrated for stress constraints that using a Taylor series to approximate the internal loads, instead of the stresses themselves, could increase the rate of convergence and reduce the need for move limits.¹⁰ They observed that internal loads are a more fundamental quantity than stresses. Venkayya's approach in formulating the optimality conditions for frequency constraints^{8,11} suggests that for frequencies modal energies may be a more fundamental quantity than the eigenvalue. A frequency constraint might be better approximated by a separate Taylor series for the numerator and denominator in the Rayleigh quotient. In fact, the concept is similar to an alternative approximation proposed by Fox and Kapoor.¹²

- **Miura & Schmit, 1978**
 - Frequencies are Highly Nonlinear
 - 2nd Order TSA
 - Generous Move Limits Offset by Added Cost
- **Vanderplaats, 1987**
 - Approximate Internal Loads Instead of Stresses
 - Loads—More Fundamental Quantity
- **Venkayya, 1983**
 - Modal (Strain) Energy Resizing
- **Rayleigh Quotient Approximation (RQA)**
 - Separate TSA for Modal Energies

Mathematical Statement of Problem.

The structural optimization problem is stated mathematically as minimizing an objective function, the weight, W , subject to constraints on response quantities, g , where \mathbf{x} is a vector of n design variables, x^l and x^u represent their lower and upper bounds, respectively, and g are the m inequality constraints. The design variables are linked to one or more of the p physical variables, represented by the vector, \mathbf{d} , through a transformation matrix, \mathbf{T} . In general the \mathbf{T} matrix may be fully populated; however, each row of \mathbf{T} is limited to only one non-zero element (so-called group linking) when reciprocal variable approximations are considered. In this case the summation in eq (4) is unnecessary. The examples below use rod and membrane elements exclusively. Their design variables are the cross-sectional properties: rod areas and membrane thicknesses.

Frequency constraints are formed using the eigenvalue, (square of the angular frequency, ω) normalized by its allowable value. The positive sign is used for upper bounds and the minus sign for lower bounds. Only lower bound frequency allowables, λ^l , are given in the following examples, since minimizing structural weight drives frequencies toward zero. Other constraints are also cast in the form of eq (3) using the positive sign and replacing the λ 's with the appropriate response quantity (Von Mises stress or displacement value).

Minimize Structural Weight

$$\min W(\mathbf{x}) \quad (1)$$

$$\begin{aligned} \text{Subject to} \quad & g_j(\mathbf{x}) \leq 0; \quad j = 1, \dots, m \\ & x_i^l \leq x_i \leq x_i^u; \quad i = 1, \dots, n \end{aligned} \quad (2)$$

Frequency Constraint

$$g = \pm \left(\frac{\lambda}{\lambda_{allow}} - 1 \right) \quad (3)$$

Design Variable Linking

$$d_k = \sum_{i=1}^n T_{ki} x_i; \quad k = 1, \dots, p \quad (4)$$

Approximate Sub-Problem

An approximation to the actual optimization problem is constructed by approximating the constraints using a first order Taylor series. If the approximate problem is solved in the reciprocal design variable space (*i.e.*, $\beta=1/x$), then the approximate constraint function is given by eq (6).

The Method of Mixed Variables uses either a direct or reciprocal variable depending on the sign of the the constraint's derivative for each design variable. This creates a convex and more conservative approximation. As generalized by Woo, the equations for the GHC are given in eqs (7) where p is a real number and n is a positive integer. When $p=0$ and $n=1$ the GHC reduces to the Method of Mixed Variables.

The approximate sub-problem formed with eqs (5), (6), or (7) is solved by a nonlinear programming optimization algorithm. Appropriate move limits are employed to insure that the design remains in the vicinity of the point about which the Taylor series was made. The move limits are applied as side constraints, eq (2), if they are more restrictive than the minimum and maximum gage constraints which are otherwise used. Move limits are typically specified as a percentage of the current design variables. Alternatively, a move limit factor, f , determines the upper and lower bounds.

Direct TSA

$$\bar{g}_j = g_{o_j} + \sum_{i=1}^n \frac{\partial g_j}{\partial x_i} (x_i - x_{o_i}) \quad (5)$$

Reciprocal TSA

$$\bar{g}_j = g_{o_j} - \sum_{i=1}^n \frac{\partial g_j}{\partial x_i} x_{o_i}^2 \left(\frac{1}{x_i} - \frac{1}{x_{o_i}} \right) \quad (6)$$

Generalized Hybrid Constraint (GHC) Approximation

$$\bar{g}_j = g_{o_j} + \sum_{i=1}^n \frac{\partial g_j}{\partial x_i} f_i(x_i) \quad r = \begin{cases} p & \text{if } \frac{\partial g_j}{\partial x_i} \geq 0 \\ p - n; & \text{if } \frac{\partial g_j}{\partial x_i} < 0 \end{cases} \quad (7)$$

$$f_i(x_i) = (x_i - x_{o_i}) \left(\frac{x_i}{x_{o_i}} \right)^r$$

Move Limits

$$\frac{x_i}{f} \leq x_i \leq f x_i; \quad i = 1, \dots, n \quad (8)$$

Rayleigh Quotient

The structural system's mass and stiffness matrices can be represented by eqs (10), where \mathbf{K}' and \mathbf{M}' are the sensitivity of the stiffness and mass, respectively, to all the elements controlled by the i th design variable. For rod and membrane elements the element stiffness and mass matrices are linear in the design variables, so that eqs (10) are exact. For frames the element matrices are functions of several dependent cross-sectional properties. If cross-sectional dimensions are used as design variables instead, eqs (10) are approximate. As Vanderplaats and Salajegheh point out, the cross-sectional dimensions are appropriate intermediate design properties for the constraint approximation even when designing for the cross-sectional dimensions directly.¹¹ The RQA below is entirely compatible with their approach of constructing constraint approximations in the cross-sectional property space.

The relationship of a natural frequency, ω , to its associated eigenvector, ϕ , and the system's stiffness and mass is expressed by Rayleigh's quotient, eq (9), where the modal strain energy, U , and the modal kinetic energy, T , are the sum of the strain and kinetic energies, respectively, from each of the elements. This is expressed for modal strain energy in eq (11) and for modal kinetic energy in eq (12). Eqs (13) defines the element energies where u_o is strain energy from undesigned elements, and t_o is the kinetic energy due to non-structural mass and undesigned elements. The gradient of a frequency constraint, used in eqs (5) or (6), is given by eq (14).

$$\lambda = \omega^2 = \frac{\phi^t \mathbf{K} \phi}{\phi^t \mathbf{M} \phi} = \frac{U}{T} \quad (9)$$

$$U = u_o + \sum_{i=1}^n u_i x_i \quad (11)$$

$$T = t_o + \sum_{i=1}^n t_i x_i \quad (12)$$

$$\mathbf{K} = \mathbf{K}_o + \sum_{i=1}^n \mathbf{K}'_i x_i \quad (10)$$

$$\mathbf{M} = \mathbf{M}_o + \sum_{i=1}^n \mathbf{M}'_i x_i$$

$$u_i = \phi^t \mathbf{K}'_i \phi \quad (13)$$

$$t_i = \phi^t \mathbf{M}'_i \phi$$

$$\frac{\partial \lambda}{\partial x_i} = \frac{u_i - \lambda t_i}{T} \quad (14)$$

Rayleigh Quotient Approximation (RQA)

Instead of using eqs (5) or (6), Taylor series approximations to the strain and kinetic energies can be used to construct the approximate constraint. In deriving eqs (15) and (16) the eigenvectors were assumed invariant with respect to changes in the design variables. In fact, Miura and Schmit recommend this assumption as a means of reducing the computational burden of calculating the second derivative of a frequency. The assumption is also implicit in Venkayya's derivation of a scaling factor for frequency constraints.¹³ The two approximations of eqs (15) and (16) are next combined to form a single approximate frequency constraint, eq (17).

The same issue of an appropriate intermediate design variable is as pertinent for eqs (15) and (16) as for constructing a Taylor series directly for the eigenvalue. Starnes and Haftka proposed that the sign of the constraint's derivative should determine the appropriate variable. A positive derivative indicates a direct variable approximation, a negative derivative signals a reciprocal variable approximation. Therefore a conservative approximation for a lower bound frequency constraint should employ reciprocal variables for the strain energy and direct variables for the kinetic energy. The reverse is true for an upper bound frequency constraint. For the former, more typical case eq (15) is replaced by eq (18).

For a lower bound frequency the approximate frequency's derivative is by eqs (19) and (20), where $\bar{\lambda} = \bar{U}/\bar{T}$. The sign of eq (19) can change as the design changes. This behavior is consistent with intuition which says that the frequency tends toward zero as the cross-sectional properties go to zero. This trait is not characteristic of TSAs to the eigenvalue in direct or reciprocal design space, nor for Woo's GHC.

Modal Strain Energy Approximation	$\bar{U} = U_0 + \sum_{i=1}^n u_i (x_i - x_{0i}) \quad (15)$
-----------------------------------	--

Modal Kinetic Energy Approximation	$\bar{T} = T_0 + \sum_{i=1}^n t_i (x_i - x_{0i}) \quad (16)$
------------------------------------	--

Approximate Frequency Constraint	$\bar{g} = 1 - \frac{U}{\lambda^l T} \quad (17)$
----------------------------------	--

Reciprocal TSA to Modal Strain Energy	$\bar{U} = U_0 - \sum_{i=1}^n u_i x_{0i} \left(\frac{x_{0i}}{x_i} - 1 \right) \quad (18)$
---------------------------------------	--

RQA gradient	$\frac{\partial \bar{\lambda}}{\partial x_i} = \frac{\left(\frac{x_{0i}}{x_i} \right)^2 u_i - \bar{\lambda} t_i}{\bar{T}} \quad (19)$	$\frac{\partial \bar{g}}{\partial x_i} = \frac{-1}{\lambda^l} \frac{\partial \bar{\lambda}}{\partial x_i} \quad (20)$
--------------	--	---

Special Case of High Non-Structural Mass

Structural designs with high non-structural mass constitute a limiting case for the RQA. Venkayya introduced modal mass ratios to characterize the degree of structural versus non-structural mass. If the mass matrix is considered as the sum of a structural mass matrix, \mathbf{M}_s , and a constant (non-structural) mass matrix, \mathbf{M}_c , then the modal mass ratios are defined in eqs (21) and (22). By definition $\eta + \gamma = 1$. In the limit as non-structural mass becomes dominant, $\gamma \rightarrow 1$ and $\eta \rightarrow 0$, the modal kinetic energy can be considered constant with respect to design changes, and the second term in the derivatives of the eigenvalue in eqs (14) and (19) can be neglected. In this case the RQA reduces to a TSA—either the reciprocal or direct variety depending on which design space was used to approximate the modal strain energy. Starnes and Haftka's hybrid constraint reduces the reciprocal TSA in this case, as well. The same reasoning for choosing the reciprocal design space indicates that it would be more successful than the direct design space for conventional TSAs when optimizing structures with a low modal structural mass ratio. A graphical illustration of this point is seen in a later figure for the beam problem.

COMPUTATIONAL CONSIDERATIONS.

The only computational penalty for using RQA is that the optimizer has to deal with explicit nonlinear instead of linear constraints. The sensitivity analysis is the same except that two gradients must be stored for each frequency constraint instead of one. Additional "bookkeeping" is required to distinguish a frequency constraint from other types in order to apply the RQA. Otherwise the method involves no more complexity than a conventional TSA.

Modal Mass Ratios

$$\text{Structural } \eta = \frac{\phi^t \mathbf{M}_s \phi}{\phi^t \mathbf{M} \phi} \quad (21)$$

$$\text{Non-Structural } \gamma = \frac{\phi^t \mathbf{M}_c \phi}{\phi^t \mathbf{M} \phi} \quad (22)$$

RQA reduces to TSA in λ as $\gamma \rightarrow 1$

Computational Considerations

- Explicit Non-Linear Constraint
- 1st Order Information only
- 2 gradients per Frequency Constraint
- Gradient of RQA can Change Sign

Three Bar Truss

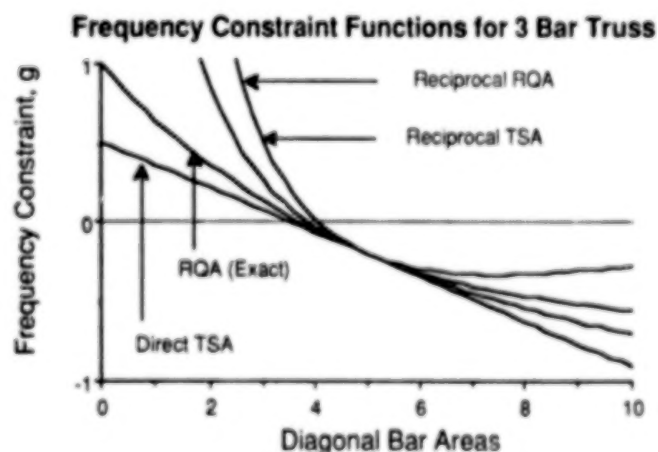
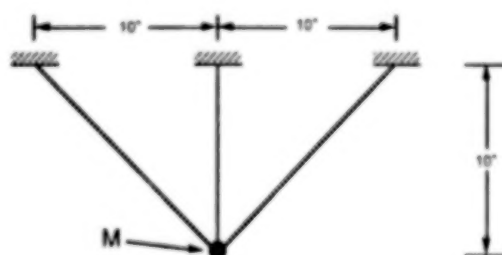
A simple three bar truss is used to illustrate the differences among approximation techniques. A 10 lb point mass is at the free node. All three bars have an elastic modulus of 10×10^6 psi, density of 0.1 lb/in³, initial areas of 5.0 in², and minimum sizes of 0.001 in². The fundamental frequency is constrained to be at least 1300 Hz. As in the remaining examples, TSAs are made in both direct and reciprocal design space. For RQA the kinetic energy Taylor series is always made in the direct design space. In reference to RQA "direct" and "reciprocal" distinguish the design space used for approximating the strain energy. Effectively no move limits were imposed, i.e., $f=10,000$ in eq (8). Due to symmetry the two mode shapes for this system are always the same: one horizontal and one vertical. Since a constant mode shape was the only assumption made in deriving the RQA, when strain energy is found with direct variables, RQA calculates the exact frequency and finds the optimum in a single iteration. Because signs of the constraint's derivatives are not all the same, a TSA in either space creates an infeasible design that is corrected the next iteration. RQA with strain energy in reciprocal space is conservative, producing only feasible designs. The initial design has $\gamma=0.51$ and the final design, $\gamma=0.65$.

The design can be controlled by a single variable by recognizing two simplifications: symmetry forces the two diagonal bars to have the same area, and because the vertical bar contributes no strain energy to the fundamental mode, it goes to minimum. The constraint functions are plotted in as a function of the single variable controlling the two diagonal bars. Using the direct RQA, the optimum area of 3.736 in² for these two bars can be calculated by hand. The conservative nature of approximating strain energy in the reciprocal space is also evident. In general the reciprocal RQA will compensate for changes in the eigenvector; however, in this instance with an invariant mode shape, it is overly conservative.

- A Direct RQA
- B Reciprocal RQA
- C Direct TSA
- D Reciprocal TSA

	A	B	C	D
1	19.14	19.14	19.14	19.14
2	10.57	11.50	10.36	0.015
3	10.57	10.67	10.56	141.3
4		10.57	10.56	24.02
5		10.57		13.30
6				10.87
7				10.57

Table 1: Iteration History (Weight)—3 DV

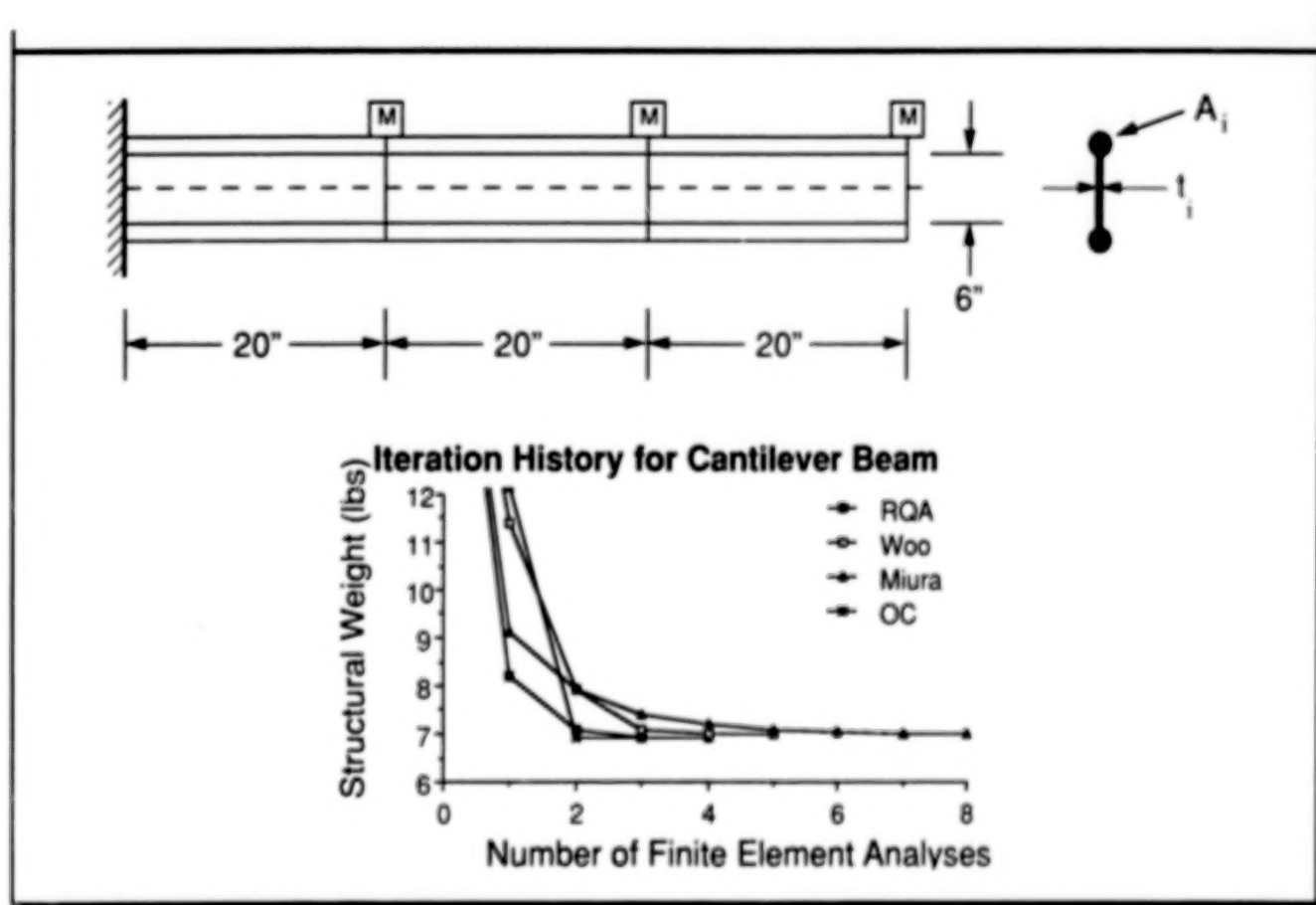


400

Cantilever Beam

The cantilever beam, originally used by Turner,¹⁴ is modelled using rod and shear panel elements. It is symmetric about the mid-plane and supports three non-structural masses, each 30 lb. Chord areas (A_1, A_2, A_3) and web thicknesses (t_1, t_2, t_3) are optimized for minimum weight subject to a minimum fundamental frequency of 20 Hz. No other constraints are applied except minimum gages of $A_i=0.01 \text{ in}^2$ and $t_i=0.001 \text{ in}$. Initial values are $A_i=1.0 \text{ in}^2$ and $t_i=0.2 \text{ in}$. Young's Modulus is $10.3 \times 10^6 \text{ psi}$, Poisson's ratio is 0.3, and the density is 0.1 lb/in^3 .

Designs were feasible at every iteration using RQA without move limits ($f=100$) and the rate of convergence was faster than for Woo's results.



Cantilever Beam Results

The final design is similar to those obtained by Turner,¹⁴ Miura,⁹ and Woo;⁵ however, the weight is slightly higher than for the latter two—entirely as a result of modelling and analysis differences. When Miura and Woo's final designs were analyzed in the small optimization program used for this paper, as well as in ASTROS*, the frequency was 19.3 *hz*. When the lower bound frequency was set to this value, the final designs were more nearly the same.

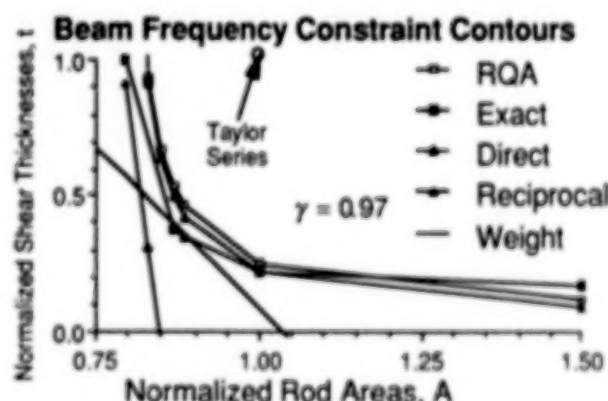
In order to examine the design space, the number of variables was reduced at a point near the optimum design. One design variable was linked to all the rod areas and one linked to the web thicknesses in the ratios given in Table 3. Contours of the resulting constraint surfaces are plotted for the approximate functions along with the actual constraint surface. The failure of the direct TSA reported by Miura and Woo is evident in the poor quality of the approximating constraint surface to the actual highly nonlinear surface. In fact since the direct TSA constitutes a linear programming problem, the optimizer always moves to a vertex in the design space, choosing to maximize the most effective variable while minimizing the rest. In the absence of severely restrictive move limits or other constraints to cut off the design space, a feasible design is never achieved. Also, because the final modal non-structural mass ratio is 0.98, the RQA closely follows the reciprocal TSA. Since the sign of both constraint derivatives is negative, Woo's GHC with $p=0$ and $n=1$ (equivalent to Fleury's Method of Mixed Variables) would be identical to the Reciprocal TSA.

	A.1	A.2	A.3	t.1	t.2	t.3	Weight	Frequency*
Turner**	0.91	0.485	0.14	0.037	0.034	0.023	7.27	19.8
Miura	0.871	0.441	0.108	0.044	0.041	0.026	7.00	19.3
Woo	0.866	0.442	0.109	0.046	0.041	0.025	7.01	19.3
RQA	0.875	0.466	0.129	0.035	0.031	0.020	6.92	19.3
RQA	0.955	0.484	0.140	0.038	0.034	0.022	7.44	20.0

*Frequencies calculated using CROD and CSHEAR elements (lumped mass) in ASTROS.

**Areas for Turner's design are the average for a linearly tapered rod.

Table 2: Cantilever Beam Final Designs



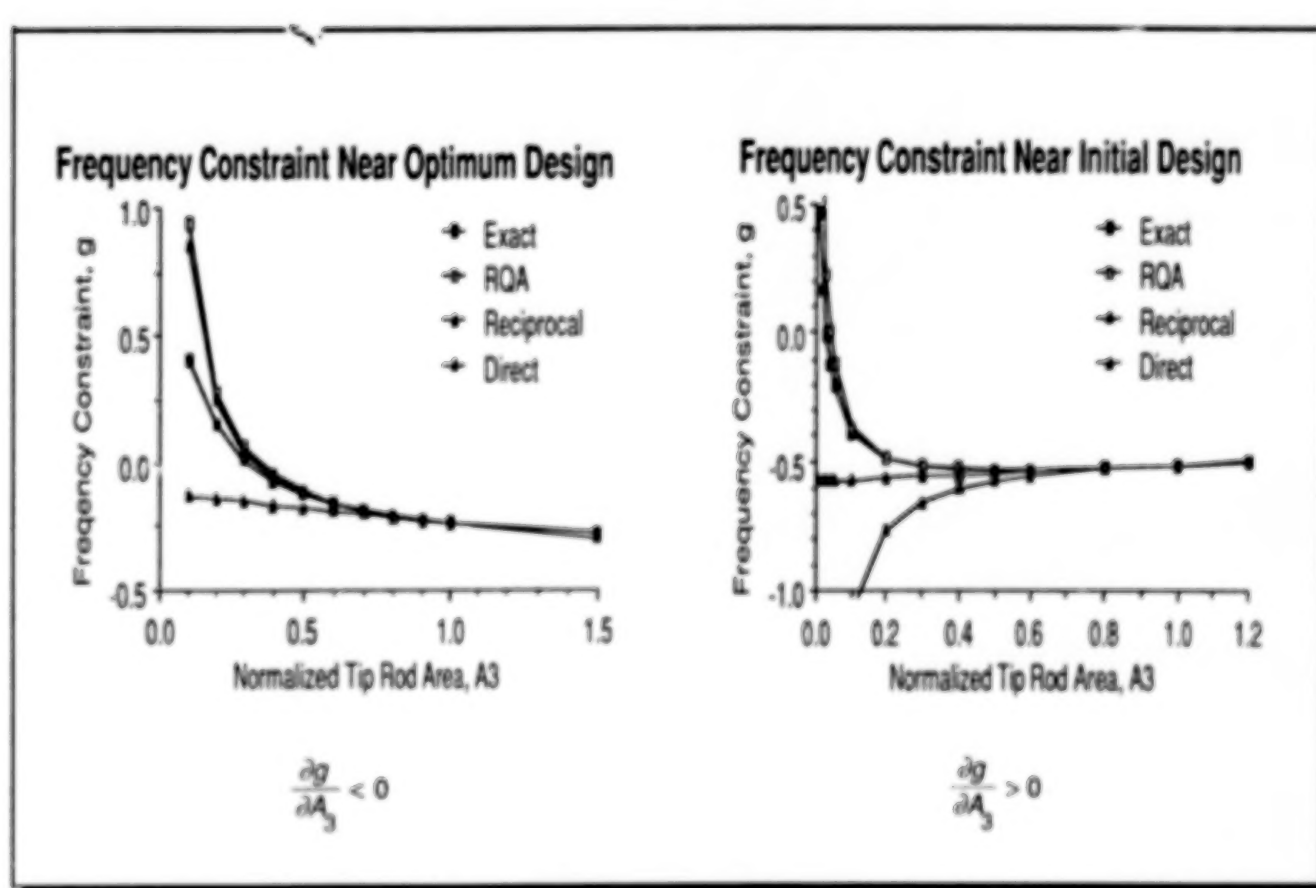
A.1	A.2	A.3
1.0	0.56	0.125
t.1	t.2	t.3
0.10	0.08	0.06

Table 3: Cantilever Beam Intermediate Design

*Automated Structural Optimization System

Cantilever Beam Single Design Variable Constraint Functions

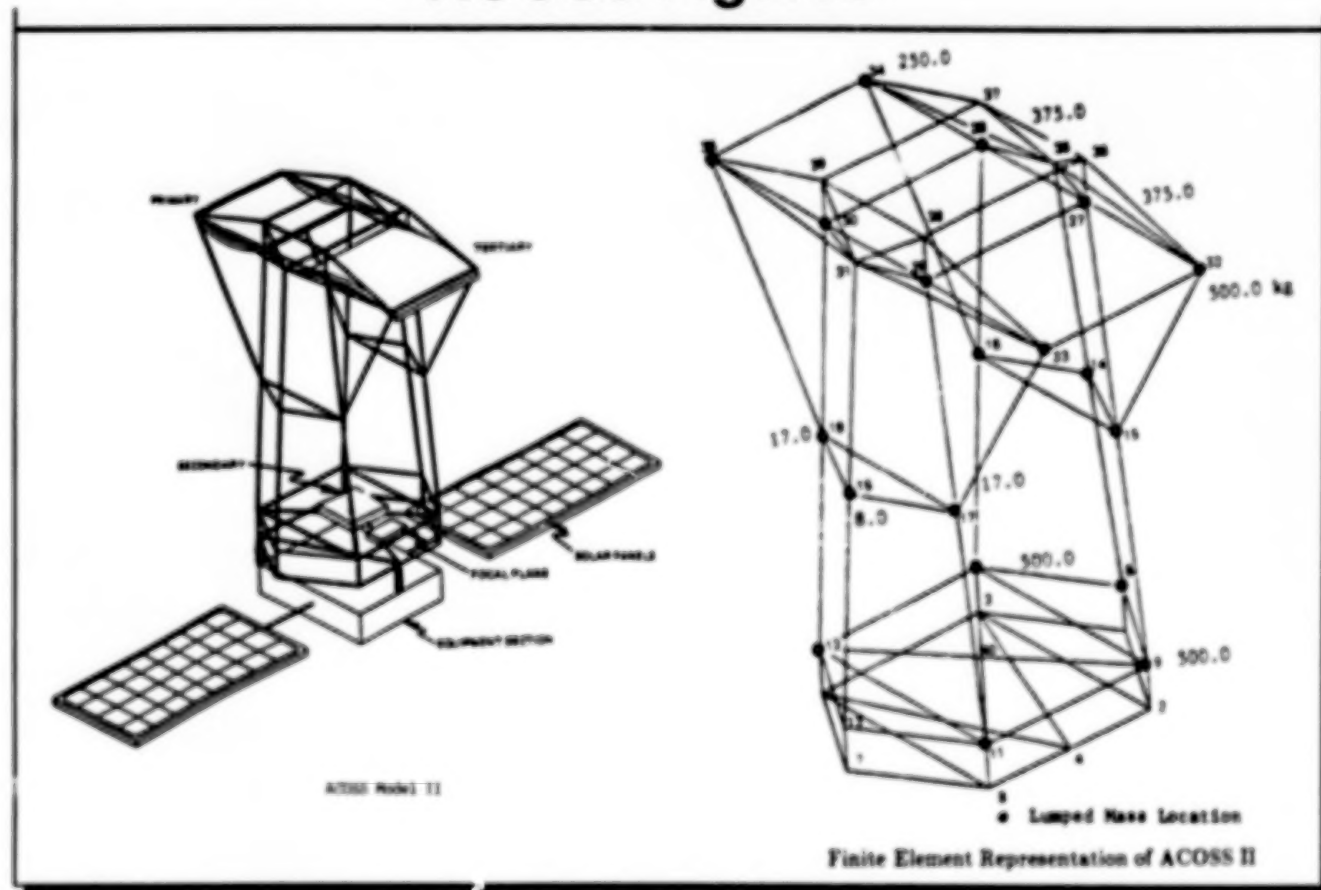
Consider next the constraint surfaces as a function of a single variable, the tip rod's area (A_3). The first plot shows a cut along the A_3 axis through the six-dimensional design space for the constraint functions near the same nearly optimum design point ($\gamma=0.97$). It reflects the same comments mentioned above. The second plot shows the same functions constructed at the initial design point ($\gamma=0.88$) where the constraint derivative with respect to A_3 is positive instead of negative. Here the difference between the RQA and other approximations stands out. The RQA closely follows the actual constraint surface. Its derivative can change sign to match the curvature of the actual surface, whereas the TSA's derivative cannot change sign. In fact, the TSA's derivative is constant in the design space in which it was constructed. The advantage of Woo's GHC is that, based on the constraint's sign, it chooses the direct TSA surface which is more conservative than the reciprocal TSA surface in this case. Neither TSA, however, represents the actual constraint surface well.



ACOSS

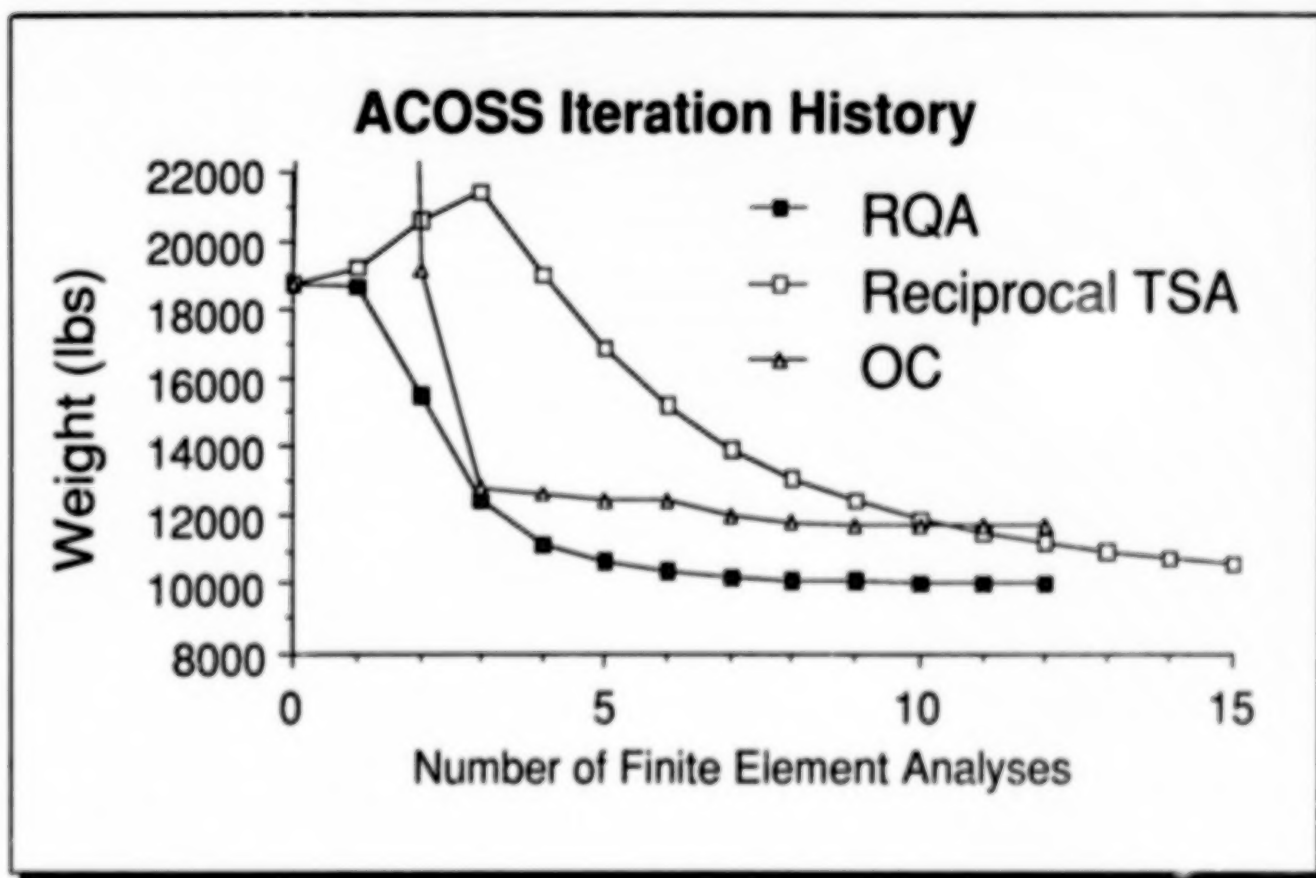
The Active Control Of Space Structures (ACOSS) model II was developed by the Charles Stark Draper Laboratory.¹⁵ The structure consists of two subsystems: (1) the optical support structure and (2) the equipment section. The two are connected by springs at three points to allow vibration isolation. In this problem the equipment section at the base was disregarded and only the optical support structure fixed at the three connection points was considered. The finite element model for this modified ACOSS II has 33 nodes (90 degrees of freedom), 18 concentrated masses, and 113 rod elements made of graphite epoxy with Young's Modulus of 18.5×10^6 psi, Weight Density of 0.055 lb/in^3 , and initial areas of 10.0 in^2 for the truss members.

ACOSS Figures



ACOSS Results

The structural weight was minimized using all 113 elements as design variables subject to a lower bound frequency of 2.0 *hz* and minimum sizes of 0.1 *in*². The results show that RQA achieves a final design significantly better than TSA or the Optimality Criteria (OC) method.¹² A reciprocal TSA fails to converge to a feasible design even with $f=1.5$. The results in the figure are for $f=1.5$ at iteration one, exponentially reduced at each iteration to a lower limit of $f=1.2$. Still, the constraint is violated ($g>0.1\%$) in the first 11 iterations and violated by more than 1% in the first 5 iterations. For RQA the move limit scale factor ($f=2$) prevented a feasible design until after the second iteration, after which all subsequent designs were feasible. With less restrictive move limits ($f=100$ initially, exponentially reduced to $f=2$) RQA's first iteration was feasible; however, some subsequent intermediate designs were violated by 1–3%. RQA still has an infeasible design after increasing the weight in the first iteration and then subsequent designs are feasible. Initially $\gamma=0.42$ and at the final design $\gamma=0.86$, showing why a reciprocal TSA eventually becomes more conservative, producing a feasible final design.



Conclusions.

A new function for approximating the frequency constraints during the solution of a structural optimization's approximate subproblem was developed. The motivation for this Rayleigh Quotient Approximation was to approximate some quantity more fundamental than the eigenvalue itself in order to improve the quality of the constraint approximation. Constructing approximations to the modal strain and kinetic energies independently results in more accurate constraint evaluation without any additional computational burden. The numerical examples demonstrate that the RQA is more conservative than other approximations and permits stable convergence without stringent move limits. Future work should be directed toward examining multiple frequency constraint problems, more direct comparisons to Woo's GHC approach, and application to space frames.

- **RQA—Frequency Constraint Approximation Function**
 - **Separate TSAs for Modal Energies**
- **Higher Quality Approximation**
 - **Generous Move Limits**
 - **Quick Convergence to Feasible Design (Conservative)**
 - **Derivative Changes Sign to Follow Constraint Surface**
- **No User Supplied Parameters**
- **Future Work**
 - **Multiple Frequencies**
 - **Frames**
 - **More Comparisons to GHC (Mixed Variables)**

References

1. Schmit, L.A.; and Farshi, B.: Some Approximation Concepts for Structural Synthesis. *AIAA J.*, vol. 2, no. 5, 1974, pp. 692-699.
2. Schmit, L.A.; and Miura, H.: Approximation Concepts for Efficient Structural Synthesis, NASA CR-2552, 1976.
3. Starnes, J.H.; and Haftka, R.T.: Preliminary Design of Composite Wings for Buckling, Strength, and Displacement Constraints, *J. Aircraft*, vol. 16, no. 8, 1979, pp. 564-570.
4. Fleury, C.; and Braibant, V.: Structural Optimization—A New Dual Method Using Mixed Variables, *I.J. Num. Methods in Engr.*, vol. 23, pp. 409-428, 1986.
5. Woo, T.H.: Space Frame Optimization Subject to Frequency Constraints, Proc. 27th AIAA/ASME/ASCE/AHS Structures, Structural Dynamics, and Materials Conference, San Antonio, TX, May 19-21, 1986, pp. 103-115.
6. Fleury, C.: Efficient Approximation Concepts Using Second Order Information, Proc. 29th AIAA/ASME/ASCE/AHS Structures, Structural Dynamics, and Materials Conference, Williamsburg, VA, April 18-20, 1988, pp. 1685-1695.
7. Vanderplaats, G.N.; and Salajegheh, E.: An Efficient Approximation Technique for Frequency Constraints in Frame Optimization, *I.J. Num. Methods*, vol. 26, 1988, pp. 1057-1069.
8. Venkayya, V.B.; and Tischler, V.A.: Optimization of Structures with Frequency Constraints, *Comp. Methods Nonlinear Solids and Structural. Mech.*, ASME, AMD-54, 1983, pp. 239-259.
9. Miura, H.; and Schmit, L.A.: Second Order Approximation of Natural Frequency Constraints in Structural Synthesis, *I.J. Num. Methods in Engr.*, vol. 13, 1978, pp. 337-351.
10. Vanderplaats, G.N.; and Salajegheh, E.: A New Approximation Method for Stress Constraints in Structural Synthesis, Proc. 28th AIAA/ASME/ASCE/AHS Structures, Structural Dynamics, and Materials Conference, Monterey, CA, April 6-8, 1987, pp. 314-321.
11. Grandhi, R.V.; and Venkayya, V.B.: Structural Optimization with Frequency Constraints, 28th AIAA/ASME/ASCE/AHS Structures, Structural Dynamics, and Materials Conference, Monterey, CA, April 6-8, 1987, pp. 32-329.
12. Fox, R.L.; and Kapoor, M.P.: Rates of Change of Eigenvalues and Eigenvectors, *AIAA J.*, vol. 6, no. 12, 1968, pp. 2426-2429.
13. Canfield, R.A.; Grandhi, R.V.; and Venkayya, V.B.: Structural Optimization with Stiffness and Frequency Constraints, *Mechanics of Structures and Machines*, vol. 17, no. 1, 1989.
14. Turner, M.J.: Design of Minimum Mass Structures with Specified Natural Frequencies, *AIAA J.*, vol. 5, no. 3, March, 1967, pp. 406-412.
15. Handerson, T.: Active Control Of Space Structures (ACOSS) Model 2, Report C-5437, Charles Stark Draper Laboratory, Inc, Sept, 1981.

**STRUCTURAL OPTIMIZATION OF FRAMED STRUCTURES
USING
GENERALIZED OPTIMALITY CRITERIA**

**R. M. Kolonay*, V. B. Venkayya*, V. A. Tischler, and
R. A. Canfield*
AFWAL/FDSRA†
Wright Patterson Air Force Base, Ohio**

*Member AIAA

† Now the Wright Research Development Center

414

ABSTRACT

This paper presents the application of a generalized optimality criteria to framed structures. The optimality conditions, Lagrangian multipliers, resizing algorithm, and scaling procedures are all represented as a function of the objective and constraint functions along with their respective gradients. The optimization of two plane frames under multiple loading conditions subject to stress, displacement, generalized stiffness, and side constraints is presented. These results are compared to those found by optimizing the frames using a nonlinear mathematical programming technique.

INTRODUCTION

Weight optimization of large aerospace structures requires the use of efficient optimization methods due to the potentially excessive number of design variables and related constraints. In order for optimization to be seriously used by the preliminary designer, the method must be able to handle multidisciplinary problems (thousands of design variables and their related constraints) and must be efficient (produce designs in hours not days).

In the late sixties and early seventies the optimality criteria approach to structural optimization was developed[1]. At that time, and in subsequent work, the optimality criterion was derived for an individual problem and although very efficient, it was criticized for its lack of generality. Recently, Venkayya[2] has generalized the optimality criteria to apply to any structural optimization problem to which the sensitivities of the objective and constraint functions can be computed. First, this paper will briefly state the optimality conditions. Next, detailed descriptions of the Lagrangian multipliers, scaling formulation along with a redesign procedure for stress, displacement, and generalized stiffness constraints applied to plane frames will be presented. Finally, the optimization results of some plane frames using the generalized optimality criterion will be given along with a comparison to results found by nonlinear mathematical programming.

PROBLEM STATEMENT

The optimization of a structure for minimum weight can be stated mathematically as:

Minimize the objective function

$$W(A) = \sum_{i=1}^m \rho_i l_i A_i \quad (1)$$

subject to the constraints

$$Z_j(A) \leq \bar{Z}_j \quad j = 1, 2, \dots, n \quad (2)$$

$$A_i^{(L)} \leq A_i \leq A_i^{(U)} \quad (3)$$

where $W(A)$ is the weight of the structure, ρ_i , A_i , and l_i are the specific weight, the cross-sectional area, and the length of the i th element respectively. The $Z_j(A)$ consist of all n of the behavioral constraints and \bar{Z}_j is the given allowable for $Z_j(A)$. The summation in equation (1) is over all m elements in the structure. However, this does not imply that all the elements are required to participate in the design algorithm. In addition to the constraints Z_j , each design variable (A_i) has upper bounds ($A_i^{(U)}$) and lower bounds ($A_i^{(L)}$) referred to as side constraints.

DESIGN VARIABLES

The design variables chosen for the plane frame are A_i , I_{iz} , and S_{iz} , where A_i is the cross-sectional area, I_{iz} is the moment of inertia about the z -axis and S_{iz} is the section modulus about the z -axis. These

variables are not independent; therefore, A_i is chosen as the primary variable with I_{ix} and S_{ix} expressed as explicit nonlinear functions of A_i in the form

$$I_{ix} = \alpha_i A_i^{n_i} \quad (4)$$

$$S_{ix} = \gamma_i A_i^{v_i} \quad (5)$$

Depending on the type of cross-section and the assumptions being made n_i will vary from 1 to 3, and v_i will vary from 1 to 2. It is important to note that this method is general and any design variable can be chosen such as width of the section, thickness of the flange, or thickness of the web of the section. This section will focus on relations between A_i , I_{ix} , and S_{ix} for solid rectangular cross-sections and a three spar box section. Three separate cases will be presented for each type of section. Each case will make varying assumptions about the width of the section, depth of the section, thickness of the flange, thickness of the web, and ratios of these quantities.

For the rectangular section in figure 1 having depth d and width b the following cases for the relations between A_i , I_{ix} , and S_{ix} are presented.

Case 1: Assume b to be constant and d is allowed to vary.

$$\begin{aligned} I_{ix} &= \alpha_i A_i^{n_i} \quad n_i = 3 \quad \alpha_i = \frac{1}{12b^2} \\ S_{ix} &= \gamma_i A_i^{v_i} \quad v_i = 2 \quad \gamma_i = \frac{1}{6b} \end{aligned} \quad (6)$$

Case 2: Assume the ratio b/d is equal to some constant C_o and let b and d vary.

$$\begin{aligned} I_{ix} &= \alpha_i A_i^{n_i} \quad n_i = 2 \quad \alpha_i = \frac{1}{12C_o} \\ S_{ix} &= \gamma_i A_i^{v_i} \quad v_i = 3/2 \quad \gamma_i = \frac{1}{6\sqrt{C_o}} \end{aligned} \quad (7)$$

Case 3: d is assumed to be constant while b is allowed to vary.

$$\begin{aligned} I_{ix} &= \alpha_i A_i^{n_i} \quad n_i = 1 \quad \alpha_i = \frac{d^2}{12} \\ S_{ix} &= \gamma_i A_i^{v_i} \quad v_i = 1 \quad \gamma_i = \frac{d}{6} \end{aligned} \quad (8)$$

Next, consider the three spar box section in figure 2. The area A_i , moment of inertia I_{ix} , and the section modulus can be expressed as:

$$A_i = bd \left\{ 2 \left(1 + \frac{t_w}{b} \right) \frac{t_f}{d} + 3 \left(1 - \frac{t_f}{d} \right) \frac{t_w}{b} \right\}$$

or

$$A_i = bdC_1 \quad (9)$$

$$I_{ix} = \frac{bd^3}{12} \left\{ \left(1 + \frac{t_w}{b} \right) \left(1 + \frac{t_f}{d} \right)^3 - \left(1 - \frac{2t_w}{b} \right) \left(1 - \frac{t_f}{d} \right)^3 \right\}$$

or

$$I_{ix} = \frac{bd^3}{12} C_2 \quad (10)$$

$$S_{ix} = \frac{bd^2}{6} \left\{ \left(\frac{1}{1 + t_f/d} \right) \left(1 + \frac{t_w}{b} \right) \left(1 + \frac{t_f}{d} \right)^3 + \right.$$

$$-\left(1 - \frac{2t_w}{b}\right)\left(1 - \frac{t_f}{d}\right)^3\}$$

or

$$S_{ix} = \frac{bd^2}{6} C_2 C_3 \quad (11)$$

Following these definitions the three cases can now be presented. Case1: The t_w , b , and t_f/d are all held constant.

$$\begin{aligned} A_i &= bdC_1 \\ I_{ix} &= \alpha_i A_i^{n_i} \quad n_i = 3 \quad \alpha_i = \frac{C_2}{12b^2 C_1^3} \\ S_{ix} &= \gamma_i A_i^{v_i} \quad v_i = 2 \quad \gamma_i = \frac{C_2}{6C_1^2 C_3 b} \end{aligned} \quad (12)$$

Case 2: b/d a constant C_4 , t_w/d , and t_f/d a constant.

$$\begin{aligned} A_i &= bdC_1 \\ I_{ix} &= \alpha_i A_i^{n_i} \quad n_i = 2 \quad \alpha_i = \frac{C_2}{12C_1^2 C_4} \\ S_{ix} &= \gamma_i A_i^{v_i} \quad v_i = 3/2 \quad \gamma_i = \frac{C_2 C_4}{6C_3 (C_1 C_4)^{3/2}} \end{aligned} \quad (13)$$

Case 3: b allowed to vary with d , t_w/b , and t_f/d held constant.

$$\begin{aligned} A_i &= bdC_1 \\ I_{ix} &= \alpha_i A_i^{n_i} \quad n_i = 2 \quad \alpha_i = \frac{d^2 C_2}{12C_1} \\ S_{ix} &= \gamma_i A_i^{v_i} \quad v_i = 3/2 \quad \gamma_i = \frac{dC_2}{6C_1 C_3} \end{aligned} \quad (14)$$

These relations for the three spar box can easily be extended to a n spar box cross-section. Also, the I-section can be show to be a special case of the spar box with $n = 1$.

CONDITIONS OF OPTIMALITY

The optimization problem defined by equation (1) can be restated in Lagrangian form as

$$\begin{aligned} L(A, \lambda) &= W(A) - \sum_{j=1}^p \lambda_j (Z_j - \bar{Z}_j) \\ p &= \text{number of active constraints} \end{aligned} \quad (15)$$

L is the Lagrangian function, and λ_j are the Lagrangian multipliers corresponding to the active constraints. A constraint will be defined as active if $Z_j = \bar{Z}_j$. Minimization of the Lagrangian function with respect to the design variable A_i gives

$$\frac{\partial L}{\partial A_i} = \frac{\partial W}{\partial A_i} - \sum_{j=1}^p \lambda_j \frac{\partial Z_j}{\partial A_i} = 0 \quad i = 1, 2, \dots, m \quad (16)$$

Equation (16) can be rewritten as

$$\sum_{j=1}^p e_{ij} \lambda_j = 1 \quad i = 1, 2, \dots, m \quad (17)$$

where e_{ij} is the ratio of constraint to objective function sensitivities and is given by

$$e_{ij} = \frac{\partial Z_j / \partial A_i}{\partial W / \partial A_i} \quad (18)$$

or in matrix form

$$\epsilon \lambda = \bar{1} \quad (19)$$

where ϵ is an $m \times p$ matrix, λ is an $p \times 1$ matrix and $\bar{1}$ is a $m \times 1$ matrix.

LAGRANGIAN MULTIPLIERS

The Lagrangian formulation introduces more unknowns in addition to the m design variables. These additional unknowns are the Lagrangian multipliers and there are as many Lagrangian multipliers as active constraints p . Thus, it is necessary to solve for $m + p$ unknowns. This section discusses some methods of solution for the Lagrangian multipliers.

Premultiplying equation (19) by $\epsilon^t \psi$ yields

$$\epsilon^t \psi \epsilon \lambda = \epsilon^t \psi \bar{1} = \bar{Z} \quad (20)$$

where the weighting matrix ψ is an $m \times m$ positive definite diagonal matrix. Here the diagonal elements of the ψ matrix are taken to be the individual weights of each element ($\psi_{ii} = \rho_i l_i A_i$). Equation (20) can now be stated as

$$H \lambda = \bar{Z} \quad (21)$$

Although the H matrix is non-singular, it is an implicit function of the final design variables. Thus, equation (21) represents a non-linear set of equations. Thus, some approximate methods are used instead of trying to actually solve for the λ s by some iterative scheme. The first approximate method considered consists of using the information at the current design and solving the equation (21) for the Lagrangian multipliers by inverting the H matrix.

$$\lambda = H^{-1} \bar{Z} \quad (22)$$

One of the drawbacks of this method is that there is no guarantee that all the Lagrangian multipliers will have the appropriate sign. This causes problems when attempting to resize the design variables. The second method considered was originally developed in 1973 by Venkayya and coworkers[3]. This method assumes that only one constraint is active at any one time. For a multi-constraint problem the λ 's simply become weighting parameters. For a single constraint equation (21) reduces to

$$\lambda = \frac{W}{\bar{Z}} \quad (23)$$

In the case of multiple constraints

$$\lambda_j = \frac{W}{\bar{Z}_j} \quad (24)$$

where \bar{Z}_j is found to be

$$\bar{Z}_j = \sum_{i=1}^m e_{ij} w_{ii} \quad (25)$$

Calculating the λ 's with this approximate method is computationally very efficient compared to inverting the H matrix. This is because w_{ii} are the weights of the individual elements and \bar{Z}_j is a simple function of the given constraint. When finding the λ s by this approximate method it is always assured that the λ s will have the necessary sign.

RESIZING ALGORITHM

Using the optimality criterion described in equation (17) an iterative resizing algorithm can be found by multiplying equation (17) by A_i^r and solving for A_i

$$A_i^{r+1} = A_i^r \left[\sum_{j=1}^p c_{ij} \lambda_j \right]^{1/\zeta} \quad (26)$$

where ζ is defined as a step size parameter and r indicates the r th iteration. For most problems $\zeta = 2$ is chosen and gives a good rate of convergence.

SCALING PROCEDURE

Once a new design has been generated by the resizing algorithm the constraint surface must be found. This is done by the use of a scaling procedure. Let \bar{A} be the current design vector with the new design found by $\bar{A} = \Lambda \bar{A}$ where Λ is the scale factor. If $d\bar{A}$ is the difference between two designs, it can be written as

$$d\bar{A} = \bar{A} - A = (\Lambda - 1)A \quad (27)$$

If the response of the structure is R , then performing a first order Taylor Series expansion on R about the current design point A yields

$$\bar{R} = R + \sum_{i=1}^m \frac{\partial R}{\partial A_i} dA_i \quad (28)$$

Substituting equation (27) for dA , dividing both sides of the equation by the response R , and realizing that $\bar{R} - R = dR$ yields

$$\frac{dR}{R} = (\Lambda - 1) \frac{\sum_{i=1}^m \frac{\partial R}{\partial A_i} A_i}{R} \quad (29)$$

In equation (29) the term $\left[\sum_{i=1}^m \frac{\partial R}{\partial A_i} A_i \right] / R$ is either ≤ 0 or ≥ 0 depending on the type of constraint being considered. For this work only stress and displacement constraints are being investigated and for these cases $\left[\sum_{i=1}^m \frac{\partial R}{\partial A_i} A_i \right] / R$ is always ≤ 0 . Now defining μ as

$$\mu = - \frac{\sum_{i=1}^m \frac{\partial R}{\partial A_i} A_i}{R} \quad (30)$$

equation (29) can be expressed as

$$\frac{dR}{R} = (1 - \Lambda)\mu \quad (31)$$

Solving equation (31) for the inverse of the scale factor Λ and defining $b = \frac{1}{\mu} \frac{dR}{R}$ gives

$$\frac{1}{\Lambda} = \frac{1}{1 - b} \quad b \ll 1 \quad (32)$$

By performing a binomial expansion and ignoring higher order terms equation (32) becomes

$$\frac{1}{\Lambda} = 1 + b \quad (33)$$

Rearranging equation (33), adding 1 to both sides, and defining β as the target response ratio equation (33) becomes

$$\beta = \frac{\mu}{\Lambda} = \mu + 1 \quad (34)$$

where β is

$$\beta = \frac{\text{New Response}}{\text{Initial Response}} = \frac{R + dR}{R} \quad (35)$$

Finally, solving equation (34) for the scale factor gives

$$\Lambda = \frac{\mu}{\beta + \mu - 1} \quad (36)$$

In the case of truss or membrane structures $\mu = 1$ and Λ reduces to $1/\beta$ which is the exact scale factor for stress and displacement constraints.

SPECIALIZATION TO BENDING ELEMENTS

In the following sections the e_{ij} , λ_j , and Λ for bending elements subject to stress, displacement, and generalized stiffness constraints will be discussed.

DISPLACEMENT CONSTRAINTS

To find the e_{ij} for displacement constraints the gradient of the constraint with respect to the design variable $(\partial Z_j / \partial A_i)$ is required. There are several methods for finding these gradients (finite difference, direct differentiation, virtual load method), but for this work the virtual load method was incorporated. The virtual load method consists of expressing the active constraint Z_j in terms of a virtual load vector F_j^t and the global displacements u . Thus, the displacement constraint $Z_j = u_j$ can be written as

$$Z_j = u_j = F_j^t u \quad (37)$$

where F_j^t is the virtual load vector in which $F_j = 1$ for $i = j$ and $F_j = 0$ if $i \neq j$. The e_{ij} can be found by first partitioning the element stiffness matrix K_i into axial K_{Ai} and bending K_{Bi} components. Next, substitute the relation $\alpha_i A_i^{n_i}$ for I_{i2} and note that $\partial W / \partial A_i = \rho_i l_i$. Then e_{ij} for a displacement constraint becomes

$$e_{ij} = \frac{f_j^t (K_{Ai} + n_i K_{Bi}) u}{\rho_i l_i A_i} \quad (38)$$

where f_j^t is the virtual displacement vector corresponding to the virtual load vector F_j^t and is obtained from the relation

$$F_j = K f_j^t \quad (39)$$

Once e_{ij} is known the Lagrangian multiplier λ_j for the j th active constraint can be found by using equation (23). The resulting λ 's are

$$\lambda_j = - \frac{W}{Z_j (\mu_{Aj} + \mu_{Bj})} \quad (40)$$

where the parameters μ_{Aj} and μ_{Bj} are

$$\mu_{Aj} = \frac{\sum_{i=1}^m f_j^t K_{Ai} u}{F_j^t u} \quad (41)$$

$$\mu_{Bj} = \frac{\sum_{i=1}^m n_i f_j^t K_{Bi} u}{F_j^t u} \quad (42)$$

For the scaling factor of equation (36) the parameter μ can be broken up into axial and bending parts μ_{Aj} , μ_{Bj} . Therefore,

$$\mu = \mu_{Aj} + \mu_{Bj} \quad (43)$$

and the scale factor for displacement constraints becomes

$$\Lambda = \frac{\mu_{Aj} + \mu_{Bj}}{\beta + \mu_{Aj} + \mu_{Bj} - 1} \quad (44)$$

$1/\beta$ which is the scale factor for membrane structures originally found by Venkayya in 1971[1]. By inspection of μ_{Aj} and μ_{Bj} and recalling the limits on n_i for bending elements, it follows that

$$1 \leq \mu_{Aj} + \mu_{Bj} \leq 3 \quad (45)$$

STRESS CONSTRAINTS

For bending elements the stress in the j th member is expressed in terms of its bending and axial components as; $\sigma_j = \sigma_{jA} + \sigma_{jB}$. The gradients of the stress constraints ($\partial Z_j / \partial A_i$) are found by the adjoint variable method which is a generalization of the virtual load method. That is, the constraints are recast in terms of a virtual load vector F_j^t and the global displacement vector u . The stress in a given member was written by Venkayya [2] as

$$\sigma_j = T_j^t Q_j \quad (46)$$

where the vector T_j is defined as

$$T_j^t = \begin{bmatrix} \frac{SGN}{A_j} & 0 & \frac{SGN}{S_j} & 0 & 0 & 0 \end{bmatrix} \quad \text{end A} \quad (47)$$

$$T_j^t = \begin{bmatrix} 0 & 0 & 0 & \frac{SGN}{A_j} & 0 & \frac{SGN}{S_j} \end{bmatrix} \quad \text{end B} \quad (48)$$

where SGN is the sign on the entries of the element force vector Q_j and S_j is the section modulus defined as $S_j = \gamma_j A_j^{3/2}$. The element force matrix can be expressed in terms of the global displacements u , the local element stiffness k_j , and a transformation matrix a_j as

$$Q_j = k_j a_j u \quad (49)$$

Now the stress σ_j can be written in terms of a virtual load vector F_j^t and the global displacements as

$$\sigma_j = F_j^t u \quad (50)$$

where the virtual load vector $F_j^t = T_j^t k_j a_j$. Unlike displacement constraints the derivative of the virtual load vector with respect to the design variable is not equal to zero ($\partial F_j^t / \partial A_i \neq 0$). This fact causes somewhat more complicated expressions for e_{ij} , λ_j and Λ . For stress constraints e_{ij} becomes

$$e_{ij} = \frac{\delta_{ij} [T_j^t \bar{Q}_j - \bar{T}_j^t Q_j] - f_j^t [K_{Ai} + n_i K_{Bi}] u}{\rho_i l_i A_i} \quad (51)$$

where δ_{ij} is the Kronecker delta and \bar{T}_j^t and \bar{Q}_j are defined as

$$\bar{T}_j^t = -\frac{\partial T_j^t}{\partial A_j} A_j \quad (52)$$

$$\bar{Q}_j = (k_{Aj} + n_j k_{Bj}) a_j u_j \quad (53)$$

Now, the Lagrangian multiplier for the j th constraint can be found as

$$\lambda_j = -\frac{W}{Z_j (\mu_{Aj} + \mu_{Bj} - \mu_j)} \quad (54)$$

where μ_{Aj}, μ_{Bj} are the same as those for the displacement constraints. μ_j is a new term introduced due to the fact that $\partial F_j^s / \partial A_i \neq 0$ for stress constraints and it is found to be

$$\mu_j = \frac{\bar{T}_j^s \bar{Q}_j - \bar{T}_j^d Q_j}{\bar{T}_j^s u} \quad (55)$$

Finally, following the derivation of equation (36) the scale factor for bending elements subject to stress constraints can be found to be

$$\lambda = \frac{\mu_{Aj} + \mu_{Bj} - \mu_j}{\beta + \mu_{Aj} + \mu_{Bj} - \mu_j - 1} \quad (56)$$

GENERALIZED STIFFNESS CONSTRAINT

If P is the generalized forces and u is the corresponding generalized displacements then the generalized stiffness constraint can be written as

$$Z_j(A) = \frac{1}{2} P_i^t u_i \quad i = 1, 2, \dots \text{load cases} \quad (57)$$

The e_{ij} , μ_{Aj} , μ_{Bj} , and λ_j can be found to be

$$\begin{aligned} e_{ij} &= -\frac{\frac{1}{2} u^t [K A_i + n_i K B_i] u}{\rho_i l_i A_i} \\ \mu_{Aj} &= \sum_{i=1}^m \frac{u^t K A_i u}{P_j^t u} \\ \mu_{Bj} &= \sum_{i=1}^m \frac{n_i u^t K B_i u}{P_j^t u} \\ \lambda_j &= -\frac{W}{Z_j(\mu_{Aj} + \mu_{Bj})} \end{aligned} \quad (58)$$

It is worthwhile to note that the generalized stiffness constraint does not require the use of the virtual load and displacement vector. This is because the information needed for the gradient of the constraint is already available and no new computations are needed.

MEETING THE CONDITIONS OF OPTIMALITY

The conditions of optimality state that the product between $e_{ij} \lambda_j$ summed over all active constraints should be equal to unity at the optimum design. The e_{ij} are the ratios of the constraint gradients to objective gradients. These gradients are taken with respect to each active design variable A_i . A design variable is considered active if it satisfies the following criteria:

1. The variable is chosen to participate in the design iteration.
2. The variable is within the given allowable limits.
3. The sensitivity of the j th active constrain with respect to the design variable A_i is negative ($\frac{\partial Z_j}{\partial A_i} < 0$).
It is important to note that this third criteria is constraint dependent.

If the design variable does not satisfy the above criteria it is considered passive and the conditions of optimality will not be satisfied for that particular design variable. That is $\sum e_{ij} \lambda_j$ may not be equal to unity at the optimum design. If the variable does not satisfy the first two criteria then the variable is simply eliminated from the design for that particular iteration. However, if the variable passes the first two criteria there is some question on how to handle the third criteria since it is constraint dependent. It is easy to see that A_i may be passive for one constraint ($\frac{\partial Z_j}{\partial A_i} > 0$) but active for another constraint ($\frac{\partial Z_{j+1}}{\partial A_i} < 0$). This raises the question of how does one deal with the e_{ij} when a member is passive relative to a particular constraint? In this work if $\partial Z_j / \partial A_i > 0$ then e_{ij} for that particular constraint and design variable was set to zero.

MODIFYING THE RESIZING ALGORITHM

When using the resizing algorithm equation (26) as it appears (that is taking the sum of all the $e_{ij}\lambda_j$) it was found that this tends to over constrain the problem. The converged optimum was well above the known optimum. This was particularly true for multiple loading conditions. Here, instead of using the entire sum for resizing the maximum value of $e_{ij}\lambda_j$ for the particular design variable was chosen. This can be interpreted as each variable being resized based on the constraint that is most critical for that particular element. This method was found to work well and allowed the algorithm to converge to the known optimum.

REDUCING THE ERROR IN THE SCALE FACTORS

Due to the Taylor Series and binomial approximations the scaling factors in equations (40,56) are only valid within certain limits. This is especially true when the structure is primarily in bending. This is because equations (40,56) do not reduce to the exact bending scale factor $(1/\beta)^{1/n}$ if axial contributions are ignored. It is desired that the limits on β extend indefinitely without allowing the error in the scale factor or the response to exceed 5%. If this can be accomplished, then no additional detailed analyses are required to scale the design to the constraint surface. Venkayya[5] achieved this by writing an interaction formula in the non-dimensional parameter space μ^* . Since the limits on μ_{Aj} , μ_{Bj} and Λ are known this is easily accomplished. The μ_{Aj} and μ_{Bj} indicate what portion of each scale factor (Λ_{axial} , $\Lambda_{bending}$) must be used to generate the scale factor for the combined axial bending case. A linear interpolation was used and the error on the scale factor and response was found to be $< 2\%$ regardless of the β . The scale factor can be represented by a linear interaction formula as

$$\Lambda = \frac{\mu_{Aj}}{\bar{\mu}_{Aj}} \left(\frac{1}{\beta} \right) + \frac{\mu_{Bj}}{\bar{\mu}_{Bj}} \left(\frac{1}{\beta} \right)^{\frac{1}{n}} \quad (59)$$

where μ_{Aj} , μ_{Bj} are the non-dimensional parameters found in equations (41,42), and $\bar{\mu}_{Aj} = 1$ and $\bar{\mu}_{Bj} = n$. One could also fit a higher order polynomial between the two ranges of Λ to totally eliminate the error, but an error $\leq 2\%$ is generally sufficient. If each element in the structure has a different n then equation (59) can be written as

$$\Lambda = \frac{\mu_{Aj}}{\bar{\mu}_{Aj}} \left(\frac{1}{\beta} \right) + \frac{\mu_{Bj}}{\bar{\mu}_{Bj}} \left(\frac{1}{\beta} \right)^{\frac{1}{n}} \quad (60)$$

where now $\bar{\mu}_{Bj} = \bar{n}$ and $\bar{n} = \frac{\mu_{Bj}}{\mu_{Aj}}$ with

$$\bar{\mu}_{Bj} = \frac{\sum_{i=1}^m \int_j^i K_{Bj} v_i}{\int_j^i v_i} \quad (61)$$

SAMPLE PROBLEMS AND RESULTS

On the basis of the preceding derivations, a computer program written in FORTRAN 77 was developed. The frames used in these examples are steel structures with a specific weight of .283 lb/cubic inch and a modulus of elasticity of 29ksi. The type of section used is I-sections and the values for α_1 , n_1 , γ_1 and v_1 are .2072, 3.0, .393, 2.0 respectively for all members. All problems were solved on a VAX 8600. For these problems the resizing was based on the generalized stiffness and displacement constraints where the scaling was done with respect to the stress and displacement constraints.

The first example optimized is a ten-story symmetric frame show in figure 3 that was reported by Tabak and Wright[4]. In this work the distributed loads used in reference [4] were replaced by concentrated load (figure 4), thus creating new nodes at the mid span of each floor. By doing this the thirty member plane frame reported in reference [4] became a forty member structure. This frame was optimized with stress constraints of 22ksi on each element and displacement constraints of two inches in the horizontal direction for all the nodes. Figure 5 shows that the math programming method converged [5],[6],[7] in seven iterations to a final weight of 35,051 pounds in 37.28 cpu seconds while the optimality criteria converged to 36,421

pounds in four iterations with a cpu time of 4.33 seconds [8]. The optimality criteria final weight is slightly higher (4%) but the cpu time is significantly less (over eight times less) than that of math programming.

The final example optimized is the 313 member frame in figure 6. This frame is subject to five loading conditions (figure 7), along with stress and displacement constraints. The displacement constraints are 4.0 inches in the vertical and 12.0 in the horizontal direction at all nodes. The limit for the stresses in each element was 29 ksi. In figure 8 it can be seen that math programming converges to a final weight of 120,419 pounds in fourteen iterations with a cpu time of 58 minutes. Where the optimality criteria converged to a final weight of 125,166 pounds in twenty-five iterations using approximately 8 minutes of cpu time. Again, the optimality criteria converges to a slightly higher weight (4% higher). The optimality criteria took a significantly large number of iterations to converge compared to math programming. This poor convergence is partly due to constraint switching. Even with the large number of iterations the cpu time for the optimality criteria algorithm is much lower than that for math programming.

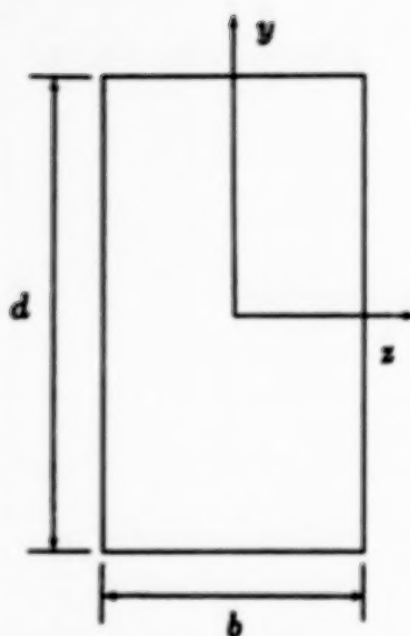
CONCLUSIONS

The generalized optimality criteria presented in this paper can be applied to any structural optimization problem and related constraints provided that the constraints and their respective gradients are available. The math programming method finds a new design by adding and subtracting gradient information to the current design. Searching from point to point can be a very long and costly procedure. On the other hand, in the optimality criteria a redesign is computed by multiplying (not adding) gradient information to the current design thus, sweeping the design space instead of performing a point search. The optimality criteria is also fairly independent of the the number of design variables, thus allowing literally thousands of independent design variables. This is not the case with math programming where an upper limit on the number of independent design variables is between three to four hundred. When this limit is exceeded computer time becomes excessive and convergence is uncertain. For these problems the math programming method although computationally heavy gave a smooth rate of convergence and overall very good results.

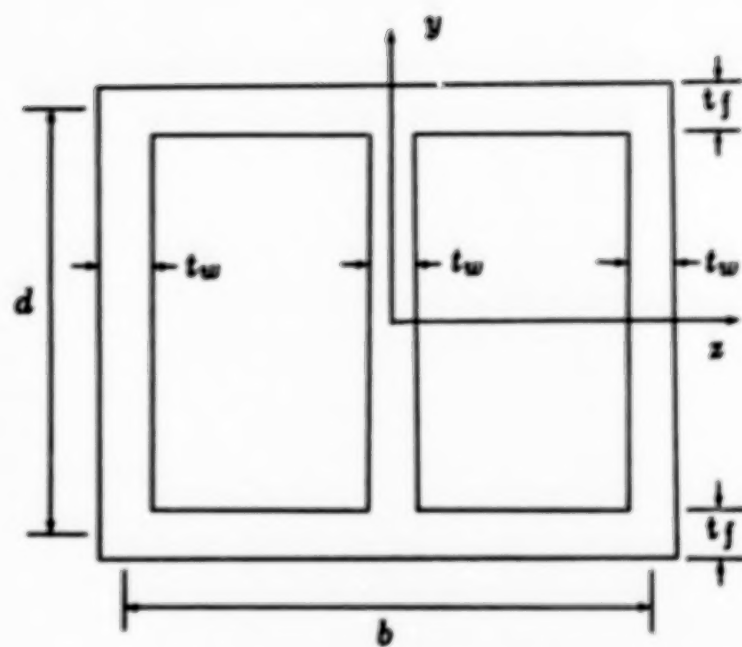
There are some disadvantages to using the optimality criteria which are evident in the sample problems. The optimality criteria, with the current implementation, converges to a 2% to 4% higher weight than that found by the mathematical programming method. Also, for the 313 member frame the optimality criteria method took a very large number of iterations to converge to the optimum. This is very undesirable since detailed analyses for large problems can become extremely expensive.

REFERENCES

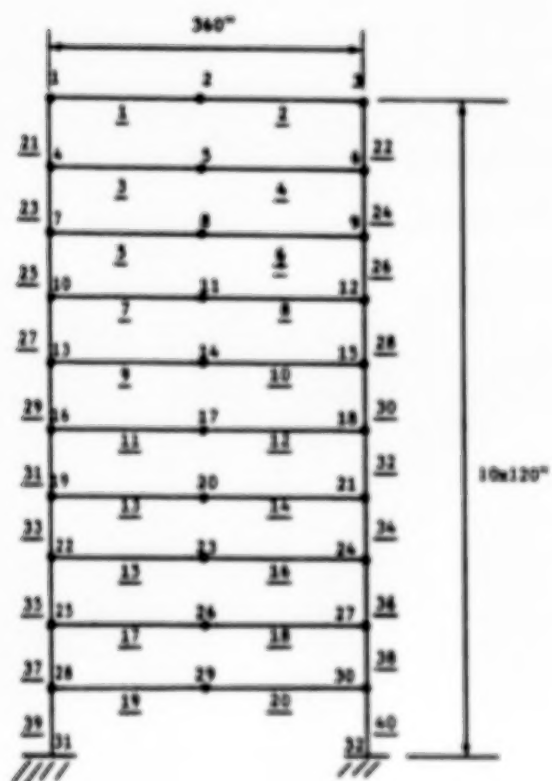
1. Venkayya V. B., "Design of Optimum Structures", Computer and Structures, pp 265-309, vol. 1, 1971.
2. Venkayya V. B., Khot, N. S., and Berke, L., "Applications of Optimality Criteria Approaches to Automated Design of Large Practical Structures", Advisor Group for Aerospace Research and Development Conference Proceeding No. 123, Second Symposium of Structural Optimization, pp3-1, 3-9, 1973.
3. Venkayya, V. B., "A Further Generalization of Optimality Criteria Approaches in Structural Optimization", International Conference on Computational Engineering Science, Atlanta, Georgia, 10-14 April 1988.
4. Todorak E. and Wright, P. M., "Optimality Criteria Method for Building Frames", Journal of Structures A, pp 1327-1337, July 1981.
5. Zoutendijk, G., "Methods of Feasible Directions", Elsevier, Amsterdam, 1960.
6. Vanderplatts, G. N., "CONMIN a FORTRAN Program for Constrained Function Minimization", NASA TMX-62-282, August 1973.
7. Schmit L. A., and Miura, H., "NASA Contractor Report", NASA CR-2552, March 1976.
8. Kolonay, R. M., "Thesis Presented in Partial Fulfillment of the Requirement for The Degree of Master of Science in the Graduate School of The Ohio State University", The Ohio State University, March 1987.



Rectangular Section
Figure 1



Three Spar Box Section
Figure 2

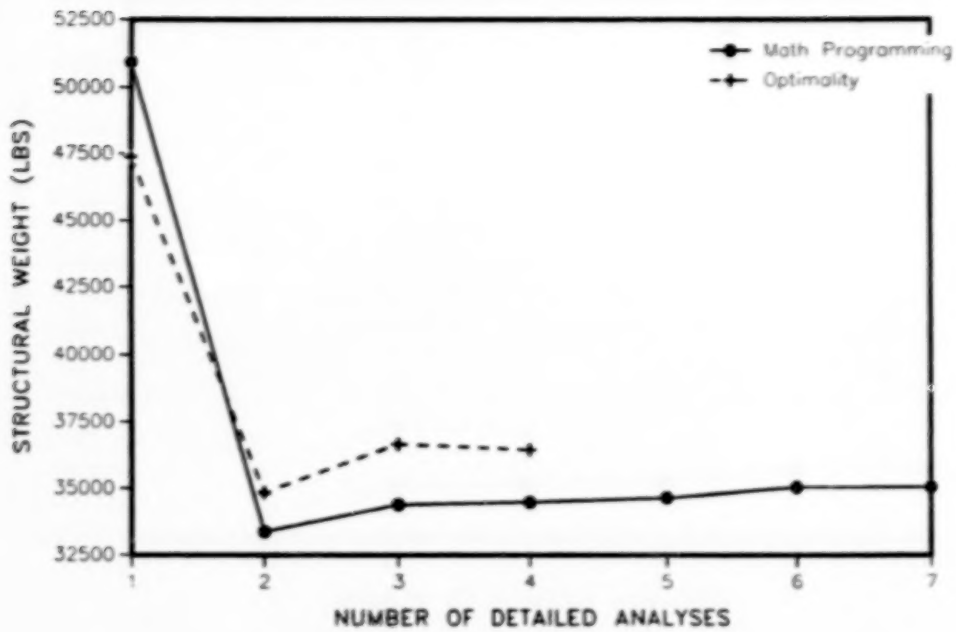


40 Member Frame
Figure 3

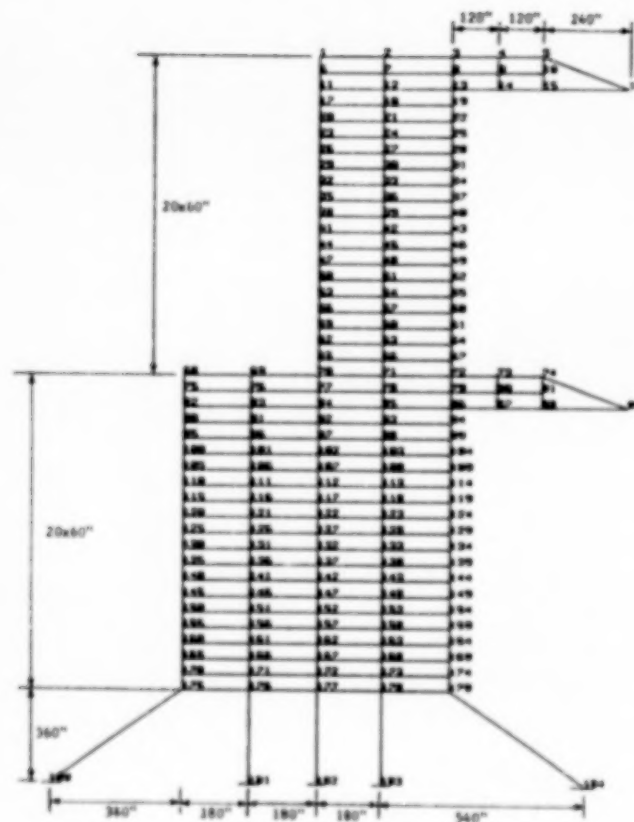
		Load case 1		Moment (inch · lbs)
Node	x-Load (lbs)		y-Load (lbs)	
1,3			-8000.	
2,			-24000.	
4,6,7,9,12			-12000.	
13,15,16,18,19			-12000.	
21,22,24,25,27			-12000.	
28,30			-12000.	
5,8,11,14,17,20			-48000.	
23,26,29			-48000.	
		Load case 2		Moment (inch · lbs)
Node	x-Load (kips)		y-Load (kips)	
1,3			-4500.	
2,			-18000.	
4,6,7,9,12			-9000.	
13,15,16,18,19			-9000.	
21,22,24,25,27			-9000.	
28,30			-9000.	
5,8,11,14,17,20			-36000.	
23,26,29			-36000.	
1	3180.			
4	6230.			
7	6080.			
10	5920.			
13	5740.			
16	5540.			
19	5300.			
22	5000.			
25	4610.			
28	4010.			
		Load case 3		Moment (inch · lbs)
Node	x-Load (kips)		y-Load (kips)	
1,3			-4500.	
2,			-18000.	
4,6,7,9,12			-9000.	
13,15,16,18,19			-9000.	
21,22,24,25,27			-9000.	
28,30			-9000.	
5,8,11,14,17,20			-36000.	
23,26,29			-36000.	
1	-3180.			
4	-6230.			
7	-6080.			
10	-5920.			
13	-5740.			
16	-5540.			
19	-5300.			
22	-5000.			
25	-4610.			
28	-4010.			

Loading Information For 40 Member Frame
Figure 4

40 ELEMENT STRUCTURE



Weight Iteration History
Figure 5



313 Member Frame
Figure 6

Load case 1			
Node	x-Load(kips)	y-Load(kips)	Moment(inch · kip)
15		-26.	
16		-30.	
88		-18.	
89		-20.	

Load case 2			
Node	x-Load(kips)	y-Load(kips)	Moment(inch · kip)
1	2.0		
6 thru 65 by 5	4.0		
68,75,82	4.0		
90 thru 170 by 5	4.0		

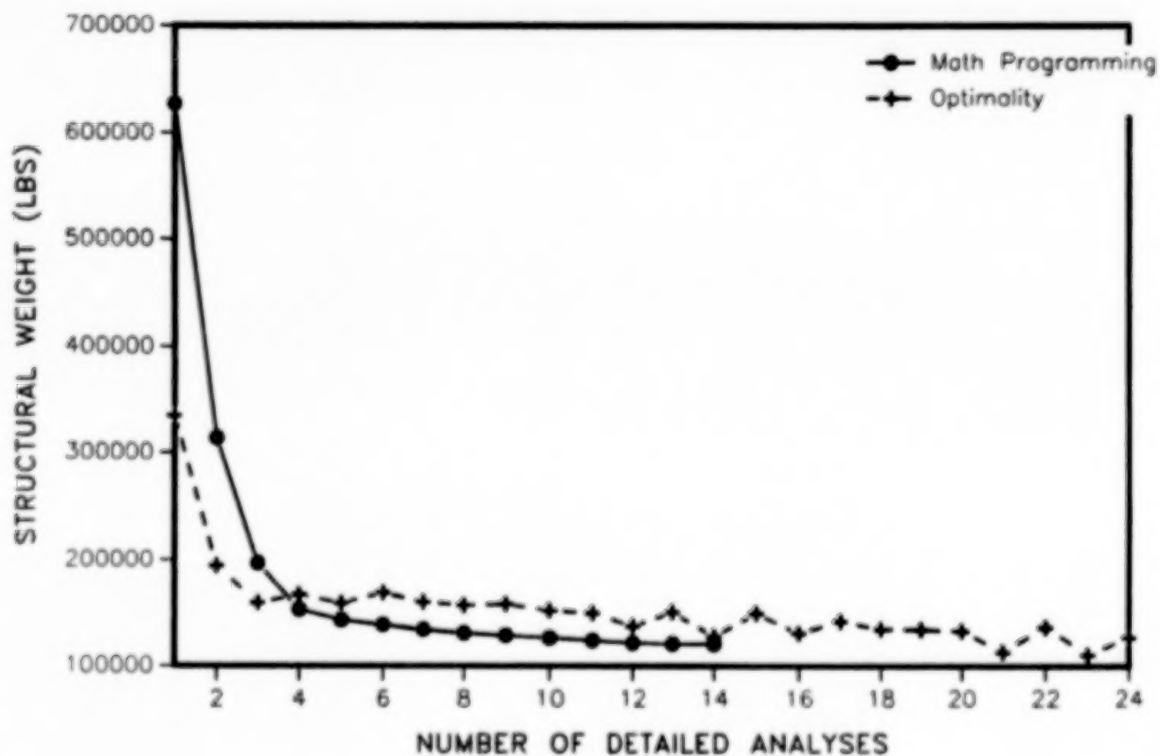
Load case 3			
Node	x-Load(kips)	y-Load(kips)	Moment(inch · kip)
5	-2.0		
16,19	-4.0		
22 thru 67 by 5	-4.0		
74,89	-4.0		
94 thru 174 by 5	-4.0		

Load case 4 = Load case 1 + Load case 2

Load case 5 = Load case 1 + Load case 3

Loading Information For 313 Member Frame
Figure 7

313 ELEMENT STRUCTURE



Weight Iteration History
Figure 8

**FINITE ELEMENT FLOW-THERMAL-STRUCTURAL ANALYSIS
OF AERODYNAMICALLY HEATED LEADING EDGES**

**Pramote Dechaumphai and Allan R. Wieting
NASA Langley Research Center
Hampton, Virginia**

**Ajay K. Pandey
Planning Research Corporation
Hampton, Virginia**

GOAL

Hypersonic vehicles operate in a hostile aerothermal environment which has a significant impact on their aerothermostructural performance. Significant coupling occurs between the aerodynamic flow field, structural heat transfer, and structural response creating a multidisciplinary interaction. A long term goal of the Aerothermal Loads Branch at the NASA Langley Research Center is to develop a computational capability for integrated fluid, thermal and structural analysis of aerodynamically heated structures. The integrated analysis capability includes the coupling between the fluid and the structure which occurs primarily through the thermal response of the structure, because (1) the surface temperature affects the external flow by changing the amount of energy absorbed by the structure, and (2) the temperature gradients in the structure result in structural deformations which alter the flow field and attendant surface pressures and heating rates.

In the integrated analysis, a finite element method is used to solve: (1) the Navier-Stokes equations for the flow solution, (2) the energy equation of the structure for the temperature response, and (3) the equilibrium equations of the structure for the structural deformation and stresses. See figure 1. Recent progress in the development of the capability is described in Ref. 1.

DEVELOP CAPABILITY FOR INTEGRATED FLUID-THERMAL-STRUCTURAL ANALYSIS FOR AERODYNAMICALLY HEATED STRUCTURES

- INCLUDE FLOW, STRUCTURAL HEAT TRANSFER AND STRUCTURAL DEFORMATION INTERACTIONS
- USE FINITE ELEMENT METHOD:
 - NAVIER-STOKES EQUATIONS FOR FLOW
 - ENERGY EQUATION FOR HEAT TRANSFER
 - EQUILIBRIUM EQUATIONS FOR STRUCTURAL RESPONSE

Figure 1

INTEGRATED FLUID-THERMAL-STRUCTURAL ANALYSIS APPROACH

The integrated fluid-thermal-structural finite element analysis approach is illustrated in figure 2 on an actively cooled scram jet engine structure. A general automated unstructured gridding technique is used to discretize the aerodynamic and coolant flow field and the structure for the thermal and structural analyses. A transient vectorized finite element algorithm is used to solve the nonlinear disciplinary equations for the solutions of the aerodynamic flow, the aerothermal loads, and the structural response. Simultaneous solution of all three disciplines is possible if required. Adaptive refinement techniques based on error indicators are applied in the analysis process to minimize the problem size and to help provide accurate and economical solutions. Several color graphic techniques are used to display the results. This integrated approach is available in a code named LIFTS, an acronym for **L**angley **I**ntegrated **F**luid-**T**hermal-**S**tructural analyzer.

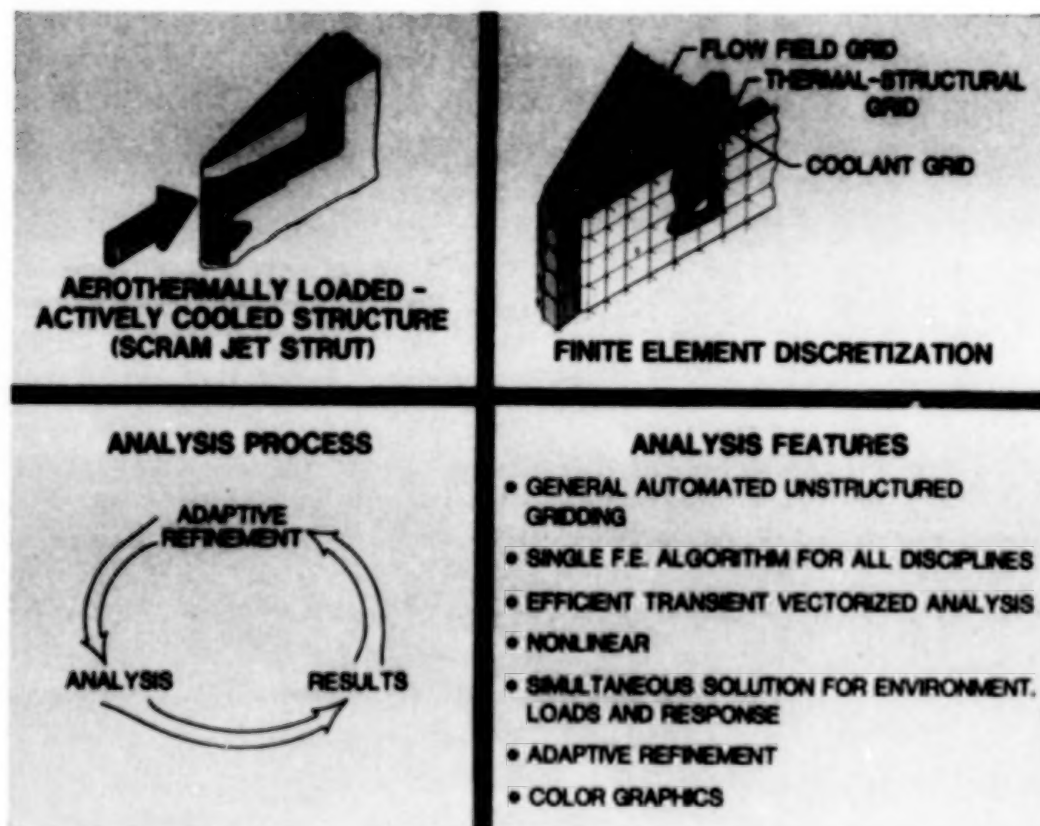


Figure 2

FLUID-THERMAL-STRUCTURAL FORMULATION

The aerodynamic flow equations are described by the conservation of mass, momentum, and energy equations. These equations can be written in conservation form as shown on the left of figure 3. The fluid unknowns are the density ρ , the velocity components u and v , and the total energy ϵ . The flux components, E and F , contain aerothermal terms such as the aerodynamic pressure, wall shear stress, and heat flux, which are of interest to the thermal structural designer.

The thermal and structural equations are also written in conservation form as shown on the right of figure 3. The first two terms in the brackets represent components of the structural equilibrium equations and the last term represents components of the energy equation for the heat transfer in the structure. Nonlinearities due to the temperature dependent material properties and large strain-displacement relations are included. Details of these fluid, thermal, structural equations are given in Ref. 2.

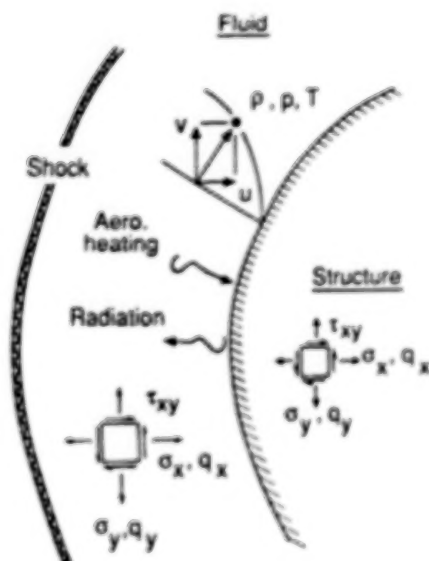
FLUID ANALYSIS

$$\frac{\partial \{U\}}{\partial t} + \frac{\partial \{E\}}{\partial x} + \frac{\partial \{F\}}{\partial y} = 0$$

$$\{U\} = \begin{Bmatrix} \rho \\ \rho u \\ \rho v \\ \rho \epsilon \end{Bmatrix}$$

$$\{E\} = \begin{Bmatrix} \rho u \\ \rho u^2 + p \\ \rho uv \\ \rho u \epsilon + pu \end{Bmatrix}$$

$$+ \begin{Bmatrix} 0 \\ \sigma_x \\ \tau_{xy} \\ u \sigma_x + v \tau_{xy} - q_x \end{Bmatrix}$$



THERMAL-STRUCTURAL ANALYSIS

$$\frac{\partial \{U\}}{\partial t} + \frac{\partial \{E\}}{\partial x} + \frac{\partial \{F\}}{\partial y} = 0$$

$$\{U\} = \begin{Bmatrix} cu \\ cv \\ \rho c_v T \end{Bmatrix}; \{E\} = \begin{Bmatrix} -\sigma_x \\ -\tau_{xy} \\ q_x \end{Bmatrix}$$

- c is fictitious damping constant
- Temperature dependent material properties
- Large strain-displacement,

$$\epsilon_x = \frac{\partial u}{\partial x} + \frac{1}{2} \left(\frac{\partial u}{\partial x} \right)^2 + \frac{1}{2} \left(\frac{\partial v}{\partial x} \right)^2$$

Figure 3

COWL AEROTHERMAL LOADS AMPLIFIED BY SHOCK-ON-LIP

Leading edges for hypersonic vehicles that experience intense stagnation point pressures and heating rates are a significant challenge to the designer. For engine leading edges, such as the cowl shown in figure 4, intense aerothermal loads occur when the cowl bow shock is intersected by an oblique shock resulting in a supersonic jet that impinges on the leading edge surface. The experimental configuration (lower left of figure), which simulates the vehicle forebody and cowl leading edge, was used to define the aerothermal loads (see Ref. 3). The schlieren photograph shows the supersonic jet interference pattern impinging on the surface of the cylinder. The interference pattern produces intense local amplification of the pressure and heat transfer rate in the vicinity of the jet impingement. The undisturbed (absence of incident oblique shock and interference pattern) stagnation pressure and heat transfer rate can be amplified by factors from 6 to 30 depending on the shock strength and the free stream Mach number (Ref. 3).

The intensity and localization of this phenomena offers a significant challenge to computational fluid dynamics codes which must accurately capture the shock interference pattern and the attendant flow gradients to accurately predict the loads. Therefore this problem and experimental results will be used to demonstrate the integrated fluid-thermal-structural analysis method.

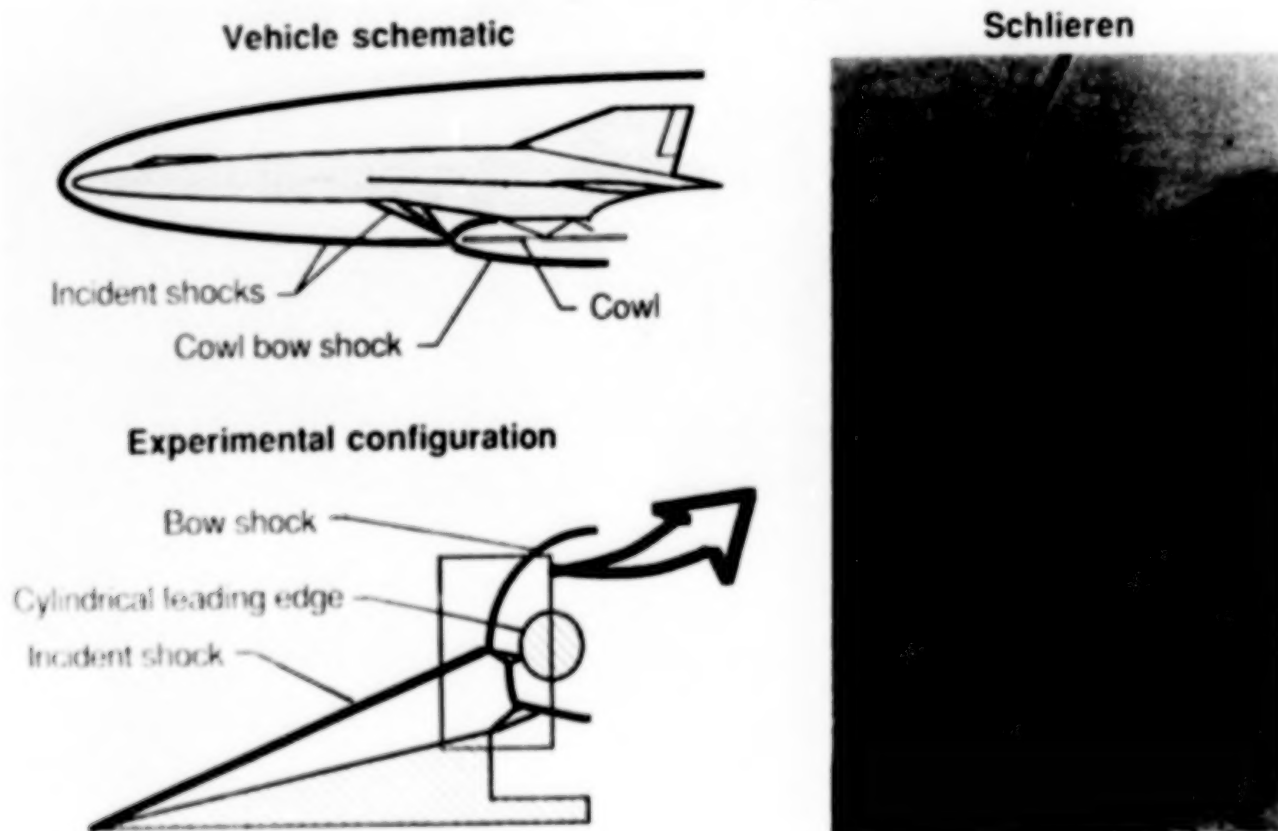


Figure 4

OBLIQUE AND BOW SHOCK INTERACTION ON CYLINDER

The supersonic jet interference pattern occurs when an oblique shock wave intersects the nearly normal part of the bow shock from the blunt cowl leading edge as shown schematically in figure 5. The intersection results in further displacement of the bow shock and the formation of a supersonic jet contained between two shear layers and submerged within the subsonic shock layer between the body and the bow shock wave. A jet bow shock is produced when the jet impinges on the surface, creating a small region of stagnation heating.

The computational technique and coupling between the fluid and the structure were evaluated using experimental results (Ref. 3) from the oblique and bow shock interaction on a three inch diameter stainless steel cylinder. The computational domain for the flow field and cylinder are shown in figure 5. The inflow conditions above and below the oblique shock are (1) Mach 8.03 flow at an angle of attack of zero degrees ($\theta = 0^\circ$) and a static temperature of 200 °R, and (2) Mach 5.25 flow at an angle of attack of 12.5 degrees ($\theta = -12.5^\circ$) and a static temperature of 430 °R. The supersonic jet impinges on the cylinder surface approximately 20 degrees below the cylinder horizontal centerline.

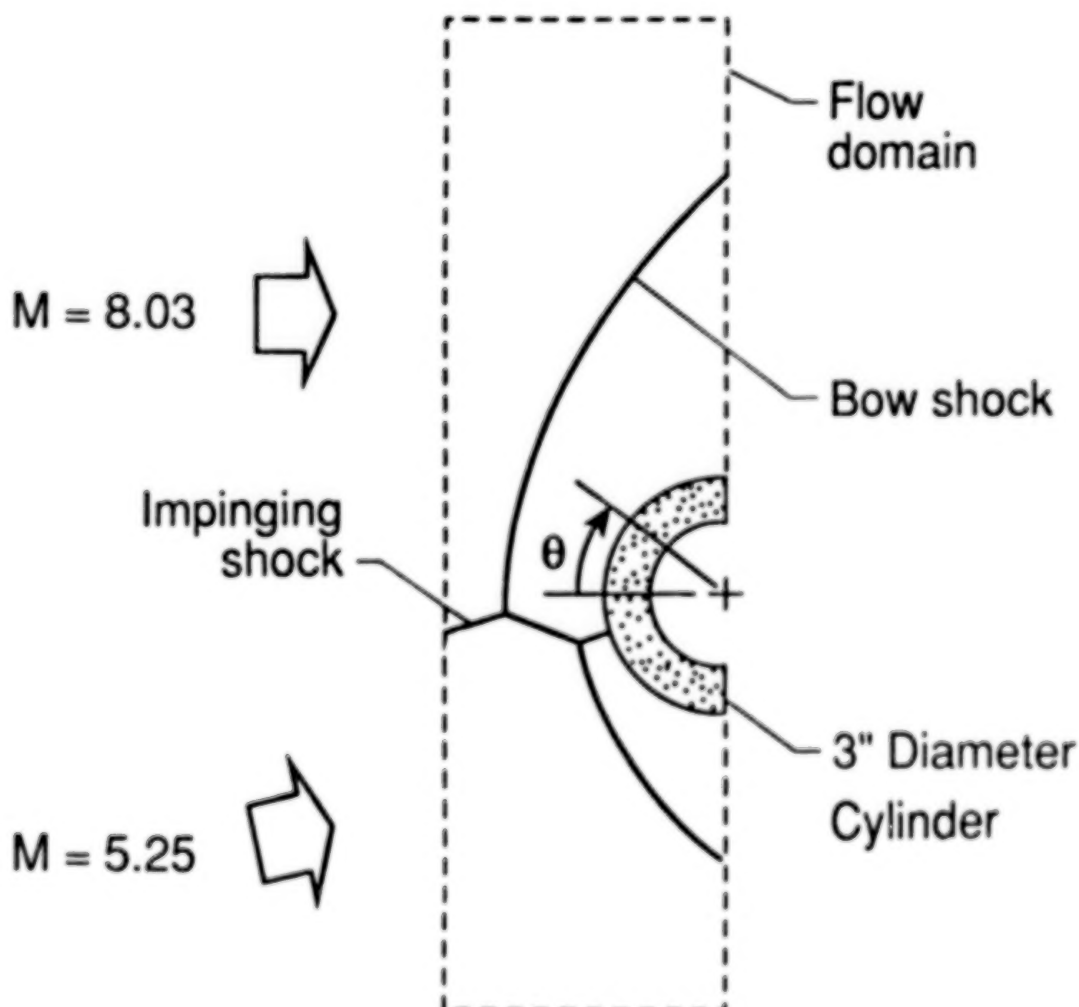


Figure 5

ADAPTIVE UNSTRUCTURED FINITE ELEMENT MESHES

The adaptive unstructured finite element remeshing technique described in Ref. 4 is used for the discretization of the flow domain to minimize the flow unknowns. Mesh adaptivity based on error indicators obviates a priori knowledge of the flow physics, which is nonexistent for this complex flow phenomena. Unstructured meshes permit adaptivity with fewer grid points than structured adaptivity. For the problem at hand, the three finite element meshes shown in figure 6 were required to obtain an accurate solution. The solution procedure starts from the uniform mesh (first mesh) which consists of triangles in the inviscid flow field and quadrilateral elements in the boundary layer region to obtaining accurate aerodynamic heating rates. As the fluid analysis proceeds, the mesh is adapted to the physics of the flow field. Elements are concentrated in the regions with large gradients (density in this case) and are removed from the regions where the gradients are small. In fact, the mesh density simulates the flow density gradients given by the schlieren shown in figure 4. The base and altitude of the triangular elements are oriented in the principal gradient directions to improve solution accuracy. The evolution of the meshes shown in the figure demonstrates the adaptive remeshing capability which provides the best flow solution with the least number of unknowns. This adaptive unstructured remeshing technique would provide similar benefits for the thermal and structural analyses and are being evaluated.

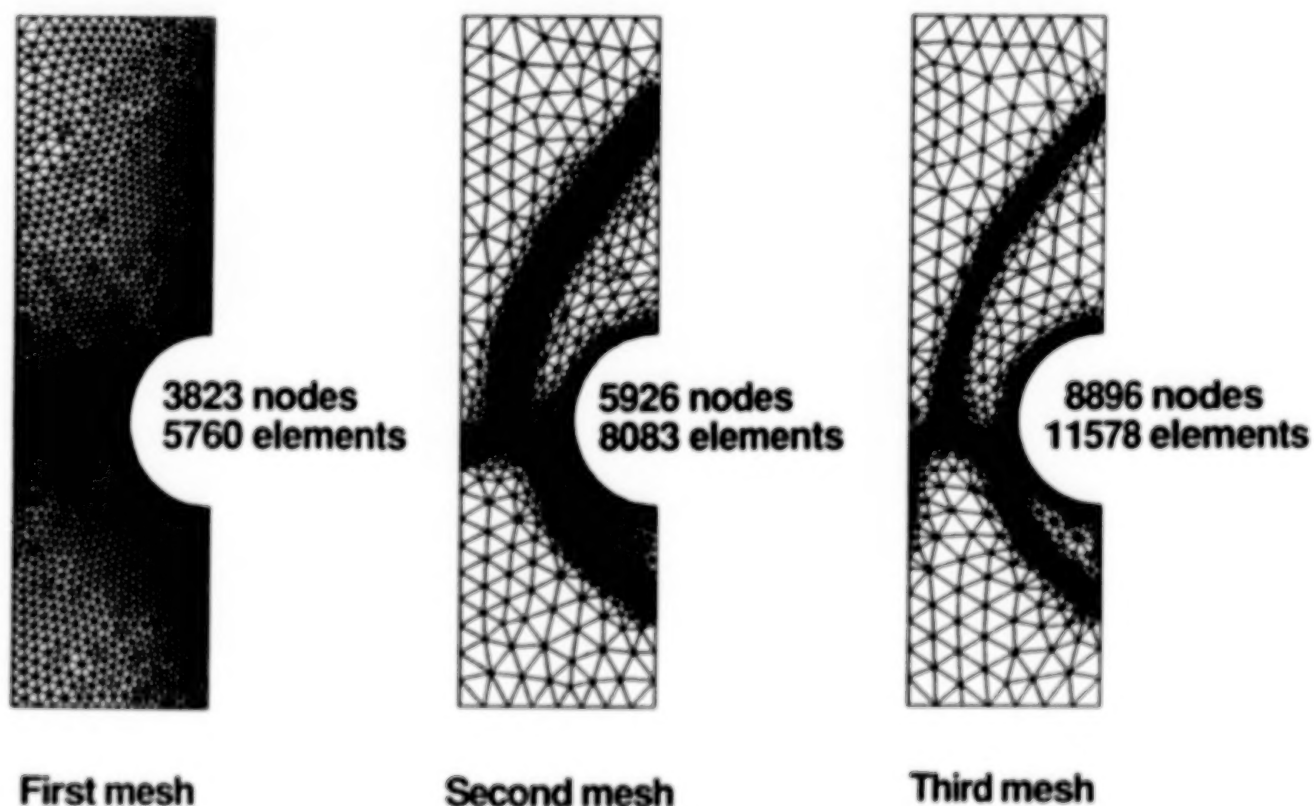


Figure 6

FLOW MACH NUMBER CONTOURS

The fluid analysis was performed using a point implicit upwinding technique described in Refs. 5 and 6. Using the crude uniform mesh (first mesh) shown in figure 6, the essential features of the flow were captured as indicated by the Mach number contours shown in figure 7. The Mach number contour scale is shown on the right of the figure. Using the density gradients from this first solution as an error indicator, the second mesh shown in figure 6 was created. The same procedure is repeated on subsequent meshes until the converged flow solution is achieved (a total of three meshes in this case).

The Mach number contours shown below demonstrate the improvement in the solution quality as the mesh is adapted. The Mach number distribution obtained on the third mesh clearly shows improved sharpness of the shock interference pattern. As described earlier the supersonic jet is submerged with subsonic regions between the bow shock and the cylinder. The Mach number in the supersonic jet is approximately two. The supersonic flow in the jet terminates through a nearly normal shock prior to impinging on the cylinder surface. The accuracy of the aerothermal loads on the cylinder surface are highly dependent on the fidelity of the shock interference pattern which is primarily an inviscid flow feature.

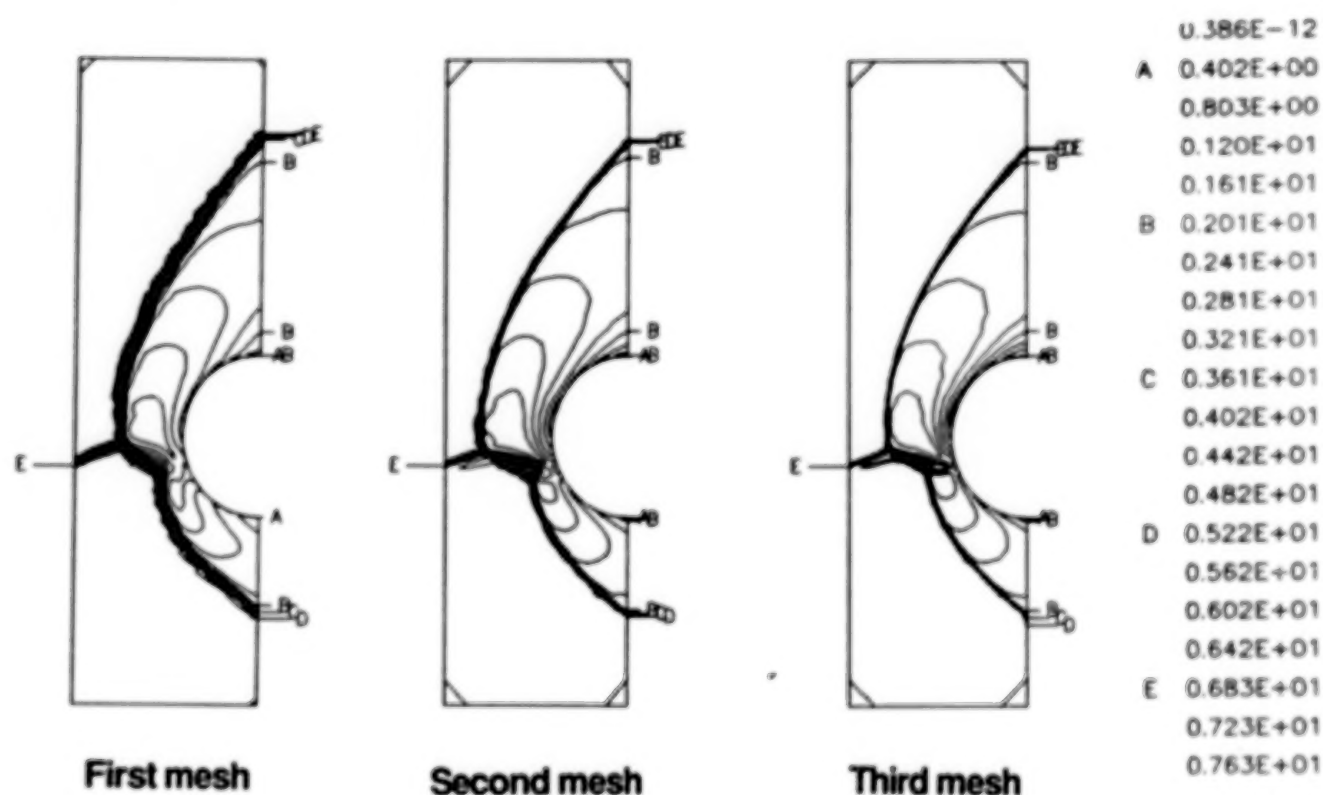


Figure 7

FLOW PRESSURE CONTOURS

The flow field pressure contours from the three meshes are shown in figure 8. The pressure contour scale in psia is shown on the right of the figure. The free stream flow pressure is 0.143 psia. The pressure increases to approximately 10 psia across the bow shock but jumps abruptly to 75 psia across the jet normal shock where the supersonic jet impinges on the cylinder. The surface pressure distribution is shown in figure 9.

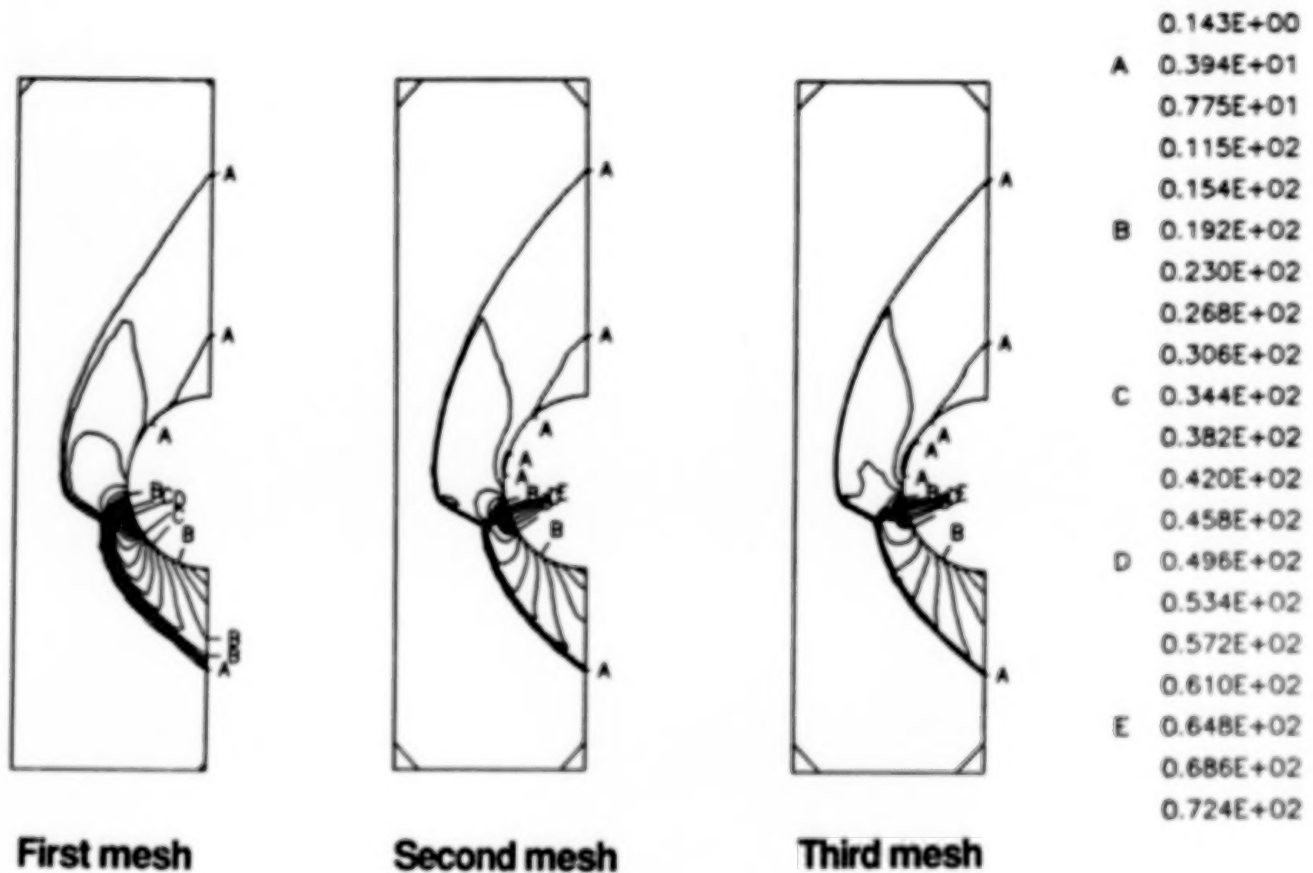


Figure 8

SURFACE PRESSURE DISTRIBUTION

The analytically predicted surface pressure distribution from the third mesh is compared with the experimentally measured pressures in figure 9. The predicted and experimental pressures are normalized by the undisturbed stagnation pressure ($p_0 = 10.61$ psia). The figure shows good agreement of the pressure distributions, peak pressure (82 ± 5 psia versus a predicted value of 75 psia) and excellent agreement of the peak pressure locations ($\theta = -19.1^\circ$ vs. a prediction of -20°). The predicted pressure distribution is applied as a static load on the cylinder for the structural analysis to be presented later.

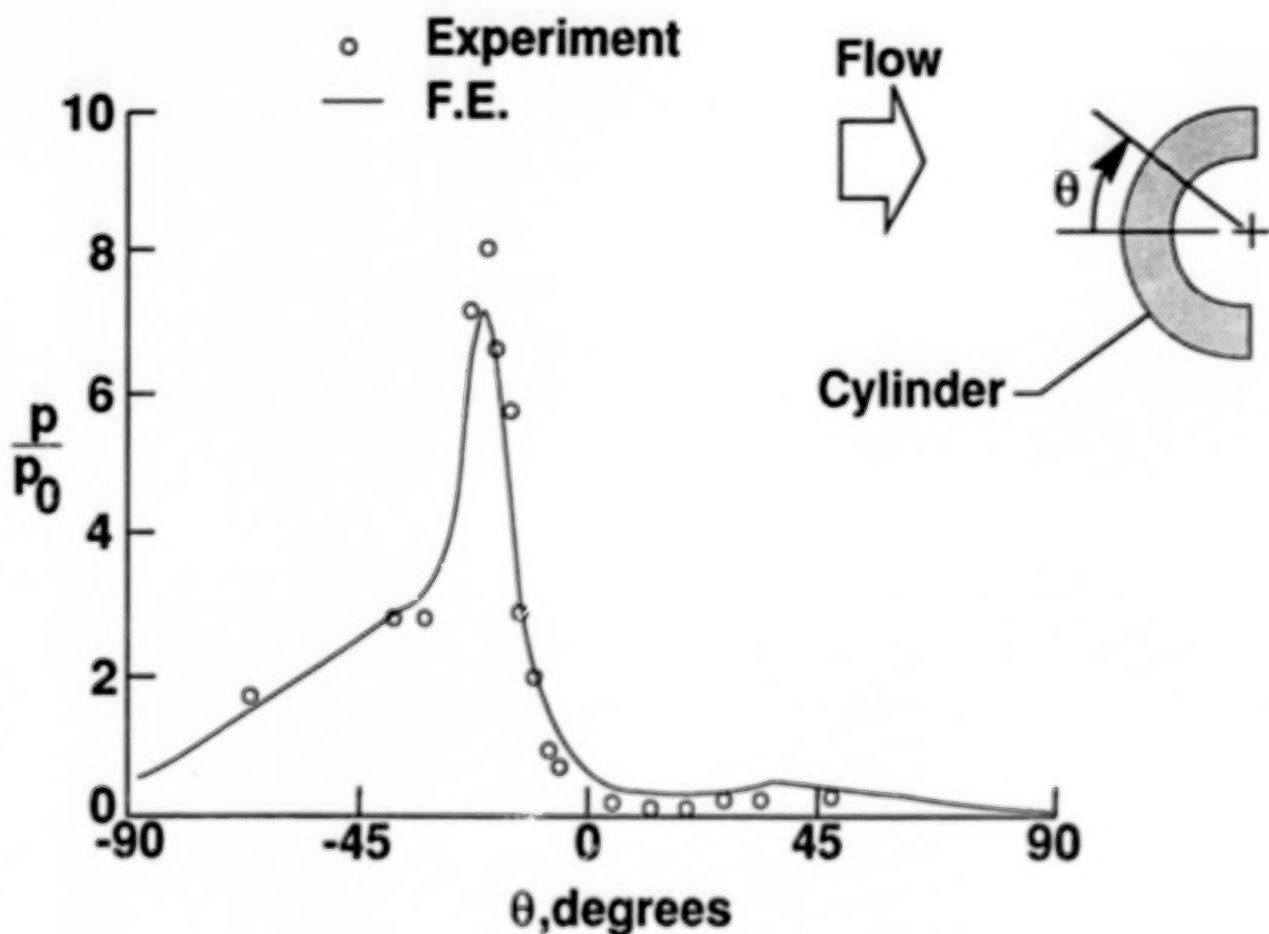


Figure 9

FLOW TEMPERATURE CONTOURS

The flow static temperature contours for the three meshes are shown in figure 10. The temperature contour scale in $^{\circ}\text{R}$ is shown on the right of the figure. The flow temperature increases abruptly from approximately 200°R to a maximum of 3000°R across the normal part of the bow shock, remains almost uniform, and drops sharply through the boundary layer to the cylinder surface temperature resulting in high aerodynamic heating rates. A more detailed view of the temperature contours in the interaction region is presented in figure 11.

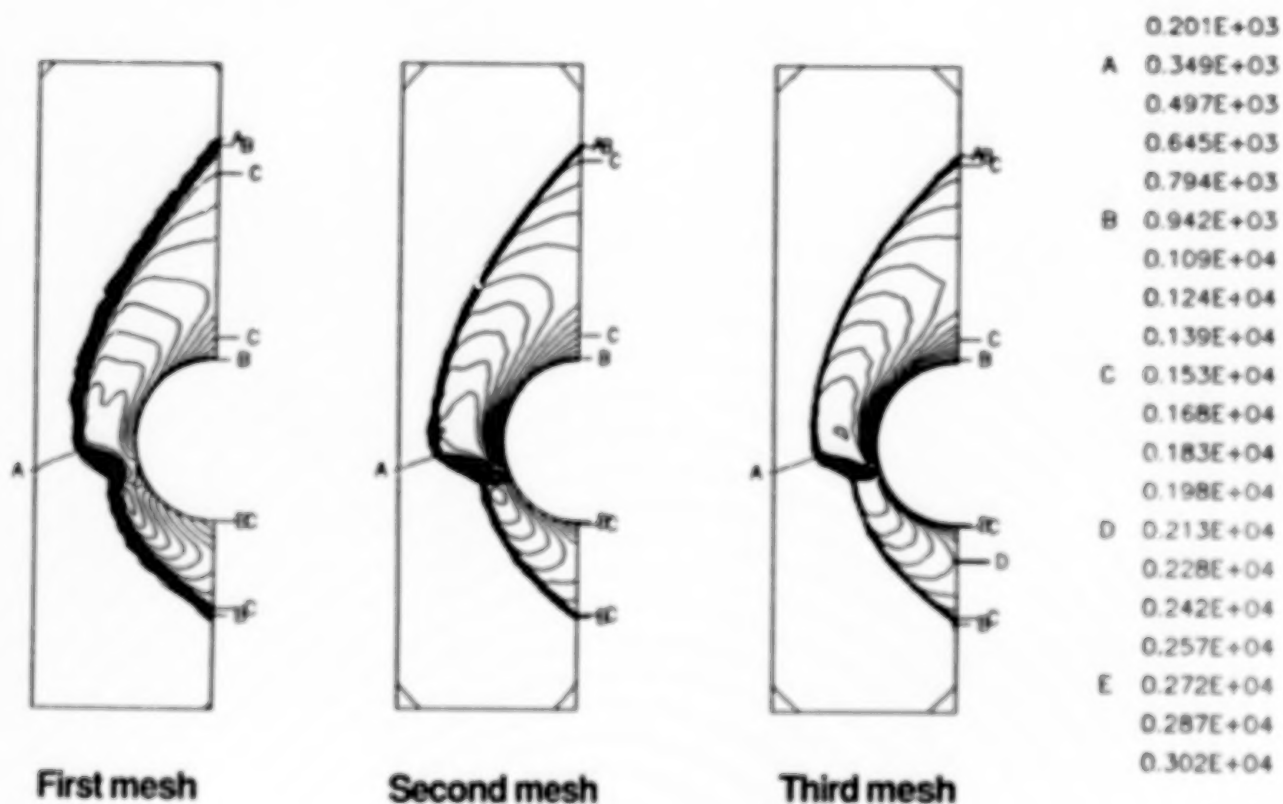


Figure 10

FLOW TEMPERATURE CONTOURS IN INTERACTION REGION

Details of the finite element mesh and the flow temperature in the interaction region are shown in figure 11. On both sides of the supersonic jet, the fluid temperature increases abruptly across the bow shocks from a relatively low temperature (200 °R and 430 °R) to approximately 2,700 °R. The temperature gradients in the shock layer (region between the bow shock and the cylinder) are relatively small except in the thin boundary layer where the temperature drops sharply to the cylinder surface temperature of 530 °R. Inside the supersonic jet, the fluid temperature increases slightly from the free stream temperature to approximately 1200 °R. As the jet stream approaches the cylinder surface, the fluid temperature increases abruptly across the jet normal shock to approximately 3,000 °R in a small stagnation region next to the cylinder surface and drops sharply to the cylinder temperature of 530°R. The high temperature gradients in this region result in a high localized aerodynamic heating rate at the jet impingement location. The severity of the temperature gradients is depicted in figure 12.

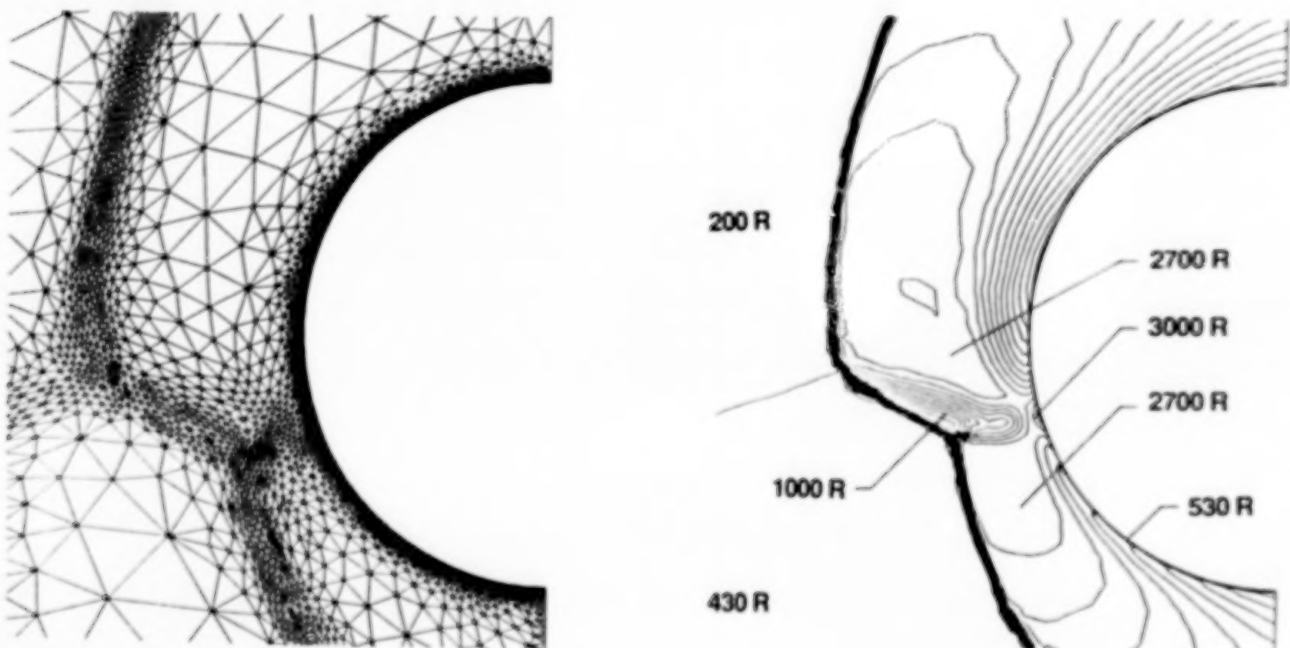


Figure 11

FLOW TEMPERATURE DISTRIBUTION

The fluid temperature distribution along a line below the supersonic jet is shown in figure 12 to highlight the severity of the temperature gradients across the shock and the thin boundary layer next to the cylinder surface. The gradient across the shock wave and boundary layer are approximately the same. These large temperature gradients require closely spaced elements for accuracy particularly in the boundary layer to accurately capture the aerodynamic heating rates. These fine meshes place severe constraints on the computational procedure since small time steps are normally required to assure solution stability. Therefore adaptive unstructured meshes, which significantly reduce the number of solution unknowns, improve solution tractability.

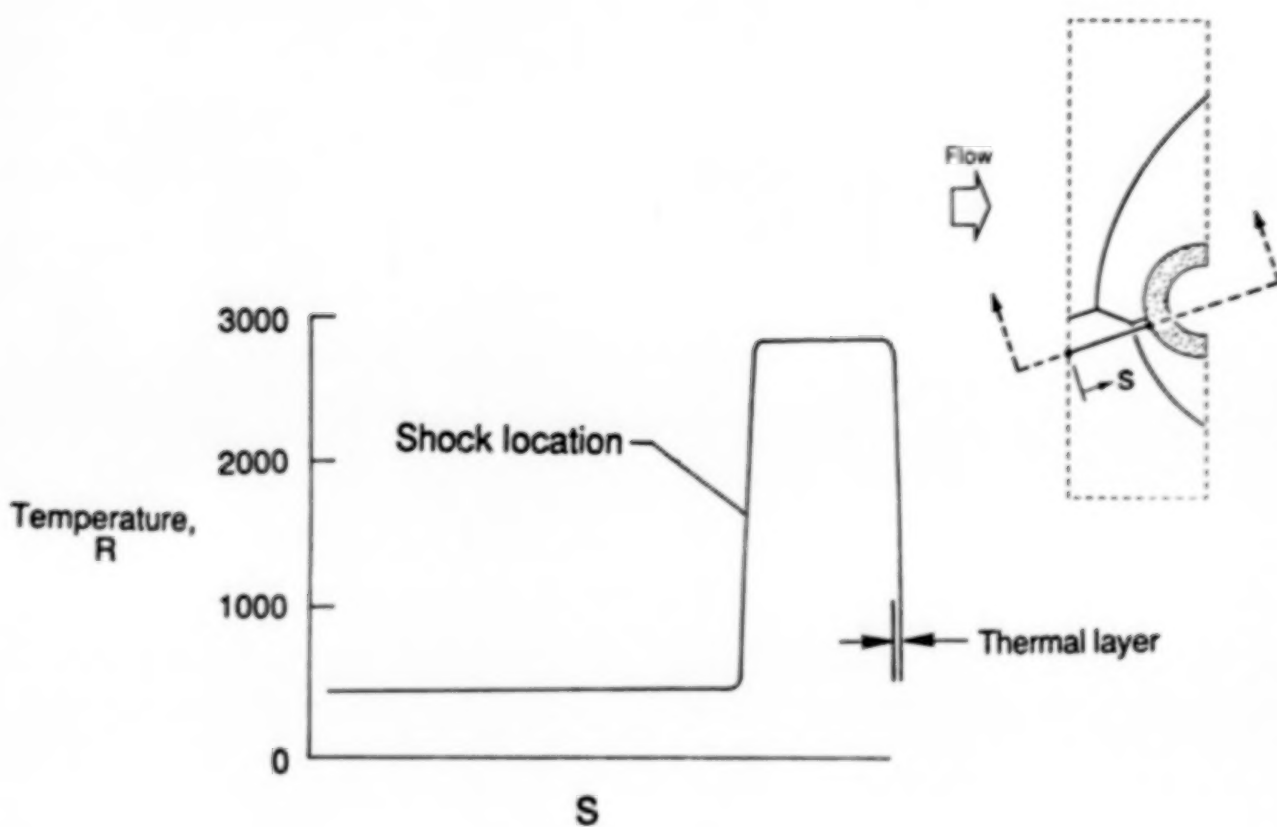


Figure 12

SURFACE HEATING RATES

The analytical and experimental heating rate distributions normalized to their respective undisturbed stagnation point heating rate are compared in figure 13. The predicted stagnation heating rate of 41.4 Btu/ft²-sec, which was obtained from a viscous shock layer solution, is lower than the experimental value of 61.7 Btu/ft²-sec (see Ref. 2). The difference between the predicted and experimental stagnation point heating rates is attributed to free stream turbulence emanating into the test stream from the turbulent boundary layer on the nozzle. Since this free stream turbulence is present during both the undisturbed (no impinging shock) and during the shock interaction test, normalization would tend to attenuate the effect of the free stream turbulence, hence providing a better comparison with the analytical predictions which do not account for any turbulence.

The heating rate distributions are in reasonably good agreement; however, the peak amplification is underpredicted as well as the heating rates between $\theta = -30^\circ$ and -55° . The underprediction is attributed to turbulence in the shear layers that bound the supersonic jet and transition of the boundary layer from laminar to turbulent. Neither of these two effects are accounted for in the analysis which is laminar. These aerodynamic heating rates are applied to the structure in the thermal analysis to predict the cylinder temperature distribution. The temperature distribution is then used in the thermal stress analysis and as a boundary condition for an updated flow analysis to account for the effect of the surface temperature on the aerodynamic heating rates.

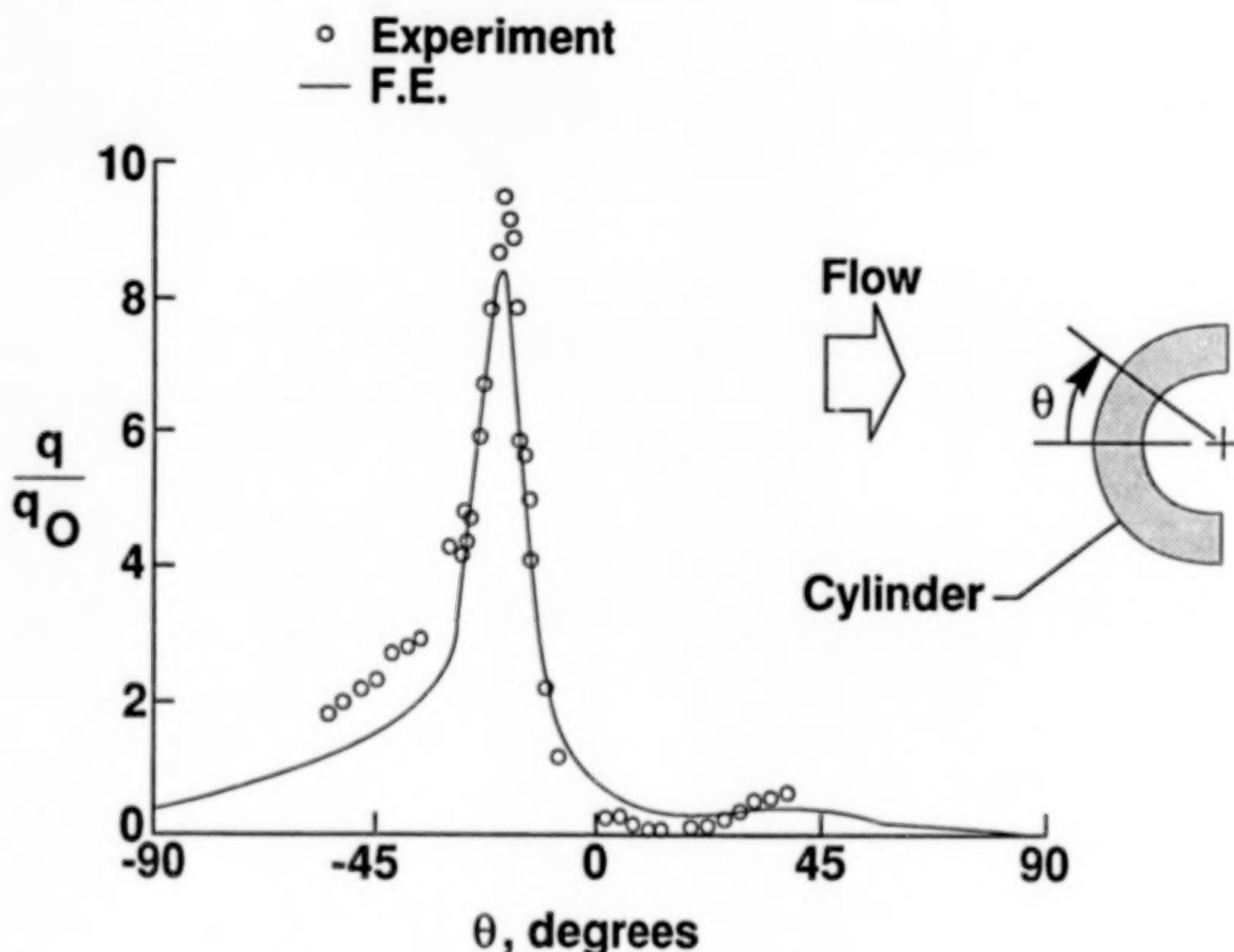


Figure 13

CYLINDER FINITE ELEMENT MODEL

The cylinder geometry, boundary conditions, and the finite element thermal-structural model are shown in figure 14. The cylinder is made of AM-350 stainless steel in which the material properties such as the thermal conductivity, specific heat, Young's modulus, thermal expansion coefficient, etc. are temperature dependent. The cylinder outer surface is subjected to aerodynamic pressure (figure 9) and heating rate (figure 13) obtained from the fluid analysis. The surface emits radiant energy to the surrounding medium at a temperature of 430 °R. The same finite element discretization is used for both thermal and structural analyses so that the difficulty in transferring data is eliminated. The mesh is graded radially from a very fine spacing at the surface to a coarser spacing on the inner surface. A common discretization is used circumferentially along the fluid and the cylinder interface to eliminate the data manipulation often required between different disciplinary analyses. Both thermal and structural analyses of the cylinder were performed using a one-step Taylor-Galerkin finite element analysis technique (Ref. 2).

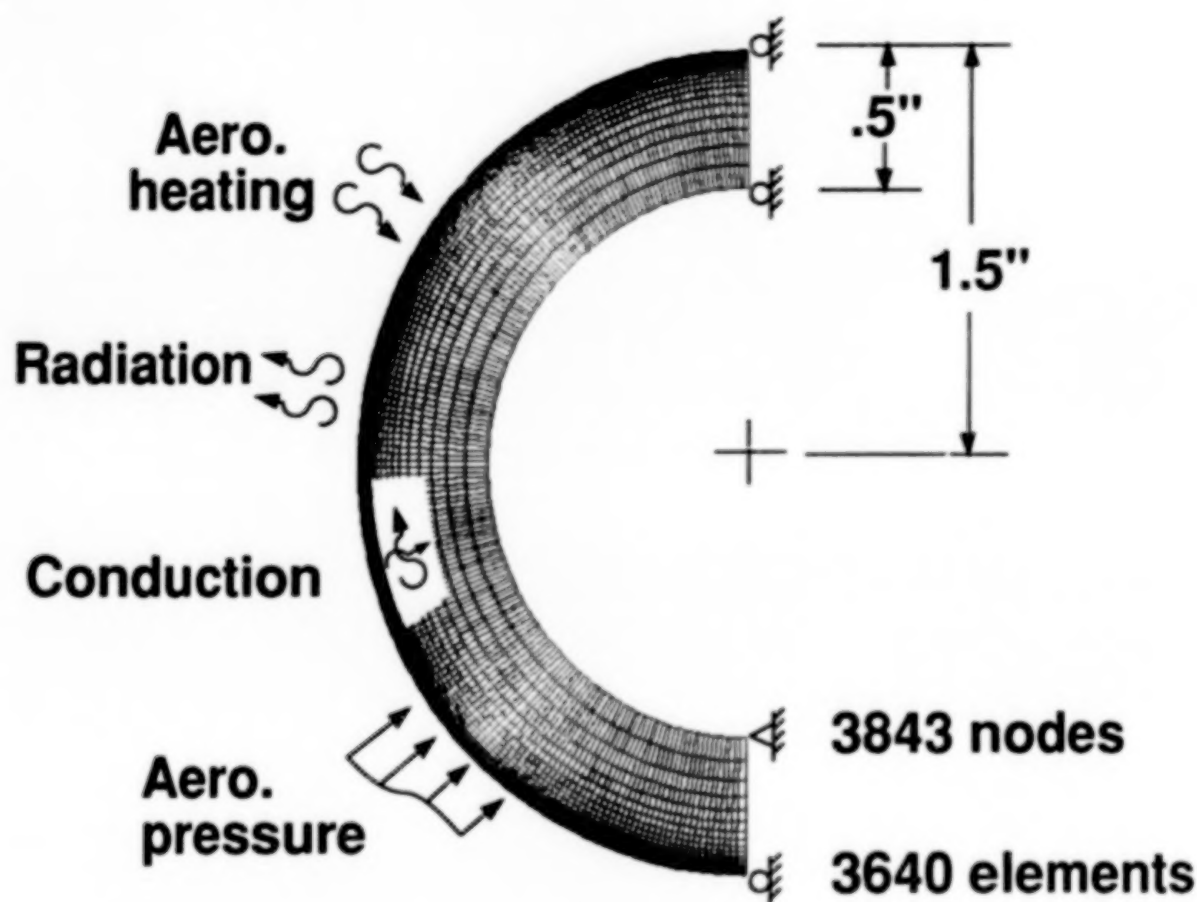


Figure 14

CYLINDER TEMPERATURE AT 0.5 SECOND

The cylinder temperature contours at 0.5 second are shown in the figure 15. The temperature contour scale in °R is shown on the right of the figure. The maximum temperature is about 1,100°R and occurs at the supersonic jet impingement location. The temperature away from this small impingement region remains at the ambient temperature of 530 °R. The intense local aerodynamic heating rates generated by the supersonic jet stream result in these high temperatures and temperature gradients in the jet impingement region after only a short exposure. The high temperature and temperature gradients result in the high thermal stresses shown in figure 16.

The response of a flight weight leading edge for the National Aero-Space Plane, which is exposed to extremely high aerodynamic heating rates during shock-on-lip conditions, is very rapid. In fact the response time is approaching the response time of the flow field and therefore may require a coupled fluid thermal analysis.

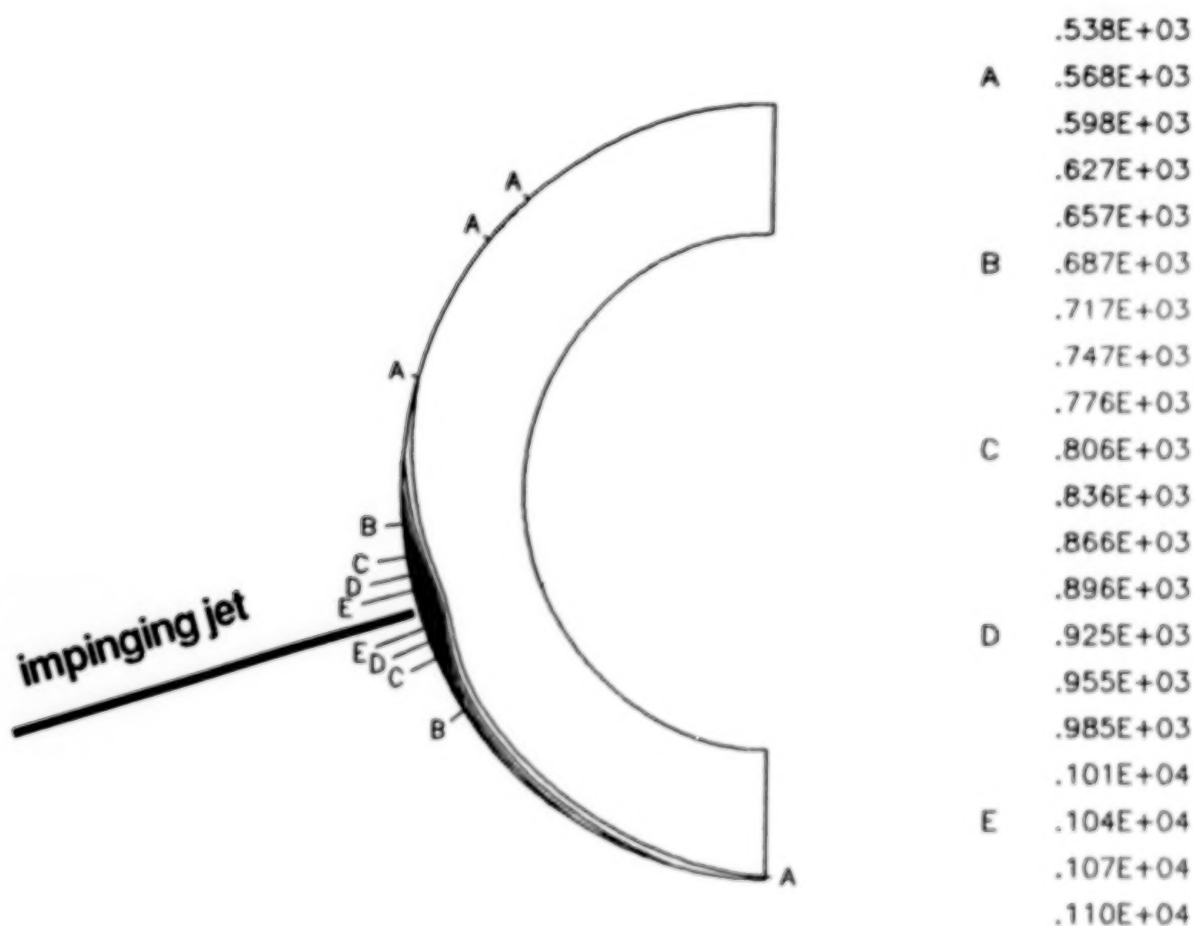


Figure 15

CIRCUMFERENTIAL STRESS ON DEFORMED CYLINDER AT 0.5 SECOND

The circumferential stress distribution superimposed on the deformed cylinder at 0.5 second is shown in figure 16. The stress contour scale in psia is shown on the right of the figure. The structural analysis was performed assuming quasi-static and plane strain behavior. The structural loads include the temperature distribution shown in figure 15 and the aerodynamic pressure shown in figure 9. The maximum deformation of 0.001 inch is radial and occurs at the jet impingement location. This maximum deformation is small and is assumed to have negligible effect on the flow field. The cylinder deformations are greatly exaggerated to highlight the deformed shape. The peak compressive circumferential stress of approximately 60 ksi occurs at the jet impingement location where the temperature and temperature gradients are maximum. The axial stresses, which are much larger than the circumferential stress, exceed the elastic limit. Hence, longer exposure with attendant higher temperature and stresses could result in permanent deformations and failure of the cylinder. Therefore a more sophisticated structural analysis, such as the capability to predict the permanent localized deformation including time dependency effects, is needed. Currently, the application of a unified viscoplastic theory for accurate prediction of the structural response at higher temperature is under investigation.

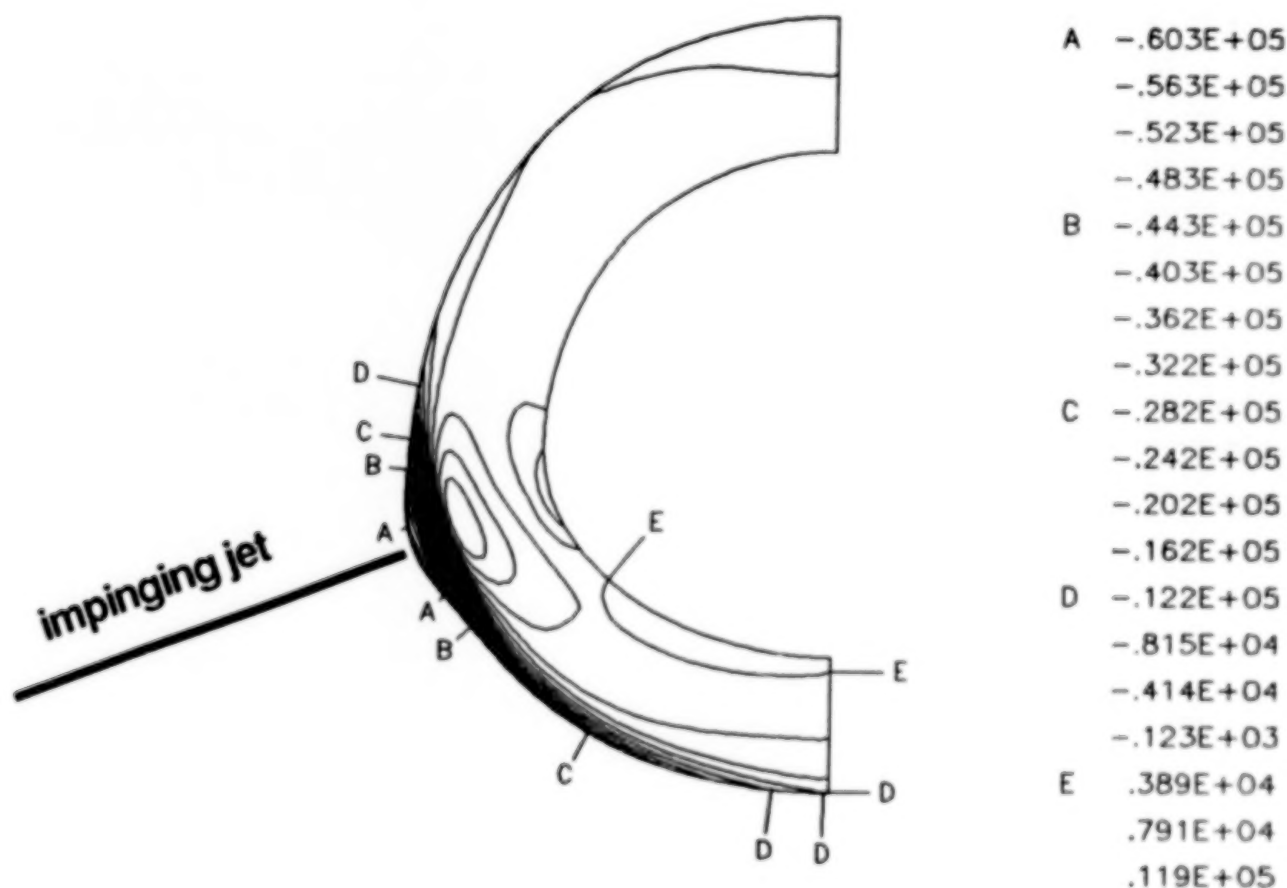


Figure 16

SURFACE HEATING RATES AFTER 0.5 SECOND OF EXPOSURE

The aerodynamic heating rates and hence the flow field are coupled to the thermal response of the cylinder through the energy equation. As the cylinder surface temperature increases, the thermal gradient through the boundary layer decreases, resulting in lower heating rates. The cylinder surface temperature after 0.5 second of exposure was used to update the aerodynamic analysis. The peak aerodynamic heating rate decreased nearly 50% from the initial heating rate at 0 second when the cylinder wall was isothermal at 530°R. The time interval of 0.5 second was selected to highlight the coupling effect between the aerodynamic flow and the cylinder thermal-structural response. A more accurate coupled fluid-thermal-structural solution can be obtained by decreasing the time interval and updating the different disciplinary analyses more frequently. Simultaneous solution of the flow field and the thermal response of the cylinder would be ideal; however, the extremely fine grid required for the flow analysis results in small time steps to insure solution stability. A time accurate transient solution would require the use of these small time steps throughout the flow solution domain and would be prohibitively expensive. The present solution avoids this dilemma by using local time stepping (time step for each element set by stability requirements) and marching the solution to steady state. This process is valid as long as the structure thermal response is much slower than the flow field response, which is usually the case.

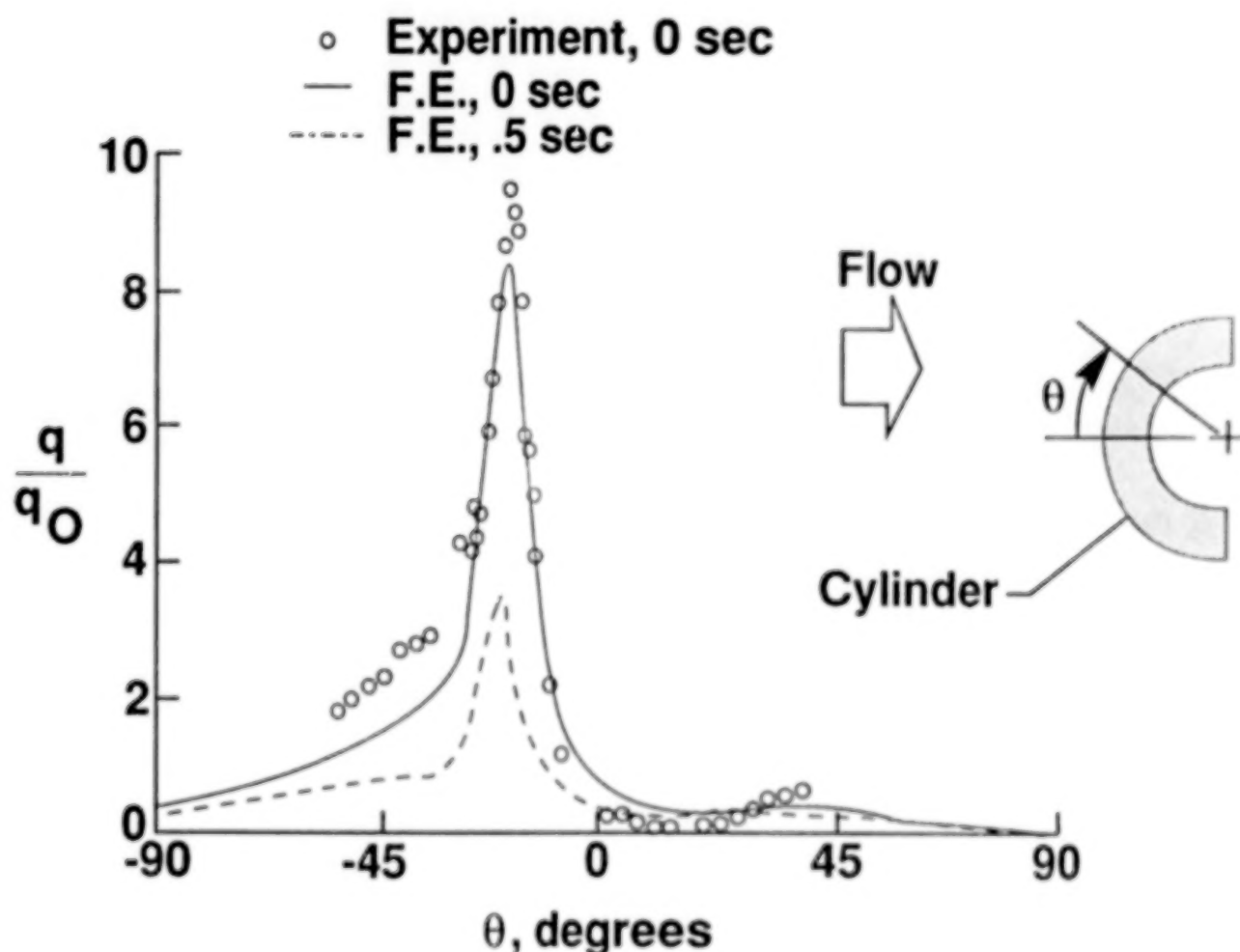


Figure 17

CONCLUDING REMARKS

An integrated fluid-thermal-structural finite element analysis approach was demonstrated for a cylinder subjected to shock wave interference heating. A general automated unstructured gridding was used to discretize the aerodynamic flow field to minimize the number of unknowns and provide an accurate and economical analytical solution. The finite element method is used in the three disciplinary analyses to facilitate the interdisciplinary data exchange. Coupling between the aerodynamic flow, the thermal, and structural response is included in the procedure; however, for Mach 8 shock wave interference on a three inch diameter stainless steel cylinder the coupling is limited to the effect of the surface temperature on the aerodynamic heating rates. The prediction of the flow behavior and the aerodynamic pressures and heating rates are in good agreement with experiment. The application has demonstrated the capability of this integrated fluid-thermal-structural analysis approach to (1) provide solutions to complex aerothermostructural behavior, (2) reduce manpower requirements, and (3) increase the computational efficiency for coupled interdisciplinary problems.

- INTEGRATED FLUID-THERMAL-STRUCTURAL FINITE ELEMENT ANALYSIS CAPABILITY DESCRIBED.
- AUTOMATED ADAPTIVE UNSTRUCTURED GRIDDING USED FOR MINIMUM PROBLEM SIZE.
- FINITE ELEMENT ALGORITHM PROVIDES SOLUTION FOR ALL THREE DISCIPLINES.
- COUPLING BETWEEN F-T-S INCLUDED FOR MULTIDISCIPLINARY INTERACTION.
- INTEGRATED F-T-S APPROACH REDUCES MANPOWER AND INCREASES COMPUTATIONAL EFFICIENCY.

Figure 18

447

REFERENCES

1. Wieting, A. R.; Dechaumphai, P.; Bey, K. S.; Thornton, E. A. and Morgan, K.: "Application of Integrated Fluid-Thermal-Structural Analysis Methods," Presented at the 16th Congress of the International Council of the Aeronautical Sciences, Jerusalem, Israel, August 28 - September 2, 1988.
2. Dechaumphai, P.; Thornton, E. A. and Wieting, A. R.: "Flow-Thermal-Structural Study of Aerodynamically Heated Leading Edges," Presented at the AIAA/ASME/ASCE/AHS 29th Structures, Structural Dynamics and Materials Conference, Williamsburg, Virginia, April 18-20, 1988, AIAA Paper No. 88-2245-CP.
3. Wieting, A. R. and Holden, M. S.: "Experimental Study of Shock Wave Interference Heating on a Cylinder Leading Edge," Presented at the AIAA 22nd Thermophysics Conference, Honolulu, Hawaii, June 8-10, 1988, AIAA Paper No. 87-1511.
4. Peraire, J.; Vahdati, M.; Morgan, K. and Zienkiewicz, O. C.: "Adaptive Remeshing for Compressible Flow Computations," *Journal of Computational Physics*, Volume 72, pp. 449-466, 1987.
5. Thareja, R. R.; Stewart, J. R.; Hassan, O.; Morgan, K. and Peraire, J.: "A Point Implicit Unstructured Grid Solver for the Euler and Navier-Stokes Equations," Presented at the AIAA 26th Aerospace Sciences Meeting, Reno, Nevada, January 11-14, 1988, AIAA Paper No. 88-0036.
6. Gnoffo, P. A.: "Application of Program LAURA to Three-Dimensional AOTV Flowfields," Presented at the AIAA 24th Aerospace Meeting, Reno, Nevada, January 6-9, 1986, AIAA Paper No. 86-0565.

**INVOLUTE COMPOSITE DESIGN EVALUATION
USING GLOBAL DESIGN SENSITIVITY DERIVATIVES**

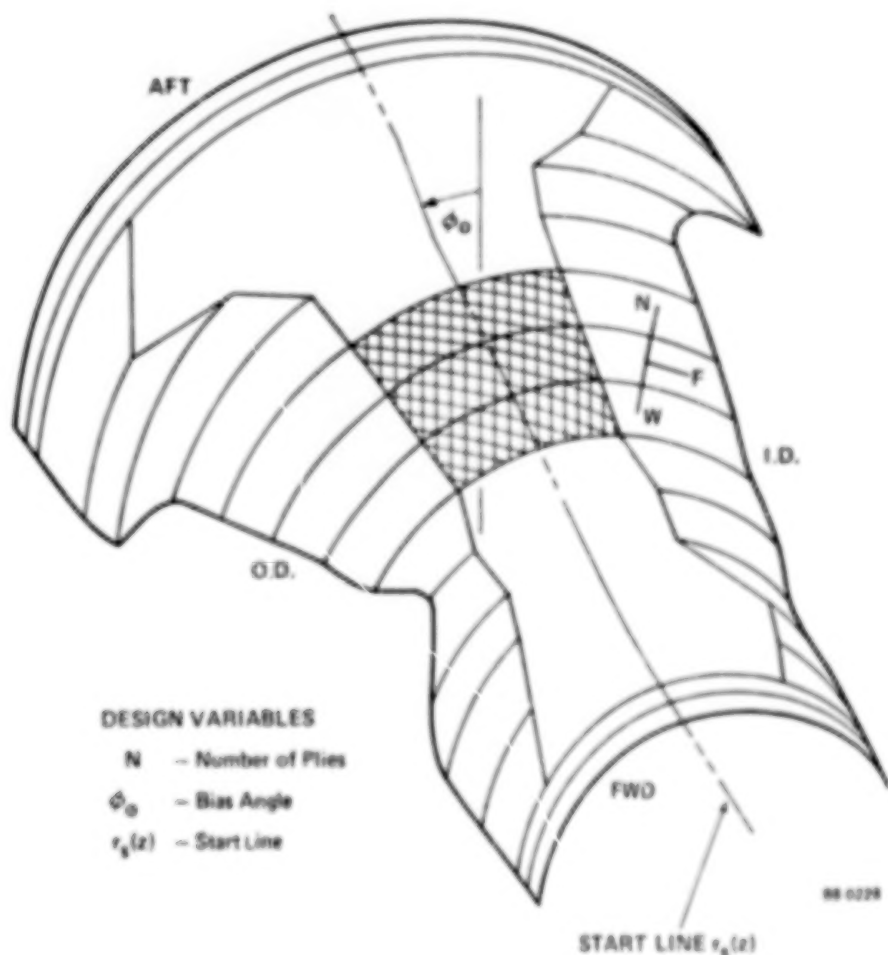
J. K. Hart and E. L. Stanton

**PDA Engineering
Costa Mesa, California**

445

Involute Composite Design Overview

The strong interaction between material architecture, processing and structural performance for nozzle components was described at an earlier NASA symposium for laminated involute composites. Since that meeting the Space Shuttle SRM nozzle has test fired involute nozzle components and progress has been made in analyzing their sensitivity to ply pattern design. The parameters that control ply pattern shape [1,2] also control tooling for the manufacture of involute composite structures. In the current CAD/CAM idiom these parameters might be called material form features and they provide a basis for global composite design sensitivity derivatives. They are not to be confused with laminate point design parameters that ignore ply continuity constraints present in finite dimension structural components with curvature. We first define the involute design problem and illustrate these commonly used approaches for composite shell structures. Then analytic sensitivity derivatives are developed and used to analyze test rings and cones with maximum stress failure criteria.

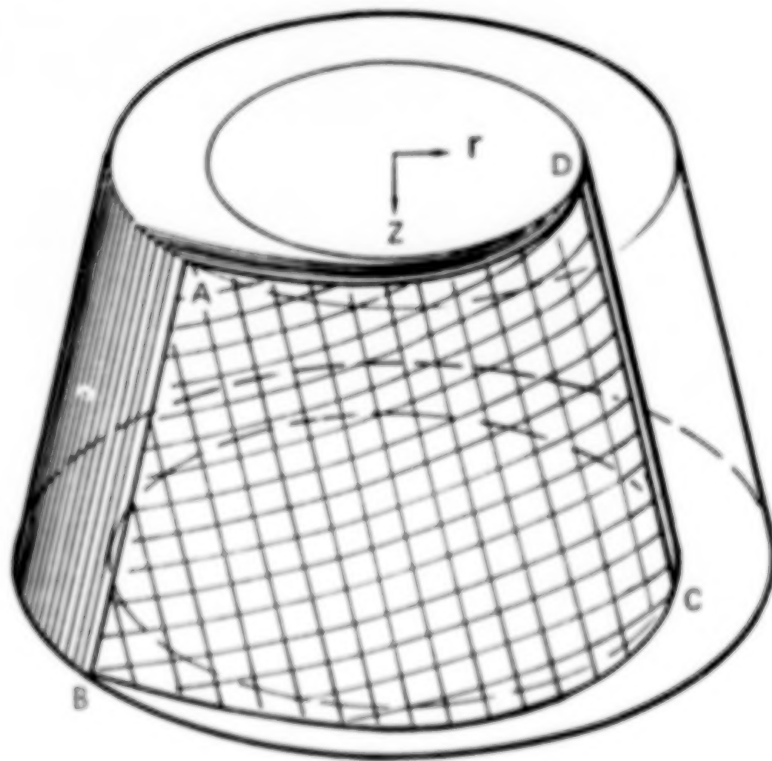


Involute Exit Cone Ply Material Distribution

The figure below illustrates the orientation of the plies in a conical section of an involute exit cone. The intersection of a ply with a plane defined by a constant Z coordinate (e.g., curves AD and BC) is an involute curve. Each ply can be mapped to an adjacent ply by a rotation of θ degrees about the axis of symmetry, where

$$\theta = \frac{360^\circ}{N}$$

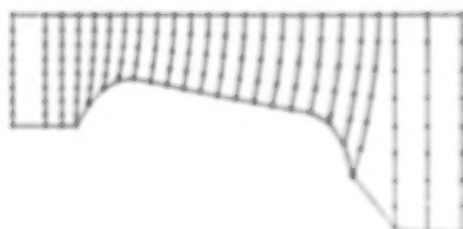
and N is the number of plies in the involute structure.



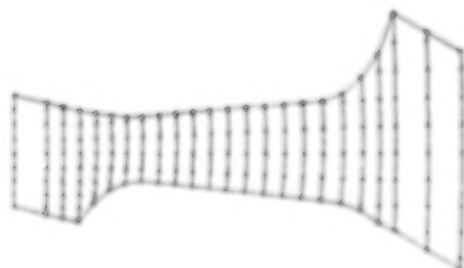
Involute Design Practice

Industrial practice in the U.S. for involute ply pattern design at one time was limited to either ID or OD start lines partly because of the geometric complexity of the problem. Both of these design approaches have one straight edge which also makes layup and inspection easier. On the negative side these patterns are more difficult to form to shape and do not insure fiber continuity in critical stress regions. An alternative approach used by PDA places the start line near the midsurface of the net part to insure fiber continuity. Typically a great many patterns are examined by trial and error using CAE tools in designing involute composite structures. Low manufacturing risk and high margins of safety during a motor firing are the figures of merit. The shape of the component, hence weight, is prescribed in most cases and rarely is this shape open to significant change. The shape of the ply pattern in contrast is open to wide variations and suggests the need for design sensitivity analyses to improve trial and error procedures and ultimately to automate the procedure.

O.D. Start-line Ply Pattern



PDA Start-line Ply Pattern



I.D. Start-line Ply Pattern



Involute Design Variables

The design space includes the ply count and the ply thickness product Nt , the helix angle ϕ_0 , and up to 6 variables defining the start line, which is a ply meridian lying in the r - z plane. These variables determine at each node three Euler angles α , γ , and ϕ which rotate the reference frame into the material frame. From these angles a strain transformation matrix is calculated and the distribution of these matrices within a finite element is used to calculate the element stiffness matrix. This is a global relation independent of finite element mesh.

DESIGN VARIABLES $\sim (X)$

$$(X) = (Nt, \phi_0, R_s(Z))$$

DEPENDENT VARIABLES \sim Euler Angles α, γ, ϕ

$$\left. \begin{array}{l} \alpha = \alpha(X) \\ \gamma = \gamma(X) \\ \phi = \phi(X) \end{array} \right\} \rightarrow [D(\alpha, \gamma, \phi)]$$

STIFFNESS MATRIX

$$[K] = \left[\int_V [B]^T [D]^T [C_m] [D] [B] |J| dV \right]$$

Design Sensitivity Formulation

The direct method of design sensitivity analysis is used. The governing equation for linear statics (equation 1) is differentiated to obtain equation 2. Equation 3 is obtained by solving equation 2 for $\{dU/dX\}$. The remainder of the effort is directed toward evaluating $\{dU/dX\}$. The finite element analysis already produces the factored stiffness matrix so it is only necessary to evaluate the part of equation 3 in parentheses. The element stiffness matrix in equation 4 and the element thermal load vector in equation 5 (only the thermal load is sensitive to material geometry orientation) may be differentiated to obtain equation 6. The differentiation is simplified because there is no shape sensitivity: the derivative of the strain-displacement transformation matrix $[B]$ is zero. The new matrices $[Q]$ and $[R]$ are functions of the elasticity matrix $[C]$, the strain transformation matrix $[D]$ and its inverse, and the corresponding derivatives, all given in equations 7 and 8. The integrands in equation 6 are developed in closed form. All sensitivity calculations and all finite element analyses are performed by a test version of the P/COMPOSITE module in PATRAN.

$$\text{Differentiate} \quad [K]\{U\} = \{F\} \quad (1)$$

$$\text{to obtain} \quad \left[\frac{dK}{dX} \right] \{U\} + [K] \left\{ \frac{dU}{dX} \right\} = \left\{ \frac{dF}{dX} \right\} \quad (2)$$

$$\text{Then} \quad \left\{ \frac{dU}{dX} \right\} = [K]^{-1} \left(\left\{ \frac{dF}{dX} \right\} - \left[\frac{dK}{dX} \right] \{U\} \right) \quad (3)$$

$$\text{Given} \quad [K] = \int_V [B]^T [C] [B] |J| dV \quad (4)$$

$$\text{and} \quad \{F\} = \int_V [B]^T [C] \{\alpha\} \Delta T |J| dV \quad (5)$$

$$\begin{aligned} \text{then} \quad \left\{ \frac{dF}{dX} \right\} - \left[\frac{dK}{dX} \right] \{U\} &= \int_V [B]^T ([Q] + [R]^T + [R]) \{\epsilon_0\} |J| dV \\ &\quad - \left[\int_V [B]^T ([R]^T + [R]) [B] |J| dV \right] \{U\} \end{aligned} \quad (6)$$

$$\text{where} \quad [Q] = [C] \frac{d}{dX} ([D]^{-1}) [D] \quad (7)$$

$$\text{and} \quad [R] = [C] [D]^{-1} \frac{d}{dX} ([D]) \quad (8)$$

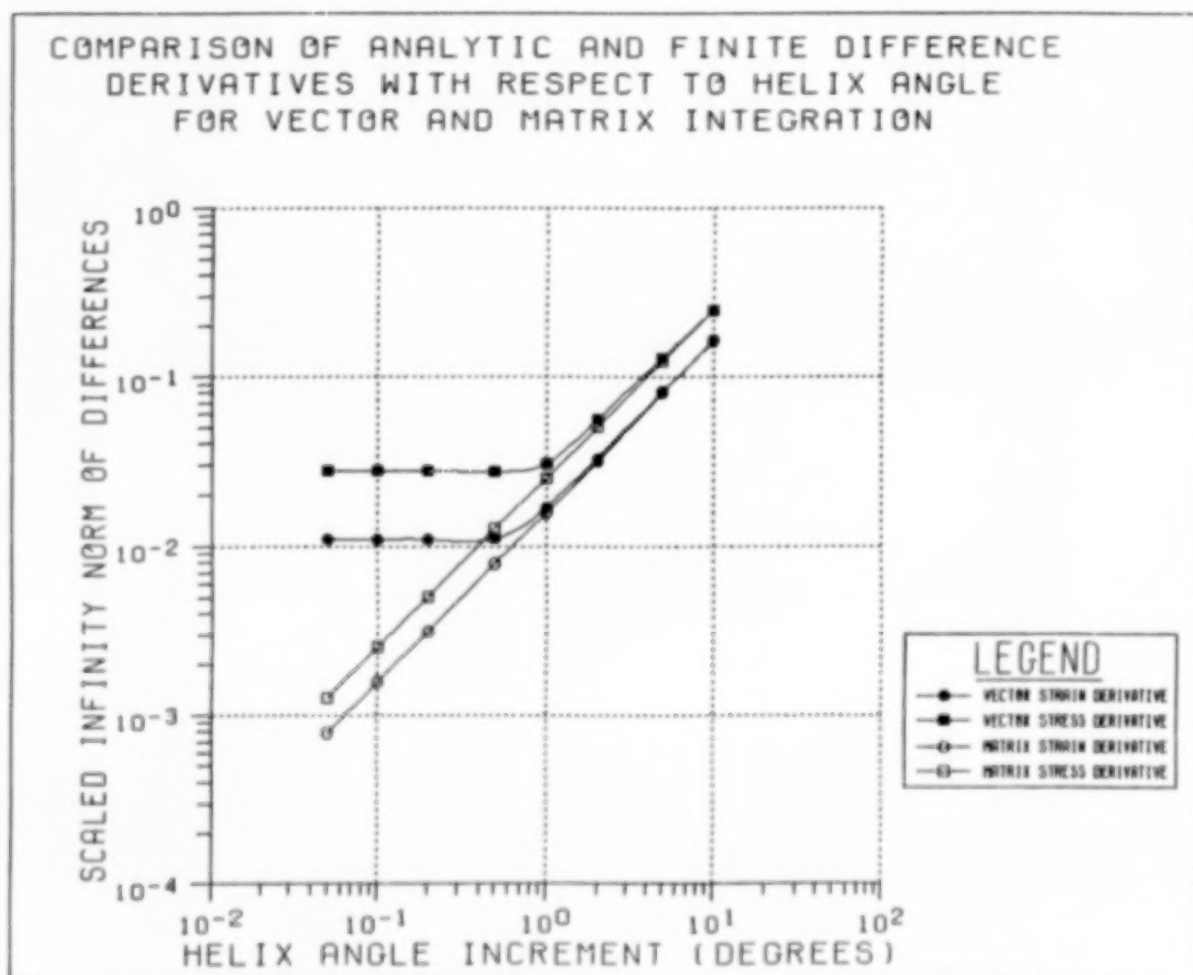
Vector and Matrix Sensitivity Integration

Originally the sensitivity integration (equation 6) was performed by inserting the $\{U\}$ vector inside the second integral and making the substitution

$$\{\epsilon\} = [B]\{U\}$$

to convert the matrix integration to a vector integration. The economy of this approach is evident, but finite difference tests show a failure to converge manifested by a "plateau" phenomenon for step sizes below a certain threshold. The onset of this deviation occurs at a step size that is too large to be attributable to round-off error. Because of this error, it was decided that matrix integration would be used for all sensitivity calculations.

The accompanying graph was generated for the helix angle design variable in a 439 degree of freedom test cone problem, and the error shown is typical.



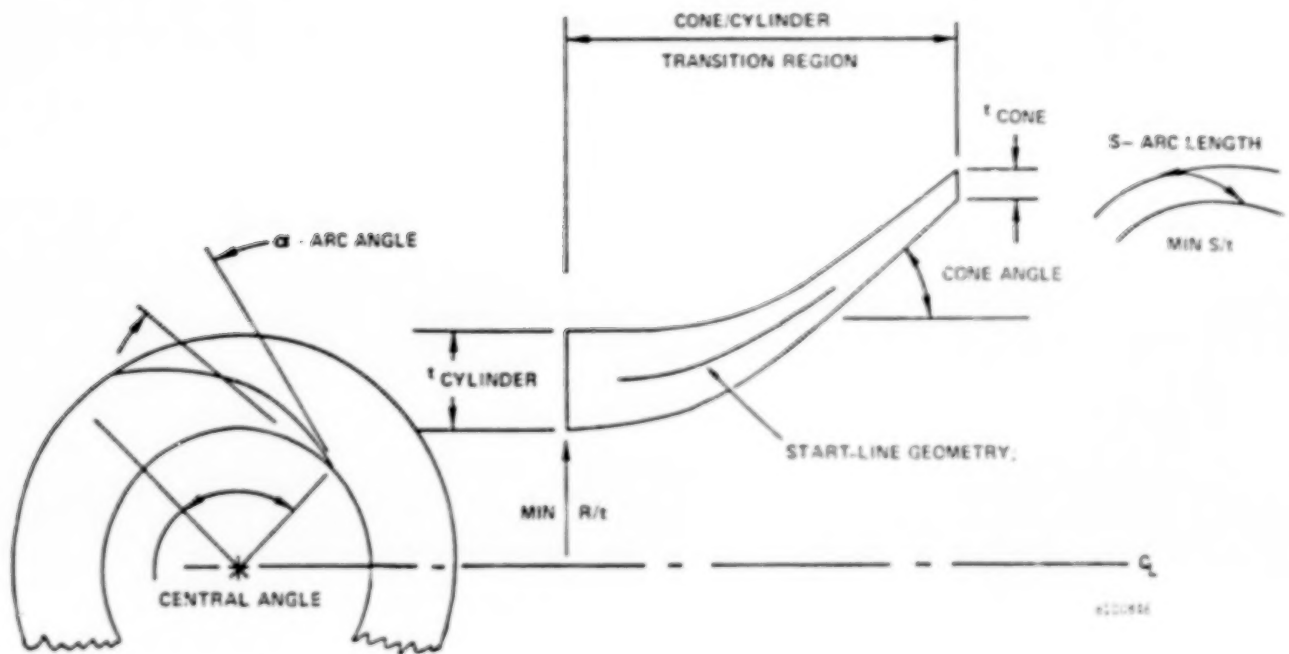
Formulation of Optimization Problem

The objective of the optimization is to minimize risk. To this end, the shape (and thus the weight) of the part are fixed and the optimization is used to find the ply pattern design furthest from the constraint surfaces, subject to manufacturing and side constraints. The mathematical formulation of the optimization problem is given below. The objective function is a slack variable β which represents the load margin (i.e., the distance between the load index and unity) to be maximized. The slack variable is added to each response constraint g_j . In addition, there are manufacturing constraints h_k which do not require the buffer of the slack variable. The Method of Feasible Directions algorithm [3] in MICRODOT is used to solve the primal form of the optimization problem. Dual methods are not used because the number of constraints is much greater than the number of design variables. Approximation concepts [4, 5, and 6] are used to formulate the sequence of approximate problems.

$$\begin{array}{ll}
 \beta \rightarrow \max & \\
 \text{Subject to} & g_j(X) + \beta \leq 0 \quad j = 1, 2, \dots, m \\
 & h_k(X) \leq 0 \quad k = 1, 2, \dots, \ell \\
 & X_i^L \leq X_i \leq X_i^U \quad i = 1, 2, \dots, n
 \end{array}$$

Manufacturing Constraints on Design Parameters

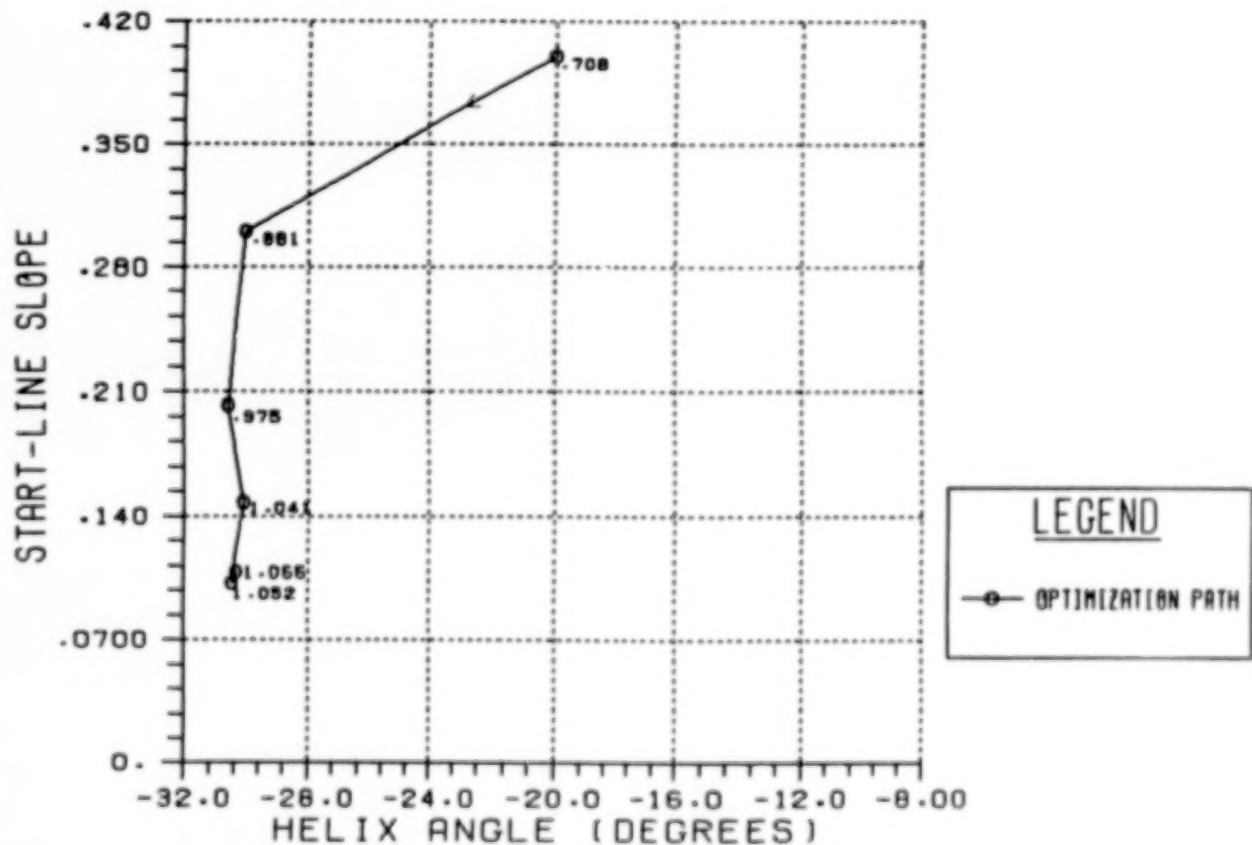
Two of the manufacturing constraints alluded to on the previous page are shown in the picture below. The central angle is the angle subtended by a ply as it extends from the inner radius to the outer radius, and the arc angle is the angle between a ply surface tangent and the circumferential direction. Good design practice for nozzle components dictates that the central angle should not exceed 120 degrees and the arc angle should not exceed 10-15 degrees.



First Optimization Sequence For Involute Ring Problem

The first optimization problem is an axisymmetric carbon-carbon cylinder having 82 degrees of freedom. The design variables are the helix angle ϕ and the slope m . Five iterations are required to increase the margin of safety from .708 at the starting point to 1.055 at the optimum.

FIRST OPTIMIZATION PATH FOR INVOLUTE RING
INTERNAL PRESSURE LOAD. MAX STRESS CRITERION
MARGIN OF SAFETY SHOWN FOR EACH ITERATION



Summary Table for First Optimization Path

The iteration history of the first optimization path is shown in Table 1. In the course of the optimization the critical stress component varies from fill tension in the outer element at the beginning to in-plane shear on the inner radius at the optimum. As the optimization proceeds, the constraint tolerance is reduced from .03 to the value of .001 required for convergence. The finite difference tests on the sensitivity derivatives were used to select move limits that would predict the response to within about 10 percent. The optimization results indicate that this choice was conservative enough.

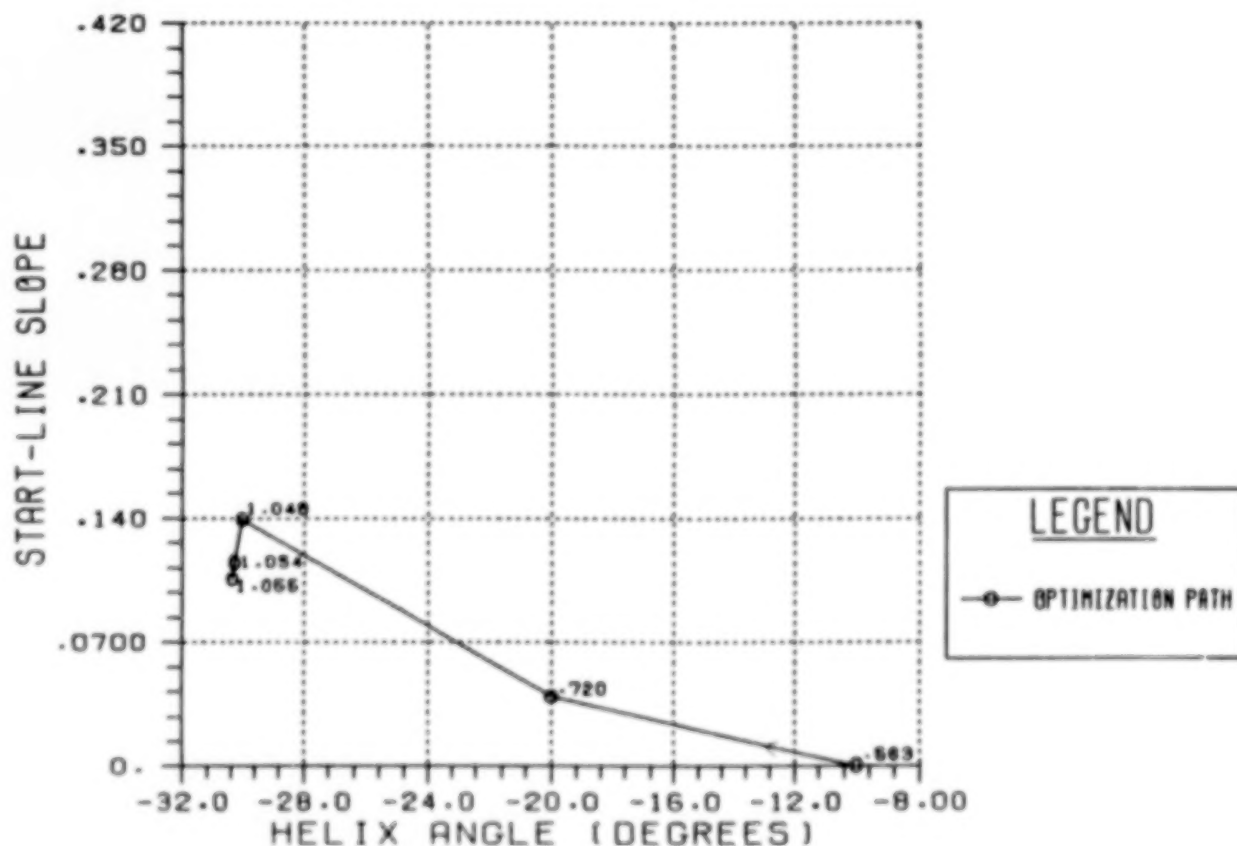
TABLE 1

Objective Function	Margin of Safety	Design Variables		Move Limits		Constraint Tolerance	Most Critical Constraint		Number of Active Constraints	Number of Gradient Evaluations	Number of Function Evaluations
		ϕ_0	m	$\Delta\phi_0$	Δm		Node	Component			
.4144	.7077	-20.000°	.4000				13	T2			
.4682	.8806	-30.000°	.3000	10°	.1	.03	25	T2	3	3	15
.4938	.9755	-30.556°	.2022	10°	.1	.03	4	S12	9	2	31
.5100	1.0409	-30.071°	.1478	10°	.1	.008	3	S12	15	2	5
.5127	1.0522	-30.440°	.1019	10°	.1	.008	3	S12	9	3	4
.5133	1.0547	-30.297°	.1086	10°	.1	.001	3	S12	3	2	2

Second Optimization Sequence For Involute Ring Problem

A different starting point is used for the same optimization problem. Here four iterations are required to increase the margin of safety from .563 at the starting point to 1.055 at the optimum. Note that the same optimum is reached in both cases.

SECOND OPTIMIZATION PATH FOR INVOLUTE RING
INTERNAL PRESSURE LOAD, MAX STRESS CRITERION
MARGIN OF SAFETY SHOWN AT EACH ITERATION



Summary Table for Second Optimization Path

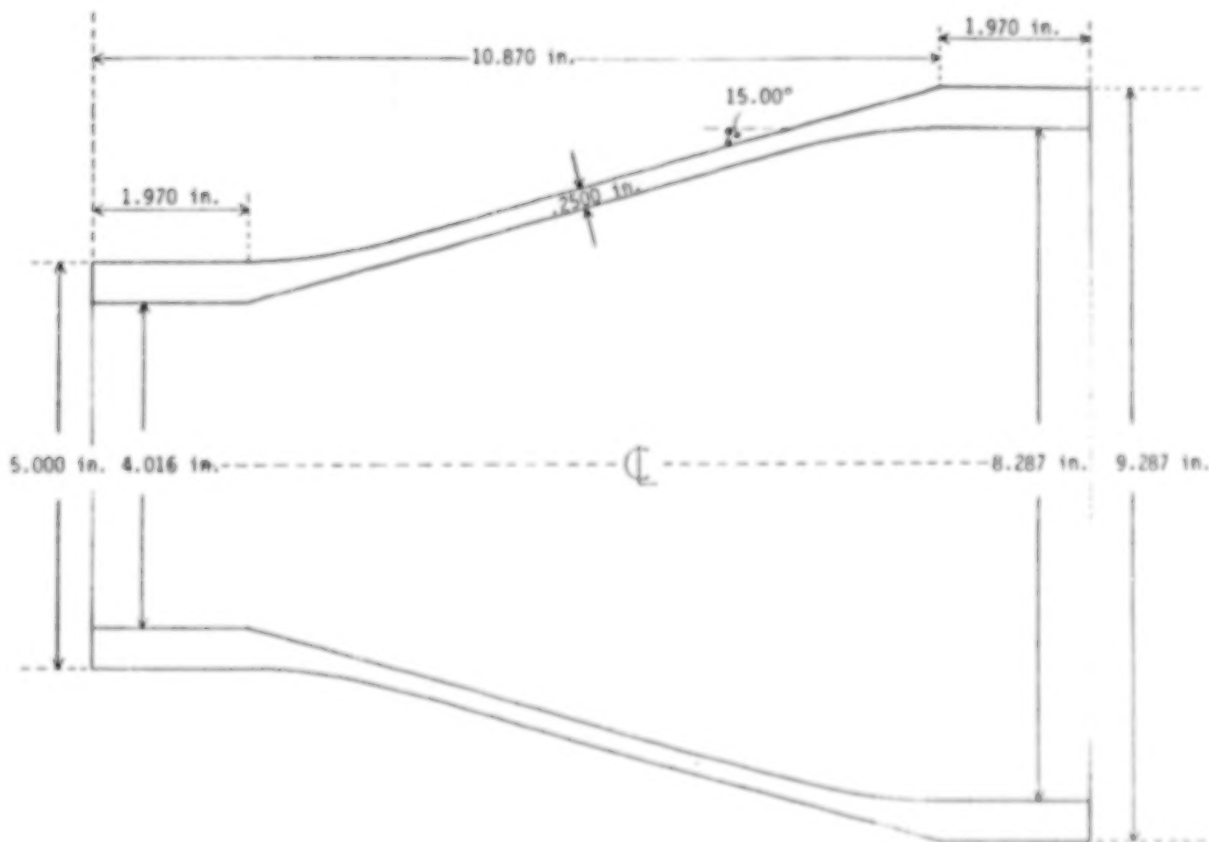
The iteration history of the second optimization path is shown in Table 2. Although the margin of safety shows greater improvement along this path, fewer iterations are required. Throughout the optimization the critical region is along the inner radius. The critical stress component varies from fill tension at the beginning to in-plane shear at the optimum. As before, the constraint tolerance is reduced from .03 to the value of .001 required for convergence. Again, the move limits appear conservative enough.

TABLE 2

Objective Function	Margin of Safety	Design Variables		Move Limits		Constraint Tolerance	Most Critical Constraint		Number of Active Constraints	Number of Gradient Evaluations	Number of Function Evaluations
		ϕ_0	m	$\Delta\phi_0$	Δm		Node	Component			
.3602	.5629	-10.000°	0.0000				2	T2			
.4184	.7195	-20.000°	.0390	10°	.1	.03	2	T2	4	2	29
.5118	1.0482	-30.000°	.1390	10°	.1	.03	1	T2	4	3	27
.5131	1.0537	-30.247°	.1144	10°	.1	.001	3	S12	3	2	5
.5134	1.0551	-30.324°	.1057	10°	.1	.001	3	S12	3	2	2

Involute Test Cone Optimization

The second optimization problem is an axisymmetric carbon-carbon test cone tested and analyzed by Stanton and Kipp [7] and having 439 degrees of freedom. The model is subjected to an axial load along the aft rim and is constrained axially along the forward rim. The design variables are the product of the ply count and the ply thickness Nt , the helix angle ϕ_0 , and four additional variables controlling the start line. The initial design is the same as the final design selected by Stanton and Kipp: it is therefore expected that the initial design is close to optimal. Four iterations are, in fact, required to increase the margin of safety from 2.653 at the starting point to 2.798 at the optimum.

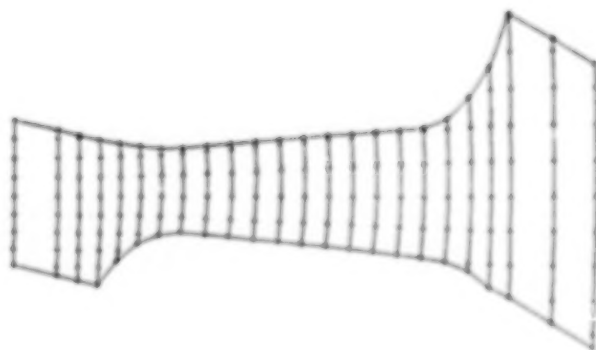


Reference and Optimized Ply Pattern

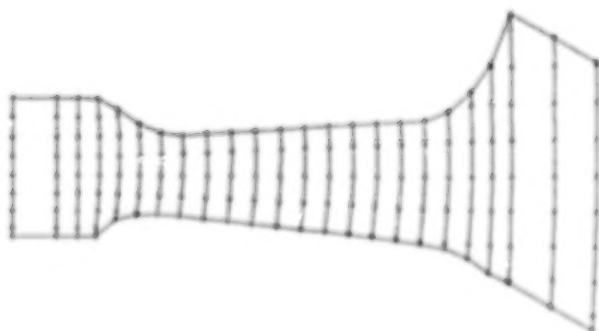
The reference ply pattern designed by Stanton and Kipp is shown below. The warp aligned test cone design with the start line following the midsurface of the shell was considered radical when it was first discussed with manufacturers. The design goal at that time was to develop the full strength of the carbon-carbon material in the critical cone-cylinder transition under axial load. That too was considered impractical but both are common practice today.

It can be seen that the shape of the optimized ply pattern in the forward region has changed considerably due to changes in the start line. In addition, the width of the ply pattern has been uniformly reduced due to the increase in the ply count and the ply thickness.

REFERENCE FLY PATTERN



OPTIMIZED FLY PATTERN



Summary Table For Test Cone Optimization Path

The optimization history for the test cone problem is given below.

(Max Stress Failure Criteria)

Iteration Number	Objective Function	Margin of Safety	Design Variables						Most Critical Constraint	
			N_t	ϕ_0	Y_1	m	Y_2	ξ_2	Node	Component
0	.7263	2.6536	2.2500	0.0000°	2.3200	3.500×10^{-2}	2.6225	.7500	48	C1
1	.7328	2.7418	2.2446	6.0972°	2.3136	7.883×10^{-3}	2.5725	.7640	53	C1
2	.7360	2.7884	2.3803	4.7420°	2.2636	2.217×10^{-3}	2.6225	.7776	48	C1
3	.7366	2.7970	2.3814	5.6872°	2.2389	1.000×10^{-3}	2.6419	.7839	53	C1
4	.7367	2.7983	2.3815	5.6538°	2.2382	1.000×10^{-3}	2.6431	.7841	53	C1

Iteration Number	Move Limits						Constraint Tolerance	Number of Active Constraints	Number of Gradient Evaluations	Number of Function Evaluations
	ΔN_t	$\Delta \phi_0$	ΔY	Δm	ΔY_2	$\Delta \xi_2$				
0										
1	.4	10^0	.05	.05	.05	.2	.001	2	3	14
2	.4	10^0	.05	.05	.05	.2	.001	2	4	32
3	.4	10^0	.05	.05	.025	.2	.001	3	2	43
4	.4	10^0	.05	.05	.025	.2	.0002	3	2	6

Conclusions

An optimization capability for involute structures has been developed. Its key feature is the use of global material geometry variables which are so chosen that all combinations of design variables within a set of lower and upper bounds correspond to manufacturable designs. A further advantage of global variables is that their number does not increase with increasing mesh density. The accuracy of the sensitivity derivatives has been verified both through finite difference tests and through the successful use of the derivatives by an optimizer.

The state of the art in composite design today is still marked by point design algorithms linked together using ad hoc methods not directly related to a manufacturing procedure. The global design sensitivity approach presented here for involutes can be applied to filament wound shells and other composite constructions using material form features peculiar to each construction. The present involute optimization technology is being applied to the Space Shuttle SRM nozzle boot ring redesigns by PDA Engineering.

- A design sensitivity capability using global material geometry variables has been developed.
- The number of global variables is insensitive to finite element mesh density.
- The sensitivity derivatives have been used successfully in an optimization context.
- The sensitivity integral calculations in vector form yielded a tangible error not shared by the corresponding calculations in matrix form.
- The global variable approach can be applied to other composite constructions using material form features peculiar to each construction.

References

1. Savage, E.E., "The Geometry of Involute Construction", JANNAF Rocket Nozzle Technology Subcommittee Meeting 1979, CPIA Publication 310, 1980, pp. 293-308.
2. Pagano, N.J., "General Relations for Exact and Inexact Involute Bodies of Revolution", AFWAL-TR-82-4053, April 1982.
3. Vanderplaats, G.N., "A Robust Feasible Directions Algorithm for Design Synthesis", Proceedings, AIAA/ASME/ASCE/AHS, 24th Structures, Structural Dynamics and Materials Conference, Lake Tahoe, Nevada, May 2-4, 1983.
4. Schmit, L.A. and Farshi, B., "Some Approximation Concepts for Structural Synthesis", AIAA Journal, Vol. 12, No. 5, May 1974, pp. 692-699.
5. Schmit, L.A. and Miura, H., "Approximation Concepts for Efficient Structural Synthesis", NASA CR-2552, March 1976.
6. Lust, R.V. and Schmit, L.A., "Alternative Approximation Concepts for Space Frame Synthesis", NASA CR-172526, March 1985.
7. Stanton, E.L. and Kipp, T.E., "Nonlinear Mechanics of Two-Dimensional Carbon-Carbon Composite Structures and Materials", AIAA Journal, Vol. 23, August 1985, pp. 1278-1284.

OPTIMIZING FOR MINIMUM WEIGHT WHEN TWO DIFFERENT
FINITE ELEMENT MODELS AND ANALYSES ARE REQUIRED

Jeffrey C. Hall
General Dynamics/Electric Boat Division
Groton, Connecticut

INTRODUCTION

Whether designing an automobile, aircraft, building, or ship, the structural engineer must consider many loading conditions and meet multiple design criteria. Arriving at a minimum weight structure which satisfies all of the design constraints requires the integration of the results from all analyses and loading conditions. This is a relatively straightforward process if all of the analyses use the same analysis model. However, if each analysis requires a separate model, each model must still vary by the same amount when the design variables change. Typically, this optimization process is further complicated when constraints from the different analyses drive the design variables in opposite directions. For example, the stress constraint from a static analysis may cause a decrease in a design variable. However, the minimum frequency constraint from a vibration analysis may cause an increase in the same design variable.

This paper discusses the FESOP (Finite Element Structural Optimization Program) program's ability to perform minimum weight optimization using two different finite element analyses and models. FESOP uses the ADS optimizer developed by Dr. Garret Vanderplaats to solve the nonlinear constrained optimization problem. The design optimization problem in the paper requires a response spectrum analysis and model to evaluate the stress and displacement constraints. However, the problem needs a frequency analysis and model to calculate the natural frequencies used to evaluate the frequency range constraints. The paper summarizes the results of both the successful and unsuccessful approaches used to solve this difficult weight minimization problem. The results show that no one ADS optimization algorithm worked in all cases. However, the Sequential Convex Programming and Modified Method of Feasible Directions algorithms were the most successful (Figure 1).

MINIMUM WEIGHT STRUCTURAL DESIGN

- *Multiple Analysis Types and Models
 - *Static, Vibration, Response Spectrum*
- *Multiple Loading Conditions
- *Conflicting Design Constraints
 - *Stress, Displacement, Frequency*
- *Different Functional Design Groups
 - *Static, Vibration*

FIGURE 1

PROBLEM

The engineer faces many conflicting requirements when designing equipment foundations. The design requirements are conflicting because a minimum weight response spectrum (stress) design will tend to decrease the structural stiffness, while a minimum weight natural frequency avoidance design will tend to increase the structural stiffness. Another problem arises from the fact that separate response spectrum and natural frequency analysis models may be required. A much finer finite element mesh may be needed in the vibration analysis to accurately determine the natural frequencies of vibration. This paper presents a multidisciplinary optimization procedure and program which has successfully integrated these analysis methods to

- (1) solve both the natural frequency and response spectrum finite element foundation models at the same time;
- (2) optimize these foundations for minimum weight while meeting both frequency avoidance and response spectrum design criteria;
- (3) arrives at producible equipment foundation designs (Figure 2).

Thus, instead of a time consuming trial and error approach to performing combined response spectrum and natural frequency avoidance foundation design, an automated process, using the FESOP computer program, now exists to arrive quickly and efficiently at producible and weight effective equipment foundations designs. The following paragraphs describe how FESOP was used to develop producible minimum weight designs.

FESOP (Finite Element Structural Optimization Program)

- *Solves Both Natural Frequency and Response Spectrum Analyses in Same Execution
- *Permits Different Finite Element Models for Each Analysis
- *Optimizes For Minimum Weight Using ADS
- *Satisfies Stress, Displacement, and Frequency Avoidance Constraints
- *Arrives at Producible Equipment Foundations

FIGURE 2

409

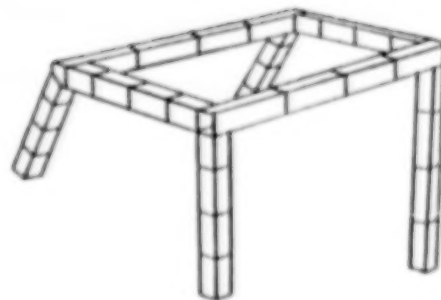
SAMPLE PROBLEM

Figure 3a is the response spectrum (stress) finite element model and Figure 3b is the vibration frequency finite element model. The response spectrum model employs the minimum number of finite elements needed to accurately assess the structure's performance, with only the equipment mass plus enough lumped masses to accurately model the foundation mass. However, the vibration model requires a much finer finite element discretization with an element mass definition but no equipment mass to accurately determine the structure's natural frequencies of vibration. Each math model, therefore, requires a separate analysis. In the normal design situation the engineer would set up the two models, run both analyses, evaluate two sets of results, change both models, rerun both models, and continue this process until the "optimum" design was established. At best this is a very time consuming and very imprecise procedure since the engineer relies only on his experience and intuition to modify the structure. In FESOP, an automated procedure exists: to read in both models, to perform both analyses, to evaluate the results of both analyses, to modify the math models as dictated by the numerical optimization program ADS, and to arrive at a producible true minimum weight foundation design while meeting all criteria.

SAMPLE EQUIPMENT FOUNDATIONS



**a - Response Spectrum
Model**



b - Vibration Model

FIGURE 3

470

ENGINEER'S FUNCTION

While FESOP improves and automates the normal design process, the engineer's knowledge is still required to achieve acceptable results. Usually two or more attempts with FESOP are required to arrive at an optimum weight equipment foundation due to the highly complex nature of the frequency avoidance problem. However, FESOP does provide an efficient means to arrive at this desirable result quickly and with little or no guesswork. In addition, by properly specifying the design constraints and variables, a truly producible structure will result.

While at first glance this would seem to be a very expensive process, in the long run the costs will be cheaper because the engineer will spend considerably less time making alterations to the design and rerunning the required analyses. He will be able to devote more cogitative effort to solving his design problem, and the design will be far superior in all aspects (Figure 4).

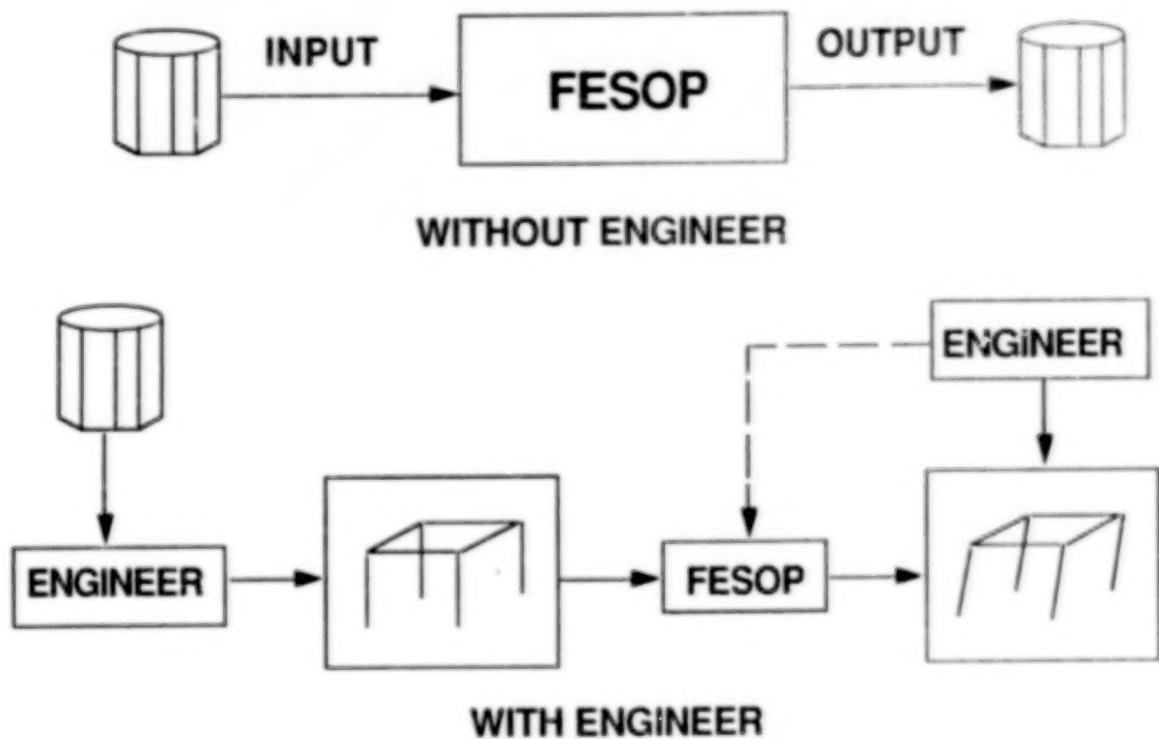


FIGURE 4

REQUIREMENTS

A combined response spectrum and vibration minimum weight design can be accomplished using many different approaches with FESOP. Some of the more important considerations for successful completion are the fineness of the finite element model; the choice and number of design variables; the choice of the optimization algorithm; the initial design of the FESOP analysis; and the producibility of the resulting structure. A number of recommended procedures have been developed to help ensure the best minimum weight design in the quickest manner possible, (Figure 5). In the following sections these important considerations are addressed, with samples of both good and bad applications to emphasize the point. Finally, a summary section discusses the successful combination of all of these features.

Fineness of Finite Element Model

Selection and Number of Design Variables

Optimization Algorithm

* - MFD, MMFD, SLP, SQP, SCP

Starting Point

- Upper or Lower Bound
- Feasible or Infeasible

Procedure

- One Step (All Constraints)
- Multiple Steps (Selected Constraints Then All)

FIGURE 5

* Defined in Figure 9.

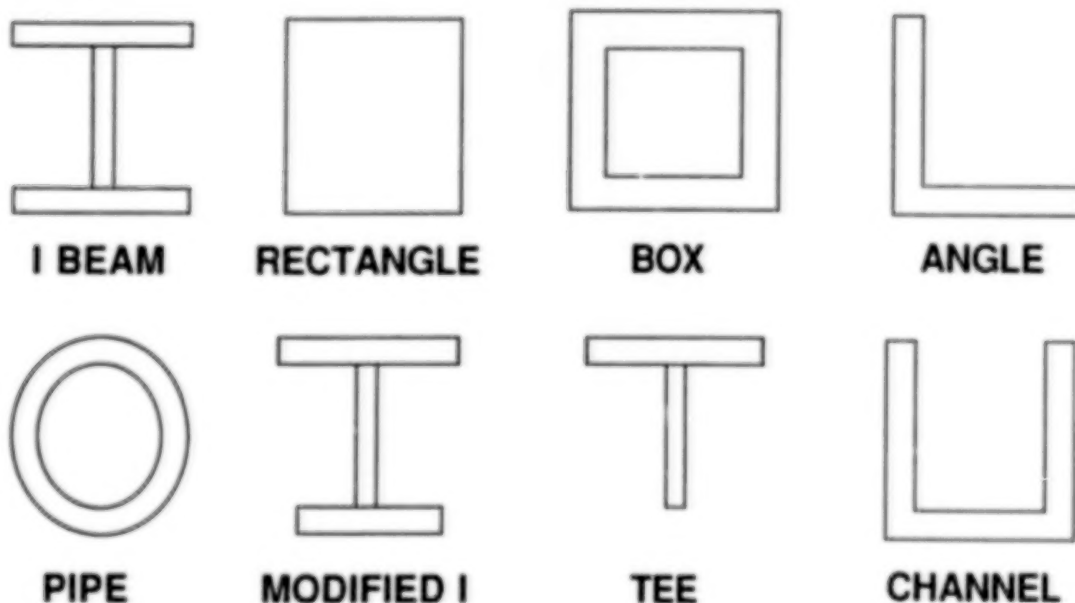
REQUIRED FINITE ELEMENT MODELS

In the sample problem, the vibration finite element model, Figure 3b, has approximately two times the number of finite elements as the response spectrum finite element model, Figure 3a. The vibration model is sufficiently complex to demonstrate a combined response spectrum and vibration foundation design optimization with FESOP. Although the discretization of the frequency model is different from that of the stress model, all of the reference data (material properties, cross-sections, eccentricities, thicknesses, etc.) must be and are identical in the two models. The reason for this is that as a design variable for one model's changes, it must change identically for the other model. The important thing to stress is that the major differences between the two models are the number of finite elements, the number of node points, and the definition of the mass associated with each model.

THE CHOICE AND NUMBER OF DESIGN VARIABLES

The choice and number of design variables affects the computer time it takes to arrive at an optimum solution; the ability of FESOP to give a true minimum weight solution; and the ability of FESOP to arrive at a producible structure. The greater the number of design variables, the more finite element solutions are required to determine the constraint gradients needed for the ADS optimizer, and consequently the longer and more costly the FESOP analysis. For example, in the sample problem every beam element box cross-section has five shape parameters: the depth, the width, the top thickness, the bottom thickness, and the side thickness (Figure 6). Thus, with the response spectrum model, there could be 16 different cross-sections (16 beam elements), with 5 design variables for each cross-section, or a total of 80 design variables. However, specifying such a large number of design variable would be ridiculous for two reasons: (1) more than 800 gradient evaluations would be required for both the models to obtain an optimum design, and (2) the resulting structure would clearly not be very producible. A more reasonable scheme would be to specify all of the horizontal members as having the same cross-section and all of the vertical or nearly vertical members having another cross-section. This would leave a total of ten design variables and only 100 gradient evaluations for a normal FESOP run. However, even in this case the structure could be very unproducible with mismatched cross-sections at the joints.

ALL WIDTHS AND THICKNESSES CAN BE DESIGN VARIABLES



Typical Beam Cross-Sections

FIGURE 6

SELECTED CROSS-SECTIONS

A better solution would be to allow only five design variables: the depth, width, and top thickness of the horizontal members; the top thickness of the vertical members; and the top thickness of the inclined members (Figure 7). The bottom and side thickness of the horizontal members; the depth, width, and bottom and side thickness of the vertical members; and the depth, width, and bottom and side thickness of the inclined members would all be dependent design variables. In this case the bottom and side thicknesses of each cross-section would equal the top thickness of the same cross-section. This would mean each box section would have a uniform thickness. The depth and width of the inclined members would be equal to the depth and width of the horizontal members, and the depth and width of the vertical members would equal each other and the width of the horizontal members. Figure 7 shows the five design variables for this case. In addition to such design variable linking for the sample foundation, the eccentricities at the joints are also linked to changes in the depth and width of the members. By doing this these eccentricities which are dependent upon the shape of the cross-section will change as the design variables change. With such limitations, the resulting optimized foundation will be very producible.

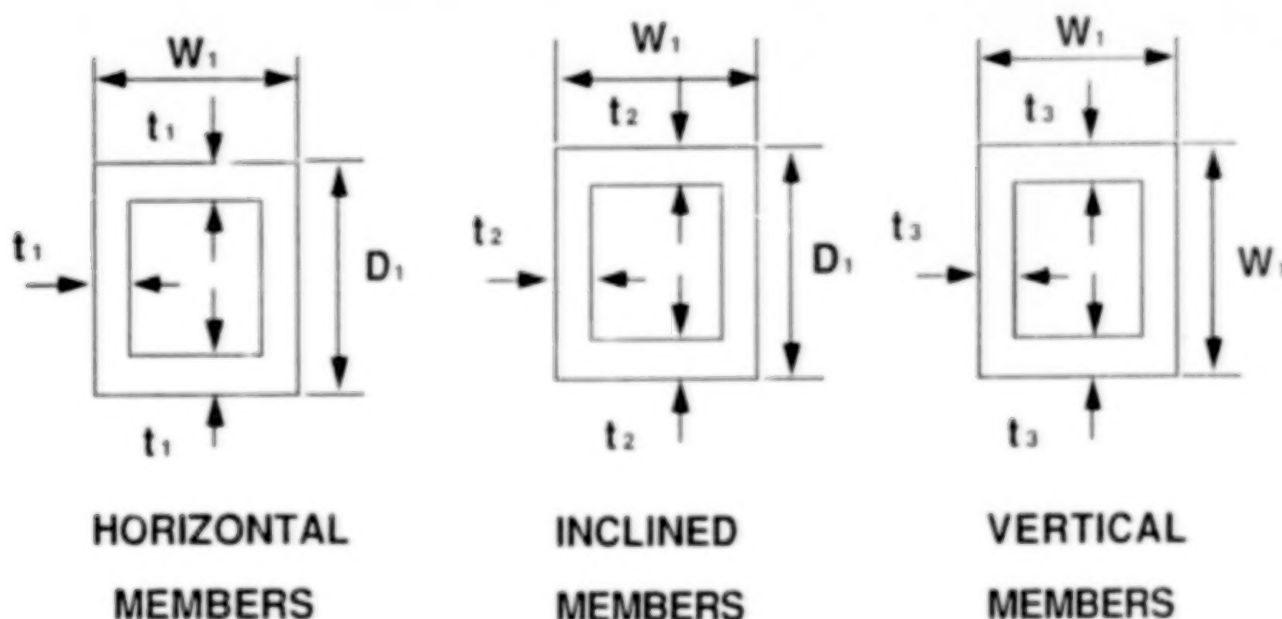


FIGURE 7

UNPRODUCIBLE OPTIMIZED STRUCTURE

Figure 8 is an example of a structure which was optimized without consideration of its producibility. The lack of linking created an impossible structure to build.

If further restrictions were made to the sample problem by making all widths and depth of each cross-section equal to the depth of the horizontal members, there would be only four design variables. And if the inclined and vertical members had the same thicknesses, the number of design variables would be three. However, because three design variables would allow very little variation in the structure, obtaining a minimum weight foundation could be very difficult. Experience has shown that with too few design variables an optimum weight foundation which satisfies all constraints frequently cannot be obtained. Therefore, it is simply too restrictive to make all of the box sections square with the same width and depth, but allowing the depth and widths to vary independently allows sufficient leeway to permit an optimum to be found. So having too many design variables or having too few design variables will both produce poor results. The best results are obtained by the judicious blend of design variables, as in this case where there are five design variables.

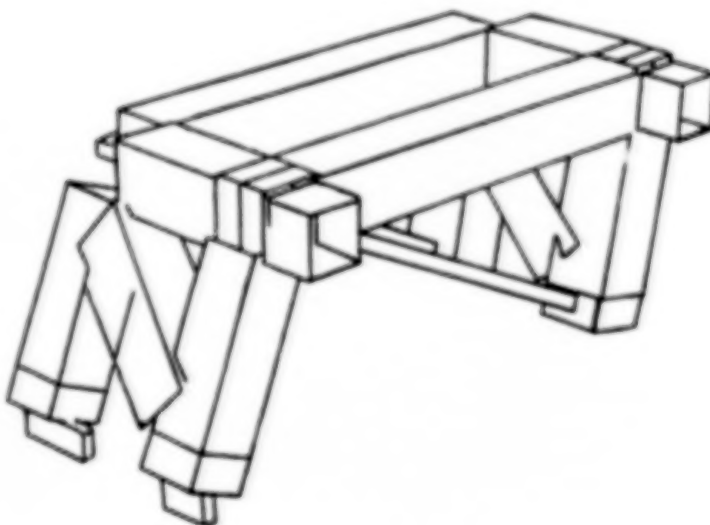


FIGURE 8

476

THE CHOICE OF THE OPTIMIZATION ALGORITHM

The ADS optimizer in FESOP offers the analyst many different optimization algorithms to choose from: the method of feasible directions (MFD), the modified method of feasible directions (MMFD), sequential linear programming (SLP), sequential quadratic programming (SQP), or sequential convex programming (SCP). (See Figure 9.) In problems with stress and/or displacement constraints, all of these methods will arrive at nearly the same minimum weight solution, with the only difference being the time it takes to arrive at the minimum weight solutions. However, with the combined response spectrum and vibration foundation design problem, which includes frequency avoidance constraints, the choice of the optimizer can make a significant difference. As will be shown, starting at the same point, two different optimization algorithms can produce two different optimum structures. In addition, both methods may not be able to produce an optimum weight foundation which satisfies all the constraints. Thus, no one algorithm will produce the best optimum all of the time. Therefore, in general, at least two of the optimizers should be used to insure the best chance of finding an optimum.

<p>MFD - METHOD OF FEASIBLE DIRECTIONS</p> <p>MMFD - MODIFIED METHOD OF FEASIBLE DIRECTIONS</p> <p>SLP - SEQUENTIAL LINEAR PROGRAMMING</p> <p>SQP - SEQUENTIAL QUADRATIC PROGRAMMING</p> <p>SCP - SEQUENTIAL CONVEX PROGRAMMING</p>
--

FIGURE 9

4 17

For the sample problem shown in Figures 3a and 3b, two different optimizers were selected to optimize for minimum weight and avoid frequencies from 80 to 120. The starting point for the optimization process was chosen as the upper limit of all design variables. Figure 10 shows the results using both the MMFD and SCP algorithms. In each case the process was started with only frequency avoidance constraints and no stress or displacement constraints. At points A and B the frequency only analysis was stopped and all other constraints were added. This is only one of the many ways to approach the problem. The SCP method arrived at a valid solution, but the MMFD method had two frequency constraint violations. With the MMFD method ADS simply could not find a way to change the design variables to eliminate the frequencies (82.0 and 114.1) within the range 80 to 120. However, Figure 10 also shows the results of using the MMFD method to avoid the frequency range of 48 to 72. In this case, the MMFD method was successful. Therefore, the analyst should always attempt more than one method when trying to avoid frequency ranges. Because the SCP method is the least expensive, I would recommend using it to start and then running the same problem with the MMFD method.

FREQUENCY AVOIDANCE USING DIFFERENT ADS ALGORITHMS

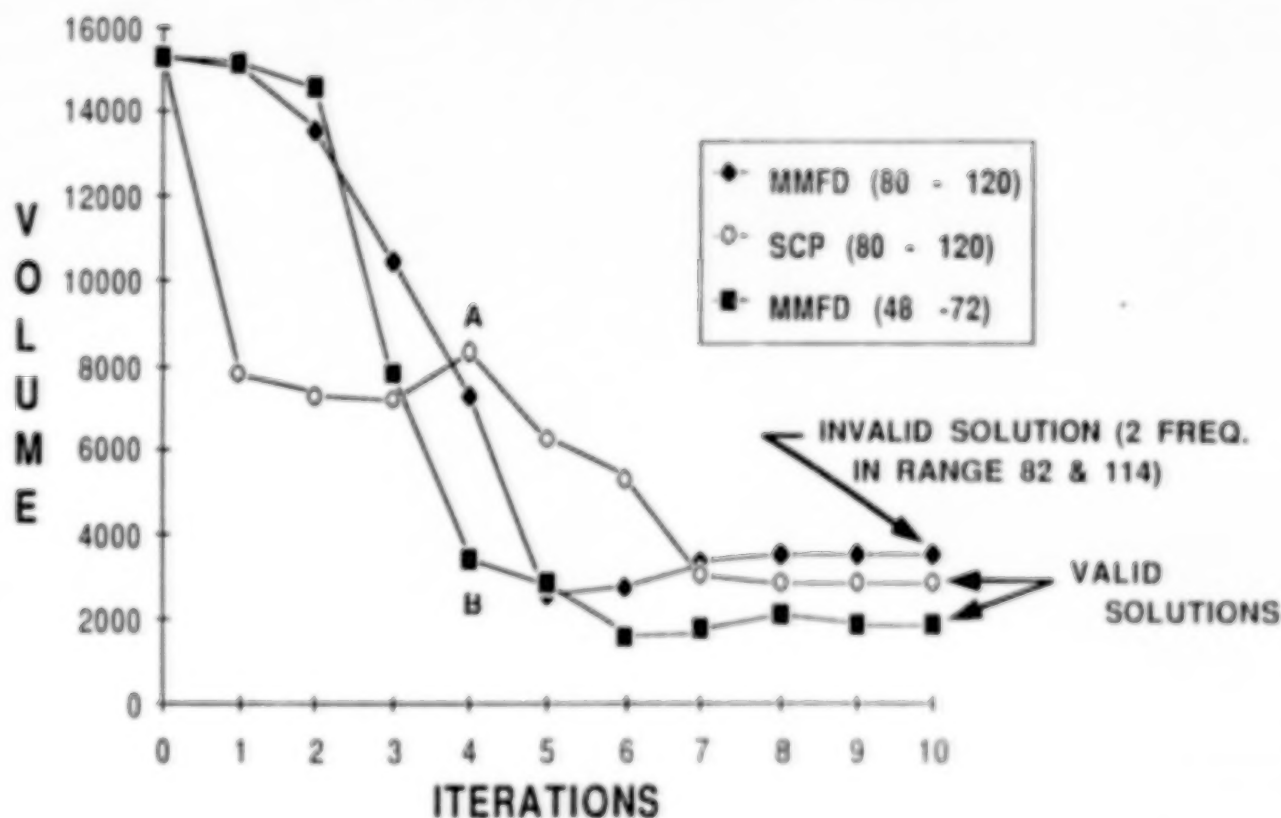


FIGURE 10

STARTING POINT FOR RESPONSE SPECTRUM AND VIBRATION FOUNDATION DESIGN

The shock and vibration foundation design optimization process can begin in any number of ways:

- (1) By applying all stress, displacement, b/t ratio, and frequency avoidance constraints from the start
- (2) By applying all constraints except the frequency avoidance constraints to obtain a fully stressed design, and by then optimizing with all constraints
- (3) By applying only the frequency avoidance constraints until a minimum weight foundation is found, and by then including the rest of the constraints
- (4) By using a minimum frequency constraint instead of a frequency avoidance constraint, and by then applying the frequency avoidance constraint
- (5) By starting with either a feasible stress design, an understressed design or an overstressed design in combination with one of the above (Figure 11).

Based upon this sample problem, no one starting procedure works best all the time, and some methods for starting almost never work and, therefore, should be avoided. In Figure 10 an understressed design was chosen for the starting point with all design variables at the upper limits. A frequency avoidance only starting procedure for the range 80 to 120 was initiated with two optimization algorithms, MMFD and SCP. Similarly, one was started to avoid the range 48 to 72 using only the MMFD algorithm. In the first case, the SCP algorithm worked and the MMFD did not, however, in the second case the MMFD algorithm worked. Looking at Figures 12 and 13 where other starting point procedures were tried, potentially better optimum solutions exist.

- (1) Apply all stress, displacement, b/t ratio, and frequency avoidance constraints from the start
- (2) Apply all constraints except frequency avoidance (fully stressed design), and then optimize with all constraints
- (3) Apply frequency avoidance only constraint, and then optimize with all constraints
- (4) Use minimum frequency only start, and then all constraints
- (5) Vary the initial design (lower or bound, feasible or infeasible) in conjunction with the first four procedures

FIGURE 11

449

In Figure 12, the SCP algorithm was used in conjunction with three different starting procedures in an attempt to arrive at an optimum weight foundation. This foundation was to avoid the natural frequencies of vibration from 48 to 72 and satisfy all stress constraints. The three approaches were

- (1) to first optimize with a minimum frequency constraint of either 48 or 72
- (2) to first optimize with only a frequency avoidance constraint (i.e. no stress or displacement constraints at the start)
- (3) to first optimize with no frequency constraints of any type (i.e. ignoring frequencies)

The first and second approaches were successful in producing an optimum weight structure; however, the optimum volumes differed significantly. In the first case, the final structure had no frequencies of vibration below 72 and a volume of 3300. In the second case (frequency avoidance only), a minimum weight structure with frequencies above and below the range was obtained, with a smaller volume of 2250. Attempting to first optimize with a minimum frequency of 48 and trying to first optimize by ignoring frequencies, both resulted in invalid solutions. For both of these cases, the final structures had unallowable frequencies within the range of 48 to 72. In these unsuccessful cases, the ADS optimizer simply could not find a way to change the design variables so as to move away from an invalid structure. This inability to move to a valid solution clearly demonstrates the need to attempt more than one approach when trying to obtain a minimum weight foundation with frequency constraints.

FREQUENCY AVOIDANCE IN RANGE 48 TO 72 USING SEQUENTIAL CONVEX PROGRAMMING

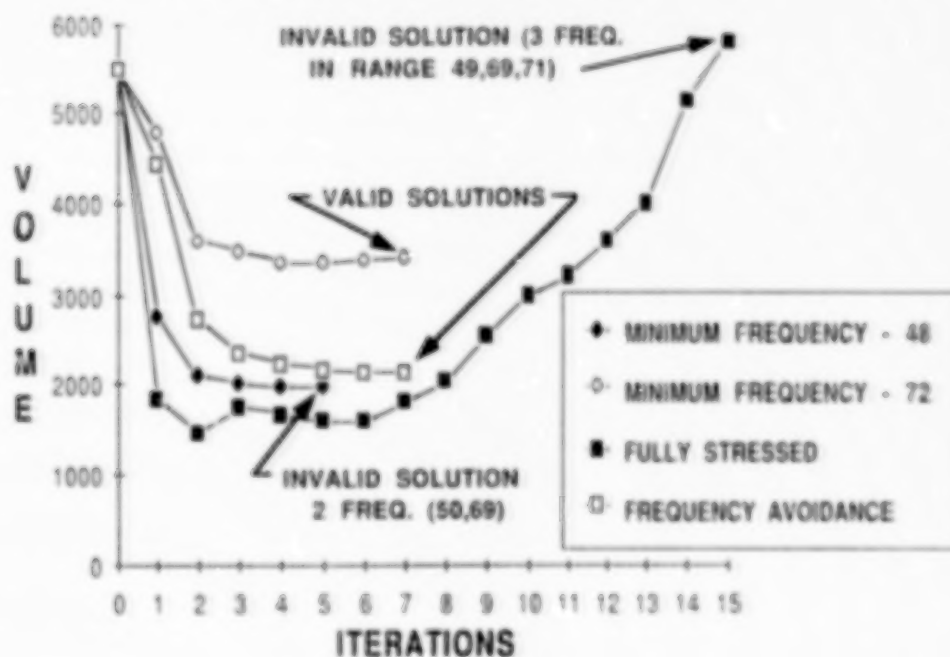


FIGURE 12

In Figure 13, two of the starting procedures employed in Figure 12 were used when trying to avoid frequencies in the range of 80 to 120. First, the SCP algorithm and a frequency avoidance only procedure was attempted. While this combination successfully obtained a minimum weight foundation with no natural frequencies in the range of 48 to 72 (Figure 12), the method was a complete failure when seeking to avoid the frequencies of 80 to 120. Similarly, optimizing with only stress constraints to start was a total failure in Figure 12, but provided two valid solutions in Figure 13, one for the SCP algorithm and one for the MMFD algorithm. The significance of this is that one starting procedure does not work all the time.

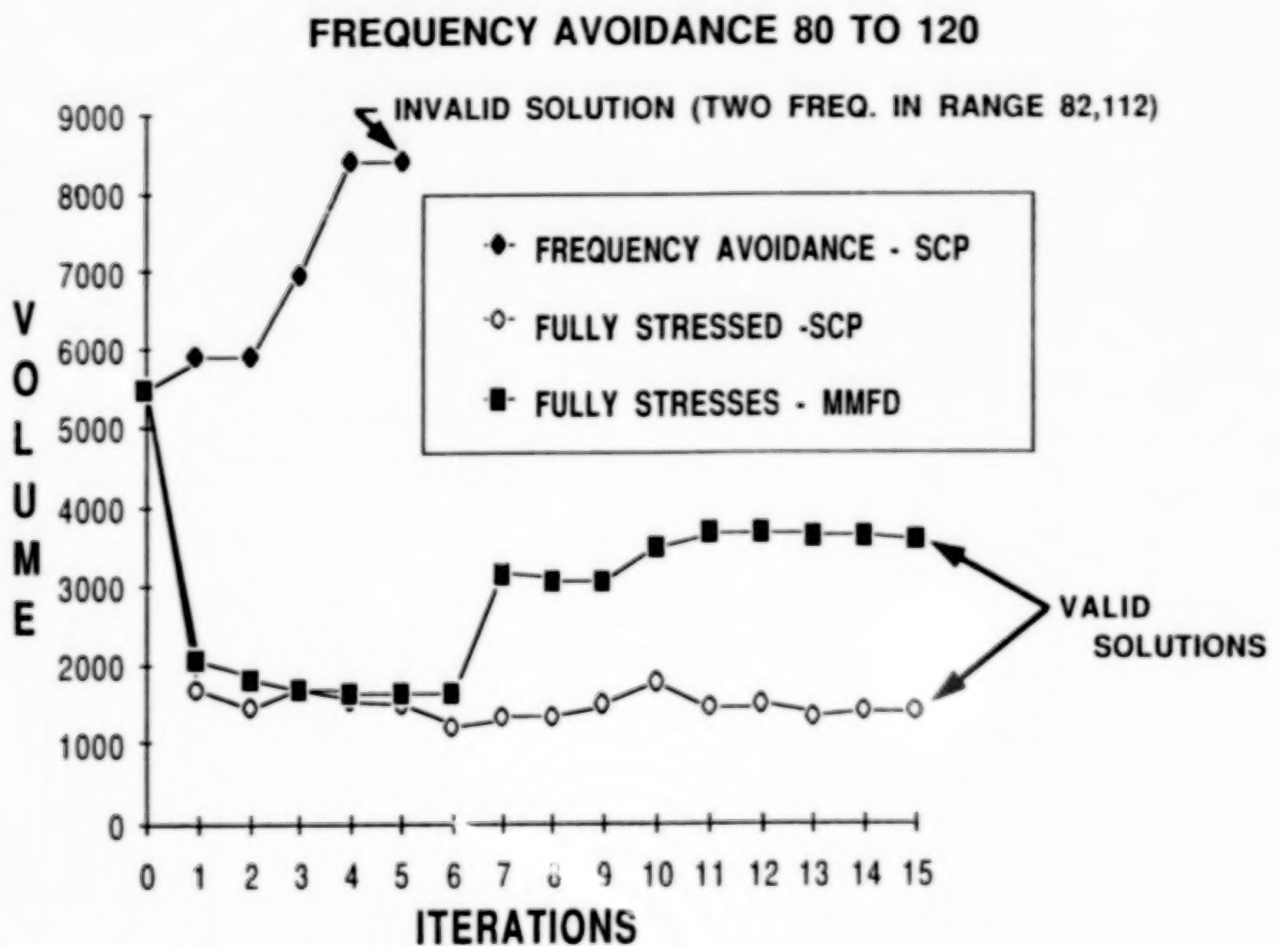


FIGURE 13

By reviewing the results in Figures 11 through 13, a number of conclusions can be drawn.

- (1) An optimum weight foundation which avoids certain natural frequencies of vibration can be found using FESOP's combined response and vibration capability.
- (2) Because of the highly complex nature of the frequency avoidance problem, a number of attempts with both different starting points and different optimization algorithms should be used to find the best optimum.
- (3) A procedure which should give a feasible optimum is to start with all design variables at their upper bound limits and perform a frequency avoidance only analysis with both the SCP and MMFD optimizers.
- (4) Next, an attempt from a reasonable design with either a frequency avoidance or maximum stress only starting point should be tried to see if a better optimum is obtained.
- (5) If no valid solution is obtained, a minimum frequency constraint for the upper bound of the allowable range should be tried. This should be the last resort because this will always result in the heaviest foundation.

Following these guidelines will help to insure the optimum equipment foundation in terms of producibility and weight.

TABLE - COMPARISON OF RESULTS

Frequency Range	Optimizer	Starting Point	Initial Constraint	Success	Objective
48 TO 72	SCP	FEASIBLE STRESS DESIGN (FSD)	$F_{min} > 48$	NO	2000
			$F_{min} > 72$	YES	3300
			$F < 48, F > 72$	YES	2250
			Stress Only	NO	5500
	MMFD	UPPER BOUND	$F < 48, F > 72$	YES	1800*
80 TO 120	SCP	UPPER BOUND	$F < 80, F > 120$	YES	2800
		FSD	$F < 80, F > 120$	NO	8300
			Stress Only	YES	1700*
	MMFD	UPPER BOUND	$F < 80, F > 120$	NO	3500
		FSD	Stress Only	YES	3300

* Best Optimum For Given Range

n° 482

PRODUCIBILITY CONSIDERATIONS

Producibility (Figure 14) is a factor which must be considered at all stages of the optimization process. The definition of the finite element model and, more importantly, the design variables must be made with producibility in mind. Otherwise, a foundation that is clearly unproducible, like the one shown in Figure 8, will result. The first step toward insuring a producible structure is to set limits on design variables which will be both reasonable and producible. However, this alone is not always enough because, during the optimization process, combinations of design variables which were not anticipated will probably result. Therefore, limits on the relationships between design variables should be made. In the sample problem the thickness of the box beams was limited to 25 percent of the cross-section width to insure that unreasonably thick box beams would not result. FESOP allows limits to be specified on the relationship between any two cross-section design variables, thus helping to insure a producible structure. In addition, as was mentioned on the choice of design variables, many design variables should be linked so as to guarantee that the changes in the structure will be uniform. This is important because it means that with design variable linking, radical size and shape changes will not take place.

- *A Primary Consideration at All Stages of the Optimization Process**
- *Vital to Definition of the Design Variables**
- *Must Also Limit Relations Between Design Variables**
- *Avoids Unproducible Structures**

FIGURE 14

RESULTS/CONCLUSIONS

Based upon the results presented, the following conclusions can be drawn:

- (1) One can successfully optimize two different finite element models and analyses with FESOP.
- (2) No one ADS optimizer works best all of the time.
- (3) Many starting procedures are possible, and each can produce different "optimums".
- (4) Producibility is a vital consideration.
- (5) The engineer's active participation is essential.

1. Report No. NASA CP-3031, Part 2		2. Government Accession No.		3. Recipient's Catalog No.	
4. Title and Subtitle Recent Advances in Multidisciplinary Analysis and Optimization				5. Report Date April 1989	
				6. Performing Organization Code	
7. Author(s) Jean-François M. Barthelemy, Editor				8. Performing Organization Report No. L-16568	
				10. Work Unit No. 506-43-41-01	
9. Performing Organization Name and Address NASA Langley Research Center Hampton, Virginia 23665-5225				11. Contract or Grant No.	
				13. Type of Report and Period Covered Conference Publication	
12. Sponsoring Agency Name and Address National Aeronautics and Space Administration Washington, DC 20546-0001 and Wright Research Development Center Wright Patterson AFB, OH 45433				14. Sponsoring Agency Code	
15. Supplementary Notes Conference Co-Chairmen: Jaroslaw Sobieski, NASA Langley Research Center Laszlo Berke, NASA Lewis Research Center Vipperla Venkayya, Air Force Wright Aeronautical Laboratory					
16. Abstract This three-part document contains a collection of technical papers presented at the Second NASA/Air Force Symposium on Recent Advances in Multidisciplinary Analysis and Optimization, held September 28-30, 1988 in Hampton, Virginia. The topics covered include: Helicopter Design, Aeroelastic Tailoring, Control of Aeroelastic Structures, Dynamics and Control of Flexible Structures, Structural Design, Design of Large Engineering Systems, Application of Artificial Intelligence, Shape Optimization, Software Development and Implementation, and Sensitivity Analysis.					
485					
17. Key Words (Suggested by Author(s)) Optimization Synthesis Systems Sensitivity Computers				18. Distribution Statement Unclassified - Unlimited Subject Category 05	
19. Security Classif. (of this report) Unclassified	20. Security Classif. (of this page) Unclassified		21. No. of pages 515	22. Price A22	

END

11—15—91